Modelling of Pulsed Electric Field Treatment on Microorganisms: Transient Electric Field and Forces Acting on Cell Membrane, Local Thermal Effects

This thesis is submitted for the degree of

Doctor of Philosophy

By

Bolin Song

In the

Department of Electronic& Electrical Engineering

University of Strathclyde

Glasgow, UK

2024

Declaration

This thesis is the result of the author's original research. It has been composed by the author and has not been previously submitted for examination which has led to the award of a degree.

Sign: 

Date: **September 2024**

Acknowledgments

I would like to express my sincere thanks and appreciation to a few people who have helped me a lot during my PhD study.

First and the most important one, I would like to knowledge my primary supervisor, Dr. Igor Timoshkin, for offering me the opportunity as his PhD student. The PhD life in the HVT research group means a lot to me and it has influenced me in a positive way for my entire life. He was always able to help me with the problems during research with his knowledge, his suggestions and decisions are trustworthy all the time not only for research but also for my life. He always encouraged me when I was feeling unconfident. I would never have finished the study and the thesis without his encouragement and guidance. There is an old saying in China which can be used to describe my heartfelt wishes: 'Teacher for one day, father forever.'

I would also like to thank Dr. Mark Wilson, Dr. Martin Given and Dr. Michelle Maclean. They helped me a lot with my experimental works. During the writing up stage, they arranged regular meetings for me to keep me motivated with writing up. Their suggestions and comments about my thesis expanded my thoughts a lot. Without their help, I cannot finish this thesis at all.

I would also like to thank my parents, my father, Xieming Song and my mother, Shuiying Xu. I know they are not good at expression. Although they could not provide academic help during my PhD, they kept supporting and encouraging me in their own quiet way.

Thanks to Dr. Qingjiang Xue who has helped me a lot in Glasgow as my best friend and roommate, it was a nice period of life to study and live with him, I will never forget that. Thanks to Mr. Hejun Tu who selflessly provided his house for me during my PhD study. Thanks to Dr. Burhan Tariq and Dr. Ting Liu, Dr. Qiteng Hong and Mrs Liping Xie, without you I would not have a happy PhD life in Glasgow. Thanks to everyone in HVT groups, it's a pleasure to be part of HVT.

Abstract

Irreversible or reversible pores could be generated in the cell membrane of microorganisms by pulsed electric field (PEF) treatment, which is generally called electroporation. Such process could be used for inactivation of microorganisms or bio-medical extraction. Both reversible and irreversible pores can be generated in bio-membranes this changes the permeabilization of the cell membrane, with the former allowing for transfection (DNA, RNA, etc.) and the latter for cell inactivation and bio fuel extraction. However, the PEF treatment is generally considered as 'non-thermal' due to the lesser significance of the thermal effect among the treatment samples. Although PEF is reported to be a non-thermal method, local heating effects which were not reported before does occur among biological cells during PEF treatment, different level of thermal excitation will be investigated in this study. Besides, the exact mechanism between the pulsed electric field and microorganisms were not fully understood. This study aimed to investigate the interaction between pulsed electric field and microorganisms, with thermal effects (local heating effects) also taken into account.

Three different novel analytical models were developed in this study: a linear model, a QuickField model and a COMSOL model. 'Hot spots' (due to local heating effects) were observed in the models and the characteristics of local heating effects were also investigated. The contribution of induced electric field strength in cell membrane and local heating effects were evaluated for electroporation process during PEF treatment. The results suggest that the significant induced electric field strength in cell membrane made the main contribution to electroporation. However, local heating effects could be significant when the treatment samples were highly conductive. The thermal force and electromagnetic force on the cell membrane were also investigated. Finally, the situation of penetrated membrane (pore was included in the cell membrane) was also modelled and it was found that

the local heating effects in the penetrated membrane were significant and could enhance the expansion of pores.

The cell nucleus was also included in the novel QuickField and COMSOL models, which were used to investigate the interactions between microorganism and external electric field, both electric field strength in membranes (cell membrane and nuclear membrane) and thermal effects were investigated. It was observed that, with nano-second PEF treatment, the induced electric field strength in the cell nucleus was strong enough to cause electroporation. Thermal effects could also be generated in cytoplasm.

The experimental works were performed using a self-built HV Blumlein generator. Different test cells were used to investigate the inactivation process of PEF treatment with different number of impulses. An alternative plasma treatment was also implemented to compare the inactivation effects between PEF treatment and Plasma treatment with the same Blumlein generator. It was found that the plasma treatment in metallic dish test cell could achieve stronger inactivation compared with PEF treatment with the same number of impulses.

List of acronyms

PEF	Pulsed Electric Field
HINS	High-Intensity narrow-spectrum
UV	Ultraviolet
DNA	Deoxyribonucleic acid
RNA	Ribonucleic acid
RF	Radio Frequency
ns-PEF	Nano second Pulsed Electric Field
AC	Alternating Current
DC	Direct Current
SS	Stainless steel
TOC	Total organic carbon content
TEM	Transmission electron microscopy
DBD	Dielectric barrier discharge
RC	Resistance and capacitance
RLC	Resistance, Inductance and capacitance
2D	Two-dimensional
LED	Light-emitting diode
HV	High voltage
Psi	Pounds per square inch

List of Tables

Table 6.3 Energy delivered to test cell with negative or positive polarity plasma treatment per impulse

Table I Test Arrangements: number of growing flasks for PEF and plasma treatment with 300,500 and 700 HV impulses

List of Figures

Figure (4.2.1) Electric potential distribution in the bio-cell model in the steady state dc conduction analysis, the reference line shows the path across which the transmembrane potential is obtained.

Figure (4.2.2) Potential differences along the reference line shown in **Figure (4.2.1)**. The voltage drops across the cell and nuclear membranes are circled.

Figure (4.2.3) Electric field distribution in the steady state DC conduction case. Zoomed in views are included to show the relationship between the electric field strength and position. The main domain was shown as uniform dark blue due to the low electric field strength in environmental fluid and cytoplasm compared with large field strength in cell membranes.

Figure (4.2.3.1) Electric field strength across the cell membrane, L represents the point moving around the circumference of the cell membrane from pole to pole with membrane thickness taken into account $(\frac{1}{2}\pi d \approx 7.8\ \mu m)$.

Figure (4.2.3.2) Electric field strength across the nucleus membrane. L represents the point moving around the circumference of the cell nucleus from pole to pole. The peaks were caused by calculation errors of software which cannot be solved in this model, thus there is no significant differences observed.

Figure (4.2.4) Current density distribution in the steady state condition.

Figure (4.2.5) Current density distribution in the steady state condition in the cell nucleus (graph obtained through zooming in a section of **Figure (4.2.4)** and changing the factor in the legend of cell nucleus from).

Figure (4.2.6) Power dissipation due to the conduction current in the steady state DC conduction case, single cell model.

Figure (4.2.7) Transient temperature increase distribution (ΔT) in 10 μs; electric field strength is 30 kV/cm.

Figure (4.2.8) Transient temperature increase distribution (ΔT) in 1 μs; electric field strength is 60 kV/cm and conductivity of fluid is 0.5 S/m.

Figure (4.3.1) transient model: Electric potential distribution, the reference line is included to show the path across which the transmembrane potential is obtained.

Figure (4.3.2) Potential differences along the reference line in **Figure (4.3.1)**. The voltage drops across the cell and nuclear membranes are circled. The values were calculated at positions on the reference line.

Figure (4.3.3) transient analysis: Electric field distribution at 1 ns. Zoomed in graph is included to show the relationship between the electric field strength and position. The main domain was shown as uniform dark blue due to the low electric field strength in environmental fluid and cytoplasm compared with the much higher field strength in cell membranes.

Figure (4.3.3.1) Electric field strength along the cell pole to pole following the arc of the membrane.

Figure (4.3.3.2) Electric field strength along the pole to pole arc of the cell nucleus membrane.

Figure (4.3.4) transient analysis: Electric field distribution at 1 ns, the maximum electric field strength in this figure is $\sim 3.1 \times 10^6\ V/m$ which facilitate a clear view of the electric field distribution in both cytoplasm and cell nucleus.

Figure (4.3.5) Current density distribution in of transient analysis in 1 ns.

Figure (4.3.5.1) transient analysis: Current density distribution at 1 ns, the maximum value of the current density in this figure was set to 2000 A/m^2 to resolve visually the current distribution in cytoplasm which allows the changes of current density in cytoplasm to be clearly observed.

Figure (4.4.1) QuickField model which includes multiple cells. Cell A and Cell B have a $0.1\ \mu m$ gap between them, the external membranes of Cell B and Cell C are in contact with one another.

Figure (4.4.2) Electric potential distribution in the steady state DC conduction simulation, the reference line is included to show the line across which the transmembrane potential is obtained.

Figure (4.4.3) Potential differences along the reference line in **Figure (4.4.2)**. The voltage drops and voltage increases across cell and nuclear membranes are circled. The values were measured at the positions on the reference line (for example: half circumference of cell nucleus).

Figure (4.4.4) Electric field distribution in the steady state DC conduction case. Reference lines were used to obtain the electric field strength of cell membranes (a), other similar reference lines were also used to obtain electric field strength in the nuclear membranes (b).

Figure (4.4.4.1) Electric field strength along the reference lines, the values were measured at the positions on the reference line (for examples: half circumference of cell nucleus. The potential drop between Cell B and Cell C was generated due to the calculation errors between boundaries and caused by software).

Figure (4.4.4.2) Electric field strength in nuclear membranes of each single cell, the values were measured at the positions on the reference line (for example: half circumference of cell nucleus), the electric field strength in transmit region is not clear on the graph as the values are negligible compared with the values in the membranes.

Figure (4.4.5) Current density distribution in the steady state case.

Figure (4.4.6) Power dissipation in the steady state case.

Figure (4.4.7) Electric potential distribution in transient field case, the reference line used to calculate transmembrane potential is included.

Figure (4.4.8) Potential differences along the reference line from **Figure (4.4.7)**. The voltage drops across the cell and nuclear membranes are circled.

Figure (4.4.9) Electric field distribution at 1 ns. The main domain was shown as uniform dark blue due to the low electric field strength in environmental fluid and cytoplasm compared with the much higher field strength in cell membranes. Reference lines (represent the environmental fluid/membrane boundary in the model) were used to obtain the electric field strength in the cell membranes (a), the same reference lines were also used to obtain the electric field strength in the nuclear membranes (b).

Figure (4.4.9.1) Electric field strength along the reference lines (electric field strength in cell membranes).

Figure (4.4.9.2) Electric field strength in the nuclear membranes of each single cell.

Figure (4.4.10) Electric field distribution at 1 ns, the maximum electric field strength of colour plot was limited to $\sim 3.1 \times 10^6\ V/m$ in order to show clearly the electric field distribution in the cytoplasm and cell nucleus.

Figure (4.4.11) Current density distribution at 1 ns.

Figure (4.4.11.1) Current density distribution at 1 ns, the maximum value was set to 2000 A/m^2 in order to show clearly the electric field distribution in the cytoplasm and cell nucleus.

Figure (5.1) General geometry of initial single cell model. The region between electrodes and fluid were used to avoid calculation errors between boundaries.

Figure (5.2) COMSOL model of a single cell, only the cell membrane was considered in the initial single cell model, the cell wall will be considered in section 5.7.2.

Figure (5.3) Electric field distribution in the treatment region at 10 μs. Horizontal and vertical axis show distance in units of μm.

Figure (5.4) Zoomed in view of the electric field distribution across the membrane pole at 10 μs (transient analysis). Axis dimensions in μm.

Figure (5.5) Zoomed in view of the electric field distribution across the membrane equator at 10 μs (transient analysis). Axis dimensions in μm.

Figure (5.6) Transient electric field strength at the membrane's pole during the first 10 μs of the PEF treatment, single cell model, and applied field is 30 kV/cm.

Figure (5.7) Temperature distribution in the single cell model at 10 μs. PEF treatment with an applied field magnitude of 30 kV/cm. Axis dimensions in μm.

Figure (5.8) Total heat source in the initial single cell model at 10 μs. PEF treatment with 30 kV/cm. Axis dimensions in μm.

Figure (5.9) Electric field distribution in the transient analysis at 10 μs; higher conductivity environmental fluid of 0.2 S/m. Axis dimensions in μm.

Figure (5.10) Zoomed in view of Electric field distribution in the transient analysis at 10 μs (at the membrane's pole). Higher conductive environmental fluid of 0.2 S/m. Axis dimensions in μm.

Figure (5.11) Zoomed in view of the electric field distribution in the transient analysis at 10 μs (at the equator), higher conductivity environmental fluid (0.2 S/m). Axis dimensions in μm.

Figure (5.12) Electric field strength at the pole during 10 μs after application of the PEF impulse. Single cell model, 30 kV/cm applied electric field strength.

Figure (5.13) Temperature distribution in the initial single cell model at 10 μs PEF treatment, 30 kV/cm applied electric field strength, higher conductivity environmental fluid (0.2 S/m). Axis dimensions in μm.

Figure (5.14) Total heat release (source) in the single cell model at 10 μs. PEF treatment with 30 kV/cm in higher conductivity environmental fluid (0.2 S/m). Axis dimensions in μm.

Figure (5.15) Electric field distribution in the transient analysis at 10 μs with higher, 67 kV/cm, applied electric field strength. Axis dimensions in μm.

Figure (5.16) Zoomed in view of the Electric field distribution at the membrane pole in the transient analysis at 10 μs; applied electric field is 67 kV/cm). Axis dimensions in μm.

Figure (5.17) Zoomed in view of the Electric field distribution at the membrane's equator in the transient analysis at 10 μs; applied cm electric field is 67 kV/ (). Axis dimensions in μm.

Figure (5.18) Electric field strength at the pole during 10 μs. PEF treatment of single cell applied electric field strength is 67 kV/cm.

Figure (5.19) Temperature distribution in the initial single cell model at 10 μs. PEF treatment with 67 kV/cm. Axis dimensions in μm.

Figure (5.20) Total heat release (source) in the initial single cell model at 10 μs. PEF treatment with 67 kV/cm. Axis dimensions in μm.

Figure (5.21) Electric field strength at the pole during 200 μs PEF treatment. Single cell model, applied field is 30 kV/cm.

Figure (5.22) Temperature distribution in the single cell model at 100 μs. PEF treatment with 30 kV/cm. Axis dimensions in μm.

Figure (5.23) Electric field strength at the pole during 200 μs. PEF treatment in the single cell model, applied field is 67 kV/cm.

Figure (5.24) Temperature distribution in the initial single cell model at 100 μs. PEF treatment, applied field is 67 kV/cm. Axis dimensions in μm.

Figure (5.25) Simplified figure illustrating calculation of the electro-mechanical forces acting upon the cell membrane.

Figure (5.26) Magnitude of the electro-mechanical force acting upon the upper part of the cell membrane in 30 kV/cm field and in low conductivity environmental fluid (0.0005 S/m).

Figure (5.27) Electro-mechanical force acting upon the upper part of cell membrane in the field with magnitude of 30 kV/cm strength and in high conductivity environmental fluid (0.2 S/m).

Figure (5.28) Electro-mechanical force acting upon the upper part of cell membrane in the field with magnitude of 30 kV/cm strength and in low conductivity environmental fluid (0.0005 S/m).

Figure (5.29) Electro-mechanical force acting upon the upper part of the cell membrane in the field with magnitude of 67 kV/cm strength in low conductivity environmental fluid (0.0005 S/m).

Figure (5.30) Electro-mechanical force acting upon the upper part of the cell membrane with 67 kV/cm field strength and high conductivity environmental fluid (0.2 S/m).

Figure (5.31) Electromagnetic force acting across the cell membrane at the lower part of the membrane, step voltage energization, external field strength is 67 kV/cm.

Figure (5.32) Step function signal used to obtain **Figure (5.31).**

Figure (5.33) The temperature-dependent conductivity of water.

Figure (5.34) Assumption of temperature-dependent permittivity of water (Real part of permittivity of water) based on data from [323].

Figure (5.35) Imaginary part of permittivity of water as a function of the temperature.

Figure (5.36) Temperature distribution in the single cell model at 1 μs. PEF treatment with 67 kV/cm electric field strength in high conductivity environmental fluid (0.1 S/m). Axis dimensions in μm

Figure (5.37) Thermal force across the cell membrane during the PEF treatment with 67 kV/cm electric field strength in highly conductive environmental fluid (0.1 S/m).

Figure (5.38) Electromagnetic force during the PEF treatment with 67 kV/cm electric field strength in highly conductive environmental fluid (0.1 S/m).

Figure (5.39) The signal of the 2 μs ramp, it rises from 0 V to a maximum constant voltage of 255 V.

Figure (5.40) Temperature distribution in the single cell model at 2 μs. PEF treatment with 67 kV/cm electric field strength in high conductive environmental fluid (0.1 S/m). Axis dimensions in μm.

Figure (5.41) Maximum Temperature obtained in the model as a function of time during the PEF treatment with 67 kV/cm electric field (voltage wave shape as shown in **Figure 5.39**) in high conductive environmental fluid (0.1 S/m).

Figure (5.42) Electromagnetic force during the PEF treatment with 67 kV/cm electric field in high conductive environmental fluid (0.1 S/m), applied voltage waveform shown in **Figure (5.39)**.

Figure (5.43) Thermal force during the PEF treatment with 67 kV/cm electric field in high conductive environmental fluid (0.1 S/m), applied voltage waveform shown in **Figure (5.39)**.

Figure (5.44) 2μs Square Wave used in the present analysis.

Figure (5.45) Temperature distribution in the single cell model at 2 μs. PEF treatment with 67 kV/cm electric field in high conductive environmental fluid (0.1 S/m), with the square voltage pulse applied. Axis dimensions in μm.

Figure (5.46) Maximum temperature during the PEF treatment with 67 kV/cm electric field in high conductive environmental fluid (0.1 S/m), square HV pulse is applied.

Figure (5.47) Electromagnetic force during the PEF treatment with 67 kV/cm electric field in high conductive environmental fluid (0.1 S/m), square 2us HV impulse.

Figure (5.48) Thermal force during the PEF treatment with 67 kV/cm electric field in high conductive environmental fluid (0.1 S/m), square 2us HV impulse applied.

Figure (5.49) Temperature distribution in the single cell model at 100 ns. PEF treatment with 1 GHz AC oscillating signal with a peak voltage of 360 V, in high conductive environmental fluid (0.01 S/m). Axis dimensions in μm.

Figure (5.50) Temperature of "hot spot" in the single cell model as a function of the treatment time. PEF treatment with 1 GHz AC oscillating signal with a peak voltage of 360 V, in high conductive environmental fluid (0.01 S/m).

Figure (5.51) Electromagnetic force as a function of time during the PEF treatment with 200 MHz AC oscillating signal in high conductive environmental fluid (0.1 S/m), AC signal frequency is 200 MHz, voltage peak value is 360 V.

Figure (5.52) A model of the membrane with a pore.

Figure (5.53) Pore in the membrane in the COMSOL model

Figure (5.54) Temperature distribution at 10 μs in the model with a pore, $\alpha = 15^{\circ}$, pore diameter d=1 nm. Axis dimensions in μm.

Figure (5.55). Temperature distribution in the pore: zoomed in view of **Figure (5.54)**. Axis dimensions in μm.

Figure (5.56) Simulation results for the single cell model with the pore in the membrane: (a) Maximum electric field in the pore as a function of α for t= 25 μs, (b) Maximum temperature as a function of the pore diameter at t= 25 μs and α=5° , (c) Maximum temperature in the pore as a function of time for different α, d=1 nm.

Figure (5.57) Electric field strength at the same location (α=0°) in the case of the electro-porated membrane (blue) and intact membrane (green).

Figure (5.58) General topology of the ellipsoidal cell model, cell wall was included in the single cell model, it will be included in further sections.

Figure (5.59) Temperature distribution in the ellipsoidal model at 2 μs with 67 kV/cm treatment, conductivity of fluid: 0.01 S/m. Axis dimensions in μm.

Figure (5.60) Maximum temperature in the local hot spot of the Spherical model

Figure (5.61) Maximum temperature in the local hot spot in the ellipsoidal model

Figure (5.62) Electro-mechanical force across the cell membrane at the lower part of the cell under step voltage energization (External field strength: 67 kV/cm).

Figure (5.63) Temperature across the cell membrane in the spherical model with AC oscillating signal, conductivity of environmental fluid is 0.01 S/m, maximum field strength is 67 kV/cm.

Figure (5.64) Temperature across the cell membrane in the ellipsoidal model with AC oscillating signal applied, conductivity of environmental fluid is 0.01 S/m, and maximum field strength is 67 kV/cm.

Figure (5.65) Single cell model with cell nucleus

Figure (5.66). Electric field strength distribution in the nucleus membrane at 500 ns.

E_0=30 kV/cm.

Figure (5.67). Electric field strength distribution in the cell membrane at 500 ns.

E_0=30 kV/cm

Figure (6.6.2) *Heraeus Labofuge* 400R centrifuge and centrifuged sample

Figure (6.6.3) Diagram of change in of light intensity during passage through a sample in the spectrophotometer. (I_0 represents the intensity of light entering the sample and I_1 represents the light emerging on the other side of the sample. L represents the light path length.)

Figure (6.6.3.1) Growth curve for culture with different concentration of nutrient based on absorbance at 680 nm wavelength. (Higher absorption of light represents the higher population of microalgae.)

Figure (6.6.3.2) Transmission result of spectrometer scanning wavelength from 400nm to 800nm. A progressive and consistent decrease of transmission can be observed at about 680 nm wavelength.

Figure (6.6.3.3) Growing cycle measurement with spectrophotometer. The graph shows growth curve behaviour over 14 days.

Figure (6.6.3.4) Cytometer used in experiment (a) and counting zones under microscope (b) which are marked in zone 1, zone 2, zone 3 and zone 4.

Figure (6.6.3.5) Growth cycle measurement with cytometer counting. The result shows the growing cycle follows the tendency of spectrometer measurement. Three groups of samples are recorded: B1, B2 and B3.

Figure (6.7.1.1) PEF treatment: 500 impulses treatment with electric field strength 70 kV/cm. Magnification x100. Both A and B were from two random locations.

Figure (6.7.1.2) PEF treatment: 1000 impulses treatment with electric field strength 70 kV/cm. Magnification x100. Both A and B were from two random locations. The large green objects were considered to be paramecium *bursana* or *amoeba* from bag provided by the company Reefphyto and couldn't be avoided, furthermore they have no effects on the experimental results in this work.

Figure (6.7.1.3) PEF treatment: 1500 impulses. Treatment with electric field strength of 70 kV/cm. Magnification x100. Both A and B were from two random locations.

Figure (6.7.1.4) PEF treatment: 2000 impulses treatment with electric field strength 70 kV/cm, Magnification x100. Both A and B were two from random versions locations.

Figure (6.7.2.1) Culture flasks of 500 and 1000 number of impulses PEF treatment samples at: (a) Day 0, (b) Day 1, (c) after 12 days.

Figure (6.7.2.2) Growth curve of PEF treatment with cuboid metallic test cell with 100 number of impulses. Abs represents the absorbance of 680 nm wavelength by microalgae, the data is recorded every 2 days. The error bars represent standard deviation. Three groups are measured and there are 3 samples in each group.

Figure (6.7.2.3) Growth curve of algae treated in the metallic test cell with 500 and 1000 impulses. Abs represents the absorbance at 680 nm, the data is recorded every 2 days. Four groups are measured and there are 3 samples in each group. The error bars represent standard deviation.

Figure (6.7.2.4) Growth curve of algae treated in the metallic test cell with 500 and 700 PEF impulses. Abs represents the absorbance at 680 nm, the data is recorded every 2 days. Four groups are measured and there are 3 samples in each group. The error bars represent the standard deviation.

Figure (6.7.4.1) Charge redistribution in microalgae with external field applied, the cell wall is not shown in this diagram as it doesn't contribute to charge accumulation and distribution during PEF treatment as discussed in Chapter 4 and Chapter 5.

Figure (6.7.5.1) HV electrode with 6-needles mounted on plate (a) and schematic diagram of test cell (b). The needles are set at the same level and the tips are just attached to the surface of samples.

Figure (6.7.5.2) Recorded waveform of voltage applied to the test cell from both metallic dish positive plasma treatment (a) and positive plastic dish plasma treatment (b).

Figure (6.7.5.3) Recorded waveform of voltage applied to the test cell from both metallic dish negative plasma treatment (a) and plastic dish negative plasma treatment (b).

Figure (6.7.5.4) Growing culture of microalgae treated with negative plasma, centrifuged and control groups after 12 days. Flasks marked as 1, 2 and 3 represent 500 impulses treatment group; Flasks marked as 4, 5 and 6 represent 1000 impulses treatment group; Flasks marked as 7, 8 and 9 represent control group; Flasks marked as 10, 11 and 12 represent centrifuged group.

Figure (6.7.5.5) Growth curve of microalgae treated with 500 and 1000 negative polarity plasma impulses. Abs represents the absorbance at 680 nm, the data is recorded at day 0 and on each day when a treatment had occurred. Four groups are measured and there are 3 samples in each group. The error bars represent standard deviation. The longer gaps between measurements occurred because of weekends when no treatments or measurements were possible.

Figure (6.7.5.6) Culture of algae treated with negative plasma impulses, at day 0 (a) and 12 days after treatment (b). There is no microalgae detected after 1000 negative plasma impulses. (Flasks marked as 4, 5 and 6). Flasks marked as 1, 2 and 3 represent 500 impulses treatment group; Flasks marked as 7, 8 and 9 represent control group; Flasks marked as 10, 11 and 12 represent centrifuged group.

Figure (6.7.5.7) Culture of algae (10 days old) after the treatment with positive polarity plasma impulses, Flasks s 1, 2 and 3: algae treated with 500 impulses; Flasks 4, 5 and 6: algae treated with 1000 impulses; Flasks 7, 8 and 9: control group; Flasks 10, 11 and 12 centrifuged group.

Figure (6.7.5.8) Growth curve of algae treated with 500 and 1000 positive polarity plasma impulses (a) and growing culture at day 9 (b). Abs represents the absorbance at 680 nm, the data is recorded at day 0 and every day after treatment. The error bars represent standard deviation. Four groups are measured and there are 3 samples in each group. There are 2 days between day 4 and day 7 as there are weekend between them.

Figure (6.7.5.9) Culture of positive plasma tests at Day 0 (a) and after 20 days (b). Flasks 1, 2 and 3: algae treated with 500 impulses; Flasks 4, 5 and 6: algae treated with 1000 impulses; Flasks 7, 8 and 9: control group; Flasks 10, 11 and 12 centrifuged group.

Figure (6.7.5.10) one example of wave shapes recorded from oscilloscope of one single impulse delivered to the test cell of negative plasma. Red line represents the moment when the breakdown is occurring. The current signal is recorded with current transformer introduced in **Section 4.5.**

Figure (6.7.5.11) one example of wave shapes recorded from oscilloscope of one single impulse delivered to the test cell of positive plasma. Red line represents the moment when the breakdown is occurring. The current signal is recorded with current transformer introduced in **Section 4.5.**

Figure I. Growing flasks of experiments in **Section 6.7.1** at Day 0. The light intensity was not measured in this experiment, however, there are gaps between these flasks and the parameters of lamps are the same, thus the light intensity could be considered as the same.

Figure II. Growth curve of algae after the plasma treatment with different number of impulses and polarity in the metallic dish. Abs represents the absorbance at 680 nm, the data is recorded at day 0 and every day after treatment. The error bars represent standard deviation. 8 groups are measured and shown in this graph.

Figure III. Growth curve of plasma treatment with different number of impulses and polarity in plastic dish. Abs represents the absorbance of 680 nm wavelength by microalgae, the date is recorded at day 0 and every day after treatment. The error bars represent standard deviation. 8 groups are measured and shown in this graph.

Figure IV. Growth curve of PEF treatment results with different number of impulses. Abs represents the absorbance of 680 nm wavelength by microalgae, the date is recorded at day 0 and every day after treatment. The error bars represent standard deviation. 5 groups are measured and shown in this graph.

Figure V. Growing curve of PEF treatment and plasma test in different containers (both positive polarity and negative polarity) with different number of impulses. Abs represents the absorbance of 680 nm wavelength by microalgae, the data is recorded at day 0 and every day after treatment. The error bars represent standard deviation. 7 groups are measured and shown in this graph.

Figure VI. One example of wave shapes recorded from oscilloscope of one single impulse delivered to the test cell of Negative Plasma with plastic dish. The current signal is recorded with current transformer introduced in **Section 4.5.**

Figure VII. One example of wave shapes recorded from oscilloscope of one single impulse delivered to the test cell of Negative Plasma with metallic dish. The current signal is recorded with current transformer introduced in **Section 4.5.** Where the red line represents the breakdown occurs.

Figure VIII. One example of wave shapes recorded from oscilloscope of one single impulse delivered to the test cell of metallic PEF treatment test cell. The current signal is recorded with current transformer introduced in **Section 4.5**.

List of publications

1. Bolin Song et al., "Local heating and stresses across membranes of microorganisms stressed with electric field," 2017 IEEE 21st International Conference on Pulsed Power (PPC), Brighton, UK, 2017, pp. 1-6, doi: 10.1109/PPC.2017.8291274.
2. Bolin Song, Timoshkin, I. V., Wilson, M. P., Maclean, M., Given, M. J., & MacGregor, S. J. (2022). Modelling of the temperature gradient across biological cell membranes stressed with pulsed electric fields. In *2022 IEEE International Conference on High Voltage Engineering and Applications (ICHVE)* Article 22337308 (IEEE International Conference on High Voltage Engineering and Applications (ICHVE)). IEEE. https://doi.org/10.1109/ichve53725.2022.9961405
3. Bolin Song, Timoshkin, I. V., Wilson, M. P., Maclean, M., Given, M. J., & MacGregor, S. J. (2023). *Electric field distribution and thermal effects in biological cells under PEF treatment*. Abstract from 15th Universities High Voltage Network Colloquium, Glasgow, United Kingdom.

Table of Contents

Chapter 1. Introduction

Different approaches to electrically assisted inactivation of microorganisms have been studied and developed with a view to their practical implementation in several industrial applications. However, the established disinfection and bio-decontamination approaches have specific limitations which restrict their suitability and economic viability, and may result in generation of undesirable by-products during the treatment. Therefore, there is a significant demand for novel methods of inactivation of microorganisms which overcome these challenges. Further development and improvement in decontamination and disinfection techniques are urgently required in areas such as food industry, medical and environmental applications.

Electrically assisted methods of rupture of biological membranes can also be used for lysis of microorganisms during such process, the cell's outer membrane breaks down, releasing its contents. It is known that several micro-organisms contain substances which could be used in food, medical and energy applications. For example, several species of green micro-algae contain carbon compounds such as triacylglycerol [1], a chemical compound which could be used for production of biodiesel fuel. Micro-algae contain different carbohydrates (including glycogen, starch, agar and cellulose), thus such rich carbohydrate content make them suitable for the production of bioethanol.

Micro-algae have a significant potential for applications not only in the field of renewable bio-diesel and ethanol production, but also in the pharmaceutical and nutraceutical industries [2].

To allow the carbohydrates which are present in micro-algae to be extracted for further use, bio-membranes of micro-algae (microorganisms) should be ruptured to facilitate the lysis process (the process of breaking down the cell membranes

through physical, chemical or enzymatic methods) to release these valuable substances for processing.

Techniques for extracting the contents of microorganisms have drawn significant research and practical interest in recent years. For example, several microorganisms have significant lipid -like compounds, including hydrocarbons, glycerolipids, and sterols [3]. Fatty acids which are present in triacylglycerols (which is the main form of lipid storage, [4]) can be used for biofuel production, which is a potential alternative to fossil fuels.

However, to achieve economic viability of production of biofuels from micro-algae, the extraction process should be made more efficient - the high cost of the extraction process is one of the main challenges that hinders biofuel production from microorganisms on an industrial scale.

One of the methods that can help to achieve this aim to improve the efficiency of extraction of fatty acids from microalgae is the pulsed electric field (PEF) process.

The first study of the PEF treatment of microorganisms can be traced back to 1967, when scientists found lethal effects after a suspension of microorganisms was treated with a high electric field [5]. After that, the theory of electroporation process was put forward when the formation of pores occurred. When a microorganism is subjected to an external electric field, pores can be generated in the cell membrane. These pores can be either reversible or irreversible, depending upon the field strength and treatment time. The electroporation process makes the PEF treatment a potential approach to the inactivation of microorganisms and field stimulated lysis which helps the extraction of cell contents.

Significant progress in the development of PEF treatment and understanding the mechanisms of interaction between the pulsed electric field and microorganisms have been achieved during the last several decades [6] [7] [8]. This process is generally considered as a non-thermal process [8], a characteristic that makes PEF

treatment desirable in several practical applications, for example in the food industry, and the PEF process continues to attract significant research attention.

Many different energization regimes and PEF chambers have been designed and investigated to improve the efficiency of the PEF process [10] [11] [12] [13]. There are also studies focused on the operational and biological factors during the PEF treatment, such as the electric field strength in the membrane, pulse wave shape, size of microorganisms and parameters of treatment samples [8].

However, the exact mechanisms of interaction between the external field and bio-cells are not fully understood. It is difficult to take into account multiple different parameters in theoretical analyses. These parameters include the cell structures, pulse wave shape, and shape of bio-cells. As local thermal effects during the PEF treatment are generally not taken into account in investigations of this treatment, the link between the electric field and thermal effects also required further investigation. Hence, a more comprehensive approach to modelling of the PEF effects in a bio-cell will be developed in this project, to help in further understanding of the electric field distribution and thermal effects during the PEF treatment with different parameters. Thereafter, the results of experimental work will be presented, which will provide data for use in the simulation models.

An overview of the content of each chapter in this thesis is given below.

Chapter 2 (Background information and literature review) provides basic background information related to the field of study in this project, to provide an understanding of the characteristics of microorganisms and the PEF treatment analysis. The technical fundamentals of PEF treatment are presented and discussed. Discussion and comparison between the PEF treatment and other inactivation approaches is included. A literature review of the PEF treatment technique, encompassing inactivation mechanisms, mathematical simulations and test chambers, is also discussed in this chapter.

Chapter 3 (Linear model of microorganisms) introduces the main principles used in the analysis of the PEF treatment of microorganisms. Initial one-dimensional mathematical models are also developed to investigate the interaction between the external electric field and bio-cells.

In Chapter 4, a 2D axisymmetric model was developed using QuickField software. This advanced model is used to investigate more detailed interactions between the external electric field and microorganisms such as: the transient electric field strength in cytoplasm, cell nucleus and thermal effects.

In Chapter 5, a more advanced (as compared with the QuickField model) 2D axisymmetric model was developed using the COMSOL Multiphysics software package. The COMSOL model provides the basis for the detailed investigation of the transient fields and forces during the PEF treatment of microorganisms. Moreover, this model allows for the application of AC signals in the PEF model treatment. The forces exerted on the microorganisms during the PEF treatment have also been investigated. The COMSOL model was also used to study the thermal effects in bio-membranes under electrical field stress, including membranes with a pore (penetrated membrane).

Chapter 6 (PEF treatment and plasma treatment of microalgae) introduces the experimental results obtained during this project. The equipment and experimental procedures are presented and discussed, as are the modelling and development of the pulse generation system used throughout this project. The obtained results are discussed and the main conclusions on the experimental part are provided at the end of this chapter.

Chapter 7 (Conclusion and future work) summarizes the novelty of this work, presents and discusses the main findings of this project and highlights the contribution of this project to the field of study (PEF treatment and modelling). Further work and potential practical applications of the results obtained in this

thesis, as well as potential challenges to their implementation, are also presented and discussed.

The Appendix introduces more complex experimental works including PEF treatment and Plasma treatment with different conductions (different test cells and different polarity of impulses), however, there may be problems with the results recorded and they are considered as not qualified compared with expected behaviour. Potential reasons are discussed in the appendix and which could be useful for further investigations.

Chapter 2. Background and literature review

2.1 Background information of microorganisms

Microorganisms were firstly observed in 1670s by *Leeuwenhoek* with his microscope, 200 years before the identification of the subject of microbiology by the famous swan-necked bottle experiments from *Pasteur* [9] [10].The estimated number of known species of them is considered as 159,000 [11]. Microorganisms are proved to be the earliest life on Earth according to investigation of fossil evidences [12], [13], 3.45 billion-year-old rocks are considered to be accreted with the help of microorganisms [14]. The dimensions of microorganisms range from ~ 200 nm to 700 µm [15] thus visually microorganisms can only be observed with a microscope. Microorganisms are basically divided into two groups: prokaryotes and eukaryotes. Eukaryotes have membrane-bounded organelles and cell nucleus, whereas prokaryotes don't and their size is normally larger than that of prokaryote microorganisms. **Figure 2.1** below shows the general differences between two types.

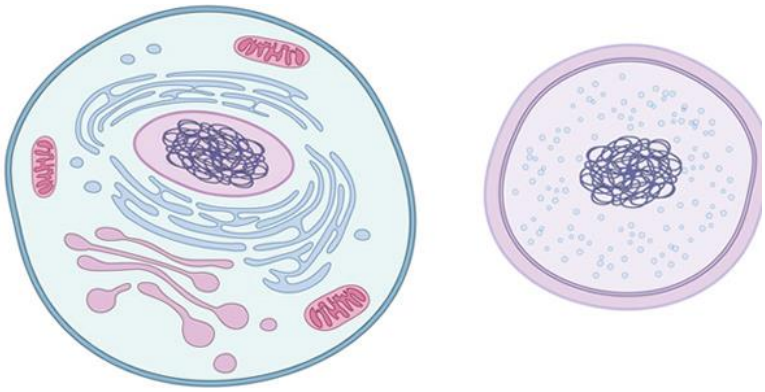

Figure (2.1) Basic structures of Eukaryote cell (left) and Prokaryote cell (right), The Eukaryote cell (left) contains membrane-bound organelles and the size is larger. Picture is taken from [16] .

In [8] the framework based on rRNA has been used to classify living organisms, as shown in **Figure 2.2**. Viruses are not included into this classification as there is a controversy – should they be considered as living species or not. Bacteria and archaea form the majority of prokaryote microorganisms. Generally, bacteria are divided into two groups, gram-positive and gram-negative bacteria according to the differences in the structure of their cell wall, for gram-negative bacteria, as they have an outer membrane and thinner cell wall, the dye used in Gram testing would not be held by them so they will show red or pink in colour, while gram-positive bacteria have a thicker cell wall, thus the stain could be retained by it and they will show blue in colour [15]. There are some microorganisms (eukaryote microorganisms) that belong to some animals and plants, such as most protists, some fungi etc. Detailed information about their structures, potential harm which they can cause to humans, their potential practical applications and inactivation technologies based on microorganisms will be introduced in the following sections.

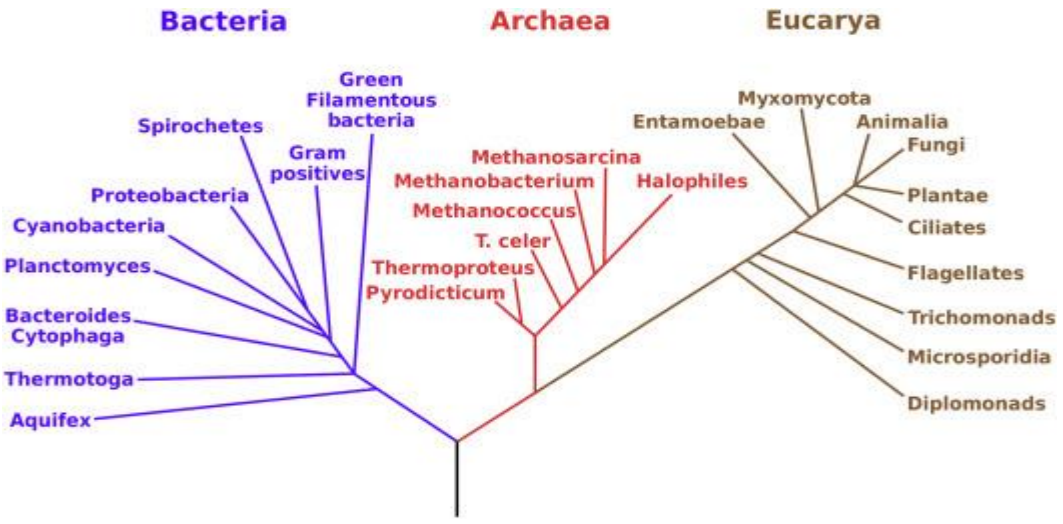

Figure (2.2) Classification of microorganisms: Carl Woese's 1990 phylogenetic tree based on rRNA data [17].

2.2 Structures of Microorganisms

The structure of microorganisms is complicated, this section will only introduce some basic and most important components commonly discussed in the literature. The parameters of these structures will also be considered in following sections focus on the simulation of interaction between electric fields and bio-cells.

2.2.1 Cell wall

The cell wall is the outermost shell of most microorganisms. Microorganisms are supported and protected by this special layer [18]. A cell wall is strong enough to keep a microorganism in its specific shape and helps to avoid the cell bursting even when the pressure on the cell can reach up to 2 atm [15].

In general, bacteria cell walls contain peptidoglycan and other polysaccharides. Gram staining shows different results as the cell wall structures are different for different bacteria. After gram staining, Gram-negative bacteria becomes colorless after washing, while, Gram-positive bacteria remain purple. This difference is caused by the structural differences between the cell walls of these two bacteria types.

Gram-positive bacteria have higher content of peptidoglycan in the cell wall than gram-negative bacteria which helps holding the stain on the cell wall during the stating process. However, gram-negative bacteria have less peptidoglycan and a thinner membrane consisting of lipid in the cell wall which can be dissolved during staining. There is no peptidoglycan in the cell walls of archaea only polysaccharide and proteins [19] [20]. For eukaryotic species, the structure of the cell wall is different, the cell wall of fungi consists mainly of chitin, glucans and proteins, while the cell wall of algae mainly consists of cellulose [21] [22] [23]. In this research, microalgae was used and cellulose wouldn’t influence the electric field distribution in cell wall when the cell was exposed to external electric field.

A cell wall is a porous permeable structure which allows for transport of small molecules among cells. The cell wall properties will be taken into account in the simulations which have been conducted in the present thesis.

2.2.2 Cytoplasmic Membrane

Membranes are one of the most critical structures in a bio-cells. There are cellular membranes, cytoplasmic membranes and nuclear membranes in bio-cells. Cytoplasmic membrane is mainly discussed in this section as the electroporation process during PEF treatment is mainly occurred in cytoplasmic membranes.

Cytoplasmic membrane is a thin layer between cytoplasm and cell wall which separates bio-cells from environmental fluids [24]. Cytoplasm is the gelatinous liquid inside the cells, detailed information will be introduced in **section 2.2.3**. The basic structure of cytoplasmic membrane is lipid bilayer with hydrophilic portions pointing outward toward cytoplasm and environmental fluid, fatty acids which point inward, there are also different kinds of proteins embedded in lipid bilayer, as shown in **Figure (2.3)** [25]. Such proteins perform the function of selective permeability and identification. Cytoplasmic membrane is a relatively weak (mechanically) structure which performs the protection function; the selective permeability of the cell membrane plays an important role in cell functioning [15].

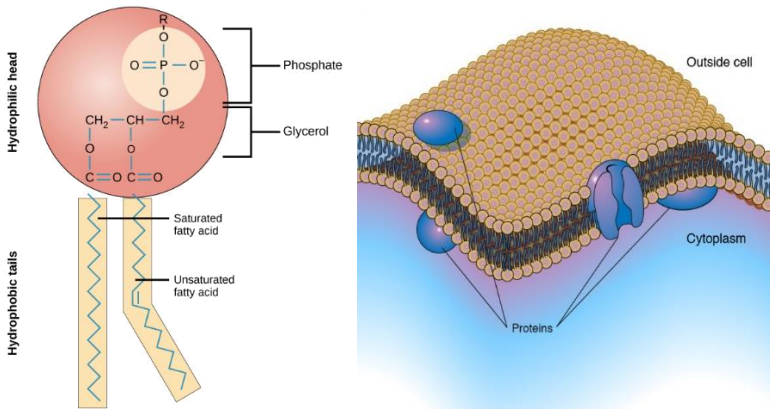

Figure 2.3 Structure of lipid bilayer and cell membrane, pictures taken from [26] [27].

Due to the selective permeability of the cytoplasmic membrane, the concentration of ions in the cytoplasm and environmental fluid outside the cell are not equal, thus a resting potential can be generated across cell membrane. The extracellular fluid has large concentration of sodium (Na+) and chloride ions (Cl−) while the cytoplasm has a large concentration of potassium ions (K+) and negative charged proteins. Although the membrane has both passive transport and active transport mechanisms, due to the different permeability of ions, the charges across the cytoplasm membrane are not equally distributed [28] [29]. The resting potential of bio-membrane will also be considered in the simulation work and detailed information about the electrical characteristics will be introduced in further sections.

The structure of the membrane makes the cytoplasmic membrane an extremely low conductive component which has significant influence on the simulation works in the later sections.

2.2.3 Cytoplasm

Cytoplasm is a gel and liquid mixture covered by cytoplasmic membrane. Cell activities mainly occur in the cytoplasm, ions and other macromolecules required or produced by metabolism are located in cytoplasm [15] [30].

Cytoplasm can be generally divided into three parts, the cytosol, cell organelles and the cytoplasmic-inclusions. Cytosol is a mixture of cytoskeleton filaments, dissolved macromolecules and water. The organelles are more complex structures covered by their own lipid bilayers, such organelles have their specific functions for cell activities, for example mitochondria is used to provide energy for cell living and endoplasmic reticulum is used to compose proteins. For prokaryote microorganisms, there are no complex organelles in the cytoplasm, cytosol is the place that cell activities occurs [31]. The cytoplasmic inclusions consists of insoluble

substances in the cytoplasm, such as glycogen, lipids and pigments. Ions, negatively charged proteins and water makes cytoplasm a relatively highly conductive medium compared with other cell structures [28]. When the cells are exposed to external electric field, ions in the cytoplasm redistribute themselves, leading to charge accumulation [6].

2.3 Benefits and hazard of microorganisms

Microorganisms exist everywhere on earth, some of them can survive even in extreme conditions. For example, cyanobacteria are the most adapted species among other bacteria, this group has been found in fossil state and is considered as the oldest known fossils (3.3 to 3.5 billion years ago) and they still exist nowadays [32]. There are also other chemolithoautorophs microorganisms adapted to high temperature up to 122℃ and high pressure up to 20 MPa [33]. As they are widely distributed, it is impossible to avoid them. It is reported that the human body contains 10 times more bacteria than human cells and many are beneficial [34]. Nowadays, humans are trying to making use of them and living in harmony with them. Other microorganisms are harmful, both aspects, the hazards related to microorganisms and their beneficial applications, will be discussed in this section.

In general, microorganisms are closely bound up with environments. They play an important role in the stability of the ecosystem. The decomposition of waste by bacteria and fungi helps to turn it to nutrients for plants or feed for animals. For example, the nitrogen in atmosphere could be taken in by plants through rhizobium [35] [36] [37]. Cellulose degradation with the help of microorganisms is also an important aspect of environmental benefits of microorganisms [38].

Some food production processes also rely on microorganisms, they are necessary for fermentation and can also be used to increase the fertility of soil to increase the yields of corps. For examples, yeasts are used in bakeries and for making yogurt, beer, wine and cheese [39] [40] [41]. Microorganisms also play an important role in

medical applications, antibiotics are extremely important and the production of them is extensive [42] [43]. Some microorganisms are used in gene engineering to produce specific proteins [44] [45] [46].

With the development of modern technology, the products produced with or stored with the help of microorganisms start to draw interest in research. Some microorganisms like microalgae and cyanobacteria have relatively high protein content which can be used as nutrients [47] [48] [49] [50] [51]. High value molecules like pigments and fatty acids are also found in microorganisms, and their extraction is also a subject of research [52] [53] [54] [55] [56].

Algae produced fuel is regarded as an alternative to fossil fuel because the released (part of it) CO_2 is removed from the atmosphere via photosynthesis when the algae grow. Although the energy used in cultivation, harvesting and processing can introduce some emissions, it is still considered as a net-zero fuel [57].

The United States Department of Energy estimated that if all petroleum was to be replaced by algae produced fuel in the U.S. it will require only 0.42% of the U.S. territory to grow the required volume of algae [58]. Several pieces of work have shown that some specific microalgae have high content of lipids which could potentially be used as a source for bio-fuel production [55] [59] [60] [61] [62]. Several methods, like high-pressure, high-temperature, mechanical and chemical approaches, have been investigated in order to extract bio-fuel content materials from algae. Pulsed electric field treatment is also being considered as an approach to extract oily content and this method is presented and investigated in this research.

Although microorganisms have multiple benefits for humans and the environment, the hazards associated with microorganisms cannot be neglected. Infectious diseases are mainly caused by microorganisms. Plague, tuberculosis and anthrax are caused by pathogenic bacteria. Malaria, dysentery and toxoplasmosis are caused by

some protozoa. Some fungi are the sources of ringworm, candidiasis and histoplasmosis [63].

Microorganisms used in food production can bring benefits when their population is at a reasonable level, however if the population/concentration increases beyond safe levels, the microorganism or sub-products produced by microorganism can be poisonous for human [64] [65] [66] [67] [68].

2.4 Inactivation methods of microorganisms

Inactivation of microorganisms is required in many practical cases [69], for example in medical applications, where bio contamination is not permitted, and it is necessary to keep a safe and clean medical environment. In the food industry, the population of microorganisms should be controlled and bio-hazardous microorganisms must be eliminated. In this section, some inactivation methods will be introduced followed by the discussion and comparison of these approaches.

2.4.1 Thermal inactivation

Thermal inactivation is one of the most widely used methods in modern industry and it has a long history. Doctors in 18th century always applied flame to metal surgical equipment or put them into boiling water before doing surgery [70]. The first thermal sterilization patent was granted to Appert in the early 19th century even though there was no knowledge of microbiology [71]. After that, in the late 19th century, pasteurization was introduced by Pasteur which is used to eliminate spoilage microorganisms. In 1920's a research paper written by Bigelow and Esty provided a relationship between treatment time and rate of death of microorganisms which is called thermal death time, later on the details of this process were investigated in [72] [78]. Models have been developed to describe the relationship between temperature and destruction rate of microorganisms [74] [75] [76]. Most organisms are sensitive to high temperature as they are composed by complex molecules and high temperature will damage the structures, and the

cell activity will be slowed down or stopped. Different microorganisms have different resistance to a specific temperature. So direct inactivation of microorganism can be achieved by exposing samples to heat in a temperature controlled environment. The autoclaves used in a laboratory are generally set to sterilize different instruments and equipment such as glass beakers at temperatures around 121 ℃.

There are also limits for thermal inactivation. Some microorganisms are quite resistant to heat, for example, *Bacillus Sporothermodurans* shows resistant to high temperature up to 120 ℃, as spores helps keep microorganisms alive during thermal inactivation processing [71]. Higher temperature or longer treatment time may solve this problem but higher temperature may also damage the nutrient and protein content of food. What's more, proteins are more sensitive to heat compared with microorganisms. Energy consumption is also a problem, higher temperature and longer time means more energy being consumed, affecting costs. Besides, the system composition of thermal sterilization is not always simple, it can be more complicated in some situations. There are generally two different approaches to thermal sterilization: moist heat and dry heat. Moist heat sterilization is normally operated under the temperature range of 121-129 ℃ with pressure required, for dry heat sterilization, higher temperature and longer treatment time are necessary, for example, for sterilization in laboratory environment, the equipment should be exposed at 121 ℃ for 15 minutes [77] [78].

2.4.2 Chemical inactivation

Chemical inactivation is also widely used in common applications. For example, alcohol has been used for sterilization for many years [69]. There are many other chemical substances which are used for inactivation, such as ozone, chlorine and iodine [79], the strong oxidation produced by these substances can cause protein precipitate, damage structures and cause dysfunction or lysis of bio-cells. Hydrogen peroxide, which is widely used in nowadays is also effective and it is less poisonous

for human beings [80]. Chemical inactivation is mainly used in the hospital environment and in large scale inactivation processes such as water purification and food sterilization.

Although chemical inactivation is effective, it has its own limits. As chemical products, every part of the processing should be strictly controlled to avoid pollution and limit hazards, which means more costs are required. Furthermore, some chemical products require a special storage environment which causes extra costs during production and inactivation process. Unexpected substances are not allowed in some applications as they may be harmful to human beings or the environment so the remaining chemical substances after treatment should be monitored [81] [82].

2.4.3 Ultraviolet irradiation (UV) inactivation

UV inactivation is widely used in water sterilization, surface disinfection, air disinfection and other large-scale treatment. The killing effects to microorganisms of UV irradiation was first recognized in the late 19th century [83]. It is an effective inactivation method for protozoa, there are no by-products generated and the results is not affected by pH and temperature [84] [85] [86]. Generally, the mechanism of UV inactivation is nucleic acid damage of the DNA and RNA of microorganisms by UV photons. Once nucleic acid is damaged, vital functions of microorganisms may be terminated, which in the end lead to cell death [87]. As a non-thermal treatment approach, the UV inactivation has many advantages compared with thermal approaches in food sterilization applications: reduced loss of nutrients, which maintain the quality of food, no toxic by-products during treatment and low energy consumption [88] [89] [90].

However, the drawbacks of UV inactivation are noticeable. From the human health point of view, excessive exposure to UV irradiation can lead to skin cancer [91] [92] [93]. UV irradiation is also considered to cause rapid aging of materials which

increase the cost of maintenance of equipment [94]. For UV inactivation in liquid samples, bad water quality may reduce the inactivation effects, biological membranes can be formed in some situations can prevent the UV irradiation from affecting the microorganisms. UV irradiation does not have a sustained effect, generally, chlorine disinfection or other methods should be used after UV irradiation treatment to maintain the sterilization results [95]. Potentially unknown changes in microorganisms may be generated due to the nucleic acid damage caused by UV irradiation which is not suitable for bio-chemical applications.

2.4.4 High pressure inactivation

High pressure processing is mainly used in food safety and preservation. It was extensively investigated since the 20th century. High-pressure treatment is conducted at ambient temperatures (to support pasteurization of food) so it helps to keep nutrients and food flavour [96]. High pressure has effects on both morphology, i.e. cell wall and membrane structures and cell activities [97]. It is reported that a pressure of 400 MPa could damage the membrane transport system of *Lactobacillus* [98]. Changes in key microbial enzymes are considered as the main reason for cell inactivation [96].

However, there are also specific drawbacks to high pressure inactivation techniques. It is a physical (mechanical) type of treatment, and the food structure potentially provides a some degree of protection for microorganisms which leads to reduction in its inactivation efficiency. So, the properties of samples play an important role in the efficiency of this type of inactivation / high pressure treatment. Also, from the technical point of view, it is challenging to develop and maintain the high pressure treatment equipment. The major challenge of the high pressure inactivation is the resistance of bacterial endospores, e.g., most vegetative cells are inactivated at 400- 600 MPa, however some spores can survive at pressures above 1000 MPa [99]. In the end, high pressure inactivation is usually combined with thermal inactivation to achieve better killing effects. In addition, in

order to provide high pressure conditions, more energy is required and this reduces its cost effectiveness [100].

2.4.5 High-intensity narrow-spectrum light inactivation

High-Intensity Narrow-Spectrum (HINS) is a newly developed technique in recent years [101] [102] [103]. Visible light, especially blue-light can be used to inactivate microorganisms. Research shows visible light with wavelength ranging from 400 nm to 420 nm has killing effects on bacteria and the inactivation mechanism is reported to be oxygen dependent [104]. Inactivation was reported due to the photoexcitation of the endogenous porphyrins of the bacteria cell, such processes can lead to the production of highly cytotoxic, oxygen-derived species [102] [105].

405nm HINS does not have the detrimental effect on humans that are found with UV irradiation. Therefore, HINS light allows people to be present while the inactivation process is underway. A study has shown the killing effects of HINS light was greater than normal infection control and cleaning activity. This research suggests HINS inactivation can be a potential choice in clinical applications [101].

The study of HINS is mainly focused on bacteria and more work is still required to confirm the mechanisms of this type of inactivation. For example, bactericidal toxicity was found in Nutrient Broth after 405-nm light treatment, the source of this should be identified, besides, some microorganism spores are also found to be resistant to the wavelength [106].

2.4.6 Pulsed electric field (PEF) treatment

Pulsed Electric Field (PEF) treatment has drawn significant interest among the food industry due to the non-thermal character of this inactivation process. In the food industry, traditional thermal processing has been commonly used to increase shelf life and maintain food safety with low processing cost [107] . The short duration of the HV pulses used in PEF makes any resulting temperature increase quite small, this helps retain nutrition and flavour of fresh food products [108]. PEF treatment

has been studied in juice processing with the juice yield increased by 67% to 75% [109]. It is also studied in applications related to plant oil, meat, eggs and even nutrition [107] [110] [111] [112] [113].

The lethal effects of a pulsed electric field on microorganisms were firstly investigated by Sale and Hamilton in 1967 [114]. Further study of the PEF treatment of cells was proposed and conducted in 1972 by Neumann, in this study it was shown that the permeability of a cell membrane can be changed after PEF treatment [115]. It was explained that the permeability changes were caused by pore formation in the membranes during the PEF treatment due to an induced trans-membrane potential, this process is called electroporation [116]. **Figure (2.4)** presents schematically the process of electroporation during the PEF treatment. After exposure to an external electric field, pores formed during the poration process make cell membrane lose the ability of selective permeability, thus substances with large molecules can be transferred across cell membranes freely. The generation of reversible pores in cell membranes during the PEF treatment can be used in many applications, such as introduction of DNA and biochemical reagents for intracellular assays [117]. However, if the trans-membrane potential is higher than a critical value, the pores will be irreversible. In the end, irreversible pores cause cell membrane rupture and cell death. The change from reversible to irreversible pore formation also depends on the treatment time and the strength of pulsed electric field **(Figure 2.5).** The irreversible electroporation can be used for bio-decontamination, food sterilization and bio-fuel production.

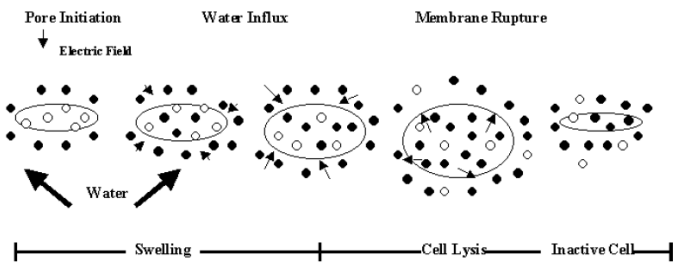

Figure (2.4) Process of cell electroporation. Picture taken from [118].

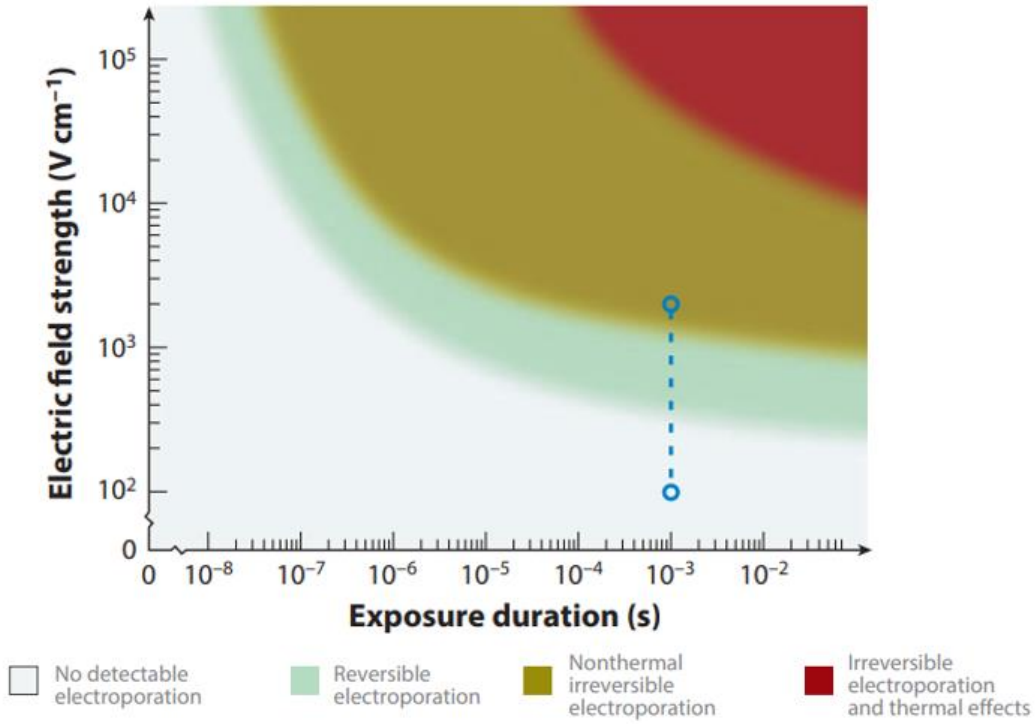

Figure (2.5) Electric field strength-Treatment duration graph. Picture taken from [119].

However, it is reported that the PEF treatment is not efficient in inactivation of the microorganism spores [120]. This limits the use of the PEF treatment in water sterilization and in some other sterilization processes of food. The exact mechanisms of interaction between the PEF fields and microorganisms are not fully understood. The molecular dynamics methods has been used to help understand the biological effects of pulsed electric field treatment [121].

In general, these applications typically use pulsed electric field with durations in the order of microseconds to milliseconds and electric field of hundreds of volts per centimetre [122].

There are also studies in which nanoseconds electric field impulses with magnitude of hundred kilovolts (ns-PEF) were used for treatment leading to changes in the permeability of intracellular structures [123] [124] [125]. AC signals have also been used in PEF treatment, where narrowband pulsed electric field with a field strength of 1 kV/cm consisting of a pulse modulated sinusoidal wave, is reported to cause intracellular effects [126]. There are also numerical studies focusing on radio frequency (RF) PEF treatment, the results show that RF PEF treatment mainly causes thermal effects [127] [128]. Studies using millimetre wave PEF show non-thermal effects on biological systems [129].

As PEF treatment is being studied in this research, the technical fundamentals, inactivation mechanisms and recent investigation of disinfection effects will be discussed in detail in later sections**.**

2.4.7 Non-thermal Plasma treatment

Non-thermal plasma treatment is an emerging technology which has gained attention during the last decade in food preservation and medical applications [130]. Plasma is considered the fourth state of matter which is a state of an ionized gas. Plasmas can be classified into thermal plasma and non-thermal plasma according to their temperature equilibrium between their constitute particles. The temperature of thermal plasma treatment can reach up to thousand degrees which can be a limitation for microorganism inactivation applications as discussed earlier. Non-thermal plasma is generated by application of an electric or electromagnetic field to a gas, with help of field energy, free electrons will be accelerated and cause ionization of gas atoms and molecules. As excited atoms and molecules will emit energy in different forms, like UV radiation, plasma is a complex state of matter with excited molecules and atoms, ions, free radicals, electrons, UV radiation and reactive oxygen and nitrogen species, moreover, all these properties show antimicrobial activity to microorganisms [131] [132] [133]. The possibility of plasma inactivation was first pointed out in the late 1960's [134]. With the development of

plasma science in the late 1990's, plasma inactivation of microorganisms started to be studied. The mechanisms of microbial inactivation by plasma is quite complex, e.g. there are DNA damage, membrane damage, protein damage and intracellular level damage. A recent study also shows indirect effects caused by plasma, such as the release of different intracellular components after plasma treatment [135].

The inactivation mechanisms of plasma are complicated due to the different forms of energy emitted during treatment: UV radiation, electric field, thermal energy, reactive oxygen and nitrogen species are generated by plasma. So, it is difficult to distinguish between different mechanisms during plasma treatment, which could be a limitation for some applications like food processing. As plasma treatment is also studied in this project (**Chapter 6**), the technical fundamentals, inactivation mechanisms and recent investigation of killing effects will be discussed in detail in **section 2.12.**

2.4.8 Discussion

Table 1. Shows all the inactivation approaches introduced in this section. The detailed advantages are compared in the table

Table 1 list of the inactivation approaches introduced in this section

	Effectiveness on spores	**Influence on sample**	**Processing conditions**
Thermal inactivation	Not effective on heat-resistant spores	May damage nutrient and protein of samples	Higher temperature means more energy consuming
Chemical inactivation	Effective to heat-resistant spores	By-products may pollute sample or be poison	Every part of processing should be strict controller

Ultraviolet inactivation	Effective to spores	Potential unknown damage may be caused	Requires more energy for damaging spores. Harmful for human body.
High-pressure inactivation	Not effective to spores or even stimulate germination of spores for some microorganism	Less damage to protein and nutrient No-by products	More energy consuming for high-pressure
Hi-intensity narrow-spectrum light inactivation	Details still need to be researched	Less damage to protein and nutrient	Not harmful for human bodies compared with UV
Pulsed electric field inactivation	Can be effective for a specific kind of microorganism	Less damage to protein and nutrient No by-products	Less energy consuming
Plasma inactivation	Effective for spores and microorganisms	By-products may pollute samples	Plasma generation and discharge should be controlled

Pulsed electric field treatment has an advantage of providing specific inactivation compared with traditional physical and chemical inactivation approaches. The PEF treatment damages the membrane structure, rather than the nucleic acid, which reduces the risk of potential unexpected damage of microorganisms in bio-medical applications.

2.5 Microorganisms used in study

One of microorganisms selected for this study is yeast *Saccharomyces cerevisiae*. These species are in the family of *Saccharomy Cetaceae*, phylum of *Ascomycota* and kingdom of Fungi [136]. It is one of the most commonly used microorganisms in fermentation processes [137]. The shape of *S. cerevisiae* cell is usually spherical or

ellipsoidal, they usually have a diameter of 5-10 µm [138]. As they are widely used in molecular biology studies and their characteristics are well documented, it will be more convenient in simulations. In addition, the *S. cerevisiae* cells also have high content of lipid, which could also provide information for bio-fuel production with this species [139] [140] [141].

The other microorganism used in this study is phytoplankton *Nannochloropsis oculata*. *N.oculata* is a species of a *Genus Nannochloropsis*. They are in the family of *Monodopsidaceae*, phylum of *Ochrophyta* and kingdom of *Chromista*. They are usually unicellular small green algae which can be found in both marine and freshwater environments [142], see **Figure (2.6)**. This kind of algae has a spherical or slightly ovoid shape, the diameter ranges from 2 to 5 µm [143] [144]. There is only one chloroplast in each cell and the main pigment is violaxanthin. These micro-algae are rich in proteins, pigments and polyunsaturated fatty acids [145]. In recent years, it has been proposed as an excellent candidate for biofuel production [146] [147]. This type of algae is chosen as it is smaller than that of the yeast, which can provide comparison of reaction to stress between these two microorganisms in simulations and experiments. They are easy to access as they are commonly used in aquaculture as feed. *N.oculata* used in experiments were obtained from Reefphyto Ltd.

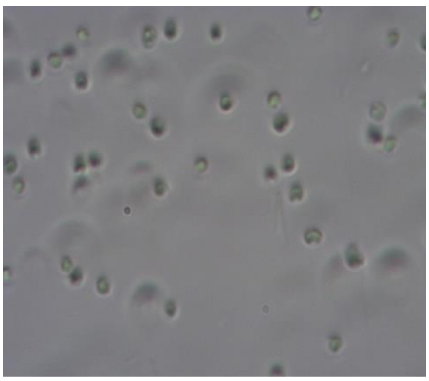

Figure (2.6) *N.oculata* cells observed under optical microscope (X100 magnification).

2.6 Electrical parameters and models of microorganisms

This section mainly introduces the development of models of microorganisms to allow the study of interactions between bio-cells and external electric field. The measurement of capacitance of erythrocyte membrane by Fricke made dielectric analysis for cells a powerful tool in biological systems research [148]. The theories used to model the dielectric properties of a bio-cell are based on Maxwell and Wagner effects and single-shell particle model, as demonstrated in **Figure (2.7)**. When a bio-cell is exposed in an external electric field, trans-membrane potential is developed across the bio-membrane because of the charge accumulation and redistribution at the cell membrane. When the induced transmembrane potential reaches a critical value the resulting electro-mechanical forces across the membrane will lead to pore formation. Details will be introduced in **section 2.8** which discusses the mechanisms of the PEF inactivation process. An early model

used to express the relationship between transmembrane potential and external electric field was proposed by Schwan in 1957 [149].

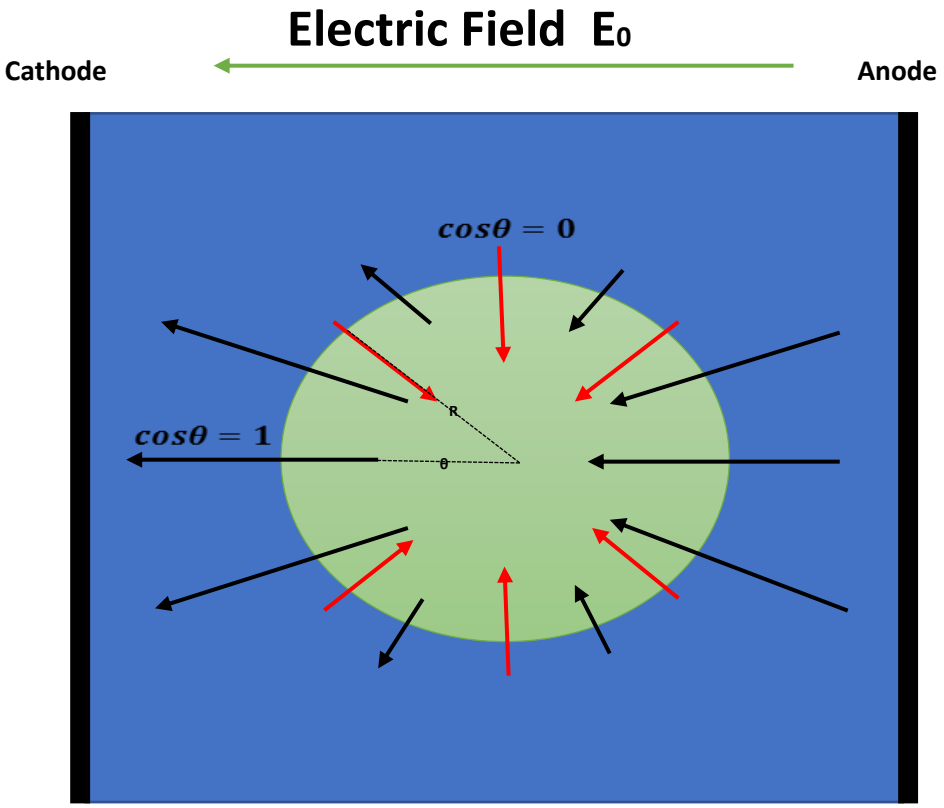

Figure (2.7). Directions of decrease of induced trans-membrane potential (black arrows) and resting potential (red arrows)

In this model the membrane of the cell is assumed to be non-conductive as stated in **section 2.2.2** before and the interior of the cell is assumed to be homogeneous [149]. The Schwan equation is expressed as:

$$\Delta\varphi = \frac{3}{2} \cdot E \cdot R \cdot \cos(\theta) \qquad \textbf{(2.1)}$$

Where $\Delta\varphi$ is the induced membrane potential (V), E is the external electric field (V/m), R is the radius of cell (m) and θ is the angle between electric field direction and the membrane wall (degree).

It can be seen from the equation that the induced trans-membrane potential is linearly dependent on the magnitude of external electric field strength and the radius of bio-cell, which means a higher trans-membrane potential will be induced across membranes of large size bio-cells. The induced membrane potential is also determined by the position on the membrane and direction of the external electric field. Therefore, the maximum trans- membrane potential will be developed on the 'poles' of the cell where $\cos(\theta) = 1$.

The dielectric constant for bio-cell is also calculated by Pauly and Schwan with this single-shell model. They also pointed out that the two sub-dispersions and Maxwell-Wagner effect (accumulation of electrical charges at the surface between two materials with different conductivity and permittivity) has only a small contribution to the total dielectric response compared with interfacial polarization. After that a two-shell model was developed and experiments have been conducted to measure the dielectric parameters of yeast cells.

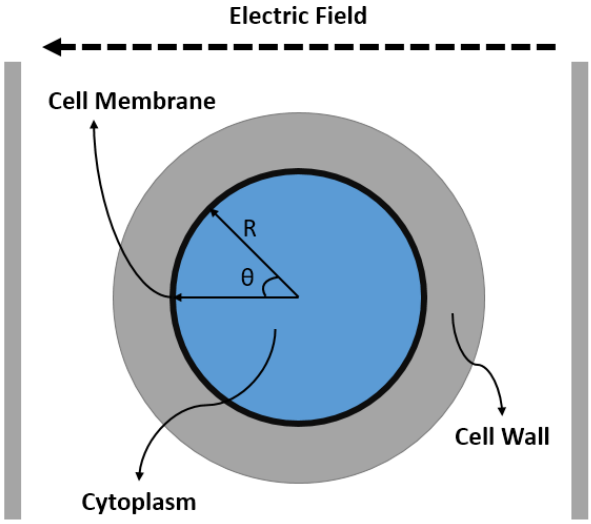

Figure (2.8) Structure of general Single cell model

The Schwan equation provided a steady-state transmembrane potential induced on spherical cells, based on this, Kotnik proposed an advanced **Equation (2.2)** with conductivity and membrane thickness included [150].

$$\Delta\varphi = \frac{3}{2} \cdot \frac{\sigma_e[3dR^2\sigma_i + (3d^2R - d^3)(\sigma_m - \sigma_i)]}{[R^3(\sigma_m + 2\sigma_e)\left(\sigma_m + \frac{1}{2}\sigma_i\right) - (R-d)^3(\sigma_e - \sigma_m)(\sigma_i - \sigma_m)]} E \cdot R \cdot \cos(\theta) \qquad \textbf{(2.2)}$$

Where σ_i represents the conductivity of cytoplasm (S/m), σ_m represents the conductivity of bio-membrane and σ_e represent the conductivity of environmental fluid (S/m), d is the membrane thickness (m). If $\sigma_m = 0$, equation will be simplified to the Schwan equation.

An analytical description of transmembrane voltage on spheroidal cells was also developed by Kotnik [150], where they confirmed that for a nonconductive membrane, membrane thickness is irrelevant to the induced transmembrane voltage. As discussed in **section 2.2.2**, a membrane consists of lipid bilayer with proteins embedded, such structures make membrane charged with ions. In [151], surface charges and resting potential were considered. The effects of surface conductance and deformation forces during membrane permeabilisation were taken into account in [151]. While in [152] [153], development of membrane potential in an ellipsoidal cell was evaluated by solving Laplace's equation with an evaluated formula valid for single confocal ellipsoidal cells instead of spherical cells. In [108] a more advanced transient model was developed which proposed the dynamics of electrical field both in a PEF treatment chamber with dielectric barriers and in a bio-membrane. In addition, a 3-stage transient process was presented and electric field strength for each phase was calculated and the transient response of membrane was calculated by an Ohmic conductivity model which provided a good reference for the PEF treatment system designs. Force analysis was also included in this research. The electromechanical effects across cell membranes when bio-cells are exposed to an electric field were studied in [151], a relationship between the forces, conductivity and pulse width was proposed. Thermal effects in microorganisms induced by an external electric field were researched in [122], with

the molecule dynamics simulations, an assumption was made that membrane thermal gradients induced by the external field may contribute to the electroporation processing.

2.7 Pulse power generation system

The source of pulsed electric field in the PEF treatment is designed, based on the pulse power technology. A typical pulse power generation system is designed to deliver a certain amount of power to the load over short period of time. With these characteristics, pulse power technology is of great importance for both civil and military applications such as radiography, electromagnetic launch, high-power microwave, free electron laser, environment protection and medical treatment [154]. In general, two steps are required for pulsed power generation. Firstly, energy should be accumulated and stored in a storage device, typically a capacitor bank, or in inductors or transmission lines. Once a required amount energy is accumulated in the energy storage device, a trigger switch is used to control the release of energy over a short period of time. Depending on the components of pulse power generation circuits, there are capacitive pulse generating circuit, inductance pulse power generating circuit and resistance-inductance-capacitive (RLC) combined pulse power generating circuit. Impulses of square waveforms, exponential decay waveforms and oscillatory decay waveforms can be generated by RLC combined circuits with different connections of components [155], square waveforms were used in this study as they could provide a more stable and controlled electric field, leading to better electroporation efficiency and cell viability, thus they were generally favoured in PEF treatment [156] [157].

2.7.1 Blumlein pulse generator

In order to obtain a nanosecond length or microsecond square pulse, instead of using the RLC combined circuit, a transmission line pulse forming network (PFN) is more suitable. The pulse generating system used in this research is designed based on the Blumlein pulse generation configuration.

Figure (2.9) shows a schematic diagram of the transmission line pulse forming network, the length of transmission line is d. In order to prevent reflections, the impedance of transmission line should be equal to the impedance of load which means a matched load is necessary. When the switch S is closed, a voltage of $\frac{1}{2}V_0$ is applied to the load and at the same time, a pulse with amplitude $-\frac{1}{2}V_0$ will travel through the transmission line to the power source, however, due to the high Impedance of charging resistors and source, which can be considered as open circuit, the pulse will be fully reflected back to the load. Finally, an impulse with period of T has been applied to the load. T can be calculated through **Equation (2.3).**

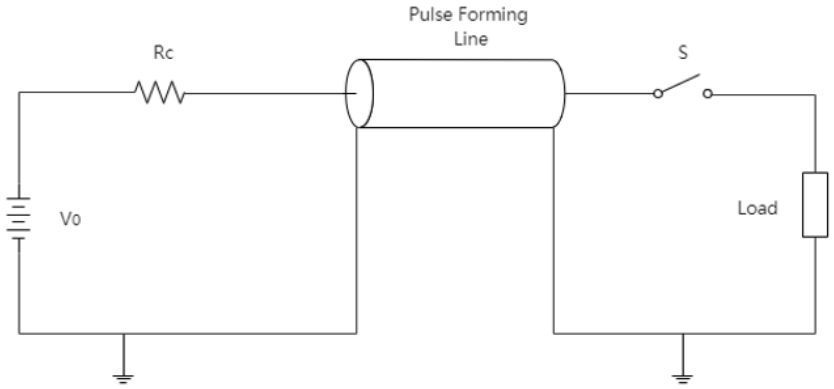

Figure (2.9) Schematic circuit diagram of a simple pulse forming line.

$$\mathbf{T} = \frac{\mathbf{2 \cdot d\sqrt{\mu_r \varepsilon_r}}}{\mathbf{c}} \qquad (2.3)$$

Where ε_r is the relative permittivity of transmission line, μ_r is the relative permeability of transmission line, c is the speed of light (m/s).

The rising time of impulse is determined by the characteristics of switch, transmission parameters and load. A drawback of this pulse forming system is the

applied voltage on the load is only half of the source. An improvement of transmission line pulse forming system is made to solve this problem by Blumlein in 1941, **Figure (2.10)** below shows the schematic of a Blumlein pulse generator [158].

As is shown in **Figure (2.10)**, in a Blumlein pulse generation circuit the load is connected between two transmission lines with the same length. If the impedance of load is twice of the impedance of each transmission line, the load is matched. When the switch S is closed, a pulse with voltage of V_0 will be transmitted to load, when it reach the load, due to the matched impedance, the pulse is half reflected back to transmission line 1 and half transmitted to line 2, resulting two symmetrical voltage pulses with $\frac{1}{2}V_0$ magnitudes but opposite polarity at the same time, creating a voltage of V_0 across the load. When they reach the end of each transmission line, then they will be reflected back towards the load. The duration of pulse T is the same as in the case of the single transmission line which can be calculated through **Equation (2.3).**

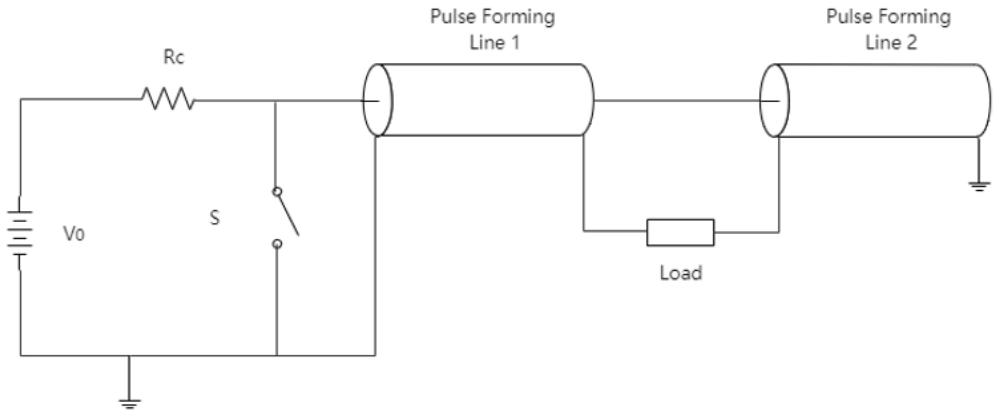

Figure (2.10) Schematic circuit diagram of Blumlein pulse generation circuit

Compared with a single transmission line pulse forming network, a Blumlein pulse generation circuit attains the same magnitude of voltage as the charging voltage.

As a flexible pulse power generation technique, improvements have been done since it was firstly developed, for example [159], a multipurpose, low cost, small size and light weight pulse generation systems was made based on the Blumlein configuration which can produce a 50ns flat top rectangular impulse with rising time and falling time less than 10 ns. The shape of impulses generated with Blumlein generator used in this study will be introduced in **Chapter 6.**

2.8 Pulsed Electric Field treatment

Although PEF treatment has been briefly introduced in previous sections, as PEF treatment is mainly studied and applied in this project so a critical review of all aspects of PEF treatment is necessary and important for the research. Therefore, this section will be focused on potential mechanisms of the PEF treatment, test chambers, and will discuss important studies on the PEF treatment conducted over past decades and in recent years.

2.8.1 Mechanisms of PEF treatment

The origin of pulsed electric field treatment can be traced back to 1960s, when lethal effects on microorganisms were firstly described by Doevenspeck [160]. After that, Sale and Hamilton critically analysed the killing effects of PEF on bacteria and yeast in 1967 and gave three conclusions [161] [162] [163]: (i) Killing effects is mainly depended on electric field strength and treatment time, (ii) Thermal effects and electrolytic products during treatment could be excluded from consideration, (iii) At least 1.0 V trans-membrane potential is required across the bio-membrane to generate pores. Since the first introduction of the PEF treatment, it attracted great interest among researchers. The theory of the PEF treatment was mainly developed in 1980s. Hulsheger, Niemann and co-workers confirmed Sale and Hamilton's results in [161] [162] [163] and developed a mathematical model for the calculation of the fraction of cells surviving after PEF treatment [164]. (PEF treatment for food

processing was firstly studied by Krupp Maschinentechinik GmbH which built a laboratory which was used to study lysis of microorganisms in liquid food stuffs and side-effects of electric pulses on food and taste under PEF treatment [160], however, due to the limitations of the pulse generator, it was nearly impossible to set repeatable electric parameters and thus really reveal the interactions between biological cells and electric field.)

The mechanism of cell lysis caused by the electric field is not fully understood. The most widely accepted model was proposed by Zimmermann in 1986: i.e. the pore formation theory which is called electroporation [165]. As charges started to be accumulated on both inner and outer sides of the membrane, the membrane is compressed, if the transmembrane voltage exceed 1 V, pores start to form across the membrane [165]. The pore formation process can be both reversible and irreversible, it depends on the field strength and treatment time. If the external electric field is applied as a short pulse, normally less than 1 μs, the membrane pores are resealable and no permanent damage is induced to the cell [166].

Study [167] also shows that the threshold electric field strength to cause membrane breakdown is determined by both cell size and cell cycle. For example, for Yeast cells treated with 4 to 5 kV/cm electric field strength, S-M phase (Synthesis phase is the period when DNA is replicated, preparing for cell division and Mitotic phase is when the cell divides) cells are more susceptible to the PEF treatment than G1-phase (Gap phase, refers to the periods of growth) cells and larger cells are more difficult to make permeable. The parameters of high voltage waveform such as rising time, peak voltage and falling time can also influence the result of electroporation.

In recent studies, intended to produce pores, μs-time pulses with field magnitude between 30 kV/cm to 40 kV/cm are generally used as PEF treatment waveforms [168] [169] [170] [171].

Other electrical and electro-chemical processes that take place during the PEF treatment also have effects on microorganisms. For example, ions can be released from electrodes due to electro-chemical reactions, such ions have been proved to have an impact on inactivation of microorganisms [172]. Ionic conduction is also a potential reason of the cell death, reports in [173] [174] show that for liquid suspension with high conductivity, the ionic conduction current can reach to hundreds of Amps.

Local heating effects during the PEF treatment may also contribute to inactivation of microorganism, however, the PEF process is usually considered as a 'non-thermal' treatment as the change in the bulk temperature of the liquid during the PEF treatment can be very small (a few degrees of Celsius only), thus typically it was assumed that local heating effects should not be taken into account.

2.8.2 Static plane-plane test chambers

A PEF treatment chamber is one of the vital components in the PEF treatment system. The test chamber is designed to house a liquid suspension to be treated and suitable electrodes to allow high voltage impulses to be applied across the chamber.

In general, there are two kind of chamber, which can be distinguished by their difference in design, namely static chamber and continuous chamber. For a static chamber, a specific amount of sample is fitted in the cavity between two electrodes. Static chambers usually can only treat a small volume of liquid each time which is not suitable for large-scale treatment processes. Continuous chambers are designed to treat larger amount of liquid as liquid samples will be flowing with a certain flow rate between the electrodes.

The early static chamber was designed by Sale and Hamilton in 1967, [114] [161] [175] as shown in **Figure (2.11)**. Two carbon electrodes are held by brass blocks and a U-shape polyethylene spacer is fitted between two electrodes as the treatment

chamber. The coolant path is designed to control the temperature of a sample during PEF treatment. The maximum treatment electric field strength is 30 kV/cm for this test chamber as air breakdown, electrical discharges, will occur above the sample if the field exceeds this value.

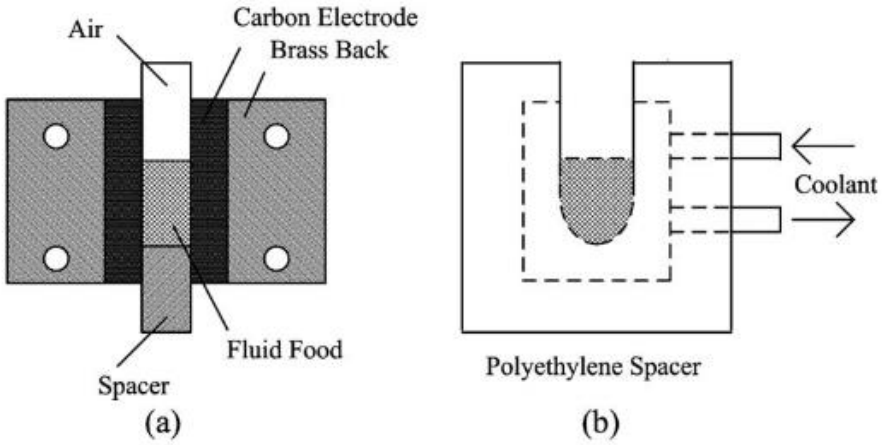

Figure (2.11) The static chamber designed by Sale and Hamilton: (a) cross section view of chamber. (b) U-shaped treatment region and coolant path. Pictures taken from [176]

In general, two parallel electrodes in the treatment chamber are required and used to generate a uniform electric field in the liquid samples. However, in the case of presence of the water/air interface in the design of treatment chamber the maximum electric field strength is limited by the flashover strength across this interface. In order to solve this problem, Dunn and Pearlaman [177] designed a new geometry of the static treatment chamber shown in **Figure (2.12)**.

The test chamber consists of two stainless steel (SS) electrodes and an acrylic Plexiglas spacer. The gap between electrodes is 5 mm. A hole is opened in one of

the electrodes to inject samples. A 5 to 25 kV/cm electric field can be applied to samples in this test cell.

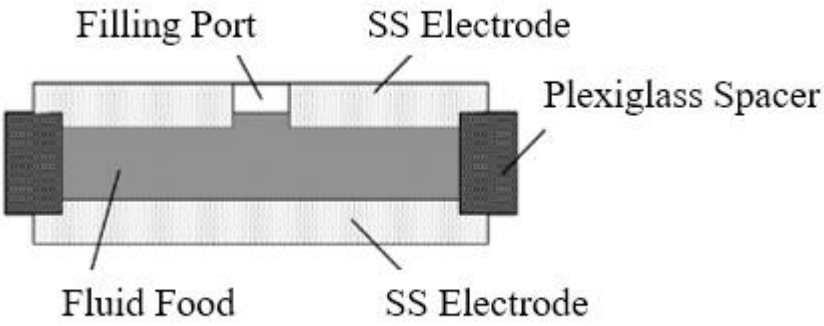

Figure (2.12) Cross section of static PEF treatment chamber designed by Dunn and Perlman, picture taken from [177].

When the electric field strength reaches 30 kV/cm, breakdown will occur due to the electric field enhancement at the edge of the electrodes. A research group from Washington State University designed a disk-shaped static PEF treatment chamber [176], as shown in **Figure (2.13)**, which can generate a high electric field up to 75 kV/cm among the sample. The probability of electrical breakdown is reduced due to the two disk-shaped, round-edged stainless steel electrodes which are polished to mirror surfaces. There are also other configurations of the PEF treatment chamber, for example a rod-rod static treatment chamber designed by Mastumoto was used to study cell destruction by underwater arc discharge [178]. Non-direct contact chamber designed by Lubiki and Jayaram in [179] was used to study inactivation of *Yeersinia enterocolitica* and it was found that *Yeersinia enterocolitica* were effectively inactivated by PEF without direct contact with metallic electrodes. Based on these well-designed test chambers, the test chamber used in this study was inspired by them with the same materials (Stainless steel with polished mirror surfaces).

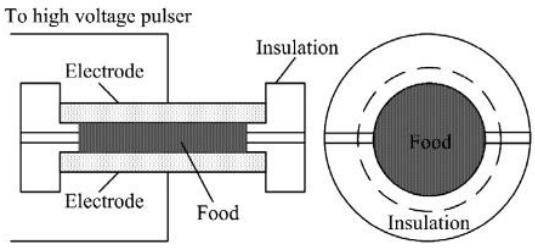

Figure (2.13) The static PEF chamber designed by Washington State University research group, picture taken from [176].

Timoshkin *et al*. in [108] proposed a static PEF treatment chamber with electrodes coated by high permittivity ceramic material. Such a design can eliminate the electro-chemical reaction between metallic electrodes during PEF treatment and reduce the by-products. For example: with aluminium electrodes, Al^{3+} can be released into liquid during PEF treatment [180], the accumulation of these ions can form bubbles thus cause undesirable dielectric breakdown [181]. Therefore, stainless steel is used in this study.

2.9 PEF inactivation of microorganisms

Several types of microorganism have been used in the PEF treatment studies including *S.cerevisiae, E.coli, Bacillus subtilis, Staphylococcus aureus, Lactobacillus and Pseudomonas. E.coli and S.cerevisiae* are the two most popular microorganisms due to their importance to the food industry and human living. With the development of bio-fuel production research, microalgae have started to draw attention among researchers, for example for lipid extraction process in which *Nannochloropsis, C. prototheocoides and Dunaliella* are used. In this section, studies of the PEF treatment on microalgae and yeast will be reviewed.

2.9.1 PEF treatment of microalgae

Study of the PEF treatment on microalgae is at an early stage and mainly focused on the feasibility of PEF induced or assisted lipid extractions.

In [182], Zbinden et *al* reported on their research on PEF-assisted lipid extraction from *Ankistrodesmum falcatus*. *Ankistrodesmum falcatus* is a green algae which is known for this lipid content and can be used as a potential feedstock for bio-fuel production which can produce around 43% lipids from ash-free dry weight. An exponentially decaying HV impulse with the characteristic decay time of 360 ns and the peak field strength of 45 kV/cm was used in this study, the test chamber was equipped with parallel-plane stainless steel electrodes. The study shows that when a specific energy of 26 MJ/kg (dry weight) was used in the PEF treatment, the samples resulted in a ~90% lysis and the lipid yield increased by 130% compared with extraction without the PEF treatment.

Axuxenochlorella protothecoides is popular among researches as it has potential to serve as source of food and energy due to the high photosynthetic efficiency of 8% [169]. In [183], a square wave impulse with 1 µs duration is used to generate a 35 kV/cm electric field across *Axuxenochlorella protothecoides* sample. According to the results, with 2 MJ/kg energy, there is a ~433% increase in release of intracellular biomass, ~400% increase in the release of total organic carbon content (TOC), ~1000% increase in the release of carbohydrates and ~500% increase in lipid yields in the case of the PEF treated samples compared with untreated samples [169]. Gottel and his research team also proposed a study with this kind of algae [183]: The samples were treated with 23-43 kV/cm field impulses with duration of 1 µs. It was found that the specific energy had more significant influence on cell lysis as compared with of the field strength. They also found that the PEF treatment did not cause spontaneous release of lipids according to fluorescence microscopy.

Nannochloropsis which has ~30 % of carbohydrates, ~20% of proteins and ~25% of total lipid has also drawn attention of researchers [184]. Several approaches have been proposed to extract valuable nutritional compounds from *Nannochloropsis such* as microwaves [185] [186], ultra-sonic treatment [187] [188] etc. The study in [184] shows that the electrically based disruption techniques, including PEF, allowed for selective extraction of water soluble ionic components, microelements, small organic compounds and water soluble proteins (~ 5.2% extraction for 1% suspensions). The impulses used in this study were HV impulses with the field strength of 20 kV/cm and duration of 4 ms. However, the extraction of pigments through PEF itself is not available, it requires additional subsequent applications, such as ultrasonic and high pressure processes [184].

There is a recent study about the PEF treatment focused on the PEF assisted extraction of polysaccharides and hydrocarbons from *Botryococcus braunii* [189]. These microalgae are able to build extracellular networks of polysaccharides and hydrocarbons which allow bio-cells to adhere as colonies. Such colonies are reported to contain over 99% C33 and C34 compounds [190]. Moreover, in general, from 25% to 40% of oil contained in these colonies can be extracted from dry weight, if under optimal conditions, the extraction rate can reach up to 86% [191]. In their research, an 80 ns duration HV impulses were applied to the sample developing a high electric field strength up to 144 kV/cm. The result shows that using energy of 25 J, ~50% of extraction of hydrocarbon can be achieved with electric field strength of 39 kV/cm and 64 kV/cm. Using 50 J energy, the extraction rate increases to 80%. They also found at lower energy level, the extraction efficiency is mainly determined by the electric field strength, and a 21.5 kV/cm field strength is not sufficient to support extraction even at high energy levels [189].

2.9.2 PEF treatment of Yeast

Qin et al studied the inactivation of *S. cerevisiae* and *E.coli* using a plate-shape static treatment chamber [192], they compared the performance of PEF treatment on *S.*

cerevisiae using different impulses, i.e. square wave impulse (~50 µs, 276.2 J/pulse) and exponential decaying impulses (~150 µs, 277.4 J/pulse), the field strength is 12 kV/cm for both conditions. The report showed a reduction of population was decreased by $\sim 10^6\ \mathrm{CFU's/mL}$ after 10 impulses. The study also showed the energy efficiency of the square wave impulse can reach to 91% and the efficiency of exponential decaying impulse is only 64%. So in [193] it was concluded that square wave impulses have better energy efficiency in PEF treatment of *S. cerevisiae*. Another study from them investigated three type of microorganisms in simulated milk ultra-filtrate liquid with impulse of peak field strength ~ 60 kV/cm and 40 µs duration. For *S. cerevisiae* a $\sim 10^5\ \mathrm{CFU's/mL}$ reduction was observed after 8 impulses. For *E.coli* and *S.aureus*, application of 30 and 40 impulses are necessary to obtain the same reduction. Therefore, Qin concluded that *S. cerevisiae* is more sensitive to PEF due to the large cell size (diameter: ~ 6 µm) compared with other two kinds of microorganisms (*E.coli*: ~2.2 µm, S*. aureus*: ~ 1 µm) [192].

Temperature, pH and water activity (a_w) was taken into account during PEF treatment on *S.cerevisiae* in [194], where the water activity is a measurement of how much water is available for biological reactions in a material, and it determines the growth ability of microorganisms. The samples were exposed to square wave shape impulses with electric field strength of 25 kV/cm, and 4 µs duration. The test chamber was continuous and the water activity of suspension being investigated ranges from 1.0 to 0.94, different microorganisms have different minimum and optimum water activity levels for growth [195].

The pH of sample being investigated ranged from 4.0 to 7.0. The treatment was undertaken under two different temperature conditions, 10 ℃ and 30℃. The results show neither pH nor water activity have significant effects on the PEF treatment results. However, the increase in temperature significantly enhanced the killing effects of PEF treatment, i.e. $10^2\ \mathrm{CFU's/mL}$ reduction observed at 30℃ after the PEF treatment [194].

The critical electric field (E_c) and critical treatment time(t_c) is studied by Grahl and Markel in [196]. **Table 2.2** below shows the critical field strength and critical treatment time for *S. cerevisiae* in different media. The research also concluded $\sim 10^5\ \mathrm{CFU's/mL}$ reduction is possible with electric field strength as low as 7 kV/cm.

	E_c	t_c
Sodium alginate	5.4 kV/cm	Below 5 µs
Ultra-high temperature(UHT) milk	4.7 kV/cm	Below 5 µs

Table 2.1 critical field strength and treatment time of *S. cerevisiae* in different media.

As mentioned in **section 2.8.1**, the sensitivity of the same microorganisms to pulsed electric field is different in different cell phases. As reported in [197] yeast cells in their logarithmic phase (a period in a bacteria growth curve where cell numbers increase exponentially) are more sensitive to the PEF treatment than cells in stationary phase (a period when the population size stabilizes, with the rate of cell division roughly balancing the rate of cell death): 75% of yeast cells in the stationary phase survived after 4 pulses with electric field strength of 30 kV/cm, for cells in the logarithmic phase, only 5% of cells survive. In [198] with 16 kV/cm electric field strength, the killing rate of yeast cell in the logarithmic phase is nearly 100% and killing rate of the cells in their stationary phase is less than 30% even for impulses with higher field strength of up to 28 kV/cm.

Transmission electron microscopy (TEM) was used to investigate the killing effects of the PEF treatment in [199], the yeast cells were exposed to 64 exponential decaying impulses with field strength 40 kV/cm and 4 µs in duration. The results supported the electroporation theory and it was found that the disruption of cellular organelles was observed more frequently than the membrane disruption.

The energy consumption during the PEF treatment of yeast varies among different studies, generally in a range of few tens to a few hundreds of kJ/litter. For a $10^5\ \mathrm{CFU's/mL}$ reduction of yeast, 84 kJ/litre energy consumption is reported in [200], while in [201], 77 kJ/litre is required to reach $10^6\ \mathrm{CFU's/mL}$ reduction. In another research, 300 kJ/litre is required to reach $10^6\ \mathrm{CFU's/mL}$ reduction [202].

2.9.3 Factors influencing PEF treatment performance

As introduced in the previous section, the electroporation process is the mechanism of the PEF treatment inactivation of microorganism, it has also been confirmed that 1 V transmembrane potential is necessary to trigger the electroporation process. The membrane potential is mainly determined by the external electric field according to Schwan equation and **Equation (2.2)** developed by Kotnik.

Based on studies about the critical electric field strength in the previous section, the critical electric field strength varies for different kind of microorganisms. For example, the critical electric field strength of *E.coli* is 14 kV/cm in sodium alginate but the critical electric field strength of yeast is only 5.4 kV/cm in sodium alginate. Besides, for the same kind of microorganism, the critical electric field strength is also different in different sample mediums. For yeast, the critical electric field strength is 5.4 kV/cm in sodium alginate and 4.7 kV/cm in UHT milk due to different conductivity.

In the previous sections, it was shown that the most frequently used pulses in the PEF process are HV pulses with square and exponential wave-shapes. A simple capacitive pulse generating circuit is enough to generate an exponential wave-shape. To generate a square wave-shape impulse, a transmission line based pulse generation circuit is preferred. Bai-lin Qin *et al* conducted a PEF study in [193] in which they investigated inactivation efficiency of different wave-shapes: exponential decaying wave-shapes, oscillatory decay pulses and square wave-shape. Three types of microorganisms were researched in [193], *E.coli*, *S.cerevisiae*

and *B.subtilis*. In this study identical peak values of voltage were used and the same amount of energy was delivered to the samples. It was found that square wave-shapes are more effective in killing effects than exponential wave-shapes. The studies also show that the oscillatory decay pulses are less effective than the exponential decay pulses with the peak field strength of 40 kV/cm and applied energy of 80 J per pulse. Because with the oscillatory decay pulses the cells were not continuously exposed to a high intensity electric field, therefore the formation of irreversible pores was reduced [193].

Qin *et al* also conducted the PEF study of treatment of yeast cells with different wave-shapes [193]. Exponential waveform and oscillating exponential waveforms were compared in the study, the results show that with peak fields of 67 kV/cm and 80 kV/cm, exponential waveform provided the best inactivation performances compared with oscillating exponential waveform. Love in [203] provided a mathematic correlation between the frequency components of pulse wave-shape and inactivation efficiency during the PEF treatment, based on the experiment results from Qin [193], they provided a quantitative way that the square impulse has better energy efficiency than other wave-shapes. In addition, square impulse also provided additional benefits: undesirable electrolysis of liquid food was minimized and solid deposits on electrodes surfaces were reduced by 80%.

Bipolar impulses are also used in the PEF treatment study [193], Bailin-Qin also made a comparison between monopolar and bipolar impulses and gave a conclusion that bipolar impulses are more efficient than monopolar impulses. The reason for that is the change in orientation of electric field, the movement of charged molecules across the membrane are changed which the enhanced electrical stress on the membrane. A similar study was conducted by Beveridge in [204], however, contradicting results were reported in the study. *E.coli*, *L.monocytogenes* and *B.cereus* were treated with both monopolar impulses and bipolar impulses. An explanation was given that the pulse duration used in the

study was relatively short (1 μs) compared with the study processed by Bailin-Qin, in which the duration was over 50 μs, so the bipolar impulses were more effective than oscillating impulses.

The characteristics of the liquid suspension such as temperature, electrical conductivity and pH also produce notable effects on the PEF treatment results as demonstrated in many studies [194] [205] [206]. As thermal inactivation is commonly used in killing microorganisms in the food industry, the suspension temperature clearly has an influence on the efficiency of the PEF treatment. Although the PEF treatment is generally considered as non-thermal, there is a temperature increase during the PEF treatment. In general, the thermal effect of the PEF treatment can be governed by the rate of energy dissipation in the liquid suspension. If a large amount of energy is delivered to the suspension over a short time, the temperature of the suspension can be increased significantly. The temperature of a liquid suspension is generally monitored in PEF treatment studies. In [206], for *E.coli*, with suspension temperature fixed to 40 ℃, a 10^2 $\mathrm{CFU's/mL}$ reduction was achieved with 20 exponential decaying impulses while 50 impulse were required for the same reduction with the suspension temperature of 30 ℃. Similar results were also given in [207]. This study also shows a good agreement with the critical membrane potential behaviour which reduces significantly with an increase in the temperature.

The electrical conductivity of a suspension also plays an important role in the PEF treatment, influencing the PEF treatment in multiple ways. First of all, higher conductivity may result in a higher trans-membrane voltage [205], thus increase the ability of electroporation process across membrane. Higher suspension conductivity also has an influence on the performance of the pulse forming networks. For a RC pulse generation network, higher sample conductivity reduces the resistance of the load which will results in a shorter pulse duration. For a transmission line based pulse generation network, higher conductivity results in a low load voltage and

reflection due to the mismatch between the load and PEF generation network impedances. From the thermal effects point of view, higher conductivity leads to more joule heating during PEF treatment and higher temperature also damages the structure of nutrient molecules which is not permitted in food industry. However, for most PEF applications in food processing, the conductivity is relatively high, in the range of 0.1 to 1 S/m [208]. In order to overcome the engineering difficulty, a non-conductive PEF test cell was designed [108], and with help of dielectric layer, the ionic conduction current through the liquid suspension can be eliminated even with high suspension conductivity which reduce the probability of production of toxic by-products such as chlorine [209].

Another factor which has an influence on the PEF treatment results is the pH of a liquid. Studies [194] [210] investigated the influence of pH on the PEF treatment of different microorganisms. Lower pH is reported to be more effective for inactivation of *E.coli* and *L.monocytogenesin*. There are also studies which show that a higher pH is more effective for inactivation of *S.enteriditis and S.senftenberg* [211] [212]. Some studies also show that pH has no effect on the inactivation process [175] [213].

What should be noticed is that, for lower pH situation, the inactivation effects should be regarded as combined effects due to both PEF and acids, as reported in [214]. It was also reported that Gram positive bacteria are more resistant to PEF treatment at neutral pH environment than Gram negative bacteria. However, in low pH environment, Gram negative bacteria shows more resistance to PEF treatment compared with Gram positive bacteria.

The size of microorganisms also has significant impact on the PEF inactivation performance. From the Schwan equation, it can be obtained that with same external electric field strength, greater voltage will be developed across the membrane of larger cell size. It has been confirmed, for example, in [192],

S.cerevisiae cells with linear dimensions of ~6 µm were more sensitive to the PEF treatment compared with *S.aureus* which have cells with linear dimensions of ~ 1µm.

The difference of Gram strain of bacteria has been introduced before. It was reported in [215] and [216] that Gram negative bacteria were generally more sensitive to PEF processing than Gram-positive bacteria. The potential reason was given in [215], due to the thick peptidoglycan layer in Gram-positive bacteria.

Several studies also investigated the influence of growth stage of microorganisms. The critical electric field for *E.coli* was given in [216]. The study demonstrated that 8 kV/cm was necessary to start PEF inactivation of *E.coli* in the stationary phase and only 2 kV/cm is required for log phase. Other studies, like [198] [206] [217], also give results show that microorganisms in stationary or lag phases shows less sensitivity to PEF treatment than microorganisms in log growth phase.

The electro-chemical reactions that occur during the PEF treatment are generally called electrolysis. These electrolysis processes produce not only metallic ions but also gaseous products such as oxygen and hydrogen. In most PEF treatment applications, stainless steel and aluminium are selected as electrodes, copper electrodes are also a selection. Cu^{2+}, Al^{3+} and $\mathrm{Fe}^{2+}/\mathrm{Fe}^{3+}$ are usually generated in suspension with such electrodes. It was demonstrated in [172] that Cu^{2+} has a high antimicrobial effect. 90% of the *E.coli* was inactivated with stainless steel electrodes, 99% and 99.9% of them was inactivated with aluminium and copper electrodes. In addition, it was reported in [180], Al^{3+} can affect the membrane electroporation process. As stainless steel has a relatively high corrosion resistance and low electro-chemical reactivity compared with other kind of electrodes [218], stainless steel is mostly used in the PEF treatment applications and experiments.

2.9.4 Discussion of PEF treatment on microorganisms

This chapter reviewed the background information about microorganisms and current inactivation methods. Fundamentals of pulse power technology are also introduced, such as pulse forming networks. Finally, a review of the PEF treatment is conducted in this chapter. The main inactivation mechanisms and experiments results are also introduced.

However, there are still not many studies focused on the analytical analysis of the processes during the PEF treatment, for example, the local heating effects and forces which lead to deformation on the membranes. Different kind of impulses and different electrical parameters can also be included in such analytical studies. Secondly, most of the studies were focused on the high electric field strength, 67 kV/cm and 80 kV/cm, lower electric field treatment of microorganisms with different number of impulses should be studied to provide more information on the efficiency of the PEF technology for some practical applications , for example for bio-fuel production.

2.10 Plasma treatment

This section provides a general overview of the principles of operation and applications of non-thermal atmospheric plasma technologies used for bio-decontamination and inactivation. In addition, the influence of different environmental factors and processing parameters will also be discussed in this section. Finally, some limitations for industrial implementation of plasma treatment will also be discussed.

Plasmas can be classified into two groups: thermal plasma and non-thermal plasma as introduced earlier. Thermal plasmas can reach temperatures up to several thousand Celsius degrees and they are usually used in metallurgical industry or chemical synthesis process. Non-thermal plasmas, with temperatures close to ambient temperature are more suitable for inactivation of microorganisms in the

food industry as the structure of nutrient would not be damaged due to high temperature.

Non-thermal atmospheric plasma offer another approach for food preservation and gained much attention during the last decade. The possibility of using plasma as a surface decontamination technology was firstly pointed out in the late 1960's [219]. However, this technique was not implemented in the food industry at that point as cold plasmas could only be obtained under vacuum and on a small scale which is expensive and not applicable in industrial settings. In the late 1990's, with development of techniques, equipment capable of generating plasmas at atmospheric pressure became available.

Plasma treatment may offer many advantages to the food industries. Firstly, it allows short treatment times, it has been reported that few seconds can cause more than $10^5\ \mathrm{CFU's/mL}$ reductions for different microorganisms, including pathogens such as *Salmonella typhimurium, S. enteritidis, Escherichia Coli* [220] [221] [222]. In addition, plasma is effective at room temperature which makes it particularly interesting for heat-sensitive products. Finally, its non-toxic nature and the reduced consumption of water and chemical agents result in a significant reduction of effluents, which is beneficial not only from an economic but also from an environmental point of view.

Although several studies have been designed to elucidate inactivation by various plasmas, the specific mechanisms leading to microorganism death are still not precisely known yet. The following sections will be used to describe potential mechanisms of plasma inactivation.

2.10.1 Mechanisms of Plasma inactivation

It is generally accepted that the reason for inactivation during the PEF treatment is the cell lysing effects. The mechanisms of plasma inactivation is more complicated. UV radiation is firstly considered as the main reason to cause cell lysis of plasma

inactivation as UV radiation always comes into being along with the generation of plasma. The non-thermal plasmas are generated by application of electric or electromagnetic field to a gas. The field causes free electrons to accelerate and ionize the gas atoms and molecules, more free electrons will be generated and excited to enhance the ionization process. In addition, excited electrons produce molecular dissociations with formation of new atoms and free radicals which lead to atoms and molecules excited to a higher energy level. When excited atoms and molecules return to energy stable state, they emit energy in the form of broad-spectrum electromagnetic radiation including UV radiation.

However, the contribution of UV radiation to killing effects in plasma inactivation has become controversial with development of plasma inactivation. Experiments shows pure argon plasmas shows greater lethal effect to *Bacillus atrophaeus* and *Bacillus subtilis* spores compared with oxygen and nitrogen plasmas which emit four times more UV radiation [223]. In [224] [225], a lithium fluoride filter or fused silica quartz plate is used between the plasma generation point and treatment region to transmit UV light but avoid the direct contact of microorganism and chemical reactive species. These studies demonstrated that the contribution of UV light to inactivation of microorganism is negligible. In addition, it is found that the transcriptional response of genes involved in UV damage repair (*uvrA, uvrB*) is unaffected while various genes involved in the response to oxidative stress are over expressed by exposing *B.cereus* vegetative cells in nitrogen plasma [226]. Such studies proved that the mechanisms of inactivation of microorganisms by UV radiation and non-thermal plasma are different. It is also agreed that reactive chemical species generated through gas ionization make contributions to the antimicrobial effect through direct and non-specific attack on various microbial structures and components, including cell membranes, DNA and proteins [227].

It has been confirmed by studies that the mechanical or oxidative damage caused to cell membranes is the main reason for the cell death caused by the plasma

treatment [130]. The electrons and excited species generated during the plasma treatment are reported to directly damage the structures of cell membranes. Electroporation phenomenon is also considered to contribute to mechanical erosion of cellular envelopes as charge accumulation occurs across bio-cells during the plasma treatment [130]. Moreover, as pores form across the cellular envelopes, they stimulate not only the release of intracellular components but also the invasion of reactive species which would damage other cellular components, such as DNA and proteins, and would accelerate the inactivation process.

The oxidative damage of cellular structures and macromolecules caused by neutral reactive species generated during plasma treatment is also considered to be one of the main reasons leading to cell death. Hydrogen peroxide is reported to be the major chemical species responsible for microorganism inactivation by plasma treatment in [131]. It has been proved that substances that chelated with reactive species can help reduce the efficiency of plasma inactivation. Thus, several sequestering agents of various reactive oxygen species have been proved to have protection on microorganism during plasma treatment [130]. Moreover, hydroxyl radicals and singlet oxygen are also proved to be the main agents involved in microbial inactivation in research [228]. Lipid peroxidation phenomena is responsible for the cell membrane damage due to the oxidative effects of these reactive species during plasma treatment which results in changes in the membrane chemical composition, ultrastructural organization and permeability, a decrease in membrane fluidity and inactivation of membrane associated enzymes [229] . Lipid peroxidation is a chain reaction which begins with the attack of unsaturated fatty acids by reactive oxygen species. Such species extract a hydrogen atom from a methylene group ($-\mathrm{CH_2}$), giving a rise of the formation of lipid radical ($\mathrm{L^*}$) which can react rapidly with an oxygen molecule to give a peroxyl radical ($\mathrm{LOO^*}$). These radicals can extract new hydrogen atoms from other lipids and become hydroperoxides (LOOH), which undergo chemical degradative phenomena to

produce very toxic degradation compounds. The damages to cell membranes through plasma treatment can be observed through electron microscopy. Size reductions, changes of shape, surface structure modification, presence of pores in membranes and envelope disruptions can be observed [230]. Determining the release of different intracellular components such as potassium ions, K^+, monitoring the entry into the cell of fluorescent dyes are alternative approaches to indirectly prove membrane damage [231].

However, cell membrane is reported to be not the only structure being damaged during the plasma treatment. In fact, those reactive species, such as single oxygen, hydrogen peroxide, nitric oxide and excited atoms and molecules generated during plasma treatment can rapidly and easily diffuse into a cell, even though the cell membrane is not damaged [232]. Which means that these species can easily react with and damage the cell structures and macromolecules inside the cytoplasm [130]. Highly selective fluorescent compounds are used for singlet oxygen and hydrogen peroxide quantification in [231] which found the singlet oxygen concentration inside *E.coli* increased steadily during 60 seconds of plasma treatment whereas the H_2O_2 content reached a maximum value after 12 seconds. Once these oxygen species exceed the critical value, the microbial cell suffers from oxidative stress which include the expression of certain genes and activation of different defense activities [233]. These researches demonstrated the occurrence of reactive oxygen species within the cells during plasma treatment, besides, the cell membrane is not the only cellular structure damaged by plasma. Atomic oxygen, hydroxyl radicals (OH^*), hydroperoxyls (HOO^*), superoxides ($O_2\ -^*$) and nitric oxide (NO) are responsible for interacting with various macromolecules in the cytoplasm during plasma treatment [234].

DNA damage is also considered to be one of the reasons causing cell death during plasma treatment. The damage to DNA is reported to be the oxidation of bases. The oxidation of DNA base leads to changes of DNA conformation, such as a

transversion between purines and pyrimidines. For example, the oxidation of guanine generates 8-hydroxy-2'deoxyguanosine (OHdG) which is a compound usually used as a marker of oxidative DNA damage. Moreover, reactive species generated during plasma treatment can also react with deoxyribose carbons which is responsible for the ruptures of DNA strand. Microarray technology is usually used to study the transcriptional process of DNA. It has been demonstrated that up to 18 genes are involved in the SOS response (which means the bacterial response to DNA damage) are over expressed during plasma treatment [235]. In [235], by studying the transcriptomic response of *E.coli* cells exposed for 2 min to an argon plasma, an intense overexpression of several genes involved in the repair of extremely damaged DNA are observed. In addition, more repair responses to damaged DNA are observed by the authors who concluded that DNA is extremely damaged during plasma treatment [235]. The existence of significant damage of DNA has also been observed through agarose gel electrophoresis techniques. For example, in research [236], after 3 minutes, a complete degradation of *E.coli* genomic DNA is observed after plasma treatment.

Not only DNA but also proteins and cytoplasmic enzymes are reported to suffer damage during plasma treatment by these oxidative reactive species. The damage of proteins and enzymes happens in several ways such as the breaking of peptide bonds, the oxidization of amino acid side chains, the production of crosslinks within proteins and aggregation phenomena which are mainly caused by formation of intra and inter-molecular disulphide bonds. The oxidation of just one amino acid in a protein can affect the function of the protein [130]. All these aspects can lead to conformation and structure changes of protein and enzymes [237]. In addition, the activity of enzymes can also be compromised by the oxidation of their cofactors. In [238], by using sodium dodecyl sulfate polyacrylamide gel electrophoresis (SDS-PAGE) technique, it is reported that proteins with high molecular weight, between 50 and 90 kDa (kilodalton) are more sensitive to plasma treatment. Moreover, an

increase of concentration of free amino acids during plasma treatment also demonstrated that plasma can also cause breaks in the proteins and liberate free amino acids. According to these damages to proteins, researchers have pointed out that plasma treatment could be more effective to bacteria compared with PEF treatment and other emerging microorganism inactivation techniques by damaging the enzymes and channel proteins involved in spore germination.

In the end, apart from the direct effects due to these reactive species, there are also indirect mechanism of action that occur during plasma treatment which lead to the formation of other cytotoxic compounds. Reports show that hydroxyl radicals (OH^*) can be generated from H_2O_2 and superoxide radicals ($O_2{}^*\_$) in the presence of transition metals such as iron or copper. The Haber-Weiss reaction is the most common reaction to occur during plasma treatment which consists the transformation of the ferric cation to ferrous cation ($Fe^{3+} + O_2{}^*\_ \rightarrow Fe^{2+} + O_2$). After that, the ferrous cation reaction with H_2O_2 to produce ferric cation (Fe^{3+}), hydro anions (OH^-) and hydroxyl radicals (OH^*) which also have antimicrobial ability. Besides, nitric oxide (NO) can also react with oxygen or superoxide radicals ($O_2{}^*\_$) to form nitrogen dioxide (NO_2), peroxynitrites ($ONOO^-$) and nitrous anhydride (N_2O_2), all these species have antimicrobial ability [239].

2.10.2 Non-thermal plasma reactors

In general, there are two approaches to generate non-thermal plasmas, by electron beam and electrical discharge. In an electron beam reactor, a separate generator is required to generate the electron beam. Usually, high voltage and a vacuum region are required to accelerate the electrons and generate the high energy electron beam [232]. The energy of electrons used to ionize gases can be much higher in the e-beam reactor than other reactors, however, it requires a special reactor and more

complicate structures, besides, the efficiency in transferring the electrons to gases is reported to be poor [240]. In the electrical discharge method, the high voltage electrodes are usually immersed in the atmospheric-pressure gas. The electrons are directly transferred to gases and energy is delivered to gas molecules immediately as they drift along the high voltage region. There are many types of electrical discharge reactors depending on the electrode configuration and electrical power supply, such as pulsed corona discharge reactor [241], ferroelectric pellet bed discharge reactor, dielectric barrier discharge reactor and surface discharge reactor [242] [243]. The pulsed corona discharge reactor is similar to the reactors used in this research so it will be introduced in following sections.

In the pulse corona method, the short-lived discharge plasma is generated by very short pulses of high voltage, applying short pulses of high voltage can prevent the plasma from going into the thermal mode and forming an arc [244] [245]. A non-uniform electric field is formed between two electrodes where their radius of curvature is the smallest. In a corona discharge reactor, the ionization is generally spread over the entire gap between electrodes so the discharge gap is able to be set as large as 10cm which makes large scale application possible [246]. In addition, there is no need of a dielectric to generate the plasma [247].

A dielectric barrier discharge (DBD) plasma reactor is basically composed of two electrodes with at least one dielectric barrier between them. A higher voltage is required to form the plasma due to the presence of the dielectric barrier, the dielectric barriers are usually quartz glass, silica glass or alumina, ceramic materials and polymer layers. DBD plasma reactors can generate a homogenous discharge between electrodes with low energy consumption. These reactors also have advantages of high efficiency and low operational cost so they are usually feasible for pollutant abatement such as CO, NO_x, as well as for ozone generation [248].

The dielectric packed bed reactor is similar to the DBD plasma reactor, but with different configuration of dielectrics. Pellets of dielectric materials are placed in the gap between electrodes. Due to the polarization of the pellets, when the pellets are exposed to an external electric field, a high electric field will be generated at the contact points between pellets [249]. The pellets can be of various materials which makes plasma-catalyst systems available with this kind of reactor. Moreover, residence time can be improved by using those pellets which lead to a higher efficiency in decomposition rates in plasma treatment on exhaust gases [250] . Research demonstrates that the residence time of dielectric packed bed plasma reactor can range from 8.9 s to 17.8s compared with pulse plasma discharge plasma reactor with only 5.4s, [251].

In a surface plasma discharge reactor, one of the electrodes is completely covered by dielectric barrier, but the other electrode is only partially covered. When the electric field is applied, the surface plasma covers the entire dielectric surface. Charge begins to build up at the dielectric surface after a few nanoseconds, which has effect of reducing the electric field outside the dielectric, eventually extinguishing the discharge [252].

2.10.3 Plasma inactivation of microorganisms

Compared with other non-thermal inactivation methods, the non-thermal plasma treatment is considered to be effectual for bacteria, moulds and yeasts [229]. In fact, studies of the effectiveness of non-thermal plasma treatment under the same experimental conditions for different microbial groups has demonstrated that the differences in non-thermal plasma treatment resistance among these microorganism are not as clear as the results observed for thermal or other non-thermal treatment results.

Microorganisms show more or less inter-kingdom and inter-species variability in non-thermal plasma treatment resistance [253]. In [254], the research finds little

difference in non-thermal plasma treatment resistance among spores of *B.cereus, G.stearothermophilus* and *B.atrophaeus*: $3.7\ \log_{10}(\mathrm{CFU})$ to $4.9\ \log_{10}(\mathrm{CFU})$ reductions are observed after a 20 min treatment with a nitrogen-based plasma, while large inter-species variations in spore resistance to heat, UV light and chemical oxidants is observed. In [255], the effectiveness of air plasma treatment of vegetative cells of 15 bacterial species and spores of 4 bacterial species were investigated. They found that after 30 s of treatment, between $4\ \log_{10}\ (\mathrm{CFU})$ to $6\ \log_{10}\ (\mathrm{CFU})$ reductions were achieved for vegetative cells while after 1min exposure under the same conditions, from $1\ \log_{10}\ (\mathrm{CFU})$ to $4\ \log_{10}\ (\mathrm{CFU})$ reduction were attained for bacterial spores. In general, vegetative cells are more sensitive to non-thermal plasma than bacteria spores. In [256], a mixture of helium and oxygen plasma is used to treat microorganisms, 0.3 min is required for *E.coli* and *S.aureus* to reach the D values (the time to reduce a microbial population by 90% or one log cycle) while, 2 min is required for *S.cerevisae* and 14 min is required for *B.subtilis* spores. Similar results are also demonstrated in [255], a nitrogen-based plasma is used and in 1 min, a 6 log cycles (period during microbial growth where the population increases exponentially) of inactivation is observed on *E.coli,P.aeruginosa,E.faecalis and S.aureus,* while 5 and 15 min are required to achieve the same inactivation levels for *Aspergillus niger* and *B.cereus* spores. Moreover, [257] reported that D values of several vegetative cells of *E.coli* and *B.subtilis* is 0.5 min and 2.66 to 8.04 min of bacterial spores of species belonging to the genus *Bacillus, Geobacillus* etc.

2.10.4 Factors influence Plasma treatment performance

There are factors reported to have influence on the inactivation efficiency of the plasma treatment. In this section, some of the factors related to the generation of plasma and properties of microorganism will be introduced.

Due to the plasma treatment conditions varying among different research studies, it is difficult to carry out a direct comparison between these factors. However, general conclusions can be drawn on some processing parameters. In general, the molecular composition of a plasma depends on the energy supplies which in turn is determined by voltage, power and excitation frequency and even on the composition and flow rate of the working gas [130]. Voltage, power and frequency are reported to have a great effect on the inactivation of microorganism as they are factors which determine the input energy, and then determine the chemical reactive species generated and their concentration. It has been demonstrated that an increase in voltage and frequencies increases inactivation rates of both vegetative cells and bacterial spores, the content of reactive chemical species, in particular, concentration of N_2^+, OH, He and O are also reported to be increased as voltage applied increases [258]. Thus, it would be advisable to use high voltages, power and frequencies for the generation of plasma. However, excessive temperature rise, potential negative impacts on samples and high costs are limitations of plasma treatment with extreme processing conditions in industrial applications [259] [260] [261] [262].

The working gas is also an important factor which has influence on the inactivation effectiveness of the plasma treatment. Various gases have been used to generate plasma, the ones most frequently used are nitrogen, oxygen, carbon dioxide, argon, helium, air or mixtures of some of these gases [130]. All of these gases give rise to plasma capable of achieving a certain level of microorganism inactivation and there is no general agreement on which one is the most effective gas. For example, in [263], *L.monocytogenes* are treated with both helium or nitrogen plasma and nitrogen-based plasmas have better inactivation results. Air-based plasma is also reported to have higher efficiency in inactivating *E.coli*. The addition of small amounts of oxygen to noble gases, such as helium, argon or nitrogen, can lead to an improvement in the inactivation effects. This effect is mainly attributed to a higher

formation of reactive oxygen species, such as hydroxyl (OH^*) and hydroperoxyl (HOO^*) radicals.

Gas moisture content also determines the inactivation effectiveness of the plasma treatment. Research studies have shown that completely dry gases are ineffective for *E.coli* inactivation [264]. In [265], an increase in the air relative humidity from 35 to 65% increased the inactivation of *S.Enteritidis* and *S. Typhimurium* from 2.5 to 4.5 log cycles and a higher concentration of hydroxyl radicals are found in the plasma. However, there are also examples showing the opposite results, in [266] when the relative air humidity increased from 52% to 81% or from 62% to 81%, the inactivation efficiency of plasma against *E.coli* and *Staphylococcus epidermidis* decreased by 87 % and 58% and this is reported to be linked to a decrease in the concentration of negative ions in the plasma. Therefore, there would appear to be an optimum moisture value for achieving a maximum antimicrobial activity. For example, the moisture content of 70% is considered to be the optimum moisture for inactivation of *Aspergillus niger* [267].

Gas flow rate is also considered to have influence on the inactivation results of plasma treatment. In [266], a steady increase in *E.coli, S.epidermidis* and *P.alcaligenes* inactivation occurs when air flow rates increased from 2 to 7 m/s, which is attributed to a linear rise in the concentration of negative ions in the generated plasma. With the plasma treatment on *L.monocytogenes* and *L.innocua*, when air was used as the treatment gas, the inactivation rate increases as the gas flow rate increases from 5 to 10 L/min, while an additional increase of gas flow from 10 to 15L/min, only a minor effect is observed on inactivation results. In contrast, gas flow rate hardly affects plasma treatment efficiency when nitrogen is used as treatment gas [268]. Studies also demonstrated that a decrease in O_3 and NO_2 generation can be caused by an increase in air flow rate from 5 to 10 L/min. According to the latest studies, at low flow rates, the number of reactive species, mainly constituted by oxygen radicals, is lower than at high flow rates, but they

have a higher average energy and, therefore, the likelihood of each one colliding with microbial cells increases, thus the antimicrobial effectiveness also increases. However, at higher flow rates the number of reactive species will be higher, but they will have a lower average energy, and their antimicrobial action would be comparatively lower [130].

The plasma treatment inactivation can also be dependent on whether the treatment is carried out directly or indirectly. In the case of direct treatment, the sample is physically located in the region where plasma is generated, therefore, the sample is intimate contact with all the photons and chemicals species produced. In the case of indirect treatment, plasma is produced at some distance from the product and the reactive species in the plasma are usually moved toward the sample using a rapid flow of the feed gas. Studies comparing the inactivation effects between direct treatment and indirect treatment demonstrated that at least 6 log cycles inactivation is observed with direct treatment on *B.atrophaeus* spores [269], however, for indirect exposures only 2.1 to 6.3 log cycles is observed, dependent on the treatment gas. There is also research which show conflicting results, it was found that indirect treatments were more effective against *E.coli* and *L.monocytogenes* than direct treatments, the authors suggested that this could be caused by the recombination of reactive radicals with a short life before reaching the microorganisms in indirect treatments, giving rise to new chemical species with strong bactericidal effects [270]. There is also some research showing no difference in effects between by direct or indirect treatment on *L.monocytongenes*, *E.coli* and *S. aureus* biofilms. The distance between the plasma generation point and samples seems to have an influence on the inactivation efficiencies of plasma treatment. Thus, in general, the antimicrobial effectiveness decreases as the distance increases [271]

2.10.5 Discussion of Plasma treatment on microorganisms

The higher resistance to non-thermal plasma treatment exhibited by bacterial spores may be due to the 'barriers' of the spores. These barriers can be caused by low water content, which reduces the diffusion of the reactive species, the high concentration of dipicolinic acid in the spore core, the very robust spore coat which makes a physical barrier to the reactive species, and the special conformation of the spore DNA, which is saturated by a group of soluble acid proteins [130] [272].

The higher resistance to non-thermal plasma treatment by yeasts and moulds compared with vegetative bacterial cells could be the result of differences in cellular structure and molecular composition between prokaryotic and eukaryotic cells. On one hand, the existence of a nuclear membrane provides a good protection for fungal DNA, on the other hand the cell wall of fungal cells are very thick and consists of rigid layers of polysaccharides, which would provide further protection to the cell [131].

In fact, studies about non-thermal plasma inactivation concentrates more on chemical reactions and reactive species generated, microorganism structures, growth conditions, such as pH and temperature, and cellular physiological state. The effect of electric field on cellular reactions is not usually taken into account. Besides, reports have shown the limitation of plasma treatment which is high microbial loads lead to a reduction of inactivation effects.

Investigating the electric field performance during plasma treatment might provide an optimization of non-thermal plasma inactivation in applications.

2.11 Discussion

This chapter reviewed background information related to this project. In the beginning of the review, basic knowledge of microorganisms is introduced. The introduction on the structure of microorganism provides background for understanding of the mechanisms of the PEF treatment from the biological point of view. After that, the benefits and microorganisms hazards sections explained the necessity of developing of the inactivation techniques. This chapter also provides the introduction and comparison of different inactivation techniques such as thermal inactivation, chemical inactivation, UV inactivation, plasma treatment and so on. Finally, a detailed review of the PEF treatment process is provided which also introduces the pulse generation systems, the mechanism of the PEF treatment and the factors influencing the treatment results. Although numerous studies have been conducted about PFE treatment and results have been published, there are still gaps in understanding of the PEF treatment process. So it is necessary to continue to study the PEF processes, which may help to optimize the applications of this technology.

Firstly, although the electroporation theory is mostly accepted by scientists, and it at assumed that this process is triggered during the study of PEF treatment, the exact mechanisms of inactivation of microorganisms by electric field effects is not fully understood.

Secondly, the PEF treatment process is generally considered as 'non-thermal' due to low bulk temperature increase of the samples during the PEF treatment. Little research has looked at possible localized heating during treatment. Therefore, the local heating effects during the PEF treatment are also necessary to be fully investigated.

Thirdly, there has not been sufficient focus on the effect of parameters, such as waveshape, on the inactivation performance of PEF treatment on microorganisms.

There are no studies focused on the difference in the mechanisms of inactivation of microorganisms using the PEF treatment with square impulses and AC high frequency oscillating signals.

Finally, because there are very high bio-fuel content microalgae discovered which provides a good alternative bio-fuel production approach, studies of the PEF treatment of microorganisms have been drawing increasing global attention in the past few years. The PEF process can be used to help to extract these oily content. To fully understand the mechanism of interaction between the electric field and microorganism, further investigation is required.

Therefore, the main objectives of the project can be summarized as follows:

- To develop a simulation model which can be used to investigate the electric field distribution and thermal distribution in microorganisms during the PEF treatment.
- To investigate the effects of different waveshapes, square impulse and high frequency oscillating signals, and to compare the effects of these HV signals on microorganisms during the PEF treatment.
- To investigate the different effects of changing parameters of the PEF treatment, such as electrical conductivities, treatment time, external field strength and cell size.
- To investigate the local heating effects at a cell during the PEF treatment and to evaluate the contribution of thermal effects during the PEF treatment process.
- To conduct the PEF treatment on microalgae with both high electric field strength and general electroporation field strength to investigate whether cell lysis be achieved by the PEF treatment in both field strength regimes.

- To conduct both the PEF treatment and Plasma treatment of microalgae with the same pulse generation system to compare the efficiency in inactivation between these two approaches.

Chapter 3. Modelling of microorganisms---Linear model

3.1 Introduction and Background

Chapter 3 is the first of three Chapters in which different models of microbiological cells will be developed, explored and discussed. This chapter is focused on a 1D model of a single cell developed using a lumped RC element circuit. This model will be called the linear model as it is based on a series configuration of RC blocks which represent different parts of the microbiological cell. More advanced models of a single cell will be developed in later chapters and the modelling results obtained from the approaches will be compared and analyzed in sections of Chapter 4 and Chapter 5.

The models which are developed in these chapters are used for simulation of the transient electric field distribution and local heating effects of a single cell during PEF treatment, as the study of bioelectrical processes requires a multidisciplinary approach.

Chapter 3 will provide background information on modelling of bio-cells stressed with an electric field and the development of the linear model which will be used to investigate the electrical properties of microorganisms during PEF treatment. As mentioned before, there will be two more models introduced in further chapters which will focus on more sophisticated analysis. These more advanced models are built with Quickfield and COMSOL. The initial analytical linear model will be mainly introduced in this chapter.

As mentioned in Chapter 2, the interactions between bio-cells and an external electric field is not fully understood. Typically, the heating effects during the PEF treatment are not taken into account in PEF models. It is problematic to develop analytical model(s) which can be used for investigation of the effect of different kind of energising signals (AC or DC signals) on local heating of microorganisms.

Therefore, investigation of the local heating effects across a single cell during the PEF treatment could be beneficial for understanding of the interactions between bio-cells and external electric fields. Such investigation using the single cell models could provide novel results in further understanding of local heating effects and transient electric field distribution across bio-cells during the PEF treatment. These results would be beneficial in optimizing the applications of the PEF treatment. Detailed information about such modelling will be introduced and discussed in Chapter 4 and Chapter 5. A brief introduction of each model will follow.

In the linear model, environmental fluid, bio-membrane and cytoplasm are included. The transmembrane potential across the cell membrane can be obtained when the external electric field is applied. This linear model has been developed and investigated in early researches about PEF treatment on biological cells [273] [274] [275]. However, these studies do not provide further investigations about how the parameters influence the transient transmembrane electric field strength of a single cell during PEF treatment.

From the electrical point of view, bio-cells can be modelled in terms of their dielectric properties. Consequently, some background information on electrical properties of bio-membranes and basic principles of electromagnetism which are used to investigate the interaction between the electric field and bio-cells will be introduced in section 3.1.1 -3.1.6 to provide the basis for the development of modelling of microorganism in this study.

3.1.1 Membrane impedance

In 1923, the capacitance of cellular membranes had been measured by Fricke [276] [277]. Fricke found that the capacitance per unit area of the cell membranes Cm was ~1 $\mu F/cm^2$. The thickness of the membrane, d, also was calculated through the results of his measurement by solving **Equation (3.1)**.

$$\boldsymbol{C_m = \frac{\varepsilon_r \varepsilon_0}{d}} \qquad \textbf{(3.1)}$$

where $\varepsilon_r$the relative permittivity of the membrane (Fricke assume this value to be 3), ε_0 is the permittivity of free space and *d* is the membrane thickness.

By solving **Equation (3.1)**, Fricke calculated the membrane thickness of cells in calf blood which was found to be *d* $\sim$ 3nm. This value is within a factor of 2.5nm, the value obtained from modern electron microscopy studies [273] [278].

Fricke's and others early measurements of the parameters of bio-cells are generally based on characteristics of cell suspensions which are not accurate enough to obtain the value of conductance of the individual cell membrane. A series of measurement were conducted by Cole and co-authors and provided the first accurate measurement of the membrane conductance by studying the squid giant axon using extracellular electrodes. According to the measurements, the nerve membrane has a resistance of $\sim 1000\ \Omega\ /\mathrm{cm}^2$ [279] [280] [281] [282] [283].

Early measurements of the membrane impedance were conducted by passing electric current through the intra-cellular electrodes and measuring the membrane potential. Such methods were also used to measure the resting potential of membrane [278] . After that, the measurement of membrane impedance becomes more direct. The linear electric properties of many cell membranes can be represented by a parallel conductance and capacitance network. The conductance represents the ionic conduction through the membrane via ion channels and the capacitance represents the isolating properties of lipid layer. With a typical cell, the conductance per unit area of membrane, G_m is considered to be $\sim 1\ \mathrm{mS}/cm^2$ and the capacitance, C_m is$\sim 1\ \mu\mathrm{F}/cm^2$ [273].

3.1.2 Cellular electric potentials

As discussed in previous chapters, there is a maintained potential difference across the membrane which is called the resting potential. It was reported that multiple parameters such as temperature, pH, extra-cellular concentration of ions and

extrinsic electric current influence the transmembrane potential. The changes in the transmembrane potential can lead to many effects on bio-cells, the most direct effect is the change of transport of charged particles across the membrane. Secretion of chemical substances can also be influenced by the transmembrane potential. Rapid changes in the membrane potential generally result from changes in conductance of the membrane to one or more ions [284]. Moreover, mechanical properties of muscle cells like eukaryotic organisms can also be influenced by changing the transmembrane potentials [285].

A large resting potential difference is observed between the extracellular and intracellular surfaces, ranging from $\sim 20\mathrm{mV}$ to$\sim 90\mathrm{mV}$. For a potential difference of $60\ \mathrm{mV}$ across a membrane with thickness of $\mathrm{d} = 8\ \mathrm{nm}$, the electric field in the membrane would be $7.5\ \mathrm{MV/m}$ according to **Equation (3.2).**

$$\mathbf{V} = \vec{\boldsymbol{E}}\mathbf{d} \qquad \textbf{(3.2)}$$

Where:

V is the electric potential in volts. E is the electric field in volts per metre. d is the distance between electrodes in metres.

Electrical breakdown in atmospheric air takes place at$\sim 3\ \mathrm{MV/m}$. So it can be observed that at $2.5\ \mathrm{MV/m}$ a strong electric field generally exists in the bio-membrane of a living cell [273].

3.1.3 Historical aspect of transmembrane potential calculations

The study of the PEF treatment of microorganisms is an interdisciplinary project which links electrical engineering and microbiology. The bio-electromagnetic terminology and basic principles of electromagnetism related to the modelling and parameters used in this project will be reviewed in this section.

When the treatment samples containing microorganism are exposed to a pulsed electric field, mobile charges (mainly ions) move along the field lines of the applied electric field. The charge movement forms the current which is measured in Amperes (A). With reference to a certain area, there will be a current density (J) which is expressed in A/m^2. Associated with the electric current, a magnetic flux density ($\vec{\boldsymbol{B}}$) also exists. **Equation (3.3)** shows the relationship between $\vec{\boldsymbol{B}}$ and the permeability ($\boldsymbol{\mu}$) and magnetic field intensity($\vec{\boldsymbol{H}}$).

$$\vec{\boldsymbol{B}} = \boldsymbol{\mu}\vec{\boldsymbol{H}} \qquad \textbf{(3.3)}$$

The link between the changing magnetic and electric fields is given by the Maxwell equation (Faraday's Law) which is **Equation (3.4).**

$$\boldsymbol{\nabla} \times \vec{\boldsymbol{E}} = -\frac{\boldsymbol{\partial}\vec{\boldsymbol{B}}}{\boldsymbol{\partial t}} \qquad \textbf{(3.4)}$$

Where $\vec{\boldsymbol{B}}$ is the magnetic flux density, $\vec{\boldsymbol{E}}$ is the electric field.

The properties of a medium influence the value of electric and magnetic field. The conduction current density ($\overrightarrow{\boldsymbol{J_c}}$) is also influenced by the conductivity of the medium ($\boldsymbol{\sigma}$), and electric field $\vec{\boldsymbol{E}}$, as shown in **Equation (3.5)**

$$\overrightarrow{\boldsymbol{J_c}} = \boldsymbol{\sigma}\vec{\boldsymbol{E}} \qquad \textbf{(3.5)}$$

The displacement current density is given by **Equation (3.6)** below, where $\vec{\boldsymbol{D}}$ is the electric flux density. **Equation (3.7)** gives the relationship between the electric flux density and electric field through permittivity **($\boldsymbol{\varepsilon}$)** of the media. According to **Equation (3.6)** and **Equation (3.7)**, an increasing electric field generates a displacement current in the direction of the electric field.

$$\overrightarrow{J_D} = \frac{\partial \vec{D}}{\partial t} \qquad \textbf{(3.6)}$$

$$\vec{D} = \varepsilon \vec{E} \qquad \textbf{(3.7)}$$

The Energy density in the electric field is represented by the Faraday's energy density equation, **Equation (3.8).** It can be seen that, the greater the applied electric field in a dielectric medium, the greater the energy density will be.

$$U_e = \frac{1}{2} \varepsilon \vec{E}^2 \qquad \textbf{(3.8)}$$

The differential form of Maxwell-Equation, **Equation (3.9)**, indicated at a point, the curl of magnetic field intensity is equal to the sum of the conduction current and displacement current densities.

$$\nabla \times \vec{H} = \overrightarrow{J_c} + \frac{\partial \vec{D}}{\partial t} \qquad \textbf{(3.9)}$$

$$\nabla \cdot \vec{D} = \rho_c \qquad \textbf{(3.10)}$$

Equation (3.10) is the Gauss' law, where ρ_c is the free charge density.

$$\vec{E} = -\nabla \varphi \qquad \textbf{(3.11)}$$

$$\nabla \cdot \nabla \varphi = \nabla^2 \varphi = -\frac{\rho}{\varepsilon} \qquad \textbf{(3.12)}$$

Equation (3.12) is known as Poisson's equation which is derived through **equation (3.11)**, **Equation (3.10)** and **Equation (3.7)**, where φ is the electrical potential, ε is the permittivity and ρ is the charge density.

$$\nabla^2 \varphi = 0 \quad \textbf{(3.13)}$$

Equation (3.13) is derived when there is no free charge ($\rho = 0$) exists in **equation (3.12),** the equation is reduced to Laplace's Equation.

The Laplace's Equation which links the electric potential and the electric field (no space charge is considered) is given by **Equation (3.14)** for 3D Cartesian coordinates [273]

$$\frac{\partial^2 \varphi}{\partial x^2} + \frac{\partial^2 \varphi}{\partial y^2} + \frac{\partial^2 \varphi}{\partial z^2} = 0 \quad \textbf{(3.14)}$$

The equations introduced in this section are generally used in modelling of the interaction between a bio cell model and electromagnetic fields in PEF studies. Previous works in the field of modelling of the membrane response to the external electric field will be reviewed in further paragraphs of this section.

The first work in which the steady-state transmembrane potential was expressed by Fricke 1953 in which an ellipsoidal shaped cell with negligible membrane conductivity (σ=0) was considered. As shown in **Figure (3.1.1)**, the cytoplasm in this model was fully charged. The transmembrane potential at the poles of the generic ellipsoidal cell was expressed by **Equation (3.15)** [286].

$$\Delta\boldsymbol{\varphi} = \frac{1}{1-n_a}\boldsymbol{aE} \quad (3.15)$$

Where $\Delta\varphi$ is the induced transmembrane potential at a pole in volts, E is the applied electric field in volts per metre, $\boldsymbol{a}$ is the semi-axis orientated in the field direction in metre and n_a is termed the depolarizing factor [287].

The depolarizing factors for spheroids and ellipsoids, which have been calculated by Stoner and Osborn, are shown in equations below [287] [288].

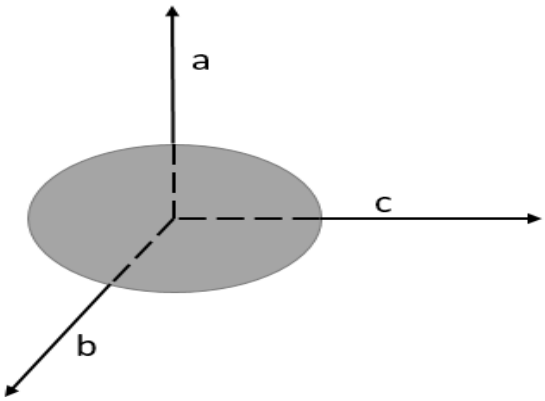

Figure (3.1.1) Ellipsoid model of single cell shows three principle axes: a, b and c.

$$n_a = \frac{\beta\delta}{\sqrt{1-\delta^2}(1-\beta^2)}(LF(LF(k,\psi) - LE(k,\psi))) \quad \textbf{(3.16)}$$

$$n_b = -n_a + \frac{\beta\delta}{\sqrt{1-\delta^2}(\beta^2-\delta^2)}LE(k,\psi) - \frac{\delta^2}{\beta^2-\delta^2} \quad \textbf{(3.17)}$$

$$n_c = -\frac{\beta\delta}{\sqrt{1-\delta^2}(\beta^2-\delta^2)}LE(k,\psi) + \frac{\delta^2}{\beta^2-\delta^2} \quad \textbf{(3.18)}$$

Where n_a, n_b, n_c depend on the axis ratios $\beta = \frac{b}{a}$ and $\delta = \frac{c}{a}$.

$$\mathrm{k} = \sqrt{\frac{1-\beta^2}{1-\delta^2}} \quad \textbf{(3.19)}$$

$$\psi = \cos^{-1}(\delta) \quad \textbf{(3.20)}$$

LF and LE are elliptical integrals that are a function of k and ψ, and they depend on the axis ratios accordingly.

$$LF(k,\psi) = \int_0^{\psi} -\frac{1}{\sqrt{1-k^2sin^2\phi}}d\phi \quad \textbf{(3.21)}$$

$$LE(k,\psi) = \int_0^{\psi} \sqrt{1-k^2sin^2\phi}\,d\phi \quad \textbf{(3.22)}$$

Where k and ψ are defined by **Equation (3.19)** and **(3.20)**, and ϕ is the amplitude angle.

Depending on the axial ratio of the ellipsoid, the depolarizing factor can be between 0 and 1.

Further investigations of the transmembrane potential of ellipsoidal cells were conducted based on the work of Fricke [286] and Stratton [289]. More detailed model of cells and cellular suspensions was developed by Schwan, Zimmermann and Neumann [290] [291] [292].

The research at that time was focused on the frequency and time dependency properties of biological materials. At present, the research continues to be focused on improving the equations developed by these researchers to specific electrical properties of cytoplasm, cell membranes and extra-cellular medium. The investigation of the effect of geometry in these models of the cell response to the electric field was also conducted: spherical shapes and non-spherical shapes were considered [293] [205] .

The main research findings which underpin the response of the cell to the external field will be introduced in further sections and will provide background information and support to the modelling of the PEF effects in a single cell conducted in the present project.

3.1.4 The Schwan Equation

H.P. Schwan developed an analytical model to calculate the trans-membrane potential of a spherical cell exposed to the external electric field by solving Laplace's **equation (3.14)** in [290]. The obtained result is called the Schwan Equation and this formula is given by **Equation (3.23)**.

$$\Delta\varphi = \frac{3}{2} ER\cos\theta \quad \textbf{(3.23)}$$

Where $\Delta\varphi$ is the induced trans-membrane potential in volts, E is external electric field in volts per metre, R is cell radius in metre and θ is polar angle with respect to direction of field in degree.

For a spherical shaped cell, a=b=c=R and hence $n_a = n_b = n_c = \frac{1}{3}$. For this case, the Fricke's equation (**Equation (3.10)**) can be reduced to the Schwan equation. Schwan assumed the conductance of the cell membrane to be zero to simplify the analysis.

3.1.5 The time dependent transmembrane potential

The Schwan Equation was obtained using the ohmic conduction approach, it was used to calculate the transmembrane steady-state potential reached after the transient period. The next major step was made in 1997 by Kotnik et al, who derived **Equation (3.24)** the time dependent trans-membrane potential depending on the geometric and electrical properties of the cell and extra-cellular medium [294]. For a bio-cell which is modelled using a membrane with finite electrical conductivity and conductive cytoplasm, surrounded by the conductive extra-cellular medium, the equation below shows the transmembrane potential in the bio membrane.

$$\Delta\varphi = f E R \cos\theta \left[1 - e^{-\frac{t}{\tau}}\right] \quad \textbf{(3.24)}$$

Where f is a function that incorporates electrical and geometrical parameters of cell which can be calculated and $\boldsymbol{\tau}$ is a time constant which also can be calculated [294].

$$f = \frac{3\sigma_0\left[3dR^2\sigma_i + (3d^2R - d^3)(\sigma_m - \sigma_i)\right]}{2R^3(\sigma_m + 2\sigma_0)\left(\sigma_m + \frac{1}{2}\sigma_i\right) - 2(R-d)^3(\sigma_0 - \sigma_m)(\sigma_i - \sigma_m)} \qquad \textbf{(3.25)}$$

where σ_m is the conductivity of cell membrane in S/m, d is the membrane thickness in metre, σ_0 is the conductivity of extra-cellular medium in S/m, σ_i is the conductivity of cytoplasm in S/m, R is cell radius in metre.

Time constant $\boldsymbol{\tau}$ is given by:

$$\boldsymbol{\tau} = \frac{RC_m}{\frac{2\sigma_0\sigma_i}{2\sigma_0+\sigma_i}+\frac{R}{d}\sigma_m} \quad \textbf{(3.26)}$$

where $\mathrm{C_m}$ is the membrane capacitance in $\mu\mathrm{F}/cm^2$. Kotnik et al assumed that C_m = $1\ \mu\mathrm{F}/cm^2$.

For the case of non-conductive membrane, $\sigma_m = 0$, the value of f tends to $\frac{3}{2}$ and the equation reduces to the Schwan equation. So the Schwan equation is valid for the case when the charging time constant of the cell membrane is much shorter than the pulse duration of the applied electric field, $\mathrm{t} \gg \tau$ when the term $1 - e^{-\frac{t}{\tau}}$ tends to 1.

Further study developed by Kotnik, solved the previous equation for the transient case [295]. The publication describes a general method for analysis of the time dependence of transmembrane potential induced by time-varying electric fields. They calculate the transmembrane potential through Laplace transforms. The transmembrane potential response as function of time was obtained [205] [294] [295].

3.1.6 PEF chamber with dielectric layers and spherical model

Timoshkin et al proposed a PEF treatment chamber with dielectric layers attached on the electrodes, as shown in **Figure (3.1.6.1)** [108]. This design of PEF chamber and calculation of electrical properties of the test chamber inspire the development of the linear model of this project which will be introduced in further sections [274]. A typical PEF treatment chamber consists of metal electrodes with sample to be treated in direct contact with them. Under certain conditions bubbles could be generated during the PEF treatment and complete electrical breakdown of the treatment sample could result. The PEF treatment chamber proposed in [274] consists of two ceramic slabs with a high relative permittivity of ~3000, in order to

avoid direct contact between the liquid and the metallic electrodes, which can minimize the conduction current.

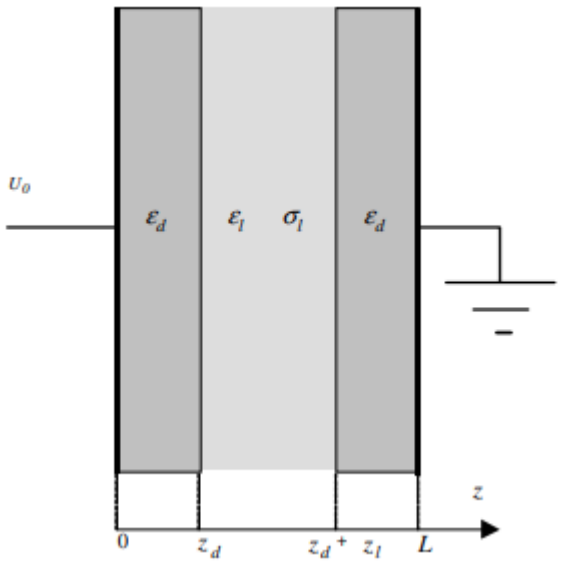

Figure (3.1.6.1) PEF chamber with dielectric layers, picture taken from [274].

In order to obtain the time-dependent effective field in the working region, Ohmic conduction approaches were used [274]. The boundary conditions used to solve these equations are similar to the linear model which will be introduced in following sections. The effective field strength is given by equation below.

$$E_0(t) = E_L e^{-t/\tau_f} \quad \textbf{(3.27)}$$

$$E_L = U_0(z_l + 2\frac{\varepsilon_l}{\varepsilon_d} z_d)^{-1} \quad \textbf{(3.28)}$$

$$\tau_f = (\frac{\varepsilon_l}{\varepsilon_d} + \frac{z_l}{2z_d})\frac{\varepsilon_0 \varepsilon_d}{\sigma_l} \quad \textbf{(3.29)}$$

Where τ_f is the characteristic field relaxation time of the test chamber in second, this time determines the time of existence of the field in the liquid due to the Maxwell-Wagner surface polarization mechanism. z_d and z_l represent the width of the treatment region and dielectric barrier respectively in metres; ε_l and ε_d represent the relative permittivity of the liquid suspension in the treatment region and dielectric barrier respectively; σ_l represents the conductivity of the liquid

suspension in siemens per metre and E_L represents the Laplacian electric field in the treatment region in volts per metre.

In order to investigate the transient potential across the cell membrane when a microorganism is put in this test chamber, a spherical model of a microorganism cell was employed.

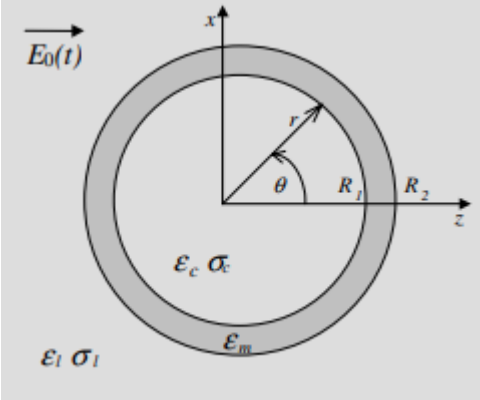

Figure (3.1.6.2) Spherical shell model of microorganism, picture taken from [274].

By applying the same Ohmic conduction approach, the time dependent maximum electric field on the membrane which, as described earlier, occurs at the poles of the membrane, can be written as **Equation (3.30)** below

$$E_{max}(t) = -A_m(t) + 2B_m(t) \cdot {R_1}^3 \quad \textbf{(3.30)}$$

Where R_1 is the radius of the cytoplasm; $A_m(t)\ and\ B_m(t)$ are coefficients relating to radius of cytoplasm $(R_1)$and the microbial cell (R_2), relative permittivity of the cytoplasm, membrane and surrounding liquid, conductivity of cytoplasm and surrounding liquid, the Laplacian electric field in the treatment region and the Maxwell-Wagner relaxation time.

By investigating the equations, the development of the electric field in the membrane was separately described in 3 distinct physical phases, the polarization process, the charge accumulation process and the Maxwell-Wagner field relaxation

process [274] [78]. **Figure (3.1.6.3)** below shows the response results. The details of the three phases will be introduced in the linear model discussion in 3.2.

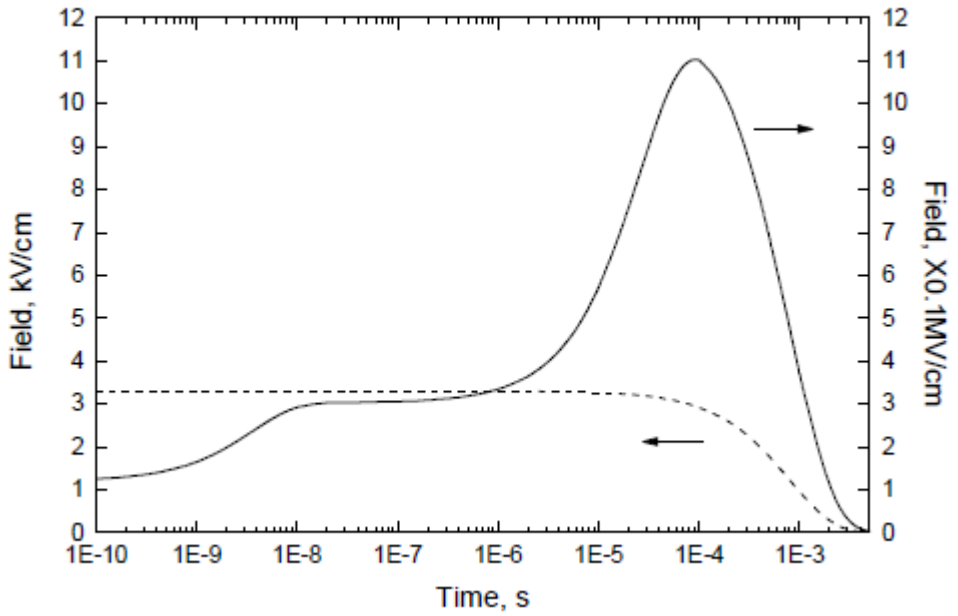

Figure (3.1.6.3) Fields in membrane (solid line) and water gap (dashed line). Picture taken from [274].

Based on this spherical model, *Si Qin et al* investigates the response of electric field build up process in membrane in [296], realistic parameters are used in the model. By changing different parameters, *Si Qin et al* also investigates the factors which influence the electric field build up process, finding out how the size of cell, thickness of membrane, relative permittivity of membrane and the conductivity of suspension have significant influence on the electric field build up process in membrane, for example: the results shows that with thicker membrane, the transient response of electrical field on the membrane at poles increases: the transient response of electrical field on the membrane could be increased twice with membrane thickness decreased from 10 nm to 4 nm [296].

3.2 Linear model

In this section, an initial linear model will be introduced to allow investigation of the transmembrane potential when the bio-cell is exposed to an external field. Some further investigations about changing parameters with this linear model will also be presented in further sections to investigate the transient electric field strength during PEF treatment of a single cell.

Figure (3.2.1) below shows the structure of the model: this linear model consists of two electrodes (Hv+ and Ground), environmental fluid (zone I, 0- Z_1 and zone V, Z_4-Z_5), membrane (zone II, Z_1-Z_2 and zone IV, Z_3- Z_4) and cytoplasm (zone III, Z_2- Z_3). l_w is the gap distance of environmental fluid between the cell membrane and electrodes (treatment suspension in PEF treatment), l_c is the thickness of the layer of cytoplasm equivalent to a diameter of an actual cell , l_w is the thickness of the layer represents cell membrane. As seen on **Figure (3.2.1)**, each zone is characterized by the conductivity of environmental fluid (σ_w) and cytoplasm (σ_c), permittivity of environmental fluid (ε_1), cell membrane (ε_2) and cytoplasm (ε_1). The conductivity of cell membrane is considered as zero for the calculation [108]. The electric field strength in the environmental fluid was represented by E_1 and E_5 while E_2 and E_4 represent the electric field strength in the cell membrane, and the electric field strength in the cytoplasm was represented as E_3. J_1 to J_5 represent the conduction current densities on the boundaries.

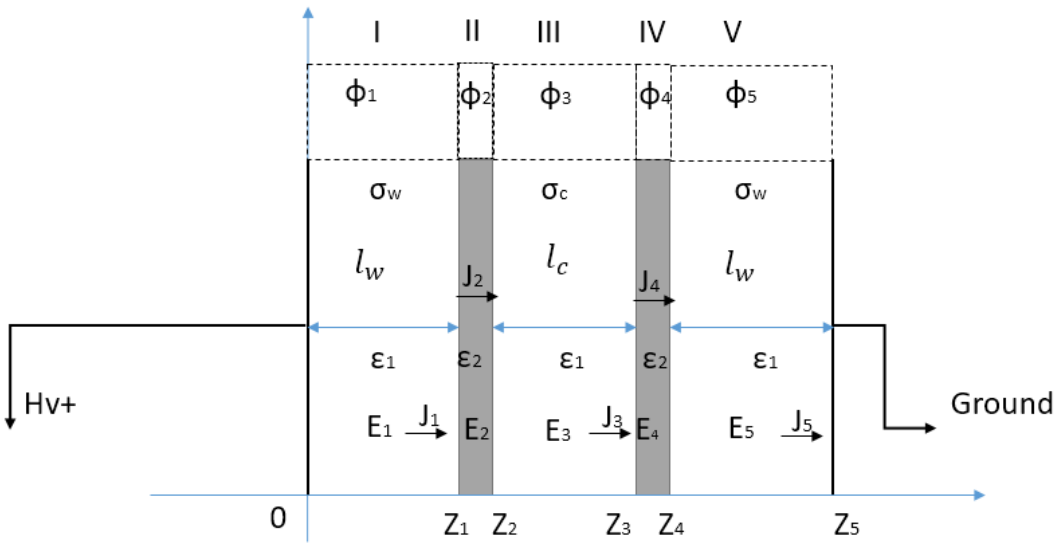

Figure (3.2.1) Constructions of linear model.

This linear model is similar to the PEF chamber model with dielectric layers in the previous section, so the response to a uniform DC step voltage can also be analyzed using the Ohmic condition approach [274]. For this method, the electrical potentials inside the environmental fluid (regions I, V), membranes (regions II, IV) and cytoplasm (region III) can be written as the equations below:

$$\varphi_1 = -A_1(t)Z + B_1(t) \quad \textbf{(3.2.1)}$$

$$\varphi_2 = -A_2(t)Z + B_2(t) \quad \textbf{(3.2.2)}$$

$$\varphi_3 = -A_3(t)Z + B_3(t) \quad \textbf{(3.2.3)}$$

$$\varphi_4 = -A_4(t)Z + B_4(t) \quad \textbf{(3.2.4)}$$

$$\varphi_5 = -A_5(t)Z + B_5(t) \quad \textbf{(3.2.5)}$$

Two boundary conditions are necessary to solve these coefficients, the first one is the electrical potentials across each interface are equal which gives equations below:

Z=0, $\varphi_0(Z_0)=U_0H\ (t)$ i**(3.2.6)**

Z=Z_1, $\varphi_1(Z_1)=\varphi_2(Z_1)$ **(3.2.7)**

Z=Z_2, $\varphi_2(Z_2)=\varphi_3(Z_2)$ **(3.2.8)**

Z=Z_3, $\varphi_3(Z_3)=\varphi_4(Z_3)$ **(3.2.9)**

Z=Z_4, $\varphi_4(Z_4)=\varphi_5(Z_4)$ **(3.2.10)**

Z=Z_5, $\varphi_5(Z_5)=0$ **(3.2.11)**

Where $H\ (t)$ is the unit step function describing the application of external potential U_0 at time $t = 0$ and Z_n is the distance from the high voltage electrodes of each cell components. This set of equations assumes that there is no distributed space charge in the dielectrics which means Laplace's equation may be applied.

Due to the conductivity of the liquid, charges move due the electric field and start to accumulate on these interfaces. This leads to the second boundary condition, which is a charge continuity condition, the rate of change of the surface charge density is equal to the difference between the conduction current densities on either side of the layers (environmental fluid and membrane layer, membrane and cytoplasm layer and membrane environmental and fluid layer represented with n).

$$J_l - J_n = \sigma_l E_0(t) - \sigma_n E_n(t) = -\frac{\partial \rho_s(t)}{\partial_t} \qquad \textbf{(3.2.12)}$$

Where $\rho_s(t)$ is the non-compensated free surface charge density at membrane represented with m and other components interfaces which is related to the electric flux density, which are represented with n.

$$\rho_s(t)=\varepsilon_n E_n(t) - \varepsilon_m E_m(t) \qquad \textbf{(3.2.13)}$$

For the linear cell model, this condition can be written as equations below:

I/II interface $J_1 + \frac{\partial \varepsilon_1 E_1}{\partial_t} = \frac{\partial \varepsilon_2 E_2}{\partial_t}$ **(3.2.14)**

II/III interface $\frac{\partial \varepsilon_2 E_2}{\partial_t} = J_3 + \frac{\partial \varepsilon_1 E_3}{\partial_t}$ **(3.2.15)**

III/IV interface $J_3 + \frac{\partial \varepsilon_1 E_3}{\partial_t} = \frac{\partial \varepsilon_2 E_4}{\partial_t}$ **(3.2.16)**

IV/V interface $\frac{\partial \varepsilon_2 E_4}{\partial_t} = J_5 + \frac{\partial \varepsilon_1 E_5}{\partial_t}$ **(3.2.17)**

Finally gives equation:

$$E_{membrane} = \frac{u_0}{a}\left\{\frac{1}{\alpha\beta} + \frac{e^{-\alpha t}}{\alpha-\beta}\left(\frac{1}{\alpha} - (T_1+T_2) + \alpha T_1 T_2\right) + \frac{e^{-\beta t}}{\beta-\alpha}\left(\frac{1}{\beta} - (T_1+T_2) + \beta T_1 T_2\right)\right\} \textbf{(3.2.18)}$$

Where the coefficients can be calculated below.

$$a = 2l_m T_1 T_2 + l_c T_1 T_3 + 2l_w T_2 T_4 \quad \textbf{(3.2.19)}$$

$$b = 2l_m(T_1+T_2) + l_c T_3 + 2l_w T_4 \quad \textbf{(3.2.20)}$$

$$c = 2l_m \quad \textbf{(3.2.21)}$$

$$\alpha = -x_1 = \frac{p}{2} - \sqrt{\frac{p^2}{4} - q} \quad \textbf{(3.2.22)}$$

$$\beta = -x_2 = \frac{p}{2} + \sqrt{\frac{p^2}{4} - q} \quad \textbf{(3.2.23)}$$

$$p = \frac{b}{a} \quad \textbf{(3.2.24)}$$

$$q = \frac{c}{a} \quad \textbf{(3.2.25)}$$

$$T_1 = \frac{\varepsilon_1}{\sigma_1} \quad \textbf{(3.2.26)}$$

$$T_2 = \frac{\varepsilon_1}{\sigma_2} \quad \textbf{(3.2.27)}$$

$$T_3 = \frac{\varepsilon_2}{\sigma_2} \quad \textbf{(3.2.28)}$$

$$T_4 = \frac{\varepsilon_2}{\sigma_1} \quad \textbf{(3.2.29)}$$

3.2.1 Parameters of microorganism used in linear model

In order to simulate the transient transmembrane potential when the model is exposed to the external electric field, the parameters of each component should be evaluated first. Parameters are determined based on references from other's research, detailed information will be introduced in the further paragraph of this section.

The electrical properties of environmental fluid which surrounds the microorganisms during PEF treatment usually varies in different PEF treatment. In general, the conductivity of sample suspension is relatively high compared with modelling studies: In [297], the conductivity of liquid suspension is set to be 0.15 S/m during the PEF treatment with microalgae, in a recent paper which is also about PEF treatment with microalgae published in 2022, the conductivity of the liquid suspension is set to be 0.17~ 0.2 S/m [298]. However, in some modelling studies [273] [299], the conductivity of the environmental fluid is set to be 10^{-4} S/m. In [274], a wide spectrum of values of conductivity of environmental fluid was investigated, it was presented that for suspension liquids used in cell manipulation procedures, the conductivity can be as low as 0.5×10^{-3} S/m. Based on published data of Kotnik *et al* [275], the values of the conductivity of environmental fluid lie in the range 10^{-3}- 10^{-2} S/m [274]. Based on these publications 0.5×10^{-3} S/m was decided to be used in the linear modelling. For the permittivity of environmental fluid, 80 is used in the linear model. This is the same as the permittivity of water, because for most common PEF treatment situation, the treatment suspension was water-based solution. In general, 80 was also commonly used in other studies about modelling of PEF treatment with microorganisms [273] [274] [275] [300].

The cell membrane is a layer between the cytoplasm and environmental fluid as introduced in chapter 2. As discussed, the basic structure of cell membrane is a phospholipid bi-layer with different types of proteins embedded. According to studies, the range of relative permittivity of the membrane was reported to be 2-10 [301] [302] [303] . In a recent paper [7], 5 was used as the permittivity of cell membrane. The permittivity of cell membrane is set to 2 in this linear model. 2 is also used in others studies [273] [274] [78]. As mentioned in chapter 2, the most important function of the cell membrane is the selective permeability which controls the ion transport between environmental fluid and cytoplasm. However, the transportation of ions is generally controlled by the channel proteins. So, in general, as the cell membrane is highly non-conducting [302], the cell membrane is considered as completely non-conducting in the linear model [304].

As introduced in chapter 2, the cytoplasm is a conductive fluid with ions, nutrients, proteins, membrane bound organelles and other essential components. All these components can affect the dielectric properties of cytoplasm. In previous studies, the values of relative permittivity of cytoplasm varies from 50 to 200 [301] [302] [303]. As the cytoplasm is water-based suspension, 80 is considered to be the permittivity of cytoplasm, this value was also used in other researches [273] [274] [78]. In terms of conductivity of cytoplasm, it is generally considered as highly conductive due to the large amount of ions [302], publications shows the conductivity of cytoplasm can be in a ranges from 0.2- 10 S/m [301] [305] [306]. In this linear model, the conductivity of cytoplasm is 1.2 S/m, as this value was also selected in others studies [7] [307].

The dimension of cytoplasm and thickness of membrane modelled with the linear model also need to be considered. The thickness of cell membrane was estimated to be ~4-10 nm [302] [308]. 5 nm was used in this linear model as the membrane thickness, this value was also used in previous studies about modelling of PEF treatment with microorganism [273] [274]. A recent paper about modelling of PEF

treatment with tumour cells used 4 nm [7] which is also close to 5 nm used in linear model. The diameter of microbial cell can vary from ~0.2 μm to ~700 μm, most of the microorganisms have a cell diameter of a few μm [308]. According to literature, the general size of yeast ranges from 5-10 μm [138], the general size of microalgae phytoplankton ranges from 2-5 μm [143] [144] .Therefore, the size of cytoplasm is considered to be 5 μm in this model which is a reasonable value to represent a phytoplankton cell.

As introduced in chapter 2, 30 kV/cm field strength is generally used in electroporation processes. Consider there is no microorganism between the electrodes, for a treatment region $\boldsymbol{l_w}$=10 μm, to obtain a 30 kV/cm electric field between 25 μm gap (the thickness of cell membrane is negligible), it is assumed that a 75 V voltage should be applied to the electrode.

Based on the parameters of previous studies and literature introduced earlier, the parameters used in the linear model are listed in the **Table 3.2.1**.

Table 3.2.1 Parameters used in the linear model. Parameters are taken from publications listed.

Parameter	Value	
Applied voltage	75 V	
Relative permittivity of cytoplasm ε_1	80	[273] [274] [275] [300]

Relative permittivity of membrane ε_2	2 [273] [274]
Relative permittivity of surrounding liquid, ε_l	80 [274]
Conductivity of cytoplasm, σ_c	1.2 S/m [7] [307]
Conductivity of environmental liquid,σ_w	0.5×10^{-3}S/m [274] [275]
Thickness of membrane, l_m	5 nm [274] [275]
Diameter of cytoplasm, l_c	5 μm [274] [143] [144]
Treatment region, l_w	10 μm

3.2.1 Results and discussion

The calculation results of linear model is obtained with Excel software. **Figure (3.2.1.1)** shows the transient electric field strength in cell membrane of linear model. The electric field build up process of cell membrane is divided into three sections by two relaxation time $\tau_c = 0.6\,ns$ and $\tau_w = 1.42\,\mu s$. The calculation and discussion of relaxation time will be discussed in further paragraphs below.

In order to show three phases clearly, a different calculation with exaggerated test parameters inputted to the linear model was processed. **Figure (3.2.1.2)** is the transient electric field strength in cell membrane obtained from the linear model with non-realistic parameters: l_c=10 μm, l_m=5 μm, the thickness of cell membrane is set as 5 μm which is 3 orders of magnitude larger than the real parameter.

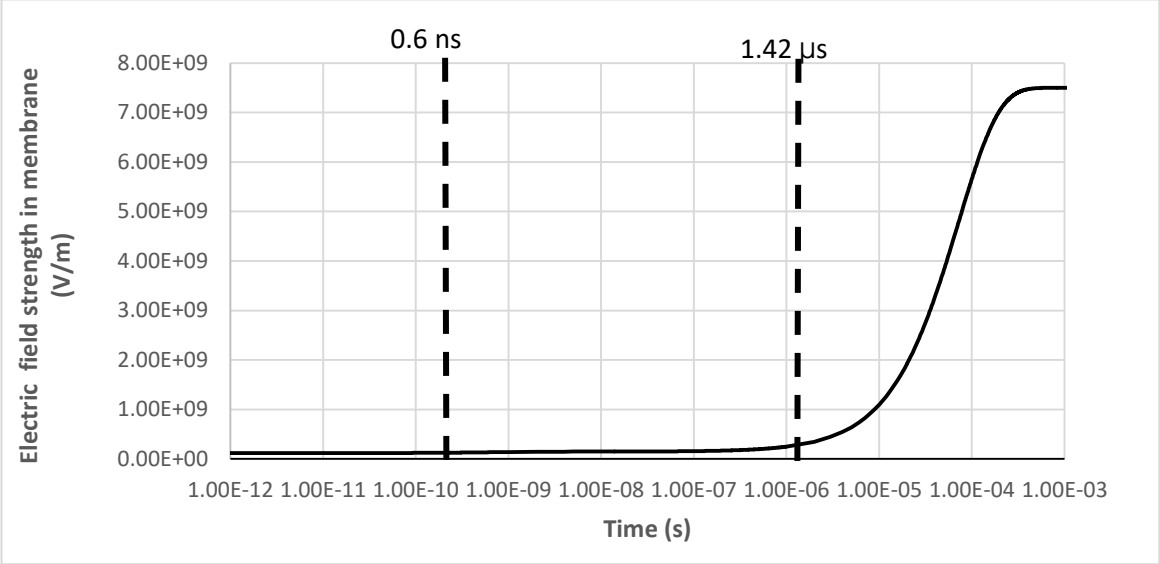

Figure (3.2.1.1) Transient response of Electric field strength in membrane of linear model with real size of microorganism (l_c=5 µm, l_m= 5 nm).

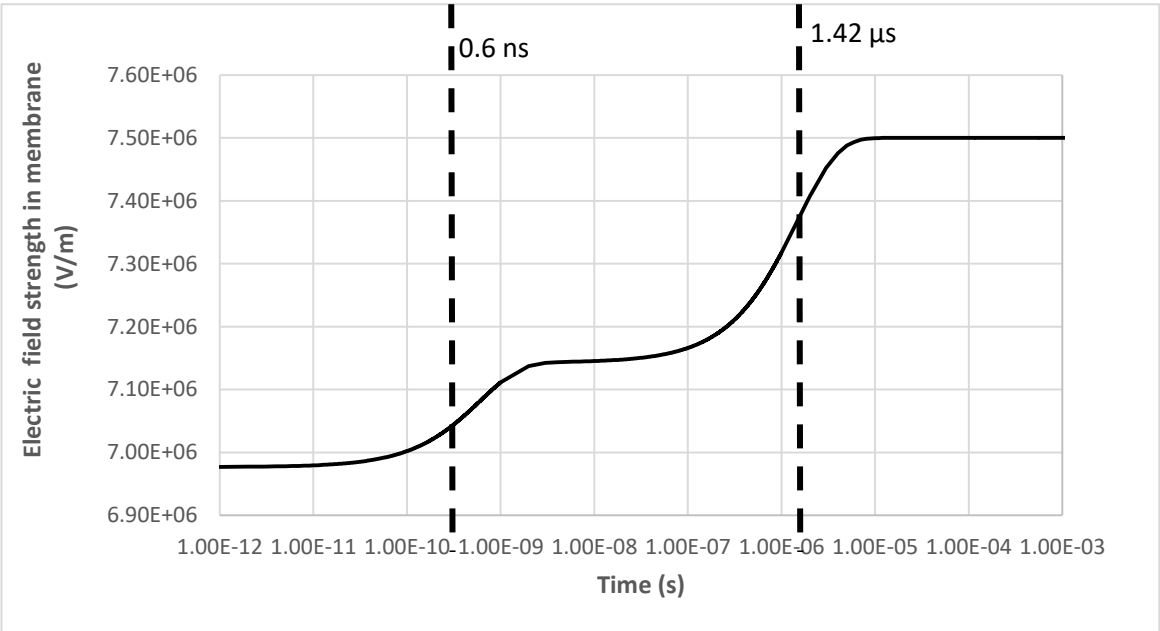

Figure (3.2.1.2) Transient response of Electric field strength in membrane of linear model with test parameters of microorganism (l_c=10 µm, l_m= 5 µm).

As can be seen from the figure, the electric field strength increase on membrane after the application of external voltage is a relative slow process. This increase is in a reasonable agreement with the result of the Pspice model mentioned in [273].

The development of electric field strength on the membrane is separately described in 3 distinct physical phases in [274].

In the first phase, the initial polarization process in the membrane after the application of voltage, is due to the dielectric characteristics of the cytoplasm and surrounding liquid, the electric field is mainly determined by the dielectric permittivity of such layers in this phase. The duration of this phase is defined by the characteristic time of highly conductive cytoplasm $\tau_c = \varepsilon_0 \varepsilon_c / \sigma_c$ which is 0.6 ns in this model.

In phase 2, free charges start to accumulate on both internal and external surfaces of membrane due to the electric field induced by the external voltage. In this phase, the characteristic time of cytoplasm and surrounding liquid mainly determines the duration of charge accumulation. As the conductivity of the environmental fluid is lower than cytoplasm, it takes a longer time to finish the charge accumulate than cytoplasm. Therefore the duration of this phase is governed by characteristic time of environmental liquid $\tau_w = \varepsilon_0 \varepsilon_l / \sigma_w$ which is 1.42 µs in this model.

In phase 3, free charges continue to accumulate on external and internal surface of the membrane and the electric field trends to reach the maximum steady state value which can be calculated from quasi-electrostatic approximation and Schwan equation, **Equation (3.23)**. As the charge accumulation has finished, there is no charge movement in both layers of membrane attached to cytoplasm or environmental fluid, the maximum field strength in this model can be calculated with equation: $E_{max} = u_0 / 2 l_m$, which is 7500 MV/m in this model, where u_0 is the external voltage and lm is the thickness of the membrane. The maximum electric field strength in the cell membrane is obtained as 7.5×10^9 V/m, as the membrane thickness is 5 nm, the voltage induced across the cell membrane is calculated as 3.75 V which is above the threshold of electroporation (1 V) as reported earlier.

3.2.2 Effects of cell properties on transient field across membrane

As discussed in the previous sections, the transient electric field strength in cell membrane with external electric field applied can be influenced by both electrical and physical parameters of bio-cells. This linear model would be helpful to investigate how these parameters influence the development of transient induced electric field in cell membrane.

3.2.2.1 Size of cells (Diameter of cytoplasm)

According to the literature in previous sections, the diameter of microorganisms varies ~0.2µm- 700 µm. In this section, several diameters of cytoplasm were selected to investigate the impact of cell dimension of the electric field.

Figure (3.2.2.1) below shows the effect of varying cell diameters on maximum field strength across cell membrane. It can be seen from the figure that for times beyond 10^{-8} s size of cytoplasm does not have significant influence on maximum field strength in the membrane. The different sizes of cytoplasm give the same field magnitude when the field build up process is finished. However, the size of cytoplasm have influence the field strength during the first phase. Biological cells with larger radii have a lower field strength during the initial phase compared with the cells with smaller radii. This result is different from a previous study which considered the maximum field strength across the membrane, and found that this field increases significantly as the diameter of the microbial cell increases [78].

In other researches discussed earlier [274] [78], a spherical single cell model was developed **Equation (3.2.30)** which gives the Electric field strength obtained with spherical single cell model using.

$$E_{\max}(t) = -A_m(t) + 2B_m(t) \cdot {R_1}^3 \quad \textbf{(3.2.30)}$$

Where R_1 is the radius of the cytoplasm, $A_m(t)$ and $B_m(t)$ are coefficients relating to radius of cytoplasm and the microbial cell [78].

Comparing **Equation (3.2.18)** obtained from linear model and **Equation (3.2.30)** obtained from other studies, it can be seen obviously that the radius of cytoplasm has a significant impact on the maximum electric field strength in the cell membrane. In some experimental studies, the results also show that microorganisms with larger cell size are more susceptible to the PEF treatment than the microorganisms with smaller size [192] [309].

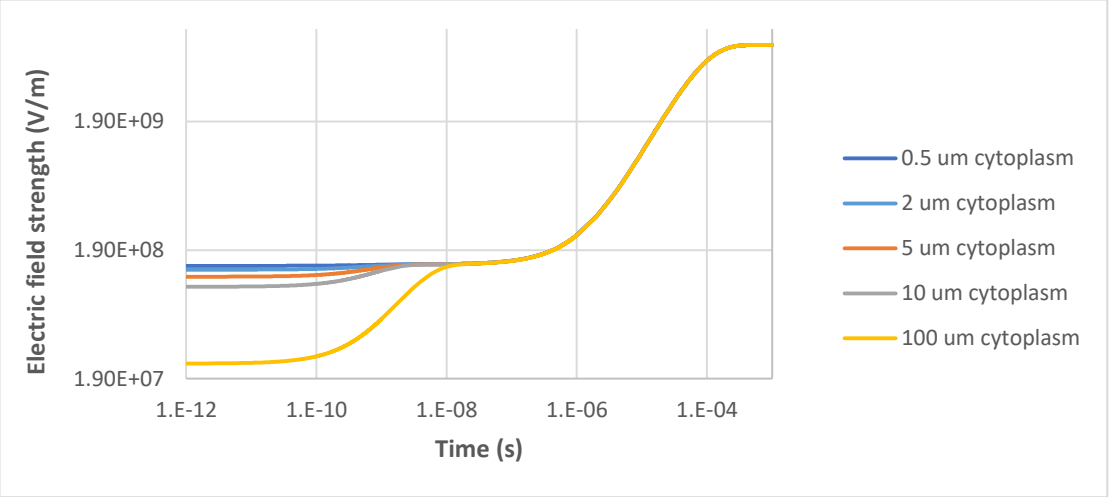

Figure (3.2.2.1) Transient electric field strength in cell membrane of linear model with different size of cytoplasm, l_c.

The results of the linear model also show that the size of cytoplasm mainly influences the phase 1 (polarization process) and phase 2 (charge accumulation process). In the linear model the size of cytoplasm firstly influences the initial induced transmembrane electric field strength due to dielectric properties but it does not significantly affects the polarization process (phase 1) because the dielectric property is govern by the materials, they have the same values of conductivity and permittivity. The cell with larger cytoplasm takes a longer time to finish phase 2 (the charge accumulation process) due to the longer travel path of charges.

In PEF treatment with pulse duration less than 1 μs, the size of microorganisms can have effects on the transient electric field strength in cell membrane. However, the linear model is not accurate enough to describe stages after dielectric polarization phases and charge accumulation phases compared with Si Qin's results in [296] where it shows higher electric field strength would be generated in cell membrane with larger microorganism. This could be one of the limitations of using the linear model to investigate the electric field strength in cell membrane during PEF treatment with different kind of microorganisms.

3.2.2.2 Membrane thickness

Figures (3.2.2.2) below show the effects of varying membrane thickness on the development of field strength build up process across cell membrane. It is obvious that, by changing the membrane thickness, there is no notable difference observed during phase 1 and phase 2. The differences occur in phase 3 which is when charge continues to accumulate on outer membrane when the charge accumulation on inner cell membrane has been finished. Because the cell membrane thickness does not influence the polarization process and charge accumulation in inner cell membrane so there is no significant difference observed during phase 1 and phase 2. In phase 3, a thinner cell membrane means higher electric field strength can be induced in the cell membrane when the charge accumulation is finished.

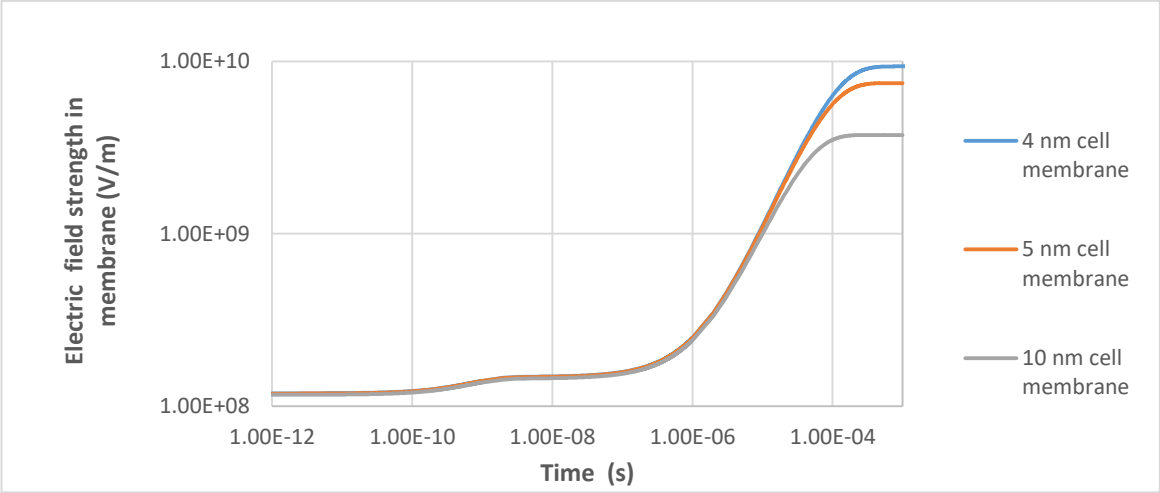

Figure (3.2.2.2) Transient electric field strength in cell membrane of linear model with different membrane thickness, l_m.

It can be obtained from the **Figure (3.2.2.3)**, that as the thickness of membrane drops the maximum electric field strength across the membrane increases. These results are in agreement with those presented by other studies [78]. However, as the value of the membrane thickness does not vary significantly for different kind of microorganisms, they are all in the range of 4-10 nm, as introduced before, the values of maximum electric field strength in cell membrane remains in the same order. The results obtained in this simulation suggested that the membrane thickness does not affect the transient value of electric field across the cell membrane significantly. Comparing these results with those obtained from **Figure (3.2.2.1)**, it can be verified that the changes in the first phase of field development

are due purely to changes in the size of the cytoplasm.

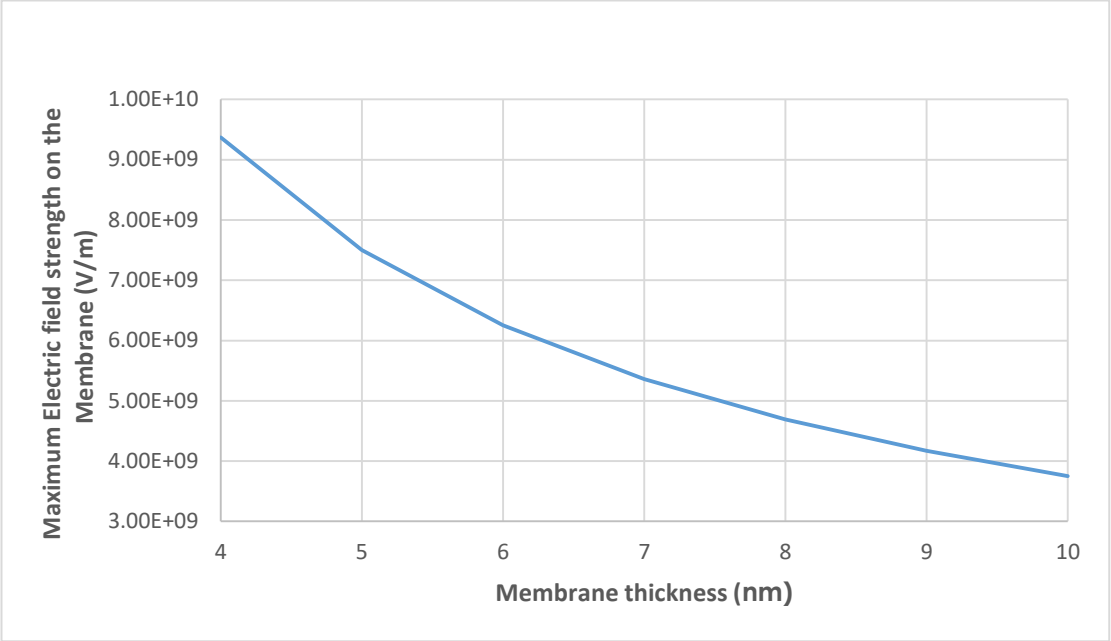

Figure (3.2.2.3) Transient electric field strength in cell membrane of linear model with different membrane thickness, l_m.

3.2.2.3 Electrical conductivity of cytoplasm

Figure (3.2.2.4) below shows the results of varying conductivity of cytoplasm over a range of values. It can be seen from the result that the conductivity of cytoplasm does not have significant impact on the maximum field strength across membrane. However, it has a minimal influence on the first stage of field strength build up in the membrane. This result is similar to previous model with dielectric electrodes [78]. As discussed in previous section, the first phase is mainly governed by the dielectric characters of cell structure, especially by highly conducting cytoplasm. The cytoplasm conductivity affects the polarization process significantly (within 1 ns). However, the maximum field strength across membrane is not influenced in later stages as the charge accumulation process in phases 2 and 3 are mainly governed by the electrical properties of membrane and surrounding liquid. Therefore, considering the electroporation process based on the calculation results of linear

model, the conductivity of cytoplasm does not insignificantly affect the transient electric field strength in cell membrane during PEF treatment. A similar result was also obtained by Si Qin with the spherical single cell model [78].

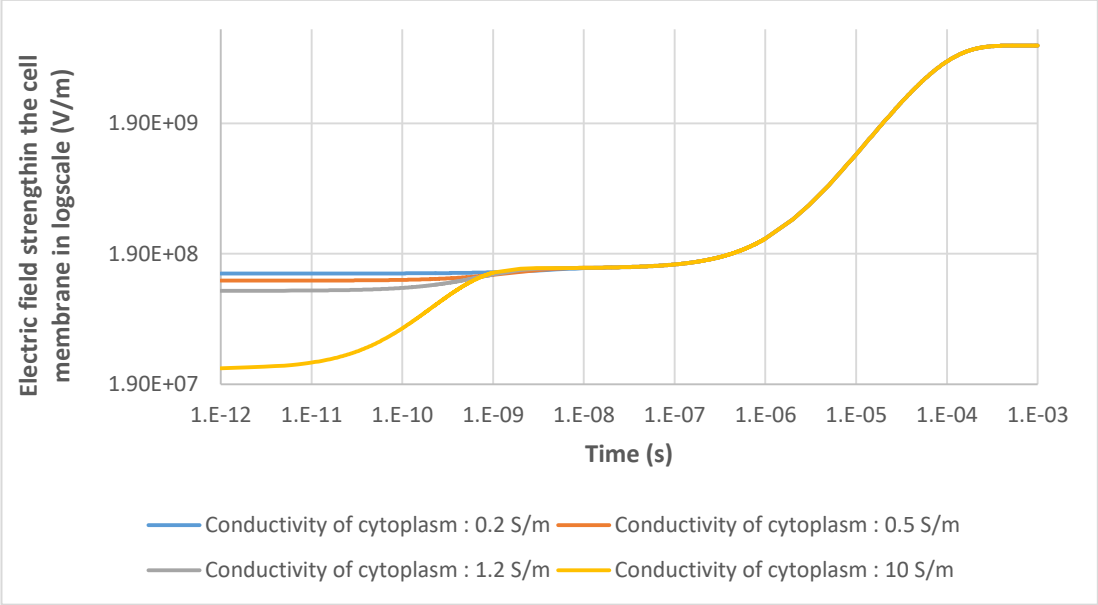

Figure (3.2.2.4) Transient electric field strength in cell membrane of linear model with different conductivity of cytoplasm, σ_c.

3.2.2.4 Relative permittivity of membrane

Figure (3.2.2.5) below shows the result of varying the relative permittivity of membrane which are close to generally used value in modelling of PEF treatment on microorganisms introduced earlier. It can be seen from the result that the maximum electric field strength across membrane is not influenced by the relative permittivity of the membrane, which is different from SiQin's model with dielectric electrodes [78]. In his model, the maximum field strength in the cell membrane reduces as the relative permittivity of membrane increases. Lower permittivity of cell membrane results in a slightly faster Maxwell-Wagner field relaxation time. However, in this linear model, as there is no dielectric electrode included, there would be no Maxwell-Wagner field relaxation process in the treatment region. (The electric field strength between electrodes would not drop).

It can be obtained from **Figure (3.2.2.5)** that the relative permittivity of membrane has a slightly impact on the field strength build up process across a membrane. A membrane with higher relative permittivity takes a longer time to reach the maximum electric field strength, this result follows the spherical model with dielectric electrodes [78]. However, as the permittivity of cell membrane cannot be controlled during PEF treatment applications and the values do vary significantly between different kinds of microorganisms, during general PEF treatment applications, the effects caused by the permittivity of the cell membrane can be ignored.

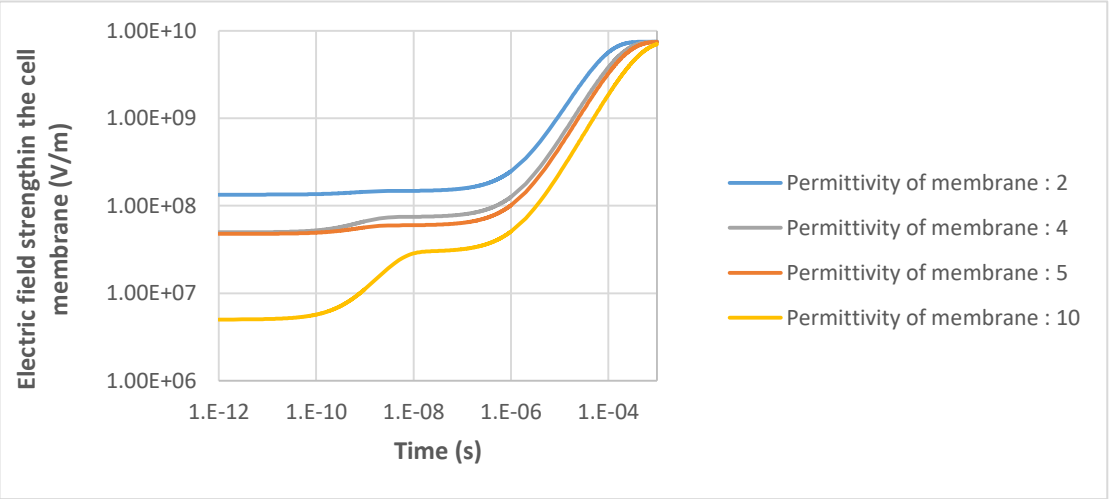

Figure (3.2.2.5) Transient electric field strength in cell membrane of linear model with different relative permittivity of cell membrane, ε_2.

3.2.2.5 Conductivity of environmental fluid

The analysis conducted in the previous section reveals how different electrical and physical parameters of microorganism influence the electric field build up process across its membrane. However, these parameters are determined by a microorganism's natural properties and they are beyond external control in practical PEF treatment. Therefore, the investigation of controllable parameters during PEF treatment is necessary to provide information and optimize the process

of PEF treatment. Conductivity of environmental fluid is a relative controllable parameter.

Figure (3.2.2.6) below shows the result of varying the suspension fluid conductivities. It can be seen from the results, the conductivity of environmental fluid has significant influence on the build-up of electric field across a bio-membrane. Models with higher conductivity of fluid takes shorter time to reach the maximum field strength compared with lower conductive fluid. However, the maximum field strength across the membrane is not influenced by the conductivity of environmental fluid. The electric field of lowest conductive liquid is still increasing when the higher conductive liquid has reached the peak value. With higher conductivity situation, the result is also different from previous study with dielectric electrodes. In previous study, with higher conductivity, the field strength across the membrane drops significantly due to Maxwell-Wagner field relaxation process which is not being observed in this model [78]. The differences between these two models should be investigated and will provide more information about PEF treatment equipment design.

The conductivity of environmental fluid mainly influences the charge accumulation process (phase 2 and phase 3). It can be observed that with higher conductivity, it takes shorter time for the electric field strength in the membrane to reach the steady state value. With commonly used conductivity of environmental fluid (0.15 S/m), the electric field strength can reach up to the steady state value at around 1 µs. 1µs impulse duration was also commonly used in electroporation applications.

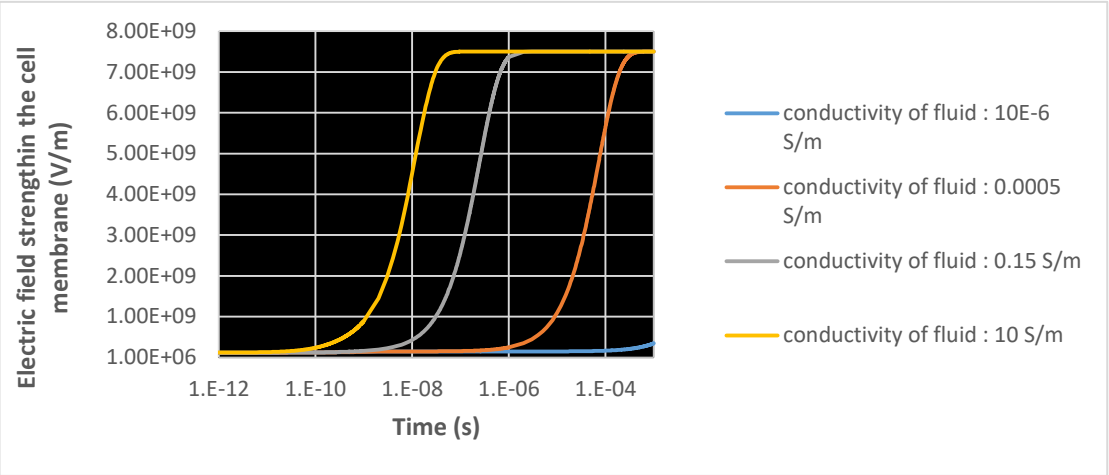

Figure (3.2.2.6) Transient electric field strength in cell membrane of linear model with different conductivity of environmental fluid (treatment region), σ_w.

3.3 Discussion

This chapter developed an initial linear model with cell membrane and cytoplasm of a single cell expressed by an external electric field strength. This analytical model was conducted using Excel in order to investigate the transient response of the induced electric field strength in the cell membrane during PEF treatment. The test cell of this linear model is conductive PEF treatment test cell. The cell membrane is represented by simple layers in this model which is considered as no conductive.

Additional analysis has also been conducted to investigate the effect of different electrical and physical properties of the microbial cell on the dynamic of transient membrane electric field. The results obtained with this model suggest that the membrane thickness has a significant impact on the maximum electric field strength in cell membrane. Other parameters such as size of the cell, electrical conductivity of environmental fluid, conductivity of cytoplasm and relative permittivity of cell membrane have less significant influence on the electric field strength in cell membrane during PEF treatment.

The results obtained from the linear model suggested that the size of cell (diameter of cytoplasm) does not have significant influence on the transient electric field

strength in the membrane during PEF treatment which is different from other studies, e.g. [78]. The previous study was developed with a spherical cell model which is different from linear model. The radius of the microorganism has significant effects on the results of the equations, which can be seen from **Equation (3.2.30).** This can be considered as a limitation of the linear model. In order to have more accurate and detailed investigation about electrical properties or further information during PEF treatment, a more advanced model is necessary.

This linear model simulates a single cell of microalgae with realistic size and parameters which is exposed to an applied 30 kV/cm electric field strength. The obtained results of transient electric field strength build up process follows other studies with different kind of models (spherical model) which support the feasibility of optimization of PEF treatment with it. However, the linear model does not take into account the size or geometry of microorganism which is a limitation during some detailed investigations. Secondly, the linear model can only calculate the transient electric field strength in cell membrane, the electric field distribution in cytoplasm and environmental fluid cannot be investigated. Thirdly, during the charge accumulating process, the thermal effects could have interactions between bio-cells or environmental fluid which is generally not taken into account during the study of PEF treatment. It would be beneficial to investigate the thermal effects during PEF treatment. Moreover, different kind of applied signals (the step impulse or oscillating signals) are hard to investigation with the linear model. So a more advanced model is necessary to overcome these problems and provide more detailed information about interactions between electric field and microorganisms during PEF treatment. The second model in this work, which is built up with Quickfield, will be introduced in Chapter 4.

Chapter 4. QuickField 2D axial symmetry model of microorganisms

The linear model of a microbiological cell developed in Chapter 3 enables analysis of the transient electric field in the cell membrane during the PEF treatment. However, this model has several limitations, one of them is: the linear model cannot provide detailed information about electric field distribution in the cytoplasm and environmental fluid during the PEF treatment. Detailed information on the electric field in the cytoplasm is important as the cytoplasm contains several cell organelles which have their own membrane structures. Thus, the electric field developed in the cytoplasm during the PEF treatment might have an effect on these cell organelles. The second limitation of the linear model is: that although this model does not include the cell nucleus it is known that the nano-second PEF treatment provides significant effect on the intra-cellular structures [123] [124] [125]. The third important limitation of the linear model is as follows: the thermal effects during the PFE treatment are not taken into account. However, the results obtained using the linear model show that there are conduction processes in the liquid media which are generated by the externally applied field and which may lead to local heating effects across the bio-membranes.

There are complex interactions between the microorganism and the electric field during PEF treatment, which include the appearance of electro-mechanical forces acting across solid-liquid interfaces, i.e. membranes, local intensive joule heating, and resulting thermal forces. The linear model is not capable of taking into account all of these effects, therefore a more advanced model was developed, to allow these local thermal and electro-mechanical effects and forces across biological membranes to be taken into account.

In the present Chapter, QuickField electrostatic software is used to develop a single cell model using 2D axisymmetric geometry, this model includes a cell nucleus.

4.1 Single cell model with cell nucleus

Considering the same type of microorganism as was used in the linear model, it was decided to develop a 2D model of a single microalgae cell. The parameters of environmental fluid and cytoplasm were identical to the parameters used in the linear model. Although the membrane is considered as a non-conductive layer, in the QuickField model, the membrane conductivity requires to be set to a small value of 10^{-13} S/m to enable operation of this software. This parameter value was also used in the previously published paper in which a COMSOL model was used [310]. The nuclear membrane has a structure similar to that of the cell membrane, both membranes have lipid bilayers and they are permeable to select ions, proteins and organic molecules [311].

Figure (4.1) shows the diagram of this single cell model. The parameters of the single cell model are listed in **Table 4.1**. The mesh show that, details information in the domain of cell membrane was investigated.

In the present model the conductivity of the nuclear membrane is set to the same value as the conductivity of the cell membrane. The same assumption was also made in study [7]. According to the literature, the size of cell nucleus is generally in the range 5- 20 µm [312] and the smallest cell nucleus was found as ~ 1 µm in Yeast. In this model, the cell nucleus was simplified as a spherical shape with conductive liquid inside and almost non-conductive nuclear membrane, the size of cell nucleus was set as 1 µm. In general, the thickness of nuclear membrane is greater than the thickness of cell membrane [313] [314]. In the present model the thickness of nuclear membrane is set to 10 nm, this value was also used in [315]. The conductivity of the cell nucleus was set to be the same as the conductivity of cytoplasm, this assumption was also made in [7] [316].

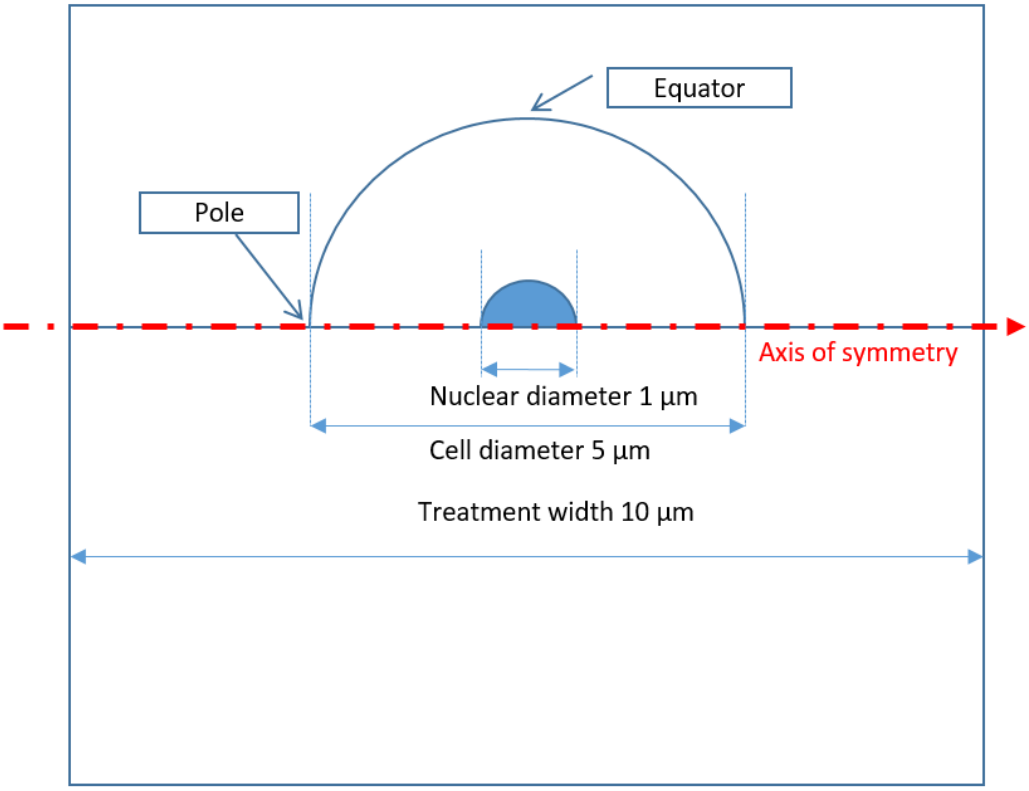

(a)

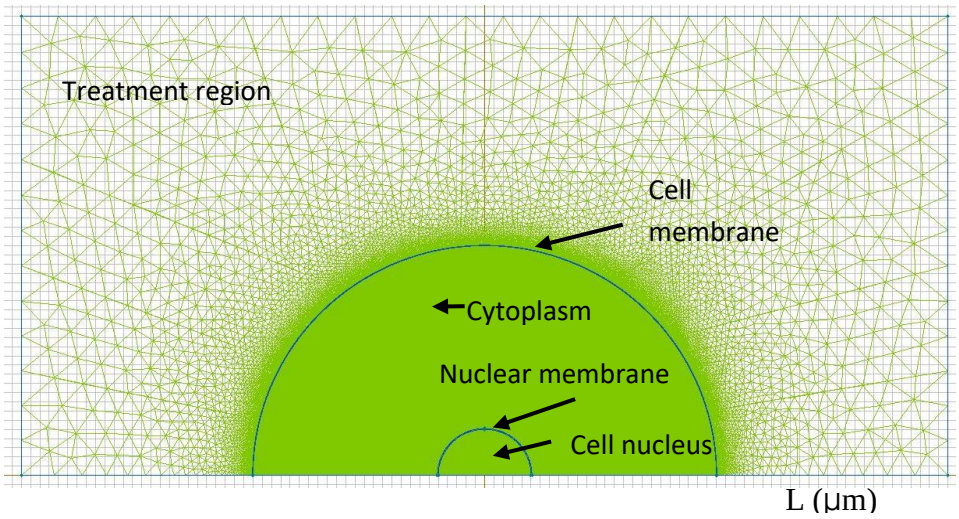

(b)

Figure (4.1) 2D model of a single algae cell: cell dimensions (a), QuickField model used for analysis of the electric field (b).

The test chamber was modelled as two parallel electrodes, with a gap of 10 µm filled with the environmental liquid, the applied voltage was 0.03 kV so the field strength of 30 kV/cm was generated in the environmental fluid (in the treatment region). This field strength is a typical electroporation field strength which was also used in the linear model.

Table 4.1 Parameters used in the 2D single cell model. Numerical values are taken from the published literature.

Parameters	**Value**
External voltage	0.03 kV
Width of treatment region	10 µm
Thickness of cell membrane	5 nm [274] [275]
Diameter of cytoplasm	5 µm [274] [143] [144]
Relative permittivity of cytoplasm	80 [274] [273]
Relative permittivity of membrane	2 [274] [273]
Relative permittivity of surrounding liquid	80 [274] [273]
Conductivity of cytoplasm	1.2 S/m [7] [307]
Conductivity of cell membrane	10^{-13} S/m [310]
Conductivity of environmental fluid	0.5×10^{-3} S/m [274] [275]
Diameter of cell nucleus	1 µm [7] [316]
Thickness of nucleus membrane	10 nm [7] [316]
Relative permittivity of cell nucleus	80 [315] [274]
Relative permittivity of nucleus membrane	2 [274] [315] [273]
Conductivity of nucleus	1.2 S/m [7] [307]
Conductivity of nucleus membrane	10^{-13} S/m [274] [275]

4.2 Steady state DC conduction results

In order to investigate the thermal effects during PEF treatment, a DC conduction approximation was used. In this steady state DC conduction analysis, only the electrical conductivity is taken into account, allowing the electric field and current density distributions to be obtained.

4.2.1 Electric potential and electric field distribution

Figure (4.2.1) shows the distribution of electric potential under steady state DC conduction conditions. It was shown that there is a potential difference between the environmental fluid and cytoplasm, also there is a potential difference between the cell nucleus and cytoplasm. However, the potential difference between the cytoplasm and cell nucleus does not change across the surface of the cell nucleus. As with the linear model, when the charge accumulation process inside the cell is completed, the charges on both side of the nucleus membrane remain steady, so the transmembrane potential across the nucleus membrane tends to be a constant value. Electric field could be generated in the nucleus membrane. The detailed representation of the potential distribution in this model is shown in **Figure (4.2.1)**.

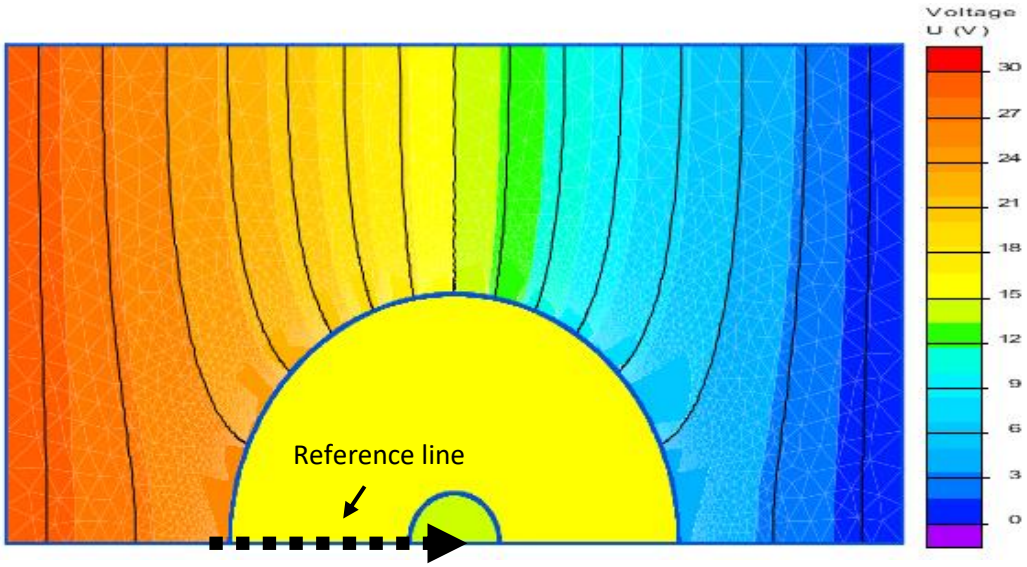

Figure (4.2.1) Electric potential distribution in the bio-cell model in the steady state dc conduction analysis, the reference line shows the path across which the transmembrane potential is obtained.

Figure (4.2.2) shows the transmembrane potential along the reference line in **Figure (4.2.1).** There are well pronounced potential differences across the cell membrane and nuclear membrane. According to the results, the transmembrane potential difference on the pole is ~ 10 V in this model, which is of the same order of magnitude as the value obtained by the Schwan Equation, 22.5 V . The maximum electric field strength in this model is $\sim 2 \times 10^9\ V/m$, which is also of the same order of magnitude as the results obtained using the linear model ($\sim 7.5 \times 10^9\ V/m$). As such, the transmembrane potential has reached the threshold of the electroporation process (~1 V). The transmembrane potential across the nuclear membrane is $\sim 0.2\ V$, which is not large enough to cause electroporation.

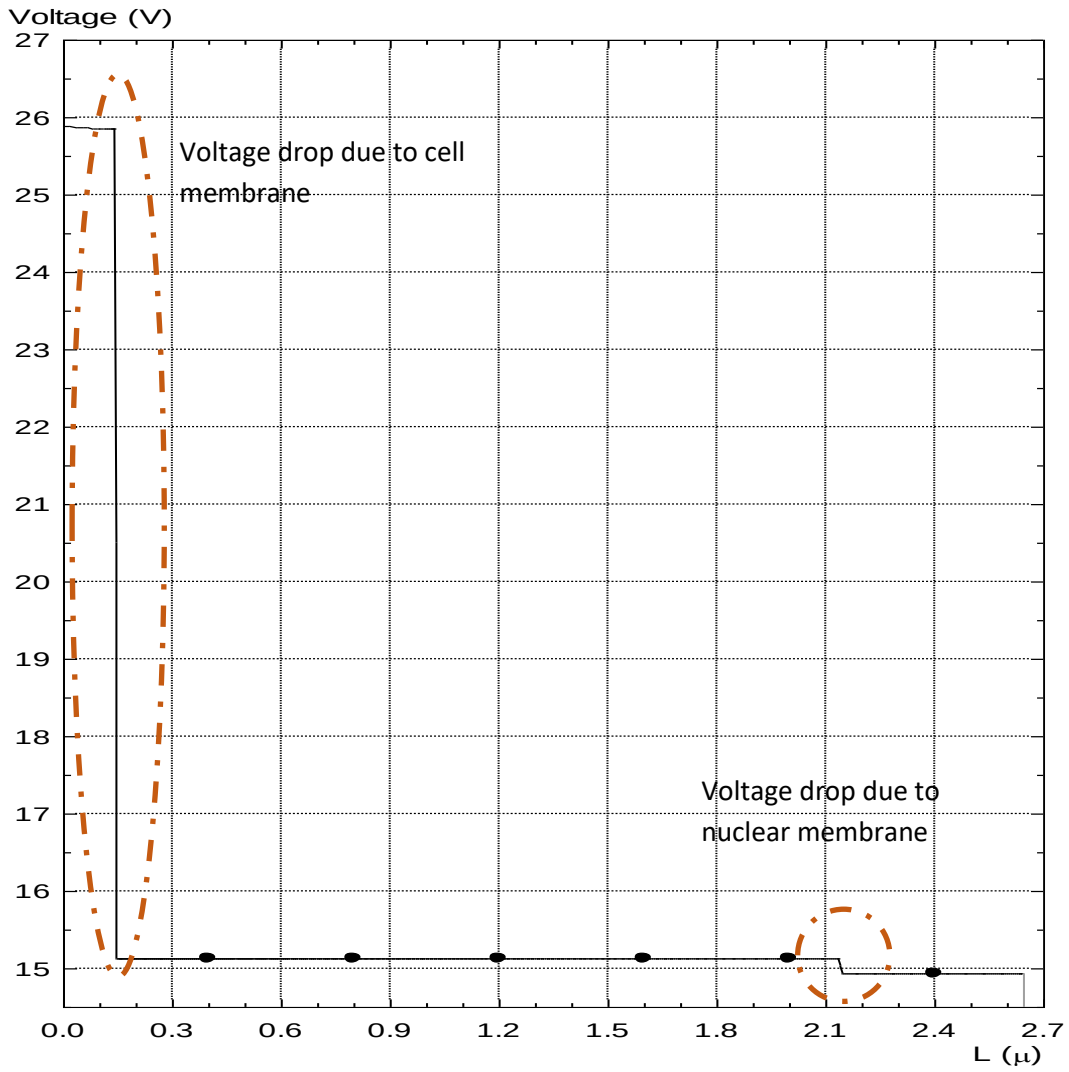

Figure (4.2.2) Potential differences along the reference line shown in **Figure (4.2.1)**. The voltage drops across the cell and nuclear membranes are circled.

Figure (4.2.3) shows the electric field distribution in the case of the steady state DC simulation. The graph shows the electric field distribution in the cell membrane, which is similar to the Schwan Equation, with its minimum value on the equator and its maximum value on the pole, **Figure (4.2.3.1)**.

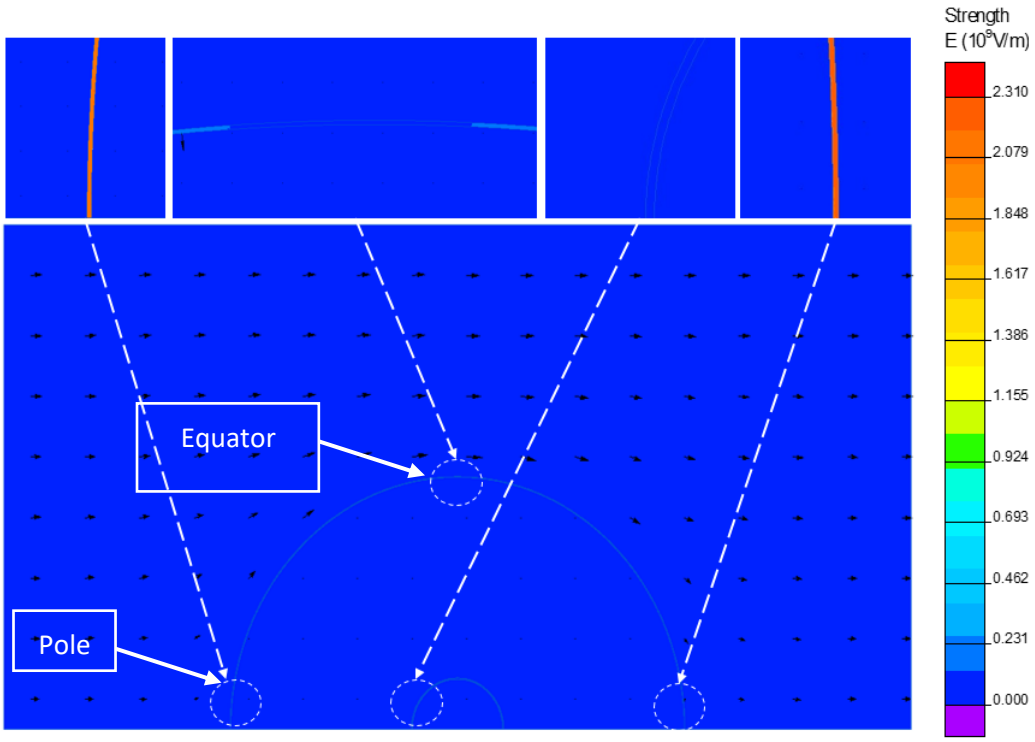

Figure (4.2.3) Electric field distribution in the steady state DC conduction case. Zoomed in views are included to show the relationship between the electric field strength and position. The main domain was shown as uniform dark blue due to the low electric field strength in environmental fluid and cytoplasm compared with large field strength in cell membranes.

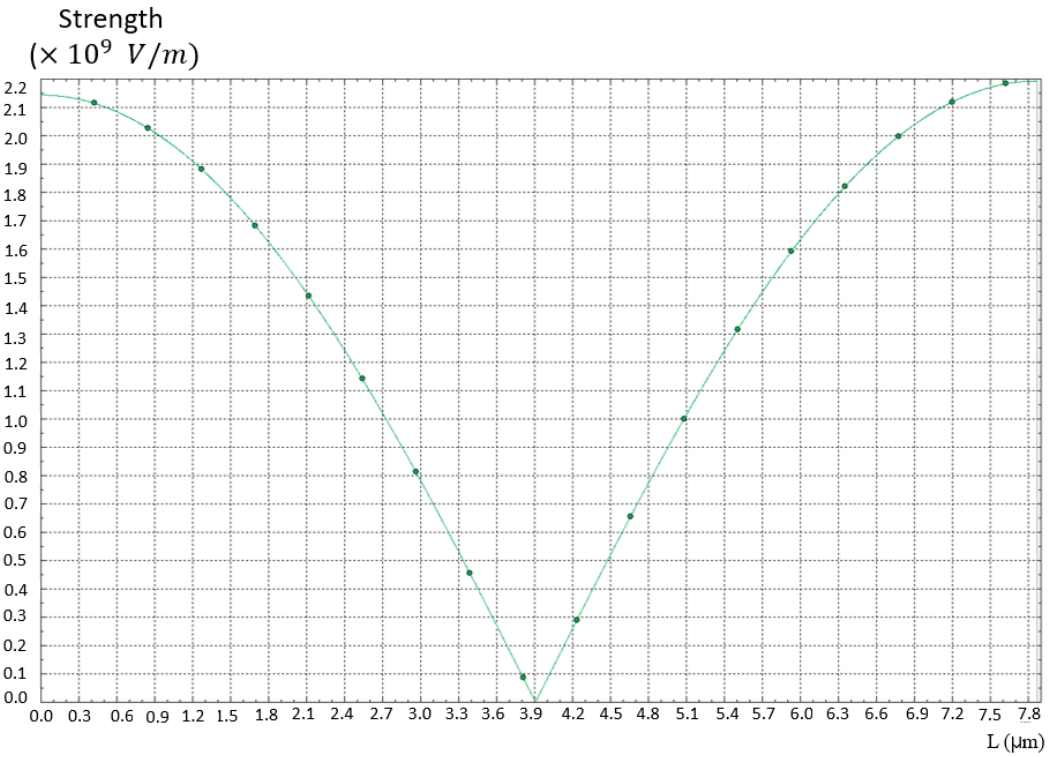

Figure (4.2.3.1) Electric field strength across the cell membrane, L represents the point moving around the circumference of the cell membrane from pole to pole with membrane thickness taken into account $(\frac{1}{2}\pi d \approx 7.8\ \mu m)$.

According to the results, the maximum electric field strength is $\sim 2.3 \times 10^9\ V/m$, which could be calculated through **Figure (4.2.2)**. The electric field strength in the cell nucleus and cytoplasm is negligible in this situation, **Figure (4.2.3.2)**.

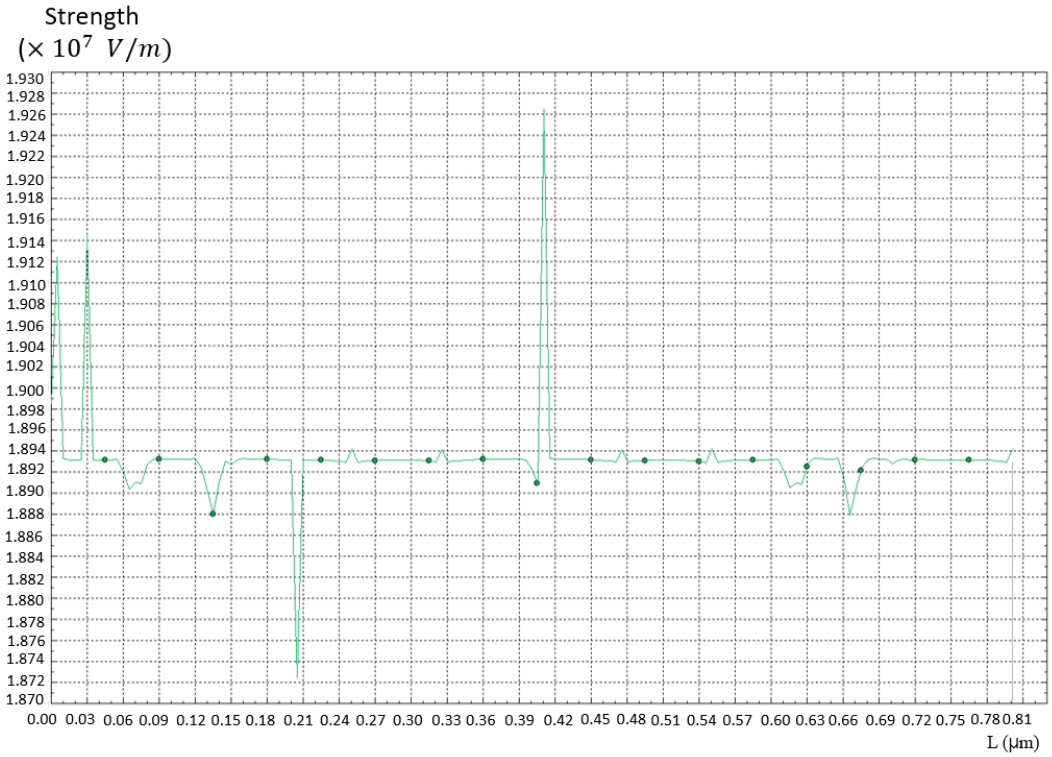

Figure (4.2.3.2) Electric field strength across the nucleus membrane. L represents the point moving around the circumference of the cell nucleus from pole to pole. The peaks were caused by calculation errors of software which cannot be solved in this model, thus there is no significant differences observed.

In the steady state analysis, the charge accumulation process inside the cell is completed, thus there would be no significant charge movement in the cytoplasm and nuclear fluid. Due to the extremely low conductivity of the cell membrane and nuclear membrane, the electric potential in the cytoplasm and nucleus is relatively stable and there is no significant voltage drop inside the cell. So, the electric field inside the cells is constant, the electric field in the nuclear membrane is uniformly distributed as shown in **Figure (4.2.3.2)**.

4.2.2 Current density and power

Figure (4.2.4) shows the current density distribution in the steady state DC conditions. It was found that the maximum current density is generated outside the membrane in the environmental fluid and its value is$\sim 2 \times 10^3\ \mathrm{A}/m^2$. Due to the joule heating caused by such a current density, there might be a 'hot spot' positioned in this area. Although the current density in the cytoplasm and cell nucleus follows the same tendency: the maximum value is outside the membrane on the equator (the poles are the positions close to electrodes), **Figure (4.2.5)**, however, the values of the current density are negligibly low: $\sim 3 \times 10^{-4}\ \mathrm{A}/m^2$ in the cytoplasm and $\sim 3 \times 10^{-6}\ \mathrm{A}/m^2$ in the nucleus.

As 'hot spots' in the environmental fluid exist during the PEF treatment, therefore, these local thermal effects may contribute to the electroporation process, causing potential structural changes which may accelerate damage (electroporation) of cell membranes.

Joule heating is the main source of such local heating; as shown in **Figure (4.2.6)** the maximum value of power released in the hot spot is $9.8 \times 10^9\ W/m^3$. This value is too high to be ignored, and detailed investigation should be conducted to understand the local heating effects.

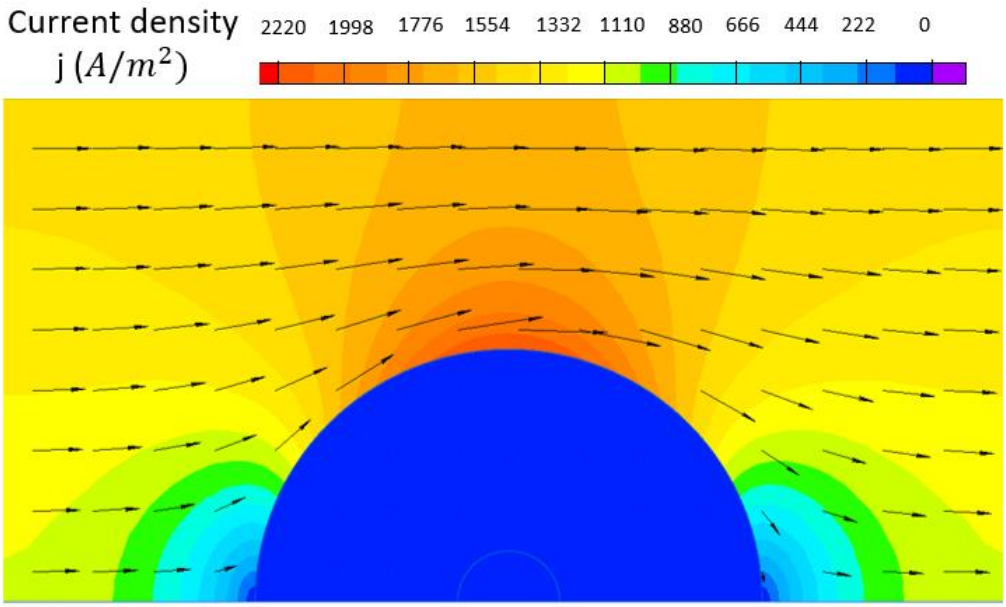

Figure (4.2.4) Current density distribution in the steady state condition.

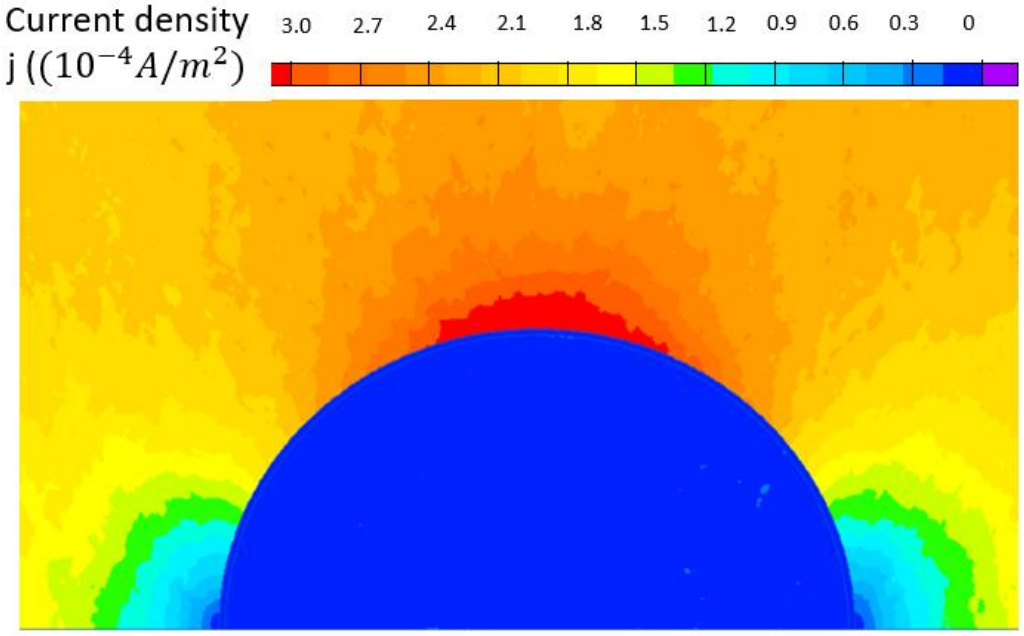

Figure (4.2.5) Current density distribution in the steady state condition in the cell nucleus (graph obtained through zooming in a section of **Figure (4.2.4)** and changing the factor in the legend of cell nucleus from).

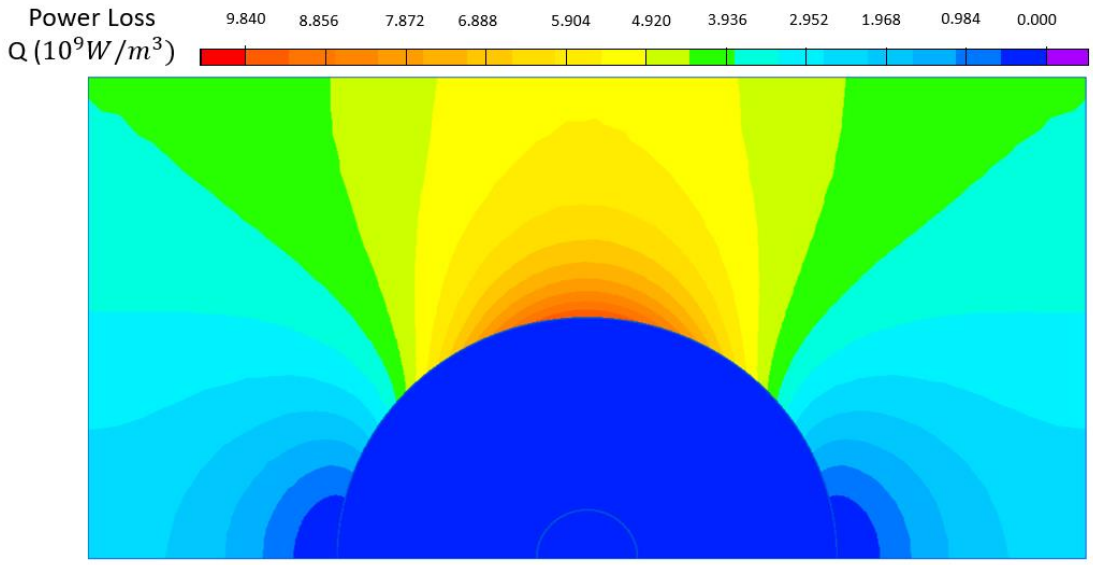

Figure (4.2.6) Power dissipation due to the conduction current in the steady state DC conduction case, single cell model.

4.2.3 Local heating effects

In order to investigate the thermal effects during this field stimulation process (PEF treatment), the transient heat transfer model can be used which is linked to the DC conduction model in QuickField software. **Table (4.2)** below introduces the thermal parameters used in this combined heat and conduction analysis.

Table 4.2 Thermal parameters, values taken from publications shown.

Parameters	Environmental fluid	Cell membrane	Cytoplasm	Nuclear membrane	Nuclear
Heat capacity at constant pressure [J/(kg·K)]	4181.3 [310] [317]	3000 [317]	4181.3 [310] [317]	3000 [317]	4181.3 [310] [317]
Thermal conductivity [W/(m·K)]	0.61 [122] [310]	0.568 [122] [310]	0.61 [122] [310]	0.568 [122] [310]	0.61 [122] [310]
Density [kg/m^3]	998.2 [310]	1100 [310]	998.2 [310]	1100 [310]	998.2 [310]

Figure (4.2.7) shows an increase in temperature due to the local heating effect discussed in **section 4.2.2**. It is shown that at the typical electroporation electric field strength (30 kV/cm), there is almost no global temperature increase in the environmental fluid however, it shows 'hot spot' in the environmental fluid. As the local heating mainly takes place in the environmental fluid, the external electric field strength and conductivity of the fluid might have significant influence on these local effects. **Figure (4.2.8)** shows the local heating effects at higher electric field strength (60 kV/cm) and higher conductivity (0.6 S/m) of the fluid – these parameters were used in [273].

Figure (4.2.8) shows that the temperature of the 'hot spot' in the environmental fluid increases by ~7 ℃ in 1 µs. The temperature increase (ΔT) in the cytoplasm and

nucleus is less than <1 ℃ and can be neglected. Typically, the local heating effects are not considered in the PEF studies because there is no significant increase in the bulk temperature of the environmental fluid (the PEF treatment is considered as a "non-thermal" process).

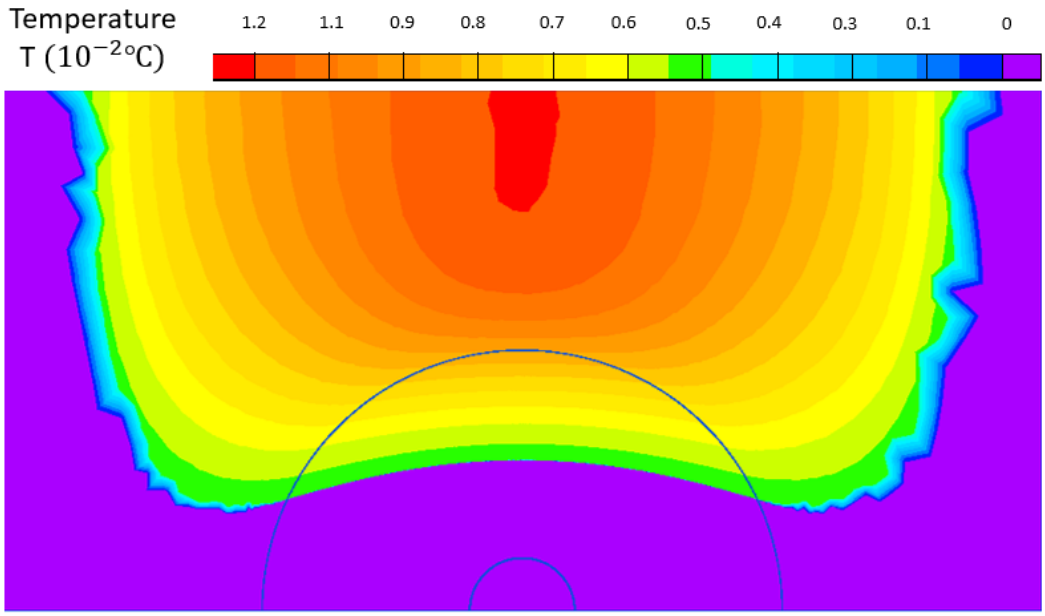

Figure (4.2.7) Transient temperature increase distribution (ΔT) in 10 μs; electric field strength is 30 kV/cm.

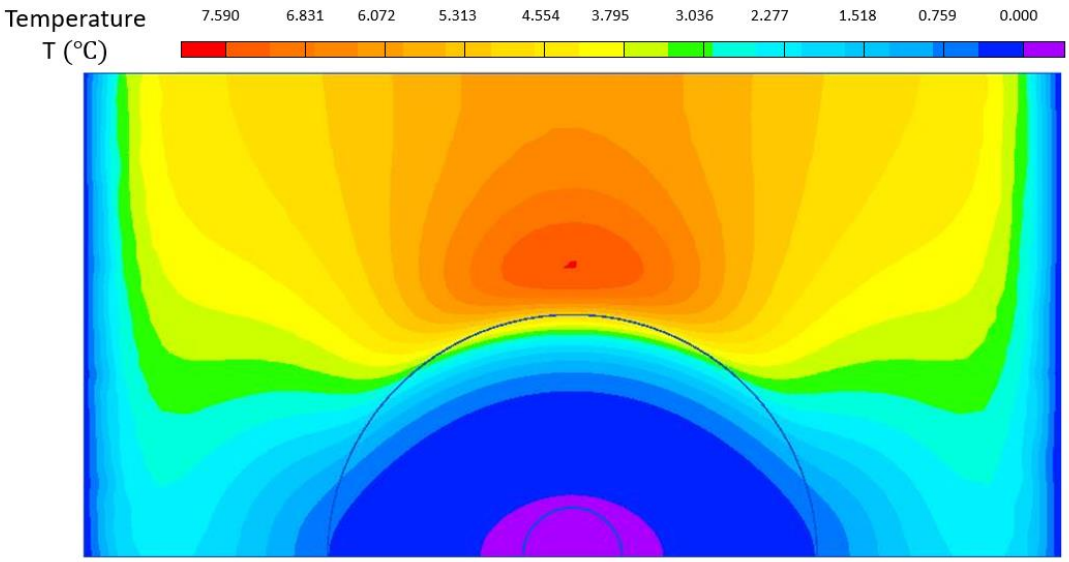

Figure (4.2.8) Transient temperature increase distribution (ΔT) in 1 μs; electric field strength is 60 kV/cm and conductivity of fluid is 0.5 S/m.

Figure (4.2.6) shows power loss is generated next to cell membrane but in **Figure (4.2.7)**, the high temperature is not at the same place, this could be caused by the coupling of thermal analysis and electrical analysis during computing by the software. Furthermore, the transient thermal effects in the case of higher electric field strength and higher conductivity of the fluid may be sufficient to cause potential damage to the cell membrane or could help to accelerate the pore formation in the membrane.

4.3 Transient QuickField analysis - single cell model

The steady state DC conduction simulation can be used to investigate the electric field and thermal effects in the steady state phase (after completion of the charge accumulation process discussed in chapter 3). However, the steady state simulation cannot be used to investigate the transient effects during the PEF process before

the field reaches its steady state phase (during the charge accumulation phase). This phase is considered to be completed within 1.42 μs for the model and parameters presented here (chapter 3). The electric field distribution and thermal effects during this phase are not well understood and required further investigation. The transient analysis (nano-second simulations) is used in this section to investigate the electric field distribution and thermal effects in the single cell model using the field strength of 30 kV/cm. It was shown in [7] that the ns PEF treatment could cause the electroporation effect and induce tensile stresses across the nucleus membrane, destroying the subcellular structures. A transient analysis could be used to investigate the field and temperature inside the cells (in its cytoplasm and cell nucleus) during the PEF treatment. In this section, the transient analysis is used, both permittivity and electrical conductivity will be included in the simulations.

4.3.1 Electric potential and electric field strength distribution

Figure (4.3.1) shows the electrical potential distribution at 1 ns in the single cell model with cell nucleus. Compared with **Figure (3.3.1)**, there are potential differences in cytoplasm and cell nucleus between regions, which is different from the steady state DC conduction results. Because the charge accumulation process inside the cell is still not completed at 1 ns, the charge distribution inside the cell did not reach its steady state.

Figure (4.3.2) shows the transmembrane potential along the reference line in **Figure (4.3.1)**. There are two significant potential drops across the cell and nuclear membranes. It was found that, in this model, the transmembrane potential difference across the cell membrane is $\sim 1.05\ \mathrm{V}$, and the maximum electric field strength is $\sim 2.1 \times 10^{8}\ \mathrm{V/m}$. This value has the same order of magnitude as the results obtained from the linear model (Chapter 3), $\sim 1.35 \times 10^{8}\ \mathrm{V/m}$, **Figure**

(3.2.1.1). Such field strength leads to a potential drop which is close to the critical value for the electroporation process ($\sim 1\ \mathrm{V}$). The transmembrane potential across the nuclear membrane is also $\sim 1\ \mathrm{V}$, which is higher than the transmembrane potential across the nuclear membrane obtained in the case of the steady state DC conduction ($0.2\ \mathrm{V}$, Figure **(4.2.2)**). This result is similar to the value of the nuclear membrane potential developed during the nano-second PEF treatment [7], which could damage the cell nucleus.

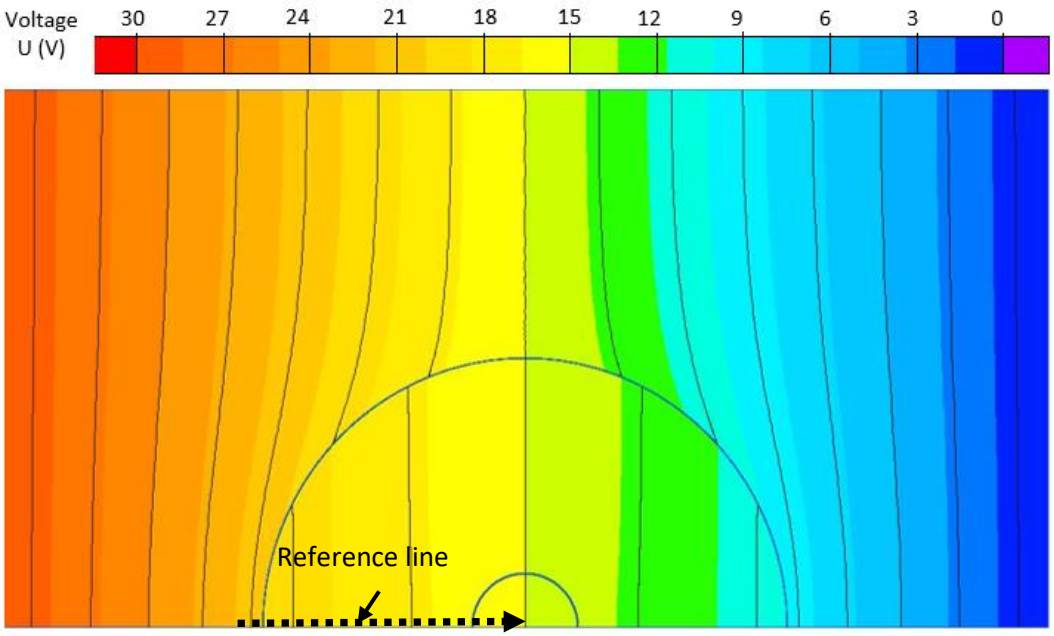

Figure (4.3.1) transient model: Electric potential distribution, the reference line is included to show the path across which the transmembrane potential is obtained.

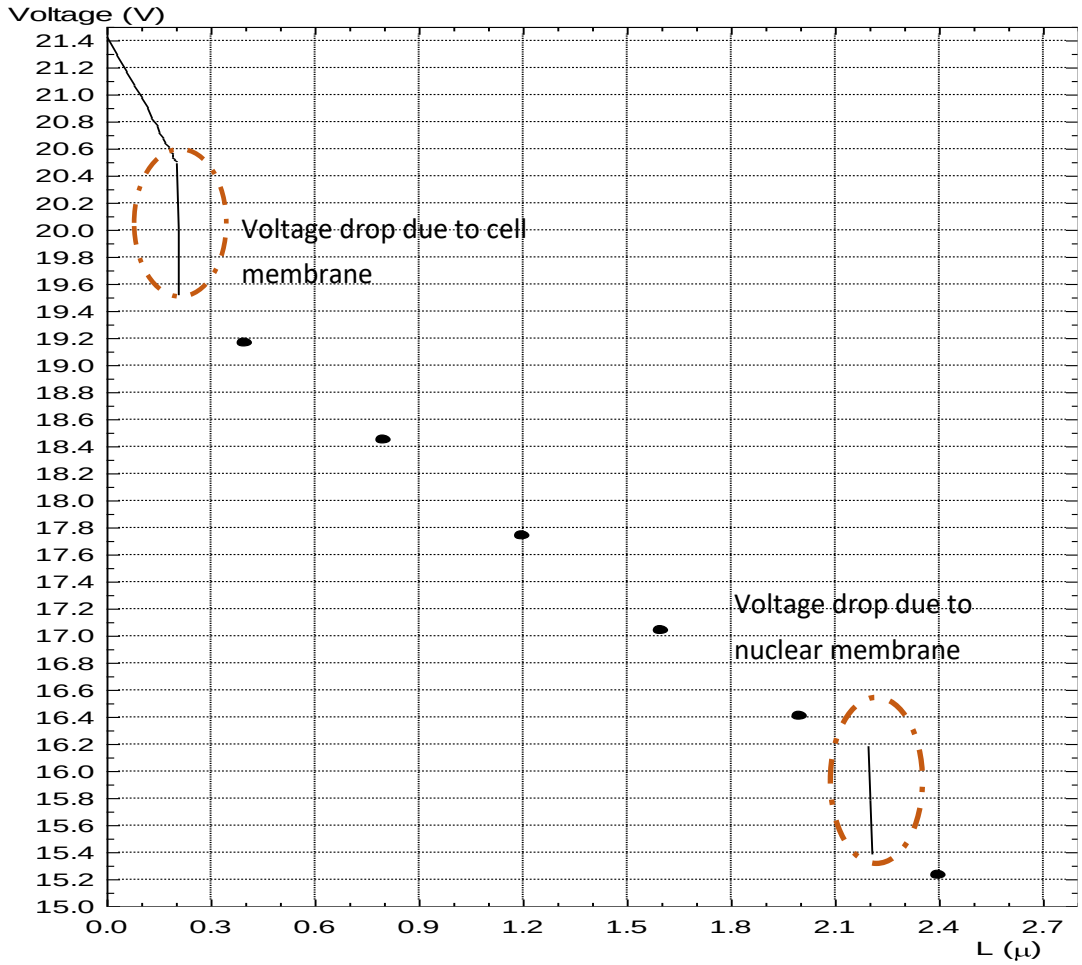

Figure (4.3.2) Potential differences along the reference line in **Figure (4.3.1)**. The voltage drops across the cell and nuclear membranes are circled. The values were calculated at positions on the reference line.

Figure (4.3.3) shows the electric field distribution at 1 ns obtained in the transient analysis simulation. The graph shows the electric field distribution in the cell and nuclear membranes, these fields follow the Schwan Equation with similar behaviour, with minimum field value achieved at the equator and the maximum value at the pole, **Figure (4.3.3.1)** and **Figure (4.3.3.2)**. According to the results, the maximum electric field strength is $\sim 2.0 \times 10^8$ V/m, which is quite close to the value obtained from **Figure (4.3.2)**. For the cell nucleus and cytoplasm, the electric

field strength is not negligible in this situation, **Figure (4.3.4)**. The graph shows a higher electric field strength in environmental fluid as compared with that in the highly conductive cytoplasm. The reason for this is as follows: 1 ns is too short for the charge accumulation process, the charges are still accumulating at each boundary of cell membrane, both in cytoplasm and environmental fluid, which affects their contributions to the electric field in cytoplasm and environmental fluid. According to the simulation results, the electric field strength in the cytoplasm and cell nucleus cannot be neglected in the nano-second PEF treatment, with $\sim 2.3 \times 10^6$ V/m strength in the cytoplasm and $\sim 8.0 \times 10^5$ V/m in the cell nucleus after 1 ns. Such a high electric field strength could help induce field effects in cell organelles, with membrane structures (such an electric field in the cytoplasm could be regarded as an external electric field applied to cell organelles with membrane structures) and might cause structural damage to these membranes.

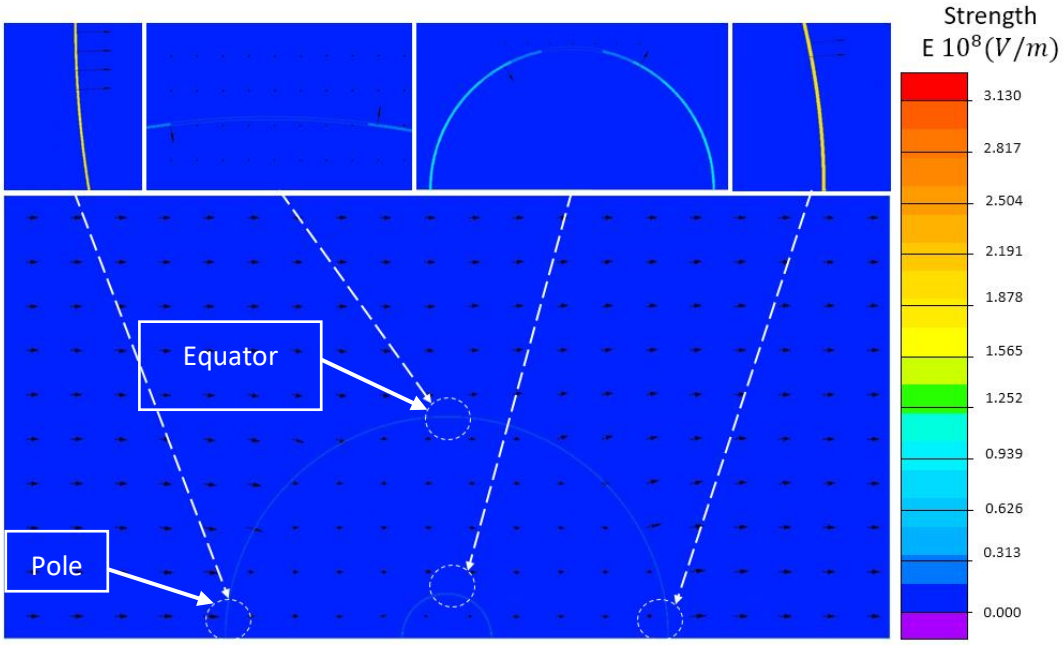

Figure (4.3.3) transient analysis: Electric field distribution at 1 ns. Zoomed in graph is included to show the relationship between the electric field strength and position. The main domain was shown as uniform dark blue due to the low electric

field strength in environmental fluid and cytoplasm compared with the much higher field strength in cell membranes.

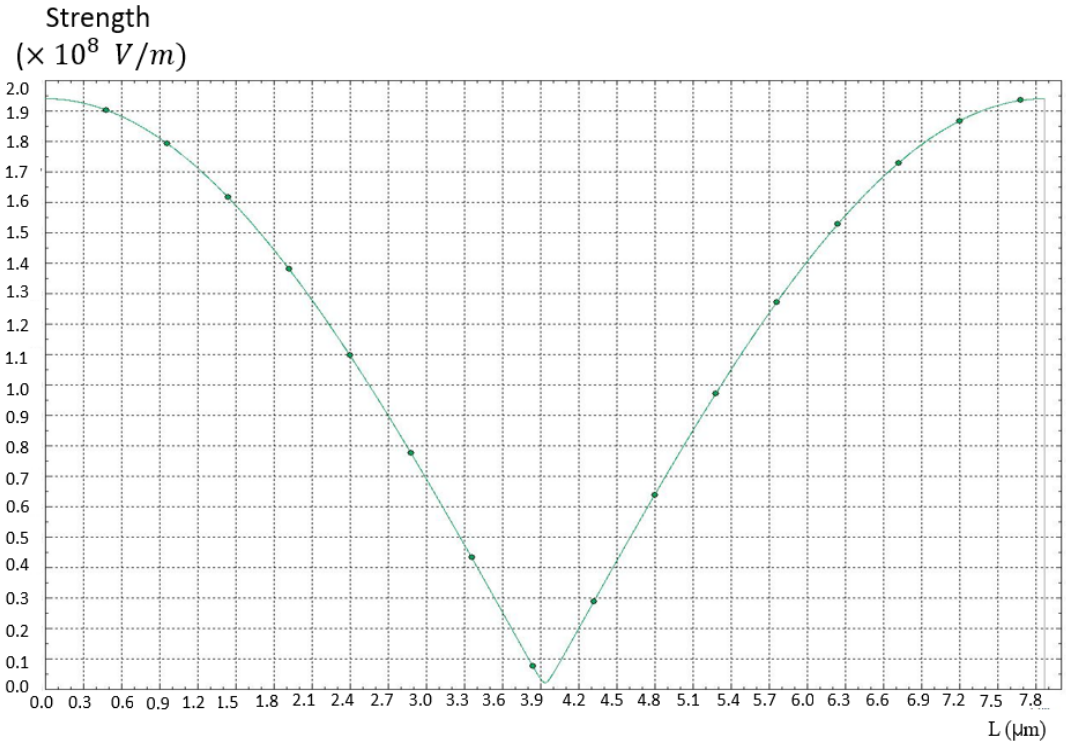

Figure (4.3.3.1) Electric field strength along the cell pole to pole following the arc of the membrane.

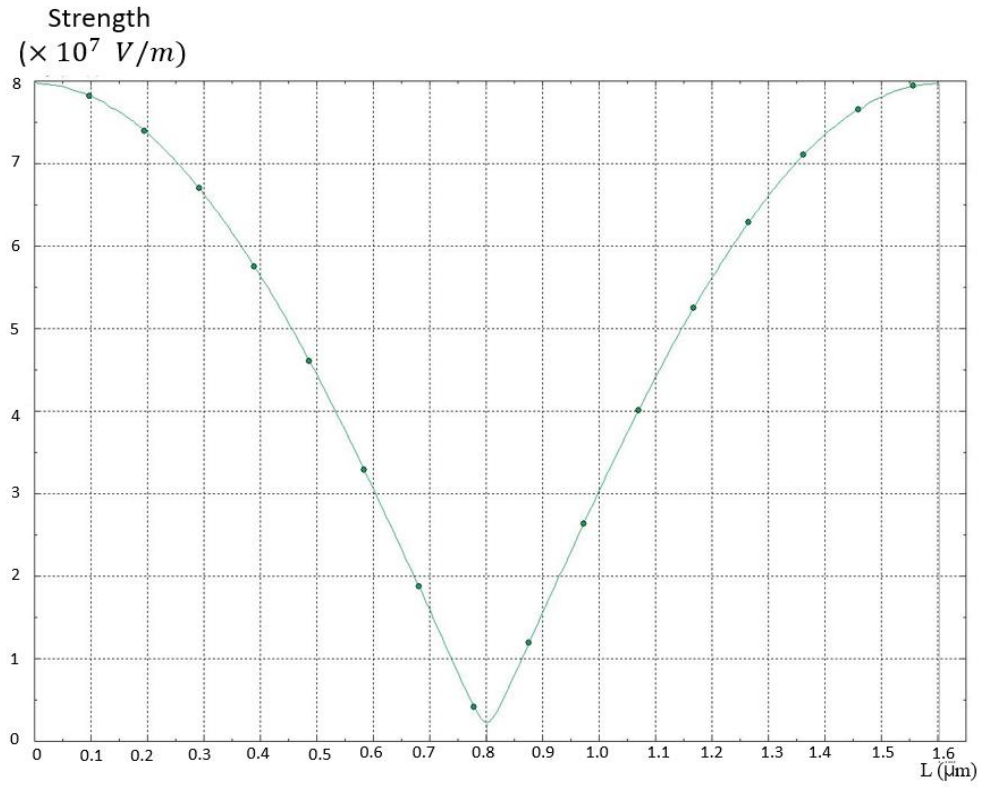

Figure (4.3.3.2) Electric field strength along the pole to pole arc of the cell nucleus membrane.

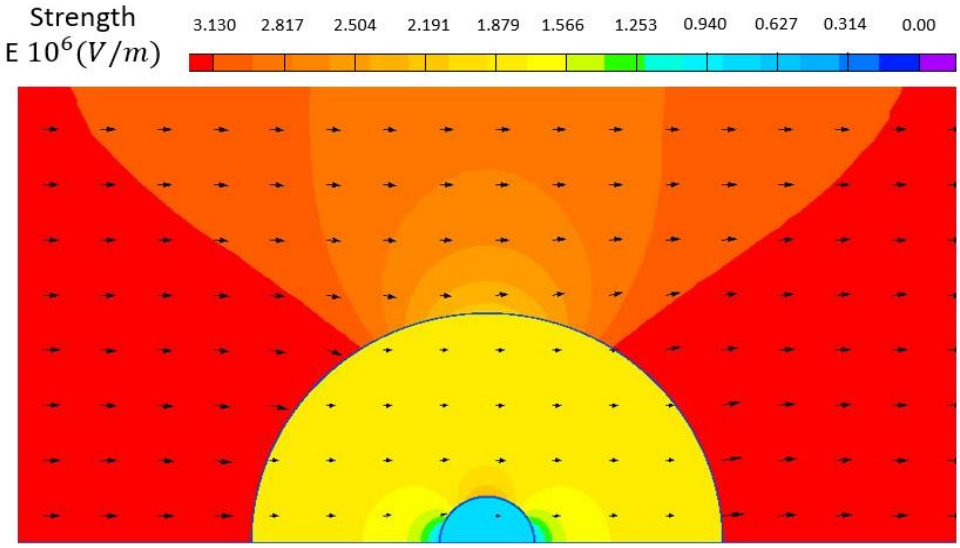

Figure (4.3.4) transient analysis: Electric field distribution at 1 ns, the maximum electric field strength in this figure is $\sim 3.1 \times 10^6\ V/m$ which facilitate a clear view of the electric field distribution in both cytoplasm and cell nucleus.

4.3.2 Current density and power dissipation

Figure (4.3.5) shows the current density distribution in the cell and around the cell. The maximum current density is generated outside the nuclear membrane in the cytoplasm with a value of $\sim 2.8 \times 10^6\ \mathrm{A}/m^2$. Thus it is expected that such current density will cause local heating effects in this region due to joule heating. The current density in the environmental fluid has a maximum value outside the membrane on the equator, **Figure (4.3.5.1)**. However, the current density is only $\sim 1.0 \times 10^3\ \mathrm{A}/m^2$ and is negligible compared with the current density in cytoplasm. The difference between the current densities in the steady state and transient analysis results from the short time of analysis, 1 ns: the charge redistribution process is not completed during this short time. However, the conductivity of cytoplasm is much larger than that of the environmental fluid, so a higher current density would be generated in cytoplasm and a more rapid charge accumulation process would occur in the cytoplasm.

The high current density in the cytoplasm could induce thermal effects and make a contribution to the electroporation process of nuclear membrane which could damage the organs of cytoplasm and cell nucleus during nano-second PEF treatment.

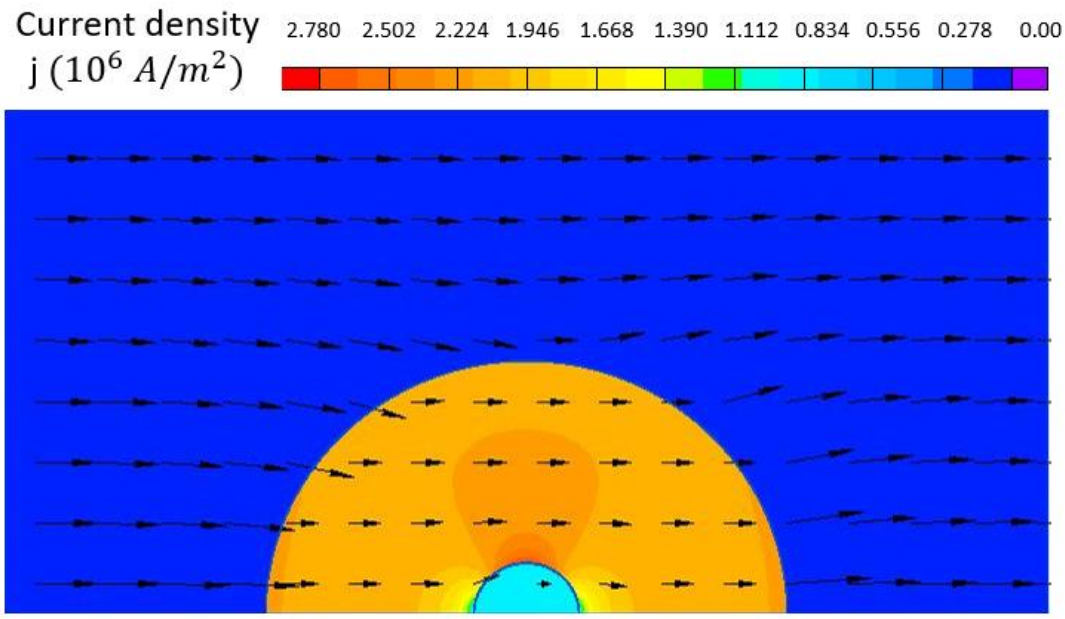

Figure (4.3.5) Current density distribution in of transient analysis in 1 ns.

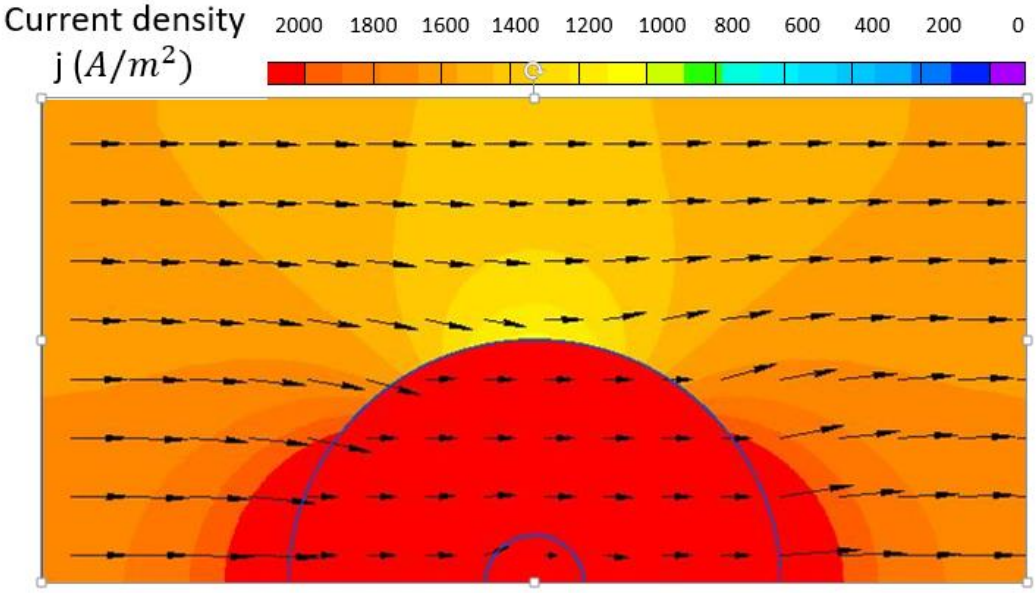

Figure (4.3.5.1) transient analysis: Current density distribution at 1 ns, the maximum value of the current density in this figure was set to 2000 A/m^2 to resolve

visually the current distribution in cytoplasm which allows the changes of current density in cytoplasm to be clearly observed.

However, the QuickField software package cannot link the transient electric field with the transient heat transfer analysis, thus the temperature distribution cannot be obtained in this simulation. This is a limitation of the QuickField model in investigating the thermal effects during the transient PEF energization regime.

4.4 Multiple cells analysis

In the practical cases, millions of microorganisms are present in the liquid medium, thus, these microorganisms could be located close to each other. Using QuickField software, any field effects which could be induced by neighbouring microorganisms were investigated. Thus the model with multiple cells was developed, this model includes 3 single cells (Cell A, Cell B and Cell C, which will be used as the appellation in further analysis of this section), with a cell nucleus present in each cell as shown in **Figure (4.4.1).**

Each cell has the same geometrical and dielectric parameters as were used in the single cell model in this chapter. The treatment region was expanded to $20\ \mu m$, so the applied voltage was set to 60 V to achieve a 30 kV/cm field strength in the treatment region. The space between cell A and cell B is 1 nm meanwhile cell B and cell C are in contact.

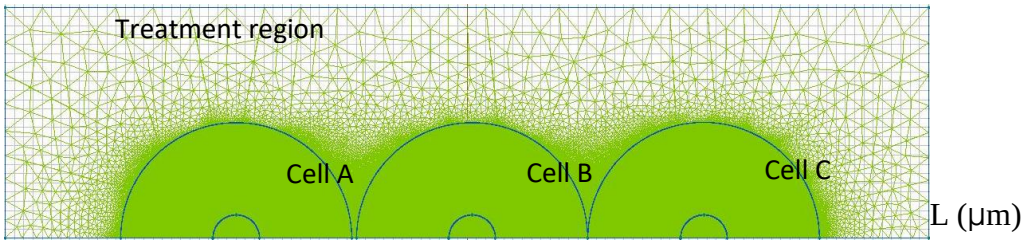

Figure (4.4.1) QuickField model which includes multiple cells. Cell A and Cell B have a $0.1\ \mu m$ gap between them, the external membranes of Cell B and Cell C are in contact with one another.

4.4.1 Steady state analysis

Figure (4.4.2) shows the electric potential distribution in the steady state DC conduction case. It was found that the potential distribution in the environmental fluid and inside each cell are the same as in the single cell model: no significant potential differences in the cytoplasm and cell nucleus. The charge accumulation processes are completed in each cell in this steady state.

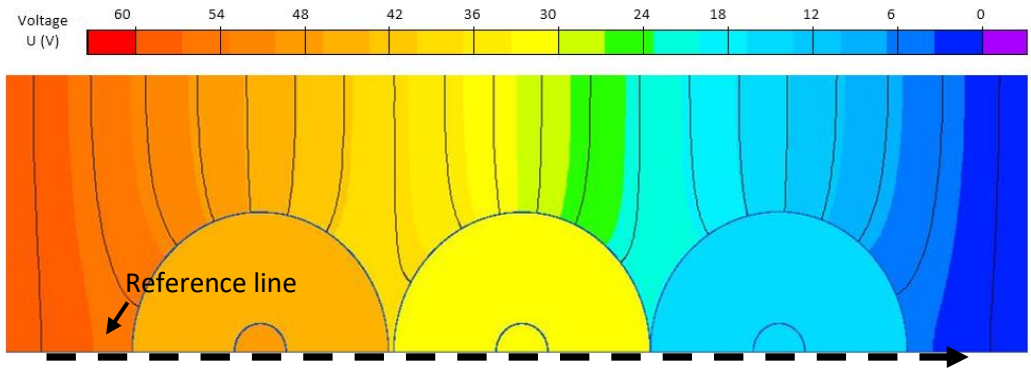

Figure (4.4.2) Electric potential distribution in the steady state DC conduction simulation, the reference line is included to show the line across which the transmembrane potential is obtained.

Figure (4.4.3) shows the electric potential obtained as a function of positions L (µm) along the reference line in **Figure (4.4.2)**. The graph shows the voltage drops at the cell membranes in each single cell and these values are high enough to cause the electroporation process, values are same at both poles
(9.5 V for Cell A, 7.2 V for Cell B and 10.3 V for Cell C). There are no significant differences between the transmembrane potentials in each single cell. However, compared with the transmembrane potential in the nuclear membrane, it is shown that the potential increases from the cytoplasm to cell nucleus and the potential drops when it goes from the nucleus to cell membrane in each single cell, as shown in **Figure (4.4.3)**. This behaviour of the potential is different from the results obtained for the single cell, and has not been reported before and requires further analysis. Furthermore, the transmembrane potentials of nuclear membranes in each cell are different and their values becomes lower values are same at both poles (1.2 V for Cell A, 0.5 V for Cell B and 0.12 V for Cell C) when the cell is getting closer to the ground electrode. For Cell A, the transmembrane potential of its nuclear membrane has reached the electroporation threshold of 1 V, which indicates that even with µS PEF treatment, the electroporation process could be triggered within the nuclear membrane, but mainly electroporation takes place in the cell membranes due to the higher transmembrane potentials.

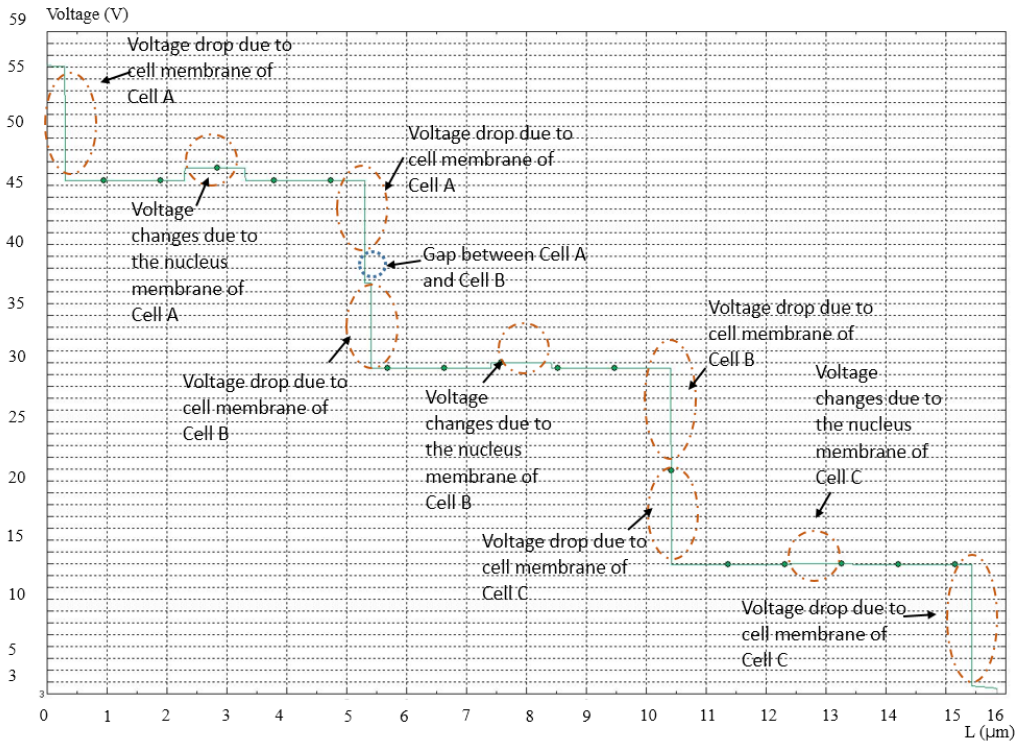

Figure (4.4.3) Potential differences along the reference line in **Figure (4.4.2)**. The voltage drops and voltage increases across cell and nuclear membranes are circled. The values were measured at the positions on the reference line (for example: half circumference of cell nucleus).

Figure (4.4.4) shows the electric field strength distribution, the maximum value is $\sim 2.1 \times 10^{9}\ V/m$ which is close to the value obtained in the single cell model and the magnitude of electric field in the cytoplasm and cell nucleus is very low ($\sim 2.2 \times 10^{-4}\ V/m$) and ($\sim 1.4 \times 10^{-5}\ V/m$) respectively. **Figure (4.4.4.1)** shows the electric field strength along the reference line (cell membranes) in **Figure (4.4.4)**, where it is obvious that the field follows the Schwan Equation and the field values are similar in each cell. **Figure (4.4.4.2)** shows the electric field strength in the nuclear membranes, the results are also similar to those for the single cell model: due to the completed charge accumulation process, the charges inside the cell are stable, and the electric field strength in the cell nucleus is constant.

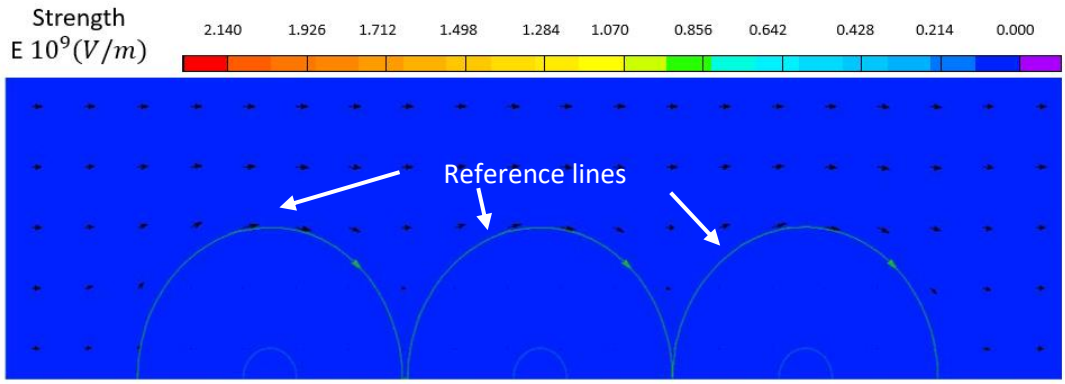

(a)

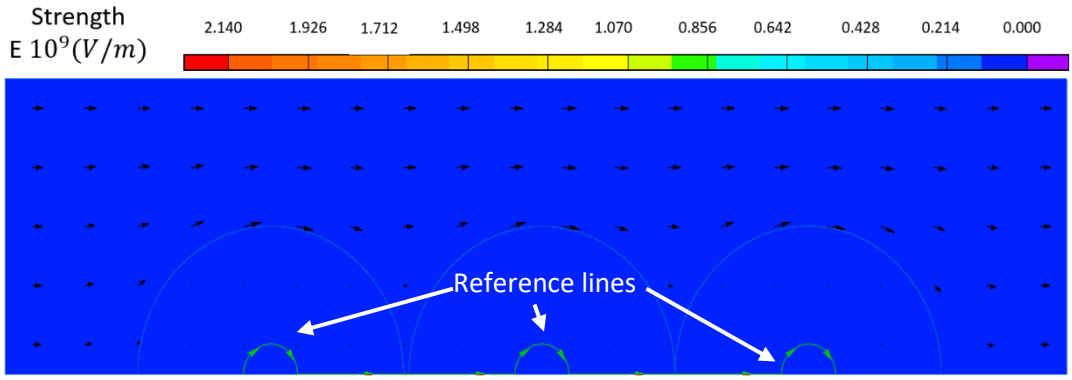

(b)

Figure (4.4.4) Electric field distribution in the steady state DC conduction case. Reference lines were used to obtain the electric field strength of cell membranes (a), other similar reference lines were also used to obtain electric field strength in the nuclear membranes (b).

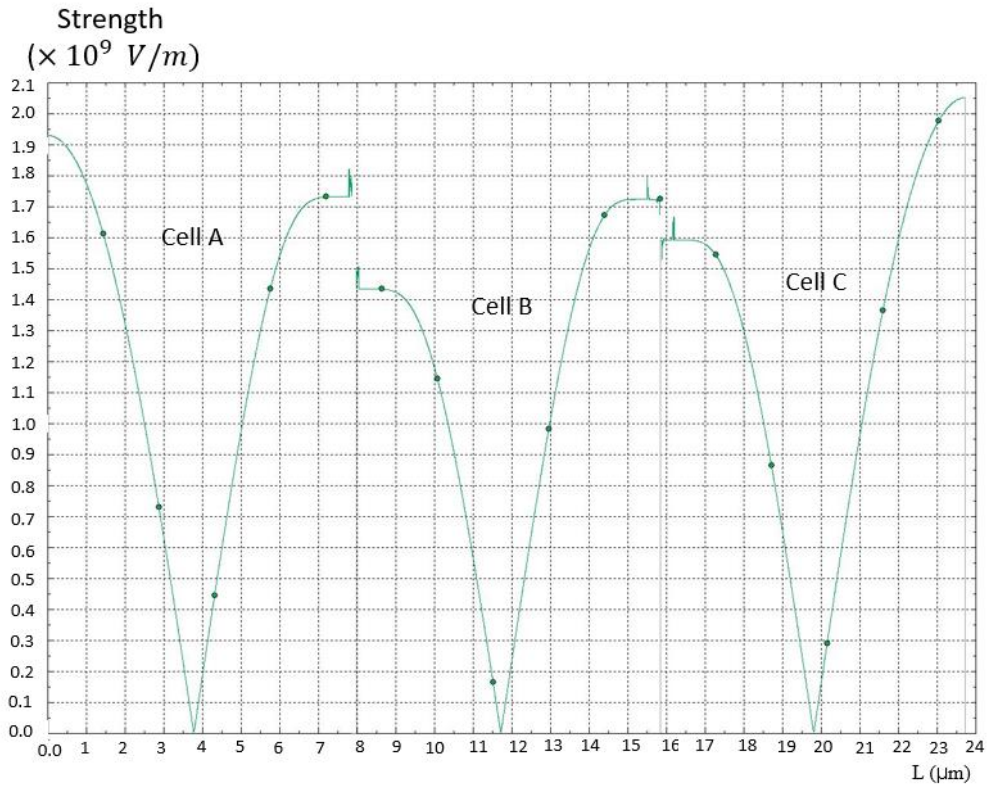

Figure (4.4.4.1) Electric field strength along the reference lines, the values were measured at the positions on the reference line (for examples: half circumference of cell nucleus. The potential drop between Cell B and Cell C was generated due to the calculation errors between boundaries and caused by software).

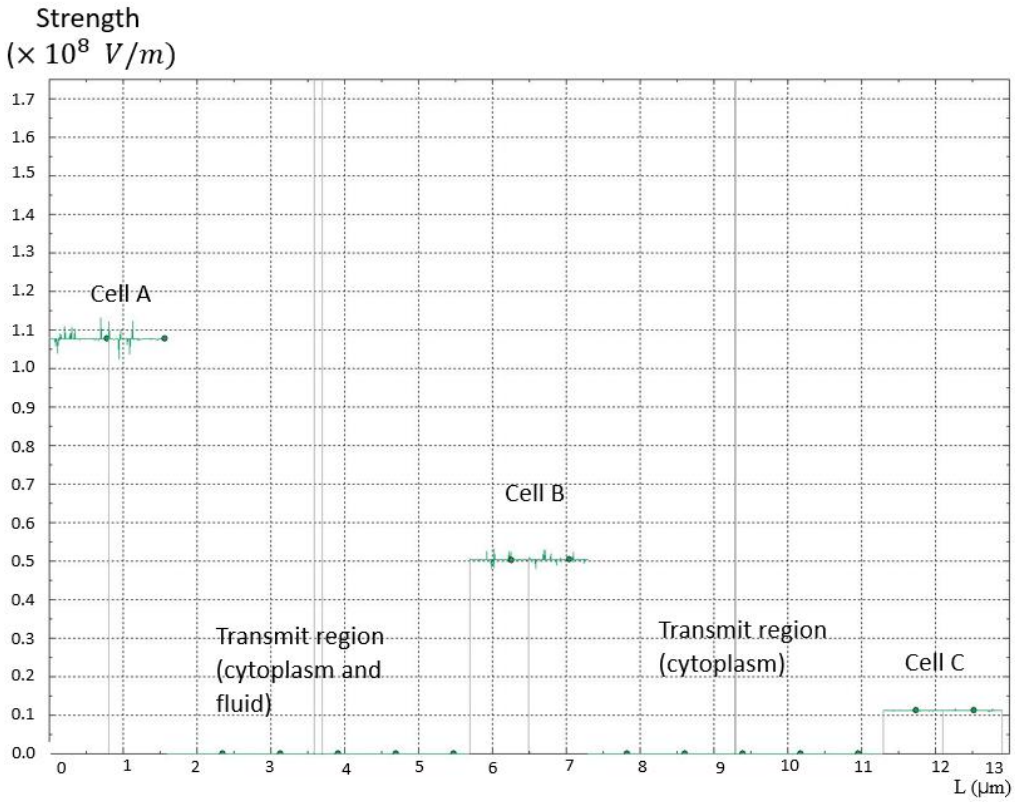

Figure (4.4.4.2) Electric field strength in nuclear membranes of each single cell, the values were measured at the positions on the reference line (for example: half circumference of cell nucleus), the electric field strength in transmit region is not clear on the graph as the values are negligible compared with the values in the membranes.

Figure (4.4.5) shows the current density in the steady state DC conduction case, there is no significant differences in the current density compared with that in **Figure (4.2.4)**, the maximum value in the multiple cells model is $2090\ \mathrm{A}/m^2$ and in the single cell model is $2220\ \mathrm{A}/m^2$. This is because the current in the steady state case flows mostly through the environmental fluid and the conductivity of this fluid in both models is the same. The current density inside each of the cells is negligible in the multiple cells model (DC steady state case).

The Increase in the current density at the poles of the three microorganisms can potentially increase the local temperature at these locations. Thus, 3 potential 'hot spots' (high intensity current density spots) were observed in this model. In general, for electroporation applications, samples with large microbial populations are treated. Thus, such 'hot spots' could lead to local temperature increases in the treated samples, and these thermal effects could be more significant in samples with higher conductivity of the fluid and at higher applied electric fields (as discussed in **section 4.2**).

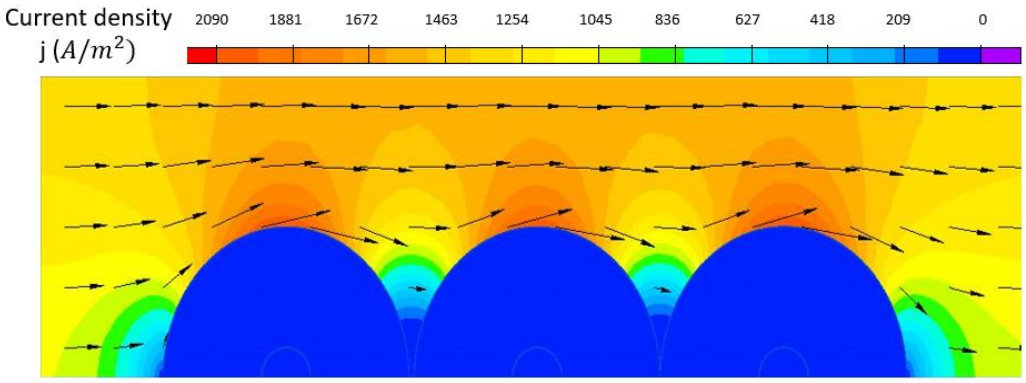

Figure (4.4.5) Current density distribution in the steady state case.

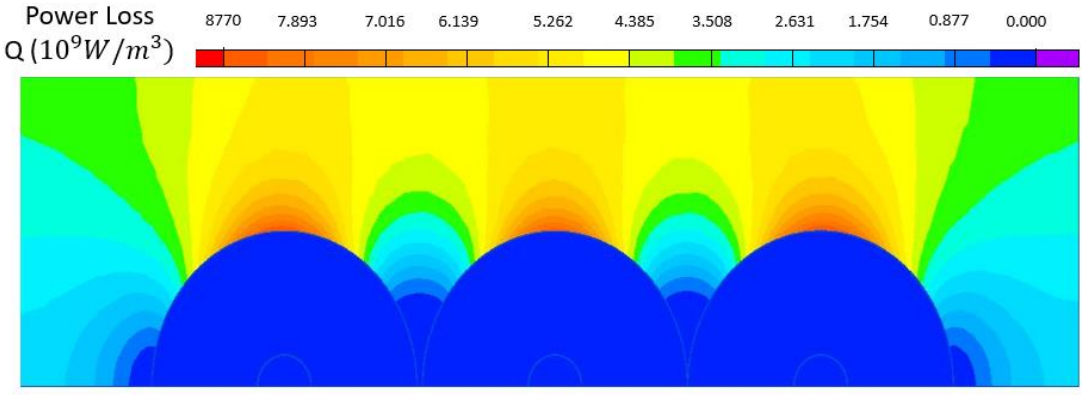

Figure (4.4.6) Power dissipation in the steady state case.

4.4.2 Transient analysis

Figure (4.4.7) shows the electric potential distribution in the case of the transient analysis at 1 ns. It can be seen that the potential distribution in the environmental fluid and inside each cell are the same as in the single cell model: there are potential drops across interfaces between the environmental fluid, cytoplasm and cell nucleus. The simulation time of 1 ns is too short for the electric field to relax due to the conduction processes in the fluid, and the dielectric properties of the cell structures play an important role in this situation. Comparing the electrical potential distribution in the cytoplasm and fluid, there is no significant difference between the results obtained using the single cell model and the multiple cell model.

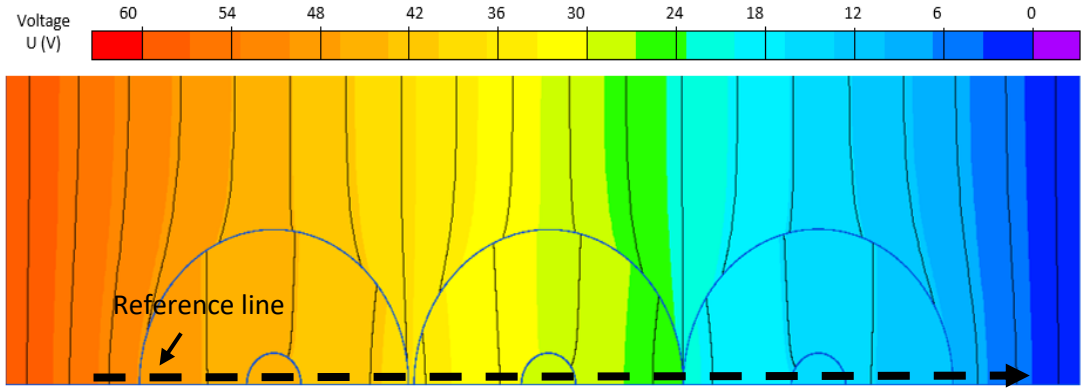

Figure (4.4.7) Electric potential distribution in transient field case, the reference line used to calculate transmembrane potential is included.

The electric potential was obtained along the reference line in **Figure (4.4.7), and** this potential as a function of positions L (μm) is shown in **Figure (4.4.8)**. The graph shows the voltage drops across the cell membranes in each single cell and the field values are high enough to trigger electroporation processes ($2-3$ V for Cell A, ~ 2 V for Cell B and $2-3$ V for Cell C). There is no significant differences between potential drops when the cell is getting closer to the ground

due to the same structures of cells and parameters. On the contrary, compared with the transmembrane potential in the nuclear membrane, there is always a potential drop (from the cytoplasm to nucleus or from the nucleus to the cell membrane) in each single cell, which is different from the results obtained in the steady state simulation. Furthermore, the transmembrane potentials in the nuclear membranes in each cell are the same (~ 1 V for Cell A, ~ 1 V for Cell B and ~ 1 V for Cell C), which is also different from the results obtained from the steady state simulation (when the cell is getting closer to the ground, the transmembrane potentials becomes lower). All transmembrane potentials of the nuclear membrane have reached the electroporation threshold (1 V).

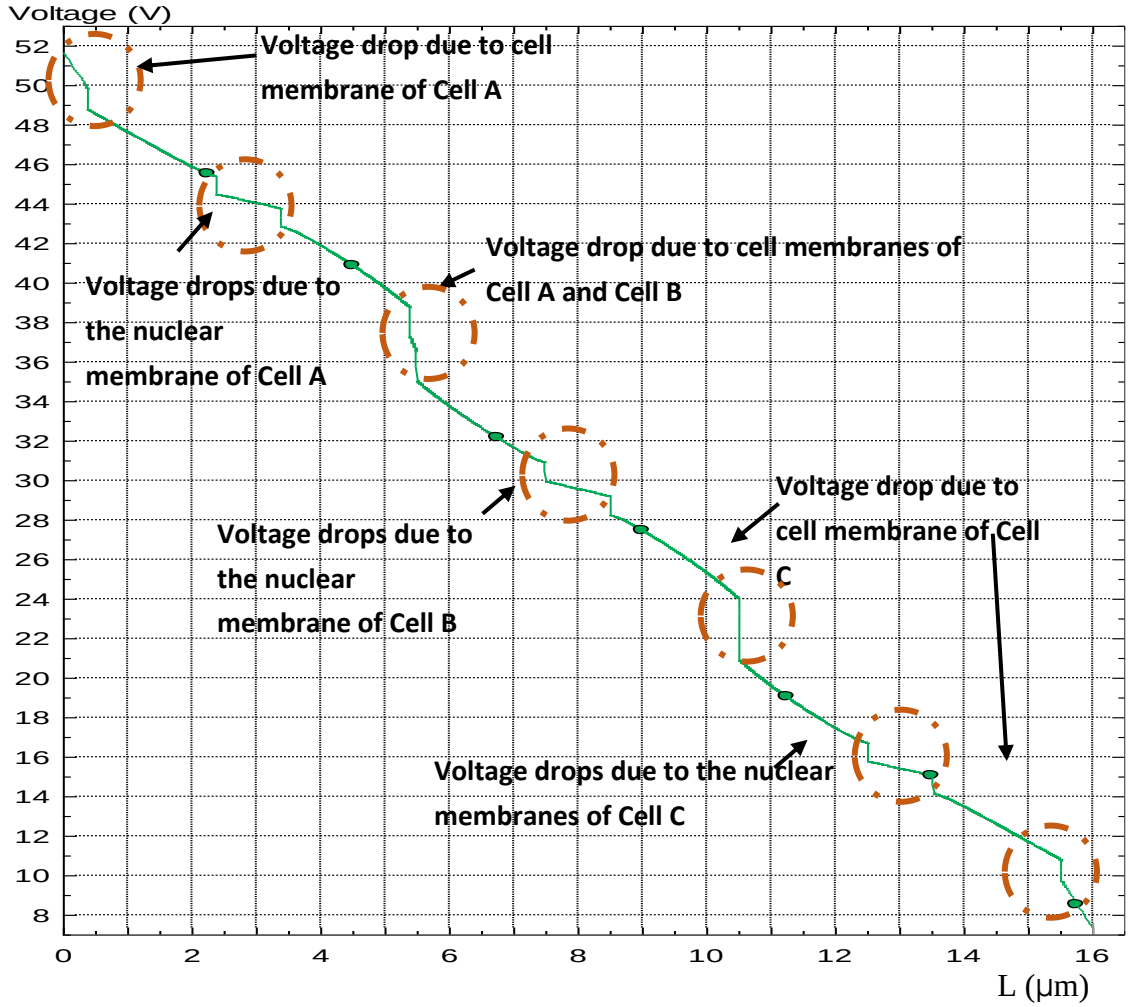

Figure (4.4.8) Potential differences along the reference line from **Figure (4.4.7)**. The voltage drops across the cell and nuclear membranes are circled.

Figure (4.4.9) shows the electric field distribution in the transient case at 1 ns. The graph shows the electric field distribution in the cell and nuclear membranes, this field follows the Schwan Equation, with minimum value at the equator and maximum value at the pole of the membranes, **Figure (4.4.9.1)** and **Figure (4.4.9.2)**. The maximum electric field strength is $\sim 3.1 \times 10^8\ V/m$, which is the same as in the case of the single cell, as shown in **Figure (4.3.3)**. For the cell nucleus and cytoplasm, the electric field strength is not negligible in this situation, **Figure (4.4.10)**. According to the simulation results, the electric field strength in the cytoplasm and cell nucleus is not negligible in the nano-second PEF treatment, the strength in the cytoplasm is $\sim 2.0 \times 10^6\ V/m$ and $\sim 7.5 \times 10^5\ V/m$ in the cell nucleus at 1 ns. These values are close to the results obtained from the single cell model, which also confirms that the electrical field in each cell in the multiple cells model is not affected by the field in other cells.

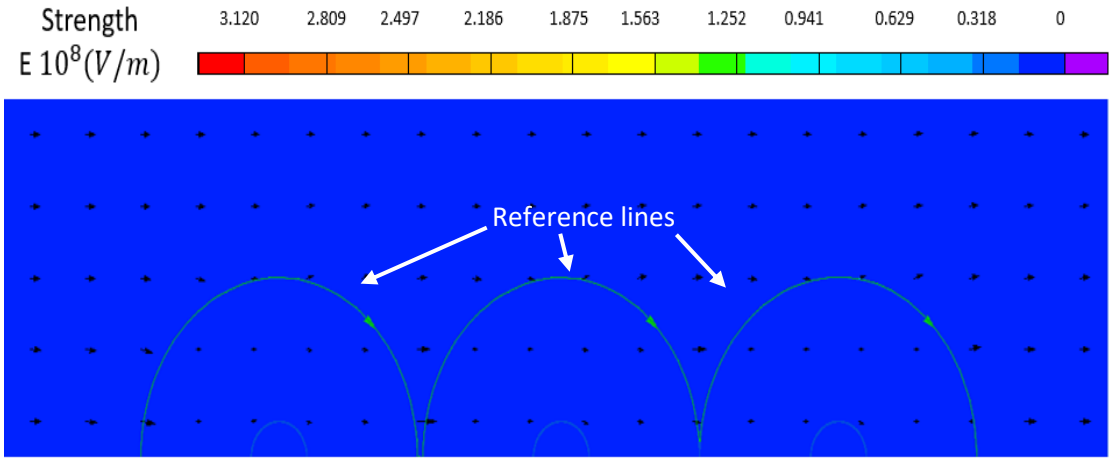

(a)

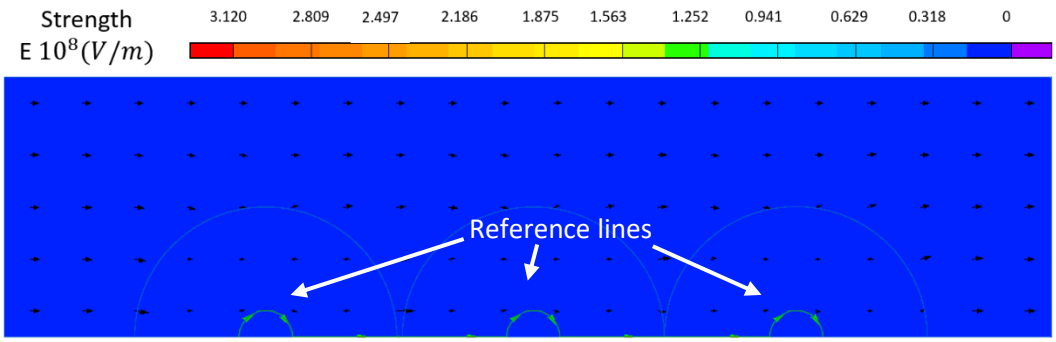

(b)

Figure (4.4.9) Electric field distribution at 1 ns. The main domain was shown as uniform dark blue due to the low electric field strength in environmental fluid and cytoplasm compared with the much higher field strength in cell membranes. Reference lines (represent the environmental fluid/membrane boundary in the model) were used to obtain the electric field strength in the cell membranes (a), the same reference lines were also used to obtain the electric field strength in the nuclear membranes (b).

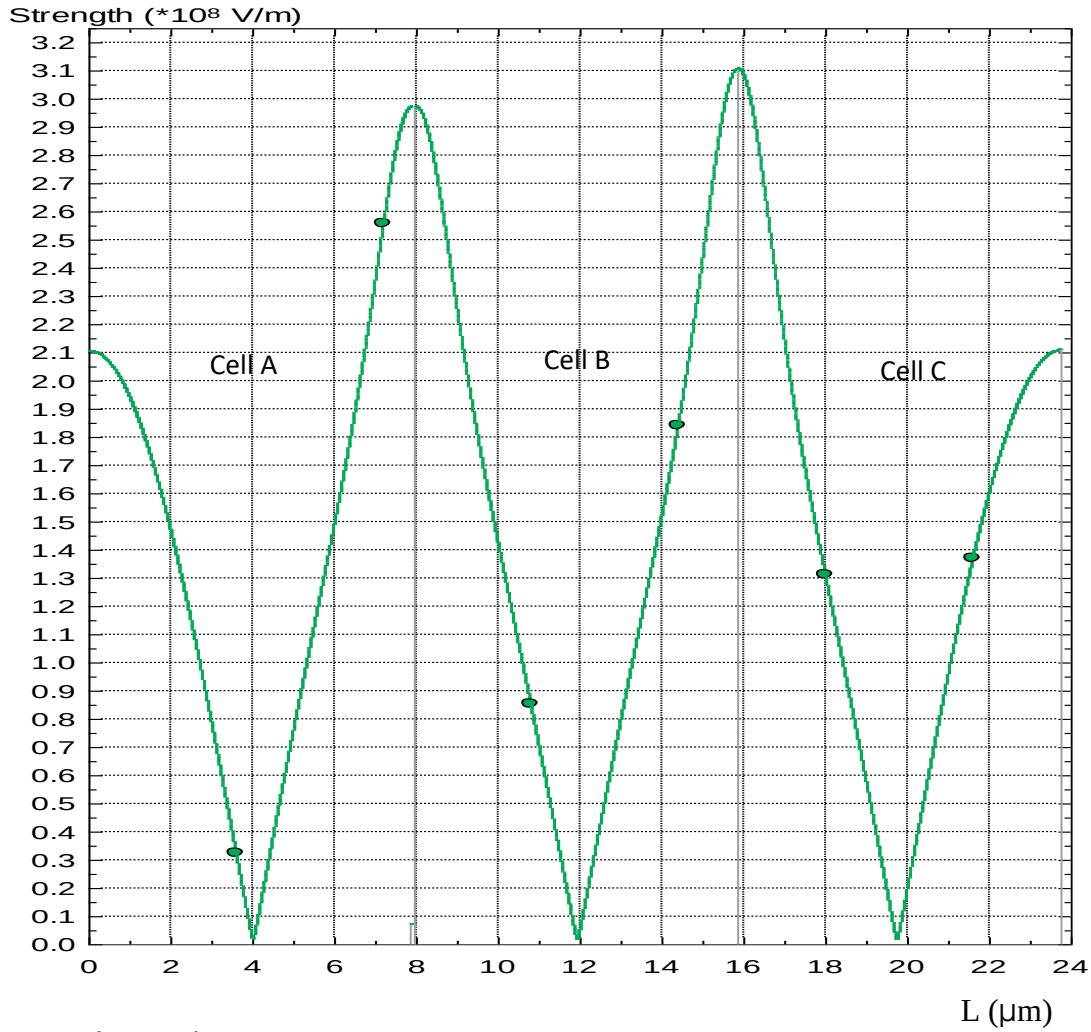

Figure (4.4.9.1) Electric field strength along the reference lines (electric field strength in cell membranes).

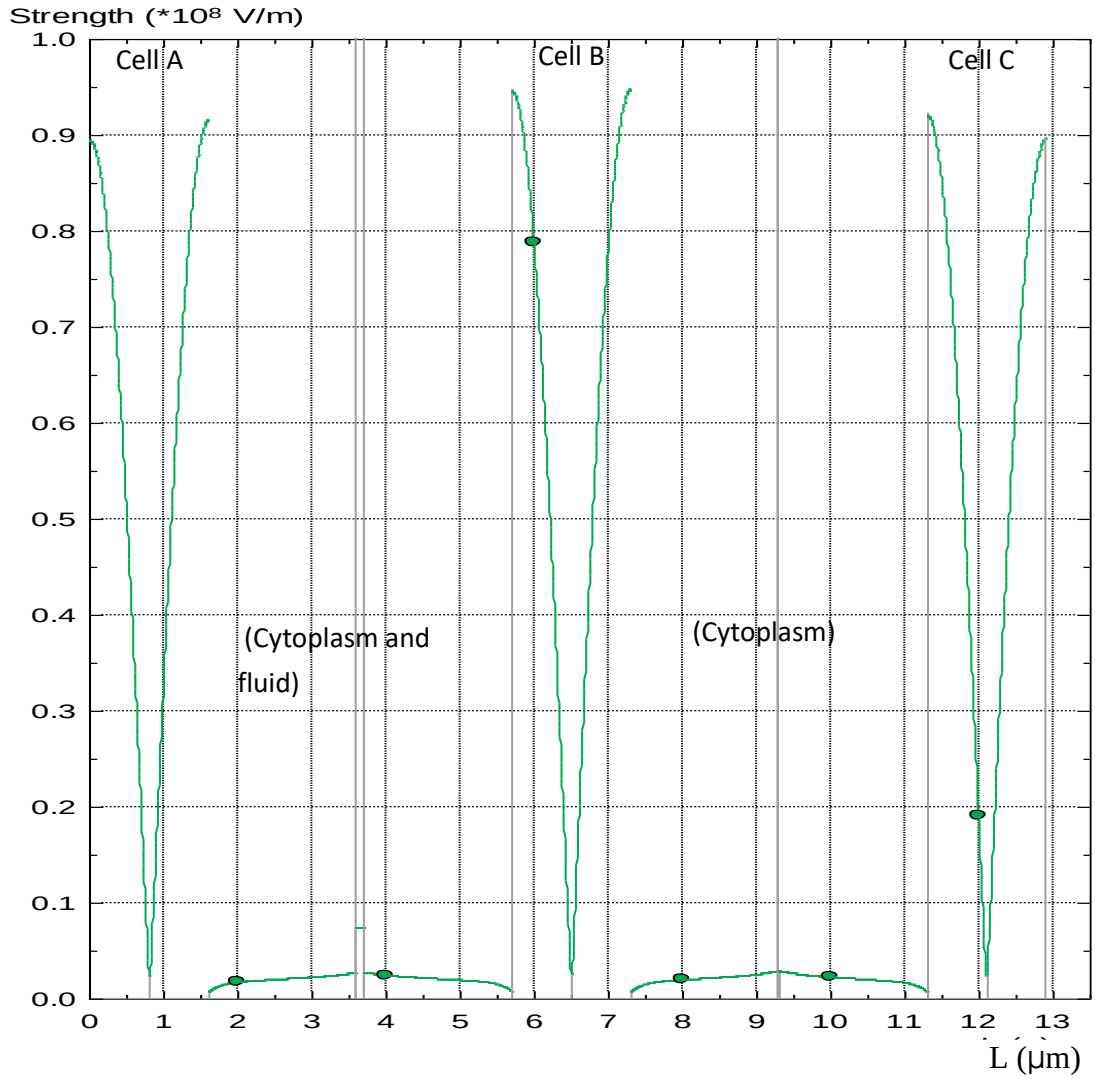

Figure (4.4.9.2) Electric field strength in the nuclear membranes of each single cell.

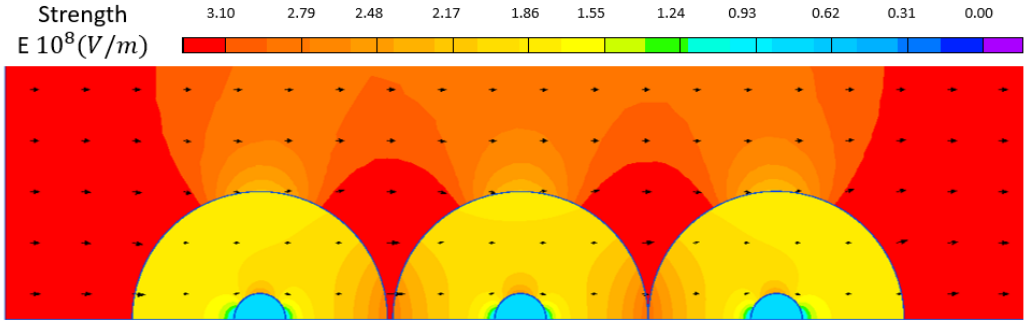

Figure (4.4.10) Electric field distribution at 1 ns, the maximum electric field strength of colour plot was limited to $\sim 3.1 \times 10^6\ V/m$ in order to show clearly the electric field distribution in the cytoplasm and cell nucleus.

Figure (4.4.11) shows the current density distribution at 1 ns. It is shown that higher current densities are generated in several positions: outside the nuclear membrane in the cytoplasm and inside the cytoplasm closer to the other cell, which is different from the results obtained using the single cell model. The number of cells does have an effect on the current density distribution in the nano second PEF treatment. Due to the joule heating, there should be local hot spots in these regions. On the contrary, the current density in the environmental fluid also shows the same tendency: with the maximum value achieved on the outer surface of the membrane, **Figure (4.4.11.1).** However, the values are only $\sim 1.0 \times 10^3\ \mathrm{A}/m^2$ and could be neglected compared with the current density in cytoplasm. The current density shows a higher value in the cytoplasm compared with that in the external fluid, this is caused by the higher conductivity of the cytoplasm compared with the environmental fluid. The high current density regions which are visible in **Figure (4.4.11)** appear at the cytoplasm at the points of contact between neighbouring microorganisms, in the region of their equator. This increase in the current density was not observed in the case of a single microorganism, **Figure (4.3.5)**. Such high current density may help to generate thermal effects and accelerate the electroporation process of the membrane or damage the cell organelles.

The high current density in the cytoplasm could induce more pronounced thermal effects as compared with the single cell model and will make contribution to the electroporation process of the nuclear membrane which could damage the organelles of the cytoplasm and cell nucleus during the nano-second PEF treatment.

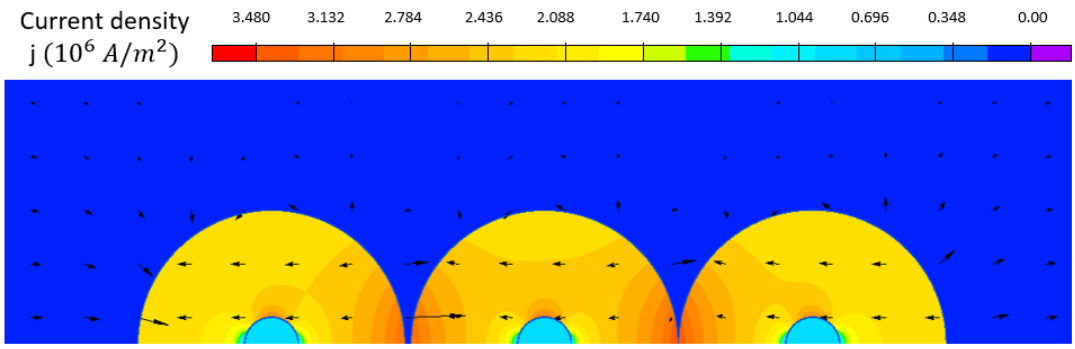

Figure (4.4.11) Current density distribution at 1 ns.

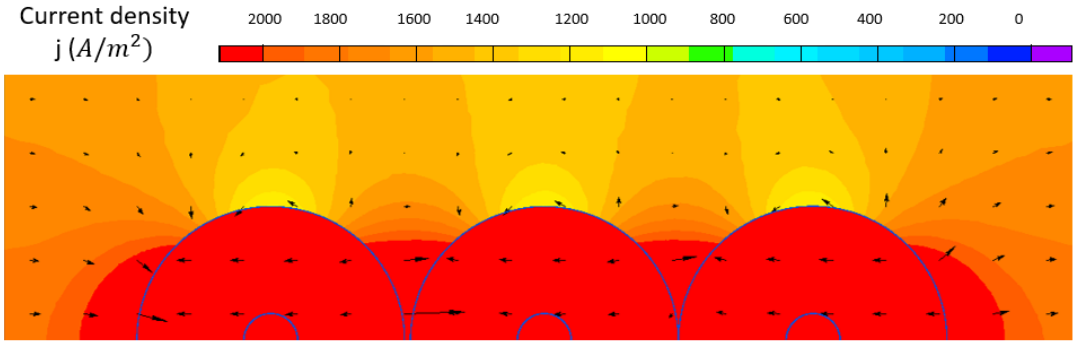

Figure (4.4.11.1) Current density distribution at 1 ns, the maximum value was set to 2000 A/m^2 in order to show clearly the electric field distribution in the cytoplasm and cell nucleus.

4.5 Summary and discussion

In this chapter, two models were developed using the QuickField software package: the single cell and multiple cells models. These models were used to investigate electric field, current density and thermal effects in the steady state and transient cases. The main results obtained in this chapter can be summarized as follows:

Steady state analysis in the single cell model

- Electric potential distribution and transmembrane potential of cell membrane and nuclear membrane were investigated and show similar results to the linear model due to the very low conductivity of

membranes, however, such field distribution would not be generated in the cell wall as it is not a membrane structure with low conductivity.

  - Electric field strength distributions were investigated, the results were consistent with the linear model and other mathematical modelling results [274] [78] [290].
  - Investigation of the current density shows that local heating effects exist in the environmental fluid during the PEF treatment and may help to enhance the electroporation process if the joule heating due to such conduction current is significant. Thus, the electroporation process would be enhanced by the thermal effects during PEF treatment of microorganisms.

- Transient analysis of single cell model
  - Electric potential distribution and transmembrane potential of cell membrane and nuclear membrane were investigated and the results show that the nano-second PEF treatment could trigger the electroporation process in the nuclear membrane. No previous investigation has focused on the interactions between external electric field and cell nucleus during PEF treatment when the thermal effects among cell nucleus and cytoplasm were investigated.
  - Electric field distributions were obtained, with the results showing that the electric field strength induced in the cytoplasm and cell nucleus could affect the organelles or structures inside cells and enhance the lethal effects of the PEF treatment.
  - Investigation of the current density shows that local heating of the cytoplasm during the nano-second PEF treatment exists and may help to enhance the electroporation process of the nuclear membrane.

- Multiple cells model
    - Both steady state analysis and transient analysis were performed using the developed multi-cell model, with the results showing that in the steady state case, the number of microorganisms might have an effect on the local heating of the environmental fluid.
    - The transient analysis demonstrated that the electrical potential and electric field inside each cell do not depend on the presence of other cells as shown in **Figure (4.4.9.1)**, however, the local heating effects in the cytoplasm were influenced by the presence of other microorganisms which could make a contribution to the electroporation process of cell membranes during the nano-second PEF treatment.

4.5.1 Limitations of QuickField model

The local heating effects during the PEF treatment should not be neglected in the case of fluids with higher conductivity and high external electric field strength. Furthermore, in the nano-second PEF treatment, the local heating effects in the cytoplasm require further investigation, as they could induce significant effects on the electroporation process of the cell or nuclear membranes. However, the heat transfer analysis in the QuickField model was not accurate as it was using the heat source generated within the steady state model. Thus, the transient temperature increase could not be obtained. Also, it is not possible to link the transient electrical results with the transient heat transfer analysis in the QuickField model, which is a limitation of this investigation of the thermal effects during the PEF treatment. To overcome these limitations of the QuickField models, COMSOL Multiphysics was used for the modelling of the transient effects during the PEF treatment of microorganisms, and this model will be presented in the next chapter. In **Figure (4.2.3.1)**, in cells B and C, electric field is higher at lower potential side but in cell A, the electric field his higher at higher potential side. The reason could be the potential increase across cells in **Figure (4.4.3)** due to the calculation error of Quickfield software, further works would be necessary to solve this problem.

Chapter 5. COMSOL model of microorganisms

5.1 Introduction

Two models which allowed for simulation of the transient electric fields in microorganisms (analytical linear model and the model implemented in the FEM simulation package Quickfield) have been developed and were discussed in the previous chapters. These models could be used to investigate the electric field build up process in the cell membrane (the analytical linear model) and the current density distribution in the treatment region (software based Quickfield model) within a single cell during the PEF treatment. However, the investigation of potential local thermal effects is not fully supported by the Quickfield software, because the transient thermal effects analysis model could not be linked to the transient electrical analysis model in the same simulation. The analysis of transient thermal effects could only be conducted using the steady state dc conduction model, therefore the results of the transient thermal analysis may not be accurate for pulsed voltages. As discussed in Sections 4.3 and 4.5, there are several other limitations associated with these models, and the different energization type of signals (DC, AC, impulsive) during PEF treatment also requires further investigation.

In this chapter, an advanced single cell model was developed to overcome these limitations of the linear and Quickfield models. COMSOL Multiphysics software was used to develop the single cell model with different geometries (ellipsoidal and spherical cells) and to study the local heating effects during the PEF treatment under different DC and AC energization regimes. Also, the transient electric field and temperature in a single pore created during the PEF treatment have been

investigated. This chapter provides detailed information and discussion on the interaction between the external electric field and microorganisms.

5.2 Development of a single cell model in COMSOL

COMSOL Multiphysics 5.1 is used in this chapter to develop a single cell model in order to simultaneously simulate the electric field and thermal effects in a cell during the PEF treatment. **Figure (5.1)** below shows the initial frame of this single cell model: The red line represents the axis of symmetry, where $r = 0$. A single cell was positioned in the middle of the environmental fluid between two electrodes, designed to provide a uniform field distribution. There are two regions between the electrodes and the environmental fluid which were present to avoid errors in the calculation of thermal effects, these regions being at the radiused electrode edges at the boundaries of electrode and environmental fluid (marked with red arrows) - thermal effects in such parts were not the concern of this model. Advanced simulation models will be presented in the following sections.

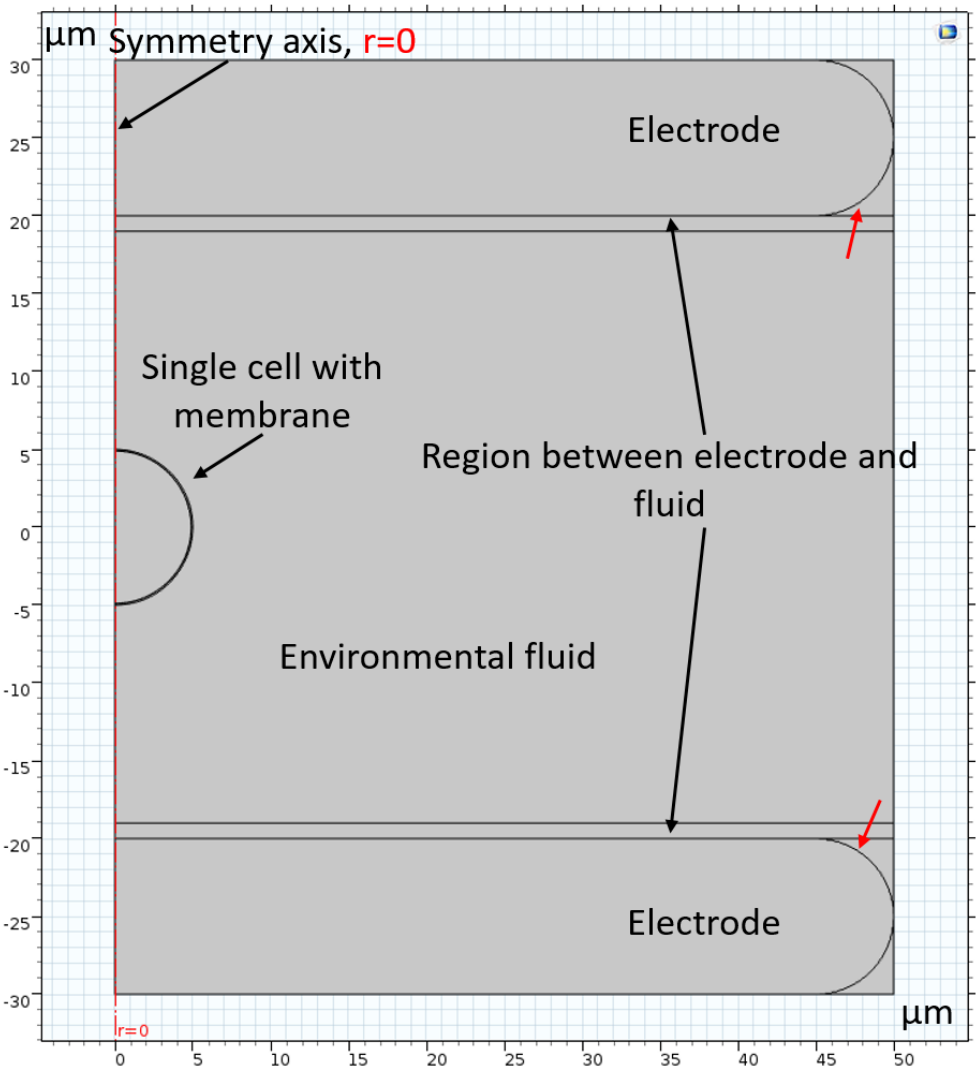

Figure (5.1) General geometry of initial single cell model. The region between electrodes and fluid were used to avoid calculation errors between boundaries.

5.3 Parameters of the microorganism used in the COMSOL model

The cell parameters which were used in the analytical linear and Quickfield models are listed in **Table (5.1).** These parameters were also used in the present chapter in the COMSOL model.

Table 5.1 Parameters used in the 2D COMSOL single cell model. Numerical values are taken from the sources cited.

Parameters	**Value**
External voltage	120
Relative permittivity of cytoplasm	80 [318], [316], [273], [300], [319]
Relative permittivity of membrane	2 [318], [316], [273], [300]
Relative permittivity of surrounding liquid	80 [318], [316], [273], [300], [319]
Conductivity of cytoplasm	1.2 S/m [7], [315], [307], [319]
Conductivity of cell membrane	10^{-13} S/m [319]
Conductivity of environmental liquid	0.5×10^{-3} S/m [275]
Thickness of membrane	5 nm [318], [315], [273], [275], [307]
Diameter of cytoplasm	5 µm [315], [273], [275], [307]
Width of treatment region (between electrodes)	40 µm

Figure (5.2) shows the general topology of the COMSOL single cell model. In order to achieve a 30 kV/cm electric field strength (typical electroporation field strength) between the electrodes, a DC voltage signal with the magnitude of 120 V was applied to the electrodes.

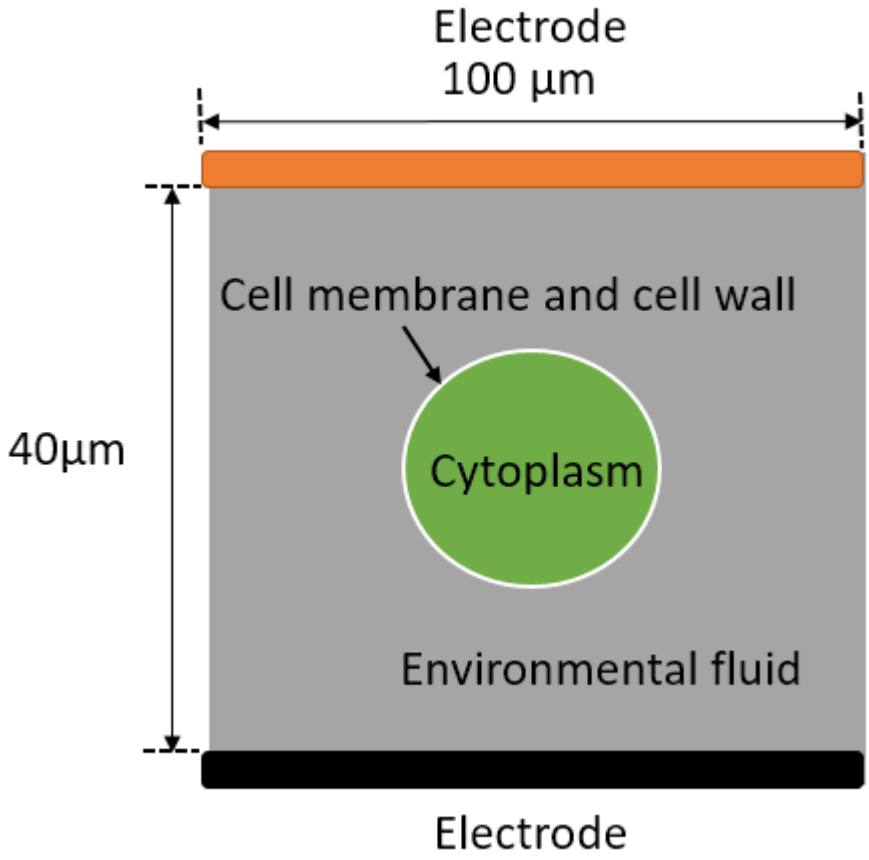

Figure (5.2) COMSOL model of a single cell, only the cell membrane was considered in the initial single cell model, the cell wall will be considered in section 5.7.2.

5.4 Transient calculation results of initial Single cell model

The electrical field distribution in the single cell after 10 µs (pulse duration) was obtained and this distribution is shown in **Figure (5.3)**. A 10 µs treatment was selected in transient analysis as thermal effects would be more significant with longer treatment time. **Figure (5.4) and Figure (5.5)** provide a zoomed view of the electric field strength distribution in the cell membrane (across the pole and equator). It is shown that the electric field strength distribution in the cell membrane follows the Schwan equation, **Eq. 3.1.4**, with maximum field strength at

the pole and minimum field strength on the equator. The maximum electric field magnitude in the membrane at 10 μs was$\sim 1.8 \times 10^9$ V/m. This value is close to the value obtained using the steady state DC Quickfield model: $\sim 2.3 \times 10^9$ V/m. The transmembrane potential across the cell membrane reached the electroporation threshold of ~ 1 V.

Figure (5.6) shows the electric field build up process during the first 10 μs of the PEF treatment. It can be seen that the field strength across the cell membrane did not reach its saturation value in 10 μs. This could be caused by the low conductivity of the environmental fluid (0.5×10^{-3} S/m). Simulation results with higher conductivity environmental fluids will be introduced and discussed in section 5.3.1.

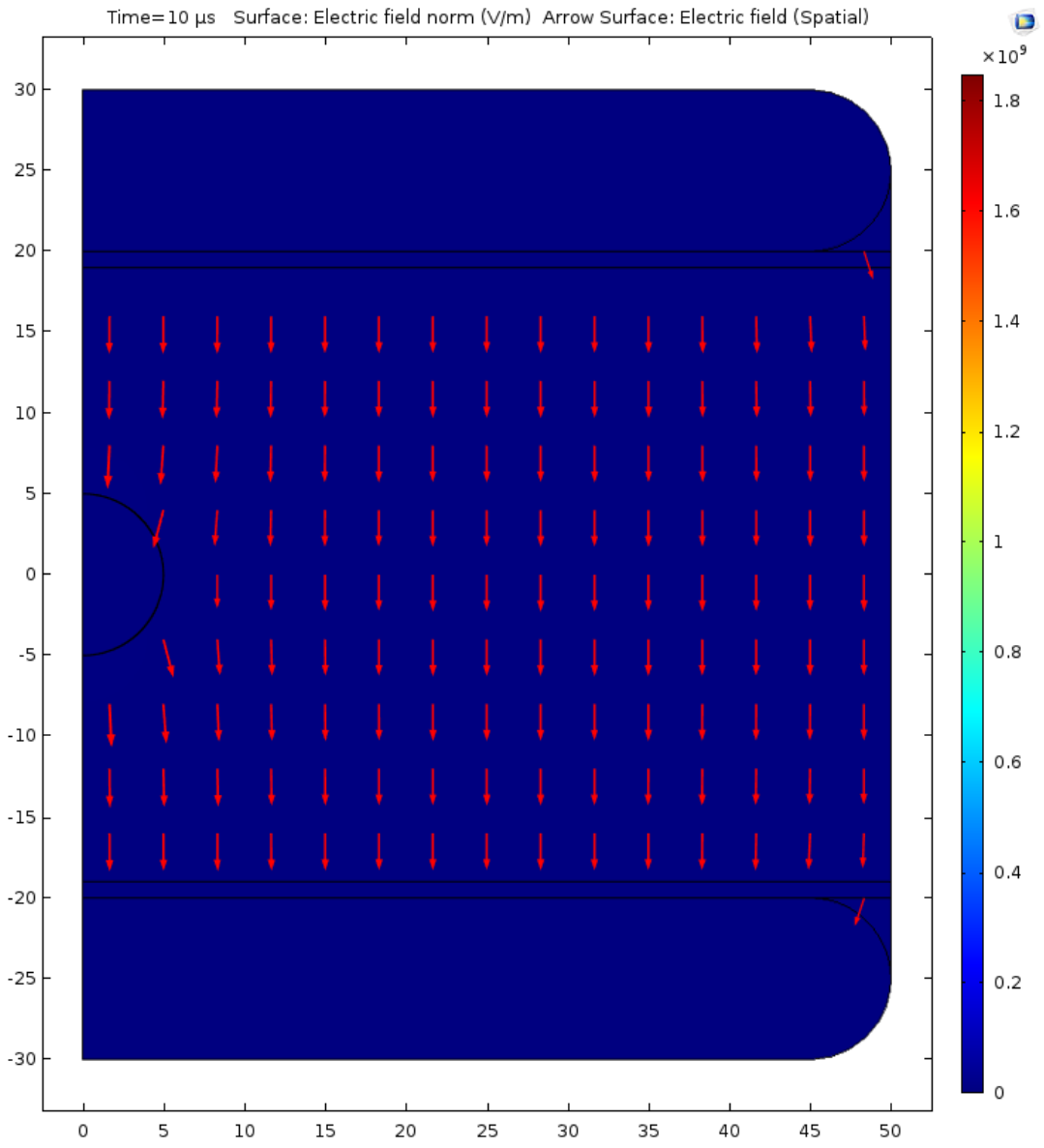

Figure (5.3) Electric field distribution in the treatment region at 10 µs. Horizontal and vertical axis show distance in units of µm.

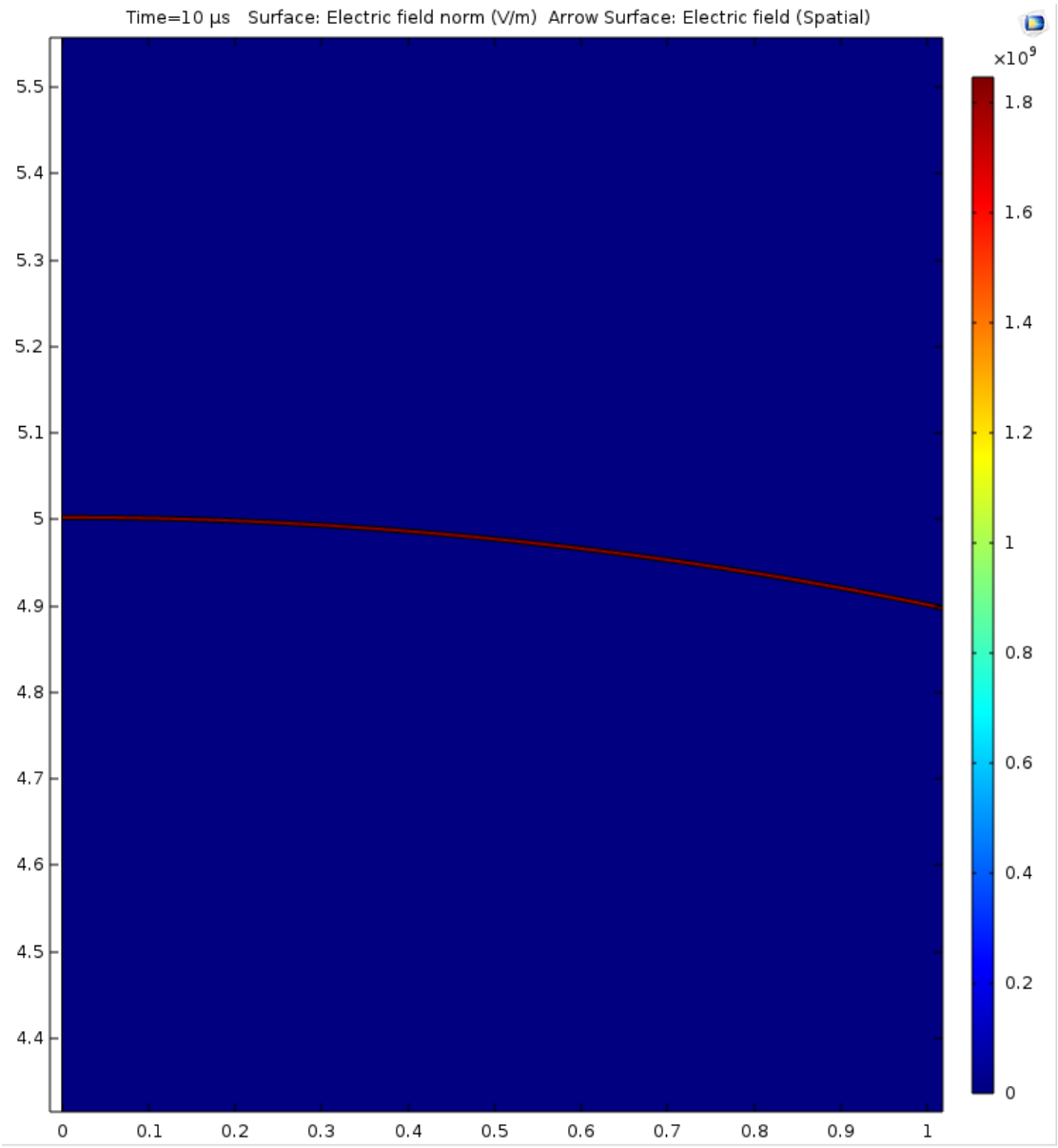

Figure (5.4) Zoomed in view of the electric field distribution across the membrane pole at 10 µs (transient analysis). Axis dimensions in µm.

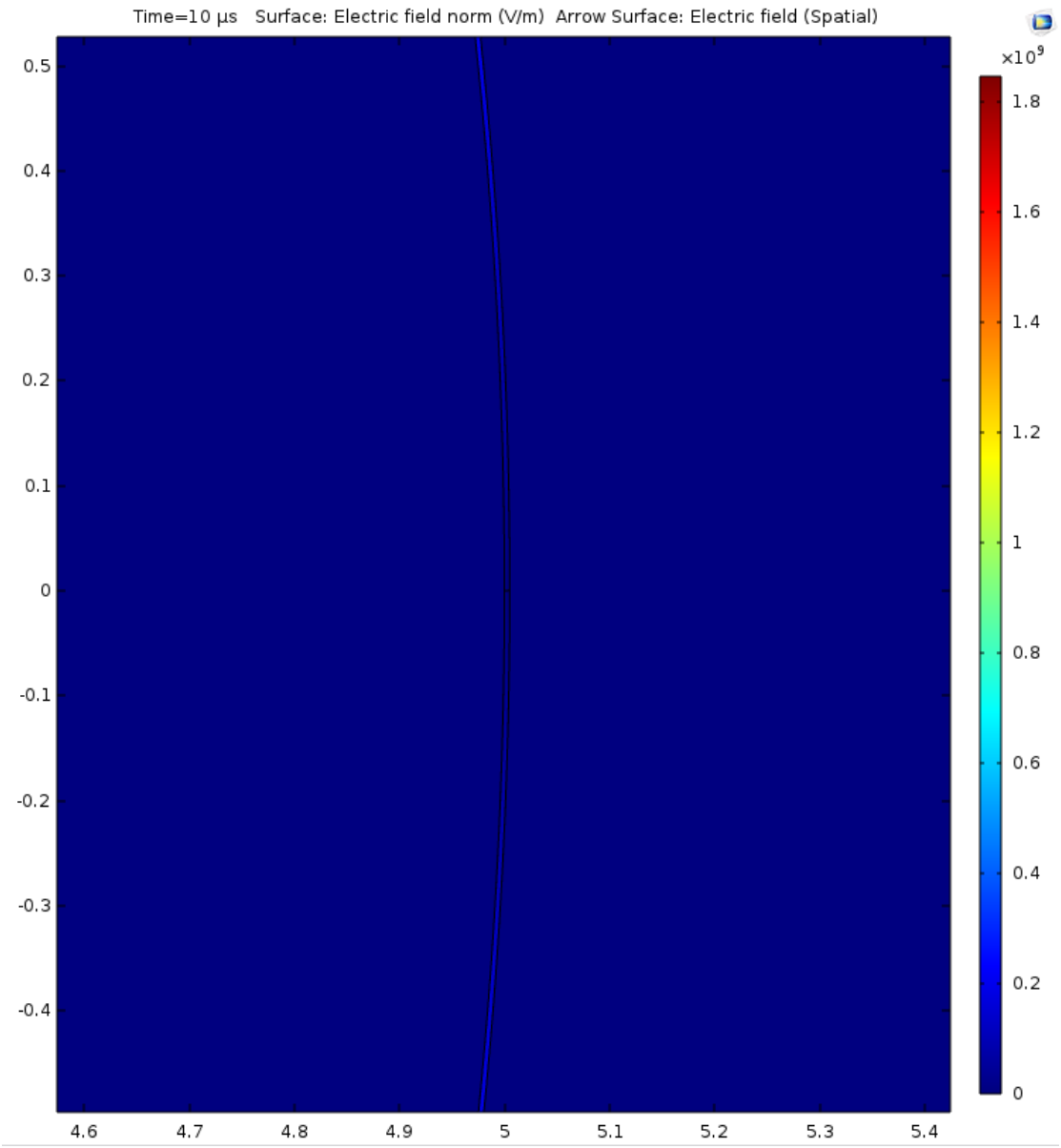

Figure (5.5) Zoomed in view of the electric field distribution across the membrane equator at 10 µs (transient analysis). Axis dimensions in µm.

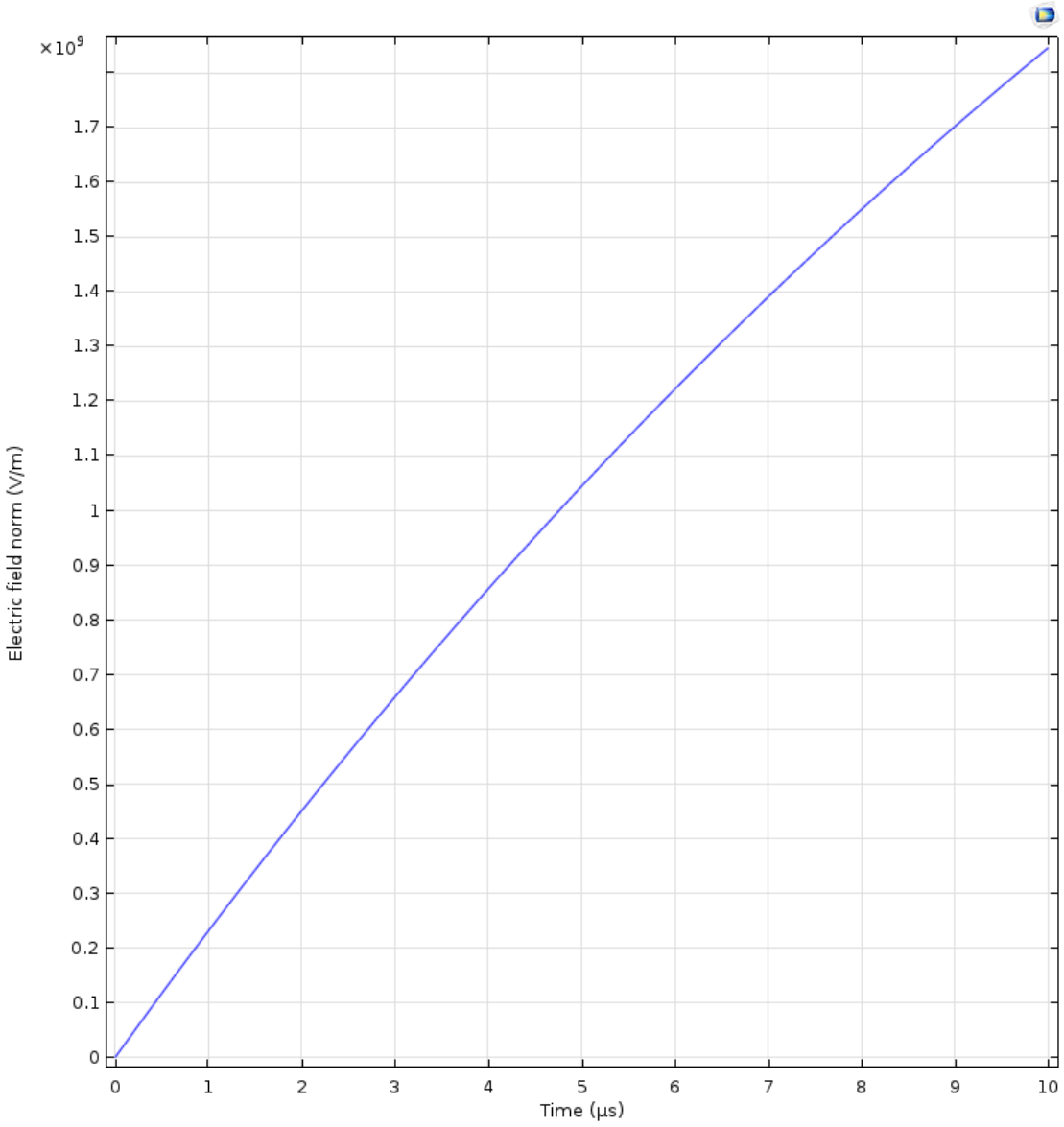

Figure (5.6) Transient electric field strength at the membrane's pole during the first 10 µs of the PEF treatment, single cell model, and applied field is 30 kV/cm.

The temperature distribution during the PEF treatment was also investigated using the COMSOL single cell model discussed in this section. **Table (5.2)** below introduces the thermal parameters used in the thermal analysis, the initial temperature is 20 °C.

Table 5.2 Thermal parameters, values taken from the sources listed.

Parameters	Environmental fluid	Cell membrane	Cytoplasm	Nuclear membrane	Nuclear
Heat capacity at constant pressure [J/(kg·K)]	4181.3 [320] [319]	3000 [320]	4181.3 [320] [319]	3000 [320]	4181.3 [320] [319]
Thermal conductivity [W/(m·K)]	0.61 [319] [122]	0.568 [319] [122]	0.61 [319] [122]	0.568 [319] [122]	0.61 [319] [122]
Density [kg/m^3]	998.2 [319]	1100 [319]	998.2 [319]	1100 [319]	998.2 [319]

Figure (5.7) shows the temperature distribution after 10 μs of PEF treatment, it can be seen that the temperature increase can be considered to be negligible (it is much less than 1 ℃ increase in 10 μs). The temperature distribution graph is necessary to be shown as it shows different positions of local heating effects even if the temperature differences are negligible. It important to investigate the details about local heating effects as a function of position, which has never been investigated before, because the local heating effects could help enhance the electroporation process, thus there might be positions where the membrane was damaged more seriously. Such temperature distribution results follow the results of the total heat source, as shown in **Figure (5.8)**, the maximum value of heat source was found to be $\sim 1.4 \times 10^{10}\ W/m^3$. Joule heating was considered as the heating source during the PEF treatment with DC impulses. The heat was mainly generated at the pole

positions outside the cell membrane as the charge accumulation process was not completed in 10 µs, due to the low conductivity of the environmental fluid. The electric field build up process, seen in **Figure (5.6)**, also supports this assumption. Compared with the steady state Quickfield model, the COMSOL model provided more detailed thermal distribution, as such changes in the local heating effect was not shown with the QuickField model.

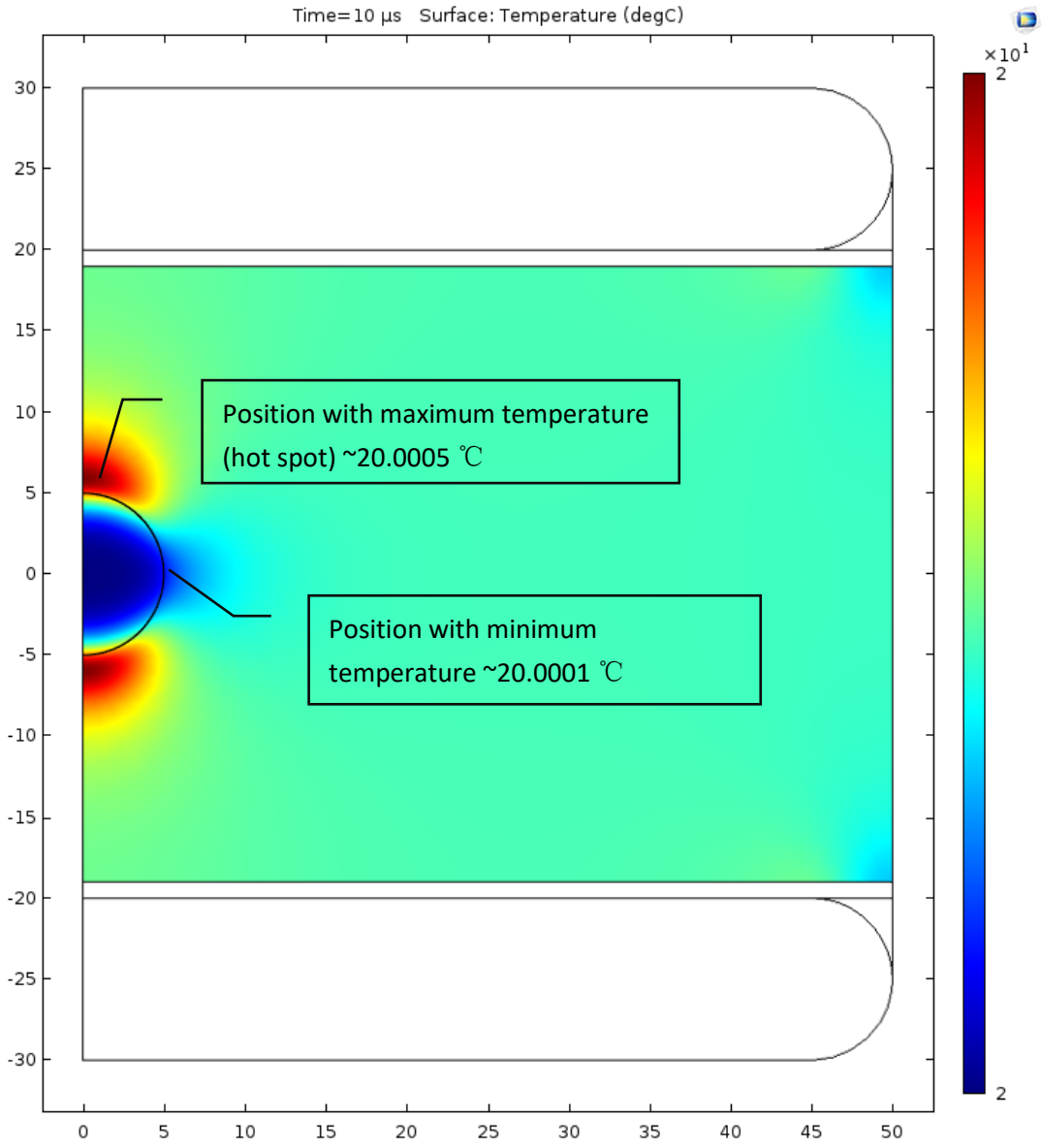

Figure (5.7) Temperature distribution in the single cell model at 10 µs. PEF treatment with an applied field magnitude of 30 kV/cm. Axis dimensions in µm.

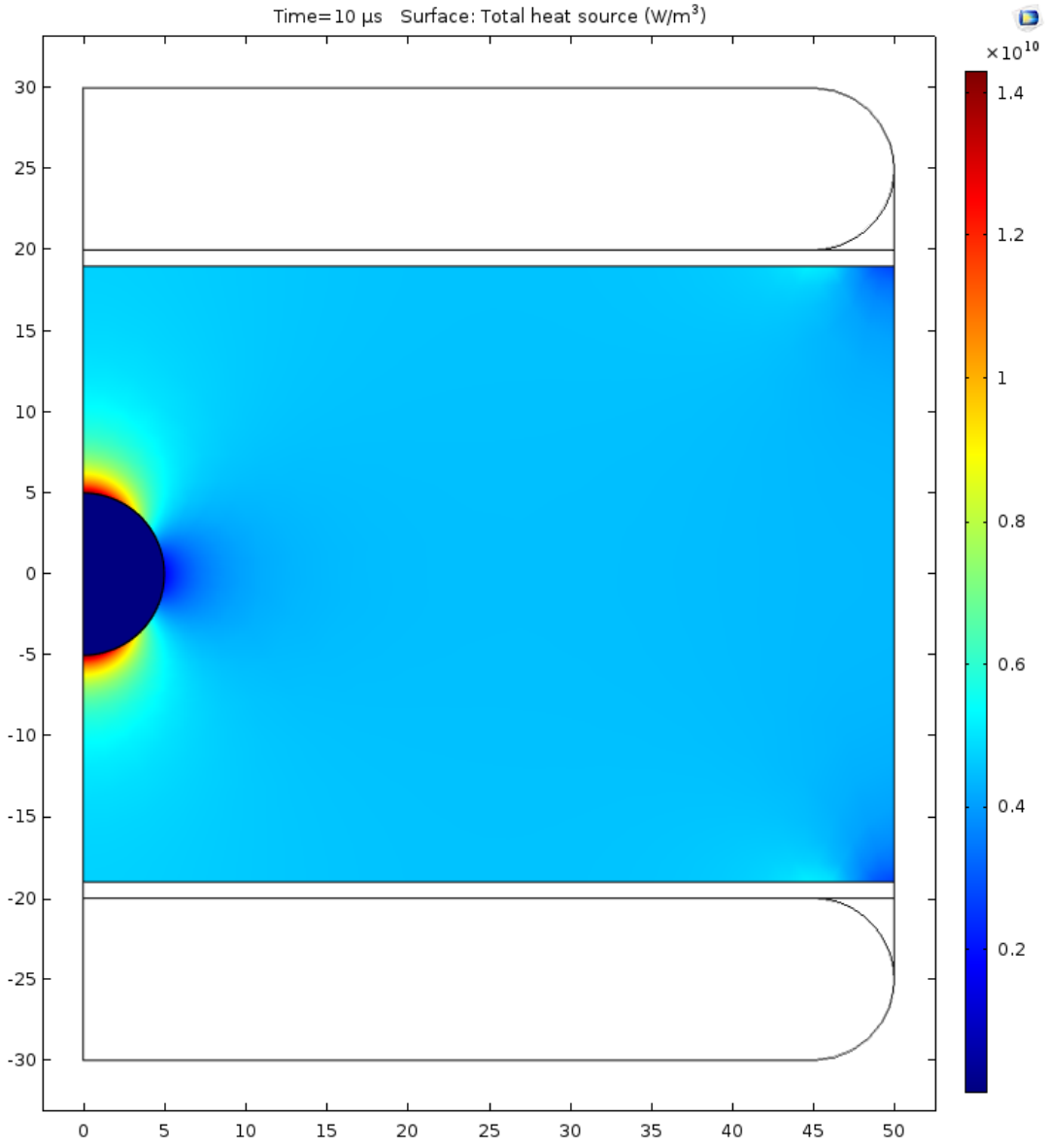

Figure (5.8) Total heat source in the initial single cell model at 10 µs. PEF treatment with 30 kV/cm. Axis dimensions in µm.

5.3 Simulation results and analyses of the single cell model with different parameters

In order to investigate the interactions between the external electric field and a single microorganism, different parameters were used in this modelling: different conductivity of environmental fluid (corresponding to different PEF treatment applications), electric field strengths higher than 30 kV/cm were also applied.

5.3.1 Results obtained with more conductive environmental fluid, 0.2 S/m

As discussed in Chapter 3, in paper [298], the conductivity of the liquid suspension was set to be from 0.17 to 0.2 S/m. The value of 0.2 S/m was used in this analysis compared to 0.5×10^{-3} S/m used previously, and the electric field strength was set to 30 kV/cm. Such high conductivity of environmental fluid and electric field strength was used in other research published in [298] to investigate the lipid bio-accessibility in *Chlorella vulgaris*, 30 kV/cm is generally used in electroporation works. It would be beneficial to investigate the electrical field distribution and local heating effects under these conditions because investigation about electrical field strength in the cell membrane and local heating effects could help explain the interactions between microorganisms and external electric field for general electroporation applications.

Figures (5.9)- (5.11) show the electric field distribution during 30 kV/cm PEF treatment in environmental fluid with higher conductivity of 0.2 S/m. Compared with the simulation results with lower conductivity fluid in **Figure (5.3)**, the maximum electric field strength in the pole obtained in this case was 2 times higher, $\sim 4 \times 10^9\ V/m$ at 10 µs, the electric field strength in the equator was ~30 kV/cm.

Figure (5.12) shows the electric field strength build up process at the pole of the membrane during first 10 µs of PEF treatment. It can be seen that the electric field strength reached the peak value at about 1 µs. Due to the higher conductivity of the environmental fluid, the charge accumulation process could be completed quicker compared with the lower conductivity fluid.

The temperature distribution is shown in **Figure (5.13).** Firstly, there is significant local heating on the equator, in the environmental fluid outside of the cell membrane, which follows the simulation results obtained using the Quickfield model. Secondly, the position of this elevated temperature region has changed

from the pole to the equator, because the charge accumulation process in the environmental fluid has been completed, and the maximum conduction current in the environmental fluid is reached at the equator in this case. Although the temperature increases by about 5 ℃ in 10 μs, and this local heating could be neglected (unlikely to impact electroporation), over longer treatment time such local heating effects could be strong enough to accelerate the electroporation process in the membrane.

Figure (5.14) shows that there was significant heat release (joule heating) ($\sim 4 \times 10^{12}\ W/m^3$) at the equator in the environmental fluid outside of the cell membrane.

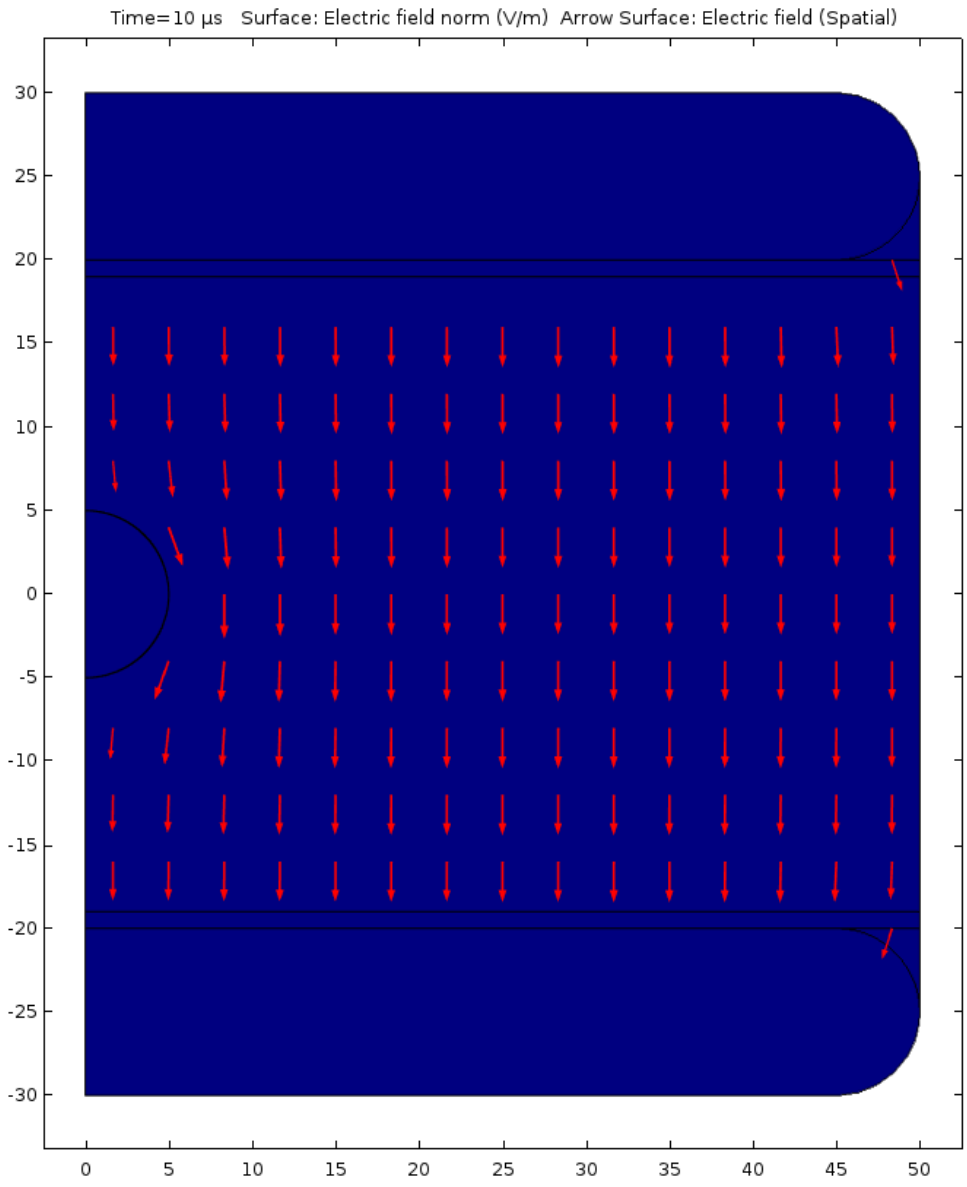

Figure (5.9) Electric field distribution in the transient analysis at 10 µs; higher conductivity environmental fluid of 0.2 S/m. Axis dimensions in µm.

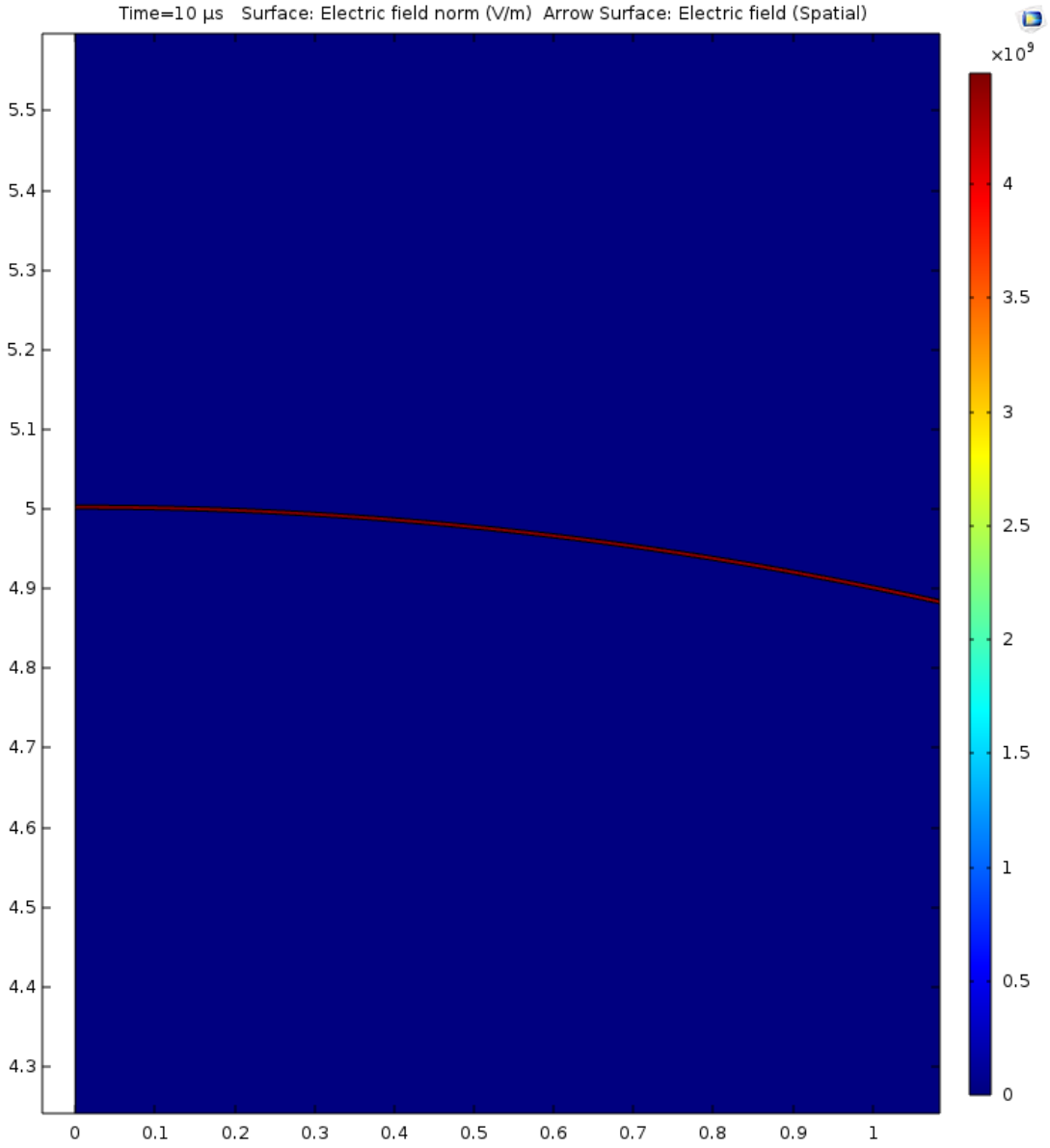

Figure (5.10) Zoomed in view of Electric field distribution in the transient analysis at 10 µs (at the membrane's pole). Higher conductive environmental fluid of 0.2 S/m. Axis dimensions in µm.

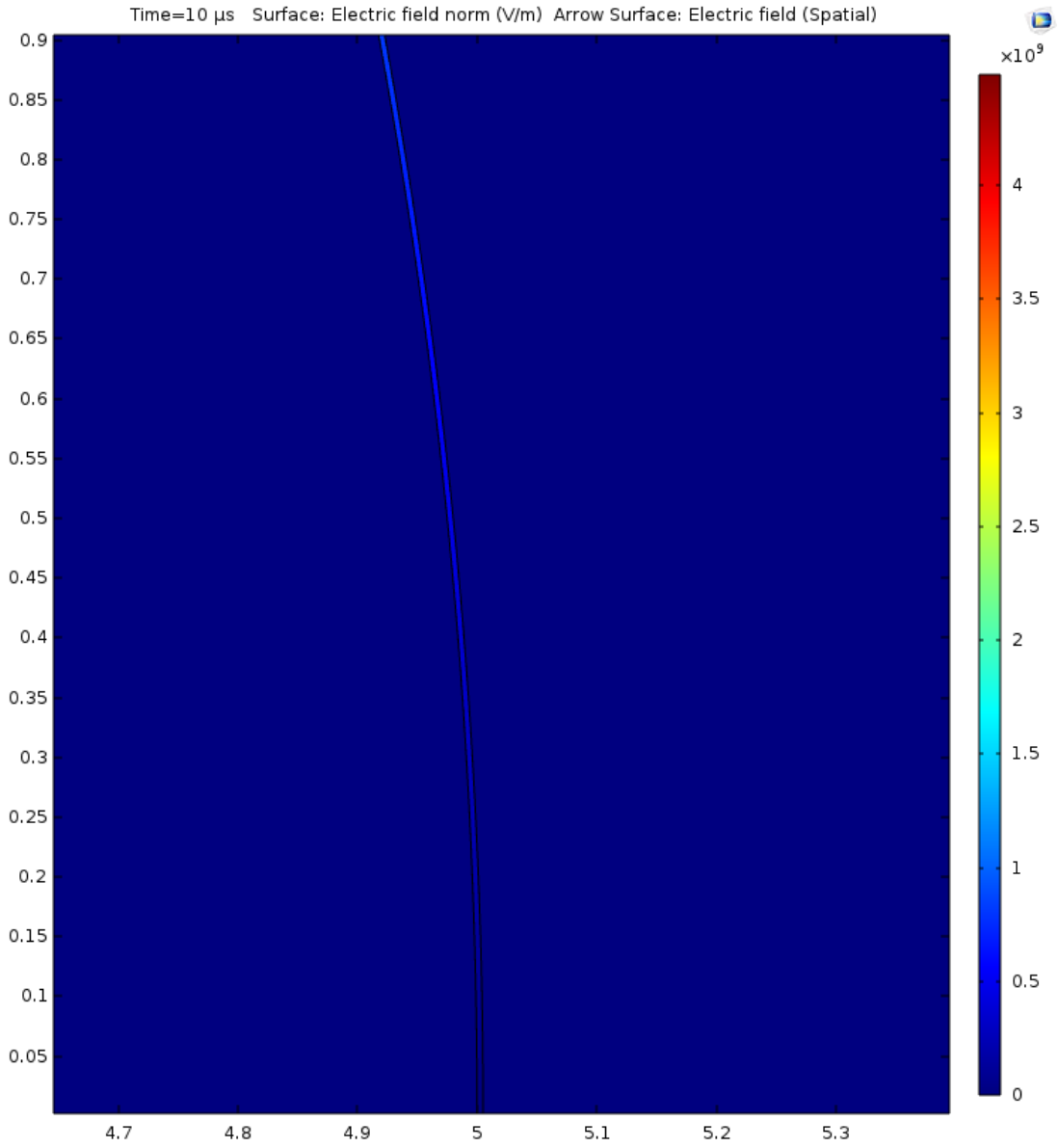

Figure (5.11) Zoomed in view of the electric field distribution in the transient analysis at 10 µs (at the equator), higher conductivity environmental fluid (0.2 S/m). Axis dimensions in µm.

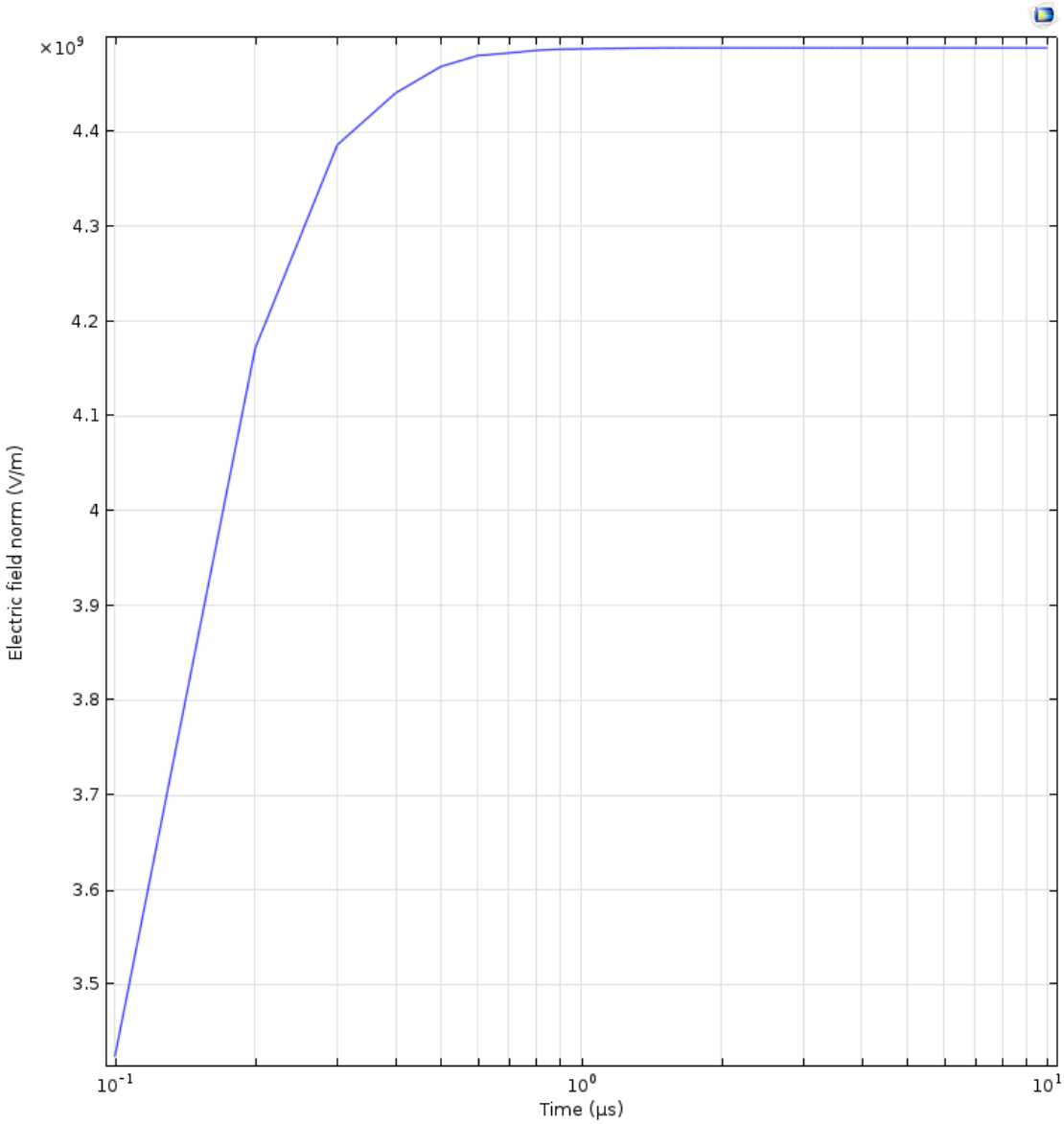

Figure (5.12) Electric field strength at the pole during 10 µs after application of the PEF impulse. Single cell model, 30 kV/cm applied electric field strength.

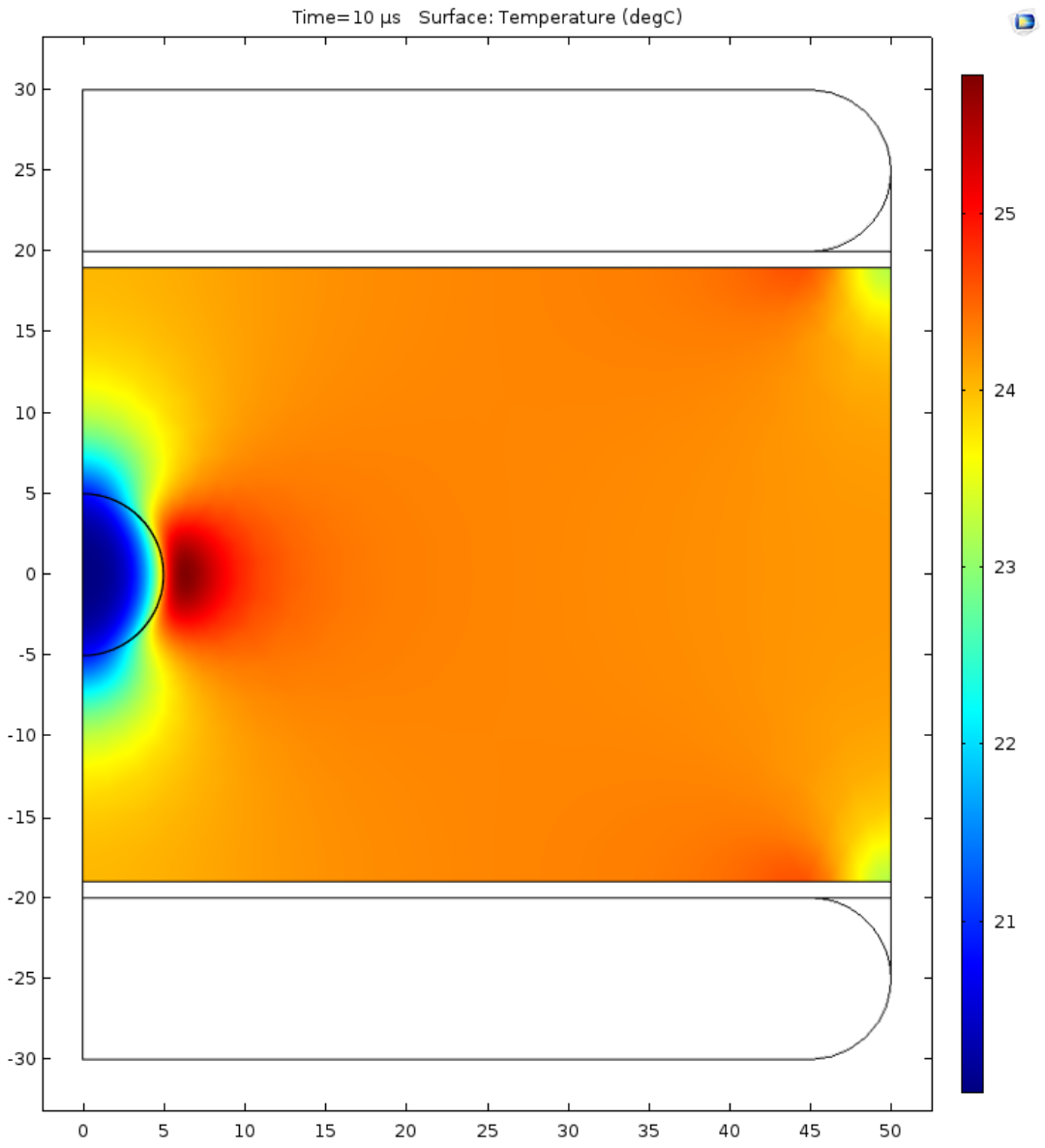

Figure (5.13) Temperature distribution in the initial single cell model at 10 µs PEF treatment, 30 kV/cm applied electric field strength, higher conductivity environmental fluid (0.2 S/m). Axis dimensions in µm.

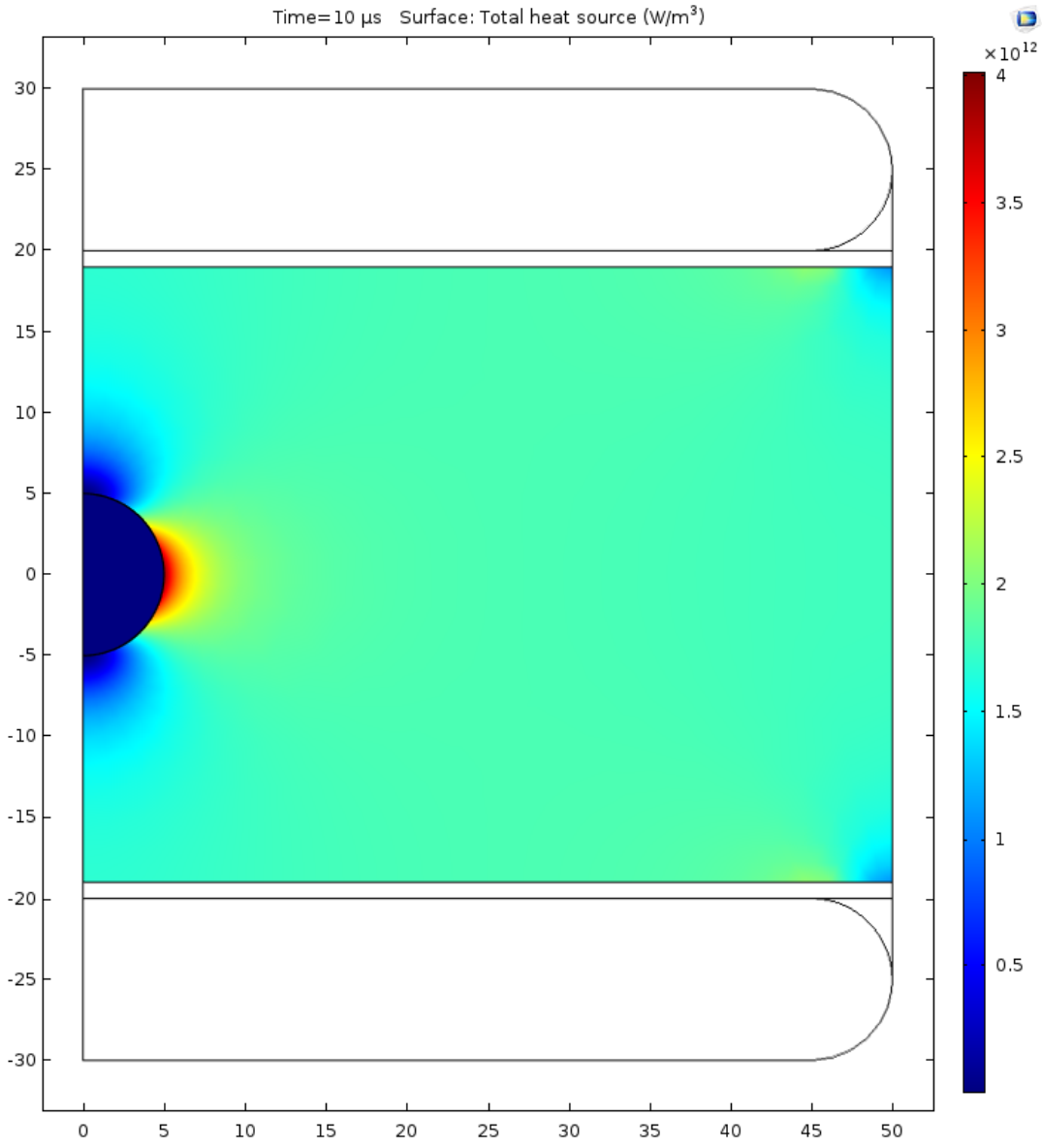

Figure (5.14) Total heat release (source) in the single cell model at 10 µs. PEF treatment with 30 kV/cm in higher conductivity environmental fluid (0.2 S/m). Axis dimensions in µm.

5.3.2 Results for electric field strength of 67 kV/cm

It has been shown in section 5.3.1 that the conductivity of the environmental fluid provides significant influence on the local heating effects in the environmental fluid during the PEF treatment. The conductivity of the environmental fluid could be

controlled in order to meet different treatment requirements. The external electric field strength could also be controlled, and in this section a higher electric field strength will be used to model the PEF treatment.

According to [181], the field strength of 67 kV/cm was used in the experimental PEF treatment of microorganisms. Following this work, the average electric field strength used in this section was 67 kV/cm, the conductivity of environmental fluid in this simulation is 0.5×10^{-3} S/m.

Figures (5.15)- (5.17) show the electric field strength distribution at 10 μs, with 67 kV/cm electric field applied. The electric field strength in the cell membrane follows the Schwan Equation. Compared with the lower field strength treatment (30 kV/cm), **Figure (5.3)- Figure (5.5)**, the electric field strength at the pole increases from $\sim 1.8 \times 10^{9}\ V/m$ to $\sim 4 \times 10^{9}\ V/m$ in 10 μs, in both cases, and the transmembrane potential reaches the electroporation threshold of ~ 1 V. The electric field strength in equator is 30 kV/cm and 67 kV/cm. However, the charge accumulation process during the 67 kV/cm field pulse was also not completed in 10 μs, as shown in **Figure (5.18)** and **Figure (5.6)**.

The thermal effects are shown in **Figure (5.19).** As compared with the result obtained for lower field strength (30 kV/cm), using the same conductivity the positions of local heated regions are the same. The temperature increases were minimal compared with the results shown in **Figure (5. 7)**. This result can also be confirmed by the heating source graphs, comparing **Figure (5.20)** and **Figure (5.8)**.

However, comparing the simulation results with the results obtained using the high conductivity environmental fluid in **section 5.3.1**, it could be noted that the conductivity of the environmental fluid has more significant effects on the electric field build up process (**Figure (5.6)** and **Figure (5.18)**) and thermal effects (**Figure (5.7)** and **Figure (5. 19)**) during the PEF treatment. The maximum heat release increased from $\sim 7 \times 10^{10}\ W/m^3$ to $\sim 4 \times 10^{12}\ W/m^3$ with the higher conductivity

environmental fluid (0.2 S/m) and lower electric field strength (30 kV/cm). So, in order to achieve the minimum thermal effects during the PEF treatment, it is important to use an optimized conductivity of the environmental fluid during the PEF treatment. Compared with the induced transmembrane potential in the cell membrane, the contribution of thermal effects during 10 μs PEF treatment could be negligible according to the simulation results with the lower conductivity environmental fluid.

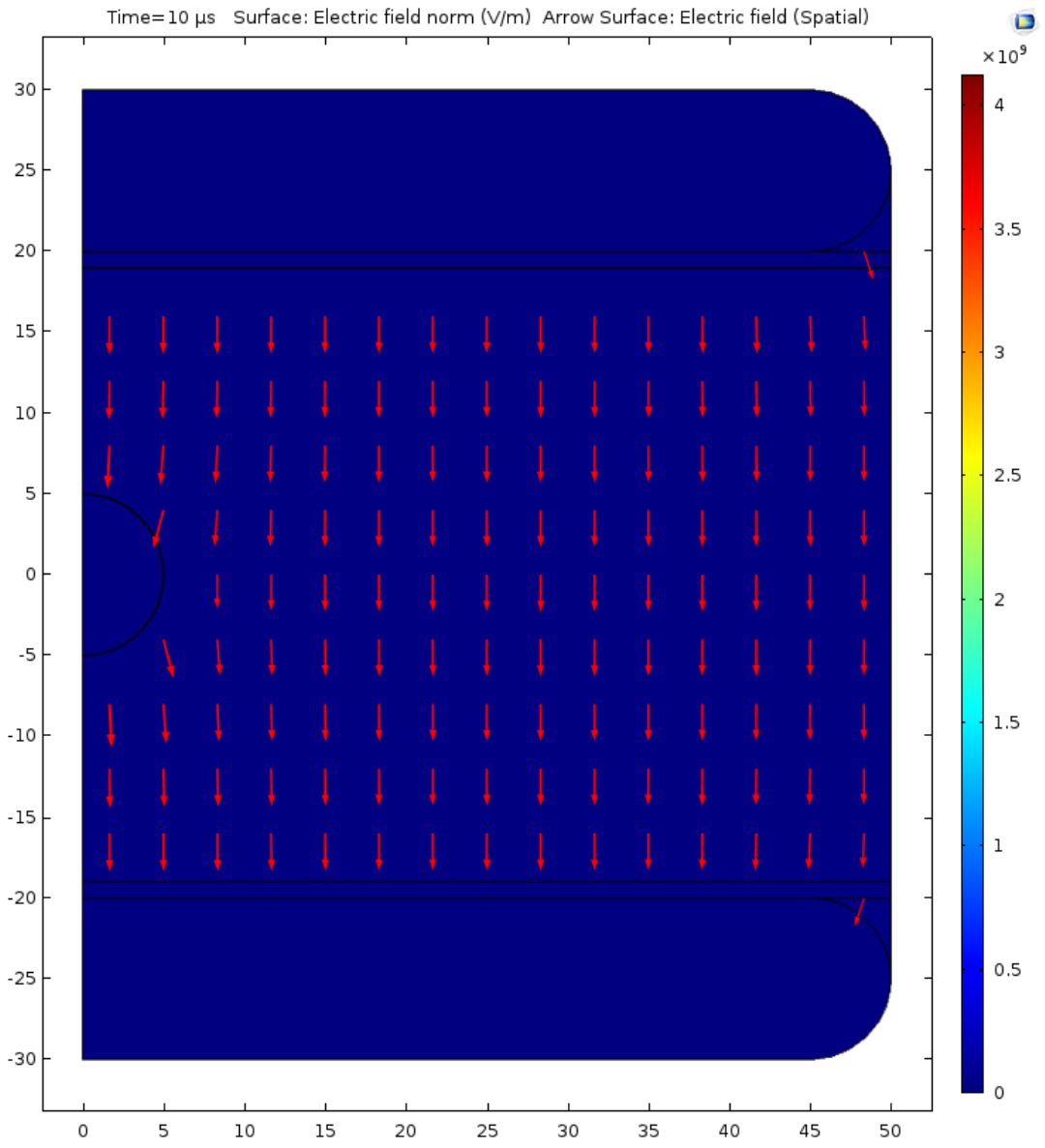

Figure (5.15) Electric field distribution in the transient analysis at 10 µs with higher, 67 kV/cm, applied electric field strength. Axis dimensions in µm.

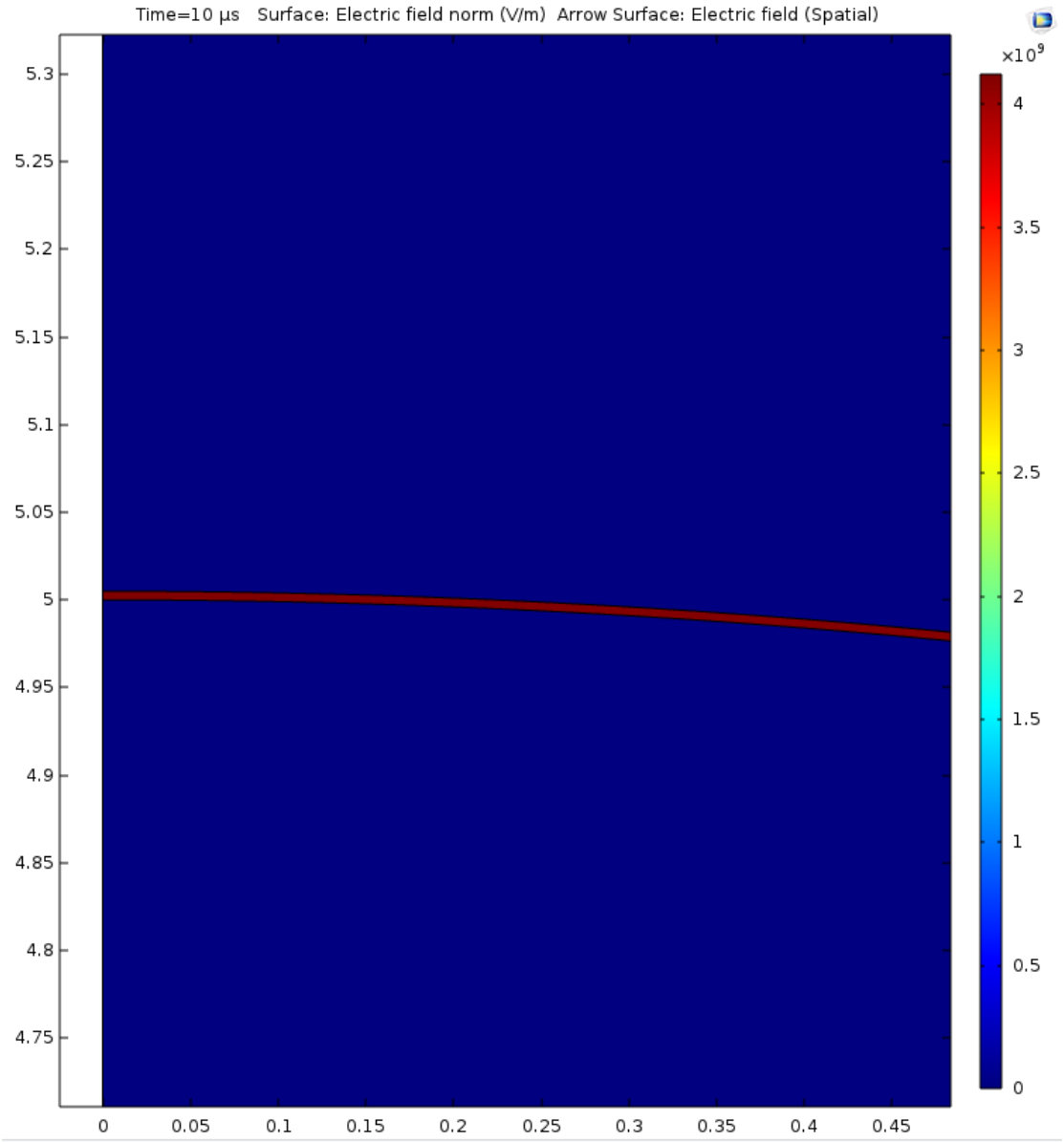

Figure (5.16) Zoomed in view of the Electric field distribution at the membrane pole in the transient analysis at 10 µs; applied electric field is 67 kV/cm). Axis dimensions in µm.

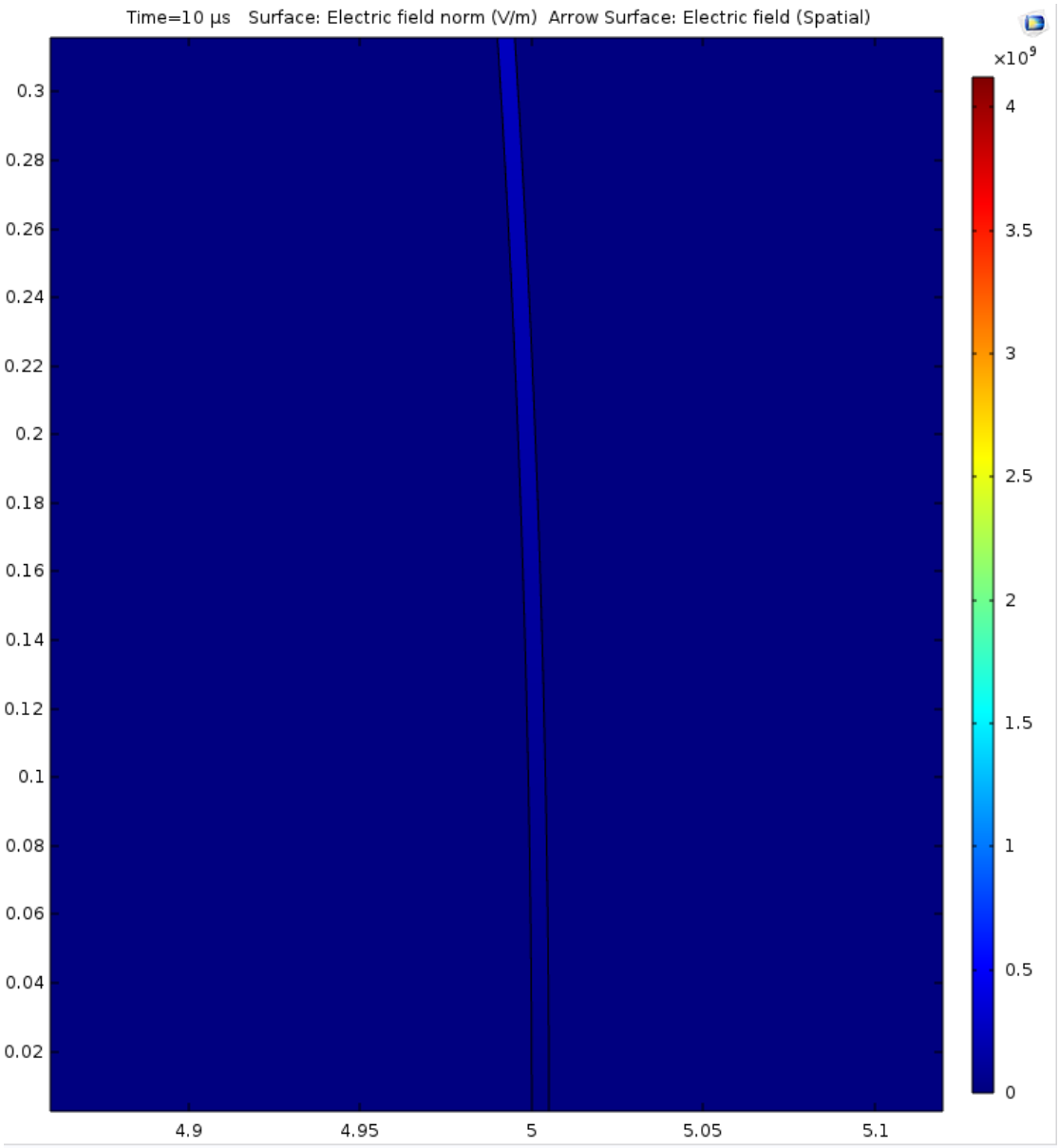

Figure (5.17) Zoomed in view of the Electric field distribution at the membrane's equator in the transient analysis at 10 µs; applied cm electric field is 67 kV/ (). Axis dimensions in µm.

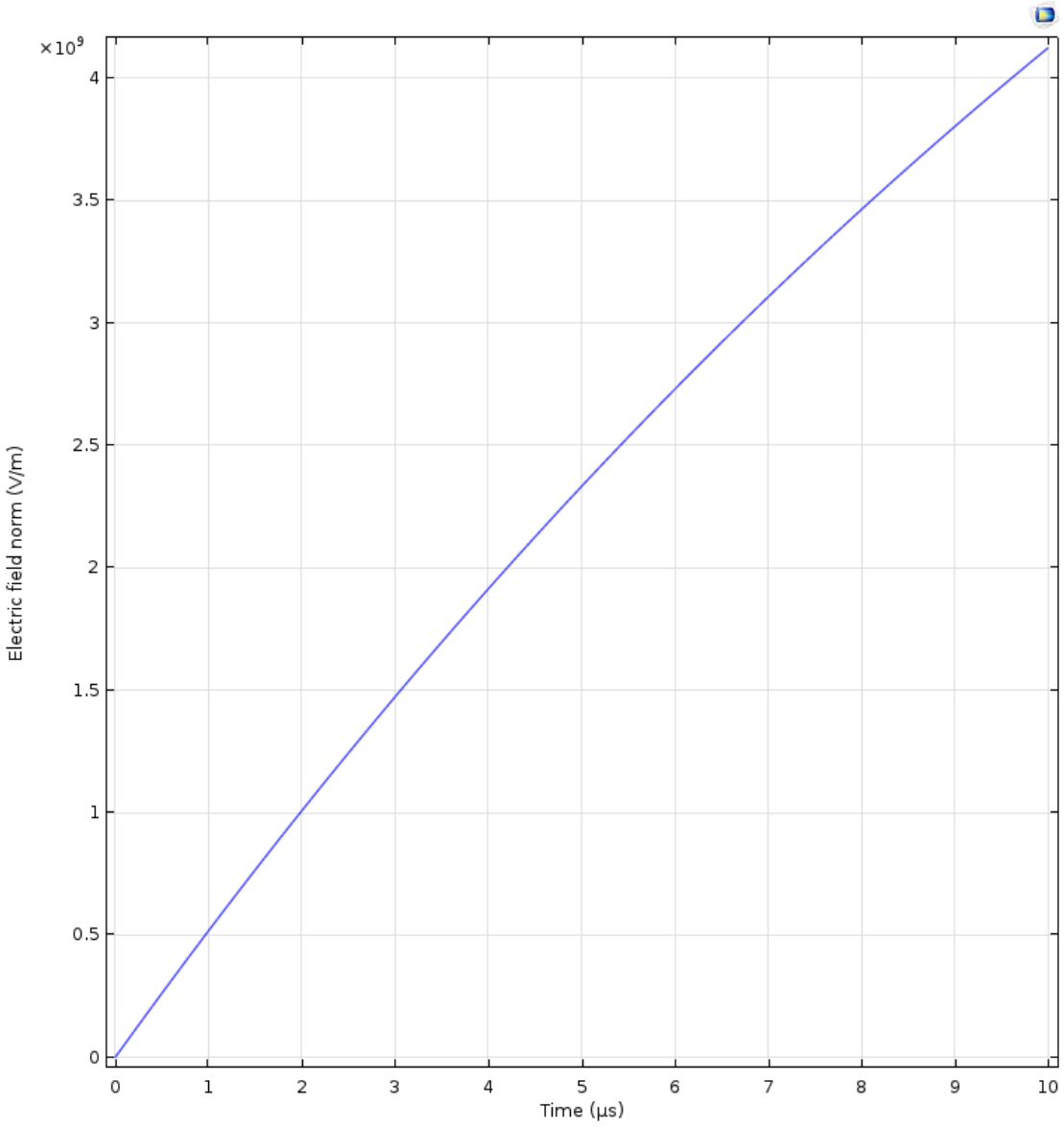

Figure (5.18) Electric field strength at the pole during 10 µs. PEF treatment of single cell applied electric field strength is 67 kV/cm.

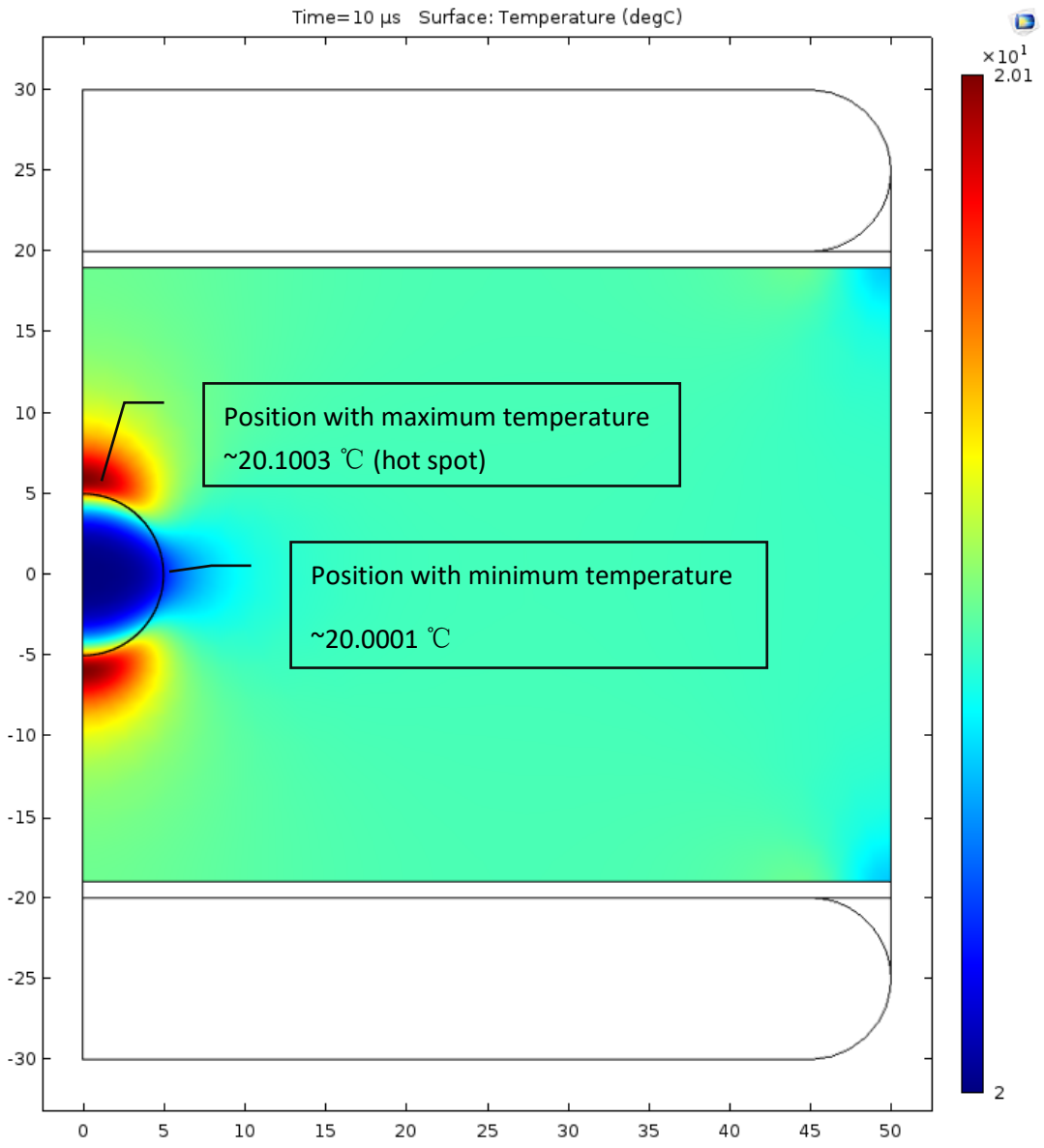

Figure (5.19) Temperature distribution in the initial single cell model at 10 µs. PEF treatment with 67 kV/cm. Axis dimensions in µm.

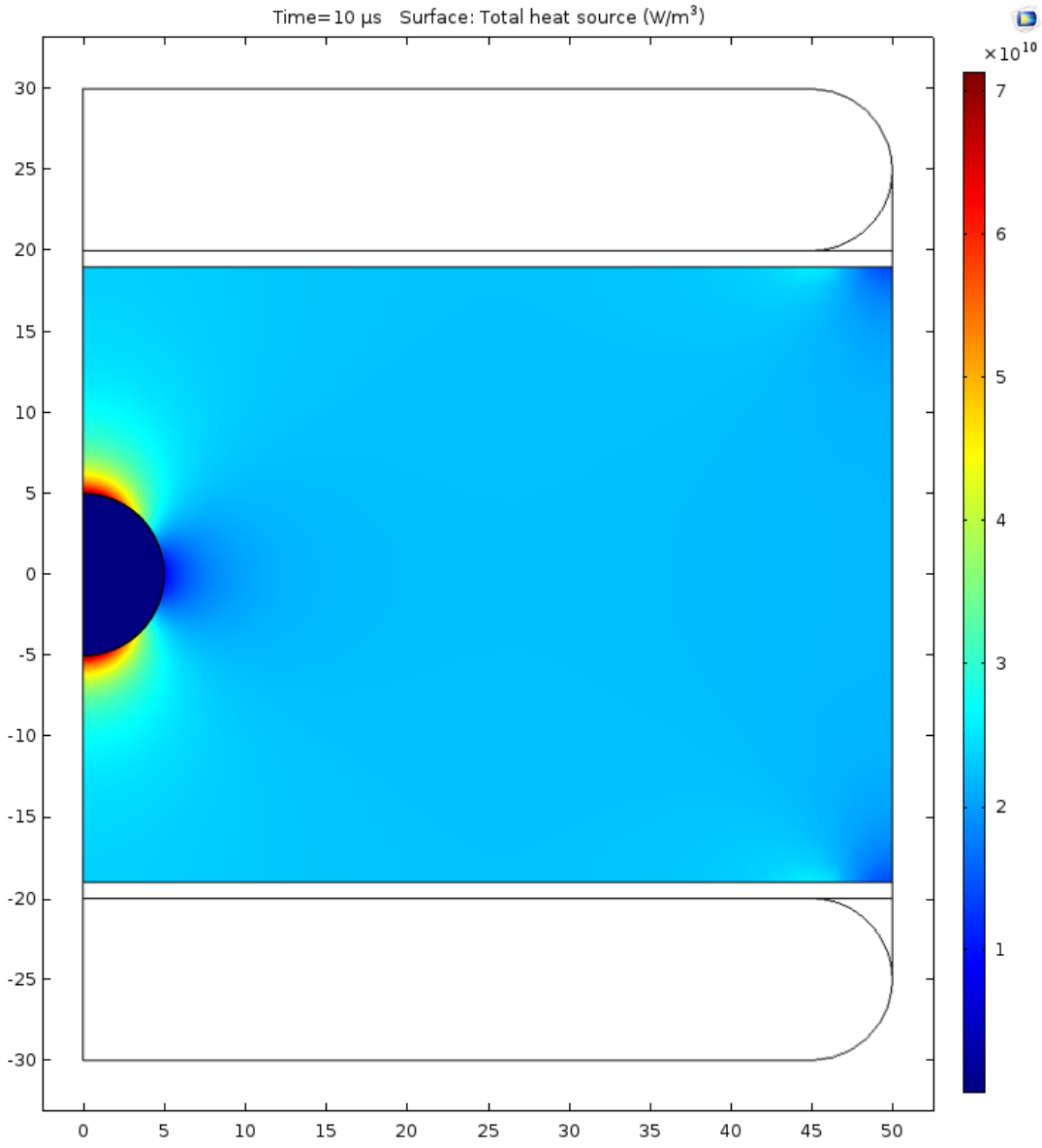

Figure (5.20) Total heat release (source) in the initial single cell model at 10 µs. PEF treatment with 67 kV/cm. Axis dimensions in µm.

5.3.3 Results for different treatment time-long-time treatment-200 µs treatment time

The simulation results presented in section 5.2 and section 5.3.2 show that, in the case of low conductivity environmental fluid, the electric field build up process could not be completed in 10 µs. Thus, it is necessary to investigate the complete

transient process and to obtain the electric field strength in the membrane after saturation. To complete this task, a longer treatment time was used in this section, and both 30 kV/cm and 67 kV/cm field strengths were applied.

Figures (5.21) and **(5.22)** show the results of the 30 kV/cm PEF treatment and the conductivity of environmental fluid is 0.5×10^{-3} S/m It is shown that the electric field strength build up process was completed at ~ 100 μs, and the peak electric field strength in the membrane is $\sim 4 \times 10^{9}\ V/m$, which is close to the results shown in **Figure (5.12)**, where the maximum field was $\sim 4.4 \times 10^{9}\ V/m$ and the conductivity of environmental fluid is 0.2 S/m. The conductivity of the environmental fluid does not have a significant effect on the maximum electric field strength in the cell membrane during the PEF treatment, but it could influence the time required for the field magnitude to reach its peak value, **Figure (5.21**) and **Figure (5.23)**. This
also confirms the results obtained using the linear model: the maximum electric field strength across the cell membrane was mainly influenced by the electric field strength applied between the electrodes, and the thickness of the cell membrane.

The positions of the local hot spots in the environmental fluid were observed to change during 200 μs PEF treatment, which is demonstrated by comparing **Figure (5.22)**, **Figure (5.24), Figure (5.19)** and **Figure (5.7)**. It could be stated that, once the charge accumulation process is completed, the local hot spots moved from the pole to the equator. However, there is no significant temperature increase in such local hot spots, due to the low conductivity of the environmental fluid.

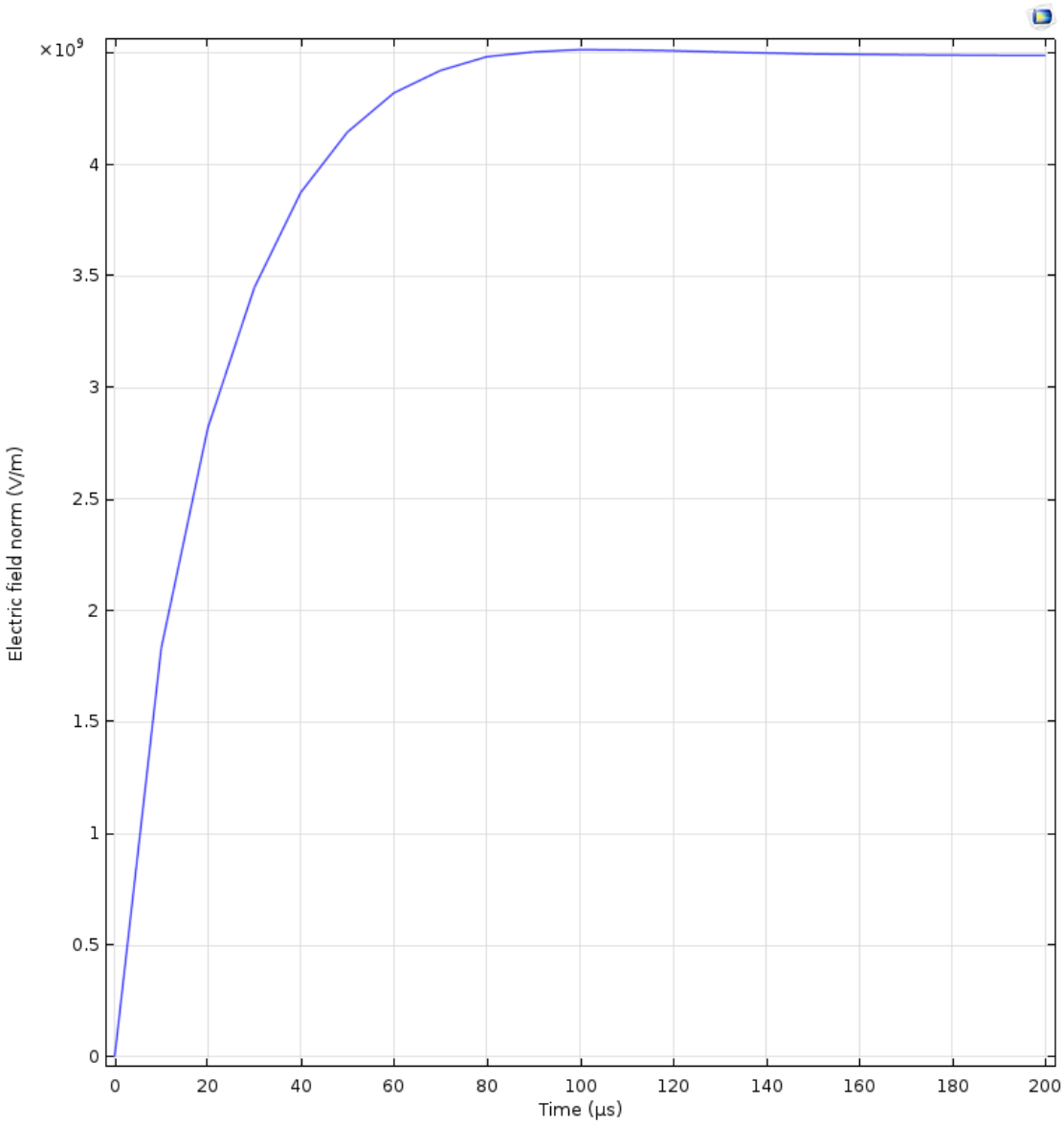

Figure (5.21) Electric field strength at the pole during 200 µs PEF treatment. Single cell model, applied field is 30 kV/cm.

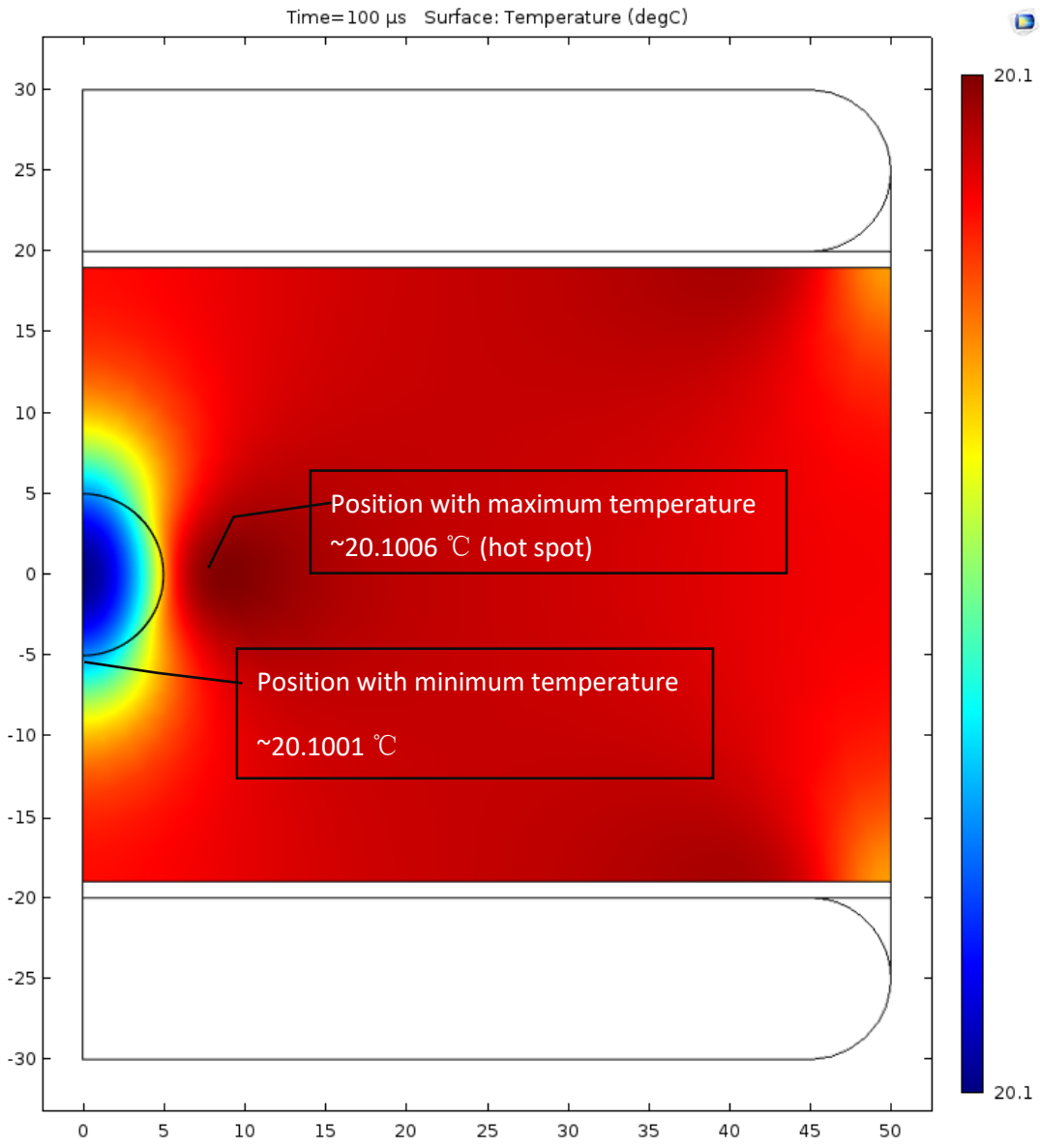

Figure (5.22) Temperature distribution in the single cell model at 100 µs. PEF treatment with 30 kV/cm. Axis dimensions in µm.

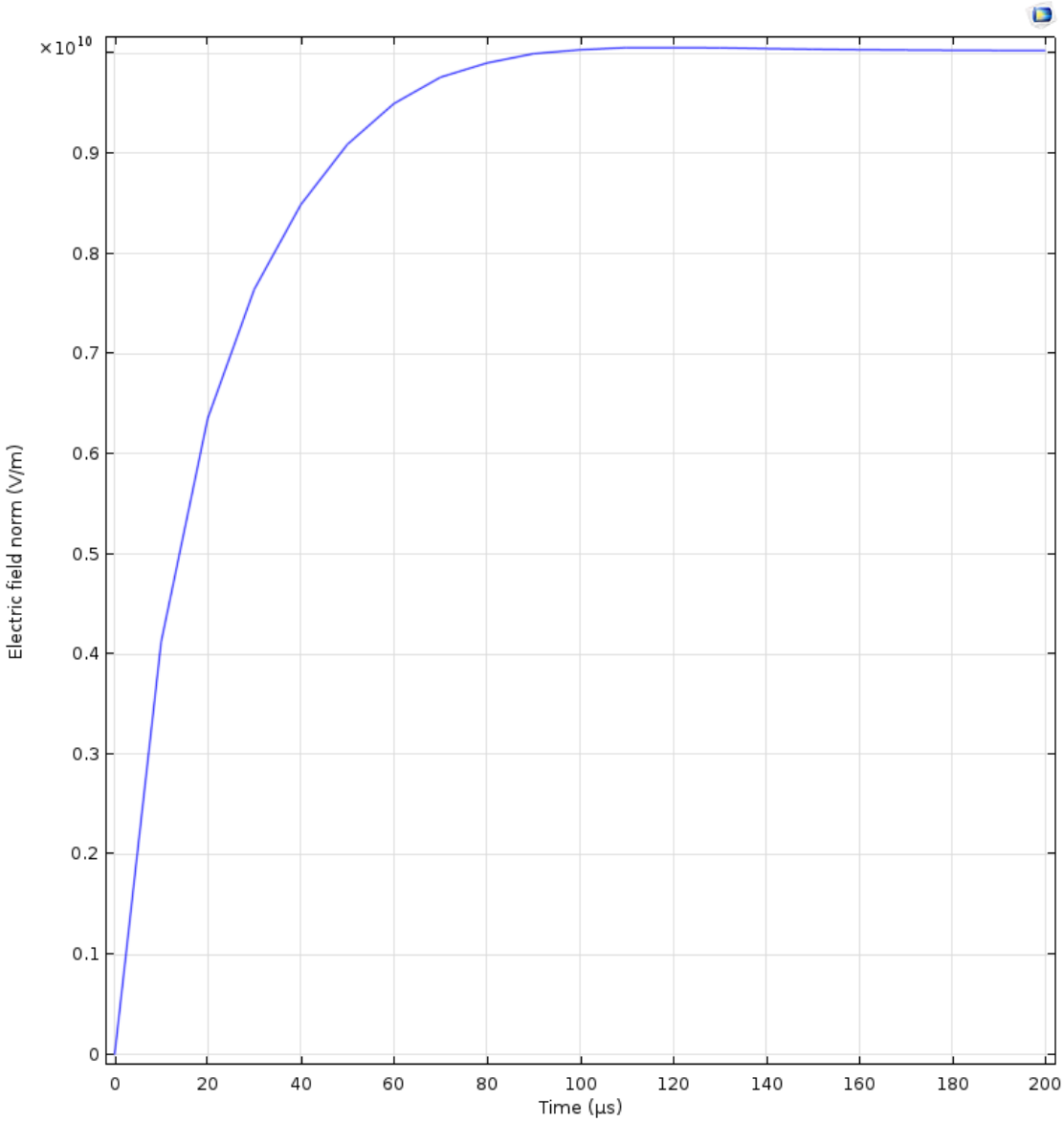

Figure (5.23) Electric field strength at the pole during 200 µs. PEF treatment in the single cell model, applied field is 67 kV/cm.

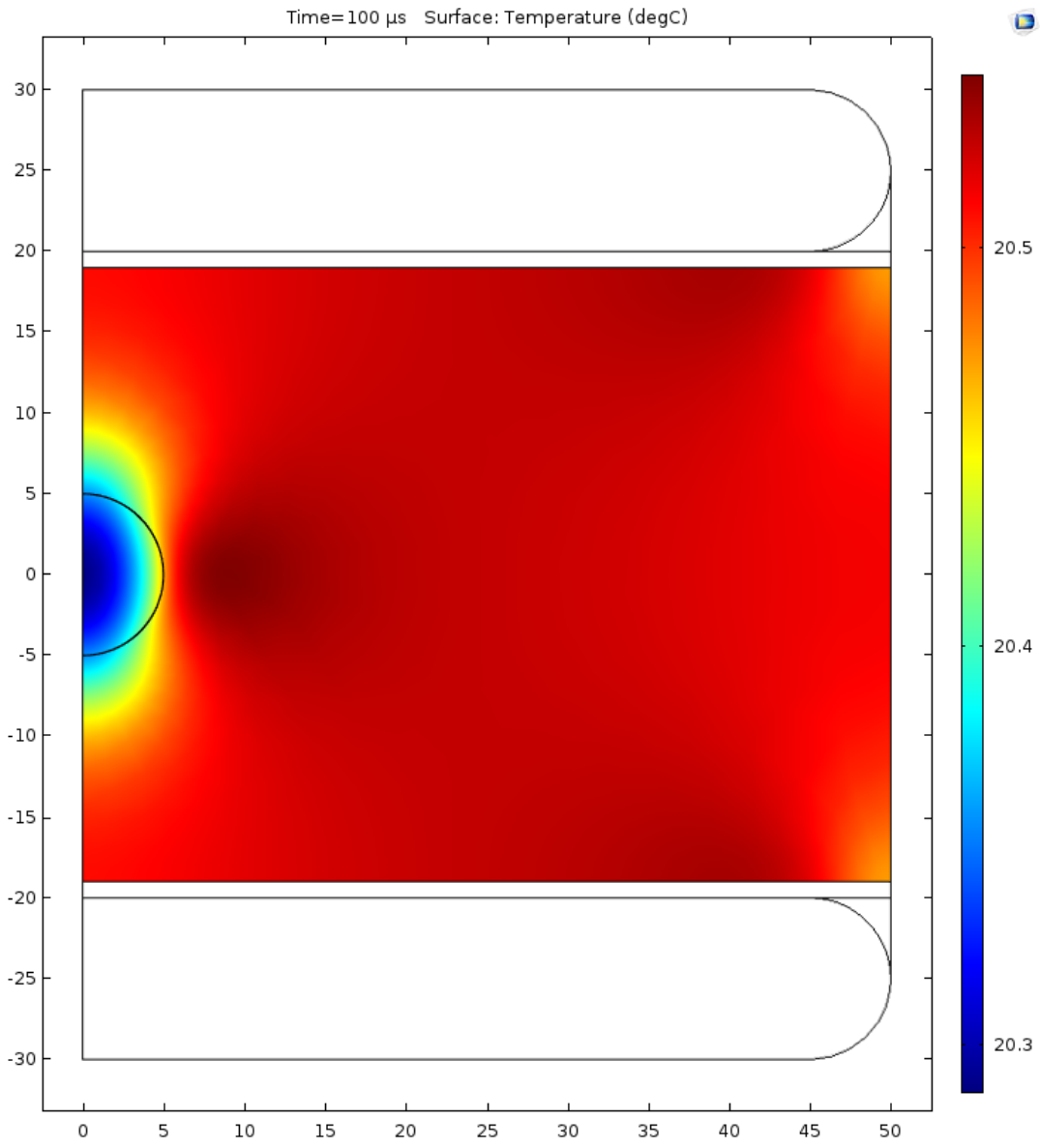

Figure (5.24) Temperature distribution in the initial single cell model at 100 µs. PEF treatment, applied field is 67 kV/cm. Axis dimensions in µm.

5.4 Forces across bio-membrane under DC impulses

The electric field strength in the cell membrane and local heating effects during the PEF treatment have been investigated in previous sections. However, due to the charge accumulated during the PEF treatment, there would be electro-mechanical forces acting on the cell membrane. Furthermore, as it was confirmed that the local

heating effects exist during the PEF treatment, the thermal forces also could help lead to membrane damage if the local temperature becomes sufficiently high. The electro-mechanical and thermal forces will be investigated in this section. Any potential effects associated with the magnetic field were not considered in this analysis.

Figure (5.25) shows a schematic diagram of the single cell model. The cell membrane was divided into two parts to calculate the electro-mechanical forces in the cell membrane. The electro-mechanical forces were generated due to the unbalanced Maxwell stresses in the dielectric cell membrane, which could promote deformation of the membrane, and even lead to membrane damage. The electro-mechanical force acting upon the upper part of the cell membrane will be investigated in this section (equal force will be acting upon the lower part of the membrane). The red arrows represent the force acting upon the cell membrane, due to the difference between the radii of the inner and outer interfaces. This difference leads to a total force acting upon the cell membrane [108] [321].

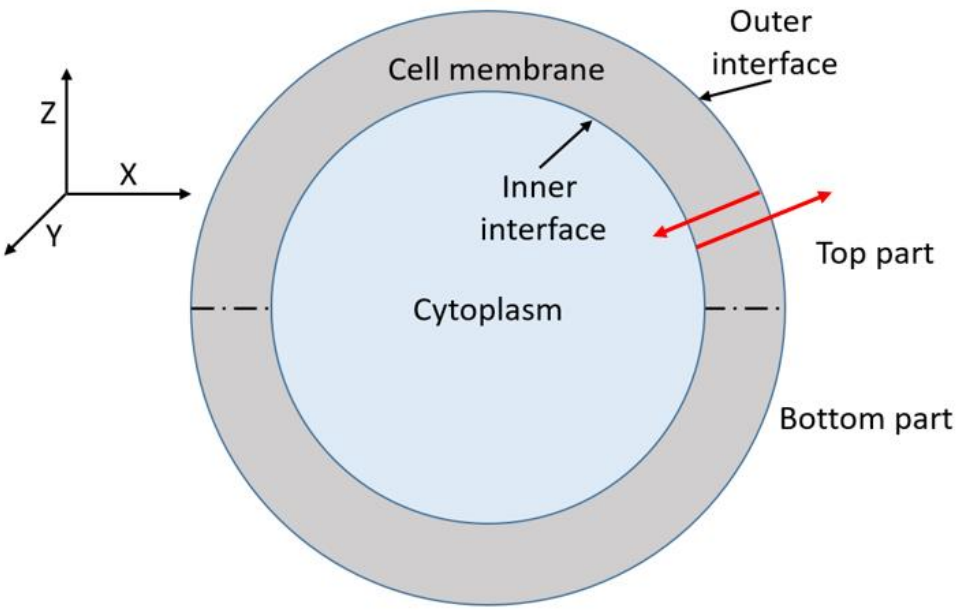

Figure (5.25) Simplified figure illustrating calculation of the electro-mechanical forces acting upon the cell membrane.

5.4.1 Electro-mechanical force in the cell membrane

The parameters used in investigating the electro-mechanical force are listed in the **Table 5.3**.

Table 5.3 Different parameters used in investigation of the electro-mechanical force in cell membrane.

Electric field strength (kV/cm)	**Conductivity of environmental fluid (S/m)**
30	0.0005 [319]
30	0.2 [319]
67	0.0005 [319]
67	0.2 [319]

Figure (5.26) shows the electro-mechanical force acting upon the upper part of the cell membrane during the 10 μs PEF treatment, with field strength 30kV/cm and conductivity of fluid 0.0005 S/m. It can be seen that, during the first 300-400 ns after application of the field, the force increases at a relatively slow rate, and this rate increases significantly after 1 μs (approximately). This functional behaviour follows the charge accumulation process. At the first stage, the charge accumulation only occurs in the cytoplasm (inner membrane interface), due to its high conductivity. Charge then starts to accumulate at the interface between the outer membrane and the environmental fluid, and the process of build-up of the electro-mechanical force accelerates.

However, the magnitude of the force starts to reduce after it reaches the maximum value $\sim 8.0 \times 10^{-7}\mathrm{N}$ in this simulation. This reduction is caused by the completion of the charge accumulation process in the cytoplasm at the outer membrane interface. It may be assumed that the electro-mechanical force should remain constant when all charge accumulation processes in both cytoplasm and environmental fluid are completed. This stable value was not shown in this plot due to the short simulation time and the low conductivity environmental fluid. It was shown that the electric field strength in the cell membrane in such low conductivity environmental fluid will reach its maximum value, as shown in **Figure (5.21)**. The force shows the positive value, which means the cell will be stretched by the forces on acting upon its upper and lower parts [108].

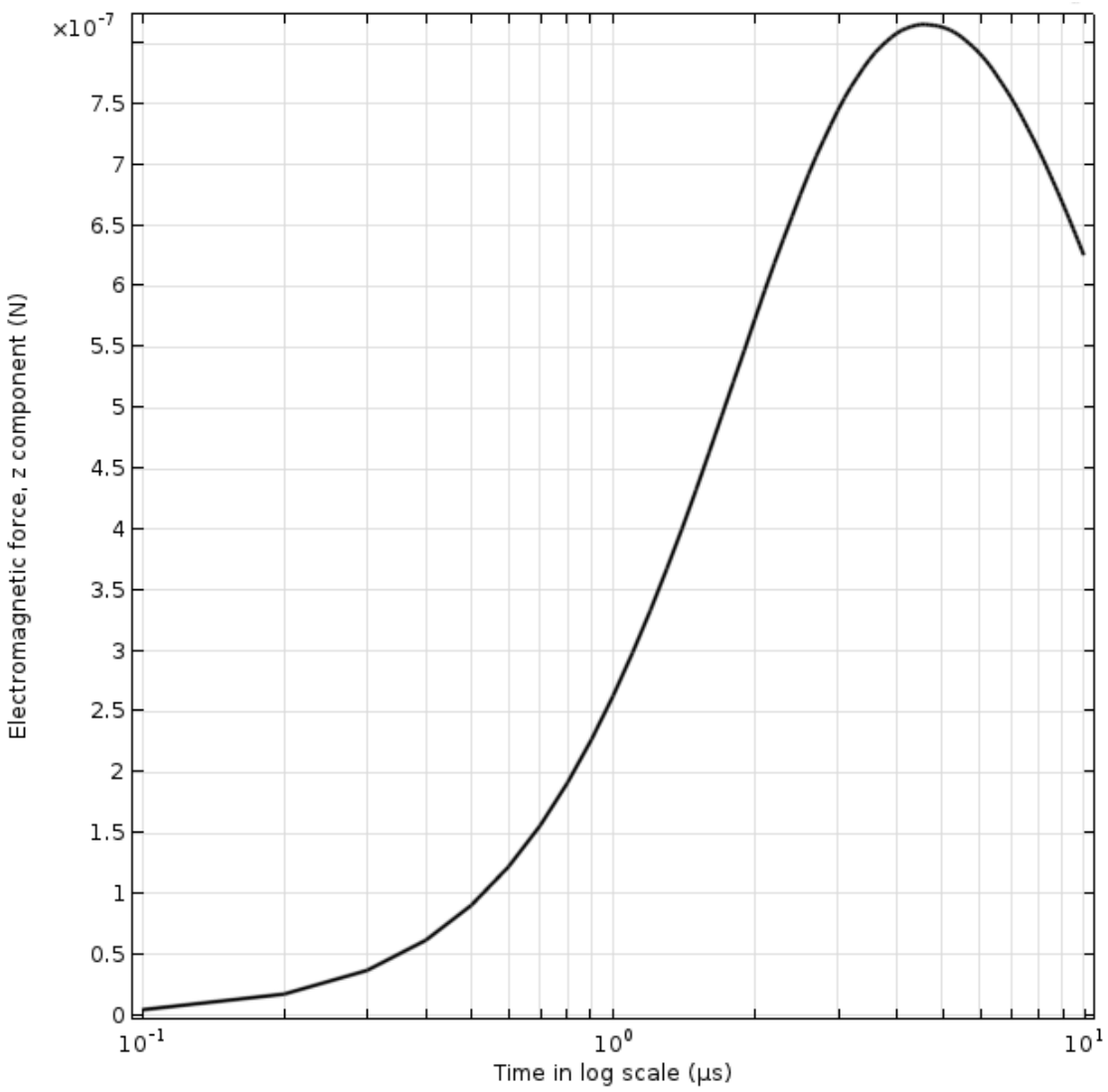

Figure (5.26) Magnitude of the electro-mechanical force acting upon the upper part of the cell membrane in 30 kV/cm field and in low conductivity environmental fluid (0.0005 S/m).

Figure (5.27) shows the magnitude of the electro-mechanical force which acts upon the membrane in the case of increased conductivity of the environmental fluid, 0.2 S/m. The electro-mechanical force reached its maximum at about$\sim -2.8 \times 10^{-7}$ N, this value is close to the value of the force obtained in [108].

The force magnitude is in the range of the typical surface tension values for the membrane, which indicates that this force may lead to membrane rupture, as discussed in [274]. The negative value of the force means that the cell is compressed by the electro-mechanical forces acting upon the upper and lower parts of the cell membrane. Besides, a force reversal (at about 0.3 μs)was observed during the early stage of the HV pulse, and such force reversal was also reported in [321], which is attributed to a high rate of voltage change, *dV*/*dt*. The voltage in the present simulation was instantly increased to from 0 V to 120 V. The peak value of the force reversal was ~$1.4 \times 10^{-8}\ N$ (Obtained through "zoom in" function of COMSOL, which cannot be clearly seen in the **Figure (5.27)**).

Figure (5.28) presents the simulation results for longer treatment time (200 μs) at 30 kV/cm field strength and in the low conductivity environmental fluid, when the charge accumulation processes were completed. Both force reversal and force stabilization effects were observed, supporting the results and assumption obtained

from **Figure (5.26)** and **Figure (5.27).**

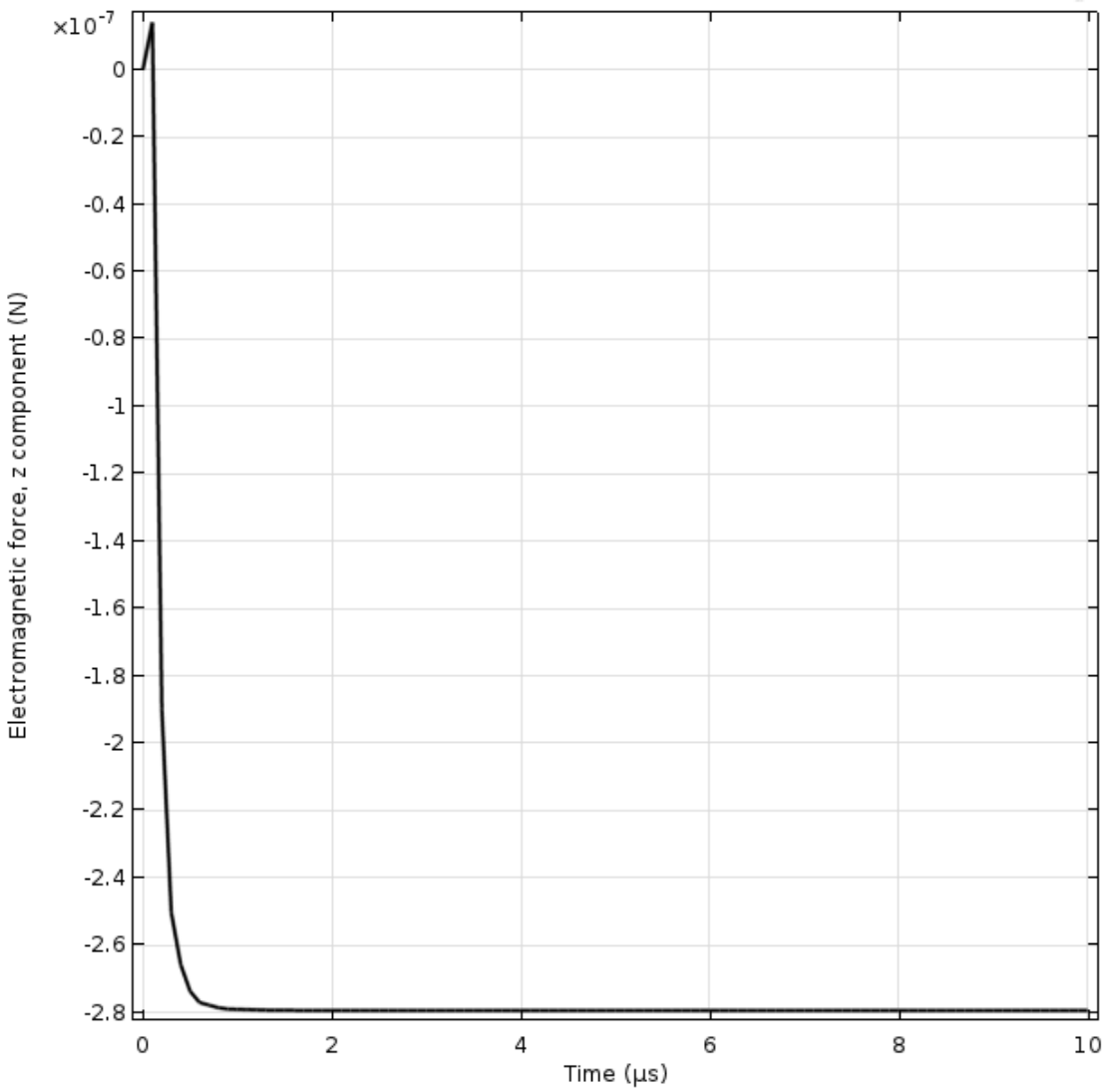

Figure (5.27) Electro-mechanical force acting upon the upper part of cell membrane in the field with magnitude of 30 kV/cm strength and in high conductivity environmental fluid (0.2 S/m).

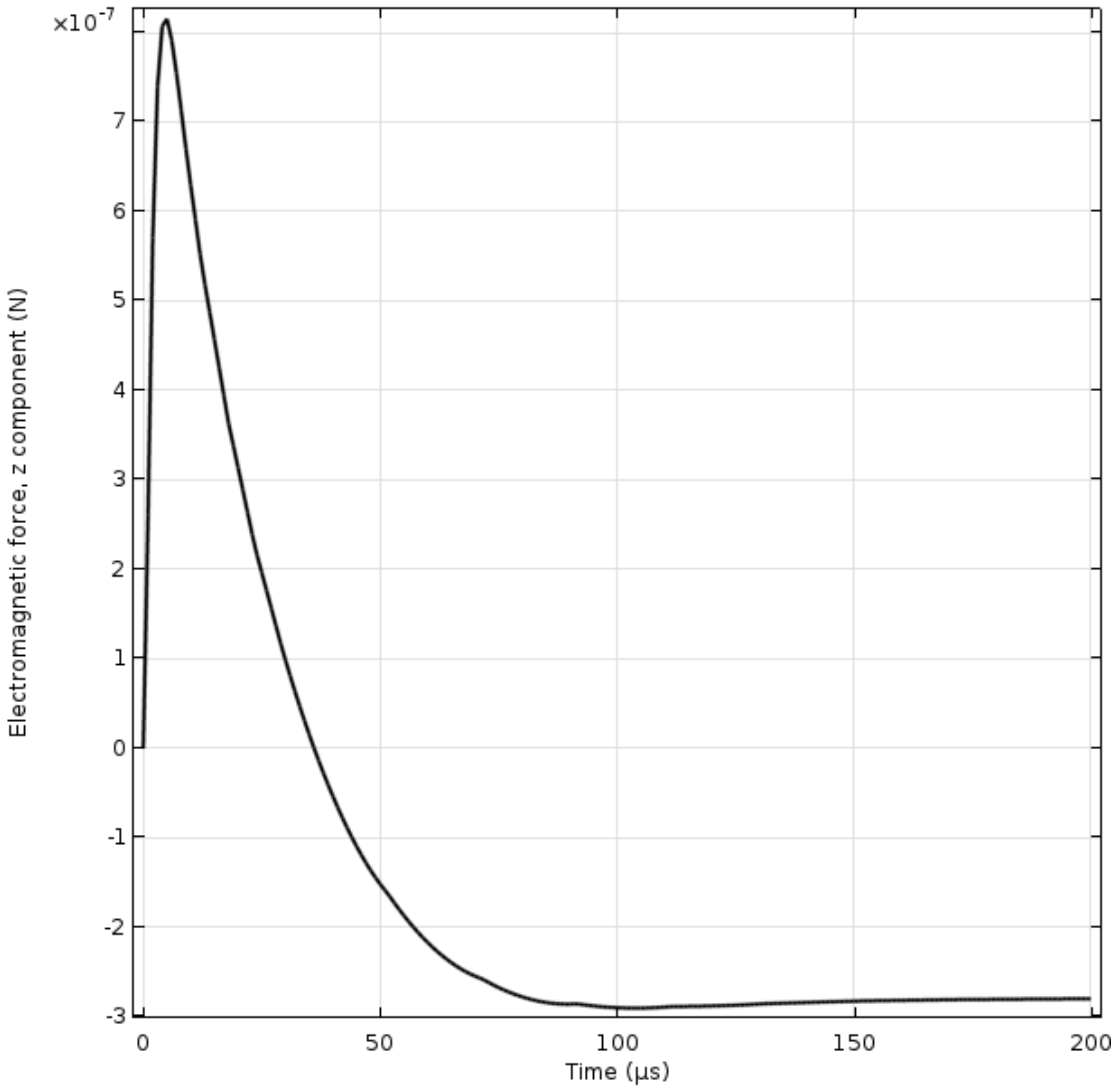

Figure (5.28) Electro-mechanical force acting upon the upper part of cell membrane in the field with magnitude of 30 kV/cm strength and in low conductivity environmental fluid (0.0005 S/m).

Figure (5.29) shows the electro-mechanical force acting upon the upper part of the cell membrane during the first 10 μs of the PEF treatment with a higher electric field strength. The force build-up process follows the results shown in **Figure (5.26),** as the conductivity and permittivity were not changed. The higher peak force $(\sim 4.0 \times 10^{-6}\ \mathrm{N})$ was caused by the higher external electric field strength.

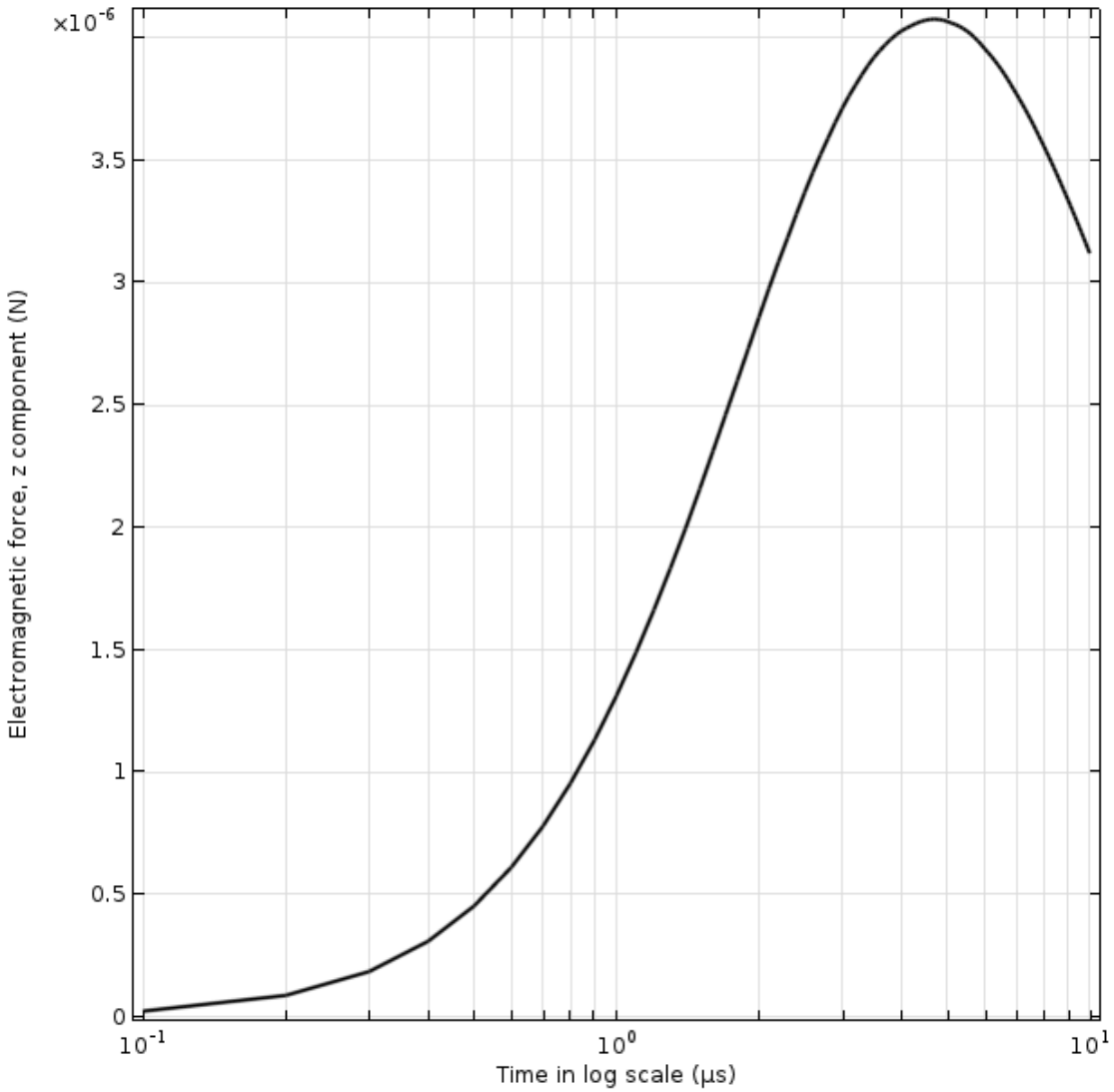

Figure (5.29) Electro-mechanical force acting upon the upper part of the cell membrane in the field with magnitude of 67 kV/cm strength in low conductivity environmental fluid (0.0005 S/m).

Figure (5.30) shows the electro-mechanical force acting upon the upper part of the cell membrane during the first 10 μs of the PEF treatment with a higher electric field strength and in more conductive environmental fluid. The stable value of the electro-mechanical force was about $\sim 1.4 \times 10^{-6}\ N$, which is increased as the applied field strength was doubled. The peak value of the force reverse was recorded as $\sim 4.8 \times 10^{-8}\ N$, which is in the same order of magnitude as obtained from **Figure (5.31)**. Such force reversal only occurred at the very beginning of the

treatment, which could be related to the charge accumulation process in the cytoplasm. Besides, the conductivity and permittivity of the cytoplasm are not changed in this simulation, so there should be no significant difference compared with **Figure (5.31)**. The increase in the value of the force is caused only by the higher applied electric field strength. This is a novel result, as such detailed investigation of the force dynamics, including the reversal of the force which is related to the charge accumulation process, has not previously been reported in the literature, to best knowledge of the author.

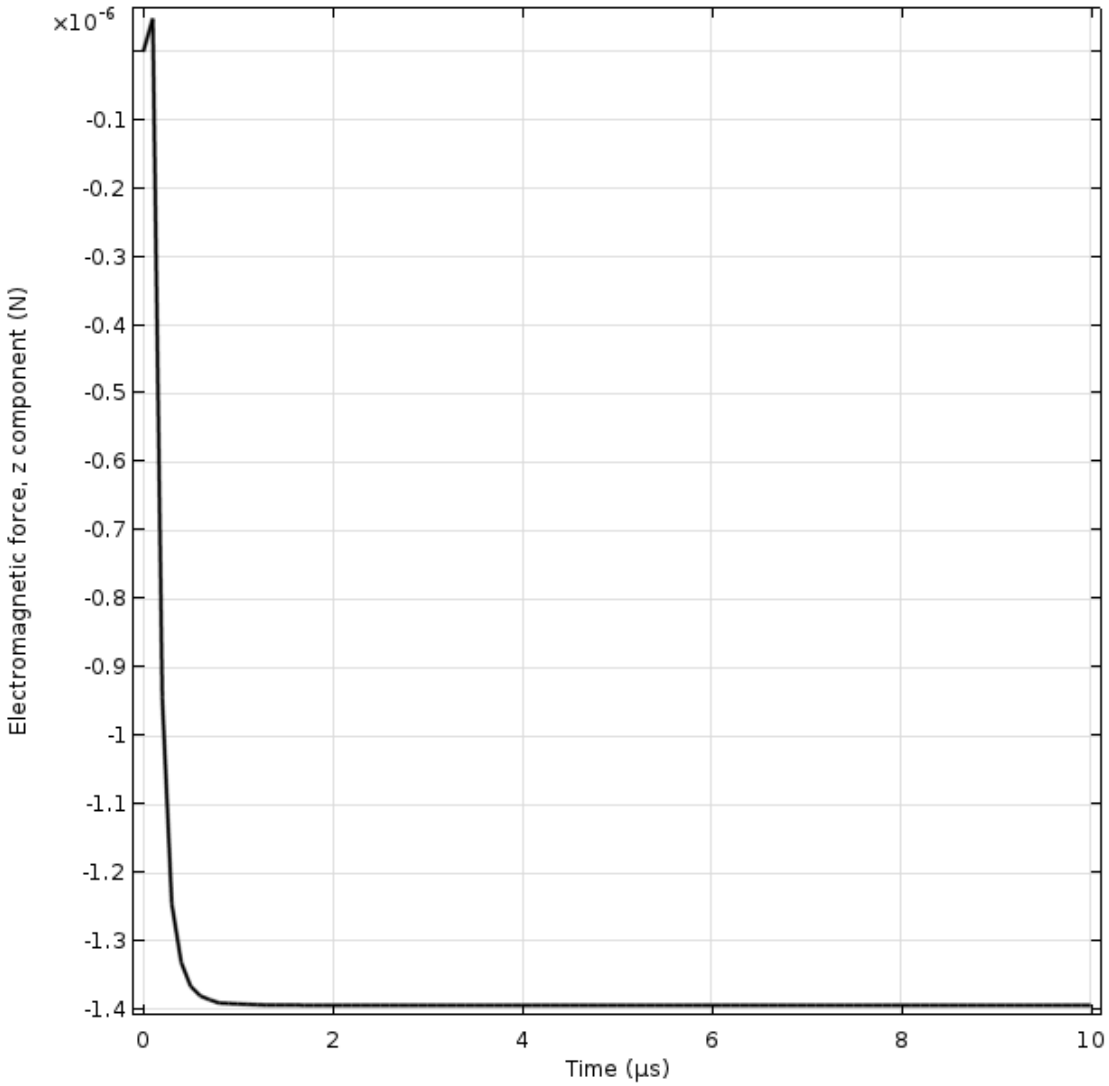

Figure (5.30) Electro-mechanical force acting upon the upper part of the cell membrane with 67 kV/cm field strength and high conductivity environmental fluid (0.2 S/m).

Figure (5.31) shows the simulation results obtained using this model. These results show the relationship between the electro-mechanical force, treatment time and conductivity of the environmental fluid. These findings have been published in [319]. The negative value of the *z*-component of the force acting upon the membrane means that the direction of force has changed and the (negative) force is directed into the negative z-direction, resulting in the stretching of the cell.

A step voltage was applied across the electrodes, as shown in **Figure (5.32)**. In this case, it was shown in **Figure (5.31)** that the conductivity of the environmental fluid significantly affects the electro-mechanical force build up process and the force reversal phenomenon: with the higher conductivity environmental fluid, the force reversal effect is not obvious. Comparing **Figure (5.31)** with **Figures (5.30)** or **(5.27),** the force reversal effect is clearly pronounced when the voltage is applied. This finding is supported by the study presented in [321]. Furthermore, it could be confirmed that the maximum electro-mechanical force at its peak was not influenced by the conductivity of the environmental fluid. A detailed investigation using a ramp voltage will be introduced in section 5.5.

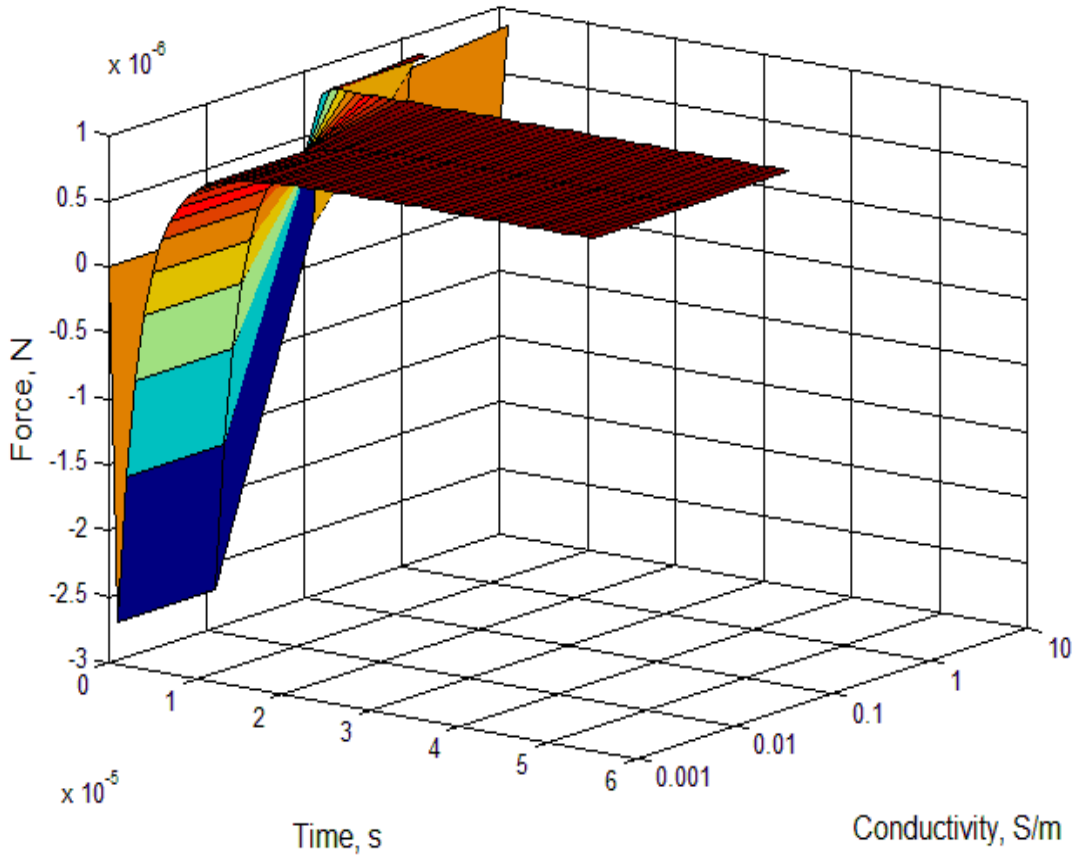

Figure (5.31) Electromagnetic force acting across the cell membrane at the lower part of the membrane, step voltage energization, external field strength is 67 kV/cm.

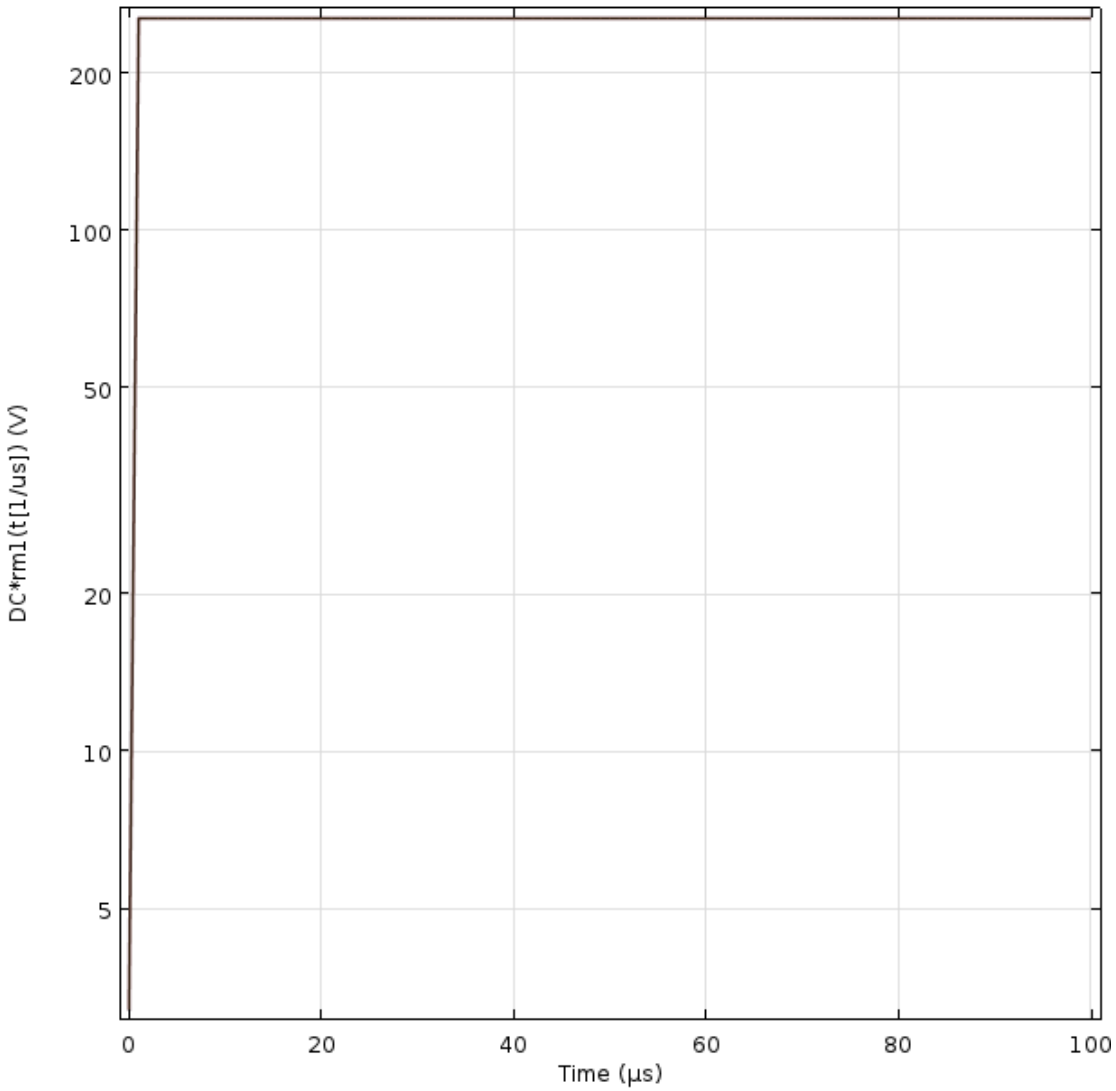

Figure (5.32) Step function signal used to obtain **Figure (5.31).**

5.4.2 Thermal stress during the PEF treatment

The electro-mechanical force was introduced and investigated in section 5.4.1, which provided a more detailed understanding of the interactions between external electric field and microorganisms. However, with higher local heating effects, there should be a thermal force, which could also cause deformation and structural damage to the membrane. Although, it has been confirmed in previous sections that the local heating effects could be negligible if the field in the fluid is close to

the typical field strength used in the PEF treatment (30 kV/cm). However, it is still beneficial to investigate the relationship between the thermal force and parameters of bio-membranes and external fluid.

It was shown that Joule heating and dielectric heating exist during the PEF treatment. In the models presented to this point, however, the joule heating due to the conduction of ions was modelled and used as the heat source when the PEF treatment was conducted using DC voltage. On the other hand, when the microorganism is stressed by AC voltage, the dielectric heating occurs and this would be considered as the main source of heat in the model. The energy delivered by the AC field is given by **Equation (5.4.1)** below.

$$Q = \omega \cdot \varepsilon_r'' \cdot \varepsilon_0 \cdot E^2 \qquad \textbf{(5.4.1)}$$

where ω is the angular frequency of the field, ε_r'' is the imaginary part of the complex relative permittivity of the absorbing material, ε_0 is the permittivity of free space and *E* is the electric field strength.

Before introduction of the obtained simulation results, the effect of the conductivity of the fluid should be further investigated, in the situation when the local heating effects are significant, since the electrical conductivity of the fluid is generally temperature dependent. In typical electroporation process, there is almost no temperature increase in the liquid, so the conductivity of all fluids in the model could be considered as constant values. However, in order to investigate the thermal force, the local heating effects should be more significant, thus it is necessary to investigate the temperature-dependent conductivities. Such analysis is also important for the further study of the effects generated by AC oscillating voltages/fields: in the case of AC field, the relative permittivity is a frequency-dependent and temperature-dependent parameter.

5.4.2.1 Investigation of temperature dependent conductivity and permittivity

As the local heating effects are mainly generated in the environmental fluid, the conductivity of the environmental fluid was considered as a temperature-dependent parameter.

Figure (5.33) shows the conductivity of water as a function of its temperature, based on [322].0

While the conductivity of water shows temperature dependency, typically the temperature of the treated fluid during the PEF process does not exceed 40 ℃ so as the structures of nutrient wouldn't be damaged due to high temperature.

In the present analysis, the treatment time is relatively short, several μs, and the simulation results also show that there is no significant increase in the temperature during the PEF treatment. Therefore, the temperature-dependency of the conductivity of the environmental fluid in this simulation was neglected.

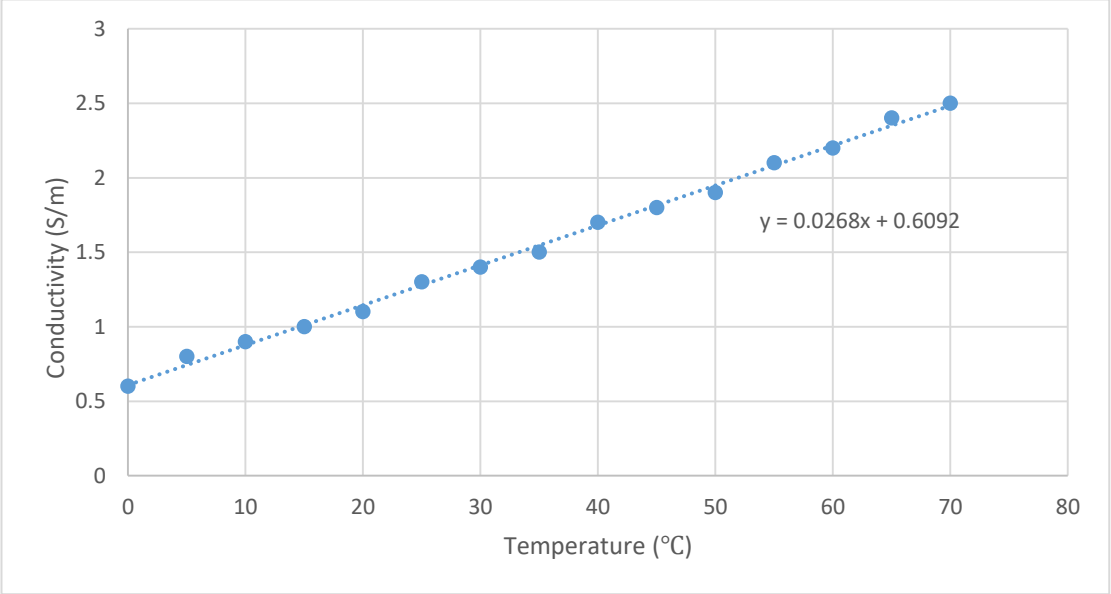

Figure (5.33) The temperature-dependent conductivity of water.

Figures (5.34) and **(5.35)** show the relative permittivity of water as a function of temperature. These graphs were plotted selecting and using specific points in [323] .

Furthermore, according to **Equation (5.4.1),** for the treatment with a specific frequency the Electric field within the membrane will be much greater than the fields in the water based cytoplasm or surrounding media. This means that the dielectric heating in these media is small and the variations in the imaginary part of the permittivity as a function of temperature will have little impact.

Compared with the dielectric heating source in the environmental fluid, the dielectric heat generated in the cell membrane should be the main source of heat which produced the local heating effects during PEF treatment in the case of AC energization, which will be confirmed in the further sections. Therefore, the temperature-dependency of the relative permittivity of the environmental fluid or cell membrane could also be neglected in the present analysis.

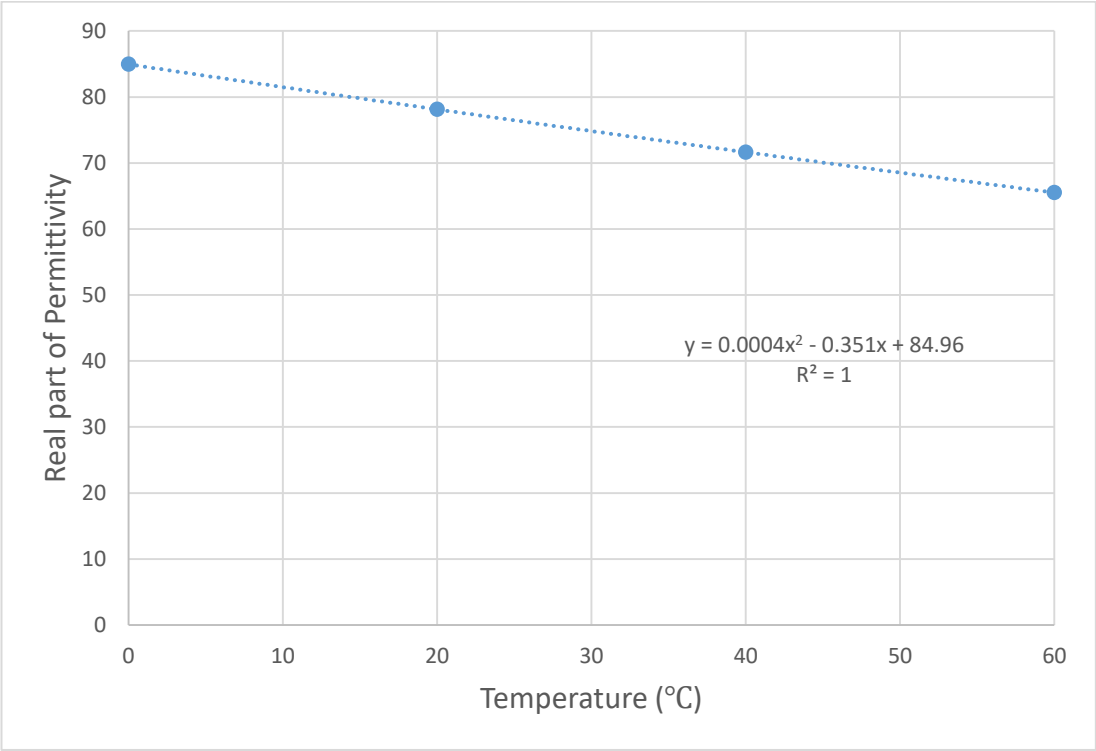

Figure (5.34) Assumption of temperature-dependent permittivity of water (Real part of permittivity of water) based on data from [323].

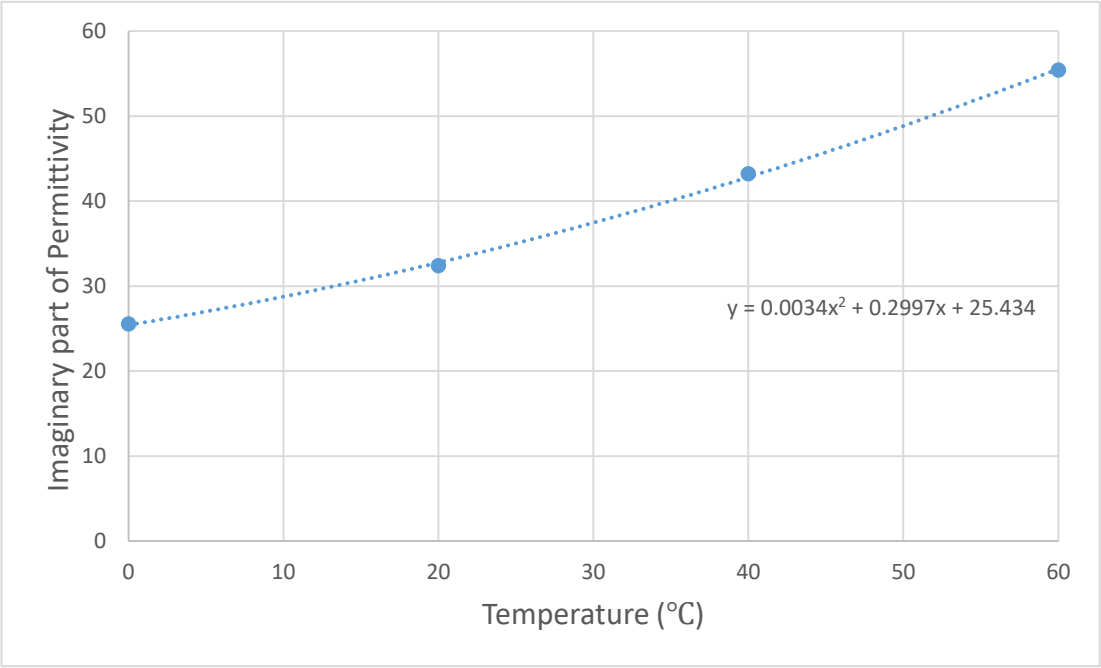

Figure (5.35) Imaginary part of permittivity of water as a function of the temperature based on data from [323].

5.4.2.2 Investigation of thermal forces under DC energization

In order to model noticeable local heating effects while not exceeding 40-60 ℃ in the local hot spots, the applied electric field strength was set to 67 kV/cm, and the conductivity of the external fluid was 0.1 S/m.

The parameters used in modelling of the thermal forces are listed in **Table 5.4**.

Table 5.4 Parameters used in the investigation of the thermal force acting across the cell membrane.

Parameters	**Membrane Young's modulus (Pa)**	**Coefficient of thermal expansion of the membrane (1/K)**	**Poisson's ratio of the membrane**
Values	125 [324] [325] [326] [327]	0.0002 [324] [325] [326] [327]	0.4 [324] [325] [326] [327]

Figure (5.36) shows the temperature distribution and local heating effects obtained in this simulation. It can be seen that after 1 μs the local temperature demonstrates significant increase with higher electric field strength and conductivity of the environmental fluid.

Figures (5.37) and **(5.38)** show the obtained thermal and electro-mechanical forces. The thermal force ($\sim 4.5 \times 10^{-12} N$) is much lower than the electro-mechanical force ($\sim 4.0 \times 10^{-7} N$). Thus, the effects caused by the thermal force which appeared during DC energization could be considered negligible in the beginning

period of PEF treatment. However, the thermal force keeps increasing as the joule heating continuously contributes to the local heating. Such thermal force would enhance the membrane structural damage with longer treatment time.

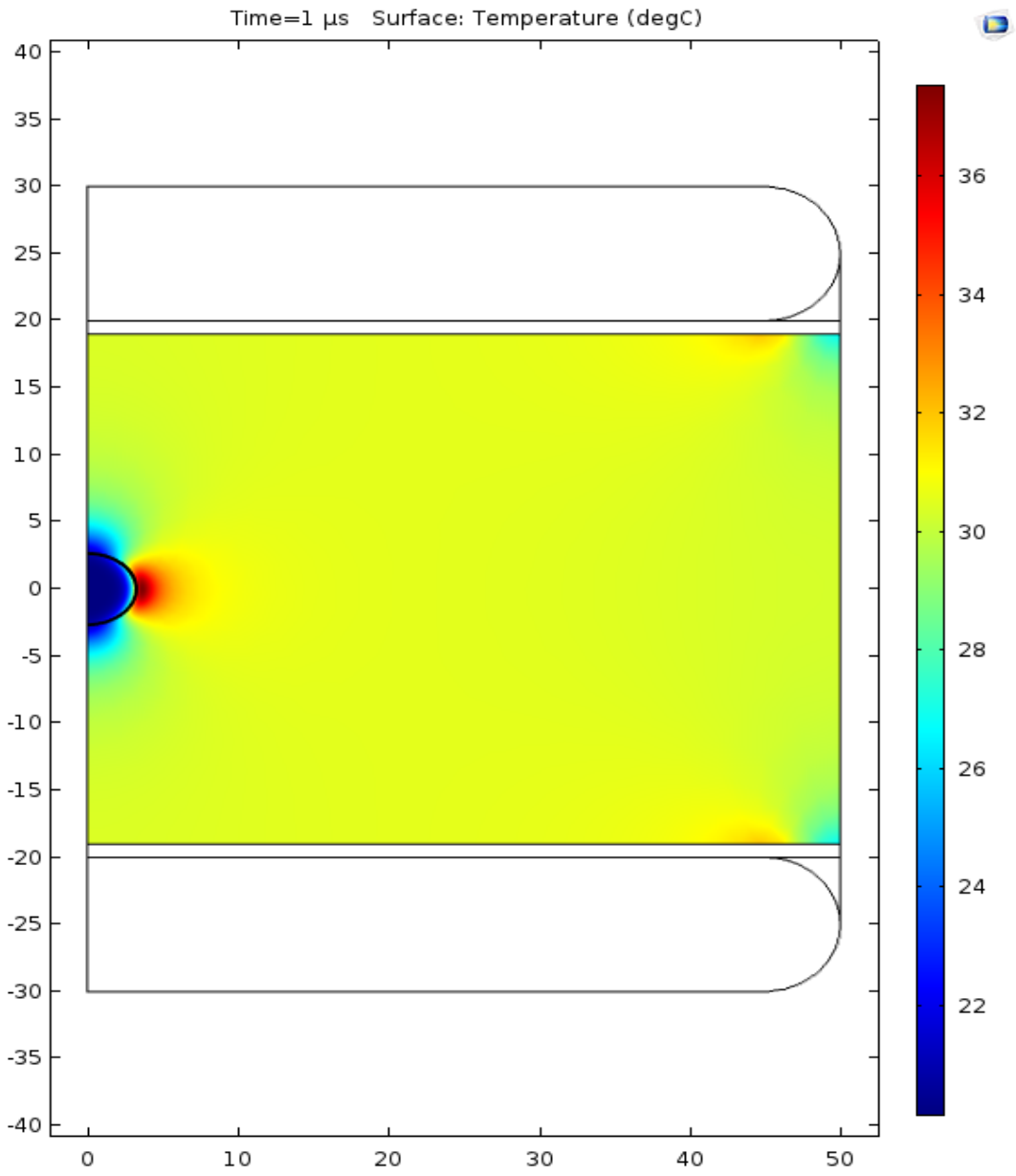

Figure (5.36) Temperature distribution in the single cell model at 1 µs. PEF treatment with 67 kV/cm electric field strength in high conductivity environmental fluid (0.1 S/m). Axis dimensions in µm

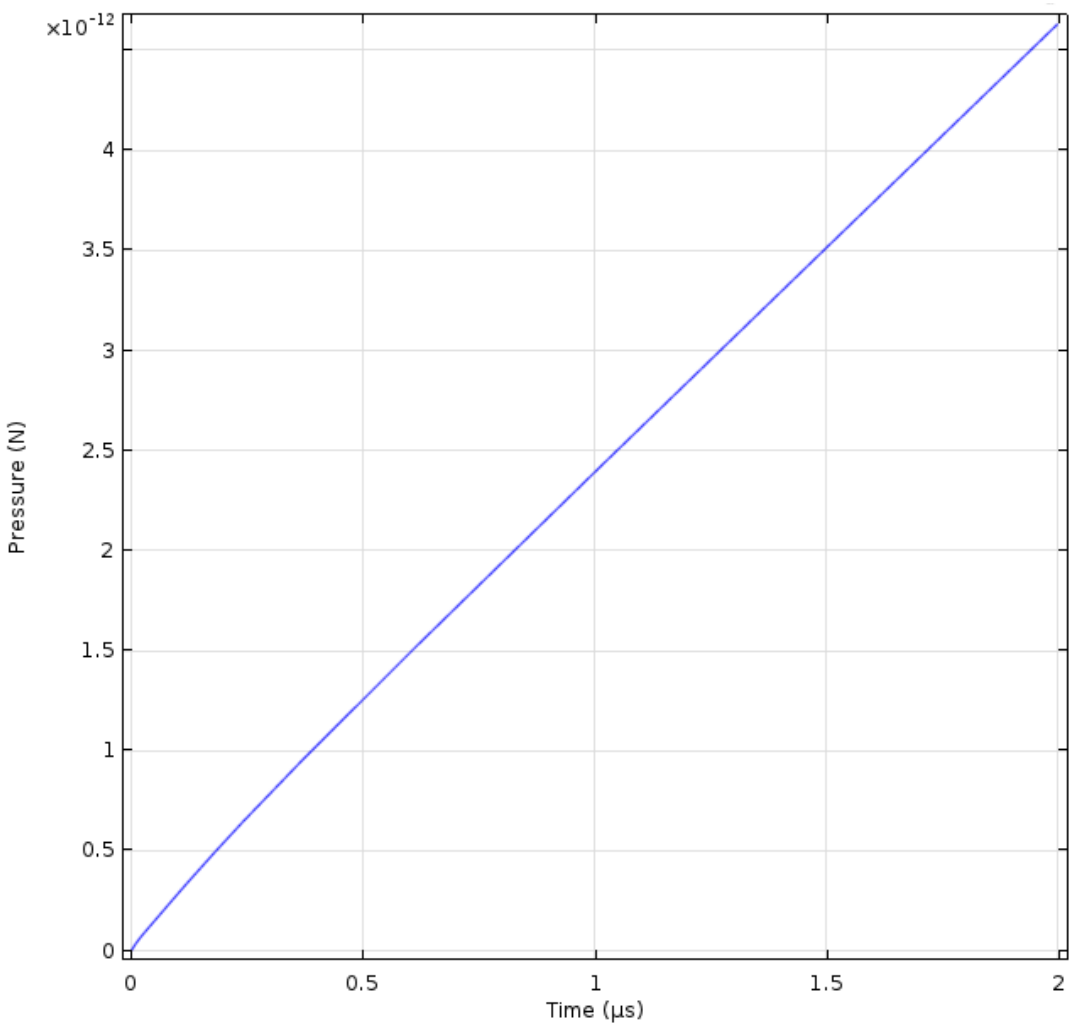

Figure (5.37) Thermal force across the cell membrane during the PEF treatment with 67 kV/cm electric field strength in highly conductive environmental fluid (0.1 S/m).

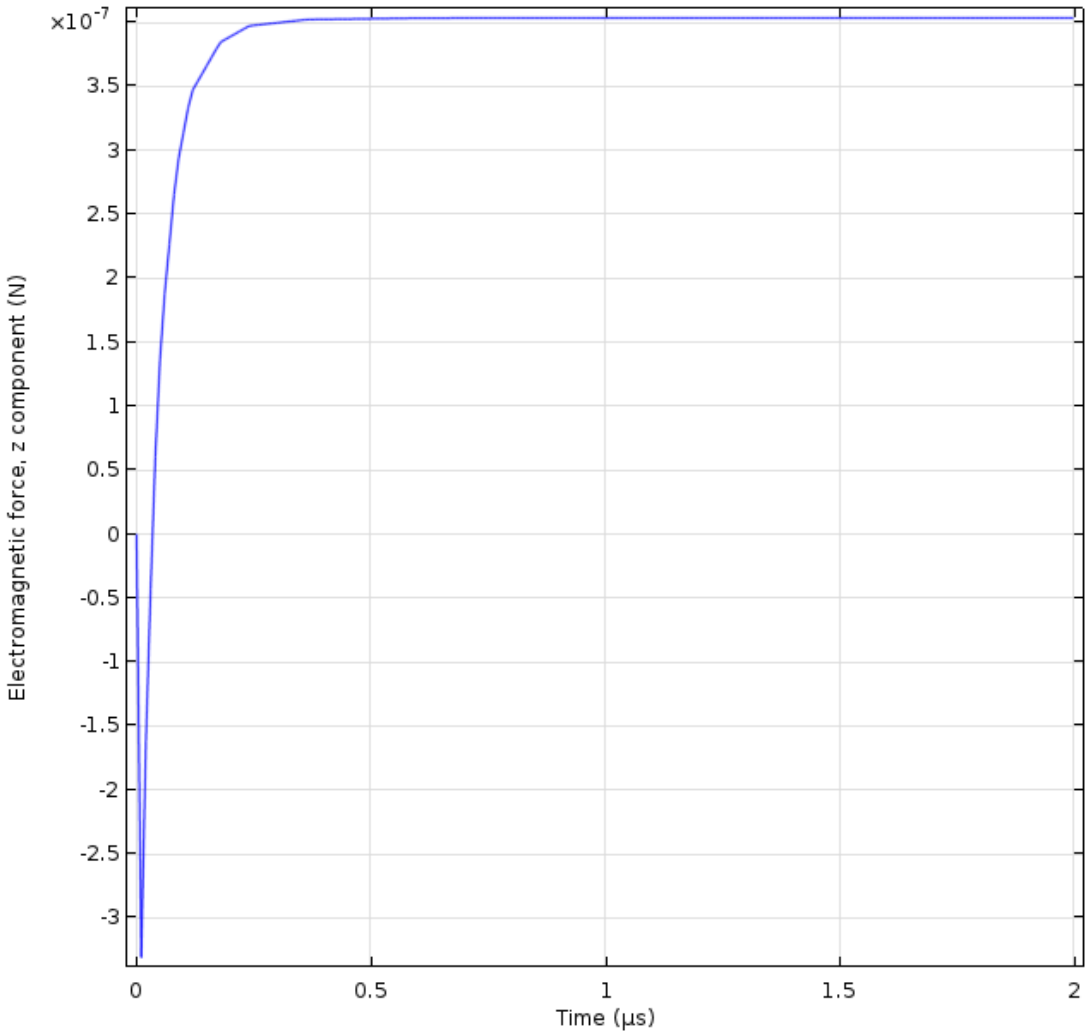

Figure (5.38) Electromagnetic force during the PEF treatment with 67 kV/cm electric field strength in highly conductive environmental fluid (0.1 S/m).

5.5 Investigation of the PEF treatment using different energisation regimes

As discussed in the previous chapters which presented the linear and Quickfield models, usually it is not easy to conduct an analysis of the field and stresses under different energization regimes, however, using COMSOL, it becomes possible to investigate how the waveforms of field/voltage signals influence the results of the PEF treatment.

5.5.1 Energisation with a ramp up to a constant field value

5.5.1.1 2μs 67 kV/cm stress with a 1μs ramp from 0 V to 255V

This section presents the results of the PEF treatment model when the liquid is stressed with a ramp rising from 0 V to 255 V in 1 µs. Followed by a constant DC stress to 2µs, the model voltage waveform (signal) is shown in **Figure (5.39).**

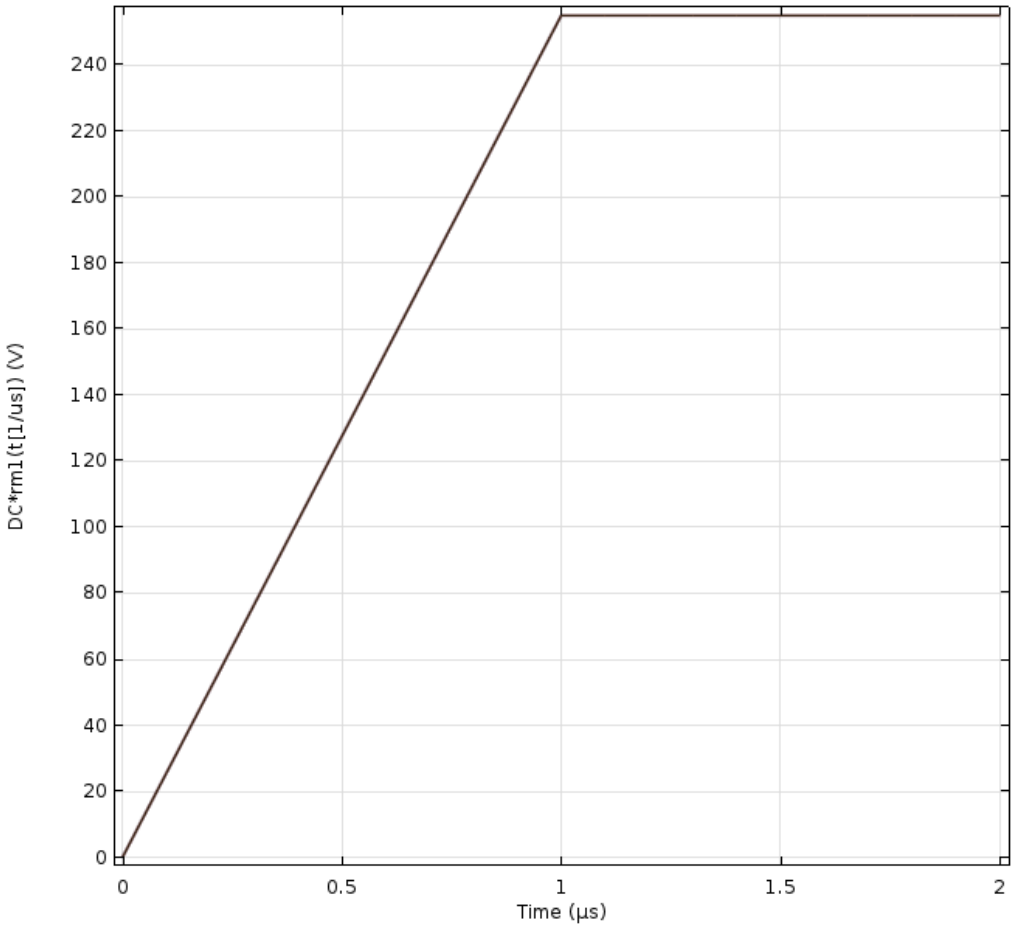

Figure (5.39) The signal of the 2 µs ramp, it rises from 0 V to a maximum constant voltage of 255 V.

The simulation results show that the electric field in the membrane reached its maximum value of $3.5 \times 10^9\ V/m$, which is close to the results obtained using the

step field impulses in the previous sections, as the maximum electric field strength in the cell membrane is mainly governed by the membrane thickness and external field strength (in the present model and approximation).

The local hot spots are observed across the outer membrane /external fluid interface at the equator of the cell (**Figure 5.40**). The maximum temperature is about 40 ℃ in this situation.

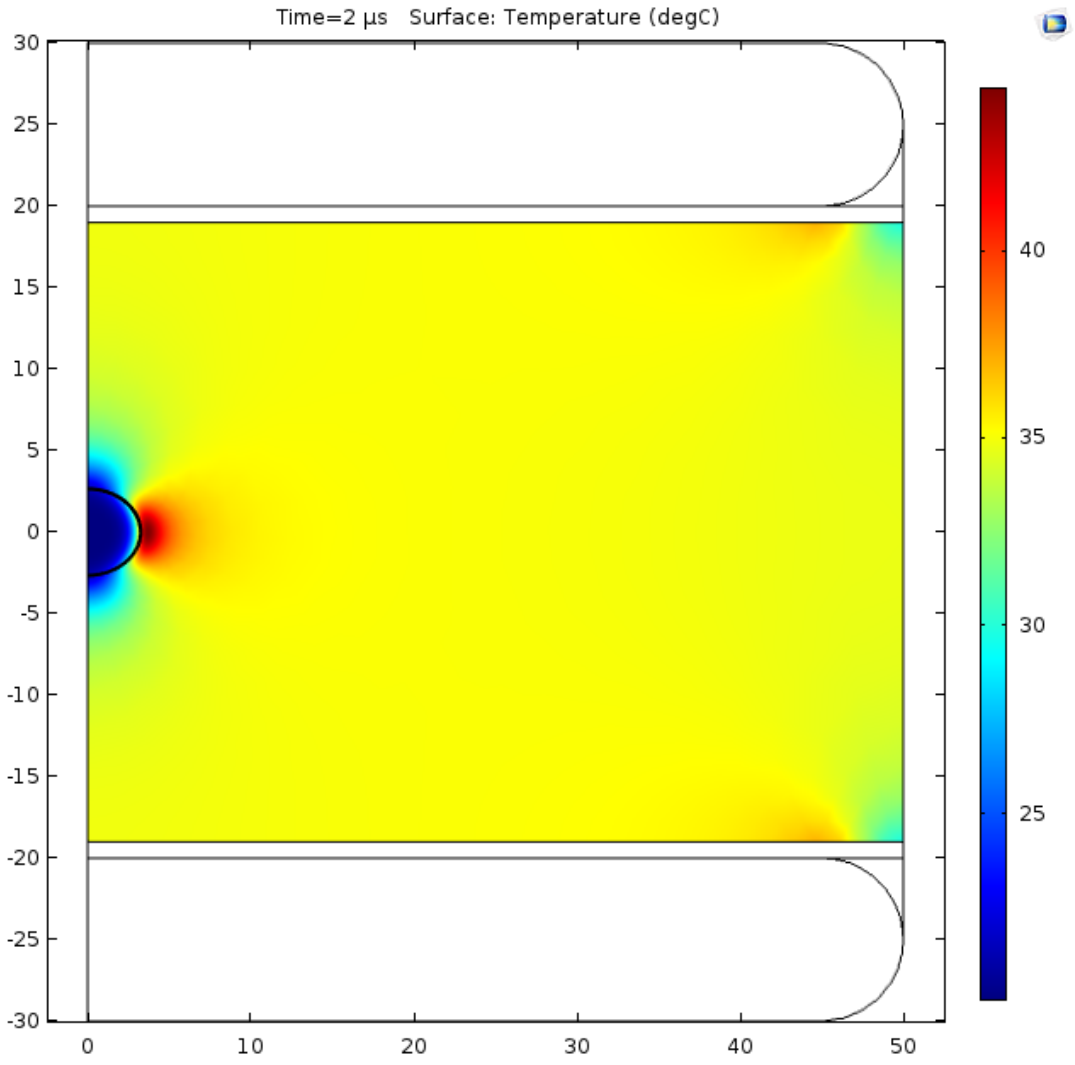

Figure (5.40) Temperature distribution in the single cell model at 2 µs. PEF treatment with 67 kV/cm electric field strength in high conductive environmental fluid (0.1 S/m). Axis dimensions in µm.

Figure (5.41) below shows the 'hot spot' temperature as a function of the treatment time, it can be seen that during the ramp stage of the treatment (up to 1 µs), the rate of temperature increase is lower than at the later stage of this process (1-2 µs) which follows the waveform characteristic of the applied field/voltage signal.

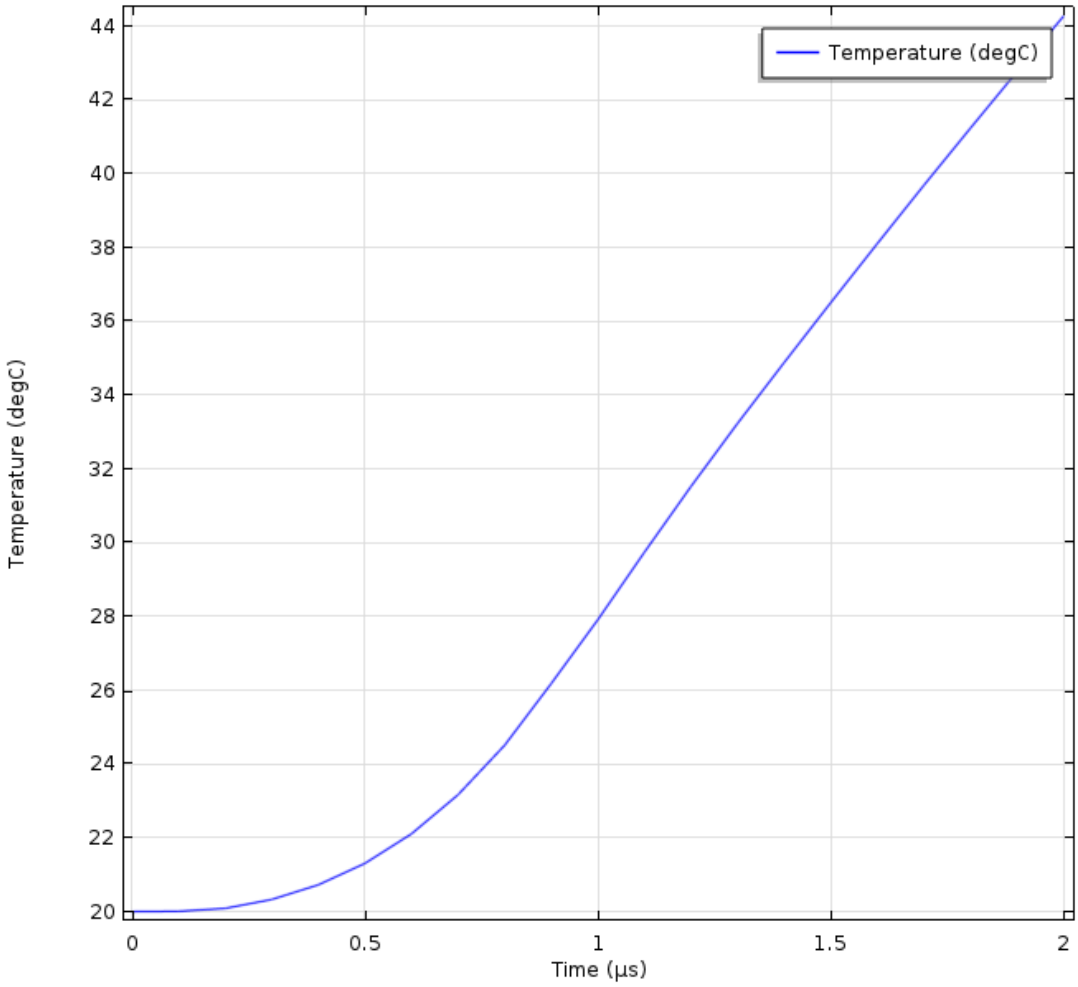

Figure (5.41) Maximum Temperature obtained in the model as a function of time during the PEF treatment with 67 kV/cm electric field (voltage wave shape as shown in **Figure 5.39**) in high conductive environmental fluid (0.1 S/m).

By comparing **Figure (5.42)** and **Figure (5.43),** it can be seen that the thermal force still can be ignored, however, there is no force reversal observed in the electro-mechanical force plot with the ramp signal applied. This could be the result of applying a voltage wave form with a fixed *dV/dt* compared with the step impulse considered in the previous sections.

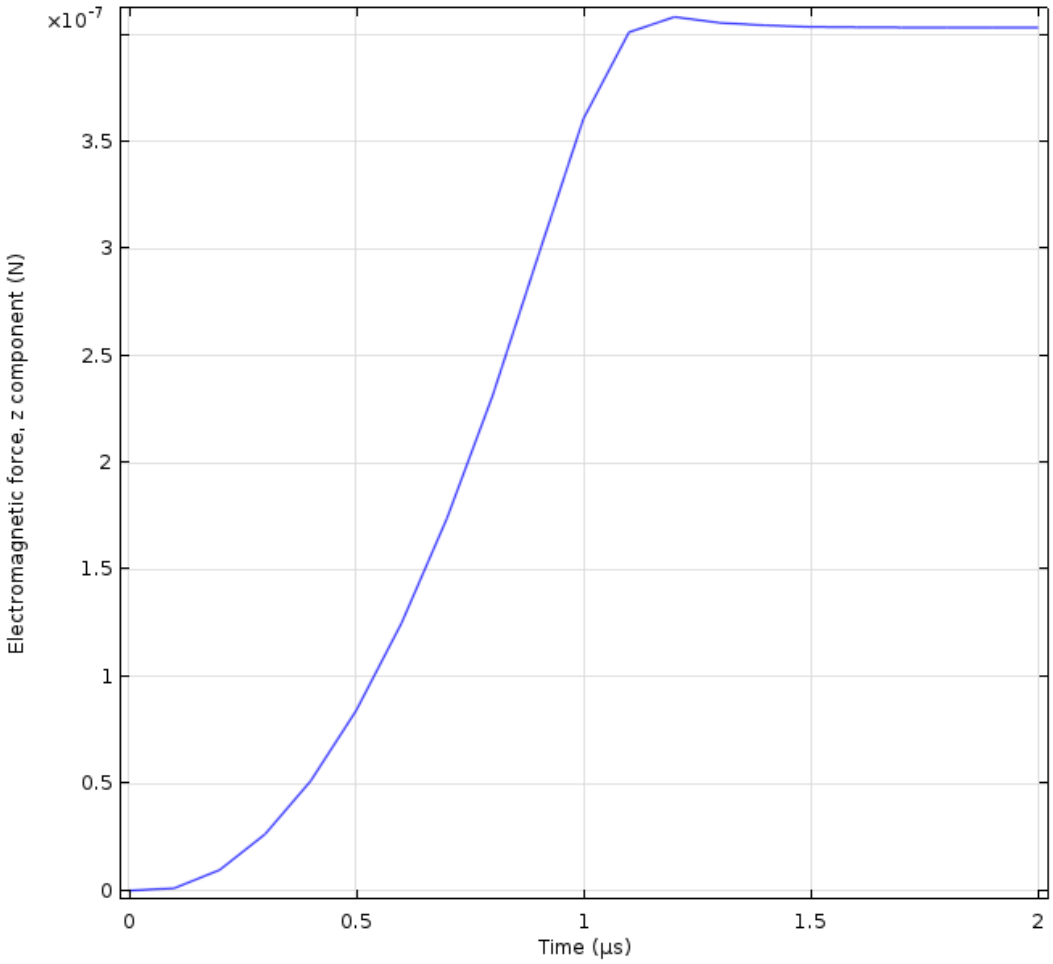

Figure (5.42) Electromagnetic force during the PEF treatment with 67 kV/cm electric field in high conductive environmental fluid (0.1 S/m), applied voltage waveform shown in **Figure (5.39)**.

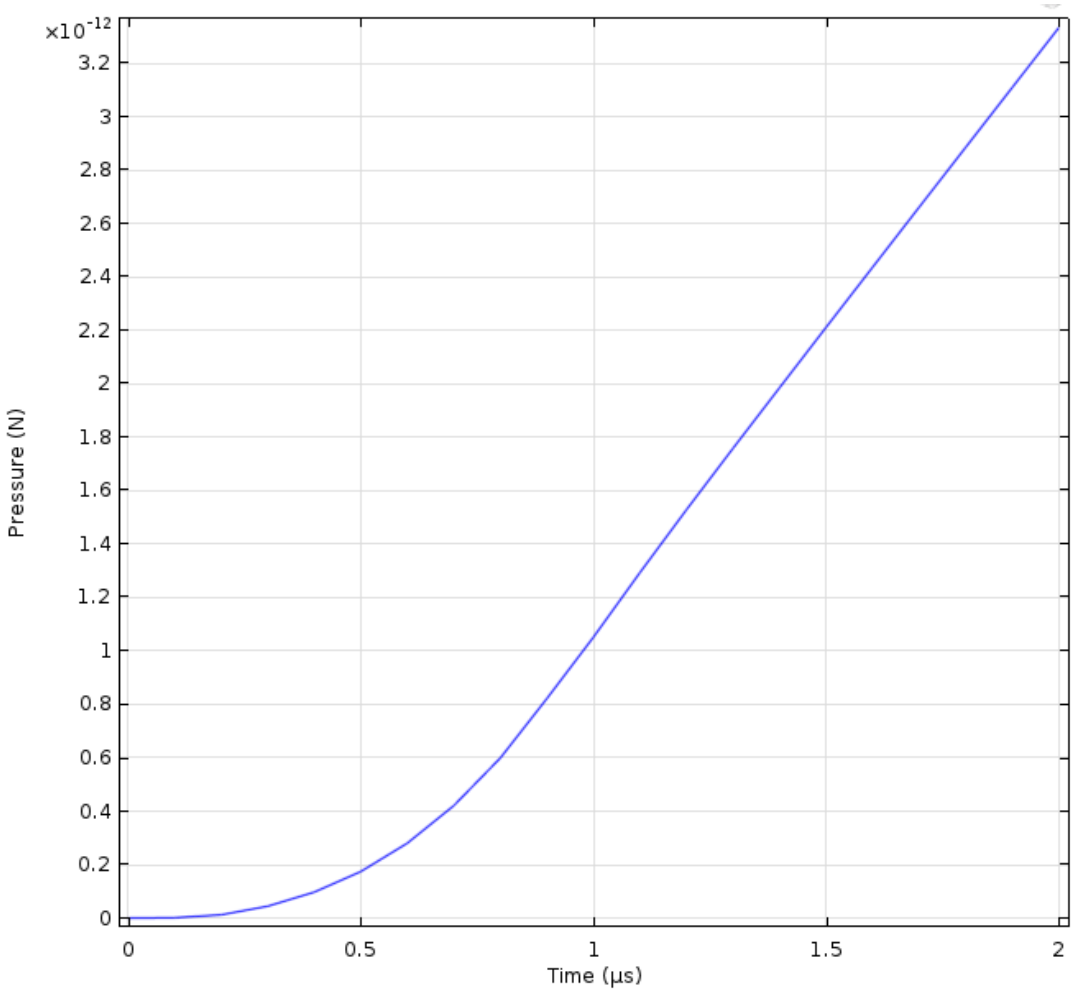

Figure (5.43) Thermal force during the PEF treatment with 67 kV/cm electric field in high conductive environmental fluid (0.1 S/m), applied voltage waveform shown in **Figure (5.39)**.

5.5.1.2 PEF treatment with 1us Square impulse field with magnitude of 67 kV/cm

Square wave PEF treatment with a rapid increase and fall of the applied field has been studied in [173] [328] [181] [329]. Thus square wave simulations would help to understand the results obtained in these studies and will provide further information about the electrical and thermal forces acting during the PEF treatment.

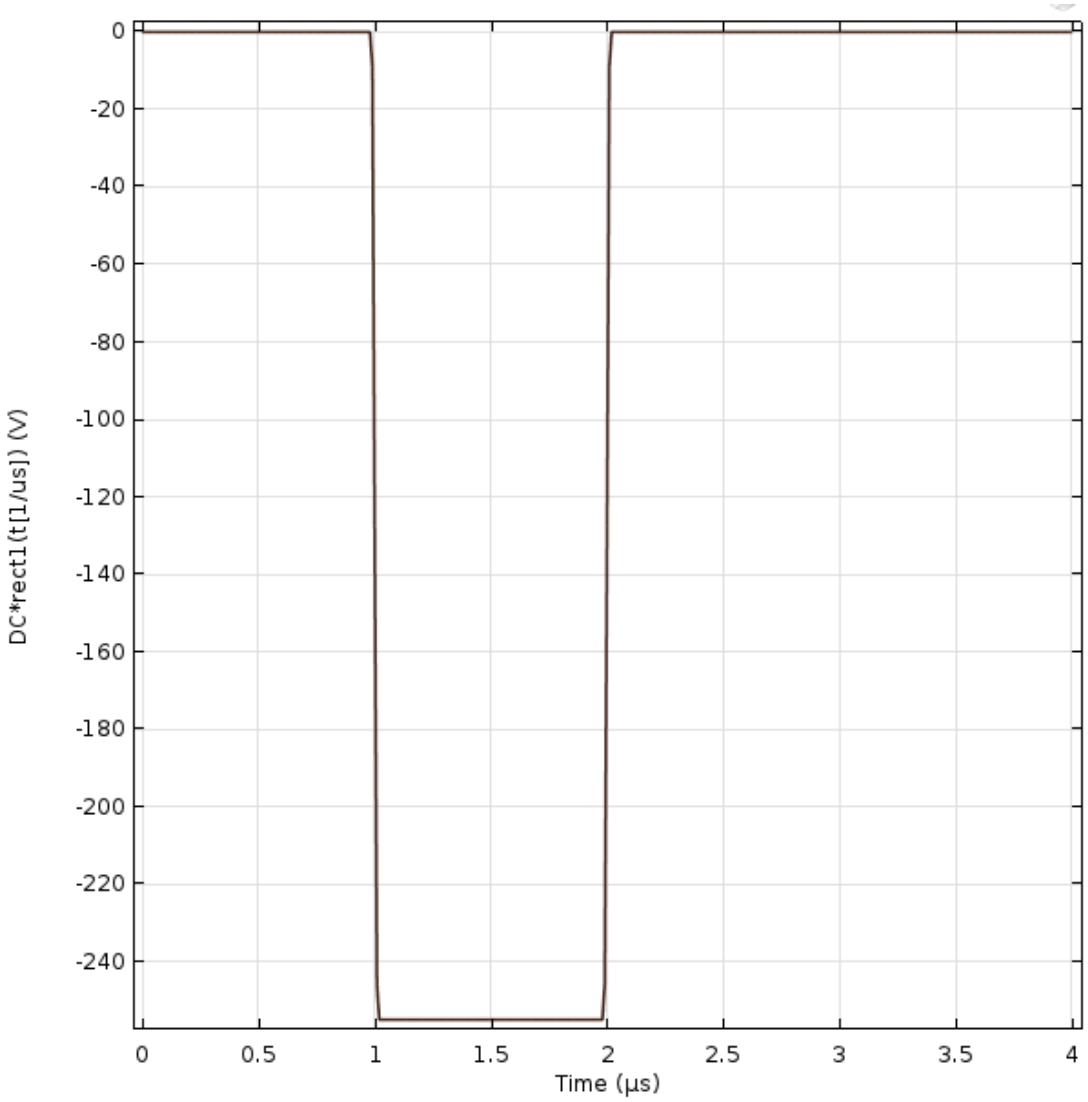

Figure (5.44) 2μs Square Wave used in the present analysis.

The square wave used in this study has a maximum of -255V and its duration is 1μs, the rate of rise (rate of fall) is 8.5×10^3 kV/μs, this is an ideal signal without noise compared with typical laboratory generated signal.

The maximum local temperature increase during the treatment is ~36 ℃ which is close to the simulation results presented in **Section 5.5.1.1** in which a voltage with a rate of rise of 255 kV/μs was used.

Figure (5.46) shows the relationship between the maximum 'hot spot' temperature and the treatment time, as the voltage drops after 2 µs, a cooling down process could be observed in the temperature plot when the heat was dissipated into the whole treatment region.

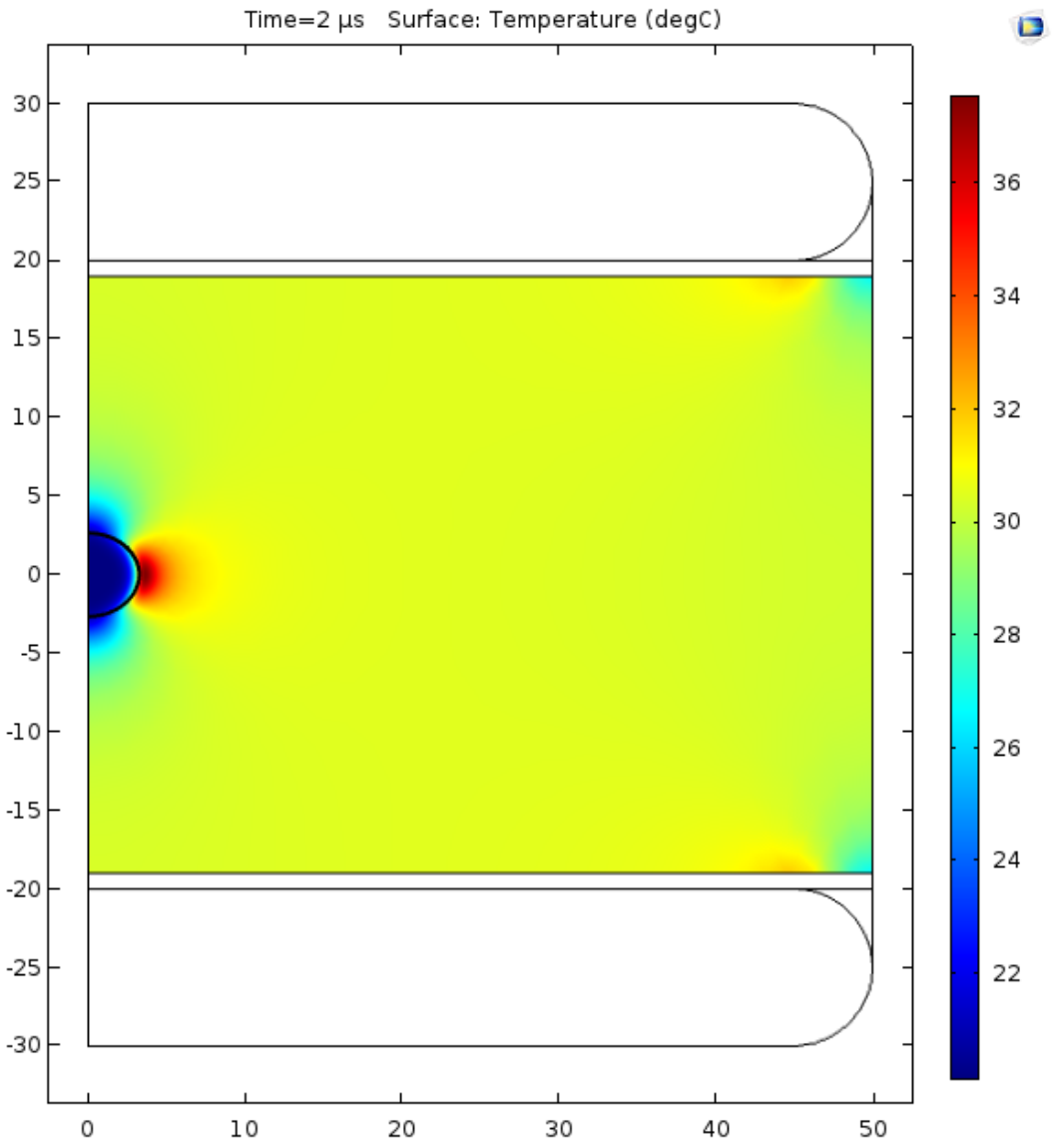

Figure (5.45) Temperature distribution in the single cell model at 2 µs. PEF treatment with 67 kV/cm electric field in high conductive environmental fluid (0.1 S/m), with the square voltage pulse applied. Axis dimensions in µm.

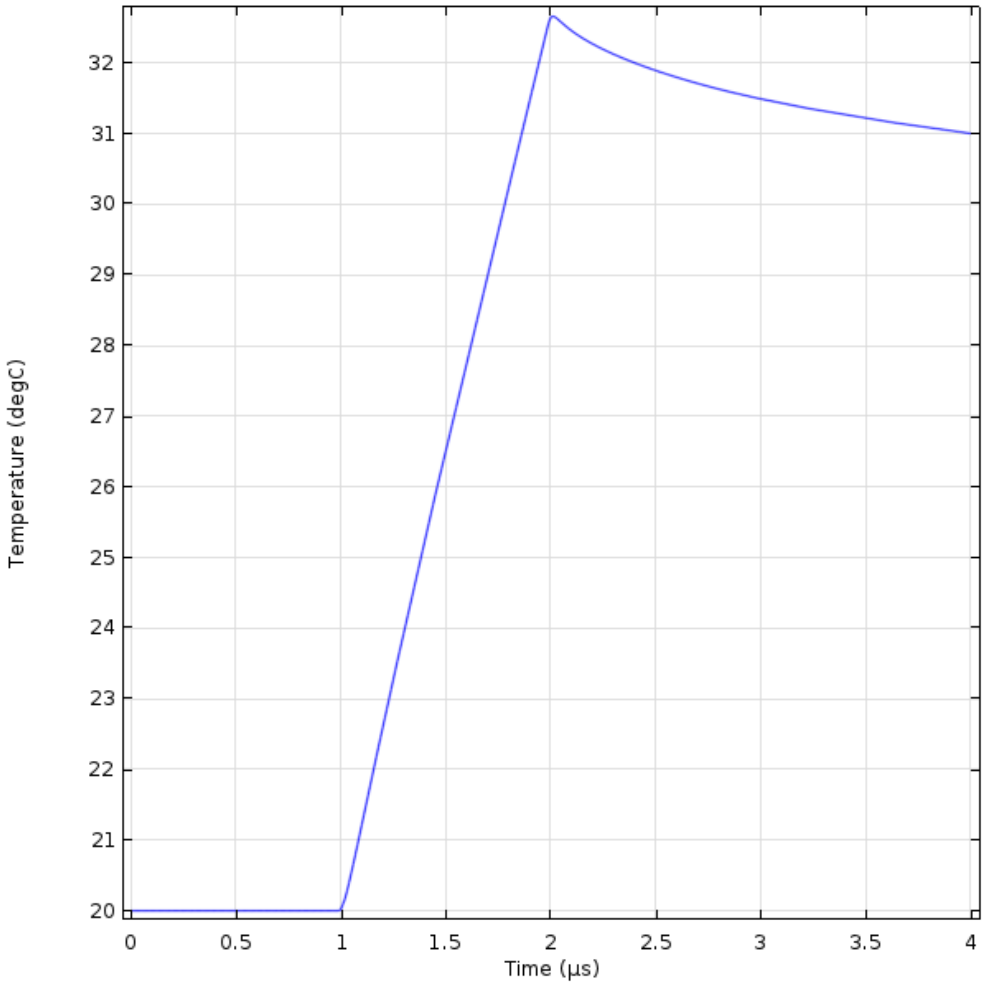

Figure (5.46) Maximum temperature during the PEF treatment with 67 kV/cm electric field in high conductive environmental fluid (0.1 S/m), square HV pulse is applied.

Figure (5.47) shows the electro-mechanical force during the PEF treatment with square 2us HV pulse. The force reversal is clearly pronounced compared with the results when the cell was stressed with the ramp voltage signal with 255 kV/µs rate of rise and DC stress discussed in other sections. This confirms the assumption that this reversal in the force direction is related to the rate of voltage rise, *dV/dt*.

Similar results were also obtained in [321], and thus it could be assumed that it's not easy to rupture the cell membrane with a short, 2us square HV impulses. However, according to **Figure (5.48)**, the thermal force is still not as significant as the electro-mechanical force due to the slight value of local heating effects.

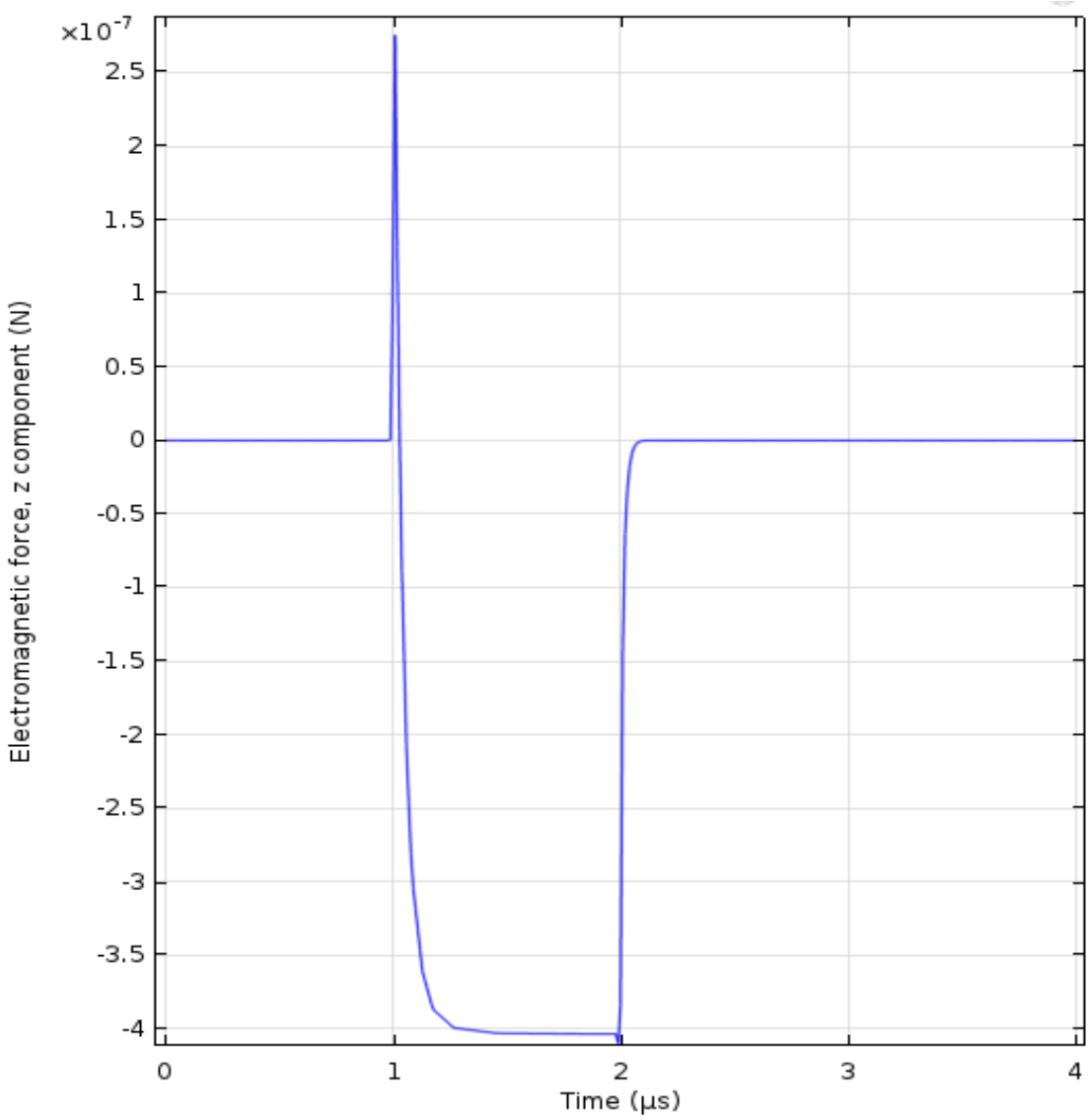

Figure (5.47) Electromagnetic force during the PEF treatment with 67 kV/cm electric field in high conductive environmental fluid (0.1 S/m), square 2us HV impulse.

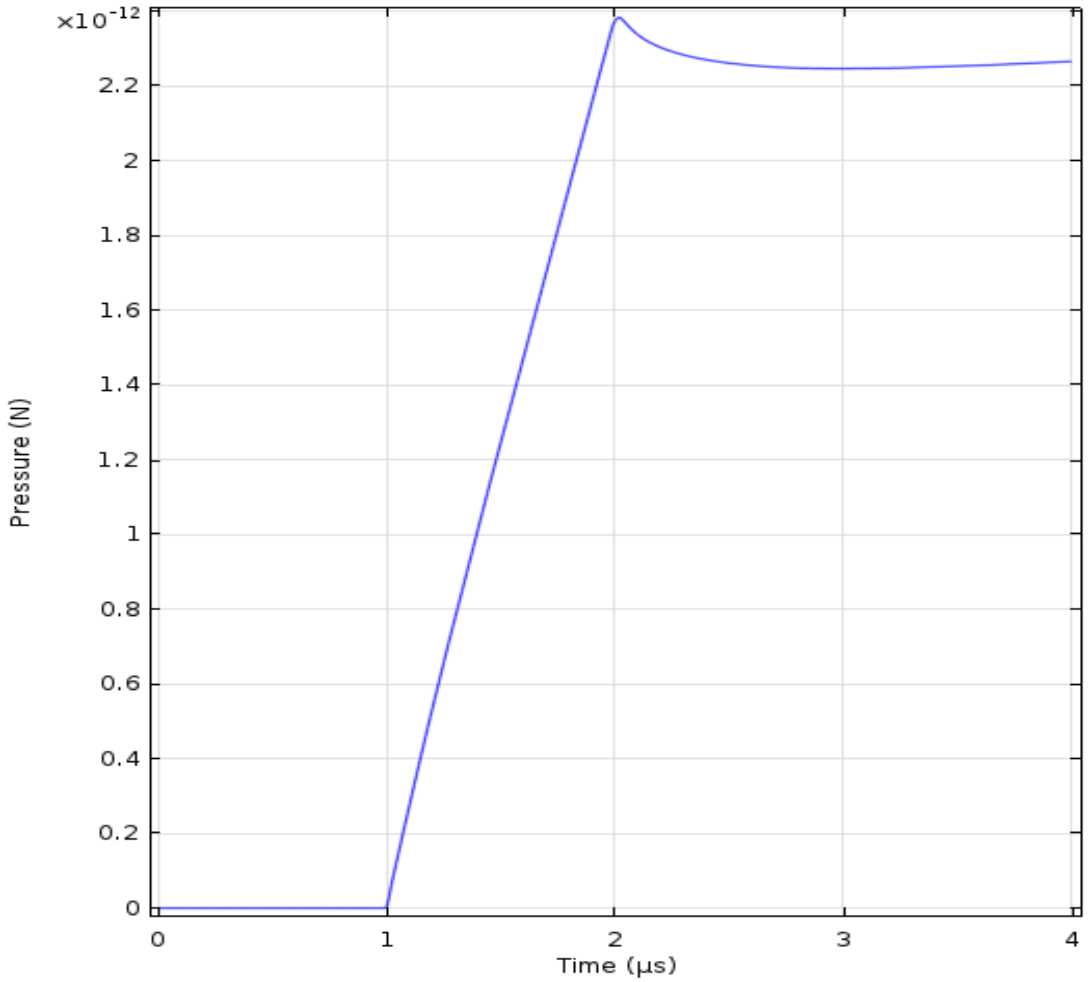

Figure (5.48) Thermal force during the PEF treatment with 67 kV/cm electric field in high conductive environmental fluid (0.1 S/m), square 2us HV impulse applied.

5.5.2 AC energization

AC oscillating voltage signals with different frequencies were used in this section to investigate the local heating effects. The simulations shows the maximum electric field strength in the cell membrane changes with the oscillating signal waveform.

The COMSOL model in which AC energization is used can be run only for 400 ns due to the limitations of the workstation (memory and processing capabilities). However 400 ns is sufficiently long enough to achieve local heating in the model and to

compare these effects with the HV step voltage/field PEF treatment. **Figure (5.49)** below shows the temperature distribution in the cell model which is subjected to the electric field with the frequency of 1 GHz. It can be seen from **Figure (5.49)** that the local heating significantly increases within only 100 ns (which is much shorter as compared with the HV step energization and the hot spot in this case is located inside the cell membrane. This is caused by the significant increase of the electric field magnitude in the cell membrane and with fast oscillating energization, the permittivity is playing a critical role in the dielectric heating instead of joule heating. The location of local hot spots follows the maximums of the electric field strength in the membrane, with maximum temperature value achieved at the poles and the minimum value observed at the equator.

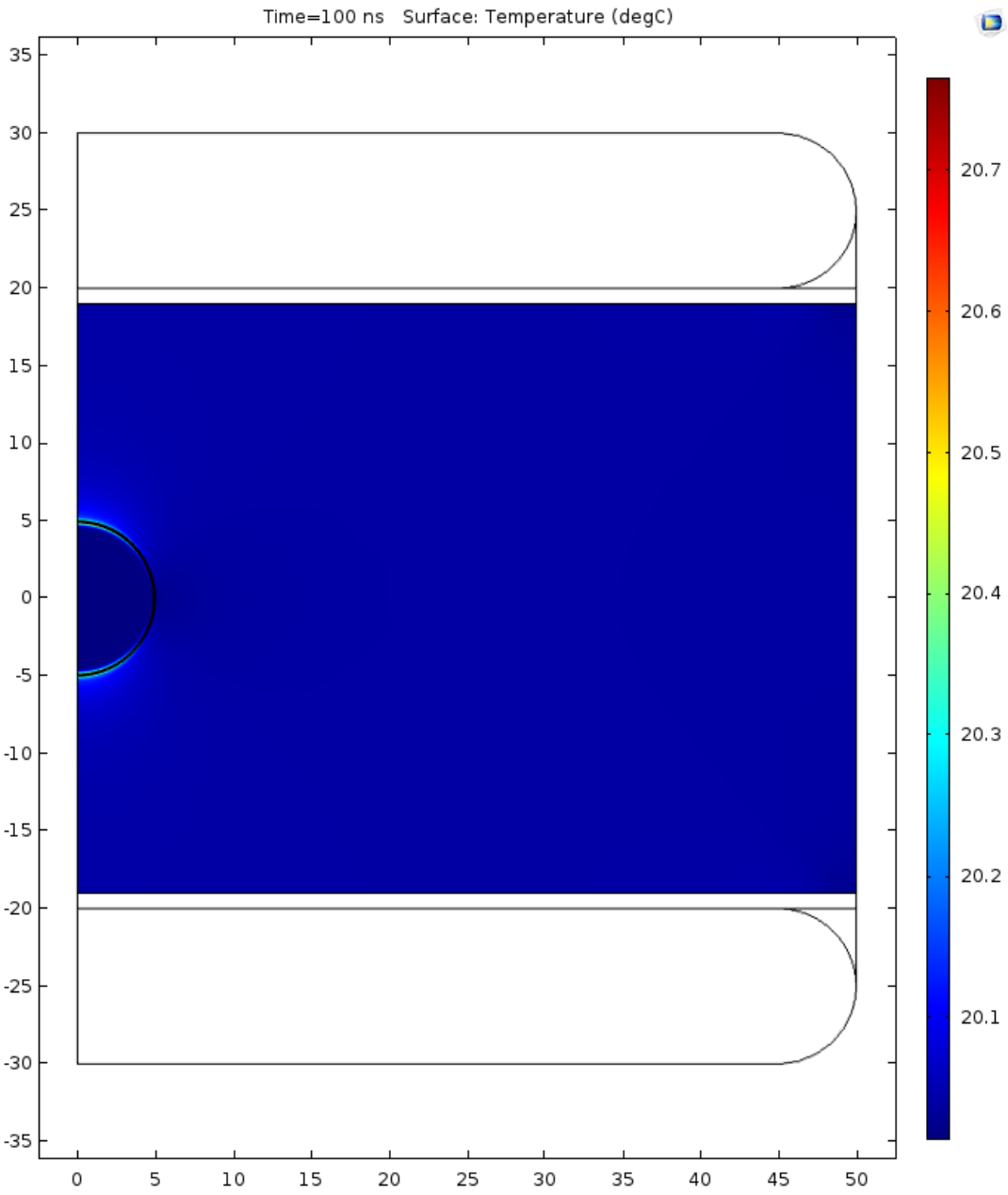

Figure (5.49) Temperature distribution in the single cell model at 100 ns. PEF treatment with 1 GHz AC oscillating signal with a peak voltage of 360 V, in high conductive environmental fluid (0.01 S/m). Axis dimensions in μm.

It can be obtained through **Figure (5.50)** below that, with higher frequency, the dielectric heating is more significant.

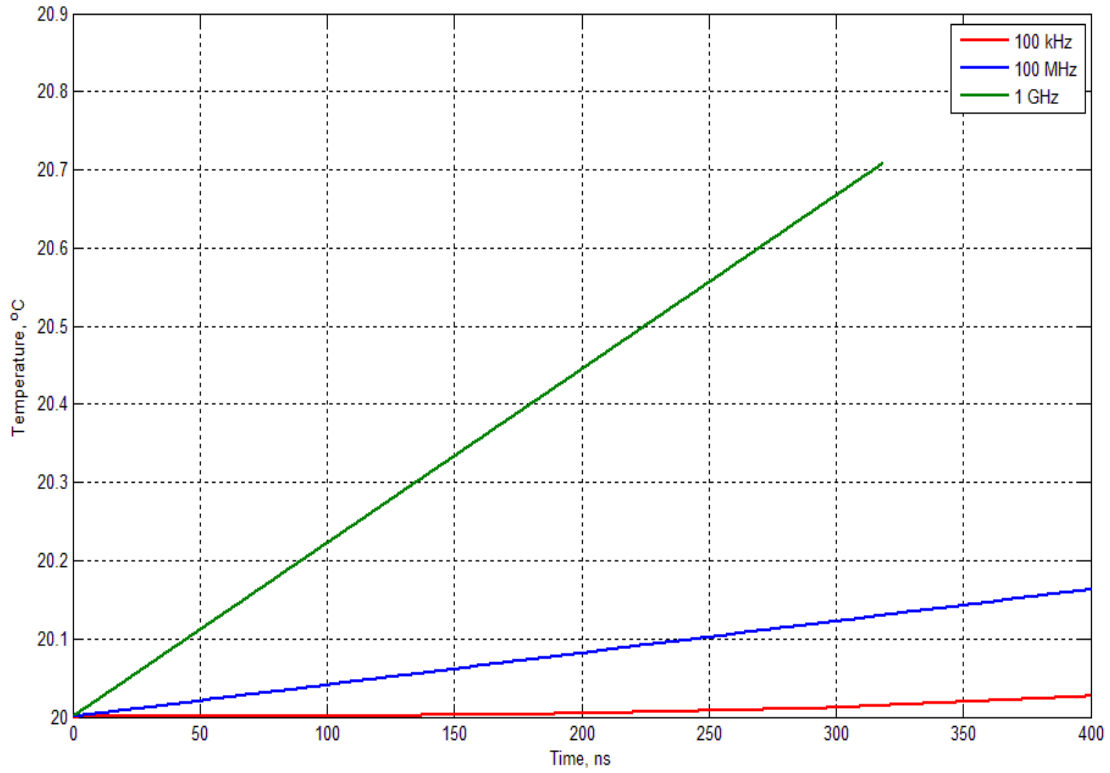

Figure (5.50) Temperature of "hot spot" in the single cell model as a function of the treatment time. PEF treatment with 1 GHz AC oscillating signal with a peak voltage of 360 V, in high conductive environmental fluid (0.01 S/m).

Figure (5.51) below shows the electro-mechanical force during the 200 MHz AC treatment, significant electro-mechanical force was observed and such force could help enhence the rapture of the cell membrane.

As the local heating at 400 ns is not significant, the thermal force again will not play a major role at this stage compared withthe electro-mechanical force. However, at longer time, the thermal effects should be more significant, thus the thermal force would help to enhance the poration and damage of the cell membrane. Nevertheless, the membrane could be damaged by the electro-mechanical force before the thermal force should start to play a noticable role .

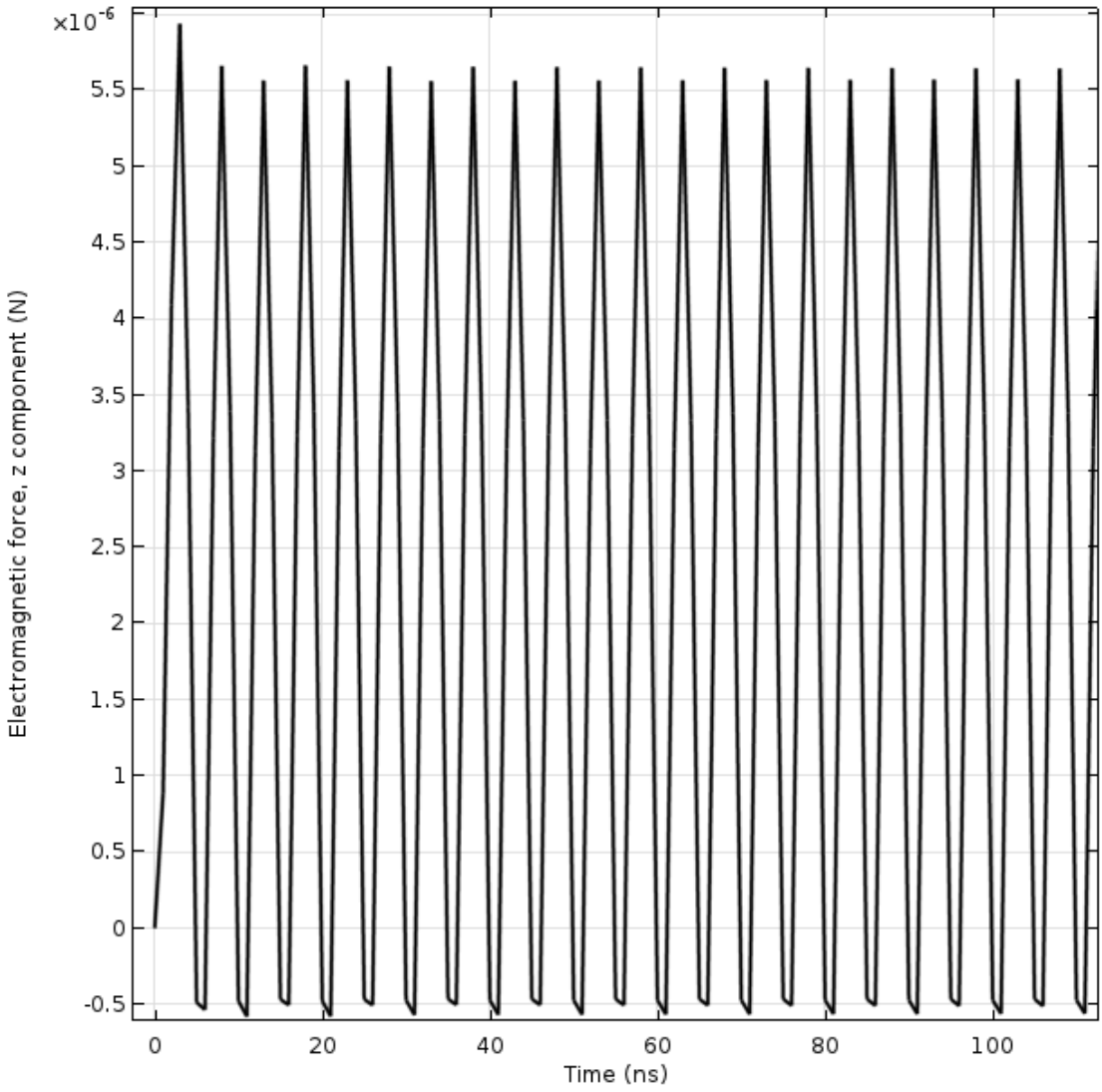

Figure (5.51) Electromagnetic force as a function of time during the PEF treatment with 200 MHz AC oscillating signal in high conductive environmental fluid (0.1 S/m), AC signal frequency is 200 MHz, voltage peak value is 360 V.

5.6 Analysis of the thermal processes in pores during the PEF treatment

Once electroporation has occurred in the cell membrane, the pores are formed in the membrane a conduction current starts to flow through these pores. To investigate the local heating effects in the membrane with pores , a single pore was introduced into the model membrane as shown in **Figure (5.52)** and **Figure (5.53)** below.

The pore can be regarded as a gap in the biological membrane filled with the conductive fluid. The pore position is defined by angle, α, between the central axis of the pore and the Y axis of the model. This angle α represents the position of the pore introduced into the membrane and changes from 0 ° (Y axis) to 90 ° (X axis). The conductivity of the fluid in the pore was set to be equal to that of the surrounding fluid, 0.1 S/m in this model, and the relative permittivity of this fluid was 80. The thermal parameters of the fluid in the pore were set to be the same as those of the environmental fluid. In order to simplify the model and the process of investigation of the membrane behaviour, the influence of the cell wall was eliminated by setting its electrical parameters to be the same as those of the surrounding fluid. Further investigation about the cell wall will be presented in this section. 25 kV/cm electric field was applied between the electrodes.

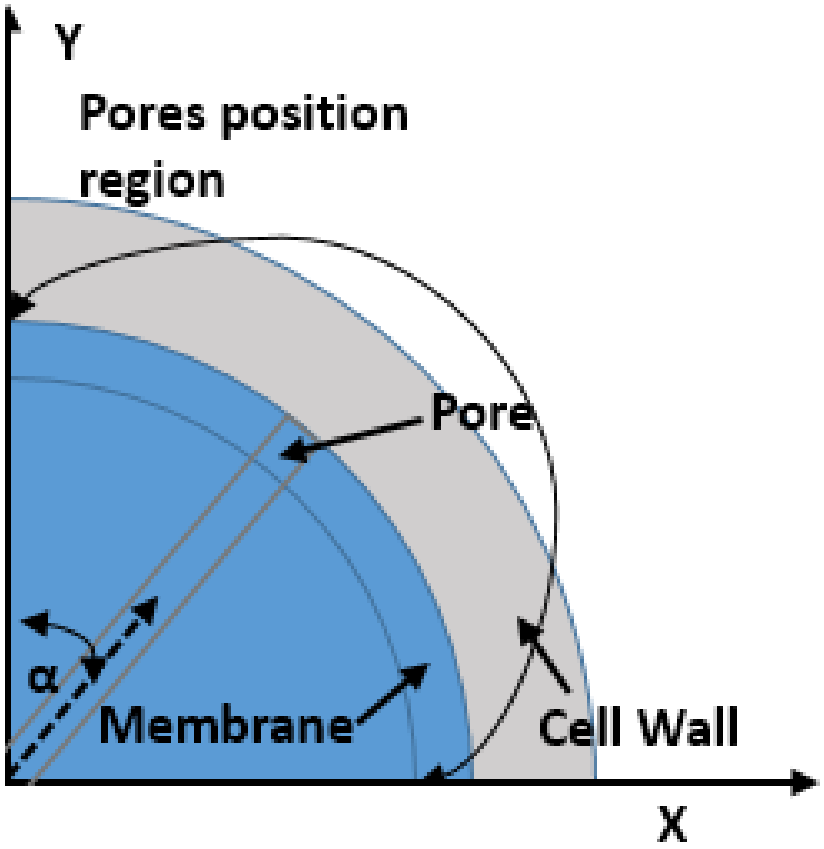

Figure (5.52) A model of the membrane with a pore.

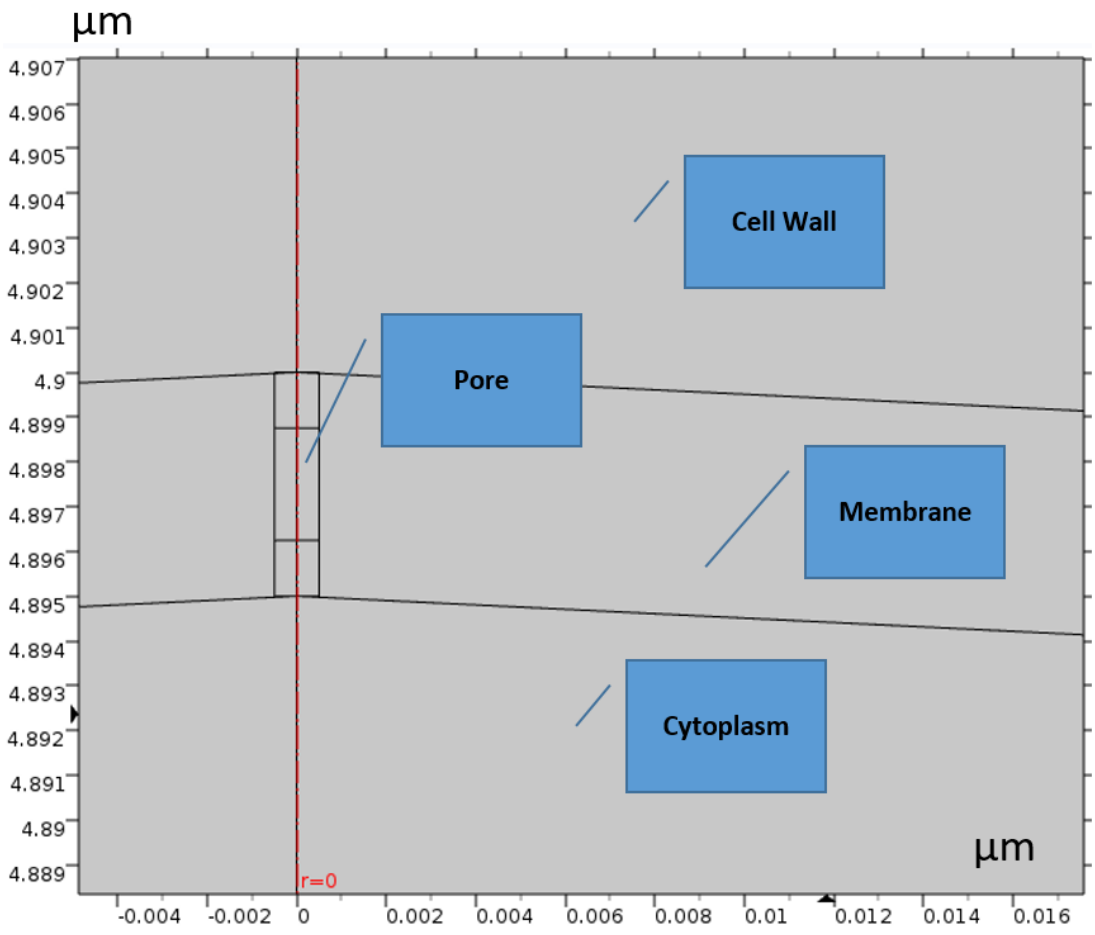

Figure (5.53) Pore in the membrane in the COMSOL model

Figure (5.54) shows the temperature distribution in the single cell model with the pore at a angle of 15 degrees. It could be observed that there are two hot spots in the treatment region: in the environmental fluid at the equator and in the pore itself which confirms that local heating could be generated in the pore.

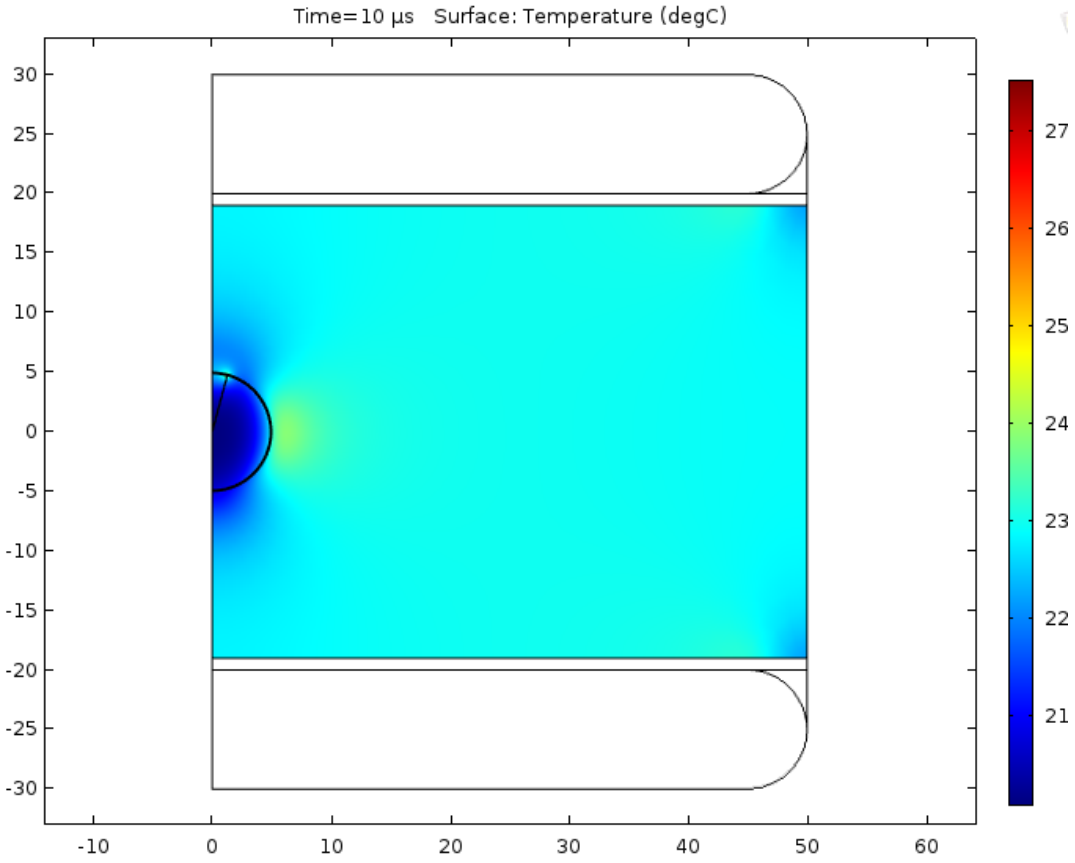

Figure (5.54) Temperature distribution at 10 µs in the model with a pore, α =15°, pore diameter d=1 nm. Axis dimensions in µm.

From the temperature distribution figures, **Figure (5.54)** and **Figure (5.55)**, it could be obtained that the existance of a pore does not influence the local heating effects in the surrounding fluid. The local heating effect in the pore is significant with temperature increasing to ~27 ℃ in 10 µs when α =15°, and the pore diameter, *d*=1 nm.

Figure (5.56) shows the effects of the pore diameter and position on the electric field and local heating effects. When α increases, the electric field strength decreases as the distribution of electric field in the membrane follows the Schwan Equation (**Eq. 3.1.4**). The pore diameter has significant impact on Joule heating in the pore, with more Joule heating occuring as the pore diameter increases.

Therefore, the formation of pores and local heating effects in these pores could make a noticable contribution to the electopration process during the PEF treatment. It was also observed that the maximum temperature in the pore saturates out at 36.1 degrees with pore diameter up to 5 nm ((b) from **Figure (5.56)**) which was never investigated and reported before.

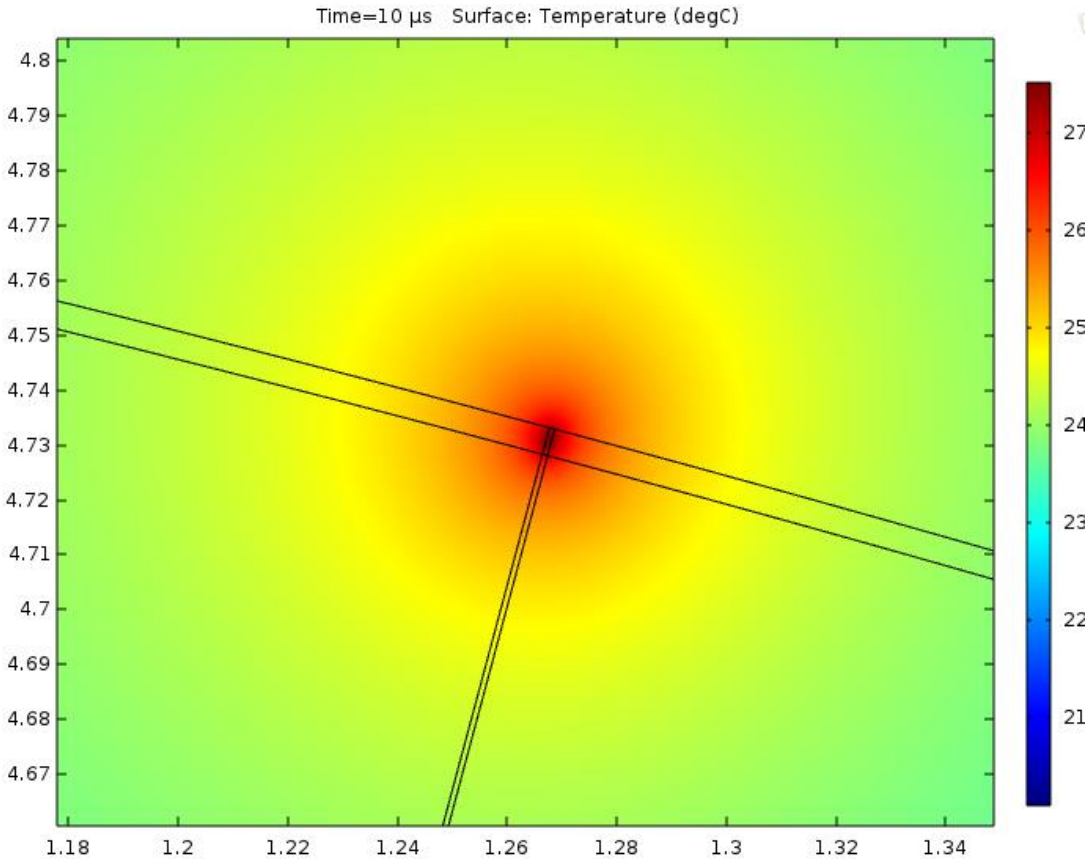

Figure (5.55). Temperature distribution in the pore: zoomed in view of **Figure (5.54)**. Axis dimensions in µm.

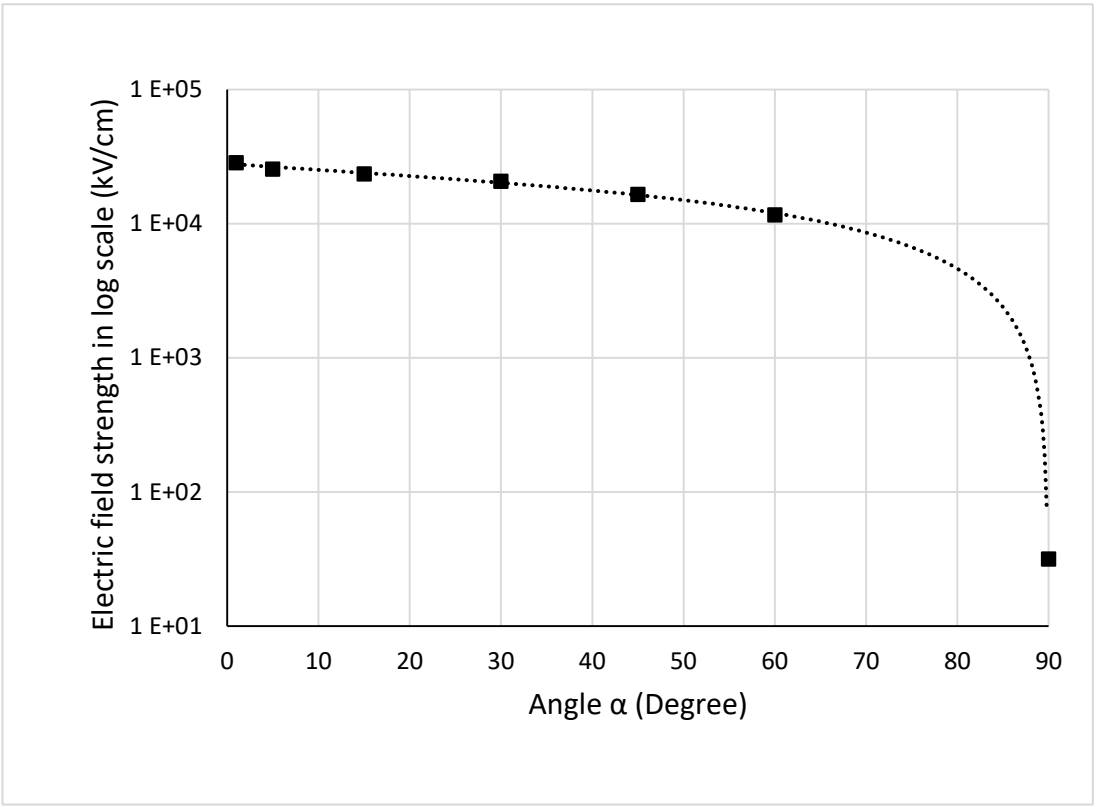
Electric field strength in log scale (kV/cm)
1 E+05
1 E+04
1 E+03
1 E+02
1 E+01
0
10
20
30
40
50
60
70
80
90
Angle α (Degree)

(a)

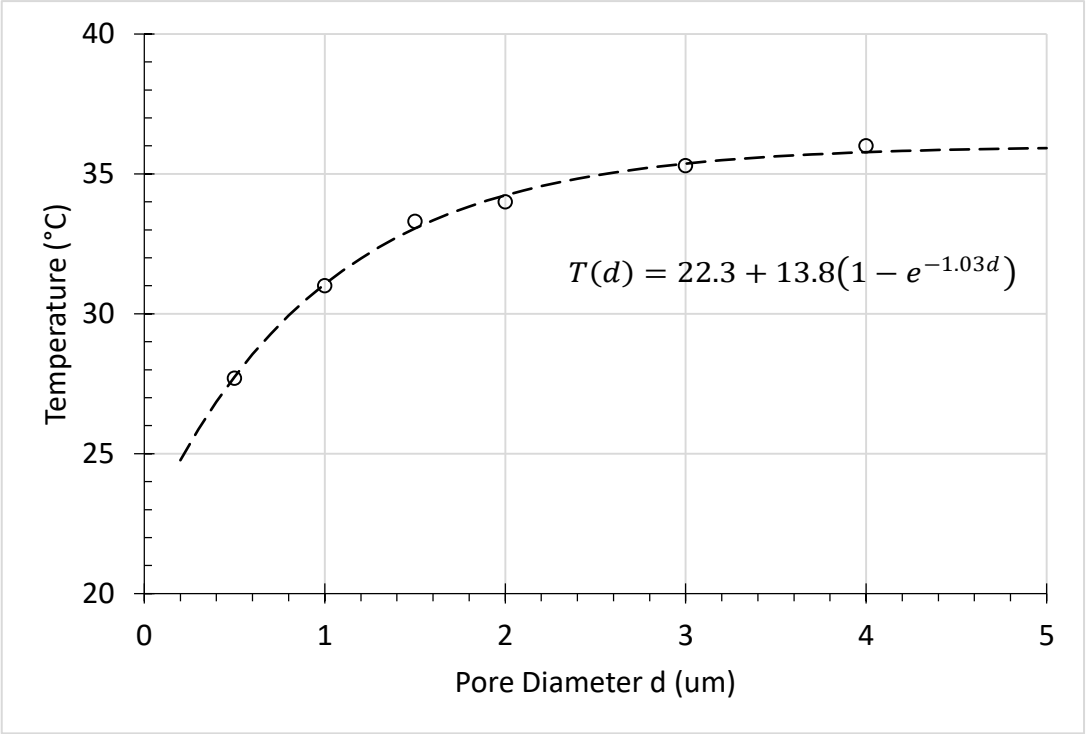
Temperature (°C)
40
35
30
25
20
0
1
2
3
4
5
Pore Diameter d (um)
$T(d) = 22.3 + 13.8(1 - e^{-1.03d})$

(b)

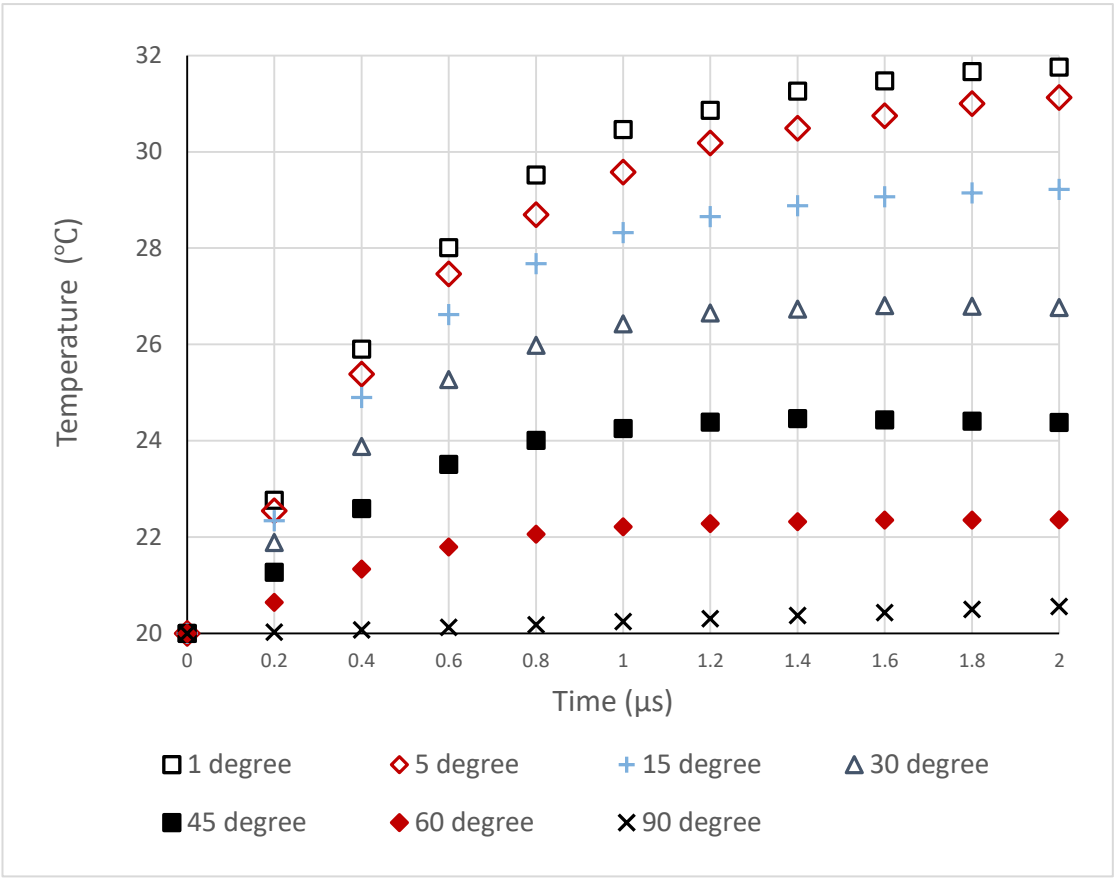

(c)

Figure (5.56) Simulation results for the single cell model with the pore in the membrane: (a) Maximum electric field in the pore as a function of α for t= 25 µs, (b) Maximum temperature as a function of the pore diameter at t= 25 µs and α=5° , (c) Maximum temperature in the pore as a function of time for different α, d=1 nm.

Figure (5.57) shows the difference in the electric field strength in the cell membrane for penetrated membrane (the membrane with a pore located at α=0°) and intact (no-pore) membrane. The graph shows that the field strength in the membrane with the pore is lower than the field strength in the intact membrane, this lower field strength is due to the conduction through the pore which leads to the reduction of the electric field in this situation.

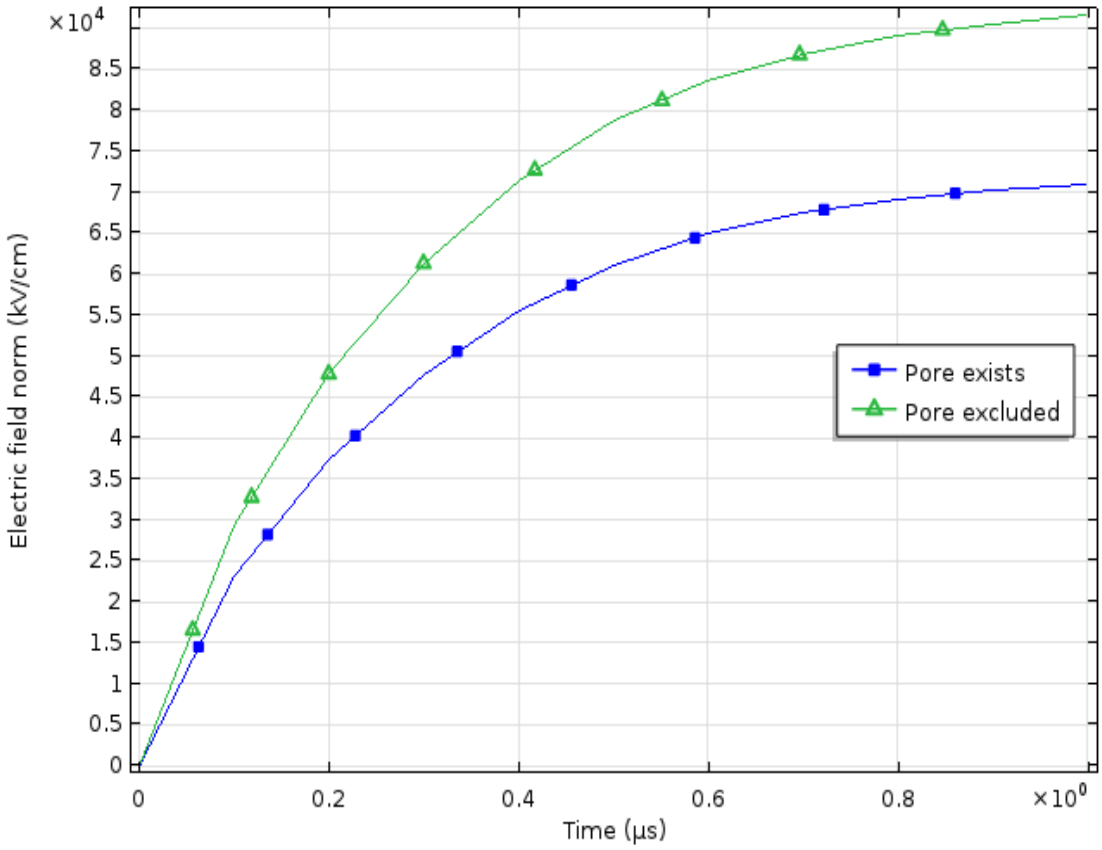

Figure (5.57) Electric field strength at the same location (α=0°) in the case of the electro-porated membrane (blue) and intact membrane (green).

5.7 Structural investigations

5.7.1 Geometry-ellipsoidal model

Ellipsoidal single cell model was built in COMSOL, to simulate the effect of the externally applied electric field on the ellipsoidal microorganisms (e.g. Yeast). The geometry parameters are listed in the **Table 5.3** below, the electrical and thermal parameters are set the same as in the spherical model. The applied electric field strength is 67 kV/cm with step voltage in this simulation, several conductivities (0.001, 0.01, 0.1,1,10 S/m) of the environmental fluid were used.

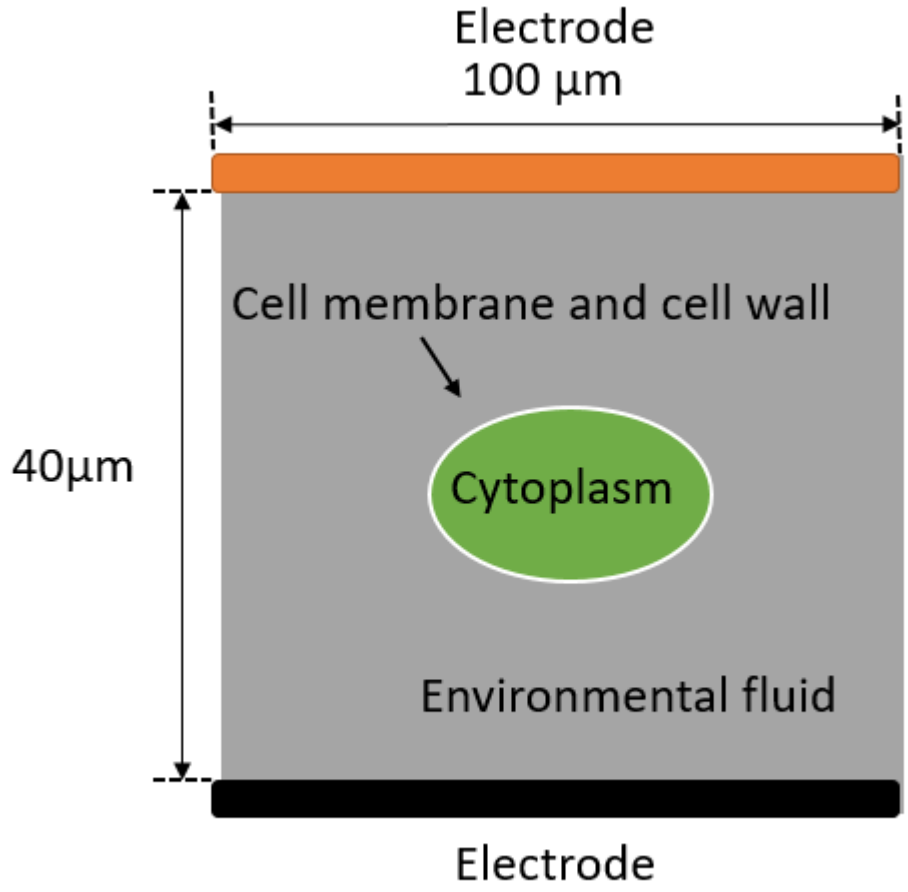

Figure (5.58) General topology of the ellipsoidal cell model, cell wall was included in the single cell model, it will be included in further sections.

Table 5.5 Geometry parameters of the Ellipsoidal model.

Geometry Design	**Ellipsoidal model**
Long axis	3.31 μm [330] [331]
Short axis	2.71 μm [330] [331]
Radius	N/A
Membrane thickness	7.5 nm [330] [331]
Wall thickness	0.1 μm [330] [331]

It can be seen from **Figure (5.59)** below that there is local heating generated at the same positions as in the spherical model (in the environmental fluid at the equator). The geometry didn't affect the local heating effects, it is only governed by the conductivity of the environmental fluid and the applied electric field strength.

Figure (5.60) and **Figure (5.61)** shows the relationship between the maximum temperature in the local hot spot and the conductivity of the fluid and treatment time for both cell shapes (spherical and ellipsoidal). In both cases similar results were obtained.

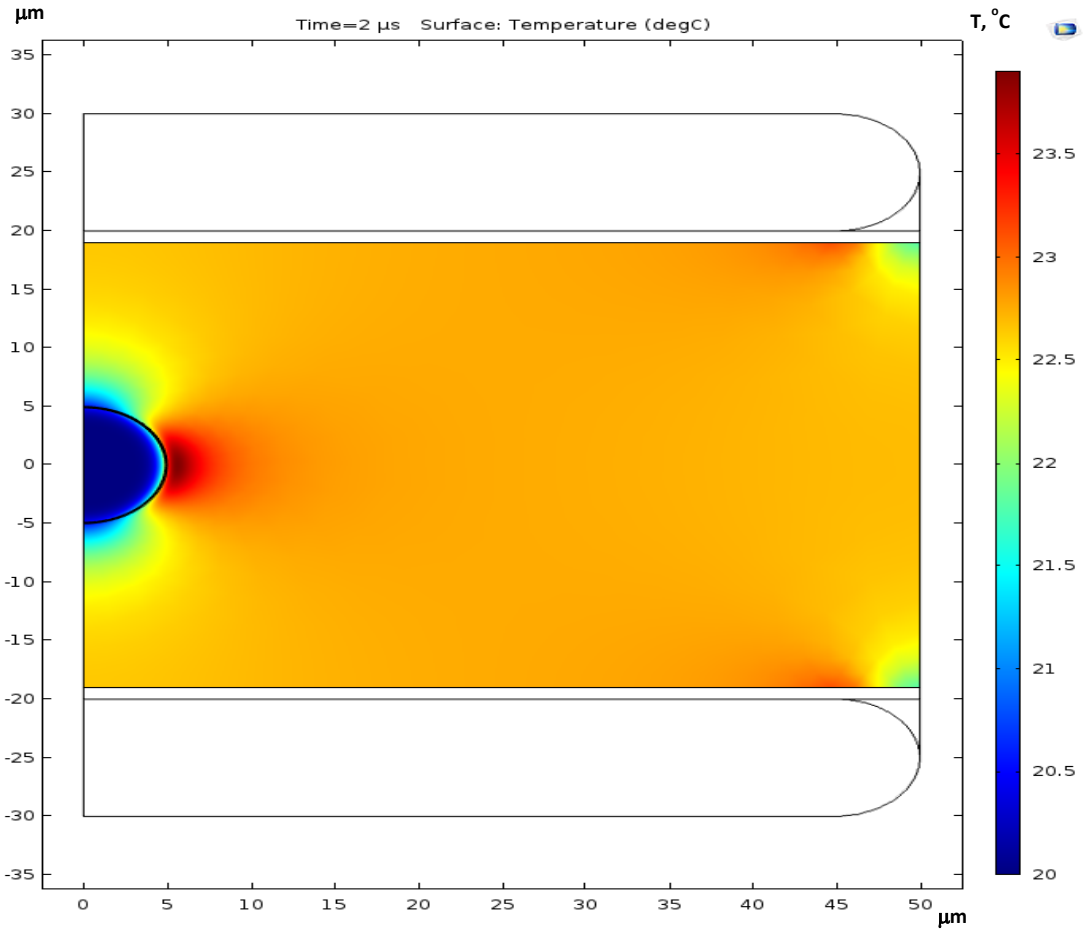

Figure (5.59) Temperature distribution in the ellipsoidal model at 2 µs with 67 kV/cm treatment, conductivity of fluid: 0.01 S/m. Axis dimensions in µm.

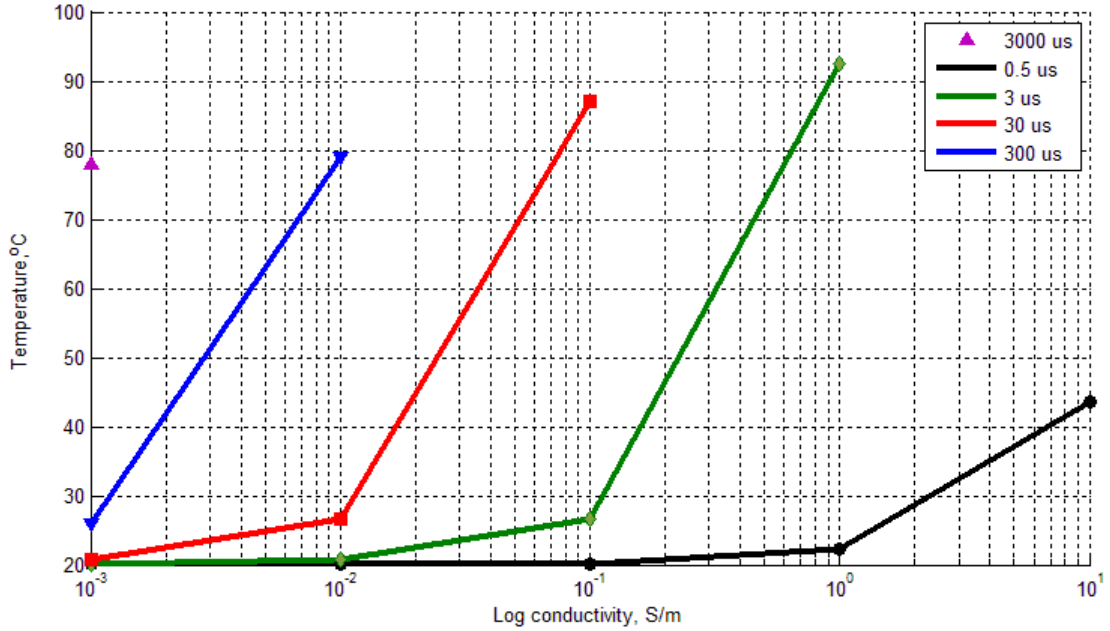

Figure (5.60) Maximum temperature in the local hot spot of the Spherical model

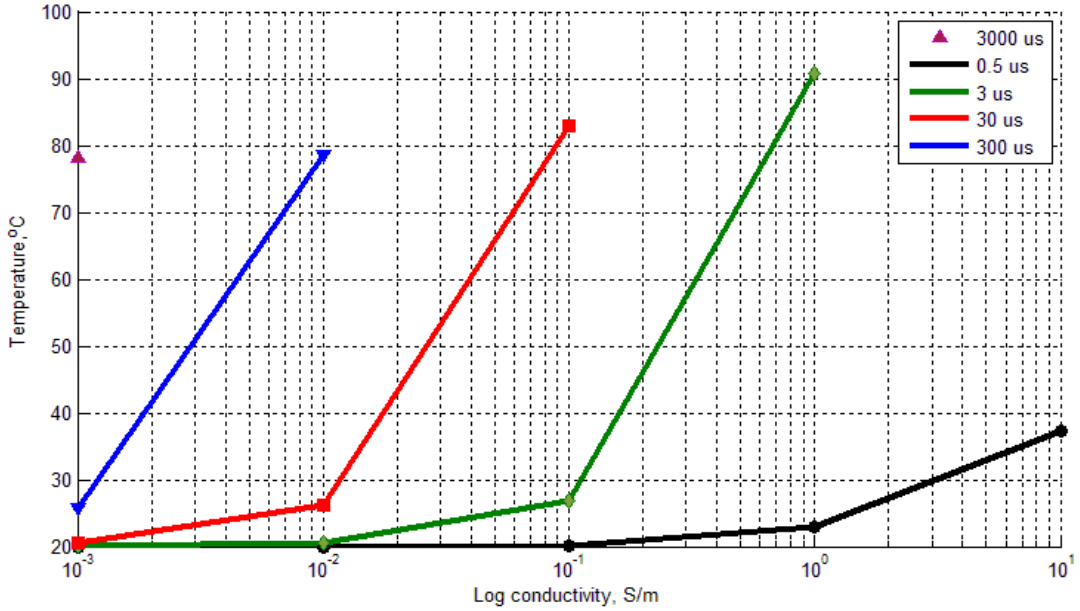

Figure (5.61) Maximum temperature in the local hot spot in the ellipsoidal model

Figure (5.62) shows the electro-mechanical force across cell membrane at the lower part of the cell obtained under step voltage energization in the ellipsoidal model. Comparing with the results presented in **Figure (5.31)**, the force reversal is also observed in this case due to *dV/dt*= 255 kV/us of the step voltage applied. The slight difference between the electro-mechanical forces was mainly caused by the different thickness of cell membrane from 5 nm to 7.5 nm.

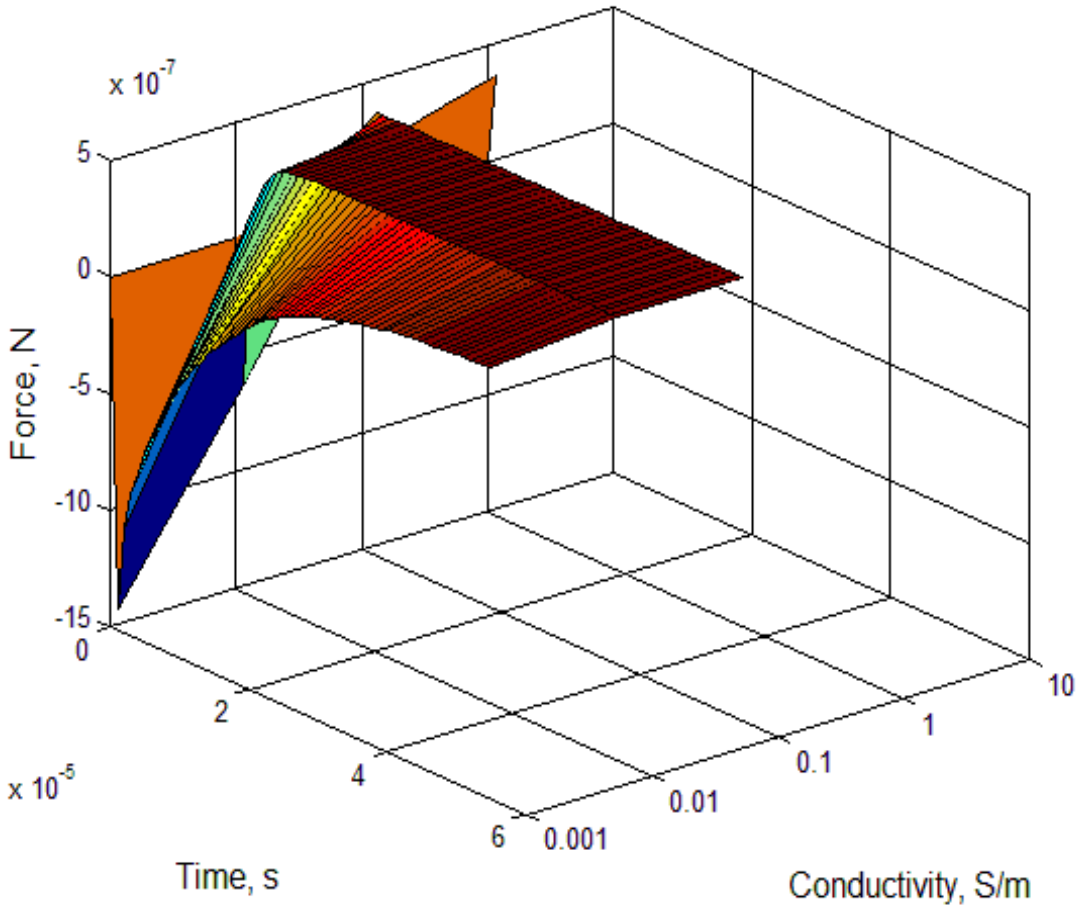

Figure (5.62) Electro-mechanical force across the cell membrane at the lower part of the cell under step voltage energization (External field strength: 67 kV/cm).

Figure (5.63) and Figure (5.64) shows the local heating effects under AC oscillating signals. It can be seen that there is only slightly difference between the values for

both models which is also caused by the slight difference in the size of the cells in these two models.

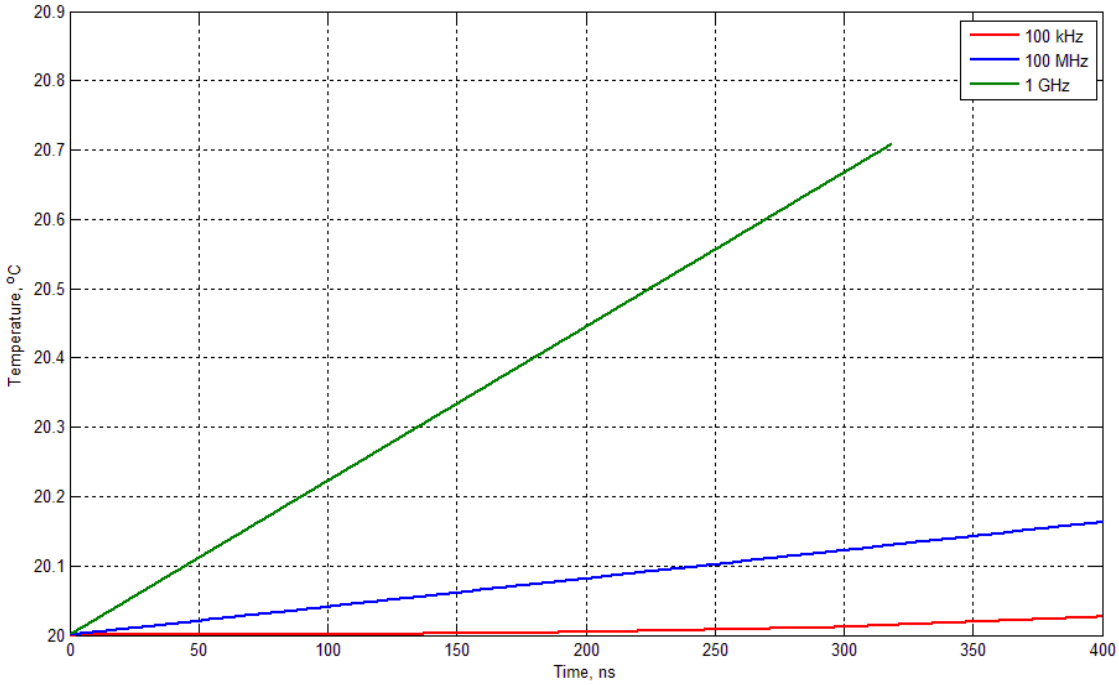

Figure (5.63) Temperature across the cell membrane in the spherical model with AC oscillating signal, conductivity of environmental fluid is 0.01 S/m, maximum field strength is 67 kV/cm.

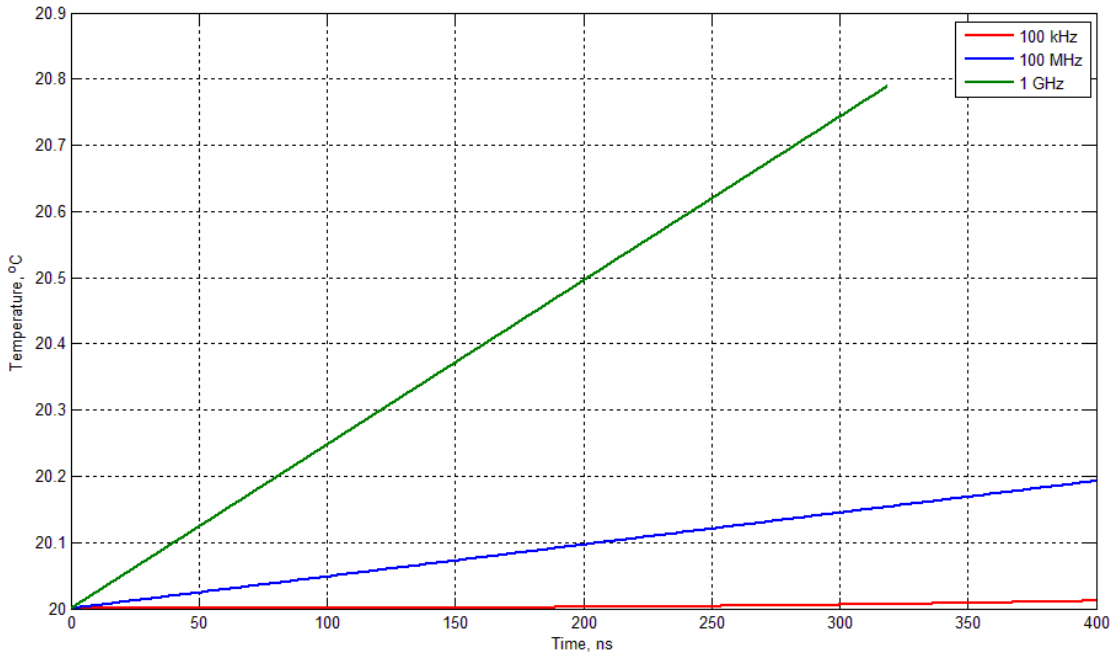

Figure (5.64) Temperature across the cell membrane in the ellipsoidal model with AC oscillating signal applied, conductivity of environmental fluid is 0.01 S/m, and maximum field strength is 67 kV/cm.

5.7.2 Cell wall and resting potential in the cell membrane

The cell wall was generally not considered in this simulation work as the ions can pass through the cell wall without limitations so the electrical conductivity and permittivity of the wall was set to the same values as the conductivity and permittivity of the environmental fluid.

It has been shown that the cell wall doesn't influence the local heating effects in the environmental fluid, as the joule heating is mainly generated in the environmental fluid according to the simulation and the electrical properties of the cell wall are set to the same values as in the environmental fluid, so the cell wall could be ignored.

The cell wall would have a slight influence on the heat absorption or deformation of the cells. However, the analysis of the cell deformation is more complex (and requires currently not well defined parameters and boundary conditions). Such analysis could be completed in future and will require further development of the cell model which is beyond the scope of the present project.

The resting potential of a cell is also included in this model, by placing a uniform surface charge with the density of $200 \times 10^{-6}\mathrm{C/m^2}$on the external surface of the membrane. However, it was found that this surface charge did not produce a noticeable effect on the maximum electric field distribution and its magnitude when the cell is stressed by strong external field.

5.7.3 Cell nucleus investigation

Using the Quickfield model introduced in Chapter 4, it is possible to include the cell nucleus in the single cell model. It was found that the electric field strength in the nucleus membrane also follows the Schwan Equation. Also, it was found that the transmembrane potential across the nucleus membrane that developed during the nano-second duration of the applied field is strong enough to cause electroporation. The cell nucleus was also included in the COMSOL single cell model to calculate the temperature distribution and electric field strength.

Figure (5.65) below shows the schematic diagram of the single cell model with the cell nucleus. The parameters of cell nucleus are listed in **Table 5.4** below, the conductivity of the environmental fluid (σ_4) is 0.1 S/m in this model.

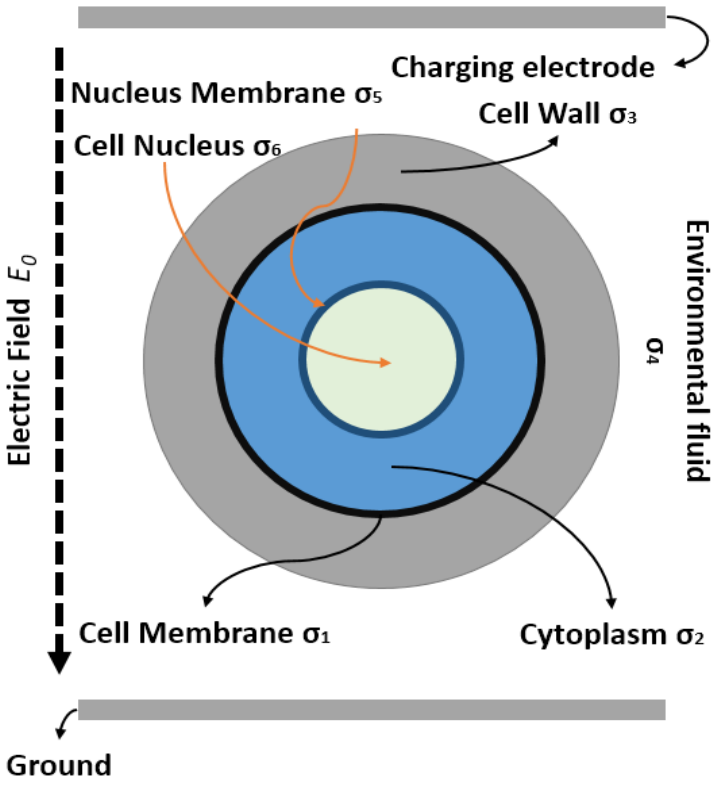

Figure (5.65) Single cell model with cell nucleus

Table 5.6. Parameters of cell nucleus in the model.

Parameters	**Value**
Relative permittivity of nucleus	52.7 [7] [318] [316] [315] [273] [275] [300] [307]
Relative permittivity of nucleus membrane	5 [7] [318] [316] [315] [273] [275] [300] [307]

Conductivity of nucleus	1.2 S/m [7] [318] [316] [315] [273] [275] [300] [307]
Conductivity of nucleus membrane	10^{-7} S/m [7] [318] [316]
Thickness of nucleus membrane	30 nm [7] [318] [316]
Heat capacity at constant pressure of nucleus membrane	545 J kg^{-1} $K^{-`1}$ [300] [307]
Heat capacity at constant pressure of nucleus	4181.3 J kg^{-1} $K^{-`1}$ [300] [307]
Thermal conductivity of nucleus membrane	0.4 J K^{-1} $m^{-`1}$ [7] [300] [307]
Thermal conductivity of nucleus	0.4 J K^{-1} $m^{-`1}$ [7] [300] [307]
Density of nucleus membrane	1100 kg m^{-3} [315] [273] [275]
Density of nucleus	998.1 kg m^{-3} [315] [273] [275]

Figure (5.66) and **Figure (5.67)** shows the electric field distribution during the PEF treatment with DC impulses, the transient results at 500 ns have been obtained using COMSOL. It was found that the electric field strength in the nucleus and cell membranes follows the Schwan Equation: with the maximum value at the pole and minimum value at the equator. All field values reach the electroporation threshold which confirms the finding made using the Quickfield model: the nano-second PEF treatment could be used to damage the cell nucleus structures. There was no local heating effects in the cytoplasm with the nanosecond PEF treatment, thus the increase in the temperature during the ns PEF treatment could be ignored, so the electroporation of the cell and nucleus membranes is mainly governed by the electric field strength induced in these membranes.

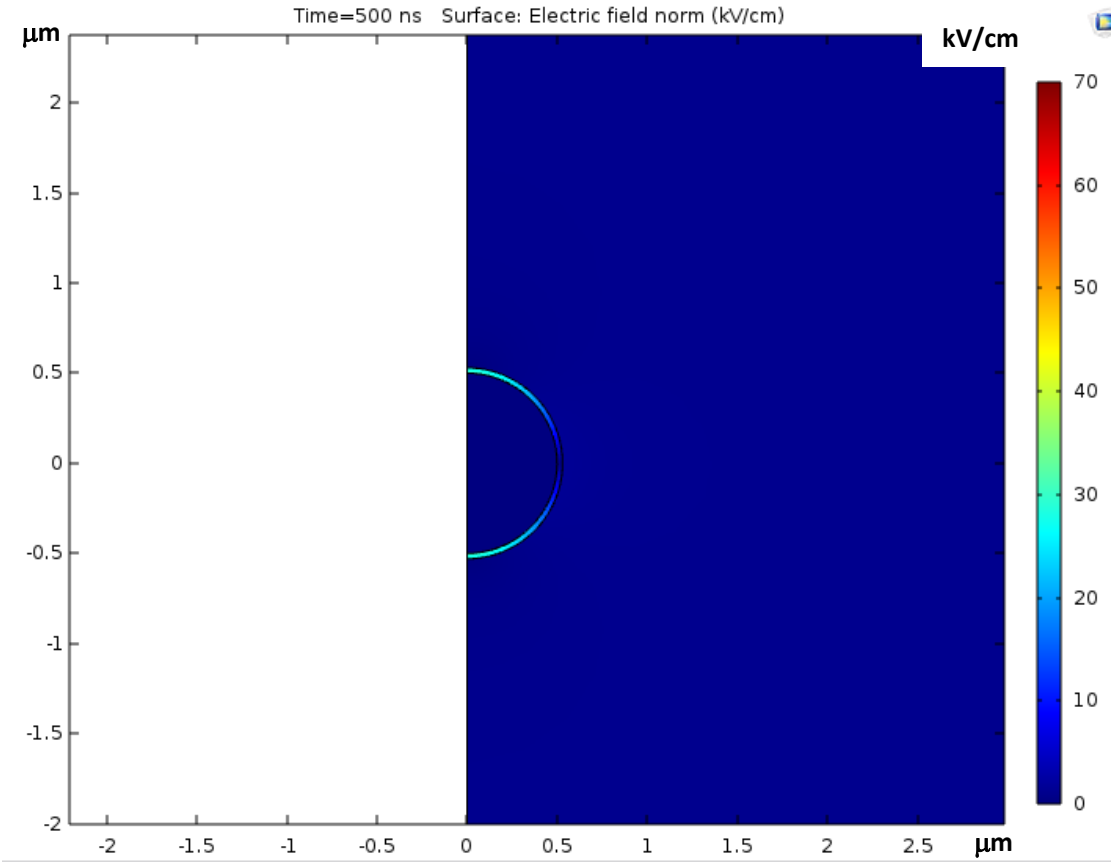

Figure (5.66). Electric field strength distribution in the nucleus membrane at 500 ns. E_0=30 kV/cm.

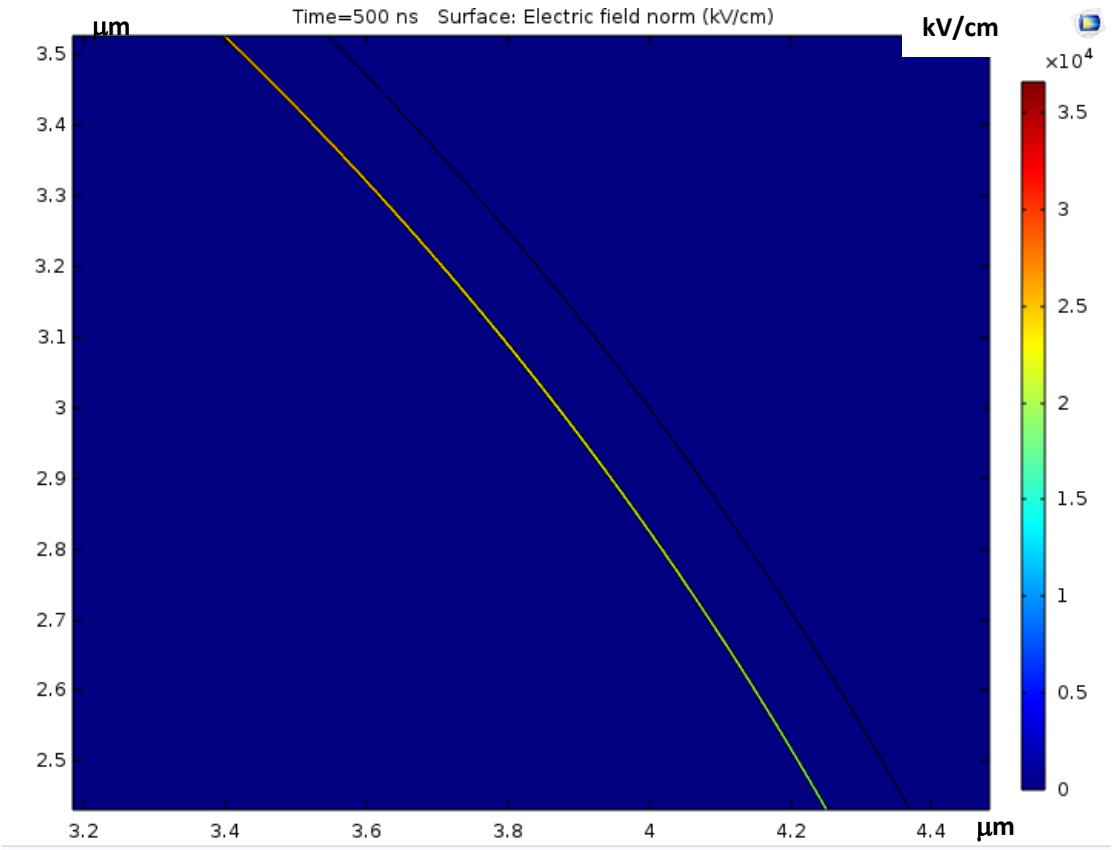

Figure (5.67). Electric field strength distribution in the cell membrane at 500 ns. E_0=30 kV/cm

Figures (5.68) and **(5.69)** below show the temperature distribution during the PEF treatment in the single cell model with the cell nucleus included. These results also support the results obtained using the Quickfield model, there were also local heating effects in the cytoplasm, however, the temperature increase was negligible. For the PEF treatment with longer time (more than 1µs in this model), as shown in **Figure (5.69)**, the local heating effects in the cytoplasm disappeared which also supports the results obtained using the Quickfield model. The transient

temperature of such local hot spots could be obtained using the COMSOL model which was not possible to model in the Quickfield model. The changing positions of the local hot spots over time can also be observed by comparing **Figure (5.68)** and **Figure (5.69),** this change is due to the charge accumulation process at the interfaces between the cell membrane and cytoplasm and environmental fluid.

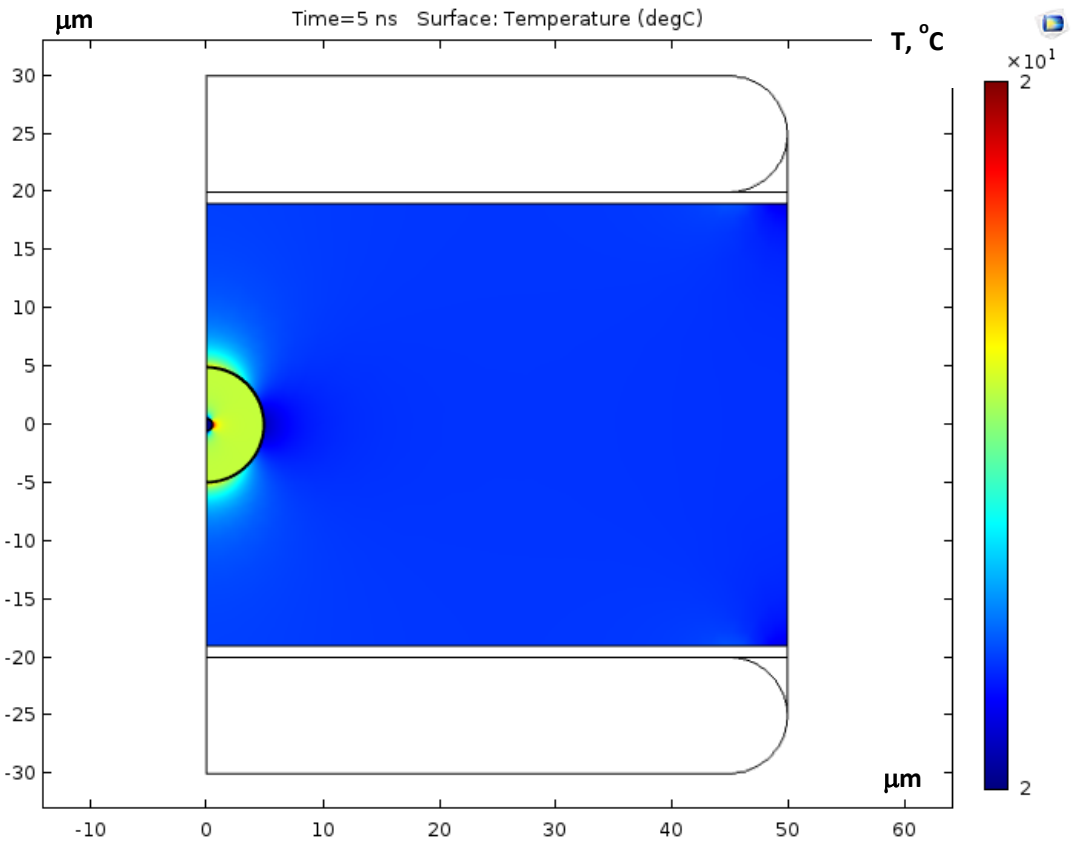

Figure (5.68). Temperature distribution at 5 ns.E_0=30 kV/cm

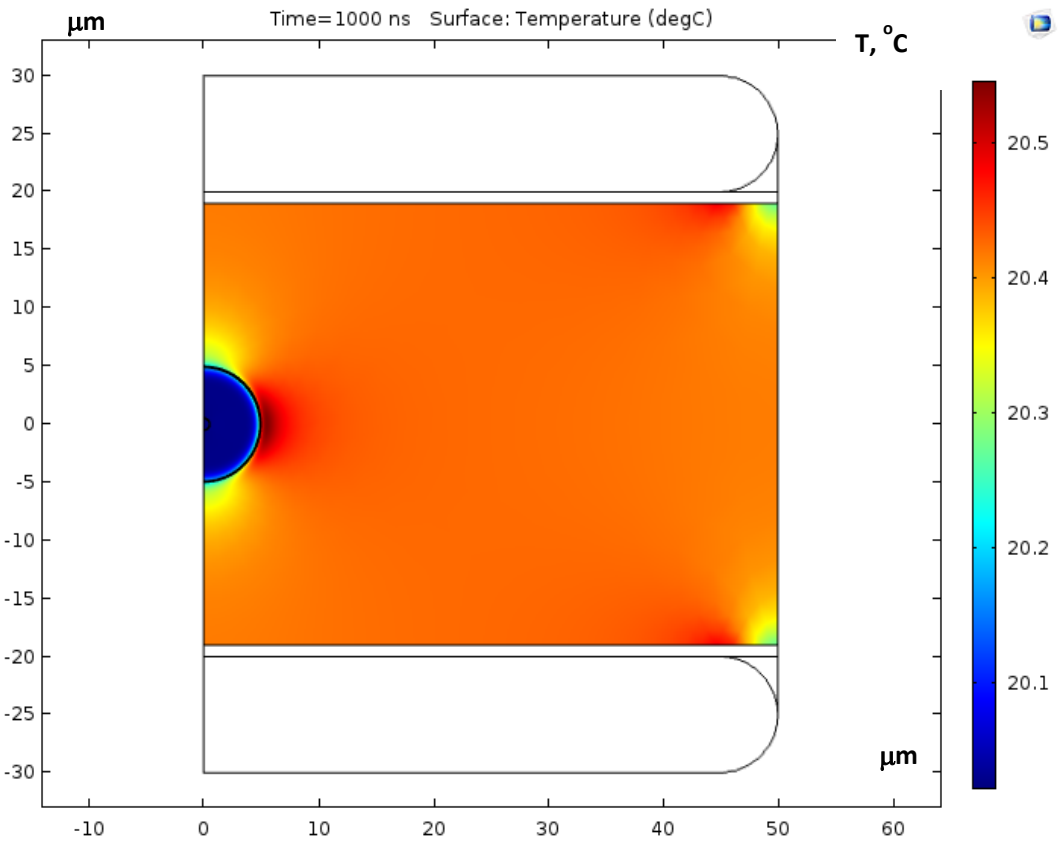

Figure (5.69). Temperature distribution at 1 µs. E_0=30 kV/cm

The electric field strength drop observed in **Figure (5.70)** follows the results obtained using the Quickfield model for the nano-second PEF treatment. When the charge accumulation process is completed, the electric field inside the cell membrane (in cell nucleus and cytoplasm) decreased as shown in **Figure (5.72)** and **Figure (5.73)**. Comparing **Figure (5.70)** and **Figure (5.71)**, it can be seen that, the electric field strength in nucleus membrane collapses after 1 µs due to the redistribution of field in the cell membrane, the dielectric properties of the cell membrane causing a behaviour similar to the system with electrodes with dielectric barrier discussed in [108] [181]. Therefore, with 1 µs PEF treatment, the cell membrane could be continuously affected by the high electric field strength which could result in pores

forming in the cell rather than the nuclear membrane. The results on the electric field strength and local heating effects support the simulation results obtained in the Quickfield model.

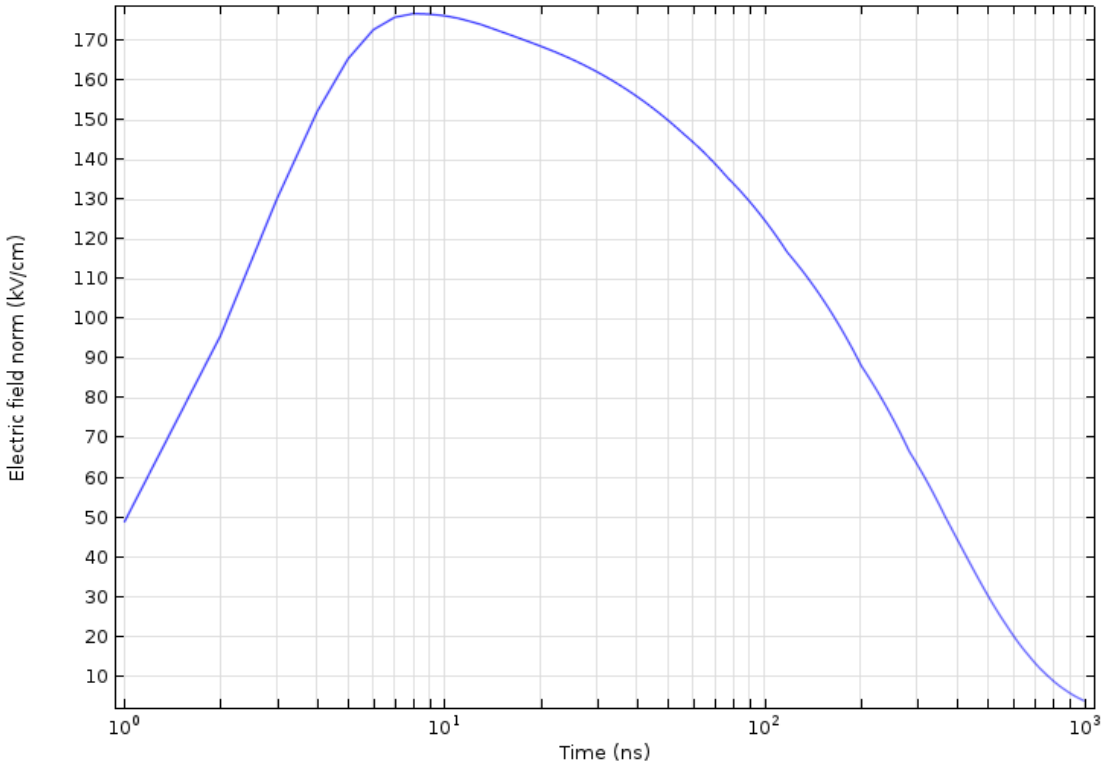

Figure (5.70). Maximum electric field strength in the nucleus membrane during 1µs PEF treatment, E_0=30 kV/cm

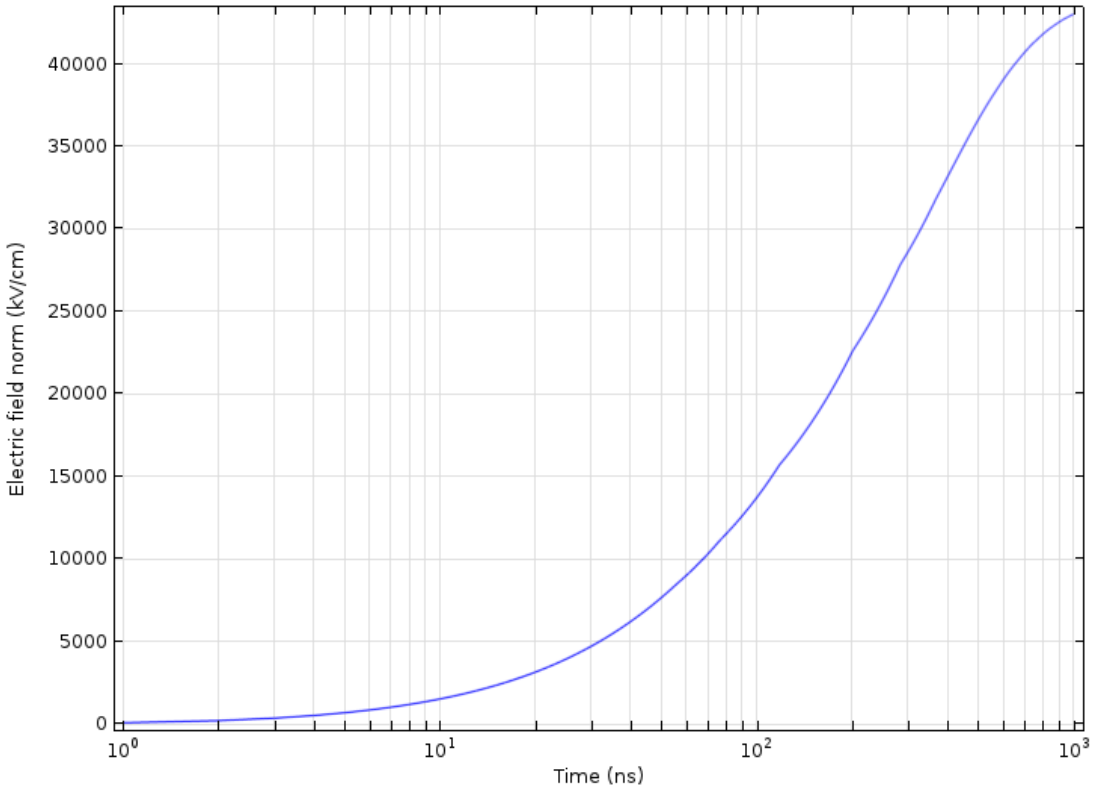

Figure (5.71). Maximum electric field strength in the cell membrane during 1µs PEF treatment, E_0=30 kV/cm

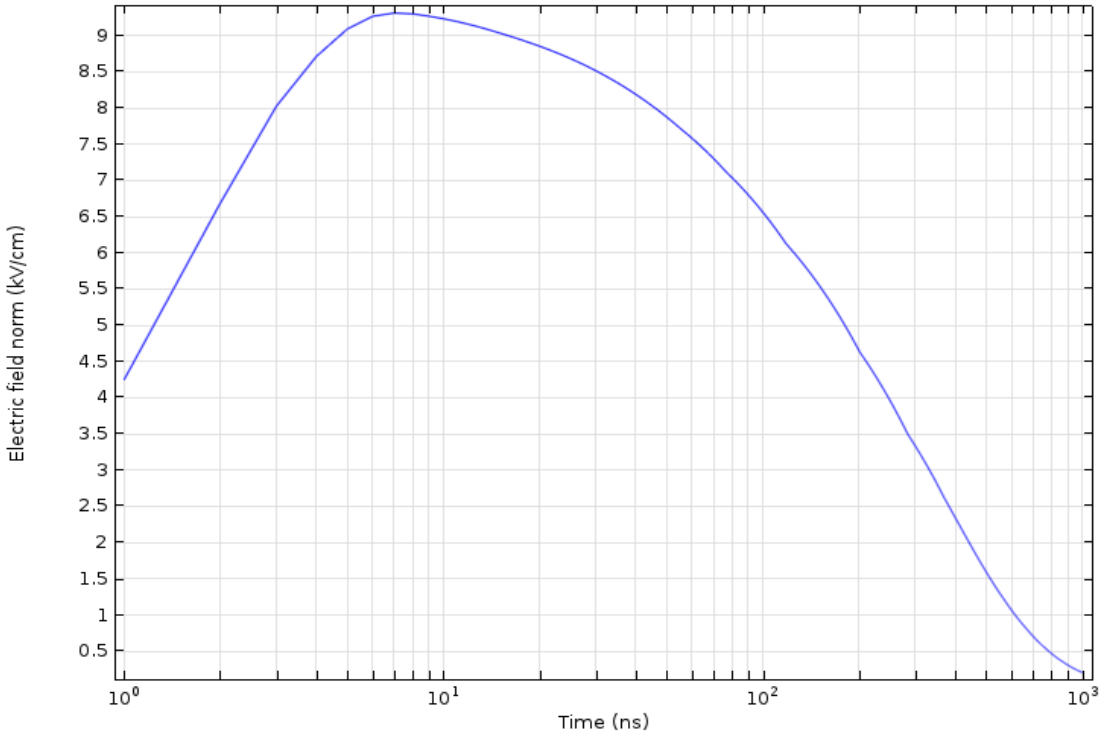

Figure (5.72). Maximum electric field strength in the cytoplasm during 1µs PEF treatment, E_0=30 kV/cm

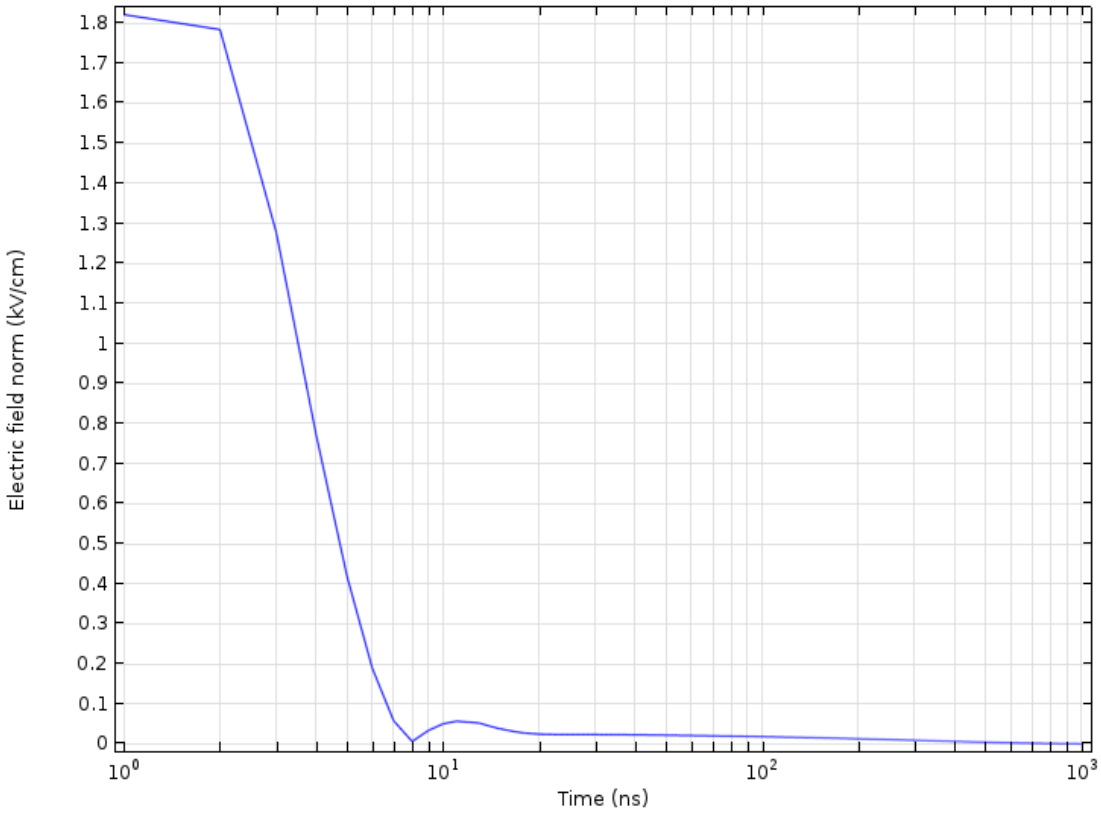

Figure (5.73). Maximum electric field strength in the cell nucleus during 1µs PEF treatment, E_0=30 kV/cm

5.8 Summary and discussions of the COMSOL simulations

A more advanced single cell model, based on multi-physics analysis, was developed in this Chapter using COMSOL software. This model was used to investigate the local heating effects and electro-mechanical forces induced by transient electric fields during the PEF treatment. Transient temperature distribution during the PEF treatment was obtained using the COMSOL model which couldn't be achieved with

the linear model or Quickfield model presented in the previous Chapters. This is a significant development in modelling of the transient thermal and electro-mechanical processes during the PEF treatment of microorganisms which couldn't be achieved with other models.

Temperature dependent parameters and resting potentials were also included in this model to increase the accuracy, however, it was confirmed that within the typical electroporation regimes, the temperature dependency of the conductivity and permittivity could be ignored. But this model provides a possibility to investigate the effect of these parameters in some specific applications in future.

Different HV signals (energization regimes) were used in this chapter. The COMSOL model allows for the analysis of the transient processes in model biological cells stressed with different voltage wave-forms: ramp signals, step voltage, square pulses and AC oscillating signals which make this model more advanced as compared with the linear and Quickfield models developed in Chapters 3 and 4.

Analysis of the conduction and thermal processes in membranes of microorganisms pores during the PEF treatment was conducted using the developed COMSOL model. Typically it is not possible to investigate these processes using simple analytical models (the linear model) or electrostatic models.

Using the single cell model developed in this chapter, differences in the conduction and heating between electro-prorated and intact membranes have been investigated which is typically not taken into account in studies of the PEF treatment of microorganisms.

The distinction between joule heating and dielectric heating in the single cell model makes the investigation of the local thermal effects more accurate. This analysis was conducted in the present chapter.

Using COMSOL model simulation results, the relationship between the electric field strength in the cell membranes and the applied electric field have been obtained directly.

With inclusion of the cell nucleus in the model, the COMSOL single cell model supports the simulation results obtained in the Quickfield model and linear model. These results confirm that the nano-second PEF treatment can induce sufficiently strong field strength in the nucleus membrane to cause the electroporation process. The thermal effects during the typical PEF treatment with low conductivity environmental fluid (~30 kV/cm) could be ignored, the PEF treatment could be considered as a non-thermal treatment. However, with higher conductivity of the environmental fluid, the thermal effects in the environmental fluid could not be ignored anymore.

Comparing AC and DC stressing, In the AC situation, the local heating effects in cell membrane are massive due to the dielectric heating caused by high electric field strength and oscillating electric field, joule heating is negligible. This could impact electroporation and lysis. For DC situation, for conditions required for electroporation and low conductivity media the local heating effects due to joule heating could be negligible.

The electro-mechanical force reversal was observed, this force reversal could help to rupture the cell structures during the PEF treatment.

The ellipsoidal and spherical models show similar electric field and temperature distributions which confirms that the electric field strength in the cell membrane was only determined by the membrane thickness and by the applied field strength

and the local heating effects are mainly governed by the external field strength and conductivity of the environmental fluid.

This COMSOL single cell model provides significant potential for further optimization of the PEF treatment with microorganisms.

Chapter 6. PEF treatment and Plasma treatment experiments of microalgae

6.1 General introduction

This chapter presents the experimental research on the PEF and plasma treatment of microalgae. Different test cells were designed and used in these tests. For the PEF treatment the standard electroporation cuvette and in-house made metallic test cell of larger volume were used. For the plasma impulsive treatment metal and plastic dishes were used with the plasma generating electrodes located above their surfaces. Detailed information on the developed test cell topologies will be provided in the following sections.

Liquid samples placed in the case of standard electroporation cuvettes were stressed with impulsive fields with magnitudes of 40 kV/cm to 45 kV/cm, while the higher electric field strength of 68 kV/cm to 70 kV/cm was achieved in liquid samples placed in the in-house made metallic test cell. For plasma treatment, high voltage impulses with magnitude of 22 kV were used to energise the plasma electrodes, this applied voltage was the same as in the case of the PEF treatment process in the PEF metallic test cell.

The results obtained include inactivation/growth curves of microalgae treated with impulsive electric fields with different magnitudes, different number of PEF impulses and different number of plasma impulses in the case of the plasma treatment. These results will help to compare and optimize the efficiency of the PEF

and plasma treatment processes with the same pulse power source (pulse generation system) and energy per pulse used.

6.2 Test cells

6.2.1 Modified Electroporation cuvette test cell

An electroporation cuvette is a plastic container made of crystal styrene with two embedded parallel aluminium electrodes. These cuvettes are used in the cuvette-based electroporation systems, they have colour coded caps which corresponds to different inter-electrode distances. For example, cuvettes with a red cap have an inter-electrode gap of 1 mm (these cells are typically used to treat bacteria), cuvettes with a blue cap have an inter-electrode gap of 2 mm (these cuvettes are used to treat yeast) and cuvettes with a green cap have a 4 mm gap between the electrodes and are generally used for treatment of mammalian cells [332].

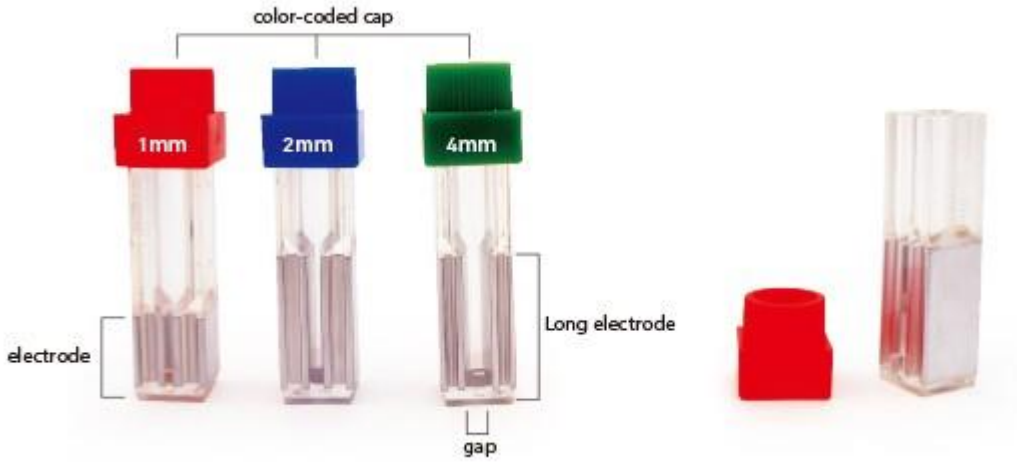

Figure (6.2.1.1) Electroporation cuvette with different thickness of gaps. Pictures taken from [332].

These electroporation cuvettes (Biotech supplied by Geneflow, UK) can be modified to satisfy the requirements of the PEF treatment for this work. Generally, the electroporation treatment requires an electric field strength of 20- 25 kV/cm. In the PEF treatment experiments planned for the project, the electric field strength was

expected to be 60-70 kV/cm. Thus, to achieve such high electric field strength, 1 mm gap cuvettes were used in the PEF tests conducted in the present study. Two holes were drilled in the plastic cuvette body to attach threaded rods to the plane aluminium electrodes embedded into the cuvette body. These rods shown in **Figure (6.2.1.2)** were connected to the output terminals of the pulse generation system. This modified test cell has to be put into a sealed chamber filled with pressurized air to avoid breakdown across liquid/gas interface in the test cell so the maximum electric field strength of 60-70 kV/cm can be achieved. Samples of algae treated in this test cell can only be used for microscope observation, as this modified electroporation test cell can only accommodate 50 µL of liquid in each test and this volume is not sufficient to provide the required population of algae to monitor their growth using the spectrophotometer measurement technique which is discussed in **section 6.7**.

In order to increase the volume of the treated samples, 4 electroporation cuvettes were connected in parallel, **Figure (6.2.1.2)**.

Figure (6.2.1.2) Modified electroporation cuvette and 4-parallel cuvettes.

However, even this increased volume of liquid samples was not sufficient to perform reliable spectrophotometric analysis and the volume of the sealed pressurized container was not sufficient to accommodate larger number of the electroporation cells connected in parallel. Thus, a standalone larger volume test cell was used to provide the increased volume of liquid samples required for the spectro-photometrical analysis.

6.2.2 Large volume metallic test cell

In order to have enough volume of samples for spectrophotometer measurement, a new larger volume test cell is required. From the previous study conducted and presented in [78], it is known that a test cell with a volume of 1.5 ml should provide

a volume of treated sample sufficient for the spectrophotometry. This larger test cell also has an open-top design which can be used to remove any bubbles before treatment. This test cell consists of two parallel plane stainless steel electrodes, a PTFE spacer which separate the electrodes and a set of 7 nylon screws which holds this whole structure together, as shown in **Figure (6.2.2.1)**.

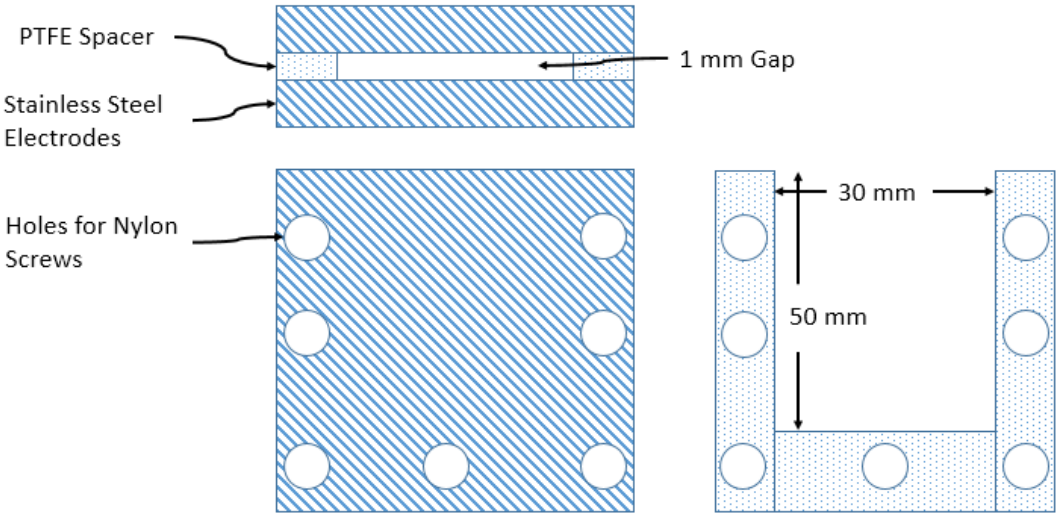

(a)

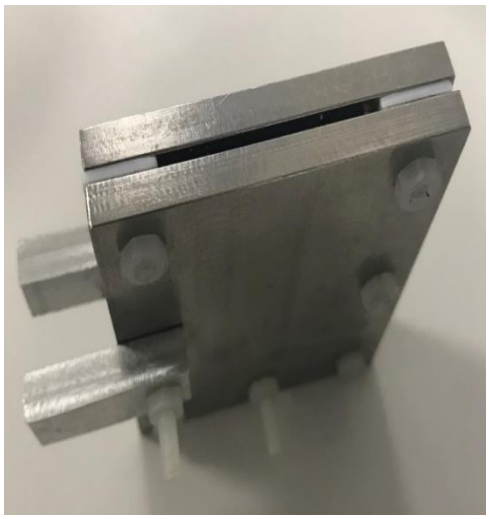

(b)

Figure (6.2.2.1) Metallic test cell. (a) Schematic diagram of metallic test cell with PTFE spacer. (b) Fully assembled metallic test cell.

The PTFE spacer remains stable during the PEF treatment and maintains the required separation when compressed with the nylon screws. Besides, compared for example with nylon, PTFE is softer which means a better seal can be achieved by compression of the electrodes and the spacer. 1.5 ml of liquid can be treated each time in the test cell and the gap is 1 mm, a 40 kV/cm electric field can be delivered to the samples.

6.2.3 Metallic dish and point HV electrodes for plasma test

The plasma discharge test cell designed for the plasma treatment consisted of the grounded metallic dish to hold a sample of liquid with a volume of 3 ml and 6 sharp point HV electrodes are located above the liquid surface to generate plasma discharges above the liquid sample. (The sharp point electrodes are general Gramophone needles which have a radius of ~ 80μm, as measured in [333].)This dish was made of stainless steel. The plasma treatment test cell is shown in **Figure (6.2.3.1)**.

(a)

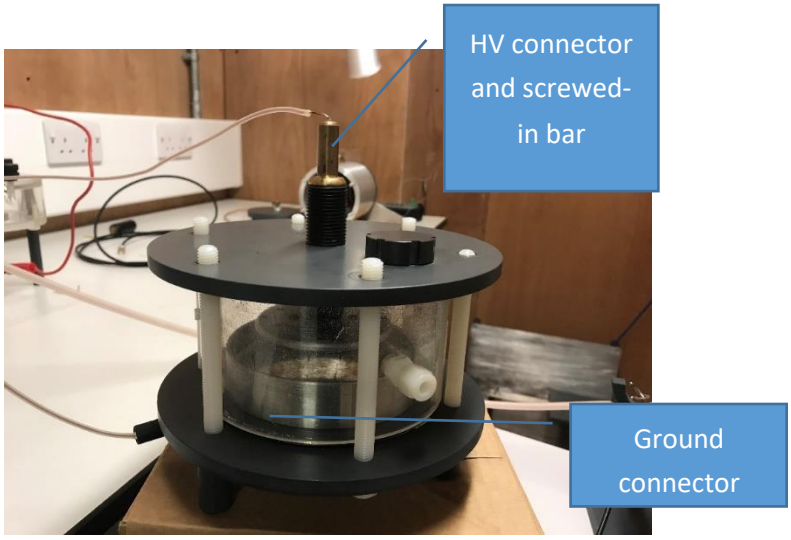

(b)

Figure (6.2.3.1) Metallic dish test cell (a) for Plasma treatment and needle-plate test chamber (b).

The output of the pulse generator discussed in **section 6.3** was connected to the HV electrode of the test chamber. The gap between the tip of the needles and the liquid surface can be adjusted by rotating the HV connector bar. The metallic sample dish was solidly attached to the grounded plate at the bottom of the test cell.

Figure (6.2.3.2) 6-needle HV electrode mounted in the test chamber above the dish with liquid sample.

The HV ring with 6 sharp needles and the grounded dish are shown in **Figure (6.2.3.2)** above. Detailed information on the plasma experimental conditions including the plasma gap and waveforms will be introduced in **section 6.7** in this chapter.

6.2.4 Plastic dish

The metallic dish with liquid sample described in **Section 6.2.3** is directly connected to the ground providing a conductive path for the current through the liquid sample in the metallic dish. Thus, the charge can be delivered directly to the sample located in the metallic dish.

Another approach adopted in the present work is based on locating the liquid sample in a plastic, non-conductive dish. In this case, the conduction current cannot go through the sample in the plastic dishes, because there is no conduction path through the liquid and plastic dish. In this case the sample in the plastic dish will be subjected to the plasma action only, as plasma will be generated above the surface of the liquid sample.

However, there will be no direct conduction through the liquid under test, so it will be possible to evaluate the efficiency of plasma treatment in both cases with and without direct conduction of current through the liquid.

The inactivation efficiency of plasma treatment in conductive and non-conductive dishes was investigated and comparison between the inactivation efficiencies achieved using the same energy per pulse and number of plasma pulses will be made.

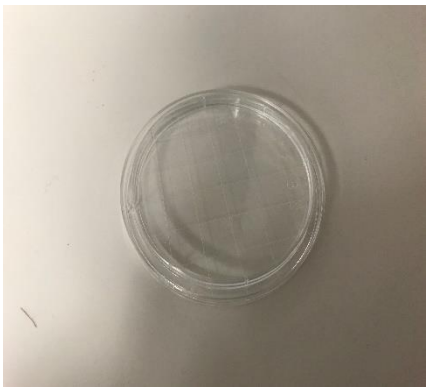

Figure (6.2.4.1) Plastic dish for plasma treatment (Petri dish)

Figure (6.2.4.1) shows the picture of the plastic dish (Sterilin Contact Plate, Thermos Scientific) used in the test. The diameter of the plastic dish is 55 mm. Liquid samples with volume of 3 ml can be treated in this plastic dish which is the same volume as the metallic dish can accommodate.

6.3 Pulse generation system for the tests

Due to a narrow, 1 mm gap between the pin HV electrodes in the PEF treatment test cell and the liquid surface, HV pulses with a peak magnitude of 6 kV are required to provide the nominal electric field strength of 60 kV/cm across the liquid sample (the nominal average field is calculated as the applied voltage, 6 kV divided by the distance, 1mm).

A Blumlein generator was designed and built (as shown in **Figure (6.3.1)**) in this project to generate 1 µs square HV impulses for the PEF and plasma treatment. According to **Equations (6.1 and 6.2)**, two 100 metre lengths of coaxial cable URM43 (total length 200m), with the characteristic impedance of Z=50 Ω and capacitance of 98 pF/m is required to generate 1 µs impulses.

$$\boldsymbol{Z = \sqrt{\frac{L_0}{C_0}}} \qquad \textbf{(6.1)}$$

$$\boldsymbol{v^2 = \frac{1}{L_0 C_0}} \qquad \textbf{(6.2)}$$

Where Z is the characteristic impedance of the coaxial cable, C_0 is the capacitance per unit length, L_0 is the inductance per unit length, v is wave speed in the coaxial cable.

The magnitude of the HV impulses can be controlled by changing the gap of the spark switch and the charging voltage, the pulse repetition rate can be adjusted by increasing or decreasing the current (power) provided by the DC power supply. In this system an AU-60 series HVDC power supply from Matsusada Precision Inc was used, which produces DC voltage from 0 kV to 60 kV. Two power supplies were used in the plasma treatment to achieve plasmas using different pulse polarities for positive and negative plasma treatment regimes**.**

Figure (6.3.1) below shows the connections between the Blumlein pulse generation system and power supply.

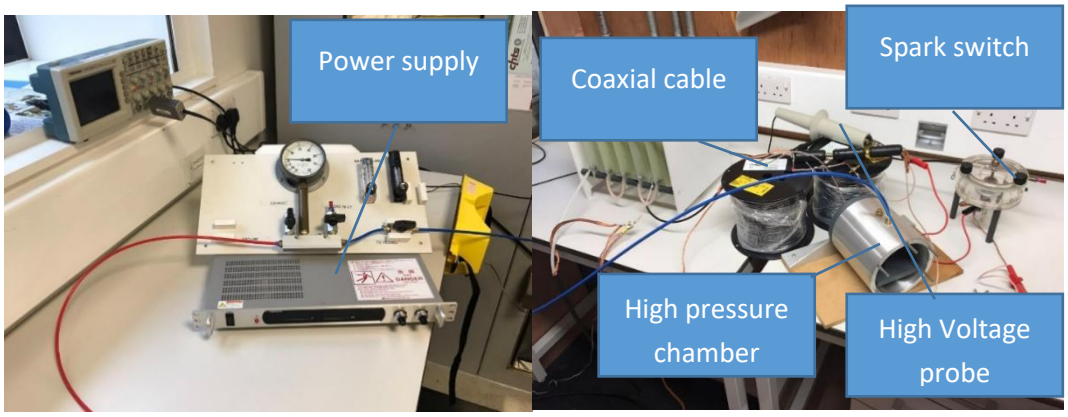

Figure (6.3.1) HVDC Matsusada Precision power supply, Blumlein pulsed power system based on URM43 coaxial cable.

The Blumlein pulse generation circuit was simulated using Pspice software before development of the practical pulsed power system in order to confirm a 1 µs impulse could be generated. **Figure (6.3.2)** shows the diagram of the generation system and the output impulse generated after triggering the spark switch (solid line square). The pulse generation system consists of 6 main parts: DC power supply (V1), charging resistor (R1), transmission lines (T1 and T2), matching resistor (R2)

and spark switch (U1). R3, R4 and C1 represents the test cells in this Pspice model. Inductances of wires used to connect different elements of the circuit are also labelled in this diagram (L1-L6). The circuit is protected through a high resistance charging resistor which is R1 left. T1 and T2 are the transmission lines which generate the HV impulse, the dashed line square shows the load which is test cell with growing microorganism samples, resistors and capacitor were used to represent the electrical properties of the microorganisms [78]. In **Figure (6.3.2)** (b), the green line represents the impulse wave shape generated by the Blumlein generator and the red line shows the input voltage.

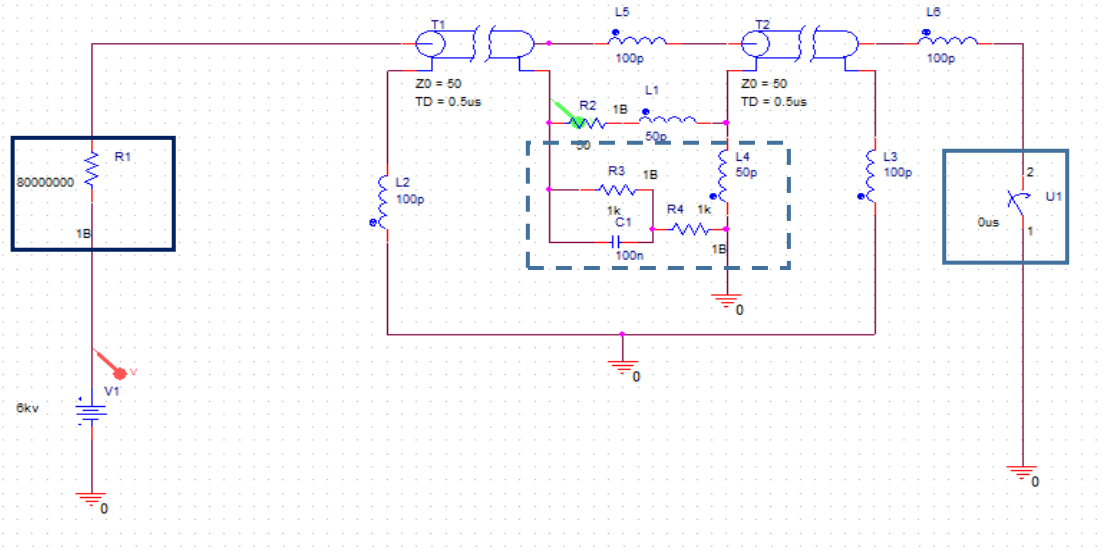

(a)

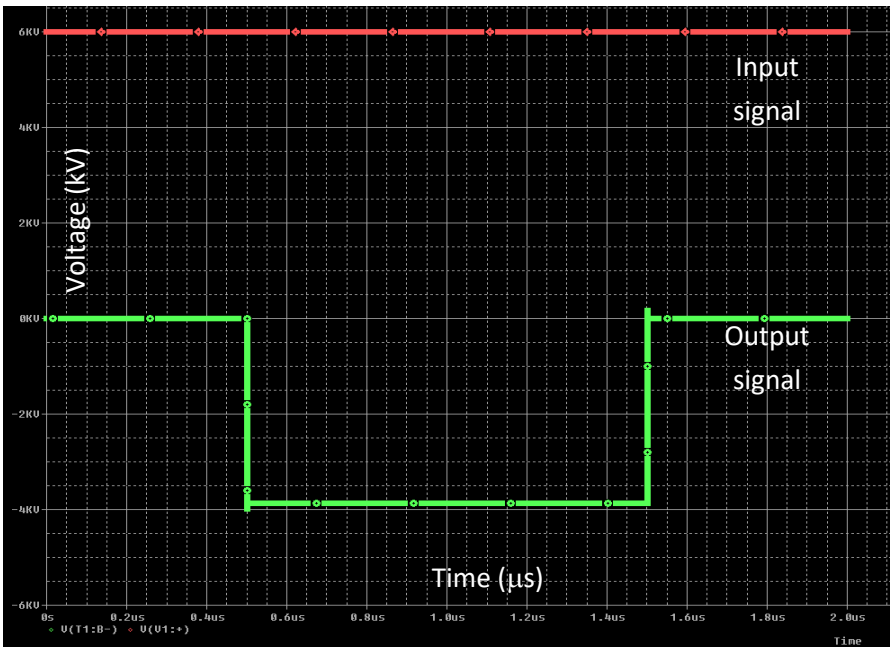

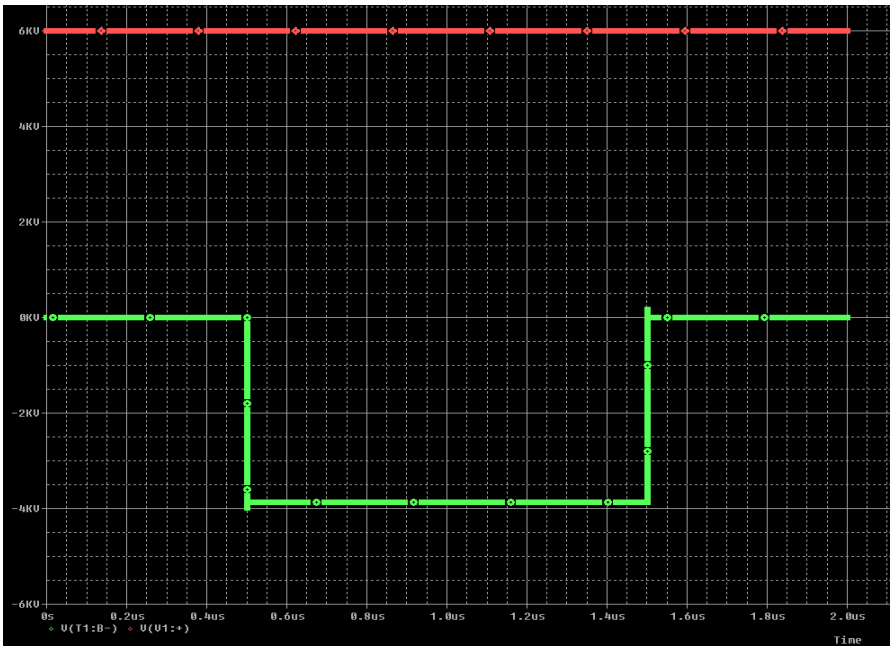

(b)

Figure (6.3.2) Pspice model of the pulsed power system (a); HV impulse generated by the model Blumlein generator (b), Red line represents input signal and green line represents output signal.

Figure (6.3.3) shows the actual output of the designed Blumlien generator used in experimental works.

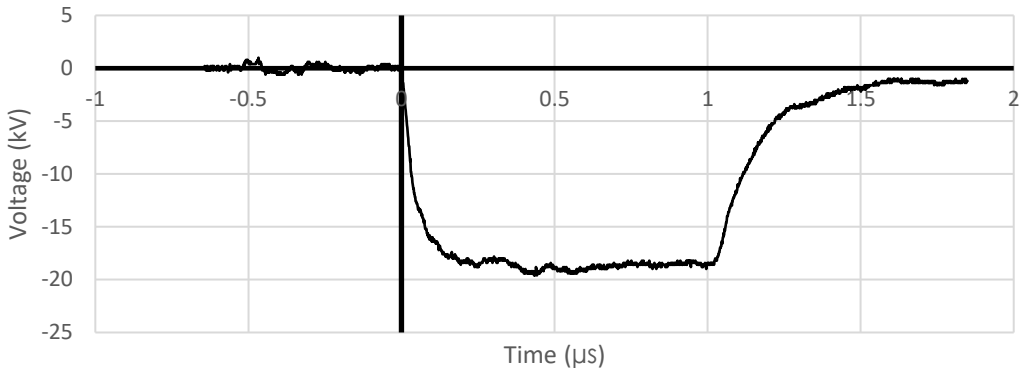

Figure (6.3.3) 1µs impulse generated with the constructed Blumlein generator.

6.4 Treatment samples and growing media preparation

Nannochloropsis Oculata Phytoplankton was selected for the PEF and plasma experiments. This microorganism has a spherical shape, and it is a single cell microalgae, with a shape which is similar to the shape used in the simulation models.

Nannochloropsis Oculata Phytoplankton requires straightforward growing conditions, and could be grown in the laboratory environment at room temperature. The lighting conditions were provided to ensure reliable growth of Phytoplankton. The lighting regime was as follows: 16 hours of light followed by 8 hours of dark (24 hours in total). The light was controlled using a timer. The flasks with Phytoplankton were located in a confined room with no windows, so the only light which was in the test box was provided by time controlled lamps. Thus the same lighting conditions were kept for all tests. The lighting parameters of the LED bulbs used in the tests were as follow: 1000 lm, 2700K colour temperature, 13W power rating of each bulb.

A photograph of samples of the Phytoplankton in glass jars and lightning system used in the tests are shown in **Figure (6.4.1)**.

Figure (6.4.1) (a) Growing culture of the samples which to be treated by PEF and plasma. (b) Flasks with growing treated and untreated samples 6 days after location into jars and placement in in the growing environment

A 10-day culture cycle was selected in these tests i.e. 10 days from seeding the treated sample into the culture liquid in jar and placing the jar in the growing box with the controllable lightning conditions and taking the final spectroscopical measurements. According to growing experiments, a 10-day culture cycle was enough to show the condition of the microalgae: with growing period, stable period

(maximum population) and decrease period. The treated Phytoplankton culture was equally distributed among the flasks with the nutrient rich growing medium and was shaken, as this provides consistent growing conditions and reliable results obtained from the spectrophotometer measurements. **Figure (6.4.2)** shows the Phytoplankton observed under the optical microscope used in the experiment.

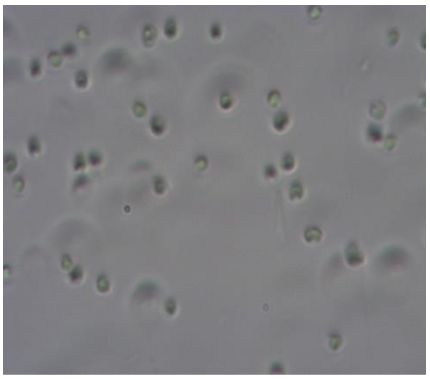

Figure (6.4.2) *Nannochloropsis Oculata* Phytoplankton observed under optical microscope: Observed in experiments of this project with magnification x100.

To culture the *Nannochloropsis Oculata* Phytoplankton in the Laboratory conditions, a culture starter sample is needed which provides faster growth rate compared with a matured sample. All the resources were obtained from Reefphyto Company.

As discussed above*, Nannochloropsis Oculata* Phytoplankton does not require strict growing conditions, the growing temperature in the current tests was room temperature, which varied during the observation period between 20 and 25 ℃. This temperature regime was sustained by the air conditioning systems in the laboratory.

A culture medium with salinity of 2.8% is required to grow Nannochloropsis *Oculata* Phytoplankton. The culture medium consists of distilled water, sea salt and growing nutrients from *Reefphyto* Company. **Figure (6.4.3)** below provides the picture of the microalgae culture starter and growing nutrient suggested for optimal growing of the phytoplankton. The growing nutrient is based on the Guillard F/2 medium and has the same nitrogen, phosphorus trace element and vitamin

content. The Guillard F/2 medium is a common and widely used seawater medium designed for growing marine algae which reduces the concentration of the original formulation (F medium) by half. The original formulation was proposed by Guillard and Ryther in 1962.

All samples of Phytoplankton were grown in 250 ml glass flasks. In order to achieve a larger contact area between the liquid sample and air, which has the potential to increase the growing speed of microalgae, 100ml was selected as the volume of the culture media.

The flasks are placed on the table as shown in **Figure (6.4.4)** to receive sufficient light.

(a) (b)

Figure (6.4.3) Culture start sample (a) and growing media (b) for *Nannochloropsis Oculata* Phytoplankton provided by the Reefphyto Ltd which were used in this experimental works.

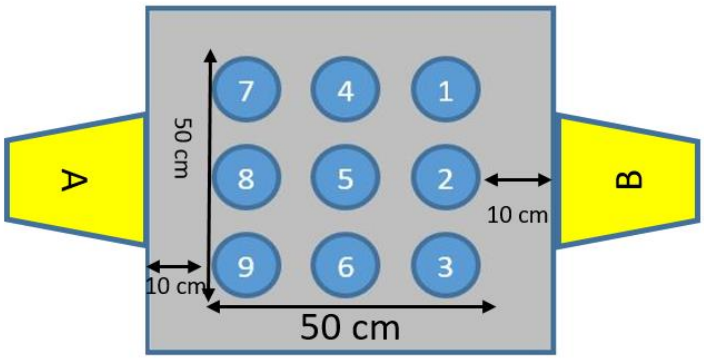

Figure (6.4.4) Positions of the lamps and flasks for the growing of phytoplankton, A and B represents lamps, the circles with numbers represents flasks.

As said earlier, a 16h/8h light/ dark cycle was used to grow Phytoplankton samples. Lightning conditions were controlled by the timers used for each lamp. The flasks with Phytoplankton samples were illuminated by 2 lamps (for the PEF treated samples) and by 4 lamps due to the larger number of flasks (for the PEF and Plasma treated samples, 51 flasks were used). LED light bulbs with same specifications - 1000 lm, 2700K colour temperature, 13W power rating, were used to provide a controllable lightning environment.

6.5 Electrical Diagnostic devices and preparation of experiment

The high voltage probe Tektronix P6015A and oscilloscope Tektronix TDS2024 were used in these experiments to monitor the impulse waveform across the test cells, **Figure (6.5.1).** The division ratio of probe used is 1000:1 and it has a bandwidth of 75 MHz, the peak value that can be measured is 40 kV, which is suitable for the PEF and Plasma treatment regimes. The probe HV terminal was attached to the output HV cable which provided impulses from the Blumlein generator to the test cell, the signal from the probe was monitored by the oscilloscope (Tektronix TDS2024 oscilloscope) which has a bandwidth of 200 MHz and a sampling rate of 2GS/s.

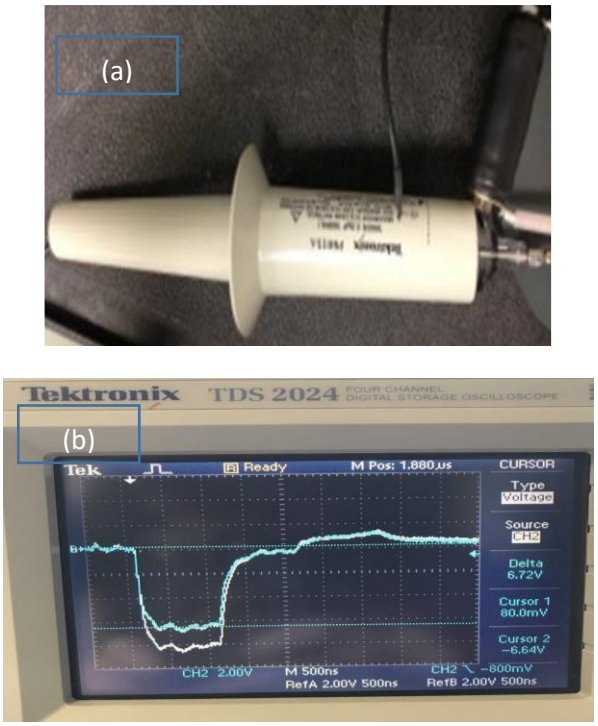

Figure (6.5.1) (a) Tektronix P6015A 1000:1 HV Probe. (b) Tektronix TDS2024 oscilloscope.

The current in the in the plasma treatment tests was measured used a Pearson current transformer model 6585 with a bandwidth of 250 MHz and sensitivity of 1 V/A, and the maximum magnitude of measurable current is 500 A. The current transformer was located between the test cell and the main ground terminal in the lab, the ground cable which connects the test cell and the main earth terminal passes through the aperture of the transformer allowing for current pulses to be measured, the output signal was recorded by the Tektronix TDS2024. In this position, the current delivered to the test chamber can be measured, as shown in **Figure (6.5.2)**.

The obtained current in the plasma treatment tests was used to calculate the energy delivered to the test cell during the discharge process.

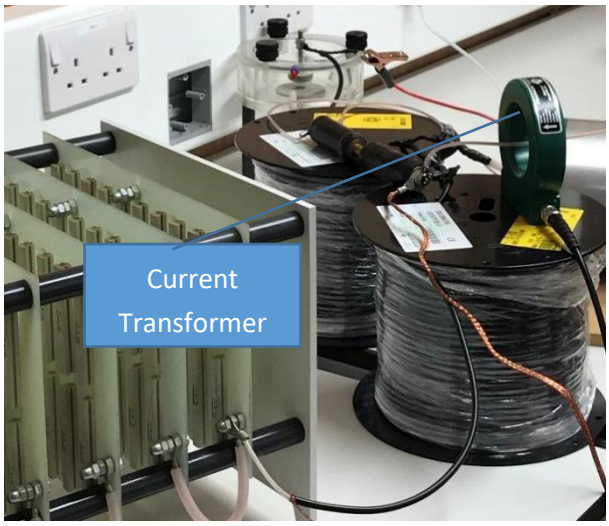

(a)

(b)

Figure (6.5.2) Pictures to show (a) current probe and (b) current recorded by oscilloscope for Plasma treatment, details of the wave shape in the oscilloscope would be discussed in **section 6.7**.

Figure (6.5.2) (a) shows the Blumlein generator with the charging current limiting resistor (on the left), the two reels of the coaxial cable, 100 Ohm load resistor (balance resistors), spark gap (transparent Perspex cylindrical cell at the back), and the Pearson current transformer located on the top of the reel with the coaxial

cable. **Figure (6.5.2)** (b) shows two HV power supplies and the Tektronix TDS2024 oscilloscope.

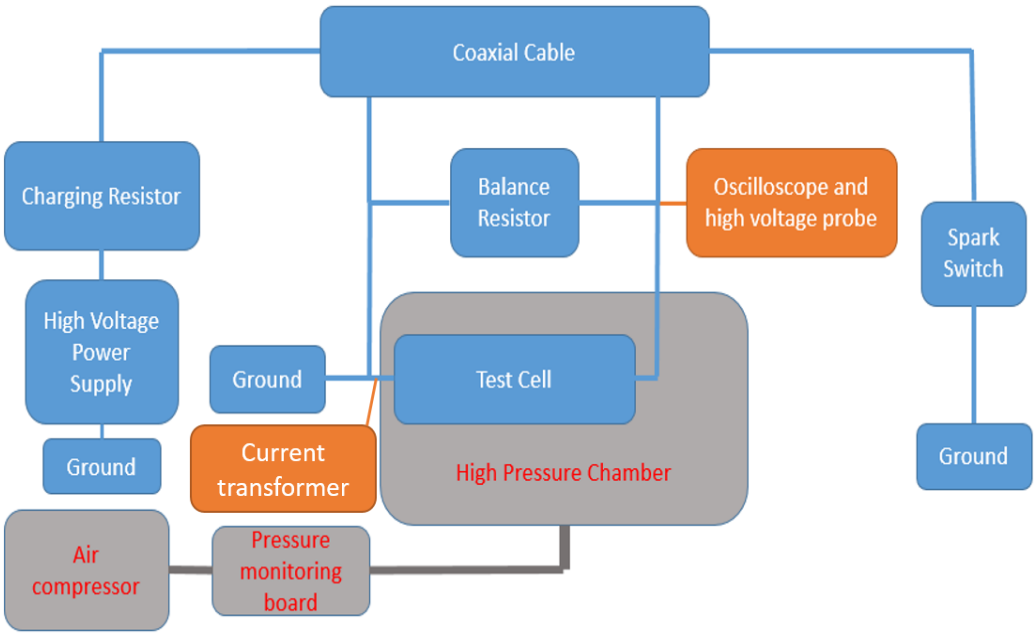

Figure (6.5.3) Block diagram of experimental system according to actual operation results, the balance resistor was set to 100 Ohm which shows better impulse in oscilloscope to provide the required impedance matching for optimal generator operation.

Figure (6.5.3) above shows the block diagram of the test system which includes the pulse power generation system and pressurized testing chamber. The pressurized chamber in which PEF test cells were located was used to avoid breakdown across interface between air and liquid between the cell electrodes, a compact table top air compressor Thorlab - PTA511-EC, was used to provide pressurized air into the sealed cell; gas pressure was controlled and monitored using the gas distribution board equipped with the valves and pressure gauge shown in **Figure (6.5.4).** The pressure of the test chamber is generally controlled between 40-50 psi, there is no specific value required as long as the breakdown could be prevented in this experiment.

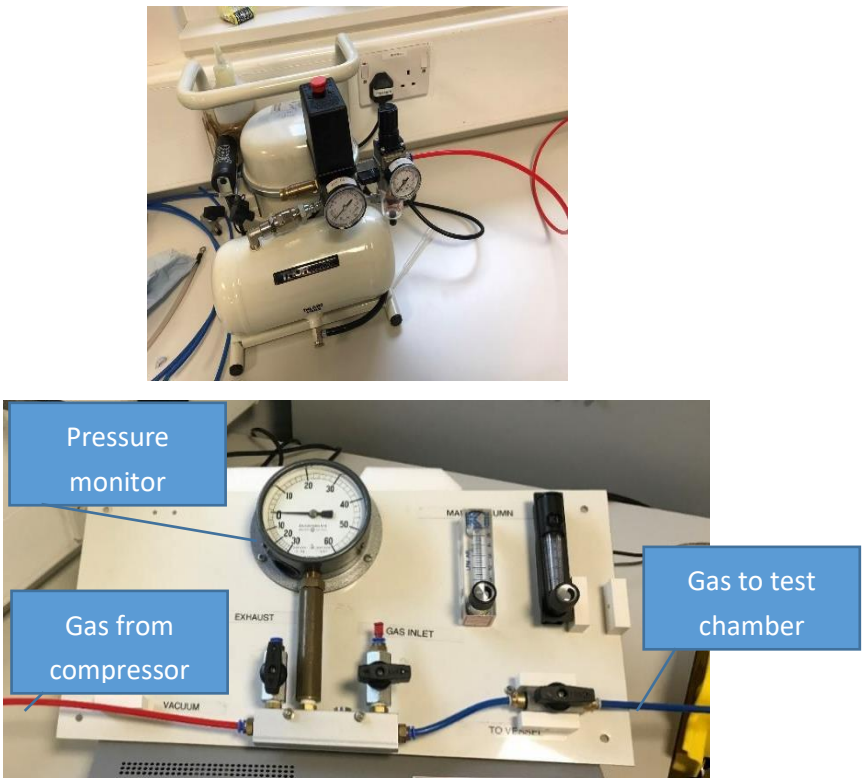

Figure (6.5.4) Air Compressor from ThorLab and gas monitoring board

Optical microscope Nikon Eclipse E400, **Figure (6.5.5)** was used for visual observations of potential changes in morphology of the algae cells after the PEF with 67 kV/cm field strength treatment. This microscope was equipped with a digital camera which was mounted on the eyepiece so that pictures taken could be saved on PC for further analysis.

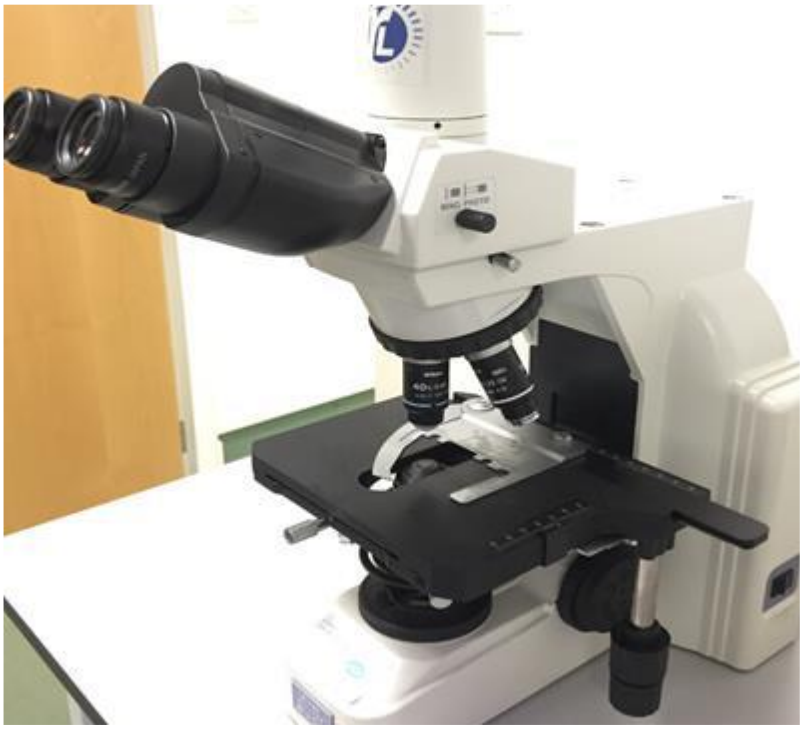

Figure (6.5.5) Microscope used in this project: Nikon Eclipse E400 microscope

The changes in the morphology of microalgae cells caused by the PEF treatment resulted in the change of the lifecycle of algae. Optical characteristics of the growing media with algae were examined using the spectrophotometer. These measurements are based on optical transparency of algae samples and this optical transparency was plotted as a function of time. With growing of algae cells the growing suspension become optically denser and the concentration of cells can be quantified by measuring the optical absorption of the culture. Liquid samples with algae were placed in transparent cuvettes which were placed in a Thermo *Spectronic Biomate 5* spectrophotometer used in these tests, as shown in **Figure (6.5.6)** below.

The detailed description of the optical tests will be provided in the following part. Pipettes were used to transfer samples between growing culture and measurement cuvettes.

Figure (6.5.6) *Thermo Spectronic Biomate 5* spectrometer and 5 mL measurement cuvettes.

6.6 Preparation works before treatment

In order to analyze the potential damage caused by PEF treatment or plasma treatment to algae, their control growing curves should be obtained first. The growing cycle of *Nannochloropsis Oculata* should be obtained to make sure that the observation period of treated samples is sufficient to cover the growing cycle of *Nannochloropsis Oculata* with the maximum population achievable in the current laboratory conditions. Secondly, the wavelength of light used to monitor the growth of algae should be selected to obtain accurate results. Thirdly, the concentration of nutrients used in the growing medium should also be confirmed. It is known that growth cultures with a higher concentration of nutrients does not provide benefits for growing of microorganisms [334] [335], algae cultures placed in a solution with a higher concentration of nutrients (15ml of nutrient solution in 100ml of growing medium) can only stay alive for 2-3 days which is too short as compared with a typical growing cycle 6 to 10 days. A shorter growing cycle makes it difficult to observe potential changes in the growth tendencies caused by the PEF treatment or plasma treatment, as such results can also be related to contaminated samples or other problems. Last but not the least, the samples during the PEF treatment should be able to withstand specific electric field strength without breakdown and energy losses due to conductivity should be minimized, therefore the samples must be

diluted with distilled water to reduce their conductivity. A sufficient number of initial cells are also necessary to achieve a good growing curve.

6.6.1 Preparation of samples and control group

As mentioned before, the dilution of the growing medium with distilled water is required to reduce the conductivity of suspension. In the attempt to find the optimal electrical conductivity of samples, different proportions between distilled water and phytoplankton have been tested. For example, at first, a 1ml algae liquid sample taken directly from the culture bag as received from Reefphyto Ltd, was added into a cuvette with 10ml of distilled water. It was found that the electric field across the electroporation cuvette filled with the liquid sample with such proportion of algae suspension and distilled water can be kept at the required value (population of algae is enough for growing curve measurement, normally 1 ml algae directly taken from bag). However, the population of algae in the diluted sample is not sufficient for growing curve measurements (it takes a long time to reach the peak population and some samples just did not show any growth). In order to achieve sufficient population of algae for the growing test and maintain the field strength in the cuvette at the same time, centrifuge was used. After extensive experimental testing it was found that the growing sample of 2 ml from the received culture bag diluted in 8 ml distilled water after centrifuging provides an optimal ratio of algae, nutrients and water.

A centrifuge *Heraeus Labofuge* 400R, **Figure (6.6.2)** was used to separate the growing media and microalgae from the received bag before dilution. The samples were centrifuged at 1800 rpm for 10 minutes, then the supernatant which contains mainly growing media was discarded and the precipitated biomass was used in further dilutions. After centrifuging, distilled water was added to the precipitated biomass, and after shaking, the sample was ready for the PEF or plasma treatment. **Figure (6.6.1)** below shows the flow diagram of the dilution progress. A control group of samples was set to estimate potential damage to algae cells caused by the

centrifuging process, this control group consisted of 2 ml samples from the received bag and 8 ml distilled water, the algae samples were diluted without centrifugation.

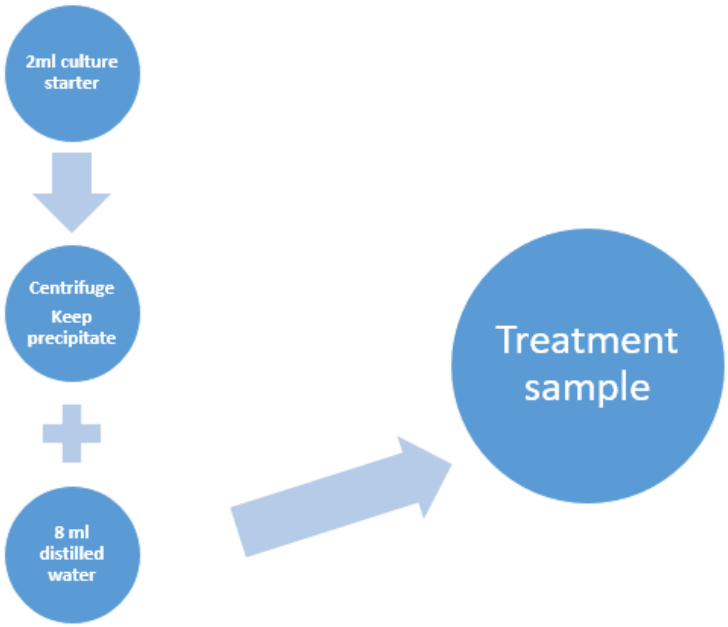

Figure (6.6.1) Brief introduction of sample preparing progress

Figure (6.6.2) *Heraeus Labofuge* 400R centrifuge and centrifuged sample

6.6.2 Recoding the transmittance or absorbance of samples with spectrophotometer

Transmittance (T) and Abs (absorbance) values are recorded by the spectrophotometer to record the absorption of wavelength. **Figure (6.6.3)** and **Equation (6.3), Equation (6.4)** below introduce the calculation of the transmittance and absorbance. The absorbance is a measure of the amount of light that interacts with the sample and which is used to analyse the population of microalgae in experiment works.

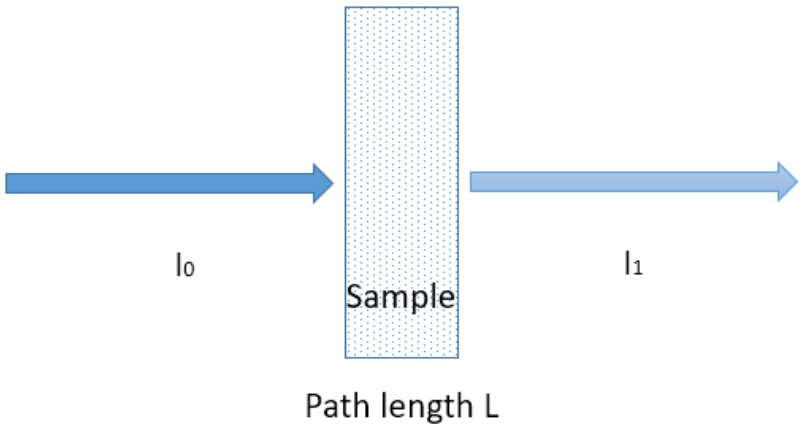

Figure (6.6.3) Diagram of change in of light intensity during passage through a sample in the spectrophotometer. (I_0 represents the intensity of light entering the sample and I_1 represents the light emerging on the other side of the sample. L represents the light path length.)

$$\boldsymbol{T = \frac{I_1}{I_0}} \qquad \textbf{(6.3)}$$

$$\boldsymbol{A(abs) = \log_{10}\frac{1}{T} = \log_{10}\frac{I_0}{I_1} = 2 - \log_{10}\%T} \qquad \textbf{(6.4)}$$

Where T is the transmission of the sample, I_1 is the light emerging on the other side of the sample, I_0 is the intensity of light entering the sample and A is the absorbance of the sample to a specific wavelength of light is shown in **section 6.6.3** (680 nm in this project).

The absorbance is recorded as “Abs” in the spectrometer measurements. This value obtained by the spectrophotometer is used to estimate the population of microalgae in this experiment. Absorbance is a measure of the capacity of a substance to absorb a light with specific wavelength. It is equal to the logarithm of the reciprocal of the transmittance **Equation (6.3)** and **Equation (6.4).** In the case of algae suspension the absorbance values were obtained at the wavelength of 680 nm. Any increase of this value means greater absorption of light with the wavelength, which can be considered as a measure of an increase in the population of microalgae.

6.6.3 Preparation of growing media and growing curve

Because the growing media includes different nutrients and salt, before obtaining the growing curves of the treated algae samples using the spectrophotometer, the potential effects caused by the growing media itself should be eliminated. Thus, the differential optical absorption spectra between the growing medium and distilled water have been obtained and the results show no significant difference between them. Therefore, it was confirmed that the effects of optical interference caused by the nutrient solution and salt are negligible and can be ignored in these experiments. Distilled water was used as the reference liquid in spectrophotometer measurements.

In order to select the wavelength at which the transparency of algae solution will be examined to plot the growth curves, 3 samples were used and their transmission characteristic in the range from 400nm to 800nm were obtained over 7 days. Thus, the growing curves were plotted and, based on their characteristics, a 680nm wavelength was selected as this gives the maximum absorption. It is known that the wavelengths in the range from 640 nm to 680 nm provide significant contribution to

the process of photosynthesis [336]. A wavelength of 680 nm represents red light which is mainly absorbed by chlorophyll α in *Nannochloropsis Oculata*. The change in absorbance is consistent from Day 0 to Day 5 compared with other wavelength (400-500nm or 600-650 nm). Therefore, the population of microalgae can be estimated based on the level of absorption (transmission) at 680nm. The testing results were recorded and plotted in **Figure (6.6.3.2)** below.

The combined results for these tests are shown in **Figure (6.6.3.1)**, it was established that 1.5 mL of nutrient in 1 L of the growing culture provides the optimal growing condition for *Nannochloropsis Oculata,* all the samples for experiments were prepared based on this proportion.

The nutrient bag was also obtained from Reefphyto Ltd, it was suggested that 1.5 ml nutrient is sufficient for 1 L growing culture. In order to reduce the growing observation cycle, other tests with higher proportion of nutrient were also conducted.

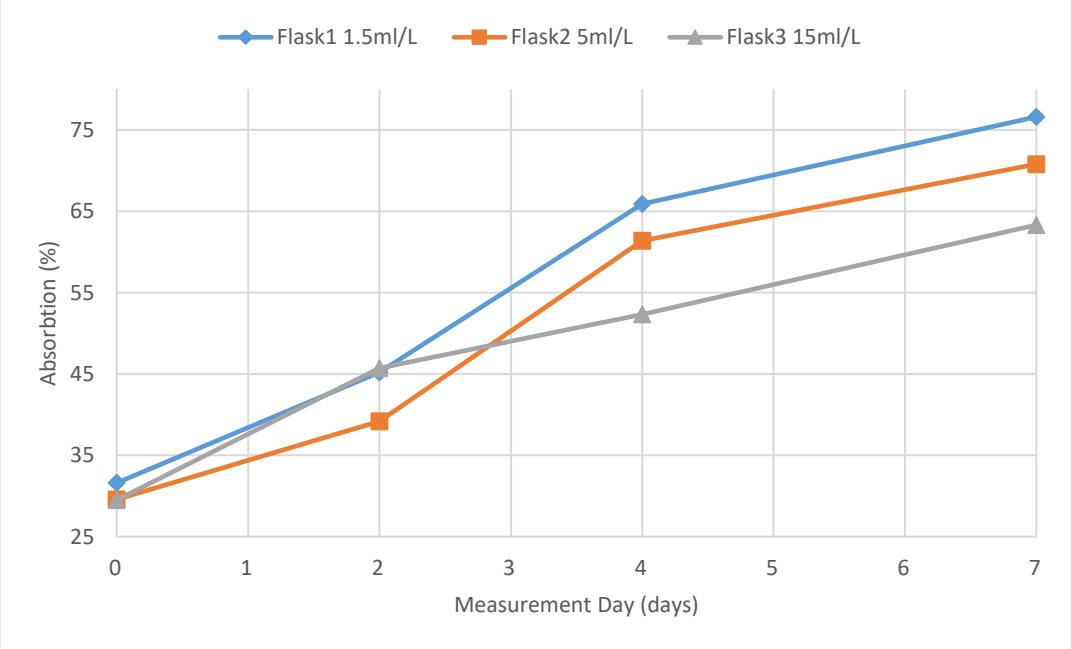

Figure (6.6.3.1) Growth curve for culture with different concentration of nutrient based on absorbance at 680 nm wavelength. (Higher absorption of light represents the higher population of microalgae.)

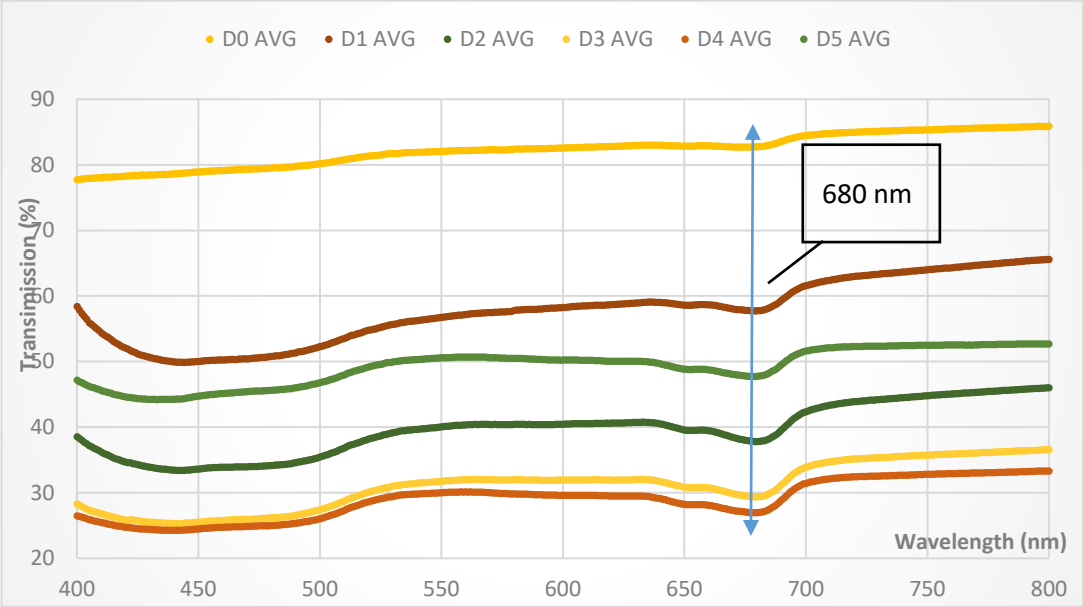

Figure (6.6.3.2) Transmission result of spectrometer scanning wavelength from 400nm to 800nm. A progressive and consistent decrease of transmission can be observed at about 680 nm wavelength.

In order to make sure the observation time after the start of the growth cycle treatment is sufficient for the algae population to reach their optimal concentration under specific growing conditions, growing curves have been measured. Cytometer counting using an optical microscope was also performed to support the results obtained using spectrophotometer measurements (optical absorption at 680 nm). It was established that measurements during 12 days provided optimal conditions for growth of the algae culture, their population started to decline after 12 days as shown in **Figure (6.6.3.3).**

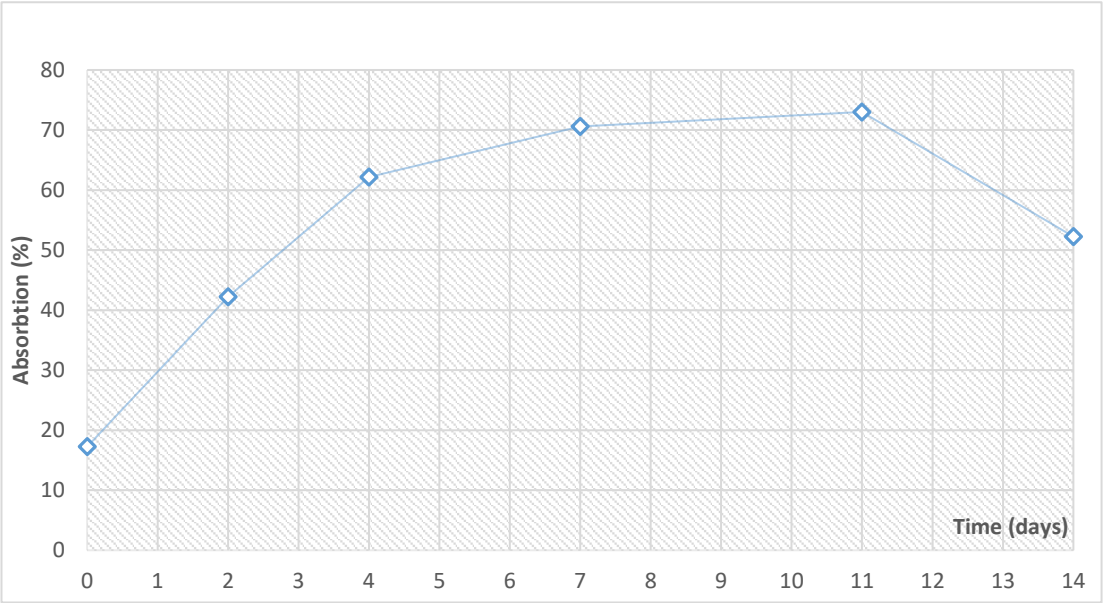

Figure (6.6.3.3) Growing cycle measurement with spectrophotometer. The graph shows growth curve behaviour over 14 days.

In order to provide a baseline for the results obtained from the spectrometer measurements, cytometer counting was used to estimate the population of microalgae following the growing curve experiments. The cytometer used in the experiments is shown in **Figure (6.6.3.4)**. By counting the number of cells in 4 corners (shown in **Figure (6.6.3.4)** (b)), the cell concentration can be calculated using **Equation (6.5)**. According to the manual of the cytometer, 10 μL of samples were taken and transferred to the cytometer with the pipette each time.

$$\text{Total number of cells } \left(\frac{\text{cell}}{\text{ml}}\right) = \text{Average number of cells in 4 grids} \times \text{dilution factor} \times 10^4 \qquad \textbf{Equation (6.5)}$$

Where the dilution factor is the ratio of the total volume of a diluted solution to the initial volume of the solute, the microalgae from samples observed under the microscope (x20 magnification) were quite clear and visible, thus further dilution was not required, and the dilution factor in the **Equation (6.5)** is 1 in this

measurement. According to the principles and design of cytometer, the number of cells included in each corner (Zone 1, 2, 3 or 4) are cells contained in 10^{-4}ml of cell suspension, so a multiplying factor of 10^4 gives number of cells in 1 ml.

(a) (b)

Figure (6.6.3.4) Cytometer used in experiment (a) and counting zones under microscope (b) which are marked in zone 1, zone 2, zone 3 and zone 4.

Figure (6.6.3.5) shows the results of cytometer measurement. Three groups of samples were measured in this experiment which are labelled as B1, B2 and B3. In B3 there is a significant drop in population at Day 12 compared with B1 and B2, most possible reason might be the influence of other microorganisms which was considered as acceptable in this experiment. Because B1, B2 and B3 shows reasonably similar growing curves from Day 0 to Day 10, besides, there was no significant population drop in B1 and B2. The total growing period for spectro-photometer measurement and cytometer measurement are different as they were not done at the same day and the growth of microalgae couldn't be stopped. In addition, the cytometer measurement were performed to support the growing period obtained through spectro-photometer measurement and therefore 1 or 2 days difference could be acceptable.

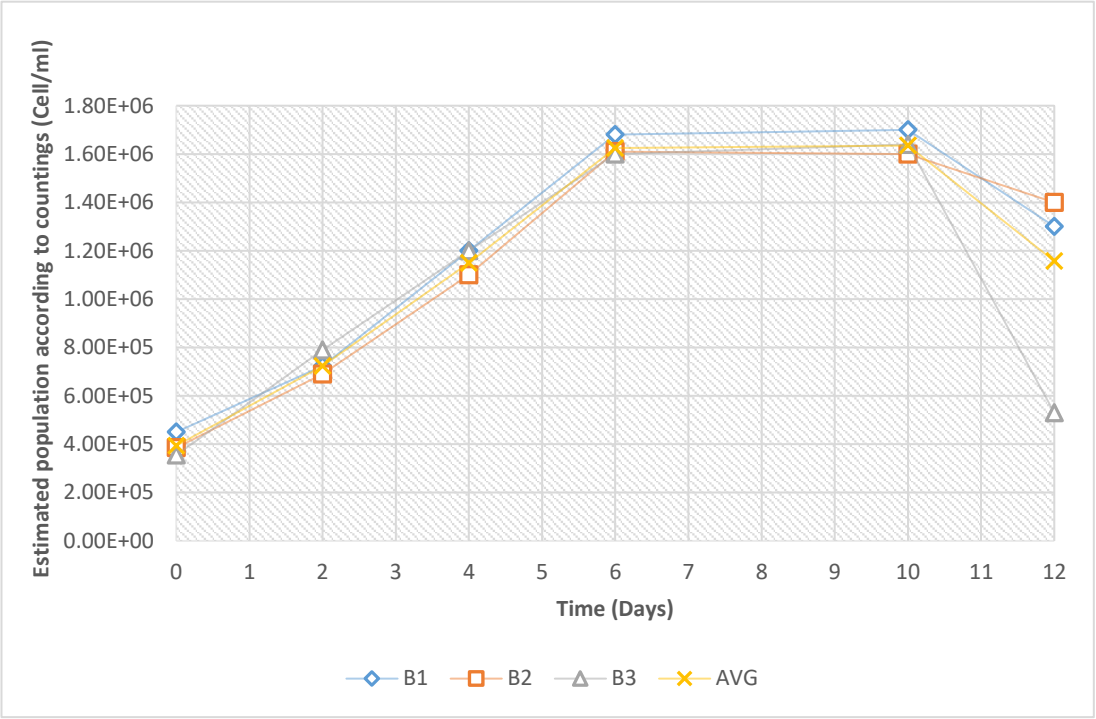

Figure (6.6.3.5) Growth cycle measurement with cytometer counting. The result shows the growing cycle follows the tendency of spectrometer measurement. Three groups of samples are recorded: B1, B2 and B3.

The **Figure (6.6.3.5)** shows the same growing tendency as obtained from the spectrophotometer measurements which supports the proposed methodology of growing microalgae in the following experiments in which the spectrometer measurement will be used.

6.7 Experiment results and discussion

In this section, the experimental methodology and the obtained experimental results will be introduced and explained.

In the PEF tests, the electroporation cuvettes which were used allow for an electric field up to 70 kV/cm to be achieved, such high electric field strength may damage membrane(s) of the microorganism, and an optical microscope was used to observe any morphological changes in algae.

As mentioned in the previous section, due to the large contact surface of the metallic test cell, the electric field strength in this test cell can reach only ~ 33kV/cm; in the tests in which this cell was used a range of number of impulses were applied to the algae samples to investigate inactivation effects caused by the PEF treatment. A volume of 1.5 mL was used for samples in these tests, and this volume made it possible to conduct the spectrophotometer measurements.

The plasma treatment is a different approach compared to the PEF treatment. Polarity of the applied HV pulses, number of impulses, materials of sample dishes (plastic or metal, which governs the current path across liquid/air interface or through the bulk of liquid), influence the treatment results even in the case when HV pulses are generated by the same Blumlein generator (i.e. the same energy is available per pulse and the same voltage level). It is important to compare the inactivation effects and results obtained using the PEF and Plasma treatment when HV impulses are generated by the same impulse source.

6.7.1 PEF treatment in the electroporation cuvette

The volume of the electroporation cuvette is only 50 µL per cuvette, as discussed before this volume is not sufficient to provide an algae population required for the spectrophotometer measurements, the cytometer measurement was also not available with electroporation cuvette test. Thus, in these tests algae were investigated using the optical microscope only. Clustering of cells was observed under the microscope with optical microscope observation.

The impulse rate was 100 impulses per minute and it was controlled by the current of the power supply. The magnitude of the pulsed electric field in the cuvette was controlled by the applied voltage to trigger the spark switch (~ 24 kV).

Algae samples were taken directly from a larger volume diluted sample and transferred into the cuvette using a pipette. In order to prevent external flashover,

the cuvettes were put in a plastic container with mineral oil. A breakdown event can be detected by monitoring the voltage and current wave shapes on the oscilloscope: each breakdown event results in a sharp increase in current captured by current transformer and the collapse of voltage across the electrodes. When breakdown occurred, the samples would be discarded as it would be hard to confirm the results were influenced by discharges or the electric field.

Figures (6.7.1.1-6.7.1.4) show the images of PEF treated algae obtained under the microscope immediately after the PEF treatment. The magnitude of the electric field was 70 kV/cm, different numbers of impulses were used to treat these samples, 500, 1000, 1500, and 2000. **Figure (6.7.1.1)** shows the visual appearance of algae treated with 500 PEF impulses, it can be seen that the phytoplankton remains in its normal shape after the PEF treatment, but several small clusters of algae are visible. When the number of impulses was increased to 2000 (from **Figure (6.7.1.2)**, **Figure (6.7.1.3)** to **Figure (6.7.1.4)** algae cells started to disintegrate, the remains of algae cells are visible in this photograph and chlorophyll from phytoplankton cells starts to leak which leads to the transparent cells. A Large numbers of cell clusters are visible, so the clustering processes intensifies with the number of the applied PEF impulses.

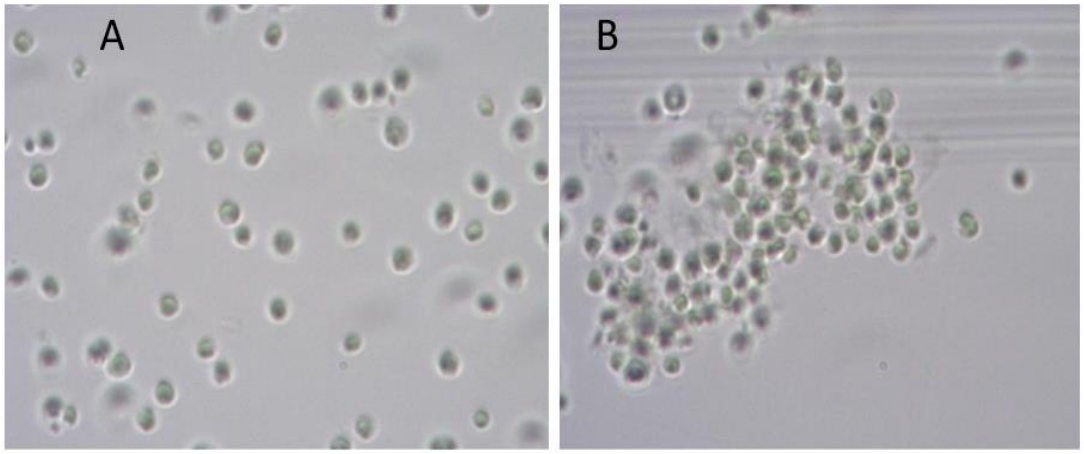

Figure (6.7.1.1) PEF treatment: 500 impulses treatment with electric field strength 70 kV/cm. Magnification x100. Both A and B were from two random locations.

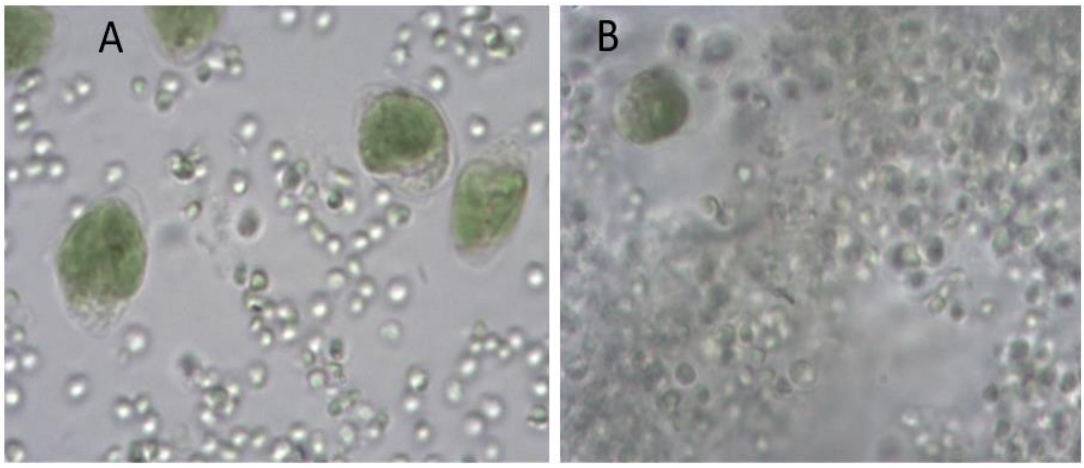

Figure (6.7.1.2) PEF treatment: 1000 impulses treatment with electric field strength 70 kV/cm. Magnification x100. Both A and B were from two random locations. The large green objects were considered to be paramecium *bursana* or *amoeba* from bag provided by the company Reefphyto and couldn't be avoided, furthermore they have no effects on the experimental results in this work.

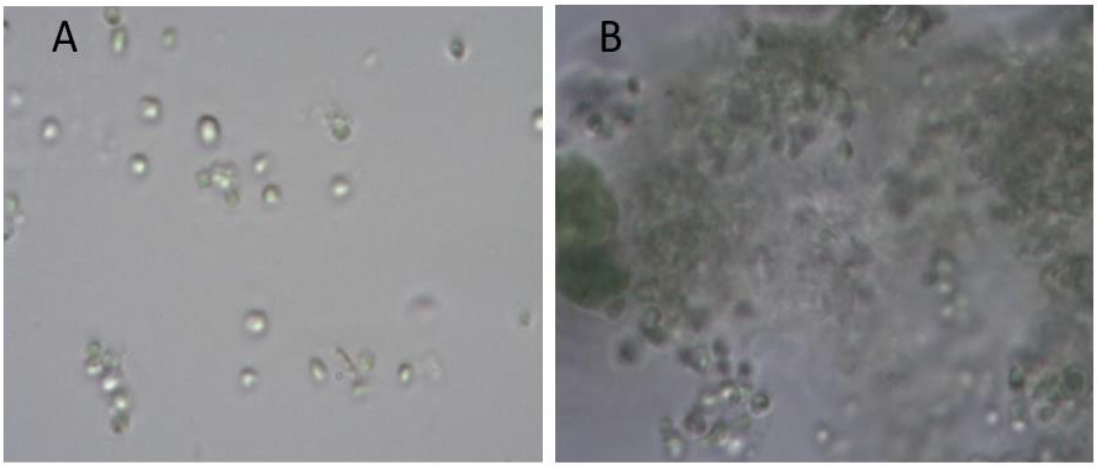

Figure (6.7.1.3) PEF treatment: 1500 impulses. Treatment with electric field strength of 70 kV/cm. Magnification x100. Both A and B were from two random locations.

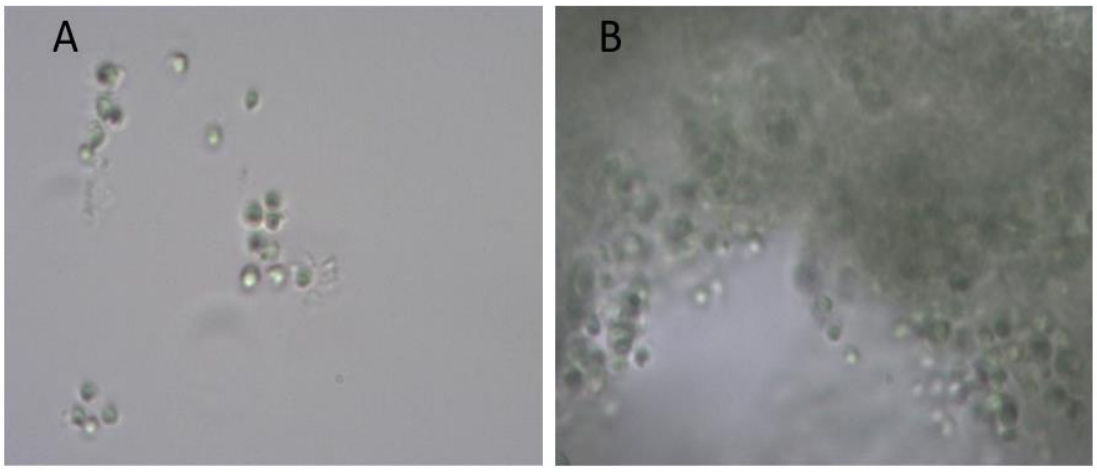

Figure (6.7.1.4) PEF treatment: 2000 impulses treatment with electric field strength 70 kV/cm, Magnification x100. Both A and B were two from random versions locations.

Also, the structural damage of the cells can be observed after the PEF treatment with high electric field strength. However, the optical observation results do not provide sufficient evidence to prove the relationship between damage efficiency and number of PEF impulses. The apoptosis process (changes of DNA and the cells become inactivated from inside) might be triggered by such high electric field, it

takes time to observe and compare cell lysis, which cannot be done in this experiment.

6.7.2 PEF treatment with metallic test cell

The PEF treatment of algae in the metallic test cell with a larger volume was conducted in order to treat the volume of samples sufficient for spectrophotometric measurements using the instrument previously used for plotting the growing curve.

Thus, treating a larger volume of algae suspension in the PEF experiments can provide reliable results on inactivation effects by monitoring the algae growing curves for different number of PEF impulses.

The tested samples of algae suspension were transferred from the prepared main sample centrifuged and diluted with distilled water to the test cell using the pipette, the pipette tip is used to stir solution to remove gas bubbles. As discussed, the PEF test cell was placed into a holder filled with mineral oil and located in the pressurized container to avoid external flashover and liquid/gas interfacial breakdown.

As previously discussed, the proportion between the nutrient solutions and distilled water has been determined to achieve sufficient population of phytoplankton for spectrometer measurements.

Due to an increased contact surface between samples and electrodes, the diluted sample cannot withstand electric fields higher than 40 kV/cm. Thus, the field with magnitude of ~ 33 kV/cm was used in the PEF tests: no breakdown events were registered in these tests.

The treated samples were transferred from the test cell to glass flasks filled with growing media using a sterile syringe.

The samples were grown at room temperature in the flasks under the growing conditions described in Section 4.4, and shown in **Figure (6.7.2.1)**.

Table (6.7.2.1) below shows the experimental arrangement (flasks and lamps) used to grow PEF treated algae suspension (samples) with 500 and 1000 HV impulses. 12 flasks in total were used to grow 3 algae samples treated with 1000 impulses, 3 algae samples treated with 500 impulses, 3 centrifuged samples for control and 3 non-centrifuged samples – also for control.

The volume of each algae suspension sample used in these tests was 3.5 mL, a sterile pipette was used to transfer each suspension from the flasks with growing culture to the spectrophotometric cuvette. After optical measurements the samples used in the cuvette were chemically sterilized and discarded.

Table 6.1 Arrangement of growing flasks of PEF treatment with 500 and 1000 impulses.

	Control sample	**Centrifuged sample**	**500 impulses**	**1000 impulses**
Number of flask	⑦ ⑧ ⑨	⑩ ⑪ ⑫	① ② ③	④ ⑤ ⑥

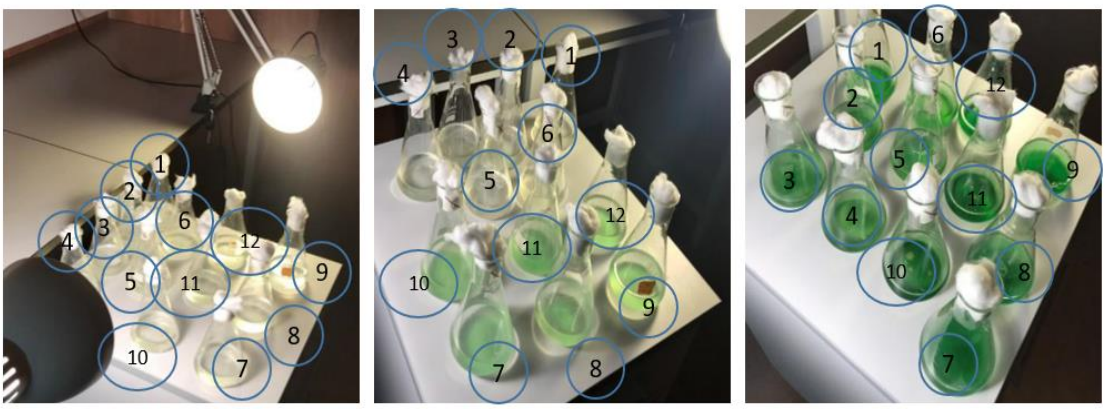

(a) (b) (c)

Figure (6.7.2.1) Culture flasks of 500 and 1000 number of impulses PEF treatment samples at: (a) Day 0, (b) Day 1, (c) after 12 days.

Figure (6.7.2.2) below shows the growing curve of samples treated with 100 PEF impulses, the growing curve shows that the inactivation effects of this PEF treatment (100 impulses, 33 kV/cm) is negligible. This field strength and pulse number are not sufficient to achieve the inactivation effect. Thus, in the next test the number of PEF impulses was increased. The results show that higher number of impulses (500, 700 and 1000) produce measurable inactivation effect at the same level of the electric field of 33 kV/cm, **Figure (6.7.2.3)**. However, according to the results this number of impulses and magnitude of the field is not sufficient to inhibit the growth of algae in the flasks completely.

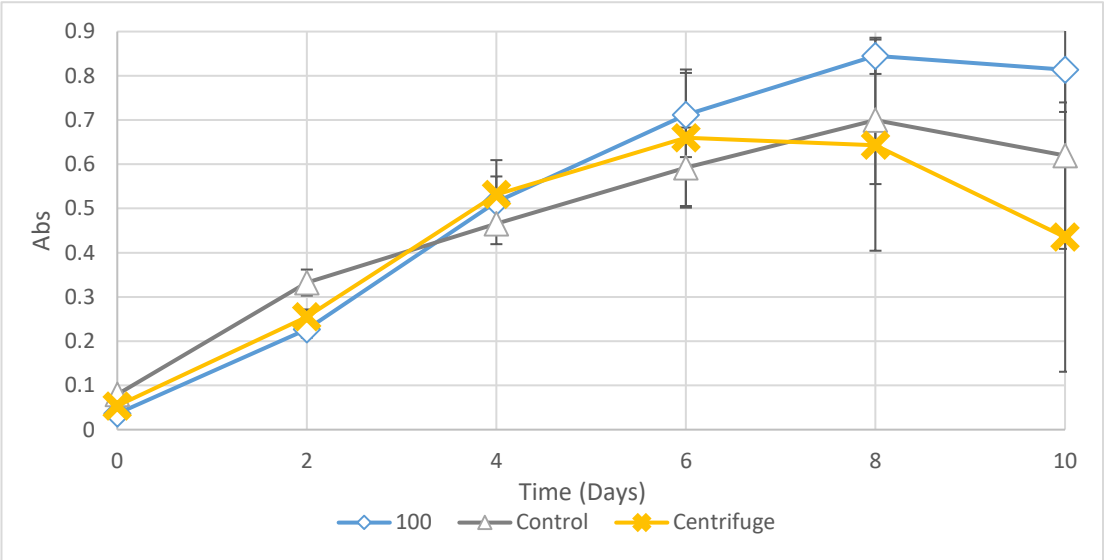

Figure (6.7.2.2) Growth curve of PEF treatment with cuboid metallic test cell with 100 number of impulses. Abs represents the absorbance of 680 nm wavelength by microalgae, the data is recorded every 2 days. The error bars represent standard deviation. Three groups are measured and there are 3 samples in each group.

From **Figure (6.7.2.2)** it can be seen that there is no significant difference between the treatment group and control groups which means 100 PEF impulses are not sufficient to cause strong and continuous electroporation process among these microalgae. There is also no significant difference between the centrifuged and control groups which suggests that the centrifugation process in this experiment does not have critical influences on the culturing of microalgae. In order to achieve inactivation, an increase in the number of impulses is necessary.

The **Figure (6.7.2.3)** shows significant differences between the treatment and control groups. Decrease in absorbance values, “Abs” of samples treated with 500 PEF impulses is observed 2 days after the treatment and the absorbance remains relatively low compared with the control groups. However, both treatment groups with 500 impulses and 1000 impulses show a slight increase in the absorbance 6 days after the treatment, which means the microalgae cannot be sterilized by 500

and 1000 PEF impulses. The centrifuged groups have a similar growing tendency to the control groups, which supports the result obtained in previous tests and confirms that the centrifugation does not have significant influence on culturing of microalgae in this experiment. By comparing the 500 impulses and 1000 impulse groups, a different growth rate can be observed 8 and 10 days after treatment. The different growth rate between two treatment groups suggested that the inactivation process of samples treated with 1000 PEF impulses is more significant. This result suggests that a greater inactivation of microalgae can be induced at this electric field strength, by increasing the number of the PEF impulses to 1000.

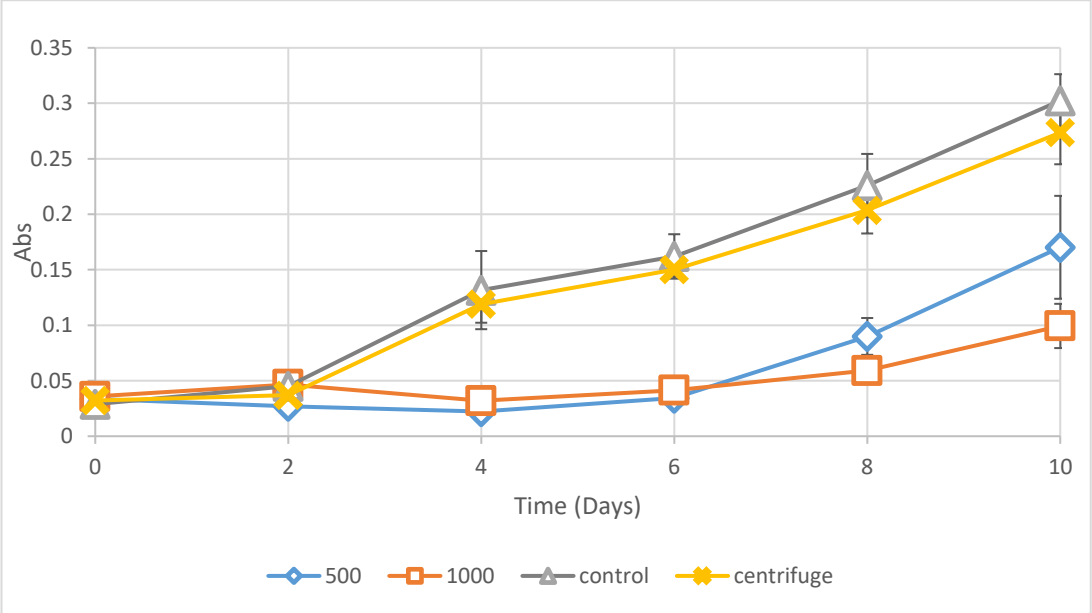

Figure (6.7.2.3) Growth curve of algae treated in the metallic test cell with 500 and 1000 impulses. Abs represents the absorbance at 680 nm, the data is recorded every 2 days. Four groups are measured and there are 3 samples in each group. The error bars represent standard deviation.

To optimize the inactivation process, it would be beneficial to confirm the minimum number of impulses which cause reliable and continuous electroporation. It was shown that the treatment with 1000 PEF impulses shows significant inactivation, however, it also consumes more energy than the PEF treatment with smaller number of impulses. Therefore, the treatment with 700 PEF impulses is selected to investigate the inactivation process. **Figure (6.7.2.4)** below shows the growing curve after 500 and 700 impulses PEF treatment.

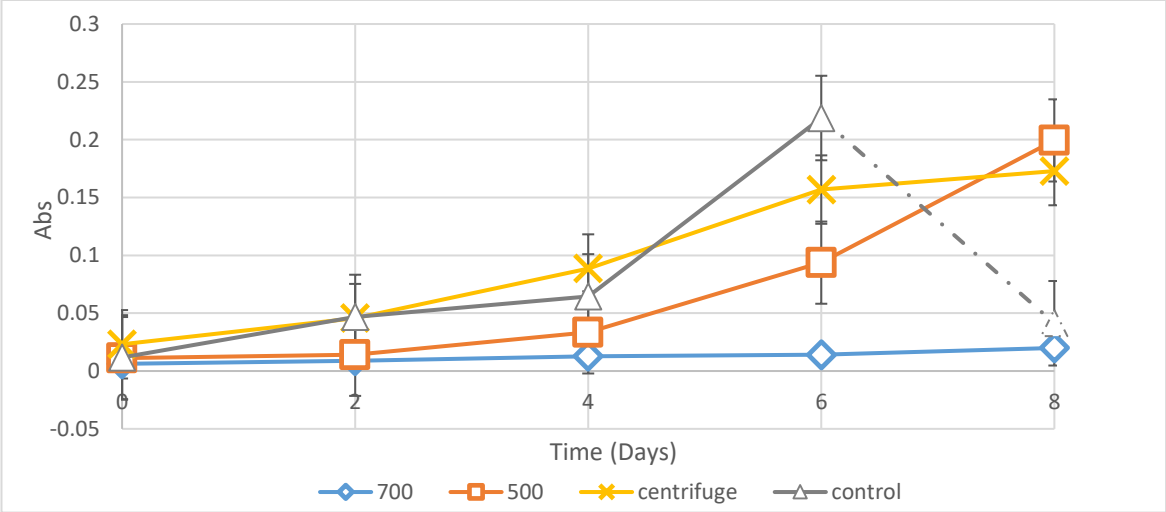

Figure (6.7.2.4) Growth curve of algae treated in the metallic test cell with 500 and 700 PEF impulses. Abs represents the absorbance at 680 nm, the data is recorded every 2 days. Four groups are measured and there are 3 samples in each group. The error bars represent the standard deviation.

This measurement was stopped after 8 days from PEF treatment due to the significant population drop in the control samples at 8 days, this could be caused by contamination or limitation of nutrient. However, the information provided within 6 days has shown a significant difference between control, centrifuge and treatment groups. This growth curve shows that 700 PEF impulses produce significant inactivation effect: there is no significant growth observed after treatment.

However, it has similar tendency as the treatment with 1000 impulses, there is a growing tendency observed after 6 days after the treatment which confirms that the PEF treatment with 700 PEF impulses cannot eliminate the microalgae but it demonstrated significant reduction in the number of algae. The result of the treatment with 500 HV impulses shows a different tendency as compared with the previous test which suggested that the inactivation effect produced by 500 PEF impulses is not stable. The control and centrifuged groups also show different growing tendencies after 6 days, this difference is not caused by the centrifugation process because the general tendencies are similar to that observed before 6 days. The difference occurs after 4 days after treatment, the two groups shows different growth rates, this might be caused by the different growing cycle of the algae when the control groups have higher growth rate and reach the maximum population faster than the centrifuged group. After that, the nutrient will be limited and this leads to decrease in the growth rate which can be observed from 6 to 8 days. The growth curve shows differences from **Figure (6.7.2.3)** as the two experiments were undertaken in different time, the original population and growing conditions from the bag were not the same, however, the deviation could be accepted in this study due to the double control groups.

6.7.3 PEF treatment with electroporation cuvette test cell and the larger test cell with metallic electrodes: summary of results

The PEF treatment of *Nannochloropsis Oculata* in the modified electroporation cuvette and in the larger test cell with metallic electrodes produced valuable results which potentially support the simulation results and predictions. A brief summary of the experimental results is provided below.

- Clustering and agglomeration of algae has been observed under the optical microscope after the algae suspension was treated with a higher electric field strength (70 kV/cm) and a significant number of impulses, 500 pulses.

This agglomeration phenomenon is enhanced by increasing the number of impulses from 500 to 2000.

- Damage to the external structure of the cell was observed under the microscope after algae were treated in the modified electroporation cuvettes. Visual examination confirms that number of damaged microorganisms does not increase significantly with number of PEF impulses, when this number increases from 500 to 2000. Such results support the results reported in the previous study [329] in which it was found that the external cell membrane is not significantly affected by the PEF treatment, however, this treatment produces the critical internal structural damage to microorganisms.
- The survival measurements based on the growing curves method could not be completed for samples treated using the modified electroporation cuvette due to its low volume (low volume of initial population of microorganisms, 50 µL, which is not sufficient for the growing curve method. In order to confirm the efficiency of the PEF treatment with such high electric field strength, further tests should be conducted, for example, using a test chamber which can be used to test large number of cuvettes at the same time to give the required population of microalgae.
- No PEF induced inactivation was observed after the treatment of algae with 100 HV impulses with the field strength of 33 kV/cm. The PEF-induced inactivation of *Nannochloropsis Oculata* was achieved in the larger test cell where the suspension was treated by 500 HV impulses with the field strength of 33 kV/cm. This inactivation effect is not significant, however, with an increase in the number of HV impulses to 700 and 1000, stronger inactivation effect was achieved.
- The global heating of the liquid during the PEF treatment is not significant. The maximum increase in the temperature of the suspension recorded

during the experiments was ~ 6 ℃. The low increase in the bulk temperature of the suspension is also reported in **section 6.7.4**.

- Significant PEF inactivation can be achieved by using 500-1000 PEF impulses with magnitude of 33 kV/cm, however, the efficiency of such PEF treatment is below the required level to confirm sterilization of Nannochloropsis *Oculata*.

6.7.4 Discussion of PEF treatment results

The results of the PEF treatment of *Nannochloropsis Oculata* using the modified electroporation cuvette and the larger test cell were presented in **section 6.7.1** to **section 6.7.3**. The obtained results and main conclusions are discussed in this section.

Firstly, the clustering of algae after the PEF treatment was observed under the optical microscope and this agglomeration is enhanced with an increase in the number of impulses from 500 to 2000. According to the simulation results and the Schwan Equation discussed in previous chapters, the maximum transmembrane potential is achieved at the poles of a single spherical cell due to the charges redistribution process in both cytoplasm and environmental fluid induced by the external electric field. Clustering may be caused by charge redistribution in the environmental fluid due to the external electric field, as shown in **Figure (6.7.4.1**). Concentration of ions increases at both sides of the cell membrane poles, in cytoplasm and environmental fluid due to the external electric field, thus the membrane's external surface become charged positively and negatively at its upper and lower poles. Thus, potentially the cells will be attracted to each other electrostatically due to charges of different polarities accumulated on their membranes and will form chains or clusters. Larger number of impulses will increase concentration of changes and thus will lead to a higher degree of agglomeration.

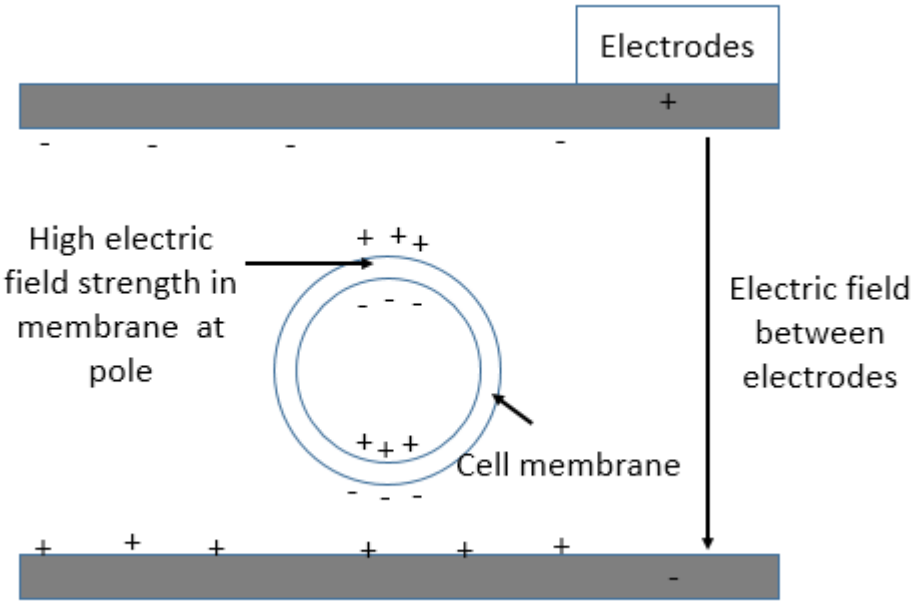

Figure (6.7.4.1) Charge redistribution in microalgae with external field applied, the cell wall is not shown in this diagram as it doesn't contribute to charge accumulation and distribution during PEF treatment as discussed in Chapter 4 and Chapter 5.

Secondly, the structural damage to the bio-cells observed under the microscope does not increase significantly with the number of impulses delivered to the samples (from 500 to 2000 HV pulses). In study [78], it was reported that no external structural damaged was produced by HV impulses with almost the same electric field strength and the same number of impulses. Such results also suggest that the main reason for PEF-induced inactivation of microalgae was not due to external membrane damage but potential internal structural damage to the cell, leading to its dysfunction.

Thirdly, inactivation during the PEF treatment was observed by plotting the growth curves, when the suspension was treated with the HV pulses produced by the

electric field strength of 33 kV/m. The maximum increase in the global temperature of the suspension due to joule heating recorded in the PEF treatment experiments is ~ 6 ℃. This is a result of using low conductivity suspensions in these tests in order to sustain the required level of the electric field across the test cell. Such low conductivity restricts the heating of treated samples. According to the simulation results, the local heating effects are not significant with HV pulses using a field strength of 33 kV/cm and the induced trans-membrane potential reaches the critical threshold value for the membrane breakdown (~1 V). Thus it can be argued that the induced electric field in the membrane leads to the cell inactivation process.

Although partial inactivation of microalgae by the PEF treatment was achieved with general electroporation electric field strength (33 kV/cm), the microorganism cannot be completely eliminated (the sterilisation criterion is not reached). There are several potential reasons for this. Firstly, there could be low field areas in the PEF test cells according to the modelling based on the same test cell as discussed in [328] . Secondly, according to the literature [337], microorganisms with different growing phases have different susceptibility to the PEF process. Thus, there might be microalgae with relatively high resistance to this electric field strength. Thirdly, sedimentation of microorganisms to the bottom of the test cell during the PEF process could also be a potential reason which influences the efficiency of PEF treatment inactivation effects. According to literature, continuous flowing chambers were more effective in inactivation than static systems [338].

6.7.5 Plasma treatment of algae suspension in metallic dish

The inactivation results of microalgae obtained through PEF treatment shows a limitation of this process: the microalgae cannot be completely sterilized even with relatively high number of PEF impulses (1000). It would be important to investigate a different approach of delivering energy to the samples. The Plasma treatment is one such approach: plasma impulses will be generated using the same pulse

generation system applied in the PEF treatment, details will be introduced in this section.

These experiments are designed for testing the inactivation effect of the plasma treatment. Plasma discharges were generated using the same source as was used for the PEF treatment i.e. the Blumlein generator, thus the magnitude of voltage and the energy available per pulse will be the same for plasma and PEF treatment. However, in this plasma treatment approach the energy is delivered into the sample by a different approach. The output from the Blumlein generator was connected to the conducting metallic plate with a number of needles which served as HV electrodes. This plate with the HV needles was mounted above the metallic dish in which a liquid suspension of algae to be treated with plasma discharges was placed. The needles were just in contact with the liquid surface, which is shown in **Figure (6.7.5.1).** The radius of the Gramophone needles used is ~ 80μm [333].

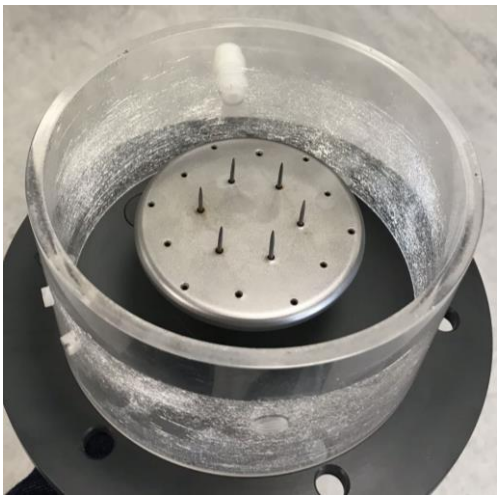

(a)

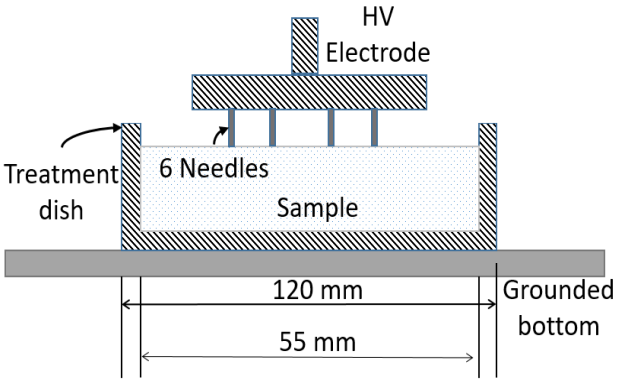

(b)

Figure (6.7.5.1) HV electrode with 6-needles mounted on plate (a) and schematic diagram of test cell (b). The needles are set at the same level and the tips are just attached to the surface of samples.

3 mL of algae suspension was placed in the metallic or plastic dish to obtain a uniform distribution of the liquid in the dish and the samples were transferred using the sterile pipette.

Two different polarities of plasma pulses were used in these plasma treatments, the polarity of the applied impulses was controlled by the polarity of the HV DC charging supply. The effect of polarity of plasma impulses on inactivation was investigated.

After the plasma treatment, the algae samples were transferred into the glass flasks with the growing medium, the growing conditions and methodology of spectrophotometer measurements were the same as in the PEF tests.

6.7.5.1 Waveforms of plasma treatment

The waveforms obtained in the plasma treatment experiments were recorded with the oscilloscope, the examples of waveform for the metallic dish and plastic dish plasma treatments will be described in this section.

Figure (6.7.5.2) below shows the recorded waveforms of the voltage applied to the test cell for positive plasma treatment for both the metallic or plastic dishes. It can be seen that, for the positive polarity metallic dish plasma treatment (a), breakdown occurs on the rising edge of the voltage impulse, which leads to the voltage collapse after breakdown. Such a breakdown event will result in a high current flowing through the test cell and the sample. The energy delivered into the sample will be investigated, and discussed in the following sections. During the positive plasma treatment in the plastic dish (b), no breakdown events occurred, and the waveform shows the full 1 µs long impulse, similar to the impulse generated in the PEF treatment in previous sections.

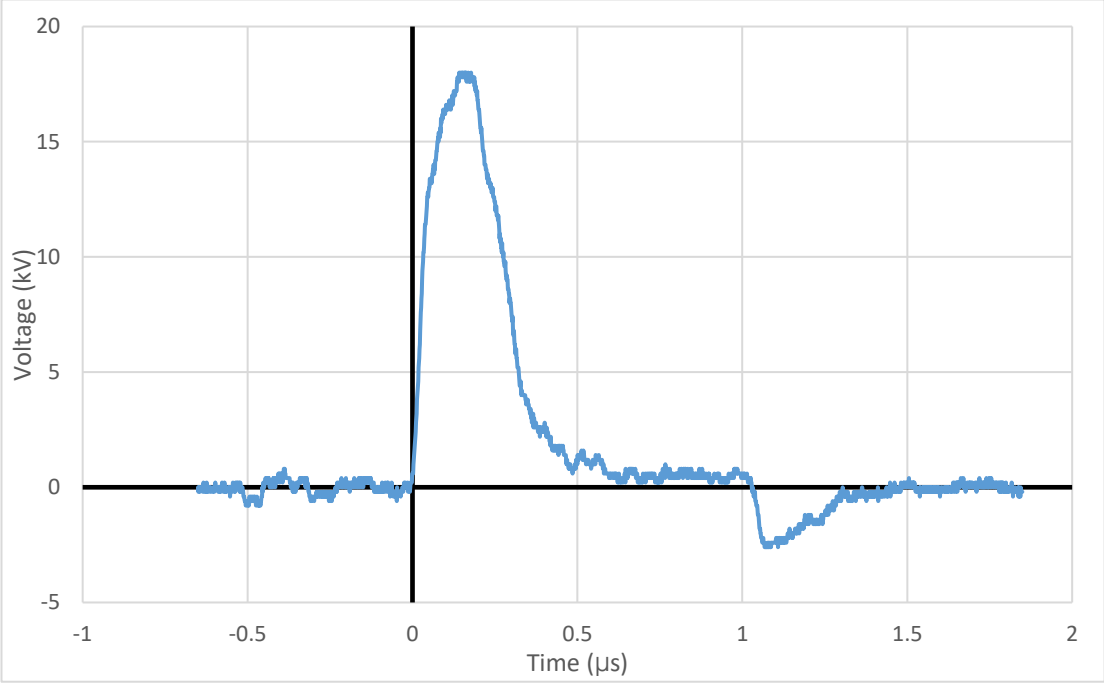

(a)

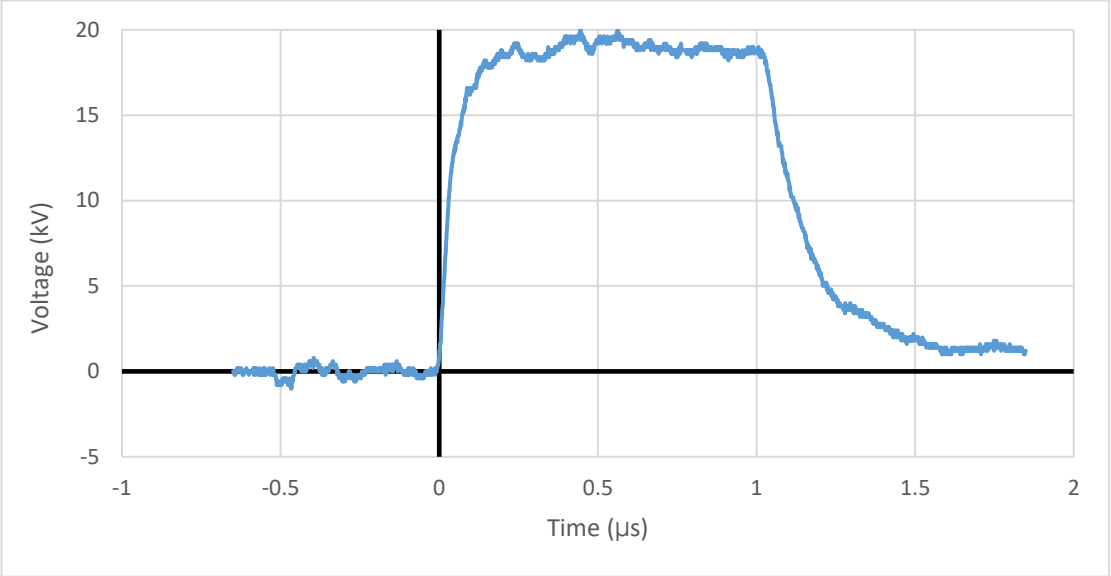

(b)

Figure (6.7.5.2) Recorded waveform of voltage applied to the test cell from both metallic dish positive plasma treatment (a) and positive plastic dish plasma treatment (b).

The waveforms of the negative plasma treatment were also recorded and are shown in **Figure (6.7.5.3)** below. There is no significant differences in voltage magnitudes in the plasma treatment regimens for the metallic and plastic dishes. In a similar manner to the positive polarity plasma treatment, there is breakdown with the metallic dish but not when the plastic dish is used during the negative plasma treatment.

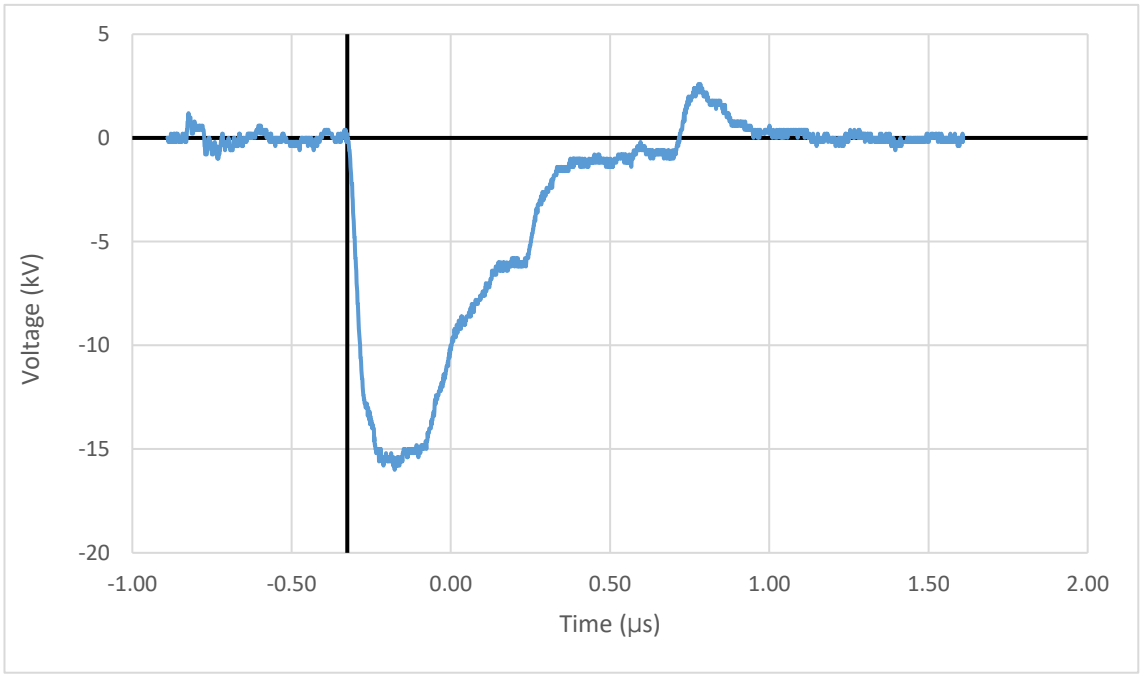

(a)

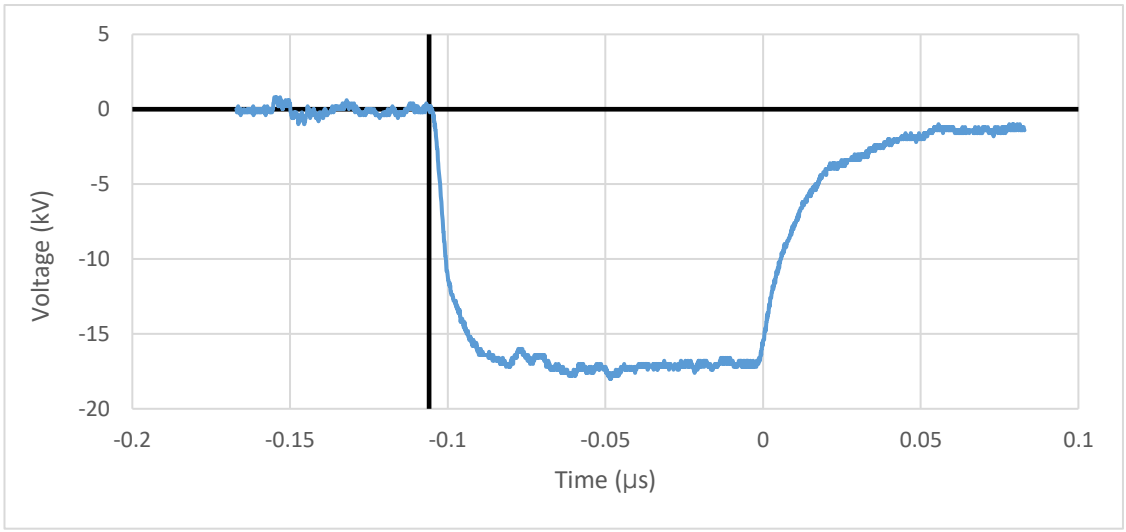

(b)

Figure (6.7.5.3) Recorded waveform of voltage applied to the test cell from both metallic dish negative plasma treatment (a) and plastic dish negative plasma treatment (b).

Plasma (corona) impulses were generated at the tips of the HV needles. 500 and 1000 HV impulses were used in the plasma treatment tests to investigate the inactivation efficiency of the plasma treatment and to compare this efficiency with the PEF treatment described in the **Section 6.7.1 to 6.7.3**.

6.7.5.2 Growing Curve of samples following Plasma treatment with metallic dish

Experiment arrangements of samples and growing curves of algae subjected to the plasma treatment in the metallic dish will be introduced in this section.

Table 6.2 Numbering of growing flasks used for negative or positive polarity plasma treatment with 500 and 1000 number of impulses

	Control sample	**Centrifuged sample**	**500 number of impulses**	**1000 number of impulses**
Number of flask	⑦ ⑧ ⑨	⑩ ⑪ ⑫	① ② ③	④ ⑤ ⑥

Figure (6.7.5.4) shows the flasks with the algae growing culture after the negative plasma treatment. Comparing the colour of treated samples with the centrifuged and non-centrifuged control groups, it is clear that 500 and 1000 plasma impulses show noticeable inactivation effects, 1000 impulses regime is more effective for inactivation phytoplankton. The growth curves of plasma treated algae samples, **Figure (6.7.5.5)**, show low absorbance (abs: 0.06 at measurement day 8), ~13 times lower in absorbance compared with control groups (abs: 0.75 at measurement day 8).

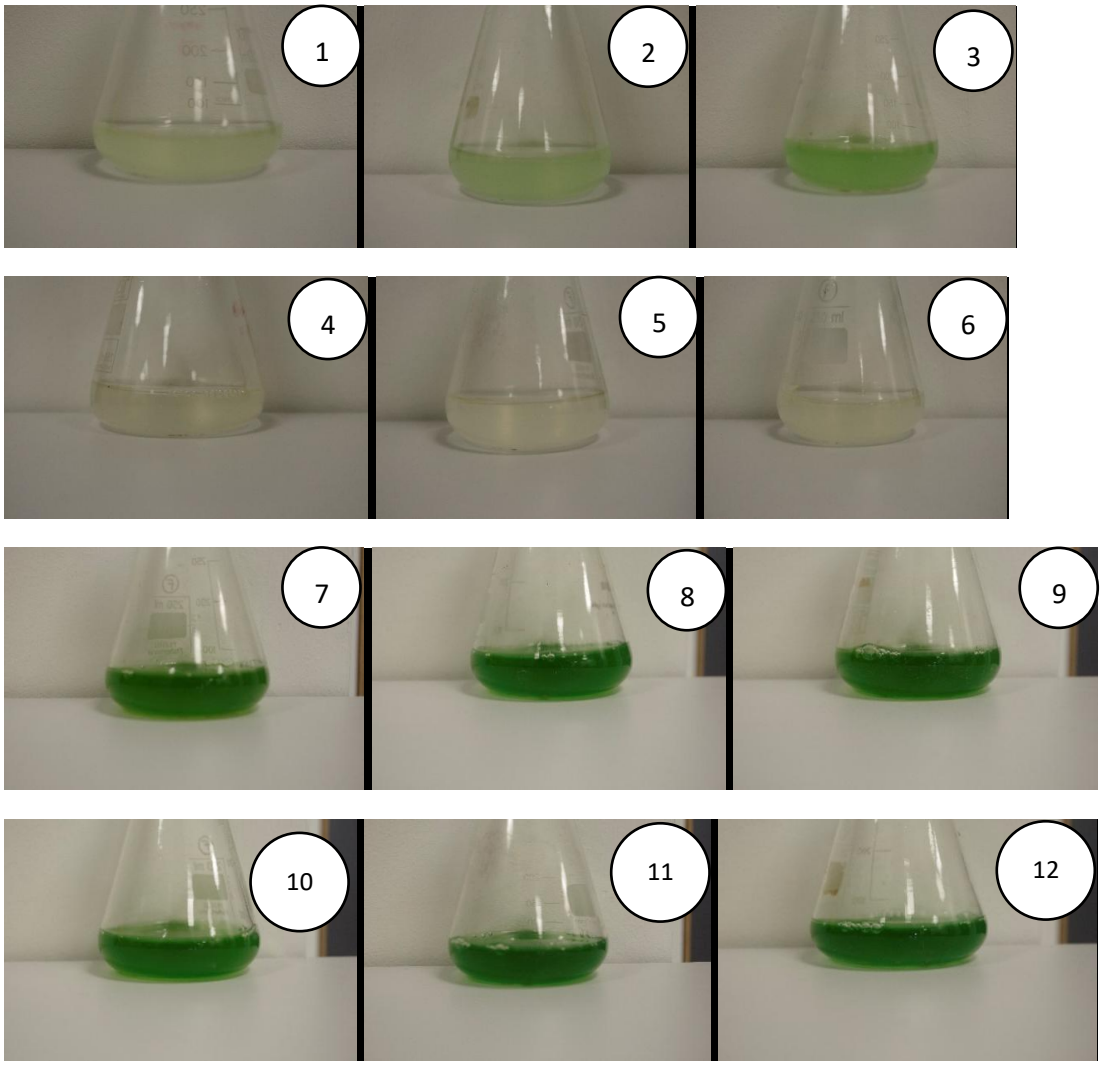

Figure (6.7.5.4) Growing culture of microalgae treated with negative plasma, centrifuged and control groups after 12 days. Flasks marked as 1, 2 and 3 represent 500 impulses treatment group; Flasks marked as 4, 5 and 6 represent 1000 impulses treatment group; Flasks marked as 7, 8 and 9 represent control group; Flasks marked as 10, 11 and 12 represent centrifuged group.

The growing curve of negative plasma treatment is shown in **Figure (6.7.5.5)**.

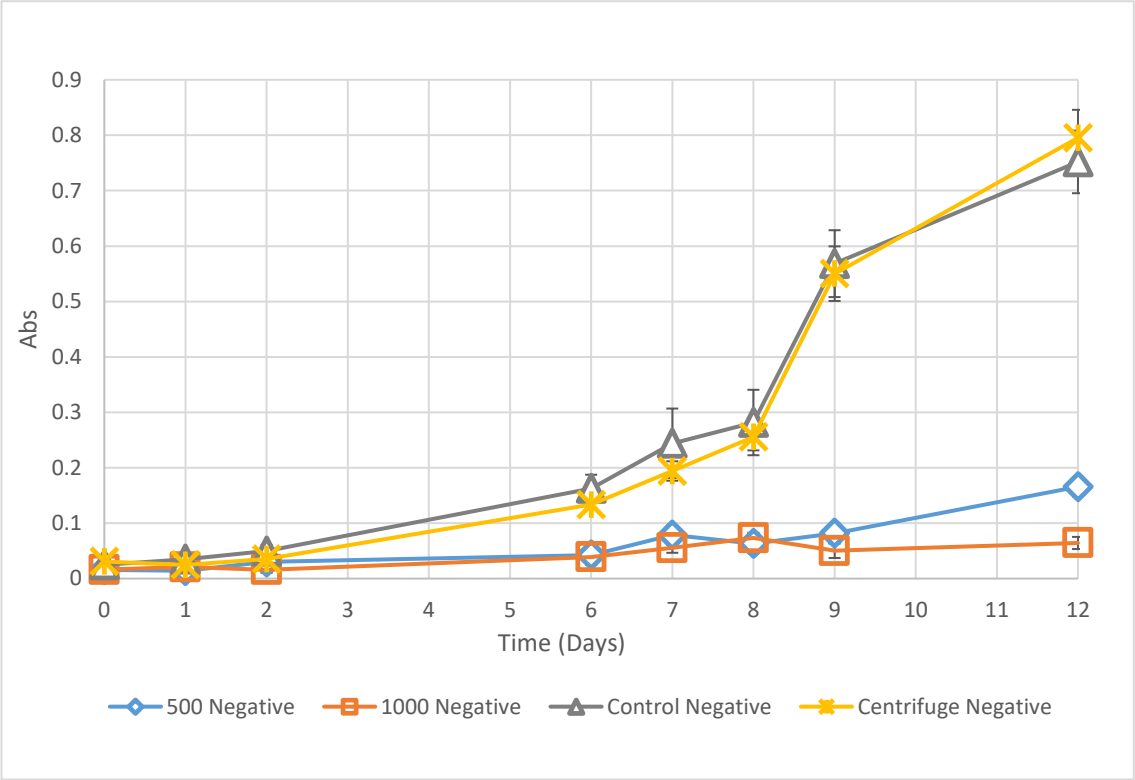

Figure (6.7.5.5) Growth curve of microalgae treated with 500 and 1000 negative polarity plasma impulses. Abs represents the absorbance at 680 nm, the data is recorded at day 0 and on each day when a treatment had occurred. Four groups are measured and there are 3 samples in each group. The error bars represent standard deviation. The longer gaps between measurements occurred because of weekends when no treatments or measurements were possible.

The growing curve of the control and centrifuged groups follow the same tendency which confirms the conclusion drawn in the PEF treatment tests: the centrifuge process does not have significant influence on the culturing of microalgae in this experiment. The growing curve of the control and centrifuged groups can be divided into two stages after treatment. The first stage is between Day 0 to Day 6. The population of microalgae increases slowly, this might be caused by changing the environment in which microalgae grow. It takes time for the metabolic system of microalgae to get used to the new growing media. Meanwhile, the synthesis of

enzyme and other metabolites also occurs when microalgae become used to a growing environment. After a slow growing period, the material basis of growing of microalgae have been fully prepared (for example, the enzymes for growing in the new growing culture has been fully prepared) and the microalgae has got used to the new growing media, then the microalgae moves into a fast growing period which is 6 days after the treatment. Such growing process follows the first two growing phases of microorganisms, the lag and exponential phases. The recording of growing curve terminated after Day 12 so there is no data about the stationary phase and death phase. It can also be observed that different number of HV impulses, 500 and 1000, affects the inactivation process of microalgae, according to the obtained growing curve. Compared with 500 impulses, 1000 impulses lead to more inactivation effects of microalgae as there is no significant increase in "abs" value after treatment. However, with 500 impulses, the "abs" value starts to increase at Day 7 which describes the growing of microalgae after the plasma treatment. 1000 negative plasma impulses have the sterilization effects on microalgae according to picture of growing culture taken after 12 days, as shown in **Figure (6.7.5.5)**.

By culturing the samples during 13 days it was shown that 500 negative plasma impulses produce the inactivation effect however, compared with 1000 negative plasma impulses, it is not strong enough to achieve sterilization as shown in **Figure (6.7.5.6)**

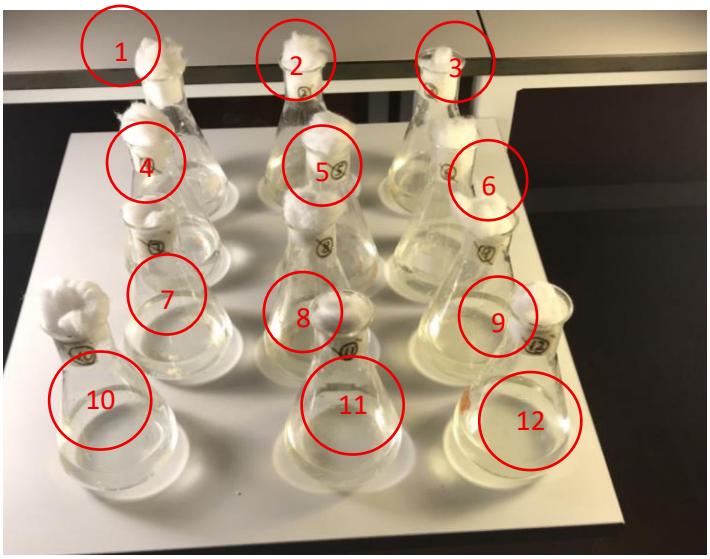

(a)

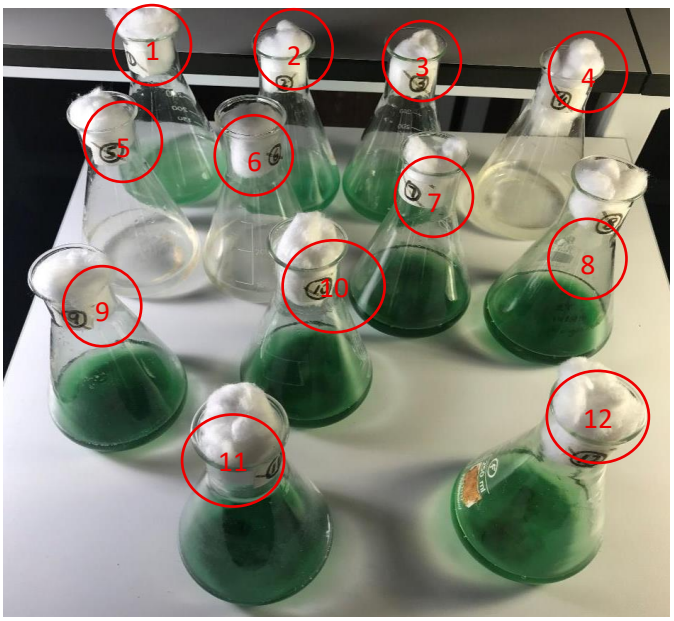

(b)

Figure (6.7.5.6) Culture of algae treated with negative plasma impulses, at day 0 (a) and 12 days after treatment (b). There is no microalgae detected after 1000 negative plasma impulses. (Flasks marked as 4, 5 and 6). Flasks marked as 1, 2 and 3 represent 500 impulses treatment group; Flasks marked as 7, 8 and 9 represent control group; Flasks marked as 10, 11 and 12 represent centrifuged group.

And the plasma treatment and corresponding growing curve were conducted and obtained using the positive plasma treatment to investigate potential plasma polarity effects. It was obtained that both 500 and 1000 positive plasma impulses result in the inactivation effect which is the same as in the case of negative plasma impulses. **Figure (6.7.5.7)** shows the condition of each growing cultures after 10 days of growth following positive plasma treatment. The measurement was done every day after treatment except weekend (between day 4 and day 7).

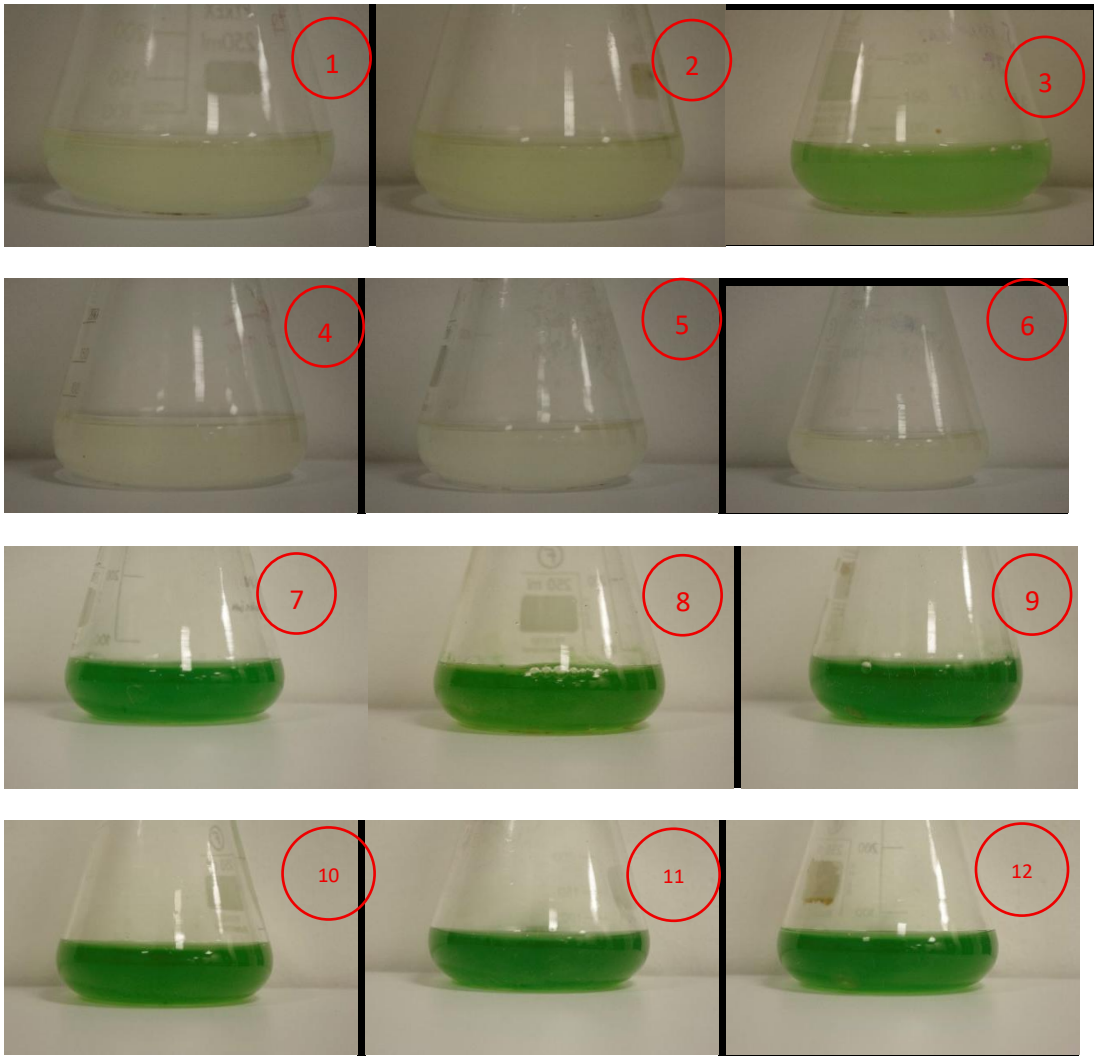

Figure (6.7.5.7) Culture of algae (10 days old) after the treatment with positive polarity plasma impulses, Flasks s 1, 2 and 3: algae treated with 500 impulses; Flasks

4, 5 and 6: algae treated with 1000 impulses; Flasks 7, 8 and 9: control group; Flasks 10, 11 and 12 centrifuged group.

The growth curve of algae treated with positive plasma in the metallic dish is shown in **Figure (6.7.5.8)**. The growing curve of the centrifuged group follows the same tendency with the control group which has been confirmed in previous sections, thus the centrifuge process does not affect growth of microalgae.

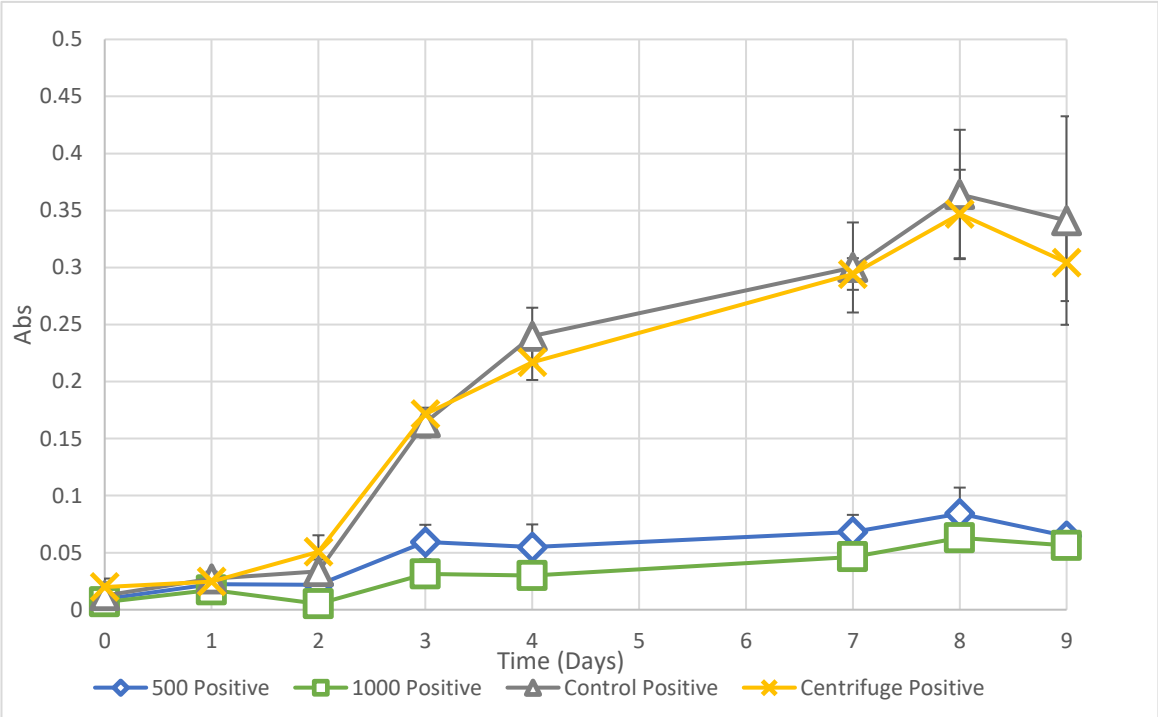

(a)

(b)

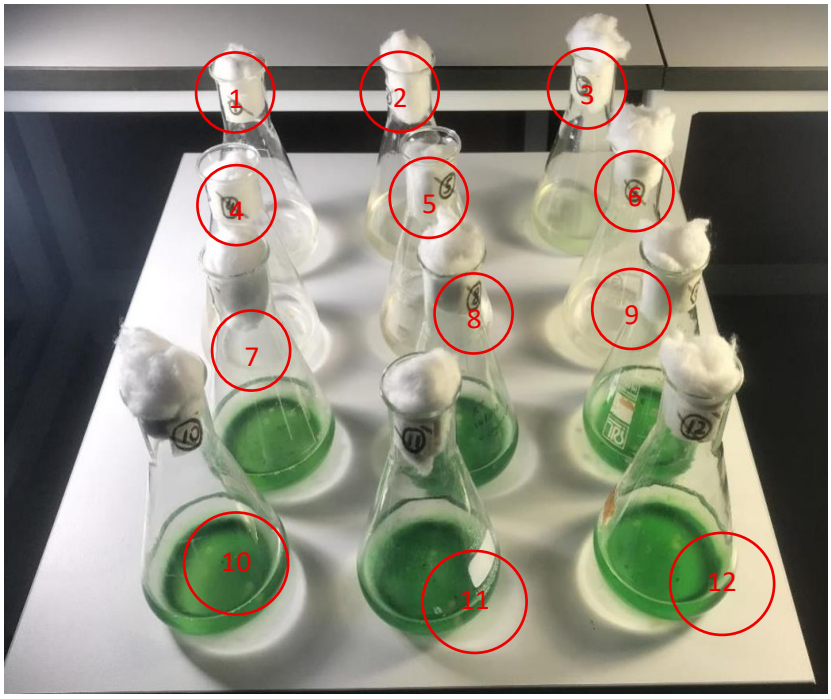

Figure (6.7.5.8) Growth curve of algae treated with 500 and 1000 positive polarity plasma impulses (a) and growing culture at day 9 (b). Abs represents the absorbance at 680 nm, the data is recorded at day 0 and every day after treatment. The error bars represent standard deviation. Four groups are measured and there are 3 samples in each group. There are 2 days between day 4 and day 7 as there are weekend between them.

(a)

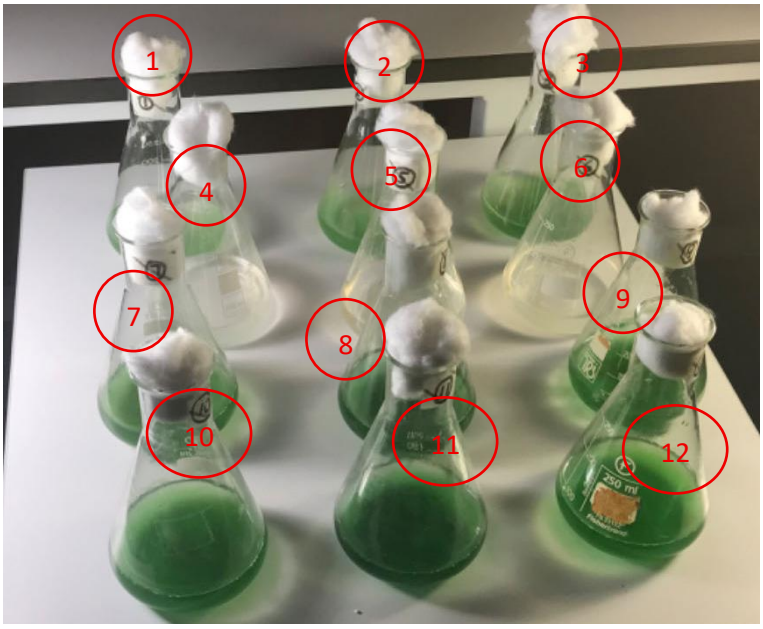

(b)

Figure (6.7.5.9) Culture of positive plasma tests at Day 0 (a) and after 20 days (b). Flasks 1, 2 and 3: algae treated with 500 impulses; Flasks 4, 5 and 6: algae treated with 1000 impulses; Flasks 7, 8 and 9: control group; Flasks 10, 11 and 12 centrifuged group.

The spectra-photometer measurement was stopped after 10 days due to no significant visible growing and significant differences between treatment and control or centrifuged group had been acquired. Besides, there were another arrangement of experimental works was planned at that time. However, after 20 days, the treatment samples with 500 impulses started growing, meanwhile, there was no microalgae alive after 1000 positive plasma impulses (Flasks marked as 4, 5 and 6)

6.7.5.3 Energy calculation of plasma treatment with metallic dish

The plasma treatment and PEF treatment result in different inactivation processes and mechanisms, the PEF treatment is based on the electric field (conduction current through the liquid is also present in this treatment method) while the plasma treatment results in generation of chemically active species above the liquid and intensive conduction through the liquid in the case of treatment in the metallic dish.

Current and voltage waveforms were obtained during the plasma treatment, these wave forms are shown in **Figure (6.7.5.10-6.7.5.11)** and can be used to calculate the energy delivered to the plasma test cell in each impulse and the total energy used for the plasma treatment. The current in the graphs transferred to voltage value shown oscilloscope through the Pearson current transformer. The total energy delivered to the test cell during the treatment can be obtained with **Equation (6.6)** below**.** The transformer is connected to a 50 Ω terminator and a 20 dB attenuator, the exact current transferred in the test chamber can be calculated through **Equation (6.7)**. **Table (6.7.5.3)** below shows the energy available in each impulse for both positive and negative polarity pulses.

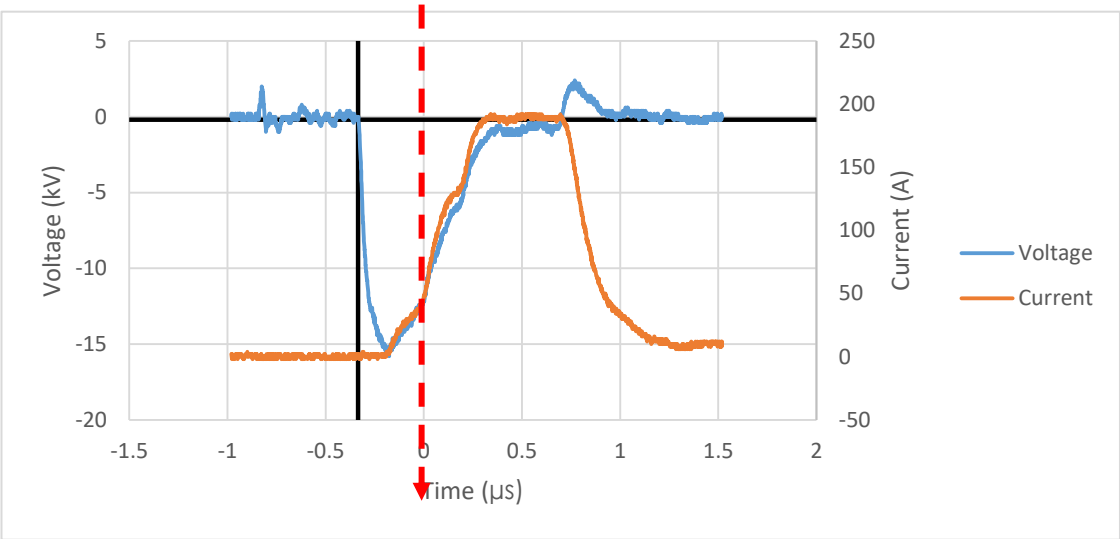

Figure (6.7.5.10) One example of wave shapes recorded from oscilloscope of one single impulse delivered to the test cell of negative plasma. Red line represents the moment when the breakdown is occurring. The current signal is recorded with current transformer introduced in **Section 4.5.**

$$\boldsymbol{E = \int V(t) \cdot I(t) \cdot dt} \qquad \textbf{(6.6)}$$

$$\boldsymbol{I = 10 \times V_C} \qquad \textbf{(6.7)}$$

Where V(t) is the transient voltage across the test cell, I (t) is the transient current though the test cell. $\boldsymbol{I}$ is the current in the test chamber in A, $\boldsymbol{V_C}$ is the voltage value recorded by oscilloscope from the Pearson current transformer in Volt.

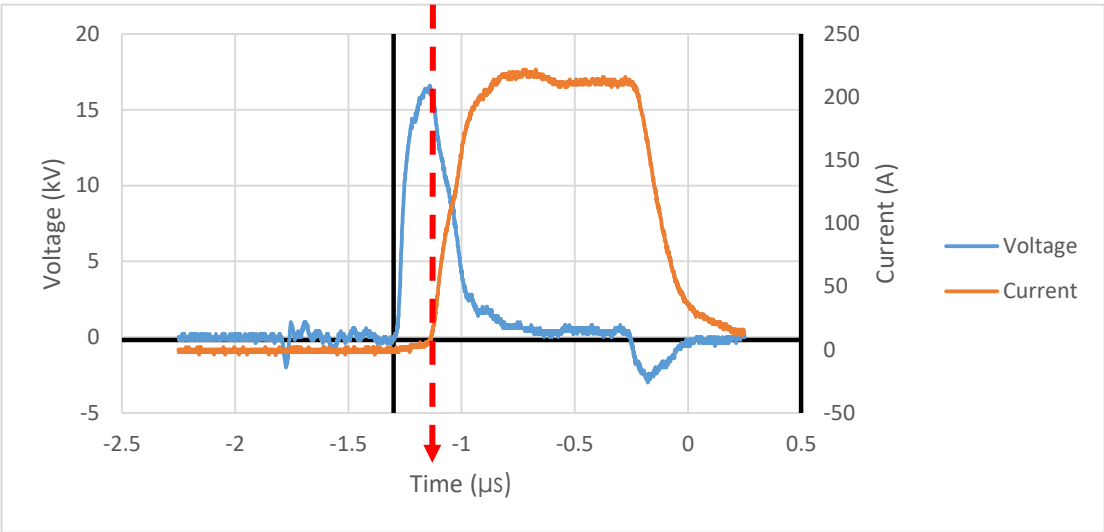

Figure (6.7.5.11) One example of wave shapes recorded from oscilloscope of one single impulse delivered to the test cell of positive plasma. Red line represents the moment when the breakdown is occurring. The current signal is recorded with current transformer introduced in **Section 4.5.**

Table 6.3 Energy delivered to test cell with negative or positive polarity plasma treatment per impulse

Wave shape samples	**Positive (Joule)**	**Negative (Joule)**
01	0.4572	0.5980
02	0.4416	0.6353
03	0.4416	0.4346
04	0.4469	0.6674
05	0.4066	0.3602
AVG	**0.44 ± 0.019 J**	**0.54 ± 0.134 J**

The growing curve shows that 500 and 1000 impulses of both positive and negative plasma polarities provide significant inactivation effects on phytoplankton. 1000 plasma impulses can lead to complete inactivation of microalgae. **Table (6.7.5.3)** shows that the energy delivered to the test cells during positive and negative plasma treatment is almost the same which results in almost the same inactivation effects for two polarities of the plasma treatment.

6.8 Plasma treatment with metallic dish and plastic dish: summary of results

There were another section which was initially planned as a more complex experimental works with both PEF treatment and plasma treatment in either metallic or plastic dish, however, in order to confirm the same treatment and growing conditions, all the experimental works were finished at one day and the time was quite tight to finish the spectrophotometer measurement. The measurement results were also not acceptable for further investigation, these experimental works were not planned to repeat due to the Covid-19. In the end, this section was included in thesis as Appendix A. Nevertheless, the recoded wave shape from oscilloscope of plasma treatment with plastic dish could still explain the differences between plasma treatment with metallic dish and general PEF treatment.

The plasma treatment provides a different approach to the delivery of energy to the samples. The plasma is generated by applying high voltage impulses to the needle electrodes above the surface of the sample which is being treated. The magnitude of the electric field is sufficiently high to generate strong electric field at the tip of the needle electrodes to cause ionization and develop plasma. The HV impulses are generated by the Blumein pulse generation system described in **Section 4.3**. A summary of the results of Plasma treatment of *Nannochloropsis Oculata* is given below.

- *Nannochloropsis Oculata* can be inactivated by the plasma treatment in the metallic dish. It was found that the inactivation effect increases with an increase in number of impulses from 300 to 1000.
- HV Impulses of positive and negative polarities were used in the plasma treatment. The inactivation efficiency was found to be same for both polarities based on the growing curve measurements and the energy calculation.
- The plastic dish and metallic dish were used in the plasma treatment. There is almost no inactivation observed (based on the growing curve of microorganisms) in the case of the plasma treatment in the plastic dish, even with the maximum number of impulses which was 1000 in these test.
- The energy dissipates through the conduction process in the liquid sample in the case of plasma treatment in the metallic dish when the needles are in contact with the liquid surface. There is no conduction current observed in the case of treatment in the plastic dish.
- The Plasma treatment in the metallic dish leads to the complete inactivation of microorganisms with 1000 impulses.
- The maximum temperature increase recorded during the plasma treatment was below ~ 10℃.
- The inactivation efficiency of the plasma treatment in the plastic dish is much lower than in the case of the metallic dish plasma treatment due to low energy delivered to the test cell. For the 700 impulses tests, the absorbance of algae suspension after negative plasma treatment in the metallic dish decreases by 20% in two days after the treatment and the absorbance of algae suspension treated with negative plasma in the plastic dish increases by 12.5% in two days after the treatment.

- The PEF treatment shows a higher inactivation efficiency compared with the plasma treatment in the plastic dish: the absorbance of algae suspension after the PEF treatment decreases by 20% in two days after the treatment.
- The Plasma treatment with 1000 impulses in the metallic dish can completely eliminate microalgae with lower energy delivered to the test cell per impulse compared with the PEF treatment. The energy delivered to the test cells is required for the inactivation process but the different processes which lead to inactivation in the case of electric field and plasma also determine the inactivation efficiency.

6.9 Discussion of plasma treatment results

The inactivation of *Nannochloropsis Oculata* using the plasma treatment was studied in this chapter. The obtained results were discussed and summarized in the previous sections. The initial motivation for these tests was an attempt to investigate potential differences in the inactivation efficiency for different approaches of delivery of energy generated by the same pulse generation system. It was found that the difference in the inactivation efficiency is significant for different methods, based on comparison of the results obtained using the plasma treatment and PEF treatment. The details of this analysis will be discussed in this section.

Firstly, the plasma treatment in the metallic and plastic dishes shows completely different inactivation efficiencies: For the 700 impulses tests, the absorbance values of the treated algae suspension (treated with negative plasma impulses in the metallic dish) decreases by 20% two days after the treatment. However, no inactivation phenomenon of microorganisms was observed after the plasma treatment with plastic dish. It is believed that the reason for this difference is the different conduction path after breakdown occurs. The samples treated in the metallic dish which is grounded by the direct contact between the dish and the

grounded plate in test chamber were subjected to the conduction current flows through the liquid during the treatment (when the HV needles are in contact with the surface of the samples). The discharge current produced by the energized needles directly propagated through the sample and the conduction current flows through the sample to the ground. Such delivery of charge directly into the samples leads to more efficient inactivation process. For the plastic dish scenario, there is no breakdown observed during the treatment, thus no conduction current flow through the liquid.

Secondly, the maximum increase in the temperature of the liquid samples measured during /after the plasma treatment was less than 10 ℃ which is not sufficient to cause denaturation of proteins. The global heating effect is therefore not the main factor in the plasma inactivation process.

According to the energy calculations, the energy delivered to the test chamber is ~0.44 J per impulse for positive plasma treatment and ~0.54 J for negative plasma treatment. It is reported that such an amount of energy is sufficient to cause the inactivation process in the case of the PEF treatment with the field strength of 80 kV/cm [78]. The energy delivered to the test cells is sufficient to cause inactivation however, the way how this energy is delivered to the samples (for example interaction between the charges and active species generated by plasma and/or electric field and micro algae) also determine the inactivation efficiency.

It can be assumed that for the effective inactivation (and potentially sterilization) process, the plasma treatment in the metallic dish is more effective as compared with the PEF treatment. From another point of view, it may be argued that the PEF treatment is more suitable for lysis i.e. extraction of valuable components for practical applications such as production bio-fuel as the microorganisms would be alive after treatment thus they could be re-used after PEF treatment for further bio-fuel extraction.

6.10 Impact of Covid Lockdowns on the Proposed Experimental Program

The original experimental program was planned to continue with comparisons between the efficiency of treatment with PEF and with plasma in plastic dishes. In the first attempt to culture algae and perform these measurements a problem developed with no significant growth of algae occurring in any of the flasks including the control flasks over a period of 12 days. The start of the Covid lockdowns at the university prevented a second attempt at these measurements and prevented any further experimental work in the project. The experimental protocol used and the results obtained have been included in Appendix A.

Chapter 7. Conclusions and future work

This chapter provides the main conclusions obtained based on the research works presented in this thesis. Several single cell models have been developed to investigate the interactions between microorganisms and an external electric field: a 1D linear model, 2D QuickField model and 3D COMSOL model. Related experimental work was also conducted during the course of this project: PEF treatment of microorganisms was conducted initially in standard, commercially available electroporation cuvettes, secondly, in the test cell with parallel plane metal electrodes developed for this study, and thirdly, microorganisms were treated by plasma discharges in metallic and plastic dishes. The main achievements of this research work are summarized in this chapter, and potential future work is discussed.

7.1 Present works and general conclusions

This research was aimed at investigation of the interactions between pulsed electric fields and microorganisms, understanding of this interaction being critically important for further development and optimization of the PEF treatment and electroporation processes. Different parameters of the PEF treatment were used in the experimental and analytical work: different electric field strength and different waveshapes/energization regimes, liquid samples with different conductivity; also different types of microorganisms (different in size and with different membrane thickness). The simulation models developed during this work will be beneficial in further investigation of the interaction between pulsed electric fields and different microorganisms.

The experimental work conducted in this research project was focused on investigation of the inactivation of microorganisms with pulsed electric fields and plasma discharges, to support the analytical studies presented in this thesis. The

main achievements of the thesis will be summarized and discussed in the following sections.

7.1.1 Modelling of microorganisms-Linear model

Chapter 3 is the first step in the modelling of the PEF treatment of microorganisms, this section as summarized previously, used analytical models and presented the linear model which was developed in this research programme.

The linear model provides an initial investigation of the interaction between the applied electric field and a single cell: the electric field strength in the cell membrane during the PEF treatment was obtained based upon realistic parameters of microalgae.

The dependency of the electric field strength in the cell membrane during the PEF treatment on time could be explained and supported by other researchers' results. The characteristics of the microorganism affect the electric field strength in the cell membrane: the membrane thickness has a significant effect on the electric field strength in the cell membrane.

The linear model was also used to investigate the transient behaviour of the electric field strength in the cell membrane during the PEF treatment. It describes the relationship between the treatment time and electric field strength in relation to the cell parameters (conductivity and permittivity of cytoplasm and environmental fluid).

However, the linear model is a one dimensional model used for the initial analytical modelling, and this model has significant limitations: the linear model could not predict an accurate relationship between the cell size and treatment time. Different types of voltage source were difficult to implement in the linear model, and the interaction between the cytoplasm and other cell structures was also not taken into account.

7.1.2 Modelling of microorganisms-QuickField 2D axisymmetric model

Chapter 4 details a more advanced single cell model, developed using QuickField software. The QuickField model could be used to investigate more complex situations: both steady state and transient electric fields could be used in this model.

The results obtained with the QuickField model could be supported by the results obtained via the linear model.

Due to the high current density, local heating effects could be observed during the PEF treatment, and such local heating effects could help to enhance the electroporation process. Local hot spots were generated in the environmental fluid treated with micro-second PEF impulses and with nano-second PEF impulses, with the local heating effects typically observed in the cytoplasm. The local heating effects are mainly influenced by the conductivity of the environmental fluid and applied electric field strength. This is the main result obtained using the QuickField model, which has not been reported in other published research work.

A multi-cell model with 3 cells was also developed using QuickField, and the results show that multiple microorganisms do not affect the electric field in their membranes and cytoplasm as compared with a single cell model.

The cell nucleus was also included in the QuickField cell model, and it was shown that during the nano-second PEF treatment, the cytoplasm and cell nucleus were affected by the applied electric field.

However, the QuickField model could not provide the transient analysis of the local heating effects due to the limitation of the QuickField software. In general, the thermal effects were not taken into account during this study of the PEF treatment of microorganisms. Therefore, a more advanced model was developed to investigate such thermal effects.

7.1.3 Modelling of microorganisms-COMSOL 2D axisymmetric model

The COMSOL model developed in Chapter 5 could be used to investigate the interaction between the external electric field and cells in more detail, and to enable comparison of these results with the QuickField model and linear model.

The COMSOL model could provide transient analysis of the thermal effects during the PEF treatment. The local heating effects obtained using the QuickField model were also obtained in the COMSOL model with the same characteristics: it was found that the hot spots are mainly affected by the conductivity of the environmental fluid and the applied electric field strength. Based upon the results of the COMSOL model, it could be stated that the global thermal effects during the PEF treatment are negligible if the applied field strength is 30 kV/cm and the conductivity of the environmental fluid is low. However, with higher field strength and higher conductivity of the environmental fluid, the thermal effects become significant.

Different energisation regimes were used in the COMSOL model, thermal effects in the case of AC signals were generated by dielectric heating, and in the case of square (DC) impulses, and it was joule heating. The dielectric heating effects could not be neglected due to the high field strength in the cell membrane, and such thermal effects could be one of the main reasons for membrane damage during the PEF treatment in the case of AC waveforms.

The resting potential and temperature dependent parameters were also investigated. Compared with the significant induced electric field strength in the cell membrane, the electric field strength due to the resting potential could be negligible. When typical electroporation field strength is used in the PEF treatment, the temperature in and around the microorganisms would not change significantly,

so the temperature dependent parameters could also be considered negligible in this case.

The cell nucleus was also included in the COMSOL model and the obtained results support the QuickField model. Furthermore, the COMSOL model provides transient thermal effects in the cytoplasm and cell nucleus during the nano-second PEF treatment, which confirms that there are local heating effects in the cytoplasm during the nano-second PEF treatment. However, in the typical electroporation process, the thermal effects could be neglected, so the local heating effects are not considered as the main reason which causes membrane breakdown or nuclear membrane breakdown.

Electromechanical forces were also investigated with the COMSOL model, the force analysis shows that the total force induced on the cell membrane during the PEF treatment is not balanced, thus the cell can be compressed. Both thermal and electromechanical forces were investigated and compared with the electromechanical force, the thermal force could be negligible, as the local heating effects are not significant in the general electroporation process.

A perforated membrane was also investigated using COMSOL: in this case, there was a pore included in the model cell membrane. It was shown that there were thermal effects in the pore and such heating effects are not negligible and could enhance the pore expansion.

7.1.4 PEF treatment and Plasma treatment experiments of microalgae

The experimental work was planned to investigate the inactivation efficiency of the PEF impulses on microalgae in different test chambers and for varying applied field strength.

A Blumlein HV impulse generator was built to provide 1 µs long HV impulses. The experimental results of the PEF treatment in the modified electroporation cuvettes show that clusters of microalgae were formed after the PEF treatment, which

suggested that charges accumulation occurs on the surface of cell membrane as modelled in Quickfield.

However, due to the low starting population of samples with the electroporation cuvette test cell, the experimental results could not show the inactivation ability (growth curve could not be obtained from spectrophotometer measurement due to the low population of samples).

With the in-house developed test cell with metallic stainless-steel electrodes, the growth curve of treated microalgae was obtained after treatment of microalgae with 1 μs long impulses with the field strength of ~33 kV/cm. The results show that the increase of the number of applied high field impulses from 500 to 1000 did increase the inactivation efficiency
(~ 41% lower 'abs' observed with 1000 impulses) of the PEF treatment of microalgae. However, the temperature difference of the solution treated with 500 and 1000 impulses was quite low: only ~6 ℃ increase was observed which suggested that the structures of valuable nutrients wouldn't be damaged during treatment. This confirms the result obtained in the simulation work: in the general electroporation process, the global heating effects can be considered negligible. For the membranes with pores during PEF treatment, further experimental works would be necessary to investigate the local heating effects in the pore which has been observed with COMSOL model in Chapter 5.

A plasma treatment experiment was also conducted, with algae solutions treated in the metallic dish and in the plastic dish. These experimental results show that the plasma treatment in the metallic dish provide the highest efficiency of inactivation of microalgae. Based upon the experimental results, the plasma treatment in the plastic dish does not show any inactivation effect. The total energy was also calculated, and it was found that the energy delivered to the test cells is sufficient

to cause inactivation, however, the way in which this energy is delivered to the samples also determines the inactivation efficiency.

7.2 Novelty and contribution to the field of study

The novel contributions to the field are summarised below.

- Three different analytical models were developed, to investigate the interactions between the bio-cell and applied electric fields.
- The local heating effects were found and investigated in the single cell model during the PEF treatment.
- Transient analysis of the single cell model was conducted using different parameters and source of HV signals.
- Electromechanical and thermal forces were investigated and compared in the investigation of the PEF treatment of a single cell (QuickField and COMSOL models).
- Multiple cells were investigated and it was found that the microorganisms were independently affected by the applied electric field.
- The resting potential and temperature dependent parameters were investigated, and it was confirmed that in the general electroporation process, these temperature dependencies in the parameters could be neglected.
- The cell nucleus was included in the model and the obtained results show that the cell nucleus membrane and cell structures in cytoplasm could be damaged using the nano-second PEF treatment.
- A single pore was included in the cell membrane model and the thermal effects in and around the pore were investigated. The results suggested that the pore would be expanded due to the thermal effects generated in the pore.
- From the experimental works it was found that the energy in the impulses applied via the same Blumlein generator, but delivered to the test samples

through different approaches (pulsed electric field and plasma in metallic dishes and plastic dishes) results in different inactivation efficiency of microalgae. The plasma treatment with metallic dish has better inactivation results compared with PEF treatment. There was no killing effects observed with the plasma treatment with plastic dish as there was no energy delivered to the test cell.

7.3 Future work

The developed COMSOL model has great potential in the investigation of PEF processes, and the deformation of a single cell could also be investigated using accurate parameters.

For the experimental works, the inactivation ability of the PEF impulses with a higher strength electric field could be investigated.

The detailed information about different inactivation efficiency in the case of different test cells and different microorganisms are also worthy of further investigation.

Appendix A: New PEF treatment and Plasma treatment with metallic dish and plastic dish

A series of additional experiments were planned to allow comparisons to be made between PEF treatment and plasma treatment where the samples was contained in plastic dishes. The first attempt to culture the algae for these experiments was unsuccessful with little or no growth occurring in any of the samples. Due to the Covid lockdowns it was not possible to make another attempt at culturing the algae to allow these comparisons to be made. However, for completeness, the obtained preliminary results have been included in this Appendix.

In order to compare the inactivation efficiency, the PEF treatment was also included in this experiment, thus comparison of efficiency of the PEF treatment, negative and positive plasma treatment in the metallic dish and plastic dish will be conducted. The control and centrifuged groups are also included to provide the baseline (control values) in these experiments. **Table I** introduces the experimental sets and number of flasks.

The procedures in these tests were the same as in experiments which have been conducted and described before, all the treatments (PEF and plasma with different polarities) are completed on the same day (Day 0) to make sure the growing conditions and population of algae are the same. The PEF test cell can only hold 1.5 mL sample and the volume of samples used in the plasma treatment was 3 mL, so the PEF treatment for each number of impulses must be conducted twice to achieve the same population of samples as in the case of the plasma treatment. It was shown that the treatment with 1000 impulses has higher inactivation however, it takes longer time to complete the treatment using this number of pulses. If the pulse repetition rate is increased, the temperature of samples and test cells also increases in the case of the 1000 impulses test, thus it is not possible to neglect the

influence of temperature in this case. Also, it was shown that 700 impulses were sufficient for effective inactivation of phytoplankton in the case of the PEF treatment. Therefore the maximum number of impulse was set to 700 in this experiment.

Table I Test Arrangements: number of growing flasks for PEF and plasma treatment with 300,500 and 700 HV impulses

	300 impulse	500 impulses	700 impulses	Control	Centrifuged
Metal dish Positive polarity	3	3	3	3	3
Metal Dish Negative polarity	3	3	3		
Plastic Dish positive polarity	3	3	3		
Plastic Dish Negative polarity	3	3	3		
PEF	3	3	3		

Figure I. Growing flasks of experiments in **Section 6.7.1** at Day 0. The light intensity was not measured in this experiment, however, there are gaps between these flasks and the parameters of lamps are the same, thus the light intensity could be considered as the same.

Figure II and **Figure III** below shows the plasma treatment with plastic dish has almost no killing effects compared with plasma treatment with metallic dish. **Figure IV** shows PEF treatment with higher number of impulses (700) is more effective, compare **Figure IV** with **Figure III** PEF treatment is more effective in inactivation effects than plasma treatment with plastic dish even with 700 impulses. **Figure V** compares all the growing curves of the tests in high number of impulses (700), it

can be seen that plasma treatment with plastic dish almost has no killing effects to the phytoplankton, both other groups show the reduction in optical absorption after the treatment. All the current through the test cell and voltage across the test cell are recorded in this experiment.

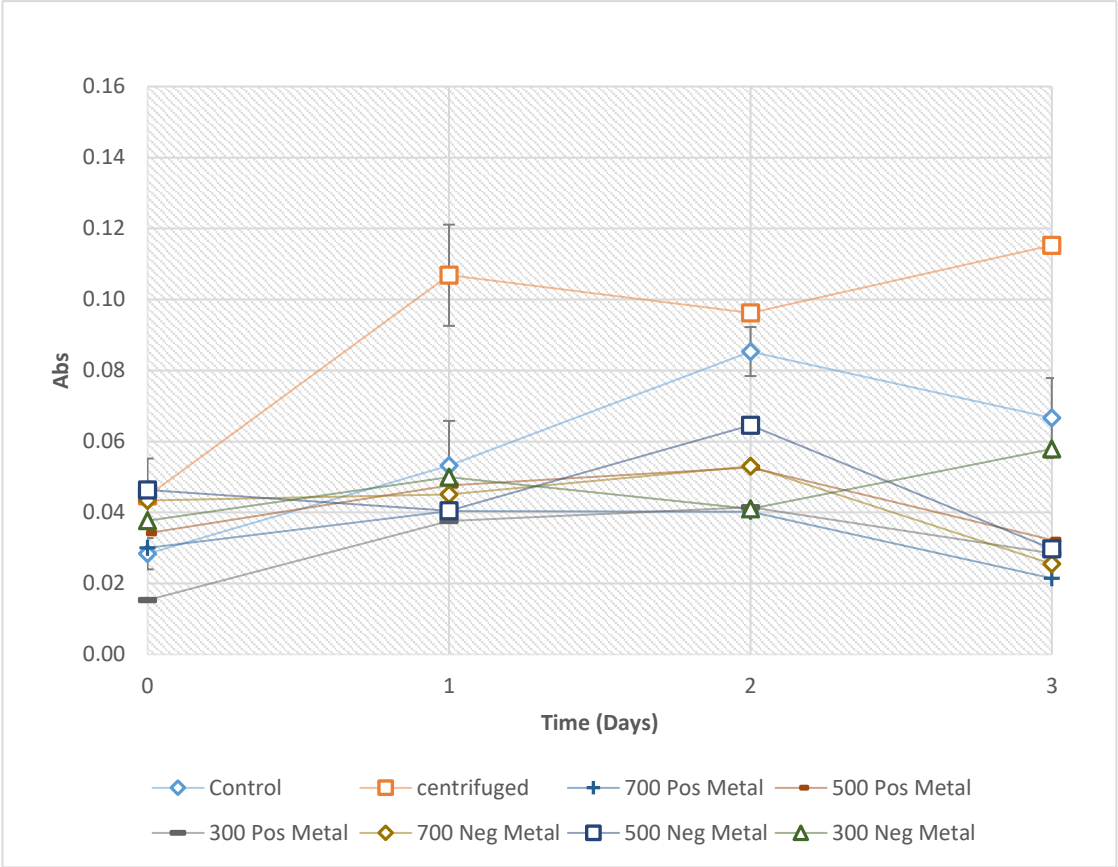

Figure II. Growth curve of algae after the plasma treatment with different number of impulses and polarity in the metallic dish. Abs represents the absorbance at 680 nm, the data is recorded at day 0 and every day after treatment. The error bars represent standard deviation. 8 groups are measured and shown in this graph.

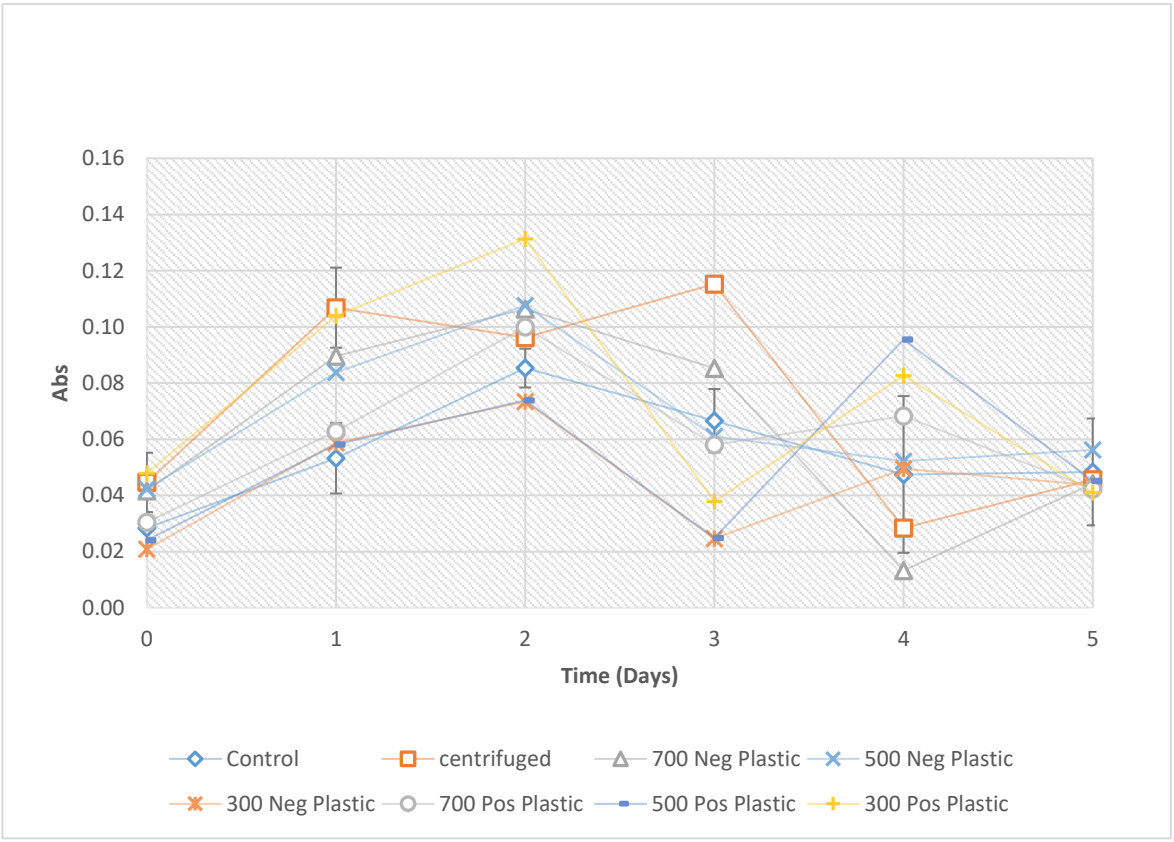

Figure III. Growth curve of plasma treatment with different number of impulses and polarity in plastic dish. Abs represents the absorbance of 680 nm wavelength by microalgae, the date is recorded at day 0 and every day after treatment. The error bars represent standard deviation. 8 groups are measured and shown in this graph.

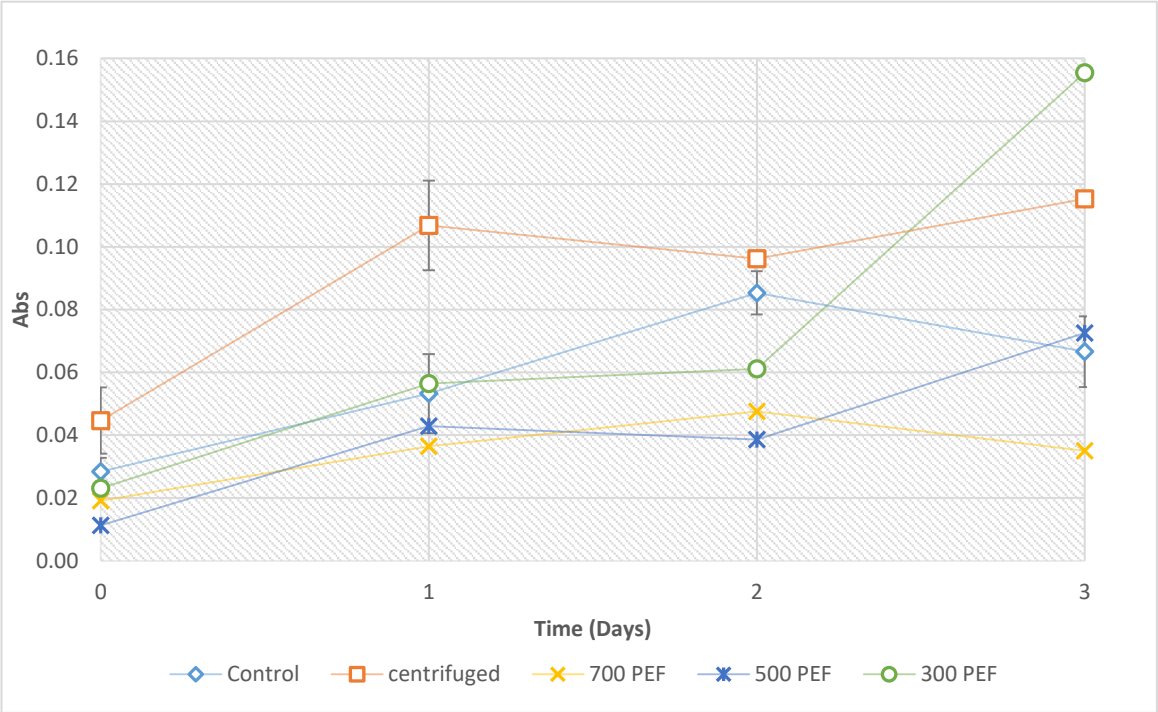

Figure IV. Growth curve of PEF treatment results with different number of impulses. Abs represents the absorbance of 680 nm wavelength by microalgae, the date is recorded at day 0 and every day after treatment. The error bars represent standard deviation. 5 groups are measured and shown in this graph.

Figure V shows the growing curve of microalgae treated with 700 impulses using different treatment methods. It can be seen that, the plasma treatment in the metallic dish shows the highest significant inactivation effect compared with other approaches. The PEF treatment with 700 impulses produces similar inactivation effect. The plasma treatment in the plastic dish does not lead to inactivation even with high number of impulses.

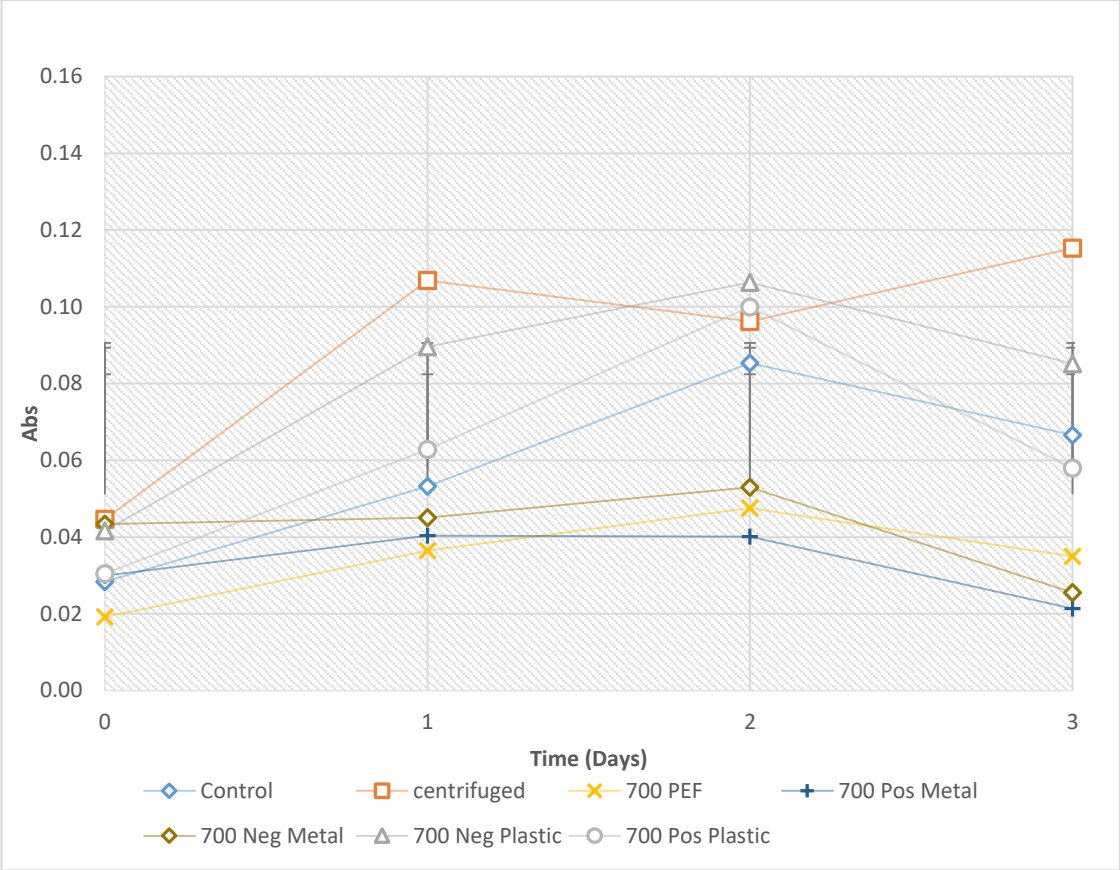

Figure V. Growing curve of PEF treatment and plasma test in different containers (both positive polarity and negative polarity) with different number of impulses. Abs represents the absorbance of 680 nm wavelength by microalgae, the data is recorded at day 0 and every day after treatment. The error bars represent standard deviation. 7 groups are measured and shown in this graph.

Energy is recorded in this experiment, **Figures VI - VIII** shows examples of voltage and current waveforms recorded in this experiment. The energy can be obtained by **Equation (6.6) and Equation (6.7)** introduced in **Section 6.7.5.**

The energy of the negative plasma treatment with the plastic dish is 0.0036 Joules per impulse, **Figure VI**. The energy of the negative plasma treatment with metallic dish is 0.7815 Joules per impulse, **Figure VII.** The large amount of energy delivered to the samples in the metallic dish during the plasma treatment could be the reason

of high efficiency of inactivation of phytoplankton in this case as compared with the plasma treatment of algae in the plastic dish.

However, the energy of the PEF treatment**, Figure VIII**, which is 1.42 Joules per impulse is higher than the energy delivered in each plasma impulse during the plasma treatment in the metallic dish.

The inactivation efficiency of the PEF treatment is not increased with an increase in the energy delivered to the samples compared with the plasma treatment in the metallic dish. This could be due to the differences in interaction between microalgae and pulsed electric field or plasma. The inactivation by the plasma treatment is a complex process at it was discussed in **Chapter 2.** Chemically active species produced by plasma treatment may lead to the high efficiency in inactivation as compared with the PEF treatment, even at lower energy delivered to the test cell during the plasma treatment.

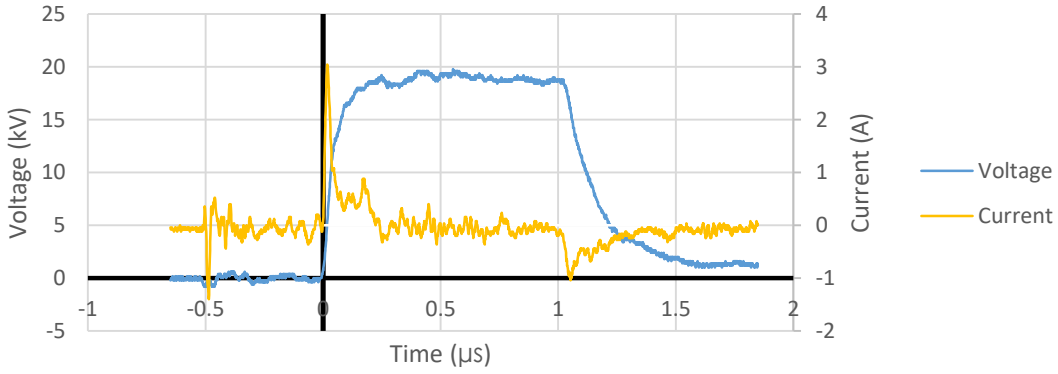

Figure VI. One example of wave shapes recorded from oscilloscope of one single impulse delivered to the test cell of Negative Plasma with plastic dish. The current signal is recorded with current transformer introduced in **Section 4.5.**

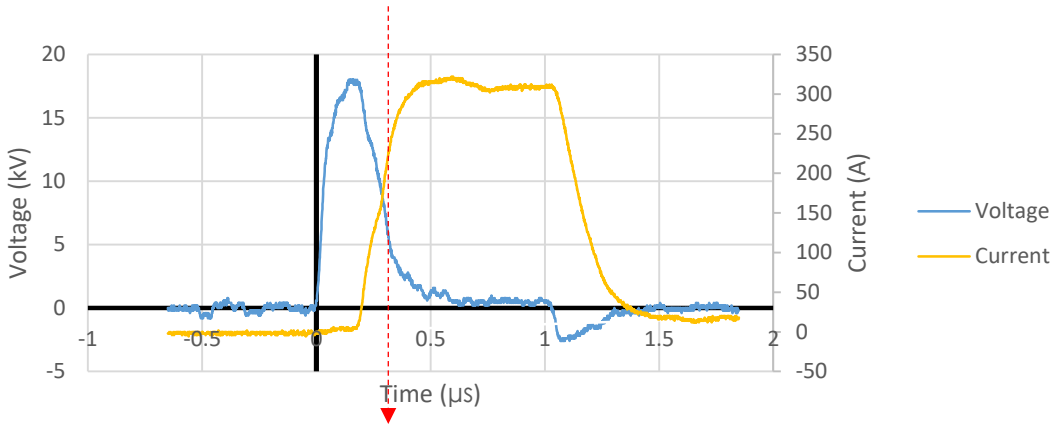

Figure VII. One example of wave shapes recorded from oscilloscope of one single impulse delivered to the test cell of Negative Plasma with metallic dish. The current signal is recorded with current transformer introduced in **Section 4.5.** Where the red line represents the breakdown occurs.

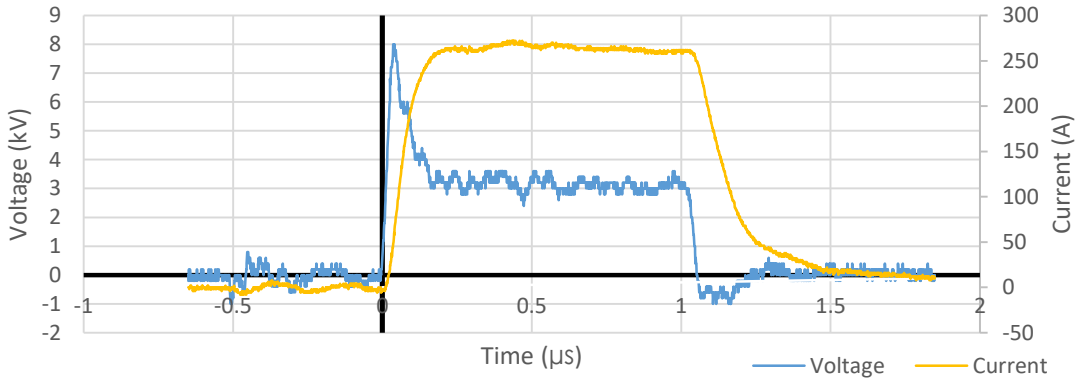

Figure VIII. One example of wave shapes recorded from oscilloscope of one single impulse delivered to the test cell of metallic PEF treatment test cell. The current signal is recorded with current transformer introduced in **Section 4.5**

Plasma treatment of algae suspension in the metallic dish showed significant inactivation effect in previous experiments. **Figure II** provides the growing curve of algae after the plasma treatment in the metallic dish for different number of impulses. It can be obtained that the plasma treatment in metallic dish with 500 impulses and 700 impulses leads to noticeable inactivation of microalgae, as the

absorbance decreases after the treatment which suggests that plasma treatment in the metallic dish with 700 impulses is sufficient to cause cell death. The plasma treatment with 300 negative impulses does not show significant inactivation effect in this experiment, however, the plasma treatment with 300 positive impulses leads to inactivation of algae.

The plasma treatment in the plastic dish does not show noticeable inactivation in this experiment, as can be seen from **Figure III**, all treated samples demonstrate the same growing tendency as the centrifuged and control samples, which is an indication that algae continue to grow after the treatment (growing curve between day 0 to day 2). The decrease in algae population at day 3 cannot be used to confirm the inactivation effect of the plasma treatment in the plastic dish as the centrifuged group also decreases at the same time. Besides, the growing curve continue to show an increase in population as the control groups at day 1 and day 2, at the same growth rate. The control and centrifuged group show a decrease in absorbance after day 2, there could be several reasons for this decrease, contamination could be the most possible reason, as there were 51 samples required to be measured each day thus the possibility of contamination would be significantly increased.

References

[1] Lakhan Kumar, Raksha Anand, Maulin P Shah and Navneeta Bharadvaja, "Microalgae biodiesel: A sustainable source of energy, unit operations, technological challenges, and solutions," *Journal of Hazardous Materials Advances,* Vol 8, no 100145, pp. 1-14, 2022.

[2] Muhammad Imran Khan, Jin Hyuk Shin and Jong Deog Kim, "The promising future of microalgae: current status, challenges, and optimization of a sustainable and renewable industry for biofuels, feed, and other products," *Microbial Cell Factories,* Vol 17, no 36, pp. 1-21, 2018.

[3] J. Leman, "Lipids, Production," from *Encyclopedia of Microbiology (Third Edition)*, Academic Press,, 2009, pp. 393-406.

[4] Marjorie Morales, Claude Aflalo and Olivier Bernard, "Microalgal lipids: A review of lipids potential and quantification for 95 phytoplankton species," *Biomass and Bioenergy,* Vol 150, no 106108, pp. 1-25, 2021.

[5] S. Ravishankar, H. Zhang and M.L. Kempkes, "Pulsed Electric Fields," *Food Science and Technology International,* Vol 14, no 5, pp. 429-432, 2008.

[6] I. V. Timoshkin, S. J. MacGregor, R. A. Fouracre, B. H. Crichton and J. G. Anderson, "Transient electrical field across cellular membranes: pulsed electric field treatment of microbial cells," *Journal of Physics D: Applied Physics,* Vol 39, no 3, pp. 596-603, 2006.

[7] C. Yao, X. Ma, K. Qian, Y. Wang and S. Dong, "Simulation and Experimental Study on the Responses of Subcellular Structures in Tumor Cells Induced by 5 ns Pulsed Electric Fields," *Applied Science,* Vol 13, no 14, pp. 1-16, 2023.

[8] Chiara Montanari, Urszula Tylewicz, Giulia Tabanelli, Annachiara Berardinelli, Pietro Rocculi, Luigi Ragni and Fausto Gardini, "Heat-Assisted Pulsed Electric Field Treatment

for the Inactivation of Saccharomyces cerevisiae: Effects of the Presence of Citral," *Sec. Food Microbiology,* Vol 10, pp. 1-11, 2019.

[9] H. Gest, "he discovery of microorganisms by Robert Hooke and Antoni van Leeuwenhoek, Fellows of The Royal Society," *Notes and Records of the Royal Society of London,* vol. 58, no. 2, pp. 187-201, 22 5 2004.

[10] B.Lee Ligon, "Biography: Louis Pasteur: A controversial figure in a debate on scientific ethics," *Seminars in Pediatric Infectious Diseases,* vol. 13, no. 2, pp. 134-141, 2002.

[11] Hawksworth.D.L., "Microorganisms," in *B. Groombridge ed. Global Biodiversity: Status of the Earth's Living Resources.*, New York, Springer Netherlands, 2012, pp. 47-54.

[12] Wladyslaw Altermann and Józef Kazmierczak , "Archean microfossils: a reappraisal of early life on Earth," *Research in Microbiology,* pp. 611-617, 21 8 2003.

[13] Thomas Cavalier-Smith, "Cell evolution and Earth history: stasis and revolution," *Philosophical Transactions of the Royal Society B: Biological Sciences,* pp. 969-1006, 29 6 2006.

[14] J. William Schopf, "Fossil evidence of Archaean life," *Philosophical Transactions of the Royal Society B: Biological Sciences,* pp. 869-885, 29 6 2006.

[15] M. Madigan, J. Martinko, K. Bender, D. Buckley and D. Stahl, Brock Biology of Microorganisms, 14th ed. Globe ed., San Francisco: Pearson Education, 2014.

[16] John A. Fuerst, "Beyond Prokaryotes and Eukaryotes : Planctomycetes and Cell Organization," Nature Education, 2010. [Online]. Available: https://www.nature.com/scitable/topicpage/beyond-prokaryotes-and-eukaryotes-planctomycetes-and-cell-14158971/. [Accessed 13 10 2022].

[17] C R Woese, O Kandler and M L Wheelis, "Towards a natural system of organisms: proposal for the domains Archaea, Bacteria, and Eucarya.," *Proc. Natl. Acad. Sci. U.S.A.,* Vol 87, no 12, pp. 4576-4579, June 15, 1990.

[18] John L. Howland, The Surprising Archaea: Discovering Another Domain of Life, New York: Oxford University Press, 2000.

[19] O. Erkmen, Laboratory Practices in Microbiology, London: Academic Press, 2021.

[20] Lisa Brown, Julie M. Wolf, Rafael Prados-Rosales and Arturo Casadevall, "Through the wall: extracellular vesicles in Gram-positive bacteria, mycobacteria and fungi," *Nature Reviews Microbiology,* vol. 13, pp. 620-630, 1 9 2015.

[21] David White, James T. Drummond and Clay Fuqua, The Physiology and Biochemistry of Prokaryotes, New York: Oxford University Press, 2012.

[22] John Webster and Roland Weber, Introduction to fungi, New York: Cambridge University Press, 1980.

[23] David S. Domozych, Marina Ciancia, Jonatan U. Fangel, Maria Dalgaard Mikkelsen, Peter Ulvskov and William G. T. Willats, "The cell walls of green algae: a journey through evolution and diversity," *Sec. Plant Physiology,* Vol 3, no 82, pp. 1-7, 2012.

[24] P. Singleton, Bacteria in Biology, Biotechnology, and Medicine, New York: J. Wiley & Sons, 1997.

[25] John F. Nagle and Stephanie Tristram-Nagle, "Structure of lipid bilayers," *Biochimica et Biophysica Acta,* vol. 1469, no. 3, pp. 159-195, 2000.

[26] National Human Genome Research Institude, "National Human Genome Research Institude," 13 10 2022. [online]. Available: https://www.genome.gov/genetics-glossary/Plasma-Membrane#:~:text=The%20plasma%20membrane%2C%20also%20called,membrane%20on%20its%20outside%20surface.. [access date: 2022 10 14].

[27] Cytoplasm and plasma membrane, "Khan Academy," [online]. Available: https://www.khanacademy.org/science/biology/structure-of-a-cell/prokaryotic-and-eukaryotic-cells/a/plasma-membrane-and-cytoplasm. [access date: 14 10 2022].

[28] Jahangir Moini, Nicholas G and MohtashemSamsam, "Chapter 2 - Cytology of the nervous system," from *Epidemiology of Brain and Spinal Tumors*, London, Academic press, 2021, pp. 41-63.

[29] Kaspar Vogt, “Chapter Eight - Diversity in GABAergic Signaling,” from *Advances in Pharmacology*, Vol 73, London, Academic press, 2015, pp. 203-222.

[30] Wolfram Weckwerth, “Metabolomics in systems biology,” *Annual Review of Plant Biology,* Vol 54, pp. 466-489, 2003.

[31] J. S. Clegg, “Properties and Metabolism of the Aqueous Cytoplasm and Its Boundaries,” *Am. J. Physiol,* Vol 246, no 2 2, pp. 133-151, 1984.

[32] J. William Schopf and Bonnie M. Packer, “Early Archean (3.3-Billion to 3.5-Billion-Year-Old) Microfossils from Warrawoona Group, Australia,” *Science,* Vol 237, no 4810, pp. 70-73, 1987.

[33] Ken Takai, Kentaro Nakamura, Tomohiro Toki, Urumu Tsunogai, Masayuki Miyazaki, Junichi Miyazaki, Hisako Hirayama, Satoshi Nakagawa, Takuro Nunoura and Koki Horikoshi, “Proceedings of the National Academy of Sciences,” *Cell proliferation at 122 ° C and isotopically heavy CH4 production by a hyperthermophilic methanogen under high-pressure cultivation,* Vol 105, no 31, pp. 10949-10954, 2008.

[34] Ron Sender, Shai Fuchs and Ron Milo, “Revised Estimates for the Number of Human,” *PLoS Biol,* Vol 14, no 8, pp. 1-14, 2016.

[35] Qi Wang, Jinge Liu and Hongyan Zhu, “Genetic and Molecular Mechanisms Underlying Symbiotic Specificity in Legume-Rhizobium Interactions,” *Frontiners in Plant Science,* Vol 9, no 313, pp. 1-8, 2018.

[36] Natasha Latysheva, Vivien L. Junker, William J. Palmer, Geoffrey A. Codd and Daniel Barker, "The evolution of nitrogen fixation in cyanobacteria," *Bioinformatics,* pp. 603-606, 1 3 2012.

[37] Masahito HAYATSU, Kanako TAGO and Masanori SAITO, “Various players in the nitrogen cycle: Diversity and functions of the microorganisms involved in nitrification and denitrification,” *Soil Science & Plant Nutrition,* pp. 33-45, 7 1 2008.

[38] Beguin P and Aubert J. P, “The biological degradation of cellulose,” *FEMS Microbiology Reviews,* Vol 13, no 1, pp. 25-28, 1993.

[39] Duccio Cavalieri, Patrick E. McGovern, Daniel L. Hartl, Robert Mortimer and Mario Polsinelli, "Evidence for S. cerevisiae Fermentation in Ancient Wine," *Journal of Molecular Evolution,* pp. 226-232, 19 11 2002.

[40] Boulton, Chris and Quain, David, Brewing yeast and fermentation, Vol 84, Oxford: Blackwell Science, 2001, pp. 205-205.

[41] J C Kolars, M D Levitt, M Aouji and D A Savaiano, "Yogurt--an autodigesting source of lactose," *N Engl J Med,* Vol 310, no 1, pp. 1-3, 1984.

[42] Murray, Patrick R, Rosenthal, Ken S and Pfaller, Michael A, Medical Microbiology, 8th ed., Philadelphia: Elsevier, 2016.

[43] Rustam I. Aminov, "A brief history of the antibiotic era: lessons learned and challenges for the future," *Frontiers in Microbiology,* Vol 1, p. 134, 2010.

[44] R. Simon, U. Priefer and A. Pühler, "A Broad Host Range Mobilization System for Invivo Genetic-Engineering-Transposon Mutagenesis in Gram-Negative Bacteria," *Bio-Technology,* Vol 1, no 9, pp. 784-791, 1983.

[45] Henry Daniell, Muhammad S Khan and Lori Allison, "Milestones in chloroplast genetic engineering: an environmentally friendly era in biotechnology," *Trends Plant Sci,* Vol 7, no 2, pp. 84-91, 2002.

[46] L O Ingram, T Conway, D P Clark, G W Sewell and J F Preston, "Genetic engineering of ethanol production in Escherichia coli.," *Applied and Environmental Microbiology,* Vol 53, no 10, pp. 2420-2425, 1987.

[47] D.Soletto, L.Binaghi, A.Lodi, J.C.M.Carvalho and A.Converti, "Batch and fed-batch cultivations of Spirulina platensis using ammonium sulphate and urea as nitrogen sources," *Aquaculture,* Vol 243, no 1-4, pp. 217-224, 2005.

[48] Richard J. Radmer and Author Notes, "Algal Diversity and Commercial Algal Products: New and valuable products from diverse algae may soon increase the already large market for algal products," *BioScience,* Vol 46, no 4, pp. 263-270, 1996.

[49] Hélène Desmorieux and Nadège Decaen, "Convective drying of spirulina in thin layer," *Journal of Food Engineering,* Vol 66, no 4, pp. 497-503, 2005.

[50] Carlota de OliveiraRangel-Yagui, Eliane Dalva GodoyDanesi, João Carlos Monteirode Carvalho and Sunao Sato, "Chlorophyll production from Spirulina platensis: cultivation with urea addition by fed-batch process," *Bioresource Technology,* Vol 92, no 2, pp. 133-141, 2004.

[51] Arnaud Muller-Feuga , "The role of microalgae in aquaculture: situation and trends," *Journal of Applied Phycology,* Vol 12, no 3, pp. 527-534, 2000.

[52] J A Del Campo, J Moreno, H Rodríguez, M A Vargas, J Rivas and M G Guerrero, "Carotenoid Content of Chlorophycean Microalgae: Factors Determining Lutein Accumulation in Muriellopsis sp. (Chlorophyta)," *J Biotechnol,* Vol 76, no 1, pp. 51-59, 2000.

[53] A.Robles Medina, E.Molina Grima, A.Giménez Giménez and M.J.Ibáñez González, "Downstream processing of algal polyunsaturated fatty acids," *Biotechnology Advances,* Vol 16, no 3, pp. 517-580, 1998.

[54] Yue Jiang, Feng Chen and Shi-Zhong Liang, "Production potential of docosahexaenoic acid by the heterotrophic marine dinoflagellate Crypthecodinium cohnii," *Process Biochemistry,* Vol 34, no 6-7, pp. 633-637, 1999.

[55] EMolina Grima, E.-HBelarbi, F.GAción Fernández, ARobles Medina and Yusuf Chisti, "Recovery of microalgal biomass and metabolites: process options and economics," *Biotechnology Advances,* Vol 20, no 7-8, pp. 491-515, 2003.

[56] Zhi-You Wen and Feng Chen, "Heterotrophic production of eicosapentaenoic acid by microalgae," *Biotechnology Advances,* Vol 21, no 4, pp. 273-294, 2003.

[57] Pavan Kumar Naraharisetti, Probir Das and Paul N. Sharratt, "Critical factors in energy generation from microalgae," *Energy,* Vol 120, no 1, pp. 138-152, 2017.

[58] E. Hartman, Interviewee, *A Promising Oil Alternative: Algae Energy.* [Interview]. 6 January 2008.

[59] Teresa M. Mata, António A. Martins and Nidia. S. Caetano, "Microalgae for biodiesel production and other applications: A review," *Renewable and Sustainable Energy Reviews,* vol. 14, no. 1, pp. 217-232, 2010.

[60] Liam Brennan and Philip Owende, "Biofuels from Microalgae—A Review of Technologies for Production, Processing, and Extractions of Biofuels and Co-products," *Renewable and Sustainable Energy Reviews,* Vol 14, no 2, pp. 557-577, 2010.

[61] Bruno Sialve, Nicolas Bernet and Olivier Bernard, "Anaerobic Digestion of Microalgae as A Necessary Step to Make Microalgal Biodiesel Sustainable," *Biotechnol Adv,* Vol 27, no 4, pp. 409-416, 2009.

[62] M.M. Mendes-Pinto, M.F.J. Raposo, J. Bowen, A.J. Young and R. Morais , "Evaluation of different cell disruption processes on encysted cells of Haematococcus pluvialis: effects on astaxanthin recovery and implications for bio-availability," *Journal of Applied Phycology,* Vol 13, no 1, pp. 19-24, 2001.

[63] Hoffmann, A. Rodrigues, Proctor, L. M., Surette, M. G. and Suchodolski, J. S., The Microbiome: The Trillions of Microorganisms That Maintain Health and Cause Disease in Humans and Companion Animals, Los Angeles: SAGE Publications, 2015.

[64] T. J. Montville and K. R. Matthews, Food Microbiology: An Introduction, 2nd ed., Washington: ASM Press, 2008.

[65] J. I. Pitt and A. D. Hocking, Fungi and Food Spoilage, 3rd ed, New York: Springer-Verlag, 2009.

[66] Lone Gram, Lars Ravn, Maria Rasch, Jesper Bartholin Bruhn, Allan B Christensen and Michael Givskov, "Food spoilage—interactions between food spoilage bacteria," *International Journal of Food Microbiology,* Vol 78, no 1-2, pp. 79-97, 2002.

[67] C. W. Blackburn, Food Spoilage Microorganism, Cambridge: Woodhead Publishing Limited, 2006.

[68] Atiqur Rahman and Sun Chul Kang, “In vitro control of food-borne and food spoilage bacteria by essential oil and ethanol extracts of Lonicera japonica Thunb,” *Food Chemistry,* Vol 116, no 3, pp. 670-675, 2009.

[69] S. S. Block, Disinfection, Sterilization, and Preservation, 5th ed, Philadelphla: Lippincott Williams & Wilkins, 2002.

[70] Bloack and Seymour Stanton, Disinfection, sterilization, and preservation 5th ed, Philadelphia: Lippincott Williams & Wilkins, 2001.

[71] J. P. P. M. Smelt and S. Brul , “Thermal Inactivation of Microorganisms,” *Critical Reviews in Food Science and Nutrition,* vol. 54, no. 10, pp. 1371-1385, 2014.

[72] W. D. Bigelow and J. R. Esty, “The Thermal Death Point in Relation to Time of Typical Thermophilic Organisms,” *The Journal of Infectious Diseases,* Vol 27, no 6, pp. 602-617, 1920.

[73] W. D. BIGELOW, “The Logarithmic Nature of Thermal Death Time Curves,” *The Journal of Infectious Diseases,* Vol 29, no 5, pp. 528-536, 1921.

[74] Micha Peleg and Martin B. Cole, “Reinterpretation of Microbial Survival Curves,” *Critical Reviews in Food Science and Nutrition,* vol. 38, no. 5, pp. 353-380, 1998.

[75] Berk and Zeki, “Thermal processing,” in *Food Process Engineering and Technology 3rd edition*, London, Academic Press, 2018, pp. 399-420.

[76] P. Mafart, O. Couvert, S.Gaillard and I.Leguerinel, “On calculating sterility in thermal preservation methods: application of the Weibull frequency distribution model,” *International Journal of Food Microbiology,* vol. 72, no. 1-2, pp. 107-113, 2002.

[77] A.Götz, A.A.Wani, H-C.Langowski and J.Wunderlich, “Food Technologies: Aseptic Packaging,” *Encyclopedia of Food Safety,* Vol 3, pp. 124-134, 2014.

[78] Si Qin, “5.3 PEF Treatment of A. platensis,” from *Pulsed Electric Field Treatment of Arthrospira Platensis and Saccharomyces Cerevisiae*, 2016, pp. 125-137.

[79] G. R. Dychdala, “Chlorine and Chlorine Compounds. In: S. S. Block ed.,” in *Disinfection, Sterilization, and Preservation. 5th ed*, Philadelphia, Lippincott Williams & Wilkins, 2001, pp. 135-158.

[80] G. McDonnell and D. Pretzer, “New and Developing Chemical Antimicrobials. In: S. S. Block ed.,” from *Disinfection, Sterilization, and Preservation. 5th ed*, Philadelphia, Lippincott Williams & Wilkins, 2001, pp. 431-443.

[81] G. A. Boorman, “Drinking Water Disinfection Byproducts: Review and Approach to Toxicity Evaluation,” *Environmental Health Perspectives,* Vol 107, no 1, pp. 207-217, 1999.

[82] S. D. Richardson and C. Postigo, “Drinking Water Disinfection By-products. In D. Barcel ó ed.,” from *Emerging Organic Contaminants and Human Health*, New York, Springer, 2012, pp. 93-137.

[83] A. Downes and T. P. Blunt, “Researches on the Effect of Light upon Bacteria and other Organisms,” *Proc. R. Soc. Lond,* Vol 26, pp. 488-500, 1877.

[84] Suphachai Nuanualsuwan, Tadesse Mariam, Sakchai Himathongkham and Dean O Cliver, “Ultraviolet inactivation of feline calicivirus, human enteric viruses and coliphages,” *Photochem Photobiol,* vol. 76, no. 4, pp. 406-410, 2002.

[85] R.L. Wolfe, “Ultraviolet disinfection of potable water,” *Environ, Sci. Technol.,* vol. 24, no. 6, pp. 768-773, 1990.

[86] Jinglan Hong and Masahiro Otaki, “Studies on Liposome-encapsulated-chemical Actinometer in UV-disinfection by Low Pressure UV Lamp,” in *2012 International Conference on Biomedical Engineering and Biotechnology*, Macau, Macao, 2012.

[87] J A Lippke, L K Gordon, D E Brash and W A Haseltine, “Distribution of UV light-induced damage in a defined sequence of human DNA: detection of alkaline-sensitive lesions at pyrimidine nucleoside-cytidine sequences,” *Proc Natl Acad Sci U S A,* Vol 78, no 6, pp. 3388-3392, 1981.

[88] E. R. Blatchley III and M. M. Peel, “Disinfection by Ultraviolet Irradiation. In S.S.Block ed,” in *Disinfection, Sterilization, and Preservation. 5th ed*, Philadelphia, Lippincott Williams & Wilkins, 2001, pp. 823-851.

[89] Theodoros Varzakas and Constantina Tzia, Handbook of Food Processing, Two Volume Set, Boca Raton: CRC Press, 2015.

[90] Elisa Gayán, Santiago Condón and Ignacio Álvarez, “Biological Aspects in Food Preservation by Ultraviolet Light: a Review,” *Food and Bioprocess Technology,* vol. 7, pp. 1-20, 2014.

[91] D. E. Brash, J. A. Rudolph, J. A. Simon, A. Lin, G. J. McKenna, H. P. Baden, A. J. Halperin and J. Pontén, “A Role for Sunlight in Skin Cancer: UVInduced p53 Mutations in Squamous Cell Carcinoma,” *Proceedings of the National Academy of Sciences of the USA,* vol. 88, no. 22, pp. 10124-10128, 1991.

[92] R. B. Setlow, “The Wavelengths in Sunlight Effective in Producing Skin,” *Proceedings of the National Academy of USA,* vol. 71, no. 9, pp. 3363-3366, 1974.

[93] B. K. Armstrong and A. Krickerb, “The Epidemiology of UV Induced Skin,” *Journal of Photochemistry and Photobiology B: Biology,* Vol 63, no 1-3, pp. 8-18, 2001.

[94] Matthew A. Roberts, Joel S. Rossier, Paul Bercier and Hubert Girault, “UV Laser Machined Polymer Substrates for the Development of Microdiagnostic Systems,” *Analytical chemistry,* vol. 69, no. 11, pp. 2035-2042, 1997.

[95] Hongwei Hu and Penghui Shi, “Research of Drinking Water Disinfection,” in *2010 International Conference on E-Product E-Service and E-Entertainment*, Henan, 2010.

[96] Montserrat Mor-Mur, Roger Escriu and Josep Yuste, “Chapter 5 - Microbiological Aspects of High-Pressure Processing,” in *Emerging Technologies for Food Processing (Second Edition)*, London, Academic Press, 2014, pp. 77-90.

[97] D. G. Hoover, C. Metrick, A. M. Papineau, D. F. Farkas and D. Knorr, “Biological Effects of High Hydrostatic Pressure on Food Microorganisms,” *Food Technology,* vol. 43, no. 3, pp. 99-107, 1989.

[98] E.Ananta and D.Knorr, “Comparison of inactivation pathways of thermal or high pressure inactivated Lactobacillus rhamnosus ATCC 53103 by flow cytometry analysis,” *Food Microbiology,* vol. 26, no. 5, pp. 542-546, 2009.

[99] D.A. Ledward, D.E. Johnston, R.G. Earnshaw and A.P.M. Hasting, “The microbe as a high pressure target,” in *High Pressure Processing of Foods*, Loughborough, Nottingham University Press, 1995, pp. 27-36.

[100] B. Mertens, “Hydrostatic pressure treatment of food: equipment and processing,” in *New Methods of Food Preservation*, New York, Blackie Academic & Professional, 1995, pp. 135-158.

[101] M. Maclean, S. J. MacGregor, J. G. Anderson, G. A. Woolsey, J. E. Coia, K.Hamilton, I. Taggart, S. B. Watson, B. Thakker and G. Gettinby, “Environmental Decontamination of A Hospital Isolation Room Using HighIntensity Narrow-Spectrum Light,” *Journal of Hospital Infection,* vol. 76, no. 3, pp. 247-251, 2010.

[102] M. Maclean, S. J. MacGregor, J. G. Anderson and G. Woolsey, “The Role of Oxygen in the Visible-Light Inactivation of Staphylococcus aureus,” *Journal of Photochemistry and Photobiology B: Biology,* vol. 92, no. 3, pp. 180-184, 2008.

[103] M. Maclean, S. J. MacGregor, J. G. Anderson and G. Woolsey, “Inactivation of Bacterial Pathogens Following Exposure to Light from A 405-Nanometer,” *Applied and Environmental Microbiology,* vol. 75, no. 7, pp. 1932-1937, 2009.

[104] M. Maclean, S. J. MacGregor, J. G. Anderson and G. Woolsey, “High-intensity narrow-spectrum light inactivation and wavelength sensitivity of Staphylococcus aureus,” *FEMS Microbiology Letters,* vol. 285, no. 2, pp. 227-232, 2008.

[105] O. Feuerstein, I. Ginsburg, E. Dayan, D. Veler and E. I. Weiss, “Mechanism of Visible Light Phototoxicity on Porphyromonas gingivalis and Fusobacterium nucleatum,” *Photochemistry and Photobiology,* vol. 81, no. 5, pp. 1186-1189, 2005.

[106] Lynne Elizabeth Murdoch, An investigation into the use of High-Intensity Narrow Spectrum light as a decontamination technology, Glasgow: University of Strathclyde, 2010.

[107] P. M. Kirthy Reddy M, “Pulsed Electric Field Technology in Food,” *International Journal of Science and Research,* vol. 3, no. 7, pp. 1144-1149, 2012.

[108] I V Timoshkin, S J MacGregor, R A Fouracre, B H Crichton and J G Anderson, “Transient electrical field across cellular membranes: pulsed electric field treatment of microbial cells,” *J.Phys. D,* vol. 39, no. 3, pp. 596-603, 2006.

[109] Nabil Grimi, Nikolai I Lebovka, Eugene Vorobiev and Jean Vaxelaire, “Effect of a Pulsed Electric Field Treatment on Expression Behavior and Juice Quality of Chardonnay Grape,” *Food Biophysics,* vol. 4, no. 3, pp. 191-198, 2009.

[110] M. Gaudreau, T. Hawkey, Jim Petry and Michael Kempkes, “Solid-State Power Systems for Pulsed Electric Field (PEF) Processing,” in *Diversified Technologies*, Bedford, 2005.

[111] B L Qin , U R Pothakamury, G V Barbosa-Cánovas and B G Swanson, “Nonthermal pasteurization of liquid foods using high-intensity pulsed electric fields,” *Crit Rev Food Sci Nutr,* vol. 36, no. 6, pp. 603-627, 1996.

[112] A.B. Jemai and E. Vorobiev, “Pulsed Electric Field Assisted Pressing of Sugar Beet Slices: towards a Novel Process of Cold Juice Extraction,” *Biosystems Engineering,* vol. 93, no. 1, pp. 57-68, 2006.

[113] S.K. SHARMA, Q.H. ZHANG and G.W. CHISM, “Development of a protein fortified fruit beverage and its quality when processed with pulsed electric field,” *J. FoodQual,* vol. 21, no. 6, pp. 459-473, 1998.

[114] A. J. H. Sale and W. A. Hamilton, “Effects of High Electric Fields on Microorganisms: III. Lysis of Erythrocytes and Protoplasts,” *Biochim.Biophys. Acta,* vol. 163, no. 1, pp. 37-43, 1968.

[115] K. R. E. Neumann, “Permeability Changes Induced by Electrical Impulses in Vesicular Membranes,” *J. Membrane Biol,* vol. 10, no. 3, pp. 279-290, 1972.

[116] U. Zimmermann, G. Pilwat and F. Riemann, “Dielectric Breakdown of Cell Membranes,” *Biophys. J.,* vol. 14, no. 11, pp. 881-899, 1974.

[117] J. C. Weaver, “Electroporation: A general phenomenon for manipulating cells and tissue,” *J. Cell. Biochem,* vol. 51, no. 4, pp. 426-435, 1993.

[118] Humberto Vega-Mercado, O. Martin-Belloso, Fu Jung Chang, Gustavo V Barbosa Ccanovas and Barry G. Swanson, “Inactivation of Escherichia coli and Bacillus subtilis suspended in pea soup using pulsed electric fields,” *J Food Process Preserv,* vol. 20, no. 6, pp. 501-510, 1996a.

[119] Martin L Yarmush, Alexander Golberg, Gregor Serša, Tadej Kotnik and Damijan Miklavčič, “Electroporation-based technologies for medicine: principles, applications, and challenges,” *Biomedical Engineering,* vol. 16, no. 1, pp. 295-320, 2014.

[120] Flavien Pillet, Cécile Formosa-Dague, Houda Baaziz, Etienne Dague and Marie-Pierre Rols, “Cell wall as a target for bacteria inactivation by pulsed electric fields,” *Scientific reports,* pp. 1-8, 01 February 2016.

[121] Wang Jianfei, Mi Yan, Yao Chenguo and Li Chengxiang, “A Review on Molecular Dynamics Simulation for Biological Effects of Pulsed Electric Field,” in *High Voltage Engineering and Application*, Chongqing, 2008.

[122] Allen L. Garner, Maxim Deminsky, V. Bogdan Neculaes, V. Chashihin, Andrey Knizhnik and Boris Potapkin, “Cell membrane thermal gradients induced by electromagnetic fields,” *Journal of Applied Physics,* vol. 113, no. 21, 2013.

[123] E.S. Buescher and K.H. Schoenbach, “Effects of submicrosecond, high intensity pulsed electric fields on living cells - intracellular electromanipulation,” *IEEE Transactions on Dielectrics and Electrical Insulation,* vol. 10, no. 5, pp. 788-794, 2003.

[124] Tina Batista Napotnik, Yu-Hsuan Wu, Martin A Gundersen, Damijan Miklavčič and P Thomas Vernier, “Nanosecond electric pulses cause mitochondrial membrane permeabilization in Jurkat cells,” *Bioelectromagnetics,* vol. 33, no. 33, pp. 257-264, 2012.

[125] K.H. Schoenbachk, R.P. Joshi, J.F. Kolb, N. Chen, M. Stacey and E.S. Buescher, “Ulrashort Electrical Pulses Open a New Gateway Into Biological Cells,” in *Power Modulator Symposium, 2004 and 2004 High-Voltage Workshop. Conference Record of the Twenty-Sixth International*, San Francisco, CA, USA, 2004.

[126] Sunao Katsuki, Naoyuki Nomura, Hideto Koga, Hidenori Akiyama, Ichiro Uchida and Shin-ichi Abe, “Biological Effects of Narrow Band Pulsed Electric Fields,” *IEEE Transactions on Dielectrics and Electrical Insulation,* vol. 14, no. 3, pp. 663-668, 2007.

[127] K. Foster, “Microwave irradiation influences on the state of human cell nuclei,” *Bioelectromagnetics,* vol. 3, no. 4, p. 325, 2000.

[128] Kenneth R Foster and Eleanor R Adair, “Modeling thermal responses in human subjects following extended exposure to radiofrequency energy,” *Biomedical Engineering Online,* vol. 3, no. 4, pp. 1-7, 2004.

[129] K. Foster, “Thermal and nothermal mechanisms of interaction of radio-frequency energy with biological systems,” *IEEE Trans.Plasma Sci,* vol. 28, no. 1, pp. 15-23, 2002.

[130] Mercedes López, Tamara Calvo, Miguel Prieto, Rodolfo Múgica-Vidal, Ignacio Muro-Fraguas, Fernando Alba-Elías and Avelino Alvarez-Ordóñez, “A Review on Non-thermal Atmospheric Plasma for Food Preservation: Mode of Action, Determinants of Effectiveness, and Applications,” *Front. Microbiol,* vol. 6, no. 622, pp. 1-21, 2019.

[131] Tobias G. Klämpfl, Georg Isbary, Tetsuji Shimizu, Yang-Fang Li, Julia L. Zimmermann, Wilhelm Stolz, Jürgen Schlegel, Gregor E. Morfill and Hans-Ulrich Schmidt, “Cold Atmospheric Air Plasma Sterilization against Spores and Other Microorganisms of Clinical Interest,” *Applied and Environmental Microbiology,* vol. 78, no. 15, pp. 5077-5082, 2012.

[132] Shawn Tseng, Nina Abramzon, James O. Jackson and Wei-Jen Lin, “Gas discharge plasmas are effective in inactivating Bacillus and Clostridium spores,” *Applied Microbiology and Biotechnology,* vol. 93, pp. 2563-2570, 2012.

[133] Beyhan Gunaydin Dasan, Mehmet Mutlu and Ismail Hakki Boyaci, “Decontamination of Aspergillus flavus and Aspergillus parasiticus spores on hazelnuts via atmospheric pressure fluidized bed plasma reactor,” *International Journal of Food Microbiology,* vol. 216, pp. 50-59, 2016.

[134] Wilson P Menashi, *Treatment of Surfaces,* US Patent 3 383 163, 1968.

[135] Qian Zhang, Yongdong Liang, Hongqing Feng, Ruonan Ma, Ying Tian, Jue Zhang and Jing Fang, “A study of oxidative stress induced by non-thermal plasma-activated water for bacterial damage,” *Appl. Phys. Lett,* vol. 102, pp. 203701-4, 2013.

[136] Cletus P. Kurtzman and Jure Piškur, “Taxonomy and phylogenetic diversity among the yeasts,” in *Comparative Genomics*, Berlin, Heidelberg, Springer, 2005, pp. 29-46.

[137] Jean-Luc Legras, Didier Merdinoglu, Jean-Marie Cornuet and Francis Karst, “Bread, beer and wine: Saccharomyces cerevisiae diversity reflects human history,” *Molecular Ecology,* vol. 16, no. 10, pp. 2091-2102, 2007.

[138] Maksim Zakhartsev and Matthias Reuss, “Cell size and morphological properties of yeast Saccharomyces cerevisiae in relation to growth temperature,” *FEMS Yeast Res.,* vol. 18, no. 6, pp. 1-16, 2018.

[139] Olga Gorte, Natalja Nazarova, Ioannis Papachristou, Rüdiger Wüstner, Klaus Leber, Christoph Syldatk, Katrin Ochsenreither, Wolfgang Frey and Aude Silve, “Pulsed Electric Field Treatment promotes lipid extraction on fresh oleaginous yeast saitozyma podzolica DSM 27192,” *Front. Bioeng. Biotechnol,* vol. 8, pp. 1-14, 2020.

[140] J. M. Galazka, C. Tian, W. T. Beeson, B. Martinez, N. L. Glass and J. H. D. Cate, “Cellodextrin Transport in Yeast for Improved Biofuel Production,” *Science,* vol. 330, no. 6000, pp. 84-86, 2010.

[141] N. A. Buijs, V. Siewers and J.Nielsen, “Advanced Biofuel Production by the Yeast Saccharomyces cerevisiae,” *Current Opinion in Chemical Biology,* vol. 17, no. 3, pp. 480-488, 2013.

[142] D. J. HIBBERD, “Notes on the taxonomy and nomenclature of the algal classes eustigmatophyceae and tribophyceae (synonym xanthophyceae),” *Bot. J. Linn. Soc.,* vol. 82, no. 2, pp. 93-119, 1981.

[143] Jin-Chywan Gwo, Ju-Yu Chiu, Chin-Cheng Chou and Hsien-Yu Cheng, “Cryopreservation of a marine microalga, Nannochloropsis oculata (eustigmatophyceae),” *Cryobiology,* Vol 50, no 3, pp. 338-343, 2005.

[144] Hanhua Hu and Kunshan Gao, "Optimization of growth and fatty acid composition of a unicellular marine picoplankton, Nannochloropsissp with enriched carbon sources," *Biotechnol. Lett.,* Vol 25, no 5, pp. 421-425, 2003.

[145] John K. Volkman, Malcolm R. Brown, Graeme A. Dunstan and S. W. Jeffrey, "The biochemical composition of marine microalgae from the class eustigmatophyceae," *J. Phycol.,* Vol 29, no 1, pp. 69-78, 1993.

[146] Liliana Rodolfi, Graziella Chini Zittelli, Niccolò Bassi, Giulia Padovani, Natascia Biondi, Gimena Bonini and Mario R Tredici, "Microalgae for oil: strain selection, induction of lipid synthesis and outdoor mass cultivation in a low-cost photobioreactor.," *Biotechnol. Bioeng.,* Vol 102, no 1, pp. 100-112, 2009.

[147] Melinda J. Griffiths and Susan T. L. Harrison, "Lipid productivity as a key characteristic for choosing algal species for biodiesel production.," *J. Appl. Phycol.,* Vol 21, no 5, pp. 493-507, 2009.

[148] H. Fricke, "The electric permittivity of a dilute membrane covered ellipsoids," *J. Appl. Phys,* Vol 24, no 5, pp. 644-646, 1953.

[149] H. P. Schwan, "Electrical properties of tissue and cell suspensions," *Adv.Biol.Med.Phys,* Vol 5, pp. 147-209, 1957.

[150] Tadej Kotnik, Feda Bobanović and Damijian Miklavčič, "Sensitivity of transmembrane voltage induced by applied electric Fields- a theoretical analysis," *Bioelectrochemistry and Bioenergetics,* Vol 43, no 2, pp. 285-291, 1997.

[151] R. P. Joshi and K. H. Schoenbach, "Electroporation Dynamics in Biological Cells Subjected to Ultrafast Electrical Pulses: A Numerical Simulation Study," *Phys. Rev. E,* Vol 62, no 1, pp. 1025-1033, 2000.

[152] J. Bernhardt and H. Pauly, "On the Generation of Potential Differences across the Membranes of Ellipsoidal Cells in an Alternating Electrical Field," *Biophysik,* Vol 10, no 1, pp. 89-98, 1973.

[153] K. Kinosita and T. Y. Tsong, “Voltage-Induced Pore Formation and Hemolysis of Human Erythrocytes,” *Biochim. Biophys. Acta,* Vol 471, no 2, pp. 227-242, 1977.

[154] Hidenori Akiyama, Takashi Sakugawa, akao Namihira, Koichi Takaki, Yasushi Minamitani and Naoyuki Shimomura, “Industrial Applications of Pulsed Power Technology,” *IEEE Transactions on Dielectrics and Electrical Insulation,* Vol 14, no 5, pp. 1051-1064, 2007.

[155] G. A. Mesyats, Pulsed Power, New York: New York: Springer, 2005.

[156] Hanifah Jambari, Naziha Ahmad Azli and M. Afendi M. Piah, “Comparison of Pulsed Electric Field Generation Techniques for Microbial Inactivation Application,” *Journal of Theoretical and Applied Information Technology,* Vol 33, pp. 22-31, 2011.

[157] Voitech Stankevic , Povilas Simonis, Nerija Zurauskiene, Arunas Stirke, Aldas Dervinis, Vytautas Bleizgys, Skirmantas Kersulis and Saulius Balevicius, *Symmetry,* Vol 12, no 3, pp. 1-14, 2020.

[158] A. D. Blumlien,, Improvements in or relating to apparatus for generating electrical impulses, UK Patent 589127, 1941.

[159] I. C. Somerville, S. J. MacGregor and O. Farish,, “An Efficient Stacked Blumlein HV Pulse Generator,” *Meas. Sci. Technol,* Vol 1, no 9, pp. 865-868, 1990.

[160] Werner Sitzmann, Eugene Vorobiev and Nikolai Lebovka, Pulsed Electric Fields for Food Industry: Historical Overview, Springer, Cham, 2016, pp. 1-20.

[161] A. J. H. Sale and W. A. Hamilton, “Effects of High Electric Fields on Microorganisms: I. Killing of Bacteria and Yeasts,” *Biochim. Biophys. Acta,* Vol 148, no 3, pp. 781-788, 1967.

[162] W. A. Hamilton and A. J. H. Sale, “Effects of High Electric Fields on Microorganisms: II. Mechanism of Action of the Lethal Effect,” *Biochim. Biophys. Acta,* Vol 148, no 3, pp. 789-800, 1967.

[163] A. J. H. Sale and W. A. Hamilton, "Effects of High Electric Fields on Microorganisms: III. Lysis of Erythrocytes and Protoplasts," *Biochim. Biophys. Acta,* Vol 163, no 1, pp. 37-43, 1968.

[164] S. Toepfl, "2.1.6 Research work on PEF application from 1980s to 2000," from *Pulsed Electric Fields (PEF) for Permeabilization of Cell Membranes in Food and Bioprocessing: Applications, Process and Equipment Design and Cost Analysis*, 2006, pp. 10-11.

[165] U. Zimmermann and G. A. Neil, Electromanipulation of Cells, Boca Raton: CRC Press, 1996.

[166] U. Zimmermann, J. Vienken and G. Pilwat, "Development of Drug Carrier Systems: Electrical Field Induced Effects in Cell Membranes," *J. Electroanal Chem,* Vol 116, pp. 553-574, 1980.

[167] Shinichiro Hojo, Kenji Shimizu, Hironobu Yositake, Masafumi Muraji, Hiroaki Tsujimoto and Wataru Tatebe, "The Relationship Between Electropermeabilization and Cell Cycle and Cell Size of Saccharomyces Cerevisiae," *IEEE Transactions on NanoBioscience,* Vol 2, no 1, pp. 35-39, 2003.

[168] M. D. A. Zbinden, B. S. M. Sturm,, R. D. Nord,, W. J. Carey, D. Moore, H.hinogle and S. M. Stagg-Williams, "Pulsed Electric Field (PEF) as an Intensification Pretreatment for Greener Solvent Lipid Extraction from Microalgae," *Biotechnol. Bioeng,* Vol 110, no 6, pp. 1605-1615, 2013.

[169] C. Eing, M. Goettel, R. Straessner, C. Gusbeth and W. Frey, "Pulsed Electric Field Treatment of Microalgae—Benefits for Microalgae Biomass Processing," *IEEE Trans. Plasma Sci,* Vol 41, no 10, pp. 2901-2907, 2013.

[170] G. A. Evrendilek, Q. H. Zhang and E. R. Richter, "Inactivation of Escherichia coli O157:H7 and Escherichia coli 8739 in Apple Juice by Pulsed Electric Fields," *Journal of Food Protection,* Vol 62, no 7, pp. 793-796, 1999.

[171] C. J. McDonald, S. W. Lloyd, M. A. Vitale, K. Petersson and F. Innings, "Effects of Pulsed Electric Fields on Microorganisms in Orange Juice Using Electric Field Strengths of 30 and 50 kV/cm," *Journal of Food Science,* Vol 65, no 6, pp. 984-989, 2000.

[172] S. E. Gilliland and M. L. Speck, "Inactivation of Microorganisms by Electrohydraulic Shock," *Applied Microbiology,* Vol 15, no 5, pp. 1031-1037, 1967.

[173] Bai-Lin Qin, Qinghua Zhang, Gustavo V and G.V. Barbosa-Canovas, "Inactivation of Microorganisms by Pulsed Electric Fields of Different Volt age Waveforms," *IEEE Transactions on Dielectrics and Electrical Insulation,* pp. 1047-1057, 6 December 1994.

[174] R. Narsetti, R. D. Curry, K. F. McDonald, T. E. Clevenger and L. M. Nichols, "Microbial Inactivation in Water Using Pulsed Electric Fields and Magnetic Pulse Compressor Technology," *IEEE Trans. Plasma Sci,* Vol 34, no 4, pp. 1386-1393, 2006.

[175] W. A. Hamilton and A. J. H. Sale, "Effects of High Electric Fields on Microorganisms: II. Mechanism of Action of the Lethal Effect," *Biochim.Biophys. Acta,,* Vol 148, no 3, pp. 789-800, 1967.

[176] K. Huang and J. Wang, "Designs of Pulsed Electric Fields Treatment Chambers for Liquid Foods Pasteurization Process: A Review," *Journal of Food Engineering,* Vol 95, no 2, pp. 227-239, 2009.

[177] J. E. Dunn and J. S. Pearlman, Methods and Apparatus for Extending the Shelf Life of Fluid Food Products, US Patent 4,695,472, 1987.

[178] Y. Matsumoto, N. Shioji, T. Satake and A. Sakuma, "Inactivation of microorganisms by pulsed high voltage application," from *Conference Record of the 1991 IEEE Industry Applications Society Annual Meeting*, Dearborn, MI, USA, 1991.

[179] P. Lubicki and S. Jayaram, "High Voltage Pulse Application for the Destruction of the Gram-negative Bacterium Yersinia enterocolitica," *Bioelectrochem. Bioenergetics,* Vol 43, no 1, pp. 135-141, 1997.

[180] T. Kotnik, D. Miklavcic and L. M. Mir, "Cell Membrane Electropermeabilization by Symmetrical Bipolar Rectangular Pulses: Part II.Reduced Electrolytic Contamination," *Bioelectrochemistry,* Vol 54, no 1, pp. 91-95, 2001.

[181] Si Qin, Igor V. Timoshkin, Michelle MacLean, Scott J. MacGregor, Mark P. Wilson, Martin J. Given, Tao Wang and John G. Anderson, "TiO2-Coated Electrodes for Pulsed

Electric Field Treatment of Microorganisms," *IEEE Transactions on Plasma Science,* vol. 44, no. 10, pp. 2121-2128, 01 June 2016.

[182] M. D. A. Zbinden, B. S. M. Sturm, R. D. Nord, W. J. Carey, D. Moore, H.Shinogle and S. M. Stagg-Williams, "Pulsed Electric Field (PEF) as an Intensification Pretreatment for Greener Solvent Lipid Extraction from Microalgae," *Biotechnol. Bioeng,* Vol 110, no 6, pp. 1605-1615, 2013.

[183] M. Goettel, C. Eing, C. Gusbeth, R. Straessner and W. Frey, "Pulsed Electric Field Assisted Extraction of Intracellular Valuables from Microalgae," *Algal Research,* Vol 2, no 4, pp. 401-408, 2013.

[184] N. Grimi, A. Dubois, L. Marchal, S. Jubeau, N. I. Lebovka and E. Vorobiev, "Selective Extraction from Microalgae Nannochloropsis sp. Using Different Methods of Cell Disruption," *Bioresource Technology,* Vol 153, pp. 254-259, 2014.

[185] Patrick Biller, Cerri Friedman and Andrew B. Ross, "Hydrothermal microwave processing of microalgae as a pre-treatment and extraction technique for bio-fuels and bio-products," *Bioresource Technology,* Vol 136, pp. 188-195, 2013.

[186] Javed Iqbal and Chandra Theegala, "Microwave assisted lipid extraction from microalgae using biodiesel as co-solvent," *Algal Research,* Vol 2, no 1, pp. 34-42, 2013.

[187] Fanny Adam, Maryline Abert-Vian, Gilles Peltier and Farid Chemat, ""Solvent-free" ultrasound-assisted extraction of lipids from fresh microalgae cells: A green, clean and scalable process," *Bioresource Technology,* Vol 114, pp. 457-465, 2012.

[188] B. Wiyarno, R.M. Yunus and M. Mel, "Extraction of Algae Oil from Nannocloropsis sp.: A Study of Soxhlet and Ultrasonic-Assisted Extractions," *Journal of Applied Sciences,* Vol 11, no 21, pp. 3607-3612, 2011.

[189] Alexis Guionet, Bahareh Hosseini, Justin Teissié, Hidenori Akiyama and Hamid Hosseini, "A new mechanism for efficient hydrocarbon electro-extraction from Botryococcus braunii," *Biotechnology for Biofuels,* Vol 10, no 39, pp. 1-9, 2017.

[190] Fred R. Wolf, Arthur M. Nonomura and James A. Bassham, "Growth and branched hydrocarbon production in a strain of Botryococcus Braunii (chlorophyta)," *J Phycol,* Vol 21, no 3, pp. 388-396, 1985.

[191] A.C. Brown, B.A. Knights and Elsie Conway, "Hydrocarbon content and its relationship to physiological state in the green alga Botryococcus braunii," *Phytochemistry,* Vol 8, no 3, pp. 543-547, 1969.

[192] Bai-Lin Qin, G.V. Barbosa-Canovas, B.G. Swanson, P.D. Pedrow and R.G. Olsen, "Inactivating Microorganisms using A Pulsed Electric Field Continuous Treatment System," *IEEE Trans. Ind. Appl,* Vol 34, no 1, pp. 43-50, 1998.

[193] Bai-Lin Qin, Qinghua Zhang, G.V. Barbosa-Canovas, B.G. Swanson and P.D. Pedrow, "Inactivation of Microorganisms by Pulsed Electric Fields of Different Voltage Waveforms," *IEEE Trans. Dielectr. Electr. Insul,* Vol 1, no 6, pp. 1047-1057, 1994.

[194] K. Aronsson and U. Ronner, "Influence of pH, Water Activity and Temperature on the Inactivation of Escherichia coli and Saccharomyces cerevisiae by Pulsed Electric Fields," *Innovative Food Sci. Emerging Technologies,* Vol 2, no 2, pp. 105-112, 2001.

[195] Loyd V Allen Jr, "Quality Control: Water Activity Considerations for Beyond-use Dates.," *Int J Pharm Compd,* Vol 22, no 4, pp. 288-293, 2018.

[196] T. Grahl and H. Markl, "Killing of Microorganisms by Pulsed Electric Fields," *Applied Microbiology and Biotechnology,* Vol 45, no 1, pp. 148-157, 1996.

[197] H. E. Jacob, W. Forster and H. Berg, "Microbiological Implications of Electric Field Effects II. Inactivation of Yeast Cells and Repair of their Cell Envelope," *Journal of Basic Microbiology,* Vol 21, no 3, pp. 225-233, 1981.

[198] D. Gášková, K. Sigler, B. Janderová and J. Plášek, "Effect of High-Voltage Electric Pulses on Yeast Cells: Factors Influencing the Killing Efficiency," *Bioelectrochem. Bioenergetics,* Vol 39, no 2, pp. 195-202, 1996.

[199] S. L. Harrison, G. V. Barbosa-Canovas and B. G. Swanson, "Saccharomyces cerevisiae Structural Changes Induced by Pulsed Electric Field Treatment," *LWT - Food Science and Technology,* Vol 30, no 3, pp. 236-240, 1997.

[200] Y. Matsumoto, T. Satake, N. Shioji and A. Sakuma, "Inactivation of Microorganisms by Pulsed High Voltage Application," from *Dearborn, MI, USA*, 1991.

[201] Q. Zhang, F. Chang, G. V. Barbosa-Canovas and B. G. Swanson, "Inactivation of Microorganisms in a Semisolid Model Food Using High Voltage Pulsed Electric Fields," *LWT - Food Science and Technology,* Vol 27, no 6, pp. 538-543, 1994.

[202] T. Ohshima, K. Sato, H. Terauchi and M. Sato, "Physical and Chemical Modifications of High-Voltage Pulse Sterilization," *Journal of Electrostatics,* Vol 42, no 1-2, pp. 159-166, 1997.

[203] P. Love, "Correlation of Fourier Transforms of Pulsed Electric Field Waveform and Microorganism Inactivation," *IEEE Trans. Dielectr. Electr.Insul,* Vol 5, no 1, pp. 142-147, 1998.

[204] J. R. Beveridge, S. J. MacGregor, L. Marsili, J. G. Anderson, N. J. Rowan and O. Farish, "Comparison of the Effectiveness of Biphase and Monophase Rectangular Pulses for the Inactivation of Microorganisms Using Pulsed Electric Fields," *IEEE Trans. Plasma Sci,* Vol 30, no 4, pp. 1525-1531, 2002.

[205] T. Kotnik and D. Miklavcic, "Analytical Description of Transmembrane Voltage Induced by Electric Fields on Spheroidal Cells," *Biophys. J,* Vol 79, no 2, pp. 670-679, 2000.

[206] U. R. Pothakamury, H. V. Mercado, Q. Zhang, G. V. Barbosa-Cánovas and B. G. Swanson, "Effect of Growth Stage and Processing Temperature on the Inactivation of E. coli by Pulsed Electric Fields," *J. Food Protect,* Vol 59, no 11, pp. 1167-1171, 1996.

[207] H. V. Mercado, O. M. Belloso, F. J. Chang, G. V. Barbosa-Cánovas and B.G. Swanson, "Inactivation of Escherichia coli and Bacillus subtilis Suspended in Pea Soup Using Pulsed Electric Fields," *J. Food Proc. Pres,* Vol 20, no 6, pp. 501-510, 1996.

[208] H. V. Mercado, O. M. Belloso, B. L. Qin, F. J. Chang, M. M. Góngora-Nieto, G. V. Barbosa-Cánovas and B. G. Swanson, "Non-Thermal Food Preservation: Pulsed Electric Fields," *Trends in Food Science & Technology,* Vol 8, no 5, pp. 151-157, 1997.

[209] H. Hülsheger and E. -G. Niemann , "Lethal effects of high-voltage pulses on E. coli K12," *Radiation and Environmental Biophysics,* Vol 18, pp. 281-288, 1980.

[210] H. V. Mercado, U. R. Pothakamury, F. J. Chang, Q. Zhang, G. V. Barbosa Cánovas and B. G. Swanson, "High Voltage Pulsed Electric Fields, pH, Ionic Strength and the Inactivation of E. coli," *Food Research International,* Vol 29, no 2, pp. 117-121, 1996.

[211] P. C. Wouters, I. Alvarez and J. Raso, "Critical Factors Determining Inactivation Kinetics by Pulsed Electric Field Food Processing," *Trends in Food Science and Technology,* Vol 12, no 3-4, pp. 112-121, 2001.

[212] R. Jeantet, F. Baron, F. Nau, M. Roignant and G. Brulé, "High Intensity Pulsed Electric Fields Applied to Egg White: Effect on Salmonella enteritidis Inactivation and Protein Denaturation," *J. Food Proc,* Vol 62, no 12, pp. 1381-1386, 1999.

[213] H. Hulsheger, J. Potel and E. G. Niemann, "Killing of Bacteria with Electric Pulses of High Field Strength," *Radiat. Eniron. Biophys,* Vol 20, no 1, pp. 53-65, 1981.

[214] X. Liu, A. E. Yousef and G. W. Chism, "Inactivation of Escherichia coli 0157:H7 by the Combination of Organic Acids and Pulsed Electric Field," *J. Food Safety,* Vol 16, no 4, pp. 287-299, 1997.

[215] G. V. Barbosa-Cánovas, M. M. Góngora-Nieto, U. R. Pothakamury and B. G. Swanson, Preservation of Foods with Pulsed Electric Fields, London: Academic Press, 1999.

[216] H. Hulsheger, J. Potel and E. G. Niemann, "Electric Field Effects on Bacteria and Yeast Cells," *Radiat. Eniron. Biophys,* Vol 22, no 2, pp. 149-162, 1983.

[217] K. H. Schoenbach, F. E. Peterkin, R. W. Alden and S. J. Beebe, "The Effect of Pulsed Electric Fields on Biological Cells: Experiments and Applications," *IEEE Trans. Plasma Sci,* Vol 25, no 2, pp. 284-292, 1997.

[218] A. Sedriks, Corrosion of Stainless Steels, 2nd ed., New York: Wiley, 1996.

[219] Wilson P Menashi, Treatment of Surfaces, US Patent 3, 1968.

[220] Shaobo Deng, Roger Ruan, Chul Kyoon Mok, Guangwei Huang, Xiangyang Lin and Paul Chen, "Inactivation of Escherichia coli on almonds using nonthermal plasma," *J. Food Sci,* Vol 72, no 2, pp. 62-66, 2007.

[221] P Muranyi, J Wunderlich and M Heise, "Sterilization efficiency of a cascaded dielectric barrier discharge," *J. Appl. Microbiol,* Vol 103, no 5, pp. 1535-1544, 2007.

[222] N J Rowan, S Espie, J Harrower, J G Anderson, L Marsili and S J MacGregor, "Pulsed-plasma gas discharge inactivation of microbia pathogens in chilled poultry wash water," *J. Food Prot.,* Vol 70, no 12, pp. 2805-2810, 2007.

[223] Kai Reineke, Katharina Langer, Christian Hertwig, Jörg Ehlbeck and Oliver Schlüter, "The impact of different process gas compositions on the inactivation effect of an atmospheric pressure plasma jet on Bacillus spores," *Innov. Food Sci Emerg Technol,* Vol 30, pp. 112-118, 2015.

[224] Hongxia Liu , Jierong Chen , Liqing Yang and Yuan Zhou , "Long-distance oxygen plasma sterilization: effects and mechanisms.," *Appl. Surf. Sci.,* Vol 254, no 6, pp. 1815-1821, 2008.

[225] Bomi Gweon, D.B. Kim, S.Y. Moon and W. Choe, "Escherichia coli deactivation study controlling the atmospheric pressure plasma discharge conditions," *Curr. Appl. Phys.,* Vol 9, no 3, pp. 625-628, 2009.

[226] M Mols, H Mastwijk, M Nierop Groot and T Abee, "Physiological and transcriptional response of Bacillus cereus treated with low-temperature nitrogen gas plasma.," *Journal of Applied Microbiology,* Vol 115, no 3, pp. 689-702, 2013.

[227] Hyun Pa Song, Binna Kim , Jun Ho Choe, Samooel Jung, Se Youn Moon, Wonho Choe and Cheorun Jo, "Evaluation of atmospheric pressure plasma to improve the safety of sliced cheese and ham inoculated by 3-strain cocktail Listeria monocytogenes," *Food Microbiology,* Vol 26, no 4, pp. 432-436, 2009.

[228] D. Bayliss, Understanding the inactivation mechanism of foodborne pathogens using cold atmospheric plasma, Loughborough University: Ph.D Thesis, 2012.

[229] Xinyu Liao, Donghong Liu, Qisen Xiang, Juhee Ahn, Shiguo Chen, Xingqian Ye and Tian Ding, "Inactivation mechanisms of non-thermal plasma on microbes: A review," *Food Control,* Vol 75, pp. 3-91, 2017.

[230] Y.-M. Zhao, S. Ojha, C.M. Burgess, D.-W. Sun and B.K. Tiwari, "Inactivation efficacy and mechanisms of plasma activated water on bacteria in planktonic state," *Journal of Applied Microbiology,* Vol 129, no 5, pp. 1248-1260, 2020.

[231] Suresh G Joshi, Moogega Cooper, Adam Yost, Michelle Paff, Utku K Ercan, Gregory Fridman, Gary Friedman, Alexander Fridman and Ari D Brooks, "Nonthermal dielectric-barrier discharge plasma-induced inactivation involves oxidative DNA damage and membrane lipid peroxidation in Escherichia coli," *Antimicrob Agents Chemother,* Vol 55, no 3, pp. 1053-1062, 2011.

[232] Sirui li, "Atmospheric Non-Thermal Plasma Discharges for Cleaning And Bio-Decontamination," *Phd thesis,* Vol University of Strathclyde, 2016.

[233] Pablo J Pomposiello and Bruce Demple, "Global adjustment of microbial physiology during free radical stress," *Adv Microb Physiol,* Vol 46, pp. 319-341, 2002.

[234] Adam D. Yost and Suresh G. Joshi, "Atmospheric Nonthermal Plasma-Treated PBS Inactivates Escherichia coli by Oxidative DNA Damage," *PLOS ONE,* Vol 10, no 10, pp. 1-20, 2015.

[235] A. Sharma, G. Collins and A. Pruden, "Differential gene expression in Escherichia coli following exposure to nonthermal atmospheric pressure plasma," *Journal of Applied Microbiology,* Vol 107, no 5, pp. 1440-1449, 2009.

[236] Young-Hyo Ryu, Yong-Hee Kim, Jin-Young Lee, Gun-Bo Shim, Han-Sup Uhm, Gyungsoon Park and Eun Ha Choi, "Effects of Background Fluid on the Efficiency of Inactivating Yeast with Non-Thermal Atmospheric Pressure Plasma," *PLOS ONE,* Vol 8, no 6, pp. 1-9, 2013.

[237] Bjoern Surowsky, Axel Fischer, Oliver Schlueter and Dietrich Knorr, "Cold plasma effects on enzyme activity in a model food system," *Innovative Food Science & Emerging Technologies,* Vol 19, pp. 146-152, 2013.

[238] Abasalt Hosseinzadeh Colagar, Hamed Memariani, Farshad Sohbatzadeh and Azadeh Valinataj Omran, "Nonthermal Atmospheric Argon Plasma Jet Effects on Escherichia coli Biomacromolecules," *Applied Biochemistry and Biotechnology,* Vol 171, pp. 1617-1629, 2013.

[239] L Han, S Patil, K M Keener, P J Cullen and P Bourke, "Bacterial inactivation by high-voltage atmospheric cold plasma: influence of process parameters and effects on cell leakage and DNA," *J Appl Microbiol,* Vol 116, no 4, pp. 784-794, 2014.

[240] M. Silindir and A. Y. Özer, "Sterilization Methods and the Comparison of E-Beam Sterilization with Gamma Radiation Sterilization," *FABAD J. Pharm. Sci,* Vol 34, pp. 43-53, 2009.

[241] Petri Ajo, Iakov Kornev and Sergei Preis, "Pulsed Corona Discharge Induced Hydroxyl Radical Transfer Through the Gas-Liquid Interface," *Scientific Reports,* Vol 7, pp. 1-6, 2017.

[242] Jae-Duk Moon, "A wire-to-wire type nonthermal plasma reactor with ferroelectric pellet barrier," *Journal of Electrostatics,* Vol 64, no 10, pp. 699-705, 2006.

[243] Tie Cheng Wang, Na Lu , Jiu Tao An, Yan Zhao, Jie Li and Yan Wu, "Multi-tube parallel surface discharge plasma reactor for wastewater treatment," *Separation and Purification Technology,* Vol 100, pp. 9-14, 2012.

[244] Mohammad Kebriaei, Abbas Ketabi and Abolfazl Halvaei, "Pulsed Corona Discharge, a New and Effective Technique for Water and Air Treatment," *Biological Forum – An International Journal,* Vol 7, no 1, pp. 1686-1692, 2015.

[245] Jie Ren, Jing-Pei Cao , Xiao-Yan Zhao, Fei-Long Yang and Xian-Yong Wei, "Recent advances in syngas production from biomass catalytic gasification: A critical review on reactors, catalysts, catalytic mechanisms and mathematical models," *Renewable and Sustainable Energy Reviews,* Vol 116, pp. 1-25, 2019.

[246] Vincenzo Palma, Marta Cortese, Simona Renda, Concetta Ruocco, Marco Martino and Eugenio Meloni, "A Review about the Recent Advances in Selected NonThermal

Plasma Assisted Solid－Gas Phase Chemical Processes," *Nanomaterials (Basel),* Vol 10, no 8, pp. 1-56, 2020.

[247] Adwek George , Boxiong Shen, Michael Craven, Yaolin Wang, Dongrui Kang, Chunfei Wu and Xin Tu, "A Review of Non-Thermal Plasma Technology: A novel solution for CO2 conversion and utilization," *Renewable and Sustainable Energy Reviews,* Vol 135, pp. 1-22, 2021.

[248] Marek Bryjak, Irena Gancarz and Katarzyna Smolinska, "Plasma nanostructuring of porous polymer membranes," *Advances in Colloid and Interface Science,* Vol 161, no 1-2, pp. 2-9, 2010.

[249] Ronny Brandenburg, "Dielectric barrier discharges: progress on plasma sources and on the understanding of regimes and single filaments," *Plasma Sources Science and Technology,* Vol 26, no 5, pp. 1-29, 2017.

[250] S. Futamura, H. Einaga and A. Zhang, "Comparison of reactor performance in the nonthermal plasma chemical processing of hazardous air pollutants," *IEEE Transactions on Industry Applications,* Vol 37, no 4, pp. 978-985, 2001.

[251] Yaolin Wang, Yanzhen Chen, Jonathan Harding, Hongyuan He, Annemie Bogaerts and Xiu Tu, "Catalyst-free single-step plasma reforming of CH4 and CO2 to higher value oxygenates under ambient conditions," *Chemical Engineering Journal,* Vol 450, no 1, pp. 1-13, 2022.

[252] Changquan Wang, Guixin Zhang, Xinxin Wang and Xiangning He, "The effect of air plasma on barrier dielectric surface in dielectric barrier discharge," *Applied Surface Science,* Vol 257, no 5, pp. 1798-1702, 2010.

[253] M. Magureanu, F. Bilea, C. Bradu and D. Hong, "A review on non-thermal plasma treatment of water contaminated with antibiotics," *Journal of Hazardous Materials,* Vol 417, pp. 1-31, 2021.

[254] Hermien van Bokhorst-van de Veen, Houyu Xie, Erik Esveld, Tjakko Abee, Hennie Mastwijk and Masja Nierop Groot, "Inactivation of chemical and heat-resistant spores of Bacillus and Geobacillus by nitrogen cold atmospheric plasma evokes distinct

changes in morphology and integrity of spores," *Food Microbiology,* Vol 45, no A, pp. 26-33, 2015.

[255] Tobias G. Klämpfl, Georg Isbary, Tetsuji Shimizu, Yang-Fang Li, Julia L. Zimmermann, Wilhelm Stolz, Jürgen Schlegel, Gregor E. Morfill and Hans-Ulrich Schmidt, "Cold Atmospheric Air Plasma Sterilization against Spores and Other Microorganisms of Clinical Interest," *Applied and Environmental Microbiology,* Vol 78, no 15, pp. 5077-5082, 2012.

[256] Kyenam Lee, Kwang-hyun Paek, Won-Tae Ju and Yoenhee Lee, "Sterilization of bacteria, yeast, and bacterial endospores by atmospheric-pressure cold plasma using helium and oxygen," *J Microbiol,* Vol 44, no 3, pp. 269-275, 2006.

[257] Shawn Tseng, Nina Abramzon, James O. Jackson and Wei-Jen Lin, "Gas discharge plasmas are effective in inactivating Bacillus and Clostridium spores," *Applied microbial and cell physiology,* Vol 93, no 6, pp. 2563-2570, 2012.

[258] Xiaohu Liu, Feng Hong, Ying Guo, Jing Zhang and Jianjun Shi, "Sterilization of Staphylococcus Aureus by an Atmospheric Non-Thermal Plasma Jet," *Plasma Science and Technology,* Vol 15, no 5, pp. 438-442, 2013.

[259] Binna Kim, Hyejeong Yun, Samooel Jung, Yeonkook Jung, Heesoo Jung, Wonho Choe and Cheorun Jo, "Effect of atmospheric pressure plasma on inactivation of pathogens inoculated onto bacon using two different gas compositions," *Food Microbiology,* Vol 28, no 1, pp. 9-13, 2011.

[260] Mahmoud Y Alkawareek, Qais Th Algwari, Garry Laverty, Sean P Gorman, William G Graham, Deborah O'Connell and Brendan F Gilmore, "Eradication of Pseudomonas aeruginosa Biofilms by Atmospheric Pressure Non-Thermal Plasma," *PLoS One,* Vol 7, no 8, pp. 1-8, 2012.

[261] G. Daeschlein, S. Scholz, R. Ahmed, R. Brandenburg, K.-D. Weltmann and M. Juenger, "Skin decontamination by low-temperature atmospheric pressure plasma jet and dielectric barrier discharge plasma," *Journal of Hospital Infection,* Vol 81, no 3, pp. 177-183, 2012.

[262] Denis Butscher, Daniel Zimmermann, Markus Schuppler and Philipp Rudolf von Rohr, "Plasma inactivation of bacterial endospores on wheat grains and polymeric model substrates in a dielectric barrier discharge," *Food Control,* Vol 60, pp. 636-645, 2016.

[263] Hyun Jung Lee, Heesoo Jung, Wonho Choe, Jun Sang Ham, Jun Heon Lee and Cheorun Jo, "Inactivation of Listeria monocytogenes on agar and processed meat surfaces by atmospheric pressure plasma jets," *Food Microbiology,* Vol 28, no 8, pp. 1468-1471, 2011.

[264] Danil Dobrynin, Gary Friedman, Alexander Fridman and Andrey Starikovskiy, "Inactivation of bacteria using dc corona discharge: role of ions and humidity," *New Journal of Physics,* Vol 13, pp. 1-13, 2011.

[265] L. Ragni, A. Berardinelli, L. Vannini, C. Montanari and F. Sirri, "Non-thermal atmospheric gas plasma device for surface decontamination of shell eggs," *Journal of Food Engineering,* Vol 100, no 1, pp. 125-132, 2010.

[266] A.C.K. Lai, A.C.T. Cheung, M.M.L. Wong and W.S. Li, "Evaluation of cold plasma inactivation efficacy against different airborne bacteria in ventilation duct flow," *Building and Environment,* Vol 98, pp. 39-46, 2016.

[267] P. Muranyi, J. Wunderlich and M. Heise, "Influence of relative gas humidity on the inactivation efficiency of a low temperature gas plasma," *Journal of Applied Microbiology,* Vol 104, no 6, pp. 1659-1666, 2008.

[268] Tamara Calvo, Avelino Álvarez-Ordóñez, Miguel Prieto, Montserrat González-Raurich and Mercedes López, "Influence of processing parameters and stress adaptation on the inactivation of Listeria monocytogenes by Non-Thermal Atmospheric Plasma (NTAP)," *Food Research International,* Vol 89, no 1, pp. 631-637, 2016.

[269] S. Patil, T. Moiseev, N.N. Misra, J.P. Mosnier, K.M. Keener and P. Bourke, "Influence of high voltage atmospheric cold plasma process parameters and role of relative humidity on inactivation of Bacillus atrophaeus spores inside a sealed package," *Journal of Hospital Infection,* Vol 88, no 3, pp. 162-169, 2014.

[270] H. Lu, S. Patil, K.M. Keener, P.J. Cullen and P. Bourke, "Bacterial inactivation by high‐voltage atmospheric cold plasma: influence of process parameters and effects on cell leakage and DNA," *Journal of Applied Microbiology,* Vol 116, no 4, pp. 784-794, 2014.

[271] T.M.C. Nishime, A.C. Borges, C.Y. Koga-Ito, M. Machida, L.R.O. Hein and K.G. Kostov, "Non-thermal atmospheric pressure plasma jet applied to inactivation of different microorganisms," *Surface and Coatings Technology,* Vol 312, pp. 19-24, 2017.

[272] Adriano O. Henriques and Charles P. Moran, Jr., "Structure, Assembly, and Function of the Spore Surface Layers," *Annual Review of Microbiology,* Vol 61, pp. 555-588, 2007.

[273] Ross MacMaster Campbell, "On the response of biological cells to pulsed electric fields," *Thesis [PhD]-University of Strathclyde,* pp. 2.9-2.10, 2006.

[274] I V Timoshkin, S J MacGregor, R A Fouracre, B H Crichton and J G Anderson, "Transient electrical field across cellular membranes: pulsed electric field treatment of microbial cells," *Journal of Physics D: Applied Physics,* Vol 39, no 3, pp. 596-603, 2006.

[275] Tadej Kotnik, Feda Bobanović and Damijian Miklavčič, "Sensitivity of transmembrane voltage induced by applied electric fields—A theoretical analysis," *Bioelectrochemistry and Bioenergetics,* Vol 43, no 2, pp. 285-291, 1997.

[276] Hugo Fricke and Sterne Morse, "The Electric Resistance and capacity of Blood for Frequencies between 800 and 4 1/2 Million Cycles," *Journal of General Physiology,* Vol 9, no 2, pp. 153-167, 1925.

[277] Hugo Fricke, "The electric capacity of suspensions with special reference to blood," *J Gen Physiol.,* Vol 9, no 2, pp. 137-152, 1925.

[278] Thomas Fischer Weiss, "Electrical Properties," from *Cellular Biophysics*, ISBN-0262231840, The MIT press, 1996.

[279] Kenneth S. Cole, "Rectification and inductance in the squid giant axon," *J Gen Physiol,* Vol 25, no 1, pp. 29-51, 1941.

[280] Kenneth S. Cole and R F Baker, “Longitudinal impedance in the squid giant axon,” *J Gen Physiol,* Vol 24, no 6, pp. 771-788, 1941.

[281] K S Cole and R F Baker, “Transverse impedance of the squid giant axon during current flow,” *J Gen Physiol,* Vol 24, no 4, pp. 535-549, 1941.

[282] K S Cole and H J Curtis, “Membrane potential in the squid giant axon during current flow,” *J Gen Physiol,* Vol 24, no 4, pp. 551-563, 1941.

[283] K S Cole and A L Hodgkin, “Membrane and protoplasm resistance in the squid giant axon,” *J Gen Physiol,* Vol 22, no 5, pp. 671-687, 1939.

[284] Shiro Takashima, Electrical Properties of Biopolymers and Membranes, Bristol, UK: Adam-Hilger, 1989.

[285] Gary C. Sieck, Leonardo F. Ferreira, Michael B. Reid and Carlos B. Mantilla, “Mechanical Properties of Respiratory Muscles,” *Compr Physiol,* Vol 3, no 4, pp. 1553-1567, 2013.

[286] H. Fricke, “The Electric Permittivity of a Dilute Suspension of Membrane‐Covered Ellipsoids,” *J. Appl. Phys,* Vol 24, no 5, pp. 644-646, 1953.

[287] J. A. Osborn, “Demagnetizing factors of the general ellipsoid,” *Physical review,* Vol 67, no 11,12, pp. 351-357, 1945.

[288] E. C. Stoner, “The demagnetizing factors for ellipsoids,” *Phil. Mag,* Vol 36, no 263, pp. 803-820, 1945.

[289] J. Stratton, Electromagnetic Theory, McGraw Hill, 1941.

[290] H. P. Schwan, “Electrical properties of tissue and cell suspensions,” *Adv.Biol.Med.Phys,* Vol 5, pp. 147-209, 1957.

[291] U Zimmermann, “Electric field-mediated fusion and related electrical phenomena,” *Biochim Biophys Acta,* Vol 694, no 3, pp. 227-277, 30 Nov 1982.

[292] E. Neumann, A. Sowers and C. A. Jordan, Electroporation and Electrofusion in Cell Biology, Springer: Plenum Press, 1989.

[293] Katherine A. DeBruin and Wanda Krassowska, “Modeling Electroporation in a Single Cell. I. Effects of Field Strength and Modeling Electroporation in a Single Cell. I. Effects of Field Strength and Rest Potential,” *Biophysical Journal,* Vol 77, no 3, pp. 1213-1224, 1999.

[294] T. Kotnik,, Feda Bobanović and Damijian Miklavčič, “Sensitivity of transmembrane voltage induced by applied electric Fields- a theoretical analysis,” *Bioelectrochemistry and Bioenergetics,* Vol 43, no 2, pp. 285-291, 1997.

[295] T. Kotnik, Damijan Miklavčič and Tomaž Slivnik, “Time course of transmembrane voltage induced by time-varying electric fields—a method for theoretical analysis and its application,” *Bioelectrochemistry and Bioenergetics,* Vol 45, no 1, pp. 3-16, 1998.

[296] Si Qin, “Pulsed Electric Field Treatment of Arthrospira Platensis and Saccharomyces Cerevisiae,” pp. 83-97, 2016.

[297] Christian Eing, Martina Goettel, Ralf Straessner, Christian Gusbeth and Wolfgang Frey, “Pulsed Electric Field Treatment of Microalgae—Benefits for Microalgae Biomass Processing,” *IEEE Transactions on Plasma Science,* Vol 41, no 10, pp. 2901-2907, 10 2013.

[298] Greta Canelli, Isabelle Kuster, Luc Jaquenod, Leandro Buchmann , Patricia Murciano Martínez, Zhen Rohfritsch, Fabiola Dionisi, Christoph J. Bolten , Paolo Nanni and Alexander Mathys, “Pulsed electric field treatment enhances lipid bioaccessibility while preserving oxidative stability in Chlorella vulgaris,” *Innovative Food Science & Emerging Technologies,* Vol 75, pp. 1-10, 2022.

[299] R.E Bruhn, P.D Pedrow, R.G Olsen, G.V Barbosa-Canovas and B.G Swanson, “Electrical environment surrounding microbes exposed to pulsed electric fields,” *IEEE transactions on dielectrics and electrical insulation,* Vol 4, no 6, pp. 806-812, 1997.

[300] K Rosenheck , “Evaluation of the electrostatic field strength at the site of exocytosis in adrenal chromaffin cells,” *Biophys,* Vol 75, no 3, pp. 1237-1243, 1998.

[301] C. L. Davey and D. B. Kell, “The Low-Frequency Dielectric Properties of Biological Cells. In D. Waltz, H. Berg, and G. Milazzo ed,” from *Bioelectrochemistry of Cells and Tissues*, Berlin, Birkauser, 1995, pp. 159-207.

[302] G. H. Markx and C. L. Davey, “The Dielectric Properties of Biological Cells at Radiofrequencies: Applications in Biotechnology,” *Enzyme and Microbial Technology,* Vol 25, no 3-5, pp. 161-171, 1999.

[303] G. Cevc, “Membrane Electrostatics,” *Biochim. Biophys. Acta,* Vol 1031, no 3, pp. 311-382, 1990.

[304] R.E Bruhn, P.D Pedrow, R.G Olsen,, G.V Barbosa-Canovas and B.G Swanson, “Electrical environment surrounding microbes exposed to pulsed electric fields,” *IEEE transactions on dielectrics and electrical insulation,* Vol 4, no 6, pp. 806-812, 1997.

[305] J. Gimsa, T. Müller, T. Schnelle and G. Fuhr, “Dielectric Spectroscopy of Single Human Erythrocytes at Physiological Ionic Strength: Dispersion of the Cytoplasm,” *Biophys J.,* Vol 71, no 1, pp. 495-506, 1996.

[306] H. P. Schwan, “Electrical Properties of Tissues and Cell Suspensions: Mechanisms and Models,” *Proceedings of 16th Annual International Conference of the IEEE Engineering in Medicine and Biology Society,* Vol 1, pp. 70-71, 1994.

[307] Hui Ye, “Kinematic difference between a biological cell and an artificial vesicle in a strong DC electric field – a “shell” membrane model study,” *BMC Biophysics,* Vol 10, no 6, pp. 1-13, 2017.

[308] M. Madigan, J. Martinko, K. Bender, D. Buckley and D. Stahl, Brock Biology of Microorganisms, 14th ed. Globe ed., San Francisco: Pearson Education, 2014.

[309] A. H. El-Hag, S. H. Jayaram, O. R. Gonzalez and M. W. Griffiths, “The Influence of Size and Shape of Microorganism on Pulsed Electric Field Inactivation,” *IEEE Trans. Nanobiosci,* Vol 10, no 3, pp. 133-138, 2011.

[310] B. Song, I. Timoshkin, M. Maclean, M. Wilson, M. Given, S. J. MacGregor, K. Satoh and H. Kawaguchi, "Local heating and stresses across membranes of microorganisms stressed with electric field," from *Pulse power conference*, Brighton, 2017.

[311] Michael L. Watson, "The nuclear envelope; its structure and relation to cytoplasmic membranes," *J Biophys and Biochem Cytol,* Vol 1, no 3, pp. 257-270, 1955.

[312] Jan Lammerding, "Mechanics of the Nucleus," *Compr Physiol,* Vol 1, no 2, pp. 783-807, 2011.

[313] S. Heyden and M. Ortiz, "Investigation of the influence of viscoelasticity on oncotripsy," *Computer Methods in Applied Mechanics and Engineering,* Vol 314, pp. 314-322, 2017.

[314] R. Hine, The Facts on File Dictionary of Biology (fourth ed.)Facts on File Science Library,, New York: Checkmark Books, 2005.

[315] Hao Qiu, Shu Xiao and Ravi P. Joshi, "Simulations of Voltage Transients Across Intracellular Mitochondrial Membranes Due to Nanosecond Electrical Pulses," *IEEE Transactions on Plasma Science,* Vol 42, no 10, pp. 3113-3120, 2014.

[316] Fei Guo, Lin Zhang and Xin Liu , "Nonlinear dispersive cell model for microdosimetry of nanosecond pulsed electric fields," *Scientific Reports,* Vol 10, no 1, p. 19456, 2020.

[317] T. Honorio, "Thermal conductivity, heat capacity and thermal expansion of ettringite and metaettringite: Effects of the relative humidity and temperature," *Cement and Concrete Research,* Vol 159, pp. 1-14, 2022.

[318] J. Neu and W. Krassowska, "Asymptotic model of electroporation," *Phys. Rev. E,* Vol 59, no 3, pp. 3471-3482, 1999.

[319] Bolin Song, Igor Timoshkin, Michelle Maclean, Mark Wilson, Martin Given, Scott J. MacGregor, K. Satoh and Hideki Kawaguchi, "Local heating and stresses across membranes of microorganisms stressed with electric field," *Pulsed Power Conference,* 2017.

[320] T. Honorio, “Thermal conductivity, heat capacity and thermal expansion of ettringite and metaettringite: Effects of the relative humidity and temperature,” *Cement and Concrete Research,* Vol 159, pp. 1-14, 2022.

[321] Robert Hebner, Kent Davey, Michael Werst, Rhykka Connelly and Colin Beal , “An Electromechanical Effect on Cell Membranes,” *IEEE Transactions on Dielectrics and Electrical Insulation,* Vol 24, no 1, pp. 666-674, 2016.

[322] Masaki Hayashi , “Temperature-Electrical Conductivity Relation of Water for Environmental Monitoring and Geophysical Data Inversion,” *Environ Monit Assess,* Vol 96, no 1-3, pp. 119-128, 2004.

[323] Peter H. Siegel, “Microwaves Are Everywhere: “Ovens: From Magnetrons to Metamaterials”,” *IEEE Journal of Microwaves,* Vol 1, no 2, pp. 1-9, 2021.

[324] V. Raicu, G. Raicu and G. Turcu, “Dielectric properties of yeast cells as simulated by the two-shell model,” *Biochimica et Biophysica Acta (BBA) - Bioenergetics,* pp. 143-148, 13 June 1996.

[325] A. Kamgoué, J. Ohayon and P. Tracqui, “Estimation of Cell Young’s Modulus of Adherent Cells Probed by Optical and Magnetic Tweezers: Influence of Cell Thickness and Bead Immersion,” *Journal of Biomechanical Engineering,* Vol 129, no 4, pp. 523-530, 2007.

[326] T. Jadidi, H. Seyyed-Allaei, M. Reza Rahimi Tabar and A. Mashaghi, “Poisson’s ratio and Young’s modulus of lipid bilayers in different phases,” *Front. Bioeng. Biotechnol.,* Vol 2, pp. 1-6, 2014.

[327] S. Youssefian, N. Rahbar, R. C. Lambert and S. V. Dessel, “Variation of thermal conductivity of DPPC lipid bilayer membranes around the phase transition temperature,” *Journal of the royal society interface,* Vol 14, no 130, pp. 1-8, 2017.

[328] Si Qin, Igor V. Timoshkin, Michelle Maclean, Mark Peter Wilson, S.J. MacGregor, Martin John Given, John G Anderson and T. Wang, “Pulsed Electric Field Treatment of Microalgae Inactivation Tendencies and Energy Consumption,” *IEEE Transactions on Plasma Science ,* vol. 42, no. 10, pp. 3191-3196, 07 May 2014.

[329] S. Qin, I. V. Timoshkin, M. Maclean, M. P. Wilson, M. J. Given and T. Wang, "Pulsed electric field treatment of saccharomyces cerevisiae using different waveforms," *IEEE Transactions on Dielectrics and Electrical Insulation,* pp. 1841-1848, 11 August 2015.

[330] Valerică Raicu, Georgeta Raicu and Grigore Turcu, "Dielectric properties of yeast cells as simulated by the two-shell model," *Biochimica et Biophysica Acta (BBA) - Bioenergetics,* pp. 143-148, 13 June 1996.

[331] Yan Mi, Shaoqin Rui, Chenguo Yao, Jin Xu, Changhao Bian and Xuefeng Tang , "Multi-parametric study of temperature and thermal damage of tumor exposed to high-frequency nanosecond-pulsed electric fields based on finite element simulation," *Medical & Biological Engineering & Computing,* Vol 55, no 7, pp. 1109-1122, 2016.

[332] Biofactory, "BIOFACT," [online]. Available: https://www.bio-ft.com/product/product.html?category=018085&id=EP-101&mode=view&sort_mode=.

[333] T. Liu, "Pre-breakdown ionization processes and impulsive breakdown characteristics of gases," *PhD thesis,* 2023.

[334] T. E. Shehata and Allen G. Marr, "Effect of Nutrient Concentration on the Growth of Escherichia coli," *J Bacteriol,* Vol 107, no 1, pp. 210-216, 1971.

[335] Justus Wilhelm Fink , Noelle A. Held and Michael Manhart , "Microbial population dynamics decouple growth response from environmental nutrient concentration," *Proceedings of the National Academy of Sciences,* Vol 120, no 2, 2023.

[336] A. Capretti, A. K. Ringsmuth, J. F. van Velzen, A. Rosnik, R. Croce and T. Gregorkiewicz , "Nanophotonics of higher-plant photosynthetic membranes," *Light Sci,* Vol 8, no 5, pp. 116-118, 2019.

[337] Shengpu Gao, Gillian D. Lewis, Muthupandian Ashokkumar and Yacine Hemar, "Inactivation of microorganisms by low-frequency high-power ultrasound: 1. Effect of growth phase and capsule properties of the bacteria," *Ultrasonics Sonochemistry,* Vol 21, no 1, pp. 446-453, 2014.

[338] Kang Huang and Jianping Wang, “Designs of pulsed electric fields treatment chambers for liquid foods pasteurization process: A review,” *Journal of Food Engineering,* Vol 95, no 2, pp. 227-239, 2009.

[339] A. L. Garner, M. Denminsky, V. Bogdan Neculaes, V. Chashihin, A. Knizhnik and n. B. Potapkin, “Cell membrane thermal gradients induced by electromagnetic fields,” *Journal of Applied Physics,* Vol 113, no 21, pp. 1-11, 2013.